CENTRAL RESEARCH LIBRARY

ORNL-4903

cy. 1

# Health Physics DIVISION

MARTIN MARIETTA ENERGY SYSTEMS LIBRARIES
3 4456 0359431 3

## Annual Progress Report

Period Ending July 31, 1973

OAK RIDGE NATIONAL LABORATORY
CENTRAL RESEARCH LIBRARY
DOCUMENT COLLECTION
LIBRARY LOAN COPY
DO NOT TRANSFER TO ANOTHER PERSON
If you wish someone else to see this document, send in name with document and the library will arrange a loan.
UCN-7969
(3 3-67)

OAK RIDGE NATIONAL LABORATORY

OPERATED BY UNION CARBIDE CORPORATION • FOR THE U.S. ATOMIC ENERGY COMMISSION

Printed in the United States of America. Available from
National Technical Information Service
U.S. Department of Commerce
5285 Port Royal Road, Springfield, Virginia 22151
Price: Printed Copy $7.60; Microfiche $0.95

This report was prepared as an account of work sponsored by the United States Government. Neither the United States nor the United States Atomic Energy Commission, nor any of their employees, nor any of their contractors, subcontractors, or their employees, makes any warranty, express or implied, or assumes any legal liability or responsibility for the accuracy, completeness or usefulness of any information, apparatus, product or process disclosed, or represents that its use would not infringe privately owned rights.

ORNL-4903
UC-41 — Health and Safety

Contract No. W-7405-eng-26

# HEALTH PHYSICS DIVISION
# ANNUAL PROGRESS REPORT

For Period Ending July 31, 1973

J. A. Auxier, Director
W. S. Snyder, Assistant Director
D. M. Davis, Assistant Director

SEPTEMBER 1973

OAK RIDGE NATIONAL LABORATORY
Oak Ridge, Tennessee 37830
operated by
UNION CARBIDE CORPORATION
for the
U.S. ATOMIC ENERGY COMMISSION

MARTIN MARIETTA ENERGY SYSTEMS LIBRARIES
3 4456 0359431 3

Reports previously issued in this series are as follows:

| | |
|---|---|
| ORNL-2384 | Period Ending July 31, 1957 |
| ORNL-2590 | Period Ending July 31, 1958 |
| ORNL-2806 | Period Ending July 31, 1959 |
| ORNL-2994 | Period Ending July 31, 1960 |
| ORNL-3189 | Period Ending July 31, 1961 |
| ORNL-3347 | Period Ending July 31, 1962 |
| ORNL-3492 | Period Ending July 31, 1963 |
| ORNL-3697 | Period Ending July 31, 1964 |
| ORNL-3849 | Period Ending July 31, 1965 |
| ORNL-4007 | Period Ending July 31, 1966 |
| ORNL-4168 | Period Ending July 31, 1967 |
| ORNL-4316 | Period Ending July 31, 1968 |
| ORNL-4446 | Period Ending July 31, 1969 |
| ORNL-4584 | Period Ending July 31, 1970 |
| ORNL-4720 | Period Ending July 31, 1971 |
| ORNL-4811 | Period Ending July 31, 1972 |

# Contents

FOREWORD . . . . . x

SUMMARY . . . . . x

**PART I. RADIATION RESEARCH AND DEVELOPMENT**

1. DOSIMETRY FOR HUMAN EXPOSURES AND RADIOLOGICAL IMPACT . . . . . 1
   - Japanese Dosimetry Program . . . . . 1
   - In Utero Exposure of A-Bomb Survivors . . . . . 2
   - Thermal Neutron Fluence Distributions . . . . . 7
   - Dose and Fluence in Isotropic and Nonuniform Fields of Radiation . . . . . 12
   - ICRU Neutron Dosimetry Intercomparison . . . . . 14
   - Improvements in Nitrocellulose Film . . . . . 16

2. SOLID-STATE DOSIMETRY RESEARCH . . . . . 19
   - TSEE Reader Development . . . . . 19
   - TSEE Detector Sensitivity and Reproducibility . . . . . 19
   - Gas Effects on TSEE . . . . . 22
   - TSEE in Personnel and Environmental Monitoring . . . . . 23
   - Fast-Neutron Dosimetry by TSEE . . . . . 24
   - TSEE Monitoring of Beta Emitters . . . . . 26
   - TLD and Film Stability Studies . . . . . 27
   - TL Detector Development . . . . . 29
   - Other Research . . . . . 29
   - Information and Educational Activities . . . . . 30

3. ATOMIC PHYSICS . . . . . 31
   - Transport of Resonance Radiation . . . . . 31
   - Decay of Resonance Photons in Argon Gas . . . . . 35
   - Quenching of Resonance Excited States with Molecules . . . . . 36
   - Mathematical Formulation of Radiation-Stimulated Biological Effects . . . . . 37

4. SPECTROMETRIC DOSIMETRY . . . . . 45
   - Organic Scintillator Research . . . . . 45
   - Distribution of Charged-Particle Stopping . . . . . 46

HPRR Neutron and Gamma-Ray Spectrum Incident on the Roof of the DOSAR ..... 47
Alpha Air Monitor Electronics ..... 47
A Convenient Counter for Measuring the Alpha Activity of Air Samples ..... 47

5. HPRR AND ACCELERATOR OPERATIONS ..... 51
Health Physics Research Reactor Operations ..... 51
High-Density Track Counting Using an Electron Beam ..... 51
Long-Lived Tritium Targets for Neutron Generators ..... 54

## PART II. FUNDAMENTAL HEALTH PHYSICS RESEARCH

6. THEORETICAL RADIATION PHYSICS ..... 58
Pion Dosimetry ..... 58
Stopping Power of Matter for Neutrons ..... 59
The Calculation of the $Z_1{}^3$-Dependent Stopping Power Contribution and its Influence on Ranges, Mean Excitation Potentials, and Shell Corrections ..... 61
An Experimental and a Computational Program for Obtaining a Relationship Between Quality Factor, $Q$, and Linear Energy Transfer, LET ..... 62
Theoretical Studies of Radiation-Stimulated Biological Effects ..... 63
The Linear Response Function of a Random Assembly of Molecules ..... 63
Complex Potential Methods for Molecular Scattering ..... 64
Rotational Resonances in Molecular Scattering of Ultra-Low-Energy Electrons ..... 64
Collisions of Alkali Metal Atoms with Atomic Oxygen ..... 66
Classical Binary Inelastic Cross Sections for Excitation and Ionization of Electrons in Atomic Systems ..... 67
High-Energy Satellites in Auger Electron Spectra from Solids ..... 68
Diffuse Scattering and Surface Plasmon Generation by Photons at a Rough Dielectric Surface ..... 70
Surface Plasmons in Cylindrical Geometry ..... 70
Primary Radiation Processes in the Physical Stage ..... 70
Surface Plasmons in Solids ..... 71

7. ATOMIC AND MOLECULAR RADIATION PHYSICS ..... 72
Interaction of Slow Electrons with Molecules in Very-High-Pressure ("Quasi-Liquid") Environments ..... 72
Long-Lived Organic Negative Ions ..... 73
Extension of Our Basic Understanding of Processes Accompanying Interaction with Matter from Simple to Complex Structures ..... 76
Threshold Electron Excitation and Compound-Negative-Ion Formation in Unsaturated Hydrocarbons ..... 76
Electron Attachment to $c$-$C_4F_8$ and $CCl_2F_2$ Below ~2 eV ..... 76
Comparison of Electron Swarm and Microwave Measurements of the Thermal Rate of Electron Attachment ..... 77
Mobilities of Thermal Electrons in $\pi$-Electron-Containing Organic Gases ..... 78
Unimolecular Decompositions ..... 80

Energy Transfer from Argon to Xenon Atoms . . . . . 81

Emission from the First and Second Excited $\pi$-Singlet States of Aromatic Hydrocarbons in Solution and Their Temperature Dependences . . . . . 81

8. INTERACTION OF RADIATION WITH LIQUIDS AND SOLIDS . . . . . 83

Photon–Surface-Plasmon Coupling in Thin Films . . . . . 83

Optical and Photoelectric Properties of Magnesium in the Vacuum Ultraviolet . . . . . 85

Optical Properties and Electron Attenuation Lengths from Photoelectric Yield Measurements . . . . . 88

Satellites in the X-Ray Emission Spectra of Li, Be, and Na . . . . . 90

Study of the Optical Properties of Solids by Ellipsometry . . . . . 91

9. ELECTRON AND ION COLLISION PHYSICS . . . . . 93

Dissociative Ionization of Molecules by Electron Impact . . . . . 93

Longitudinal Diffusion Coefficients and Drift Velocity Measurements in $H_2O$ and $D_2O$ . . . . . 96

Mass Analysis of Negative Ions Produced in Swarm Experiments: Ion Clustering Reactions in Water Vapor . . . . . 96

Thermal Energy Electron Attachment Rate Constants for Some Polyatomic Molecules . . . . . 98

Collisional Ionization of Cesium by Molecules: Determination of Molecular Electron Affinities . . . . . 99

Electron Impact Studies of Some Cyclic Hydrocarbons . . . . . 99

Low-Energy Induced Sputtering of Alkali Halides . . . . . 101

Properties of Constituents of Possible Superconductors . . . . . 101

A Chemical Accelerator for Studying the Collisional Behavior of Large Molecules: $SF_6 + CO_2$ . . . . . 102

10. PHYSICS OF TISSUE DAMAGE . . . . . 103

Electron-Slowing-Down Studies . . . . . 103

Optical Properties of Organic Liquids . . . . . 104

Radiation Interactions with Nucleic Acid Bases . . . . . 106

Optical and Electronic Properties of Chlorophyll . . . . . 108

**PART III. MEDICAL PHYSICS AND INTERNAL DOSIMETRY**

11. A MODEL FOR EXPOSURE TO A SEMI-INFINITE CLOUD OF A PHOTON EMITTER . . . . . 110

12. ESTIMATION OF DOSE AND DOSE COMMITMENT TO THE BLADDER WALL FROM A PHOTON EMITTER PRESENT IN URINE . . . . . 115

13. DOSE FROM PHOTON EMITTERS DISTRIBUTED UNIFORMLY IN THE TOTAL BODY AS A FUNCTION OF AGE . . . . . 119

14. ESTIMATES OF DOSE RATE TO GONADS OF INFANTS AND CHILDREN FROM A PHOTON EMITTER IN VARIOUS ORGANS OF THE BODY . . . . . 125

15. A HUMAN METABOLIC MODEL FOR $^{14}C$-LABELED METABOLITES USEFUL IN DOSE ESTIMATION . . . . . 130

16. AN EXPERIMENTAL MOCKUP OF THE SNYDER-FISHER PHANTOM . . . . . 131

17. MEDICAL X-RAY DOSE ESTIMATION PROGRAM . . . . . 133

## PART IV. URBAN RESEARCH

18. BACKGROUND . . . . . 139

19. PROGRAM IN URBAN RESEARCH . . . . . 140

Migration and Fertility: A Study of the Social Factors Involved . . . . . 140

Changes in Population and Employment as Processes in Regional Development . . . . . 140

Correlates of Childlessness and Expectation to Remain Childless: U.S. 1967 . . . . . 140

Measuring Patterns of Urban Growth . . . . . 141

The Decentralization of Manufacturing Employment . . . . . 141

The Prospects for New Cities: The Historical View . . . . . 141

An Urban Classification Scheme: The Development of a Simple Urban Model . . . . . 141

Selected Factors Influencing City Growth 1960–1970 . . . . . 142

Poverty and Migration from Rural to Metropolitan Areas . . . . . 142

Labor Mobility and Urban Growth in the Atlanta Metropolitan Area . . . . . 142

Effects of Crowding and High Population Density: An Annotated Bibliography with Permuted Title and Simple Author, Title, Key Word, and Taxonomic Indices . . . . . 143

A Statistical Processing System for the Public Use Samples . . . . . 143

## PART V. CIVIL DEFENSE RESEARCH

20. STRATEGIC DEFENSE . . . . . 144

Soviet Civil Defense Studies . . . . . 144

Strategic Considerations in Planning a Counterevacuation . . . . . 145

Mapping of Population Density . . . . . 146

Expedient Shelter Survey . . . . . 154

Blast Resistance of Expedient Shelters . . . . . 160

Measurement of Shock Overpressure in Air by a Yielding Foil Membrane Blast Gage . . . . . 162

21. EFFECTS ON CIVILIAN SYSTEMS FROM HIGH-ALTITUDE DETONATIONS . . . . . 166

Surges Induced in Transmission Systems . . . . . 166

Effects of EMP on the Supervisory Control Equipment of a Power Station . . . . . 167

The Stability of the Electric Power System in a Nuclear Electromagnetic Environment . . . . . 168

Effects of Electromagnetic Pulse on Radio Communications . . . . . 169

The Voltage Induced in Infinite, Lossless, Two-Wire Transmission Line by Parallel Finite Current Sources . . . . . 170

22. EMERGENCY PLANNING FOR ACCIDENTAL RADIOACTIVITY RELEASES FROM A LICENSED NUCLEAR FACILITY . . . . . 172

Time Available to Institute Emergency Procedures . . . . . 172

Chemical Prophylaxis . . . . . 172

Improvised Respiratory Protection . . . . . 174
Dose and Deposition Estimation . . . . . 174

**PART VI. EDUCATION AND INFORMATION**

23. EDUCATION AND VOCATIONAL TRAINING . . . . . 175

24. HEALTH PHYSICS INFORMATION SYSTEM . . . . . 178

**THESES, PAPERS, PUBLICATIONS, AND LECTURES**

THESES . . . . . 179

PAPERS . . . . . 180

PUBLICATIONS . . . . . 183

LECTURES . . . . . 191

# Foreword

This annual report covers the research efforts of the Health Physics Division during the period from August 1, 1972, through July 1973. As has been the case in the past, the work of the Applied Health Physics sections is reported separately, by calendar year. The latest, for calendar year 1972, is ORNL-4894.

The content of this report is a series of abstract-type summaries with references and figures added. The references, chiefly to open literature publications, give the complete work, and the reader is invited to contact directly the authors, group leaders, or section chiefs.

The retirement of Dr. Morgan as Director of the Health Physics Division occurred approximately one year ago, and this was the occasion for some reorganization. Waste disposal research was transferred out of the Division, and the Civil Defense Research and Urban Research sections were added. This is the first annual report to include accounts of the research of these two sections.

There have been a number of organizational changes within the Division, the most noteworthy being perhaps the broadened scope implied by the new title of the Medical Physics and Internal Dosimetry Section and the addition of two senior persons to the staff of the former Internal Dosimetry Section. Although one can never truly replace a former leader such as Dr. Morgan, the program of the new section indicates that his emphasis on reducing medical exposure is represented by the constructive studies reported below. Education and informational activities of the Division are now combined in the Education and Information Section. Because of the increased emphasis on the environment and the accompanying responsibilities for monitoring and interpreting the data, the personnel of the Applied Health Physics sections have been strengthened and some new programs are developing.

The programs during the past year have emphasized the interdisciplinary nature of health physics, and cooperative programs are under way or under active development with the Biology and the Environmental Sciences divisions, the UT-AEC Agricultural Experiment Station, and several other organizations. It is too early for some of these efforts to be reported here, but the reader will have no doubt of the serious effort represented by the contributions contained herein.

The Division has reviewed its past performance and has developed a plan of goals and objectives for the next several years. Although the plan provides specific guidance, it represents a dynamic program which can be responsive to major changes in national needs. The Division expects its future goals to be relevant to the significant problems of health physics research and practice, as in the past, and it will maintain the highest standards of the profession.

# Summary

## PART I. RADIATION RESEARCH AND DEVELOPMENT

### 1. Dosimetry for Human Exposures and Radiological Impact

Techniques are presented for entering particles (or photons) of nondirectional radiation fields into Monte Carlo transport calculations of depth dose in the body and for normalizing the depth dose in the body to the particle fluence of the field. Depth-dose distributions in a cylindrical man-type phantom exposed to isotropic fields of monoenergetic neutrons are presented and compared with depth-dose distributions from broad, monoenergetic beams of neutrons. The investigation of depth-dose distributions in the body from nondirectional radiation fields is important in estimating dose to internal organs, both in radiation protection and in Japanese A-bomb survivor studies. Depth-dose distributions are also presented for neutron and gamma-ray spectra and angular distributions typical of those from a fission-type nuclear weapon. Application of these results in estimating dose to survivors exposed in utero is discussed. Additional calculations of the thermal neutron fluence in the body are also presented for broad, monoenergetic beams of 0.025-eV to 14-MeV neutrons incident on the body. These thermal neutron fluence distributions provide some guidelines for investigators considering the use of neutron irradiation in therapeutic treatment of neoplastic soft tumors.

The overall accuracy of methods used to calculate shielding factors for Japanese A-bomb survivors who were exposed in concrete structures and the incidence of acute radiation effects or symptoms in Japanese A-bomb survivors exposed to fallout rain in Hiroshima are also reported.

Improvements have also been made in preparing nitrocellulose films used as alpha particle detectors in radon progeny personnel dosimeters. Strong and durable films with a thickness of 10 to 20 $\mu$ have been prepared using a solution of nitrocellulose, dioctyl phthalate, and tetrahydrofuran. The track density, as determined with a spark counter for these films, is linear with alpha particle fluence up to several thousand counts per square centimeter.

### 2. Solid-State Dosimetry Research

Research and development work on sensitivity, stability, and reliability of sensitive integrating radiation detectors based on thermally stimulated exoelectron emission (TSEE) from ceramic beryllium oxide, and improvements of the TSEE readout instrumentation, have reached a point where these detectors have been used successfully in environmental and personnel dosimetry field tests. The detectors also show promise for low-energy beta radiation dosimetry ($^3H$) in gases and liquids. Their response characteristics in mixed fast-neutron and gamma radiation fields have been further investigated, and methods to determine the direction and effective energy of incident neutrons have been developed.

Extensive further laboratory and field tests concerning the stability of photographic films, TLD, and other dosimeters confirmed that the film dosimeter cannot be used in humid and warm climates in which even LiF:Mg,Ti (unlike some other TL phosphors, such as $CaSO_4$:Dy) may exhibit considerable fading. Other studies on TLD included an encouraging system for fast-neutron dosimetry based on the dispersion of finely powdered sensitive phosphors in pellets of high-melting (>450°C) hydrogenous organics, such as *p*-sexiphenyl, and the use of improved phosphors in area monitoring. As in previous years, substantial efforts have also been devoted to information and education activities in the solid-state dosimetry field; the compilation of critical reviews; and assistance to international organizations, such as the International Atomic Energy Agency, World Health Organization, and Organization of American States.

### 3. Atomic Physics

An equation for the transport of resonance radiation is derived and shown to be in reasonable agreement

with an experiment on the argon 1048-Å resonance radiation conducted in parallel with the theoretical development. At pressures greater than 1 torr, where collisions are frequent, the derived transport equation is equivalent to that of Holstein and Biberman. In the pressure region from 0.02 to 0.5 torr there is substantial disagreement between the present work and theory that assumes complete redistribution in frequency, that is, takes the emission profile to be equal to the absorption profile.

Resonance radiation transport is an important factor in studies of energy pathways following charged-particle excitation of noble gases. Another pathway which recently emerged in importance appears to be dissociative recombination of ion pairs, which gives birth to additional resonance states. We have found that our time-resolved spectroscopy is a valuable technique for study of this nonlinear effect, important to laser technology. Quenching of resonance states has been measured with a direct rate of decay method; rates are found to be in excellent agreement with theory for the case of energy transfer from the resonance states $Ar(^1P_1)$ and $Ar(^3P_1)$ to ethylene.

We continue to pursue a generalized approach to radiation dosimetry aimed at predicting the probability of effect $i$ appearing in species $j$ as a function of time $t$, that is, $P_{ij}(t)$. Important aspects of this program are the modeling of various biological effects in several species and comparison of the results in the dynamical models with experimentally measured $P_{ij}(t)$. A model has been developed for cell survival with encouraging results. Efforts are now under way on the generalization of the Katz track effect model so that kinetics of repair and the time history of the radiation exposure are properly incorporated. Additional modeling done with the existing data on production of cataracts in mice has been sufficiently encouraging to suggest new experiments for further testing.

### 4. Spectrometric Dosimetry

The goals of the Spectrometric Dosimetry Group are the evaluation and design of spectrometers for application to radiation protection. This year, these studies were expanded to include work with dosimetry systems using detectors that produce pulse-height distributions. Work in the design of electronic circuits needed both for the detectors studied and in support of other programs has continued. The continuing program to develop improved organic scintillators for neutron detectors has provided improved techniques of synthesis and purification of *p*-sexiphenyl. Preliminary measurements of light yield show this scintillator to be more efficient in producing light than anthracene. The apparatus to measure the distribution of energy losses of low-energy protons has been tested and calibrated. The first measurements will use selected hydrocarbon foils that are now being cast. Neutron and gamma-ray spectrum measurements in support of the other programs within this section continue. Emphasis for the past year has been on neutron spectrum measurements made as a function of incident angle upon the roof of the DOSAR Control Building. A simplified technique for alpha spectroscopy of air samples was developed. An electronic circuit was designed and tested for use with an alpha air monitor that is under development in the Radiation and Safety Surveys Section of the Division.

### 5. HPRR and Accelerator Operations

The principal activity of this group is the operation of the Section's radiation facilities in support of research in dosimetry, radiation biology, other radiation effects, and nuclear safety. Research activities in the group included the continued development of long-lived neutron generator targets and the evaluation of track densities in Kimfoil (10 $\mu$) by the transmission of 14-keV electrons through etched holes in the foil.

The Health Physics Research Reactor continues to play an important role in the efforts to correlate radiation dose with biological effect. Scientists from the ORNL Biology Division, UT-AEC Agricultural Research Laboratory, and several other laboratories comprise the list of "most frequent" users. In addition, the HPRR is also used for nuclear engineering studies and for nuclear safety through the dosimetry intercomparison studies which are designed to evaluate nuclear accident dosimetry systems.

Target research has centered on the parametric study of palladium-silver foils as an agent for replenishing tritium to the "target-site" region of neutron generator targets. These targets make it possible to provide 14-MeV neutrons for dosimetry and for radiation biology studies requiring long exposures to relatively high yields of neutrons. At this point, the half-life of self-replenishing targets has been increased by 75%.

The section's 20-keV electron accelerator was used successfully to evaluate the density of fission-fragment tracks in 10-$\mu$ Kimfoil (tracks appear as small holes in Kimfoil) over a wide range. These hole densities are normally determined by using a "jumping spark" counter, but this technique is limited currently to approximately 3000 holes/cm$^2$. By using 14-keV elec-

trons, which penetrate only the holes, it is possible to measure in the range of 10 to 100 times larger hole densities.

## PART II. FUNDAMENTAL HEALTH PHYSICS RESEARCH

### 6. Theoretical Radiation Physics

**Theoretical dosimetry.** Additions have been made to our PION-1 computer code which may be used to calculate depth-dose curves for pion beams incident on various targets. These additions allow for the presence of multiregional targets of varying composition; we have incorporated range straggling and an improved method of treating multiple Coulomb scattering. The Bethe theory of the stopping power of matter for charged particles has been generalized to include the neutron as a projectile. The theory of the $Z_1^3$-dependent contribution to the stopping power of matter for charged particles has been cast into simple formulas which apply in a comprehensive manner to all targets. We have evaluated the influence of the $Z_1^3$ contribution to theoretical stopping power on the evaluation of mean excitation potentials and shell corrections; we find that the former are changed relatively little ($\lesssim 1.5\%$) for a wide range of materials, but use of the $Z_1^3$ contribution results in rather dramatic changes in the shell corrections. A rationale for determining $Q$-LET relationships from controlled animal experiments has been proposed.

**Theoretical atomic and molecular physics.** An approximate expression has been obtained for the dielectric response function of a randomly distributed system of molecules. The resulting response function describes in a qualitative fashion both electron-hole pair excitations and plasmons. This result has relevance to the recent observation of collective electron modes in liquid water by workers in the Interaction of Radiation with Liquids and Solids Group. The complex optical potential approach to multichannel scattering in atomic and molecular systems has been applied to a study of low-energy electron collisions with linear molecules in the energy region where rotational and vibrational excitations of the target molecules are important. The existence of rotational resonances in molecular scattering of ultra-low-energy electrons has been studied using a simple model of a molecular dipole coupled with an electron having energy less than, but approaching, the first rotational threshold; a rotational resonance is found. We have evolved simple procedures for fitting classical binary collision cross sections, most nearly valid in the region of large momentum transfer, with other data on cross sections which are appropriate in the region of small momentum transfer; this is done by requiring that the generalized oscillator strength corresponding to this composite cross section shall obey the Bethe sum rule. Calculations of excitation and charge-transfer cross sections in neutral atom-atom collisions have been carried out in a three-state approximation. The charge-transfer cross sections obtained agree generally with those obtained from the Landau-Zener theory at low velocities but agree with those obtained from the Born approximation at high velocities.

**Theoretical radiation physics of solids.** The theory of the process by which an Auger electron created in a solid may acquire the plasmon energy has been studied; the results seem to be in reasonable agreement with experiment considering the uncertainties which exist in the Auger lifetime, a parameter which enters the theory in an important fashion. Processes of this character may yield important information about charged particle track structure in condensed media. We have derived formulas for diffuse scattering and conversion to surface plasmons of photons incident on a plane, microscopically rough dielectric surface, for arbitrarily large electronic damping processes in the dielectric. Surface plasmon eigenmodes for plasmas in infinite circular cylinder geometry have been considered; dispersion relations have been derived and evaluated numerically using the full set of Maxwell's equations for the fields. Collective modes in this geometry may have relevance to the properties of long chain molecules of biological significance. A review of physical processes which may occur in condensed matter at early times ($<10^{-13}$ sec) following the passage of a swift charged particle has been made. A review article describing the properties of the dynamic electron polarization modes associated with surfaces of simple solids has been published.

### 7. Atomic and Molecular Radiation Physics

The results of a recent study on the capture of slow electrons by molecules embedded in very-high-pressure gases are presented and discussed. Electron attachment to $O_2$ to form $O_2^-$ at thermal and near-thermal energies has been studied in mixtures with nitrogen (up to 26,000 torr), ethylene (up to 17,000 torr), and ethane (up to 17,500 torr). The observed large changes in the magnitude of the attachment rate for the formation of $O_2^-$ with increasing density of these three media are very different, demonstrating the profound effect and importance of the environment on the electron attach-

ment process. A lifetime of $\sim 2 \times 10^{-12}$ sec has been estimated for $O_2^{-*}$ from these studies.

The lifetimes $\tau$ of a number of organic long-lived ($\tau > 10^{-6}$ sec) negative ions – formed via nuclear-excited Feshbach resonances at thermal and near-thermal electron energies – have been measured as a function of electron energy and have been theoretically treated and related to the respective molecular structures. Thus the lifetime data for the $NO_2$-containing disubstituted benzene derivatives indicated that the $\tau$ for these molecules depends on the electron donor-acceptor properties of the substituent groups and the intramolecular interaction between them, which is a function of their relative position around the benzene periphery. From a mass spectrometric study of "key" organic molecules, it has been concluded that $NO_2$-containing benzene derivatives, CN-substituted organic molecules, higher aromatic hydrocarbons, strained structures, and organic molecules containing the functional groups –COCO–, –COCH(OH)–, –COOH, and =CHCHO capture thermal and near-thermal electrons very efficiently (often with a cross section $>100$ Å$^2$) and – in the absence of competing dissociative attachment processes which are usually very fast – form long-lived parent negative ions via nuclear-excited Feshbach resonances.

Our understanding of slow-electron–molecule interaction processes, especially of the process of short-lived ($\tau \lesssim 10^{-13}$ sec) compound-negative-ion formation, has been extended to a number of complex molecular structures of radiobiological interest, such as the benzene *N*-heterocyclic molecules and the unsaturated hydrocarbons (e.g., neopentane, *n*-hexane) for which threshold electron excitation spectra have been obtained.

The mobility $\mu$ of thermal electrons in $\pi$-electron-containing organic molecules (linear, cyclic, and aromatic hydrocarbons) was found to decrease with increasing number of doubly occupied $\pi$ orbitals. For linear hydrocarbons with two doubly occupied $\pi$ orbitals, $\mu$ increases with increasing separation of the two $\pi$ orbitals. On the basis of this work, double-bonded systems can effectively thermalize slow electrons, a property which increases with increasing number of doubly occupied $\pi$ orbitals.

Finally, fluorescence emission from the second excited $\pi$-singlet state has been observed for eight aromatic hydrocarbons in fluid media. The temperature dependence of this emission has been studied in detail and allowed deduction of general conclusions as to the radiative and nonradiative deactivation processes from the first and second excited $\pi$-singlet states of these molecules.

## 8. Interaction of Radiation with Solids and Liquids

The Interaction of Radiation with Solids and Liquids Group studies the ways in which photons and high-energy charged particles interact with matter in the condensed phases. From these studies we hope to understand eventually the ways in which energy is deposited along the track of any ionizing radiation, and the subsequent ways in which the energy is dissipated, in biological materials. It is becoming increasingly apparent that plasmon excitation is an important factor. It is known that volume plasmons are created in bulk material, and these have been studied extensively in previous years. This year, however, the emphasis has been on the investigation of surface plasmons since it is thought that these too may be important in macromolecules such as DNA. Surface plasmons may be excited by attenuated total reflectance. Using this technique we have determined the optical properties of silver and the dependence of the surface plasmon dispersion curves on surface roughness. The decay of surface plasmons into one-electron excitations was seen as an increase in the photoelectric yield. Surface plasmons may also be excited when photons interact directly with microscopically rough surfaces. This has been observed in magnesium as a decrease in the reflectance at the surface plasmon energy, and theory, developed in the Theoretical Radiation Physics program, has been used to obtain surface roughness parameters for the surface. An increased photoelectric yield was also observed by this method in magnesium at the surface plasmon energy. X-ray emission from lithium, beryllium, and sodium was studied for volume plasmon involvement. In each case a single satellite was observed below and a single satellite above the main emission band under study. The low-energy satellite was associated with volume plasmon creation, but the high-energy satellite originated from double ionization decay and did not show any volume plasmon involvement.

The accurate determination of optical properties and electron attenuation lengths requires different techniques depending on their magnitudes. We have developed a method of obtaining the refractive index $n$ and the extinction coefficient $k$ or electron attenuation length $L$ from the photoelectric yield from an infinitely thick photoemitter as a function of photon angle of incidence. This method may be more accurate than other techniques when $n$ is close to, but less than, unity and $k$ and $L$ are small.

Preliminary values for the optical constants of lithium have been obtained by the ellipsometry method.

### 9. Electron and Ion Collision Physics

Electron impact ionization phenomena are of fundamental importance in radiation physics and chemistry studies. A new experiment has been constructed to study the dissociative ionization process in detail. Both the kinetic energies and angular distributions of the ionic products resulting from electron impact ionization of molecules are being examined. These studies shed light on the symmetries and positions of the molecular state involved in the dissociation process and in addition are of fundamental importance to radiation chemistry and dosimetry, since the nature and distribution of the final products of irradiation will be determined by the energies and angular distributions of the primary dissociation products.

Electron transport, ion molecule reactions, and ion clustering reactions have been studied in water vapor from 0.1 up to 3 torr. A complete picture of the fate of slow electrons and ions in water vapor is obtained from these studies. Large and unexpected differences are observed between $H_2O$ and $D_2O$.

Studies of the electronic and ionic properties of a large number of organic and inorganic molecules are reported with direct relevance to theoretical chemistry, radiation chemistry, dosimetry, analytical chemistry, and superconductivity.

Last but not least, electron affinities of molecules are being determined with a new collisional ionization experiment. The technique is yielding quite useful results for many polyatomic molecules.

### 10. Physics of Tissue Damage

Additional electron-slowing-down studies have been carried out using dysprosium-doped aluminum oxide sources. Measurements have been made using both polished and unpolished samples to study what effects surface roughness may have on the electron spectrum. No difference in spectral characteristics was observed between the two forms.

The study of the influence of source thickness on the slowing-down spectra has continued with measurements of the spectra exhibited by thin gold films on a beryllium backing. The structure seen earlier at the *LMM* Auger energy shows up clearly for the thin sources.

The optical and dielectric properties of the liquids benzene, pyridine, quinoline, and 2-ethylnaphthalene have been obtained in the energy region between 4 and 10.6 eV from transmission cell measurements and a Kramers-Kronig analysis. The structure in the optical properties is interpreted in terms of excitations involving the $\pi$ and $\sigma$ electrons.

Previously obtained optical and dielectric properties of the nucleic acid base guanine in the energy region between 14 and 80 eV have been supplemented by a study of these properties down to 4 eV through a combination of reflection and transmission measurements. The energy-loss function calculated from these data agrees reasonably well with that obtained from direct measurements of the electron energy loss by others.

A study has been initiated on chlorophyll in an attempt to improve the understanding of the optical and electronic processes involved in photosynthesis, in particular, how the chlorophyll molecules interact with each other and with surrounding protein molecules, in situ. Since it is known that, in general, organic molecules absorb more strongly in the ultraviolet than in the visible, it is necessary to know the optical properties over an extended energy range in order to understand the processes occurring in photosynthesis in the visible region. Preliminary measurements have been made on chloroplasts between 2 and 22 eV. Several absorption peaks were observed in this region, two of which are reported for the first time.

## PART III. MEDICAL PHYSICS AND INTERNAL DOSIMETRY

### (Chapters 11–17)

The dose from a semi-infinite cloud of a photon-emitting radionuclide is an idealization of an exposure situation, but it is a useful one, particularly for noble gases of long radioactive decay half-times, for example, $^{85}Kr$. An analysis of absorbed dose to body organs for monoenergetic photons emitted in an infinite cloud is presented in the report "A Model for Exposure to a Semi-Infinite Cloud of a Photon Emitter." A method is described also which provides estimates of absorbed dose to organs by use of calculated depth-dose profiles in the phantom. Dose from photons emitted in the decay of a real radionuclide could be obtained by interpolation from the results of this research.

The bladder is one of the more variable organs of the body, and dose per photon from an emitter present in the urine may differ by up to an order of magnitude during the course of a filling. The report by Snyder and Ford on "Estimation of Dose and Dose Commitment to the Bladder Wall from a Photon Emitter Present in Urine" presents an analysis of the practical implications for the clinician of varying the many parameters of the

problem. Surprisingly simple rules are formulated which can save up to 50% or more of the dose if it is possible for the clinician to increase the output of urine or to begin the administration when the bladder is partly filled.

Doses to the organs of infants and children from photon emitters present in their bodies are reported below for two cases of special interest, namely, when the source is uniformly distributed in the body (Hilyer, Hill, and Warner) and also when the source is in the gonads (Snyder and Ford). By the reciprocity theorem the latter dose is used to obtain estimates of genetic dose rate for sources in a variety of organs. These results, as well as those reported previously, show marked increases in dose per photon as age decreases.

The study of the metabolism of carbon and its dosimetry is one example among many of the models constructed for estimation of dose needed for the revision of ICRP Publication 2. The report "A Human Metabolic Model for $^{14}$C-Labeled Metabolites Useful in Dose Estimation" presents a model which allows for a compartment of slow biological elimination as has been indicated in several long-term experiments.

A study is reported which was undertaken to determine the feasibility of calculating absorbed dose to internal organs from external sources of x-ray beams. The objective was to obtain a complete set of basic dosimetry data for selected monoenergetic beams incident on a spatial grid from which one could construct certain organ doses from typical diagnostic x-ray exposures of specified average energy or energy spectrum and varying field size and location. Photon energies chosen for this initial study were 30, 55, and 80 keV, and the organs of primary interest were the gonads, thyroid, lenses of the eye, and the red bone marrow.

## PART IV. URBAN RESEARCH

### (Chapters 18 and 19)

The research program of the Urban Research Section is primarily aimed at studying national urban growth patterns, determining the principal factors affecting such patterns, and evaluating the effects of alternate policies upon population distribution. This research is intended to assist the Department of Housing and Urban Development in developing systematic national trends and projections of changes in the size and characteristics of local area populations. Such trends and projections can assist policy makers by identifying possible futures under varying sets of assumptions.

The presence of the demographic expertise available for immediate response to the AEC is especially significant because of the need to know the population densities within given distances of every reactor on a 24-hr work-residence basis. Additionally, as Dr. Weinberg has stated, "The possibility of using waste heat from power reactors... depends critically on long-term trends in population and industrial densities, and our ability to project these trends for at least ten years." The evaluation of environmental impacts of reactor siting further requires consideration of the present and projected demographic characteristics of the population surrounding present and proposed nuclear installations. Because the data and program development have been primarily made possible by HUD funds to the Urban Research Section, the AEC has been able to utilize this expertise at very low cost.

Thus, the research on population and employment growth in small areas nationwide being done in the Urban Research Section funded by HUD is invaluable to the AEC because data, programs, and expertise concerning small area projections on a nationwide basis are available:

1. for providing estimates of population in regard to reactor siting,
2. for indicating location of population at any given time, which, when combined with meteorological and geological data, provides estimates of the population at risk in the event of a nuclear release or for civil defense planning purposes,
3. for providing input for impact statements, and
4. for providing estimates of energy requirements in each region based on the energy-using characteristics of the present and projected populations of each area which can be translated into adequacy of resource availability.

## PART V. CIVIL DEFENSE RESEARCH

### (Chapters 20–22)

Because of the usefulness and impact of the ORNL translation of the 1968 Soviet Civil Defense manual, the translation and editing of two other Soviet manuals, *Civil Defense* (1970) and *Use of Shelters in Civil Defense*, has been undertaken. Studies of the Soviet city evacuation system have led to a shift of the U.S. Civil Defense program to emphasis on contingency city evacuation planning. United States superiority in transportation, housing, and food resources are important strategic assets in a confrontation leading to city

evacuation. However, a contingency follow-on construction program for permanent shelter must be part of the U.S. evacuation plan to prevent its neutralization by deliberate false alarms.

The 1970 U.S. census data have been analyzed to determine population density distribution as part of the evacuation studies. Curves of cumulative population vs population density have been determined. Approximately half the U.S. population lives at a density greater than 1000 people per square mile, and about one-fourth at a density greater than 5000 per square mile. Programs to produce isometric projections of population density for cities have been developed and have demonstrated the shortcomings of the conventional elliptical normal distributions for many analyses.

A survey of all the available designs of expedient shelters in the literature was made with the best designs to be included in a handbook. The designs are intended to be constructed by average rural and small-town families from locally available materials in 48 hr or less. A survey of building materials indicates that there would be inadequate amounts of conventional lumber to build the required shelters in a crisis. However, 70% of the population lives in OBE (Office of Business Economics) areas which have more than ten times the amount of standing timber required to build small-pole shelters for all the OBE residents. Door-covered trenches and other designs can accommodate the population in treeless regions. A preliminary evaluation indicates that rural and suburban residents would also have enough tools to build the necessary expedient shelters.

Six designs of expedient blast shelters were tested in a 500-ton TNT explosion. All models showed surprisingly high resistance to blast, believed due to earth arching. The small-pole shelter survived 29 psi, and it is estimated from the roof deflection that it would easily survive 50 psi. The door-covered trench survived 5 psi. A spinoff from the field tests and previous shock tube studies was the development of a very cheap (~$50) but accurate (±10%) blast gage employing the plastic deformation of an aluminum-foil membrane.

The surges induced by a representative electromagnetic pulse (EMP) in typical transmission lines and control circuitry of distribution systems have been calculated by means of comprehensive computer codes. The effects of such calculated surges on typical electrical systems have been studied. In particular, a study of the effects of EMP on supervisory control equipment indicates that electromechanical relays will operate reliably when subjected to EMP-induced surges, whereas relays with semiconductor components will likely be damaged or operate falsely. Countermeasures have been recommended.

The stability of the electric power network is being investigated from the standpoint of EMP vulnerability. Present results indicate that the extensive nature of a high-altitude EMP can cause widespread temporary loss of load with a resulting loss of synchronism in the power system.

The vulnerability to EMP of the various types of civil defense radio communications has been assessed, and specific hardening procedures have been recommended. Additionally, theoretical work on the currents and voltages induced in idealized systems has continued. In particular, the total voltage across a long, lossless, two-wire transmission line has been shown to vanish when the current sources are parallel to the line.

Calculation of fission product release from a severely damaged nuclear power plant indicates that there is adequate time for effective emergency procedures to be instituted. A number of possible chemical prophylactic compounds for radioiodine are discussed. The compound of choice is potassium iodate ingested just prior to or within ½ hr after exposure. The prophylactic iodine compound can be incorporated in a tag attached to the electric meter of each residence. The inhalation of radioactive aerosols can be reduced by 85% by improvised respiratory protection consisting of two layers of dry bath towel.

## PART VI. EDUCATION AND INFORMATION SECTION

The AEC health physics training program included fellowship students from the University of Kentucky, the University of Tennessee, Vanderbilt University, and the Georgia Institute of Technology. These students reported to ORNL for summer on-the-job instruction in applied and research health physics.

Division personnel visited numerous colleges and universities to give seminars on various research problems of current interest.

The Health Physics Division provided research facilities and advisors for Oak Ridge Graduate Fellows, AEC Fellows, and USPHS Fellows who were conducting thesis research.

Teaching assistance was given to the University of Tennessee for its program in radiation physics. Assistance and consultation were given to several other schools that are interested in establishing health physics courses or health physics programs in their science departments. The Division cooperated with ORAU in the presentation of a ten-week course in applied health physics. Tours were also given for several college groups visiting ORNL.

Under the new Cooperative Training Program for Health Physics Technologists at the B.S. level, 12 students reported to the Division for 12 weeks of training. Due to a shortage of funds, this program will continue only on a much reduced basis for the immediate future.

The Health Physics Information System was designed and became operational as a pilot program. This system, which uses the hardware and software of the Environmental Information System and the Nuclear Safety Information Center, will be expanded as interest and available manpower warrant.

# Part I. Radiation Research and Development

F. F. Haywood

## 1. Dosimetry for Human Exposures and Radiological Impact

George D. Kerr

T. D. Jones
J. S. Cheka
H. W. Dickson
W. F. Fox
S. B. Lupica
D. G. Willhoit[1]
J. J. Shonka[2]
S. L. Chu[3]

### JAPANESE DOSIMETRY PROGRAM

Atomic bomb survivors from Hiroshima and Nagasaki residing in the United States have been estimated to number about 500 with about one-third located in the Los Angeles area. Little is known at present concerning the radiation exposure of these survivors. Some detailed information is available on 69 of the survivors in the Los Angeles area. In about one-half of these cases, the data were sufficient to estimate a radiation dose to the survivor. In order to establish a shielding factor and hence to estimate a radiation dose to the remaining survivors, additional data will be necessary to pinpoint their location with respect to the hypocenter of the bomb. Other survivors in the Los Angeles area will be included in this study as soon as possible. At the request of the Atomic Energy Commission, a dosimetry study of those residing in the Los Angeles area has been started in cooperation with the Office of the Chief Medical Examiner-Coroner for the County of Los Angeles and the Atomic Bomb Casualty Commission in Japan.

Because of uncertainties in the overall accuracy of the method used in Japan to estimate the radiation shielding factors of concrete structures, a study was undertaken at ORNL by the staff of the Radiation Research and Development Section and two visiting Japanese shielding experts. The structure used in this study was the Control Building of the Health Physics Research Reactor (HPRR). Neutrons and gamma rays incident on the control building from the HPRR have spectra similar to those from a fission-type nuclear weapon. The angular distribution of the neutron and gamma radiation, as measured on the roof of the DOSAR Control Building,[4] did not give calculated values in good agreement with measurements inside the building, so a new approach was made. In this study, shielding factors were calculated by the method used in Japan and were compared with experimentally obtained shielding factors at 34 different locations inside the Control Building. The experimental shielding factors were obtained from dose measurements made both inside and outside the Control Building. For both neutrons and gamma rays, the difference between the calculated and experimental shielding factors was 20% or less at 22 of the 34 locations. Results of this study have provided a means of estimating shielding factors for areas within a thick concrete structure. Methods which have been developed will be applied to cases in Japan. It is felt that these methods should provide shielding factors accurate to within a factor of 2 in all cases and accurate to within 20% in many cases.[5]

---

1. Consultant, University of North Carolina.
2. Consultant, Georgia Institute of Technology.
3. Alien Guest, Atomic Energy Council, Taiwan, Republic of China.
4. *Health Phys. Div. Annu. Progr. Rep. July 31, 1972*, ORNL-4811.
5. Y. Okamoto, H. Yamada, J. S. Cheka, and H. H. Hubbell, Jr., *A Technique for the Estimation of Radiation Exposure to Japanese Survivors Shielded by Reinforced Concrete Structure*, ORNL-CF-72-10-1 (Feb. 5, 1973).

To make a realistic estimate of the dose to internal organs of survivors in which radiation effects have been observed, a knowledge is required of the dependence of depth dose in the body with both the energy and angular distribution of the incident radiation and the body size. Comparisons of depth dose for the idealized cases of isotropic and plane-beam irradiation of the body are discussed elsewhere in this report.

One additional category of survivor has received some attention during the last year. This category includes those who lingered in the induced-activity region near the hypocenter and/or were in one of the several outlying districts where the "black" fallout rain was experienced. In the past, the levels of these exposures were thought to have been extremely low and, thus, second-order contributors to doses of most individuals; however, the black rain problem has been considered only on a macroscopic scale and has usually been assumed, perhaps prematurely, to be a second-order effect. The black rain fell on some outlying provinces in irregularly shaped patterns and generally on people who were exposed to unimpressively low levels of initial radiation, so in most cases the fallout rain was the primary mode of exposure.

It was expected that particulates from the fallout rain would be removed quickly from the skin and clothing of those survivors experiencing precipitation heavier than a moderate sprinkle or a light drizzle. Instead, some of the particulates deposited by light precipitation may have been washed into and captured by the hair and clothing where they could have become an important contributor to the dose of an individual survivor; however, it seemed that black rain dose levels were extremely low for those survivors not experiencing beta-ray burns[6] on the upper convex portions of their bodies. Evidence from several individual medical observation histories now casts considerable doubt on the accuracy of this assumption.

Because of the small black rain population, it is desirable to classify radiation symptoms so as to maximize the size of the subpopulations. This task is somewhat complicated by the fact that some survivors experienced minor symptoms only, some experienced major symptoms only, and some experienced both minor and major symptoms. Rather than try to combine data from these somewhat unparallel subpopulations, it is believed that the information revealed by this study can best be illustrated by the negative approach of Table 1.1, in which a comparison is made of the number of survivors in the black rain population (EP) and in the control population (CP) who reportedly showed no easily observable response to initial major and/or minor effects.

**Table 1.1. Report "nonincidence" of initial radiation effects**

| Initial exposure (rads) | EP (287 survivors) (%) | CP (16,045 survivors) (%) |
|---|---|---|
| <1 | 37.8 | 99.0 |
| 1–10 | 30.6 | 96.4 |
| 10–20 | 24.4 | 95.4 |
| >20 | 9.8 | (null set) |

**Table 1.2. Specific symptom vs ratio of EP to CP incidence**

| Symptom | EP:CP incidence |
|---|---|
| Fever | 10 |
| Vomiting | 14 |
| Diarrhea | 22 |
| Sore throat | 42 |
| Sore mouth | 47 |
| Sore gums | 53 |
| Gingival bleeding | 29 |
| Purpura | 33 |
| Epilation | 15 |

From an extensive set of data regarding symptoms, one can also form the ratios EP:CP of symptom incidence in those exposed to the black rain to symptom incidence in the control population shown in Table 1.2. Although some of the individual ratios may be unreliable, a definite trend is established; for fever (13.56% of EP), diarrhea (22.04% of EP), and epilation[7] (68.64% of EP), the respective ratios EP:CP of 10, 22, and 15 should be reasonably accurate.

## IN UTERO EXPOSURE OF A-BOMB SURVIVORS

For dose-specific correlation of selected biological responses such as thyroid carcinoma and investigation of effects of radiation on survivors who were in utero (at time of exposure) in Hiroshima and Nagasaki, a complete description of the internal dose distributions

6. In fission product decay, a beta particle is liberated in each act of radioactive disintegration, and because the mean path length of beta particles relative to that of neutrons or photons is quite short, beta burns are often used as a crude biological dosimeter. Beta burns were restricted to upper convex portions of survivors' bodies in order to exclude those receiving burns from small particulate deposition trapped in a recession such as an ear.

7. These manifestations were selected because incidence rates were high enough to include sizable subpopulations of the "black" rain survivors.

is desirable. Results were presented[8] for the contribution to dose from (1) the neutron field and (2) photons produced by neutron interactions inside the phantom, for truncated right circular cylinders having heights of 60 cm and radii of 6, 12, and 15 cm, corresponding to the neck and adult human torso. Dose patterns to the same phantoms from gamma rays produced exterior to the phantoms were given in 1971.[9]

The widespread FORTRAN version of GTISO,[10] a subroutine for the production of isotropic direction cosines specifically designed for use in breakup kinetics of nuclear reactions, was used to describe the velocity components of incident photons from the isotropic (by assumption) radiation field.

Since 1971, it has been discovered that GTISO (although working perfectly for the use for which it was designed) breaks down if used to predict the direction cosines of incident photons. Documentation of GTISO has not been found, so it has been difficult to check the algorithm. For this reason, the following algorithm was developed and substituted for GTISO in the source subroutine.

Let us consider the problem of choosing direction cosines $\alpha$, $\beta$, and $\gamma$ for particles intersecting the surface of the truncated cylindrical phantom at the point $P_2$ having spatial coordinates $X$, $Y$, $Z$ and let $\theta$ be defined as the angle between **D**, the assumed direction of a particle, and **N**, the inwardly directed surface normal (shown in Fig. 1.1), so that:

$$\mathbf{N}\cdot\mathbf{D} = |\mathbf{N}| \cdot |\mathbf{D}| \cos\theta = -(\alpha X + \beta Y) . \tag{1}$$

From the definition of isotropic, that is, having physical properties that are the same regardless of the direction of measurement, it is essential that the angle of incidence (relative to the surface normal) be selected from the uniform distribution of solid angle $\Omega$ rather than uniformly with planar angle $\theta$. In general (no longer referring to Fig. 1.1), the differential element of solid angle $d\Omega$ subtended at a point $P$ by an element of surface $da'$ is defined by (1) drawing a straight line from every point on the periphery of $da'$ to the point $P$ and (2) drawing a sphere of radius $S$ having $P$ as its center such that $S$ is equal to the length $PQ$, where $Q$ is the centroid of $da'$. The cone of lines from $da'$ to $P$ intersects an area $da$ on the surface of the sphere. Now referring to Fig. 1.1, the differential unit of solid angle subtended around $P_2$ which includes all angles between $\theta$ and $\theta + \Delta\theta$ is

$$d\Omega = \frac{da}{S^2} = \sin\theta \, d\theta \, d_4 , \tag{2}$$

but

$$\Omega = \int_0^\theta \int_0^4 d\Omega = 2\pi(1 - \cos\theta) , \tag{3}$$

so that

$$\theta = \arc\cos\left(1 - \frac{\Omega}{2\pi}\right), \tag{4}$$

where $0 \leqslant \Omega \leqslant 2\pi$ (uniformly). This establishes $0 \leqslant \theta \leqslant \pi/2$, but $\theta$ is now a nonuniform distribution. The angle $\phi$, varying uniformly between zero and $2\pi$, is the angle of rotation about the surface normal, and $\psi$ represents

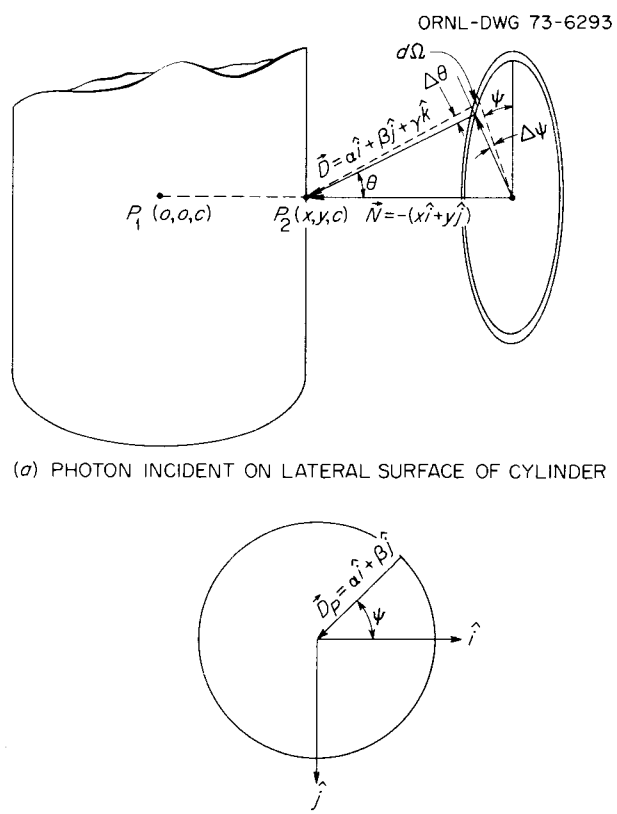


**Fig. 1.1. Diagram showing direction cosines for photons isotropically incident on truncated cylinder.**

8. *Health Phys. Div. Annu. Progr. Rep. July 31, 1970*, ORNL-4584.

9. *Health Phys. Div. Annu. Progr. Rep. July 31, 1971*, ORNL-4720.

10. R. R. Coveyou, personal communication.

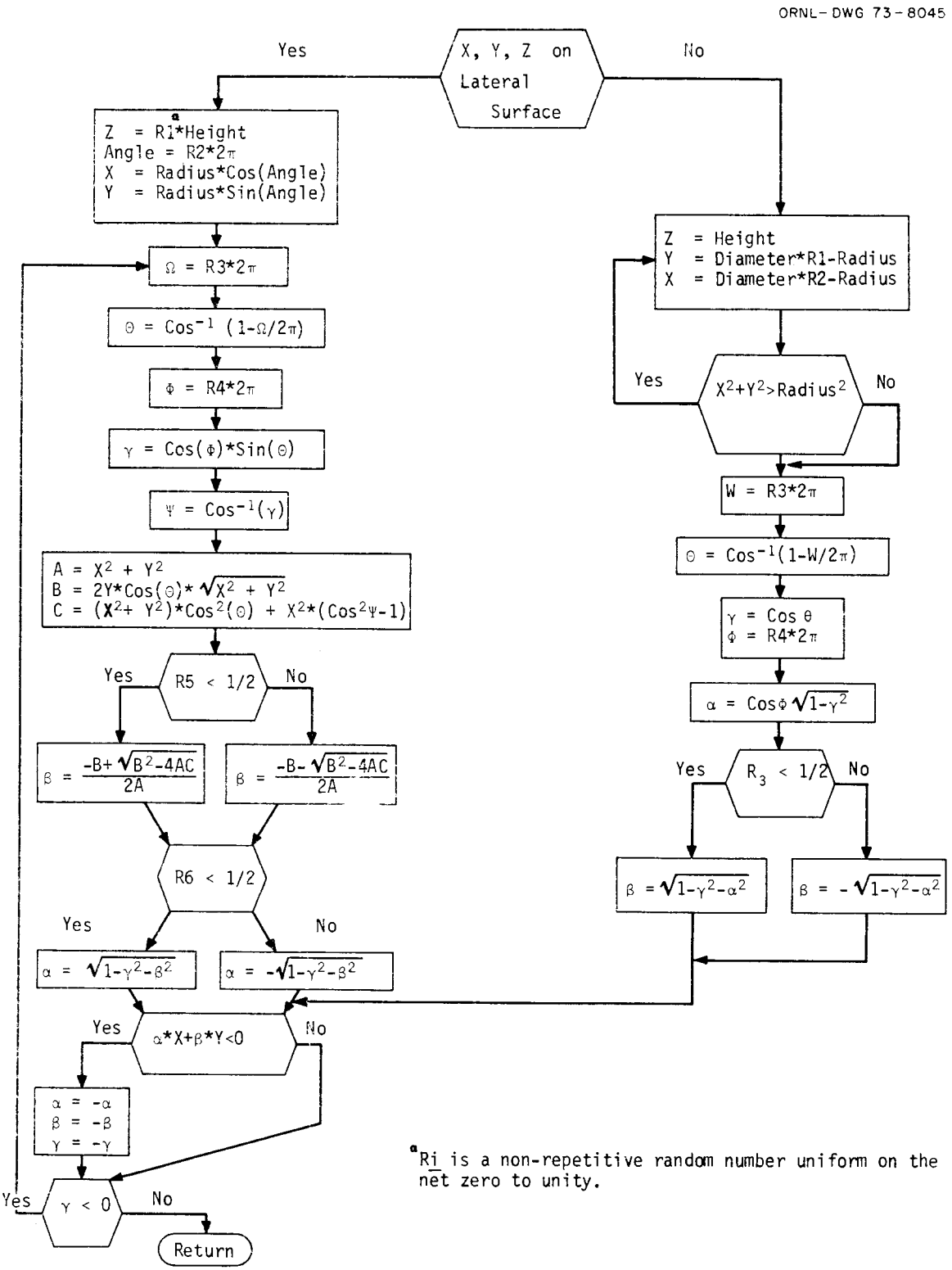


**Fig. 1.2. Flow chart for direction cosines isotropic in half space.**

the angle between the projection, in the $YZ$ plane, of $\theta$ and $+Z$. Now,

$$\cos\psi = \gamma = |\mathbf{D}| \sin\theta \cdot \cos\phi = \sin\theta \cos\phi \,, \tag{5}$$

and using Eqs. (1) and (5) plus

$$\alpha^2 + \beta^2 + \gamma^2 = 1 \,, \tag{6}$$

we establish

$$\alpha^2 + \beta^2 = 1 - \cos^2\psi \tag{7}$$

and

$$-(\alpha X + \beta Y) = \sqrt{X^2 + Y^2}\cos\theta \tag{8}$$

and consequently obtain a quadratic equation of the form

$$A\beta^2 + B\beta + C = 0 \,, \tag{9}$$

where

$$A = X^2 + Y^2 ; B = 2Y\cos\theta\sqrt{X^2 + Y^2} ; \text{and} \quad C = (X^2 + Y^2)\cos^2\theta + X^2(\cos^2\psi - 1). \tag{10}$$

Equation (9) is solved for $\beta$ and

$$\alpha = \pm\sqrt{1 - \gamma^2 - \beta^2} \quad \text{(see Fig. 1.2).} \tag{11}$$

If the photon is incident on the top of the phantom

$$\mathbf{D} \cdot (-\hat{k}) = |\mathbf{D}| \cos\psi = \cos\psi = -\gamma \,, \tag{12}$$

and if incident on the bottom

$$\cos\psi = \gamma \,, \tag{13}$$

and if $dW$ is defined similarly to $d\Omega$ in Eq. (2),

$$\theta = \arccos(1 - W/2\pi) \tag{14}$$

and

$$\phi = R_1 \cdot 2\pi \,, \tag{15}$$

where $R_1$ is a random number uniformly distributed on the net zero to unity. Now $\psi$ is a uniform distribution and from

$$\mathbf{D}_p \cdot (\hat{i}) = |\mathbf{D}_p| \cos\phi = \alpha \tag{16}$$

and Eq. (7)

$$\alpha = \sqrt{1 - \gamma^2 \cos\phi} \tag{17}$$

and

$$\beta = \pm\sqrt{1 - \gamma^2 - \alpha^2} \,. \tag{18}$$

This algorithm is shown in flow chart form in Fig. 1.2.

The energy spectral distribution[11] shown in Fig. 1.3 was used to compute dose distributions, shown in Fig. 1.4, to the phantom shown in Fig. 1.5. From these distributions and those presented in 1970, it appears that fetal size and directional orientation of the mother are relatively unimportant (especially in the first trimester of pregnancy and only become important for an extremely late stage of fetal development), because the dose distribution curves are relatively flat across the fetus, ensuring a nearly constant level of exposure. The thyroid gland is not centered in a sagittal plane through the neck, and consequently, unlike the fetus, is not exposed uniformly. Orientation of the survivor is still not very important because contributions to the radiation field are nearly symmetrical with respect to direction.

11. E. A. straker and M. L. Gritzner, *Neutron and Secondary Gamma-Ray Transport in Infinite Homogeneous Air*, ORNL-4464 (December 1969).

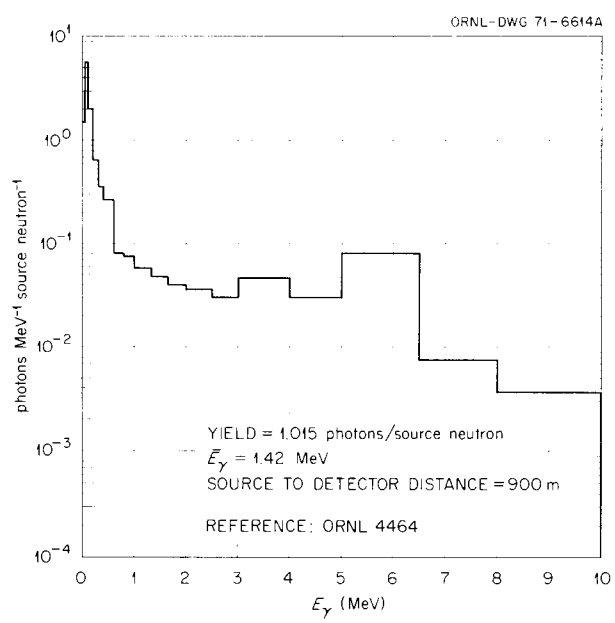


**Fig. 1.3. $4\pi R^2$ photon energy spectrum produced by a distant nuclear explosion in an infinite air medium.**

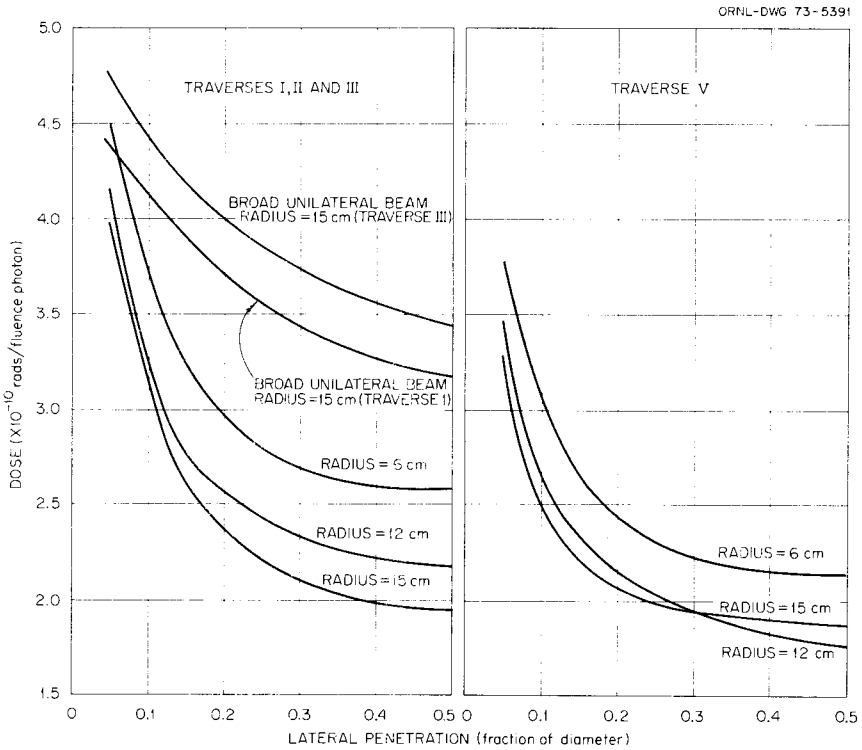


**Fig. 1.4. Dose from $2\pi$ isotropically incident photons having an energy spectral distribution equivalent to that of an atomic bomb.**

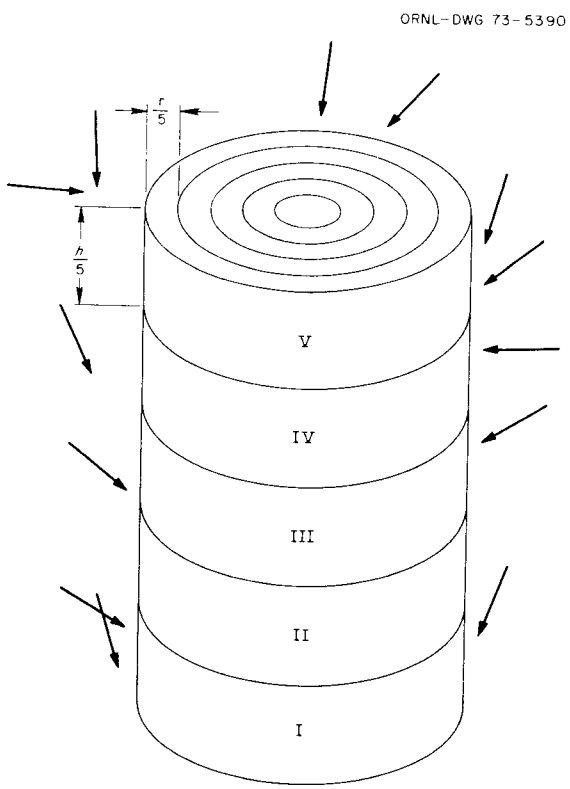


**Fig. 1.5. Phantom for averaging of dose from a $2\pi$ isotropic field of radiation.**

## THERMAL NEUTRON FLUENCE DISTRIBUTIONS

Since 1936, investigators have considered the use of neutron irradiation for therapeutic treatment of neoplastic soft tumors.[12] Doses to these tumors can be increased greatly by localized injection into the tumor of $^{10}B$, $^{6}Li$, $^{235}U$, or some other isotope having a high thermal neutron cross section. In the past, therapeutic applications have often been discouraging because of the rapidly decreasing thermal neutron fluence with increasing depth from the air-tissue interface. These decreases have usually caused ulcerating skin reactions at tumor sublethal doses,[13] thus limiting treatment to within 2.5 cm of the surface.

The phantom shown in Fig. 1.6 was used in the computation of dose and thermal fluence as functions of beam penetration depth and distance from the path of the unattenuated radiation. Depth doses as functions of energy along the center of the beam are shown in Fig. 1.7.

To maximize the "advantage doses," it is necessary to consider (*a*) the dose from neutron-produced recoil ions in the phantom (Fig. 1.7), (*b*) dose from neutron-produced photons inside the phantom, and (*c*) the "advantage dose ratio" gained by injection of one of the thermal neutron receptive isotopes. Fairchild and Goodman[14] state that the advantage dose is a significant parameter which determines the type of tumors that can be treated. They also state that the higher the advantage factor, the higher the ratio of tumor lethal dose to tissue tolerance dose that is obtained, and unless a tumor is acutely radiosensitive, an advantage dose of more than unity is necessary. Figures 1.8–1.12 give thermal neutron fluence distributions for the evaluation of component *c*, the advantage dose ratio.

12. G. L. Locher, *Amer. J. Roentgenol.* **36,** 1 (1936).
13. J. O. Archambeau, V. Alcober, W. Calvo, and H. Brenneis, *IAEA Neutron Symposium*, Report No. SM-44/20 (1963).
14. R. G. Fairchild and L. H. Goodman, "Development and Dosimetry of an 'Epithermal' Neutron Beam for Possible Use in Neutron Capture Therapy. II. Absorbed Dose Measurements in a Phantom Man," *Phys. Med. Biol. II,* No. 1, 15–30 (1966).

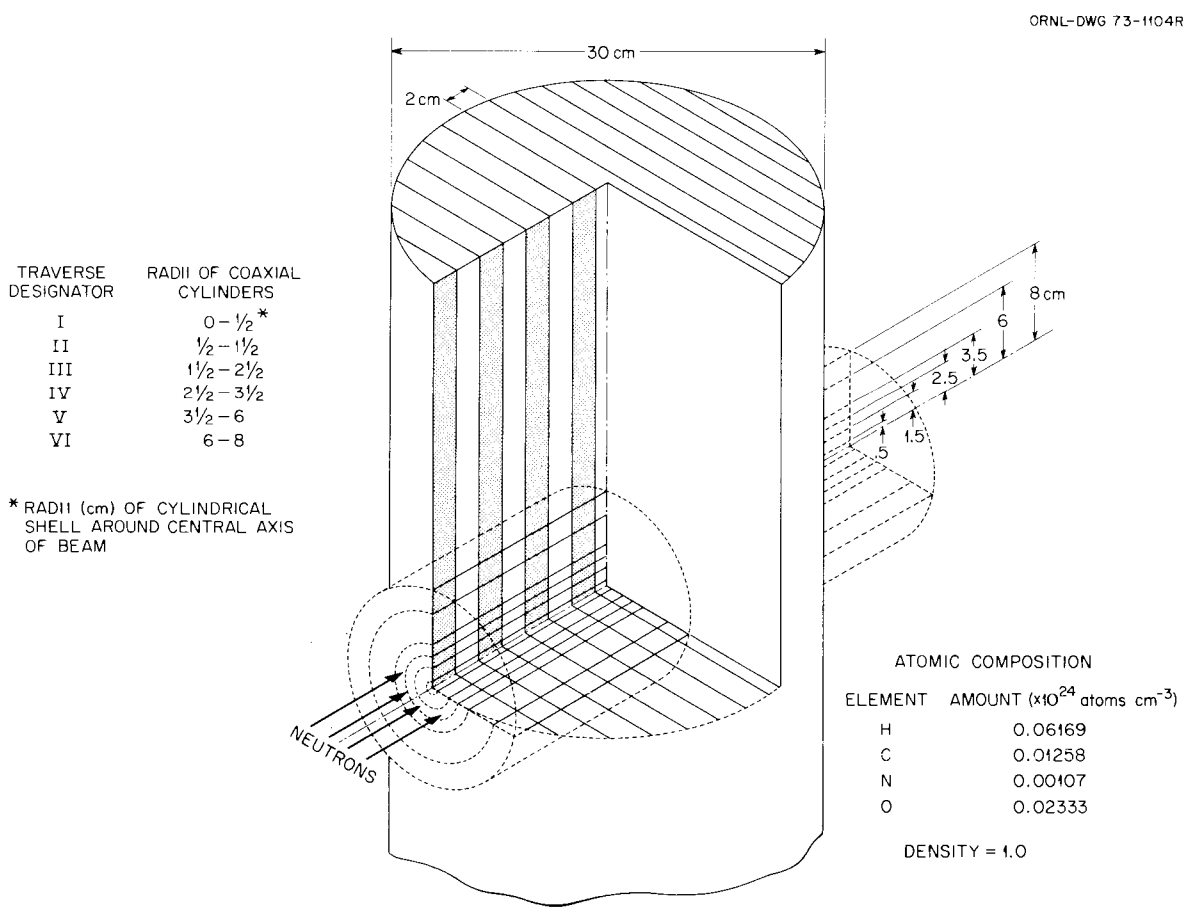


**Fig. 1.6. Cylindrical phantom for calculation of thermal fluences.**

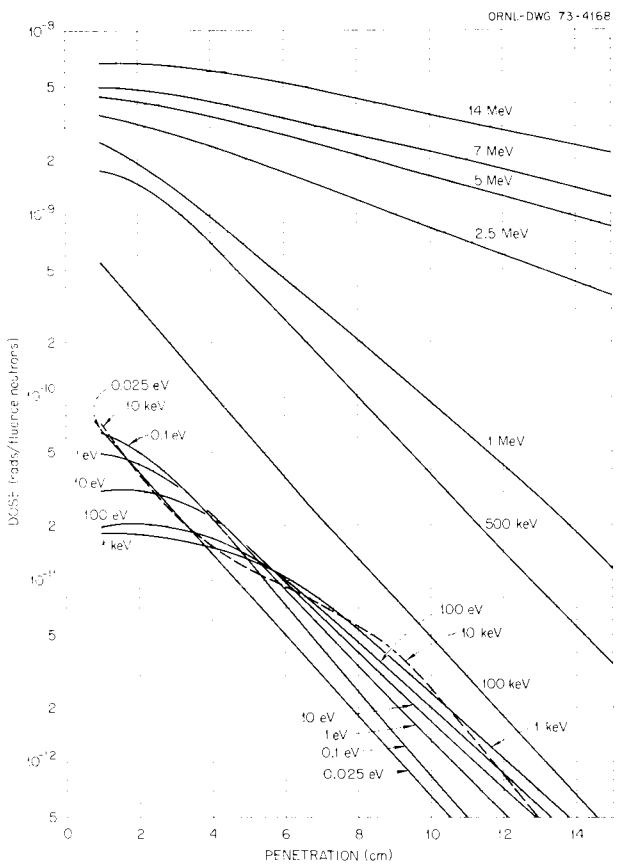


Fig. 1.7. Dose from neutron-produced recoil ions along the center of a collimated neutron beam. Beam radius = 2.5 cm.

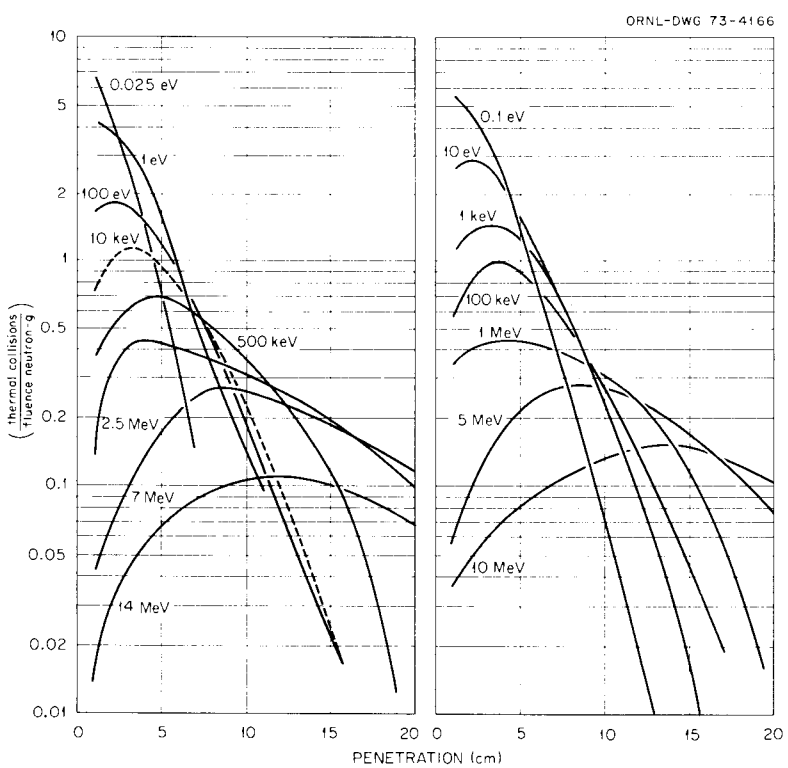


Fig. 1.8. Thermal neutron activity along the center of a collimated beam of monoenergetic neutrons.

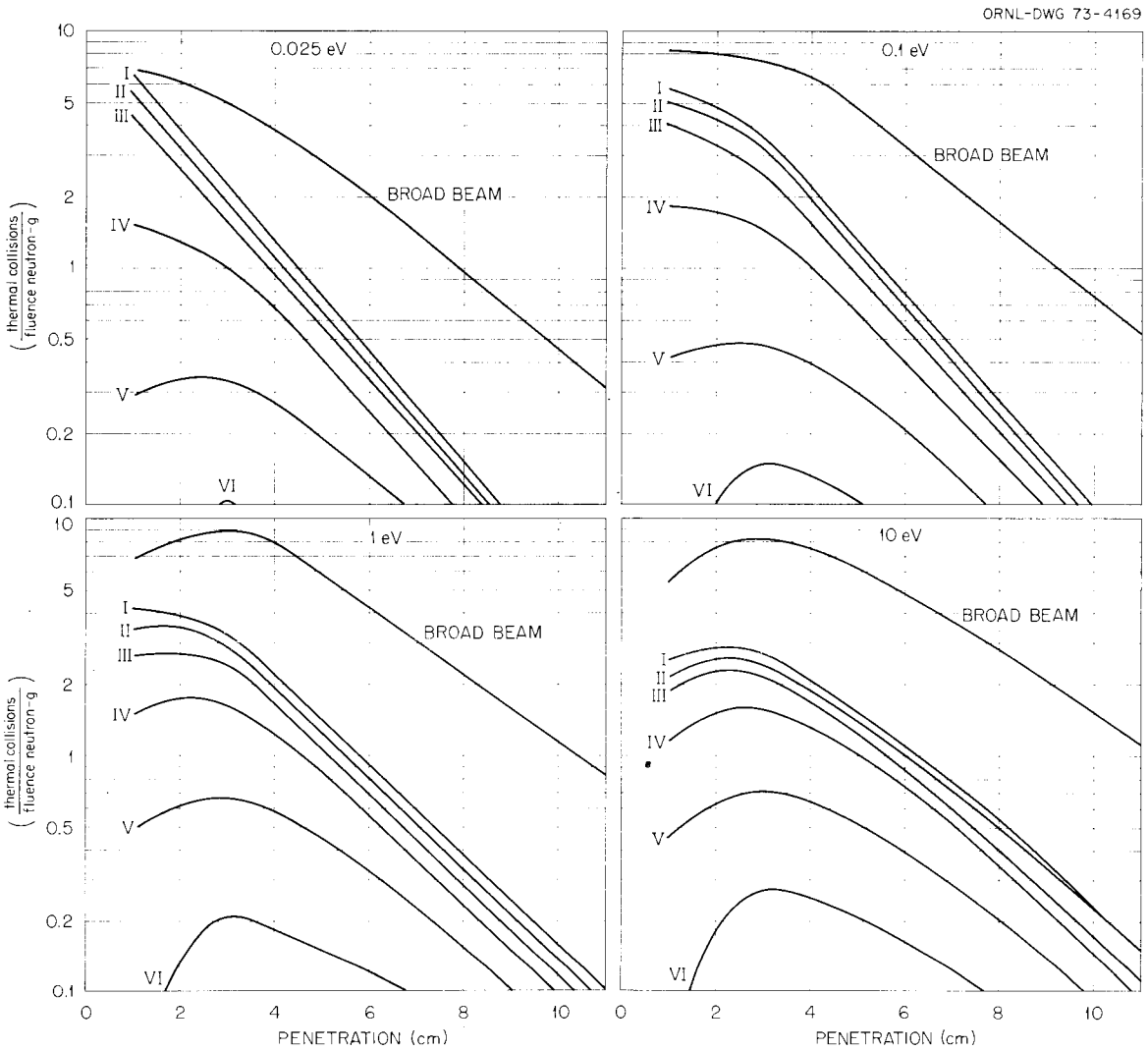


**Fig. 1.9. Thermal neutron activity produced by a collimated beam of monoenergetic neutrons.** Roman numerals locate traverses in the phantom.

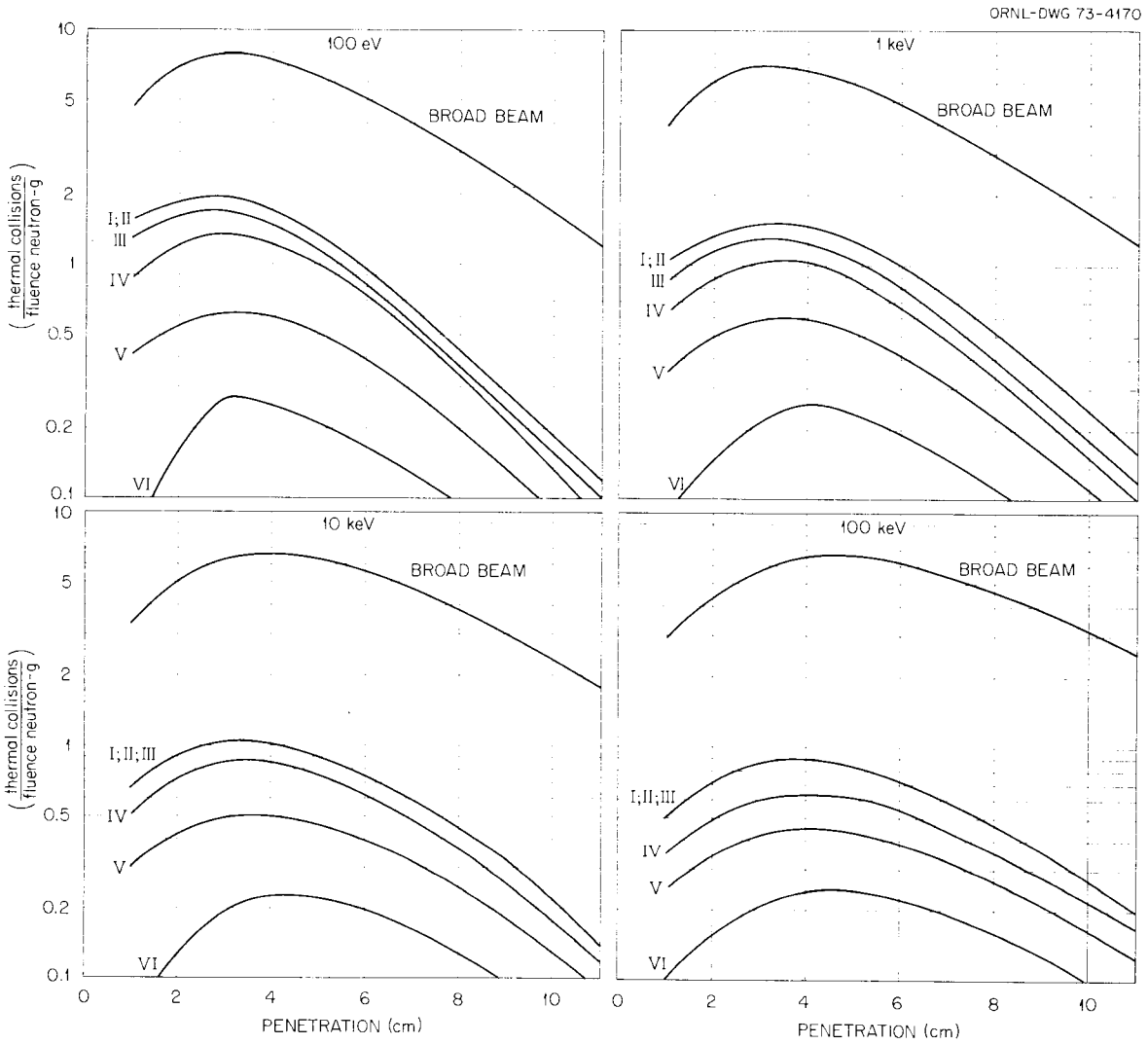


**Fig. 1.10. Thermal neutron activity produced by a collimated beam of monoenergetic neutrons.** Roman numerals locate traverses in the phantom.

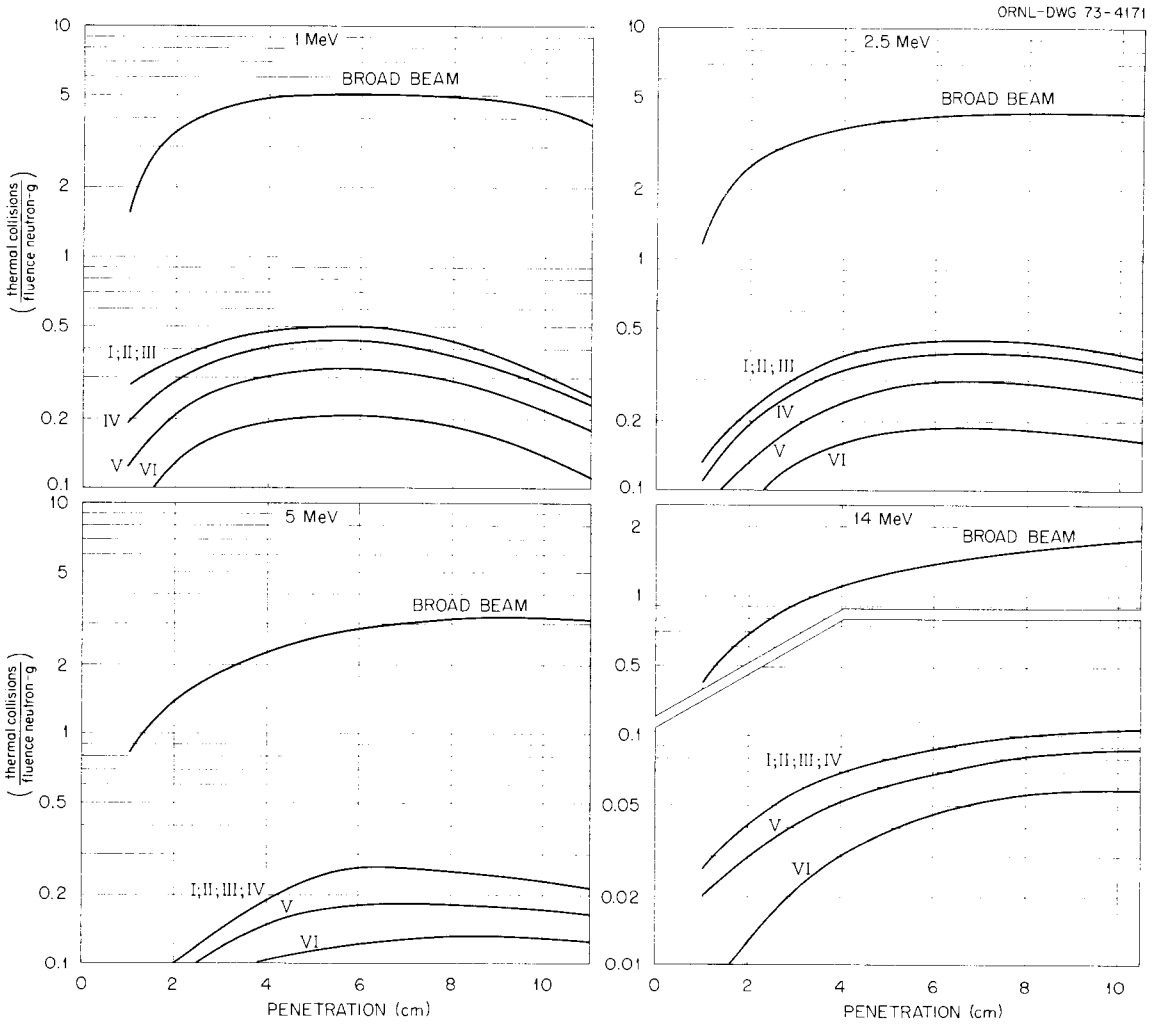


**Fig. 1.11. Thermal neutron activity produced by a collimated beam of monoenergetic neutrons.** Roman numerals locate traverses in the phantom.

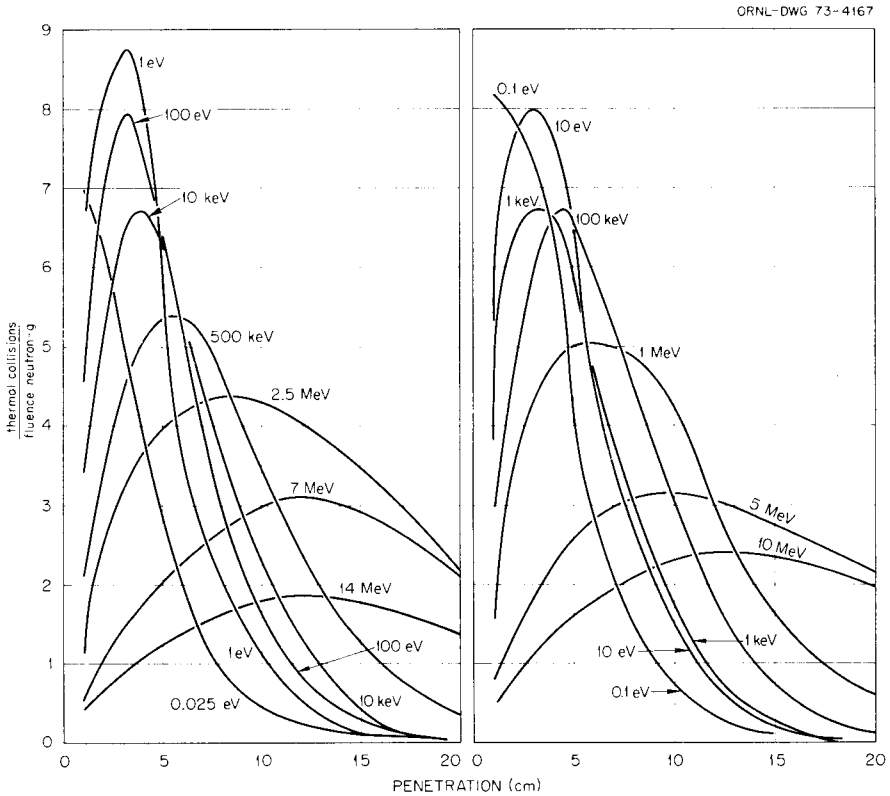


**Fig. 1.12. Thermal neutron activity from a broad beam of monoenergetic neutrons.**

The improved depth dose and thermal fluence distribution curves resulting from deeper penetration of the more energetic energy beams (Figs. 1.9–1.12) should help resolve many of the problems of rapid neutron attenuation.

## DOSE AND FLUENCE IN ISOTROPIC AND NONUNIFORM FIELDS OF RADIATION

Particle fluence[15–17] is defined as the number of particles which enter a sphere per unit cross-sectional area of that sphere. Following this definition, it is well to consider a list of special exposure situations which include:

1. a spherically shaped detector immersed in a uniform radiation field,
2. a spherically shaped detector immersed in a nonuniform radiation field,
3. a detector of arbitrary shape immersed in a uniform radiation field, and, finally, the most general exposure situation,
4. a detector of arbitrary shape immersed in a nonuniform radiation field.

Exposure situations 1 and 2 involving spherically shaped detectors, which may be mechanical, electronic, biological, etc., are usually encountered only in carefully designed and controlled laboratory experiments; thus, the fundamental definition of fluence is a "laboratory definition" and is difficult to apply to generalized calculational systems comprised of nonspherical detectors immersed in nonuniform radiation fields, such as occur in Monte Carlo transport calculations where it is desirable to assume a specific number of particles incident on a detector of arbitrary shape. This perplexing fluence situation is especially troublesome for personnel exposures such as the A-bomb survivors in Hiroshima and Nagasaki. However, if we specify a *uniform radiation field* to be one where the fluence is constant over the projected area of the detector normal

15. *Protection against Neutron Radiation*, NCRP Report No. 38, p. 43 (Jan. 4, 1971).
16. *Neutron Fluence, Neutron Spectra, and Kerma*, ICRU Report No. 13, p. 1 (Sept. 15, 1969).
17. J. A. Auxier, W. S. Snyder, and T. D. Jones, "Neutron Interactions and Penetration in Tissue," in *Radiation Dosimetry*, vol. I, Academic, 1968.

to the beam, then the existing definition of fluence usually suffices. Such a field may originate from a point, line, plane, or volume source positioned a large distance from the detector; a monodirectional unilateral or bilateral beam of radiation; or a half-space or infinite-space isotropic radiation field corresponding to a uniform cloud source of radiation in a system having a good geometry. For calculational analog exposure conditions other than these, the present definition of fluence is usually inadequate.

Let us now study the most general exposure situation, that is, (4), a detector of arbitrary shape immersed in a nonuniform radiation field, and try to formulate a perfectly general definition of fluence that under simple conditions reduces to the present definition. Clearly, an analog of any complex radiation field can be established in the space of interest by superposition of an infinite number (or fewer) of monodirectional unilateral beams. The fluence for any one such beam can be computed by dividing the number of particles from that beam intersecting the detector by the area that the detector projects on a plane normal to the monodirectional path of the radiation. To extend this simple beam concept, let us integrate all such monodirectional beams over all possible solid angles where a differential unit of solid angle is denoted by $d\Omega$. Let us also assume that the intensity of a specific beam of monodirectional radiation corresponds to some differential unit of solid angle and denote it by $\phi_\Omega$. The corresponding projected area on a plane normal to the monodirectional path of the particles will be designated by $A_{p,\Omega}$. The mean projected surface area, obtained by integrating, over all solid angles, the products of the monodirectional projected areas and their corresponding intensities, is:

$$\bar{A}_p = \frac{\int_{\Omega=0}^{4\pi \text{ steradians}} (A_{p,\Omega}) \cdot (\phi_\Omega) \cdot d\Omega}{\int_{\Omega=0}^{4\pi \text{ steradians}} (\phi_\Omega) \cdot d\Omega}, \qquad (1)$$

and the generalized definition of fluence becomes:

$$\phi = \frac{N}{\bar{A}_p} = \frac{N \int_{\Omega=0}^{4\pi \text{ steradians}} (\phi_\Omega) \cdot d\Omega}{\int_{\Omega=0}^{4\pi \text{ steradians}} (A_{p,\Omega}) \cdot \phi_\Omega \cdot d\Omega}, \qquad (2)$$

where $N$ is the total number of particles intersecting the surface of the detector in one or more locations; however, if we specify that the detector must have a convex-shaped geometry in order to simplify the calculation of $A_{p,\Omega}$, then

$$A_{p,\Omega} = \int_A \cos\theta \times dA = \cos\theta \int_A dA = A \times \cos\theta \ , \qquad (3)$$

$$\phi = \frac{N}{\bar{A}_p} = \frac{N \int_{\Omega=0}^{4\pi \text{ steradians}} (\phi_\Omega) \cdot d\Omega}{A \int_{\Omega=0}^{4\pi \text{ steradians}} \cos\theta \cdot \phi\Omega \cdot d\Omega}. \qquad (4)$$

Equation (2) is equivalent to the following concept: The fluence for the complex field can be obtained by multiplication of the total number of particles intersecting the surface of the detector by the integral, over all solid angles, of the intensities of the monodirectional beams divided by the integral, over all solid angles, of the intensities of the monodirectional beams weighted proportionally to the projected surface area of the detector, normal to that particular beam.

For a radiation field uniform in all directions, the analog beam intensities $\phi_\Omega = \phi_c$ are constant, and the differential unit of solid angle, which is independent of field uniformity, is seen from Fig. 1.13 to be

$$d\Omega = \sin\theta \, d\theta \, d\psi \ , \qquad (5)$$

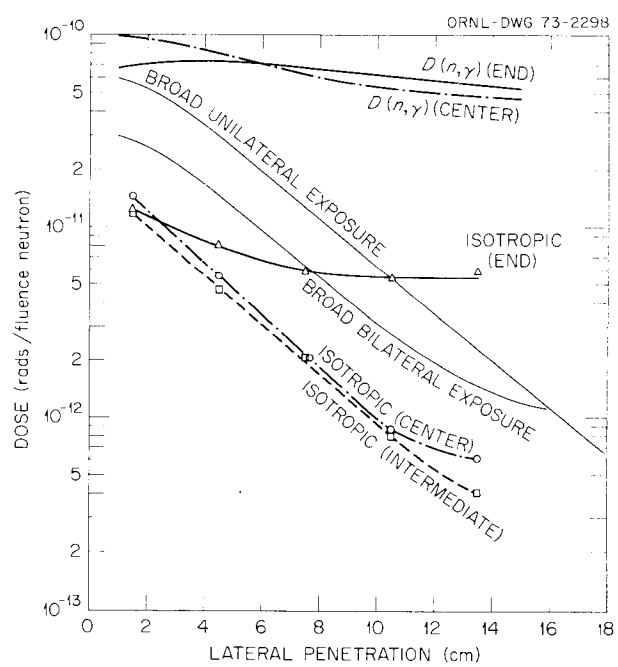


**Fig. 1.13. Dose from recoil ions produced by 0.025-eV neutrons incident on a cylindrical phantom.**

so that the *mean projected surface area* becomes

$$\bar{A}_p = \frac{A}{4\pi} \int_{\theta=0}^{\pi/2} \int_{\psi=0}^{2\pi} \cos\theta \sin\theta \, d\theta \, d\psi = \frac{A}{4}, \qquad (6)$$

and the fluence is

$$\phi = \frac{4N}{A}. \qquad (7)$$

If a detector is immersed in such a uniform field and is also assumed to have a spherical geometry, then the general definition of fluence is found to be identical to the reigning definition.

Let us define a detector whose volume approaches a point, position it in infinite space, and surround it by a field of radiation, infinite in extent and uniformly directed with respect to solid angle orientation. Since the definition of isotropic is *having physical properties that are the same regardless of the direction of measurement*, and because it is obvious that particles passing near this point-sized detector must also have directions of travel that are uniformly distributed per unit of solid angle, then we will call the radiation field *isotropically incident* on the detector. Now, let us assume a convex-shaped body having infinite mass, assume that its volume occupies half space, and place it tangential to a very small detector having some infinitesimal unit of volume. The body of infinite mass provides infinite shielding in half space, but the direction cosines of the particles incident from the unobstructed half space must remain the same as they were for that hemisphere for infinite space. It should be mentioned that this problem is similar to that of computing the number of first collisions to a differential unit of detector volume explained by Ritchie.[18] Ritchie says, "It seems plausible that the effect of an isotropic flux of particles incident on a phantom, e.g., from a very large source cloud, may be represented in a straightforward Monte Carlo analog calculation by merely choosing points of entry uniformly in the hemisphere of inward directions. Contrary to intuition, it turns out that it is necessary in this case to 'weight' the incident particle by the factor cos $\nu$, where $\nu$ is the angle between the inward normal to the surface at the point of entry and the velocity vector of the incident particle. Alternative, one may choose from a distribution proportional to cos $\nu \, d\hat{\Omega}$ where $d\hat{\Omega}$ is an arbitrary interval of solid angle." Ritchie's cosine factor is actually a correction factor which accounts for slant incidence. When this factor is applied as directed by Ritchie, the normalization to fluence should utilize the entire surface area of the convex-shaped detector as opposed to the mean projected surface area. For isotropic and other uniform fields of radiation where the angular intensities are constant, it is usually preferable to choose the angular incidence strictly as a function of solid angle and then to normalize to fluence by use of the mean projected surface area. In fact, if in this case we assume an additional weighting factor of cos $\theta$, then this corresponds to a point source moved in from infinite space and positioned on the lateral surface of the detector, because the direction cosines are now skewed from those of the original paths of entry of the isotropically incident particles.

Using the above logic and assuming a detector of finite dimensions immersed in a field of radiation, the Monte Carlo analog is established by the computer code which transports the particles to the differential units of volume to calculate dose distributions inside truncated cylindrical phantoms irradiated by infinite space isotropic and half-space isotropic fields of radiation. The normalizing fluence was found to be

$$\phi = \frac{4N}{A} = \frac{4N}{2\pi R^2 + 2\pi RH} = \frac{2N}{\pi R(R+H)}, \qquad (8)$$

where $R$ and $H$ are the radius and height, respectively, of the truncated cylinder. The direction cosines were chosen according to the algorithm presented in the section on In Utero Exposure of A-Bomb Survivors, and some of the results are shown in Figs. 1.14–1.19.

## ICRU NEUTRON DOSIMETRY INTERCOMPARISON

The Dosimetry for Human Exposure Group participated in the International Neutron Dosimetry Intercomparison (INDI) being conducted at the Radiological Research Accelerator Facility (RARAF) of Brookhaven National Laboratory and Columbia University. INDI is sponsored by the International Commission on Radiation Units and Measurements. Measurements including both neutron and gamma doses for several source energies in air and in a water-filled phantom are to be intercompared over a period of a year as dosimetrists, both in the United States and other countries, participate in groups of two or three at a time.

The RARAF utilizes a 4-MeV Van de Graaff accelerator to generate neutrons used in the intercomparison.

18. R. H. Ritchie, "Isotropic Incident Flux in Monte Carlo Calculations," *Health Phys.* 24(5) (1973).

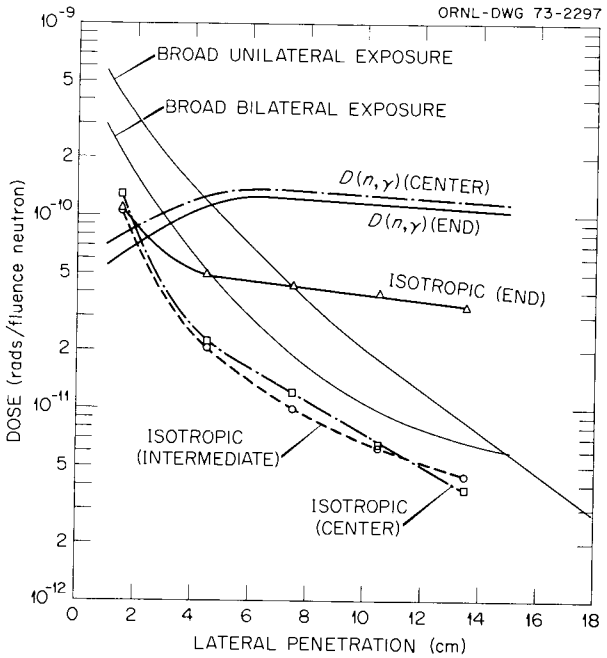


Fig. 1.14. Dose from recoil ions produced by 100-keV neutrons incident on a cylindrical phantom.

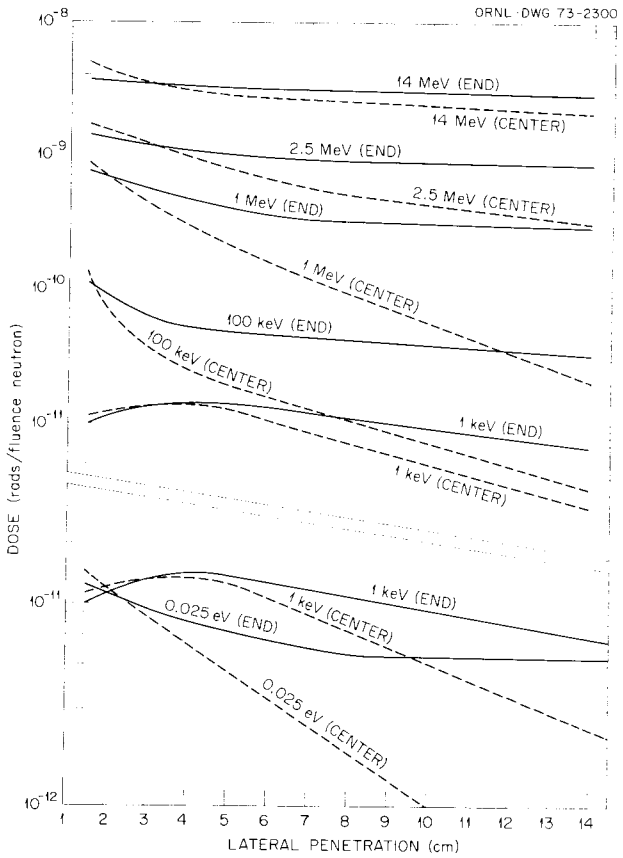


Fig. 1.16. Dose from recoil ions produced by monoenergetic neutrons isotropically incident on a cylindrical phantom.

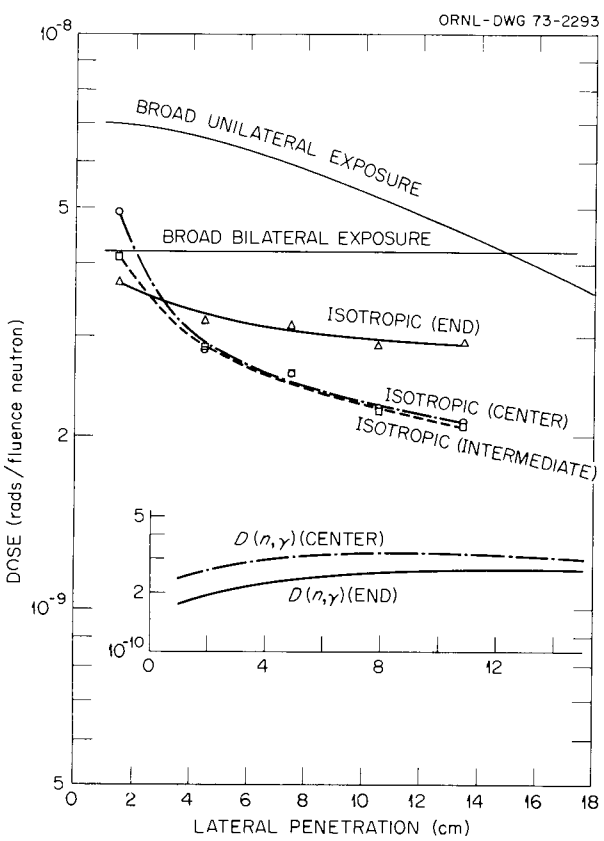


Fig. 1.15. Dose from recoil ions produced by 14-MeV neutrons incident on a cylindrical phantom.

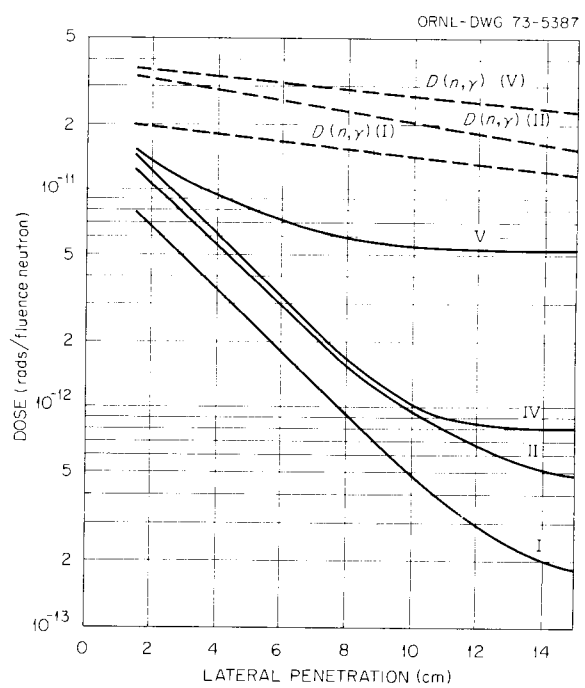


Fig. 1.17. Dose from recoil ions produced by 0.025-eV-neutron half space isotropically incident on a cylindrical phantom.

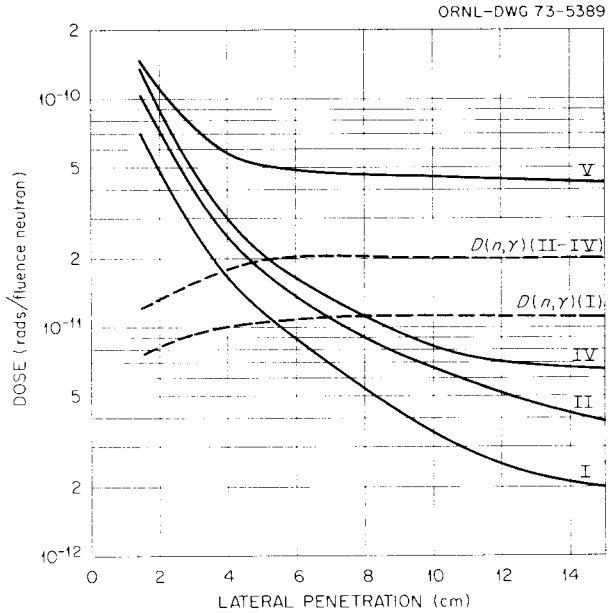


**Fig. 1.18. Dose from recoil ions produced by 100-keV-neutron half space isotropically incident on a cylindrical phantom.**

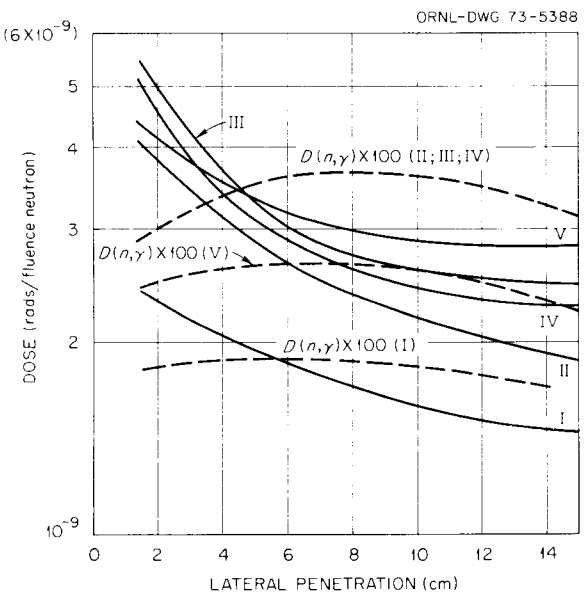


**Fig. 1.19. Dose from recoil ions produced by 14-MeV-neutron half space isotropically incident on a cylindrical phantom.**

The reactions in Table 1.3 were used during our measurements. In addition, a $^{252}$Cf source of nominal mass of 2 mg was used to generate a fission spectrum.

The experimental arrangement is shown in Fig. 1.20. All tissue kerma rates in free air were measured at the 30-cm position. Doses in the phantom were measured at depths of 5, 10, and 20 cm corresponding to 25, 30, and 40 cm, respectively, from the target. Free air measurements were made for all the sources listed in Table 1.3 and for the $^{252}$Cf source; however, measurements within the phantom were made only for the 15.4- and 5.5-MeV sources. The phantom was an open-topped Lucite cube filled with distilled water and having outside dimensions of 30 cm and walls 0.64 cm thick.

**Table 1.3. Neutron sources measured at INDI**

| Reaction | Neutron energy (MeV) | Energy spread (± %) | Max kerma rate at 30 cm (rads/hr) |
|---|---|---|---|
| $^{3}$H($d,n$)$^{4}$He | 15.4 | 4 | 40 |
| $^{2}$H($d,n$)$^{3}$He | 5.5 | 7 | 80 |
| $^{3}$H($p,n$)$^{3}$He | 2.1 | 5 | 20 |

Gamma kerma and dose rate were estimated from measurements made using a "Phil" Geiger counter[19] with a lithium shield to reduce the thermal neutron response. This dosimeter was chosen because of its insensitivity to neutrons and because its small size made it convenient for measurements within the Lucite cube.

Neutron kerma and dose rates were estimated from measurements made with an in-phantom Hurst proportional counter.[20] This counter was used with a multichannel analyzer to record the pulse-height spectrum on paper tape for subsequent computer analysis.

The results of the intercomparison will be submitted to the ICRU Neutron Dosimetry Intercomparison Committee by all participating groups. This will be followed by the preparation of the formal Committee's Report which will be submitted to the ICRU for possible publication.

## IMPROVEMENTS IN NITROCELLULOSE FILM

When an alpha particle impinges on a cellulose nitrate film, some point track damage occurs. The track-damage "points" of the film etch more rapidly than the remainder of the film when agitated in a caustic solution (25% 1.239 sp gr KOH maintained at 40°C). When the films are thin enough, the tracks will etch completely through them, and they can then be counted using the spark counting technique.[21]

19. E. B. Wagner and G. S. Hurst, *Health Phys.* **5**, 20 (1961).
20. W. A. Mills and G. S. Hurst, *Nucleonics* **12**(8), 33 (1954).
21. W. G. Cross, private communication.

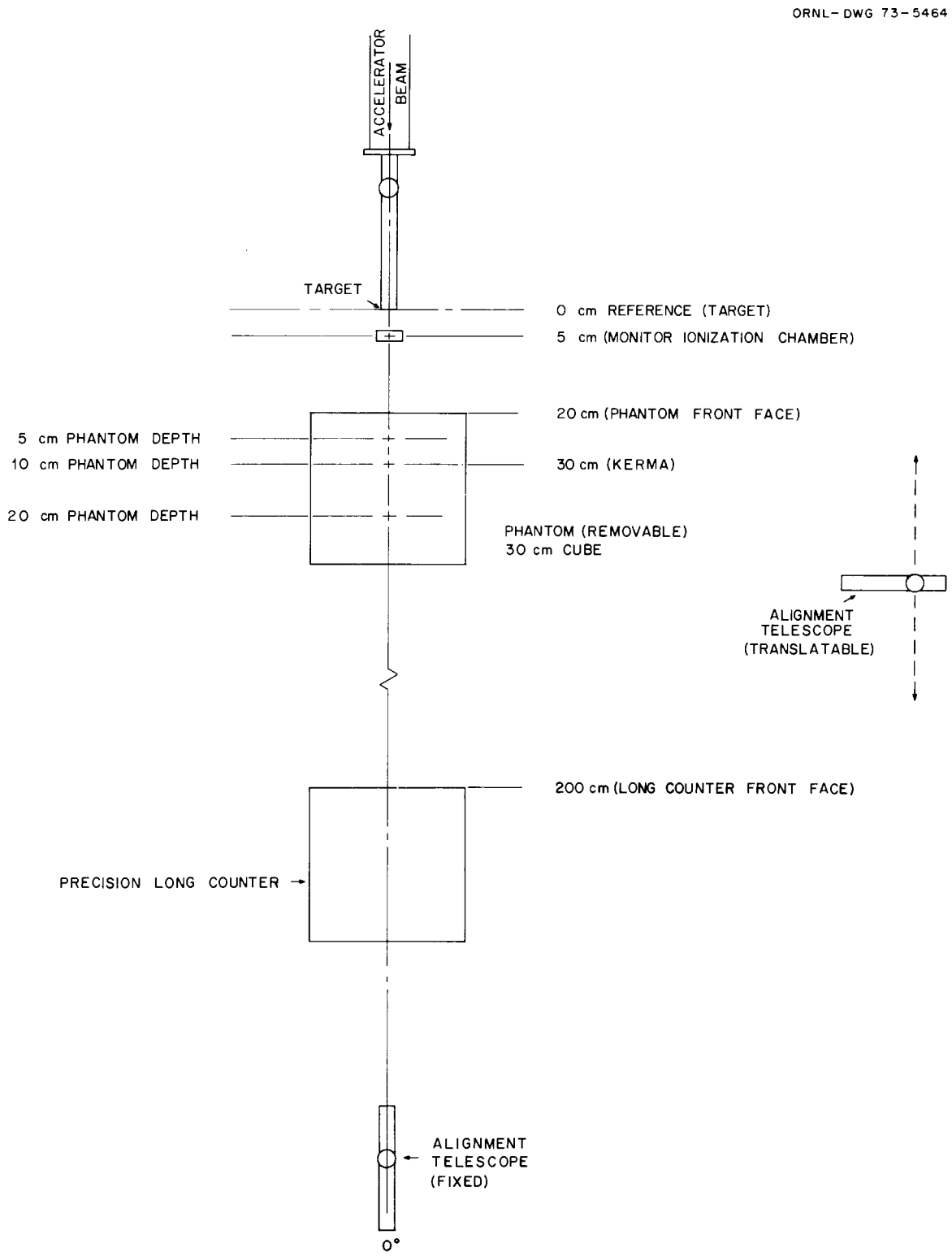


Fig. 1.20. Intercomparison apparatus arrangement, top view.

One problem has been in the making of a thin nitrocellulose film with a reproducible thickness of 10 to 20 $\mu$. The desired characteristics are that it be sensitive, strong, and durable and yet capable of registering high track densities from alpha particles. Most films used for this purpose have one or more undesirable characteristics.

Many investigators have made nitrocellulose film from a solution by slow evaporation of one or more solvents such as ethyl acetate, ethyl alcohol, and possibly other alcohols. These films had plasticizers included. Using Parlodion or a highly nitrated nitrocellulose powder from Hercules Powder Company, films were prepared according to literature formulas. These films did not meet our criteria and were therefore unsatisfactory.

Tetrahydrofuran (THF), a lower-boiling (66°C) and faster solvent, was tried, although no previous reference to the use of THF with nitrocellulose film was found in the literature. Films made without a plasticizer had poor properties, such as strength, hardness, and endurance in 25% KOH. The addition of the single plasticizer DOP, dioctyl phthalate,[22] in with the THF solution of Hercules nitrocellulose led to the production of a film with all the desired characteristics. For these thin (10 to 20 $\mu$) films, the optimum etching time is between 105 and 135 min in 25% KOH solution at 40°C; moreover, the films were still intact at the end of 3 hr of etching. The track density, as determined with a spark counter for these films, was linear with alpha particle fluence up to several thousand counts per square centimeter before reaching saturation, but still responded in the 10,000 to 15,000 counts/cm$^2$ range.

---

22. D. N. Buttrey, *Plasticizers*, Cleaver-Hume Press Ltd., 2d ed., 1957.

# 2. Solid-State Dosimetry Research

Klaus Becker

M. Abd-el Razek[1] F. F. Haywood[2]
J. S. Cheka J. S. Nagpal[1]
K. W. Crase T. D. Tham[1]
R. B. Gammage

## TSEE READER DEVELOPMENT

To overcome some of the problems related to extraction of exoelectrons from ceramic BeO detectors, a gold cup sample holder has been incorporated into the reader. A negative voltage is applied to the cup both to accelerate the exoelectrons and to help neutralize the remaining positive charge on the BeO. This greatly increases the reproducibility and sensitivity of the response.

The exoelectron emission from the same detector before and after applying the voltage is shown in Fig. 2.1. The effect of the applied voltage is to produce a smoother and more reproducible thermally stimulated exoelectron emission (TSEE) curve. The sensitivity enhancement is shown in Fig. 2.2 as a function of voltage. Furthermore, without the accelerating voltage a memory effect is observed, wherein the sensitivity of the detector changes with the time elapsed since the last readout. Negative or positive changes in a detector's response can be obtained which depend on the thermal history. The memory effect is nearly eliminated with the accelerating voltage, as is seen in Fig. 2.3.

## TSEE DETECTOR SENSITIVITY AND REPRODUCIBILITY

Procedures for maximizing the sensitivity of the ceramic BeO disks (Brush Beryllium Corporation Thermalox 995, 12.5 mm diameter) which have been used in most of our recent TSEE studies have been investigated further; the data in Table 2.1 show that 1000 to 2000 exoelectron counts per milliroentgen of gamma radiation per square centimeter of emitting surface are obtained after heat sensitization at 1450°C, followed by "stabilization" in liquid water.

Apparently, there are differences in sensitivity dependent on the lot number of the purchased product. The sensitivity shows a general increase over extended periods of heat treatment. The recommended recipe for detector preparation is to heat the detectors for 100 hr or more at 1450°C and then to stabilize them in water (or water vapor at saturation pressure) for ~100 hr before drying at 500°C. If impurities in the water are allowed to dry onto the BeO surface, spurious effects are introduced. Washing in alcohol is, therefore, recommended before the final drying.

The improved TSEE counter has operated successfully for several thousand readings, during which time the short- and long-term stability characteristics of the detectors have been studied. Repetitive readings of a detector in one day can increase the response by up to 15%, due probably to outgassing of the detector surface. The effect is transient, and after exposure to air for several hours the sensitivity returns to the original value. If a detector is read only once or twice per day, the response to a standard dose is invariant; for five detectors each read a total of 30 times over a period of 18 days, the average standard deviation is 4%. Under these conditions, the intragroup standard deviation has been in many instances within ±10%. The long-term

**Table 2.1. Sensitivity of Thermalox 995 BeO**

| Storage time at 1450°C (hr) | Mean response (counts $mR^{-1}$ $cm^{-2}$) |
|---|---|
| 100 | 860 |
| 160 | 1377 |
| 264 | 1296 |
| 586 | 1697 |

1. Alien guest.
2. Dual capacity.

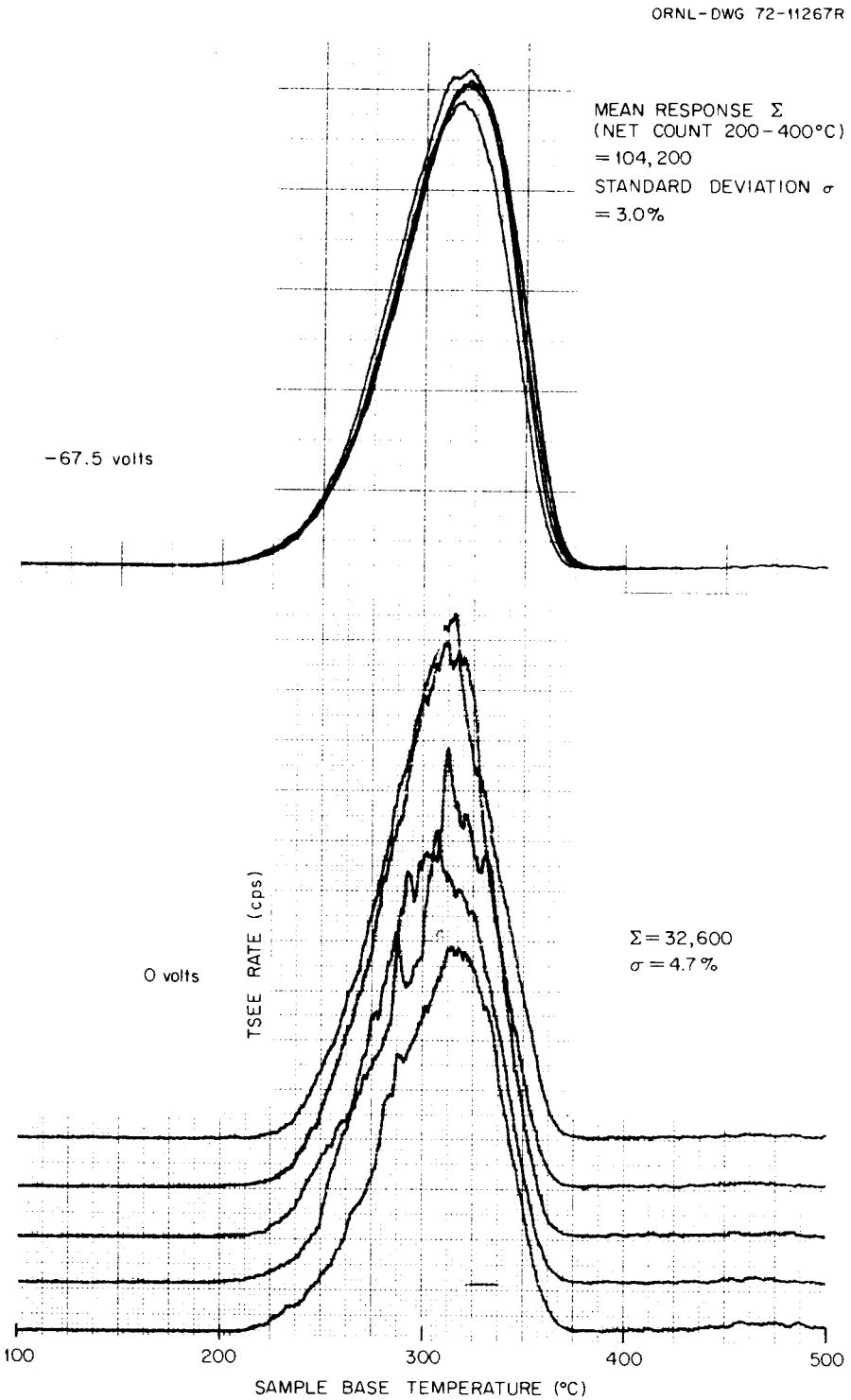


Fig. 2.1. TSEE curves of the same ceramic BeO detector, repeatedly exposed to 250 mR gamma radiation with and without an accelerating voltage on the gold cup sample holder.

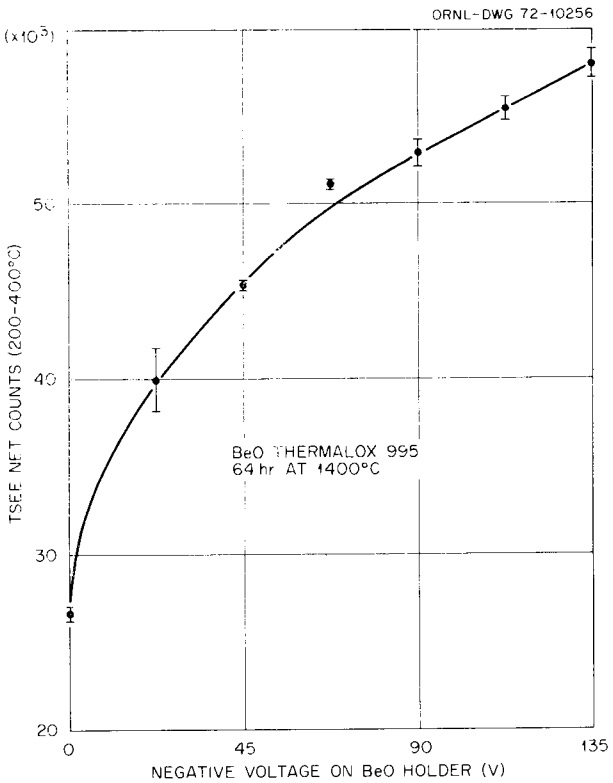


**Fig. 2.2. Mean TSEE response from three readings at different accelerating voltages, applied to the back of the same BeO detector during readout after exposure to a constant gamma radiation dose.**

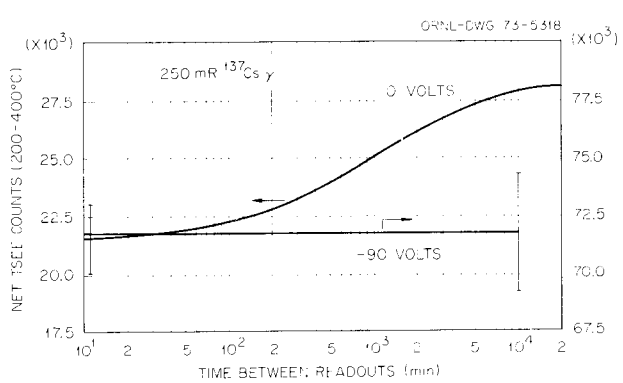


**Fig. 2.3. Effect of elapsed time since the last readout on the TSEE response of the same BeO detector, with and without the application of an accelerating potential on the gold sample holder.**

stability of two different batches of heat-sensitized and stabilized detectors was checked at the beginning and end of an eight-month storage period; the mean response changed by ≤2%, indicating that slow aging effects are absent after the initial stabilization has been accomplished. For many dosimetric applications, therefore, some selected and well-stabilized BeO detectors exhibit an acceptable degree of reliability. A calibration curve for a group of 6 detectors randomly selected from a batch of 38 detectors is shown in Fig. 2.4.

The postirradiation fading characteristics are being investigated currently. The preliminary findings are that fading is minimal under normal laboratory conditions of temperature and humidity. At 30°C and 95% relative humidity, fading of up to 10% occurs within a few hours, followed by little additional change. Many other parameters have been studied for their influence on the TSEE characteristics of ceramic BeO. For example, several types of spurious dirt and adsorption effects have been identified. Methods have been devised for minimizing the undesirable and optimizing the desirable effects. These developments will be the subject of a detailed report.[3]

The detector's sensitive surface should not be touched with hard objects or plastics or exposed to any other potentially contaminating or tribosignal-inducing agent. A substantial effort has been directed toward finding suitable detector holders, which for different applications will protect the BeO disks from scratching, contamination, and exposure to light. The detectors can be mounted in a rack made of Lucite, such that

3. R. B. Gammage and J. S. Cheka, ORNL-TM in preparation.

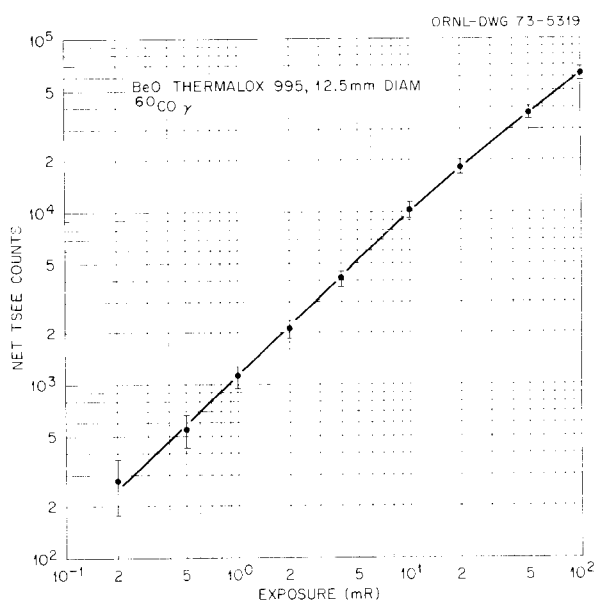


**Fig. 2.4. Gamma radiation calibration curve for Thermalox 995 BeO.** At each exposure the mean response for 18 readings, 3 on each of six BeO detectors, is shown together with the intragroup standard deviation.

physical contact is made only with the base and outer rim of each disk. Loading can be accomplished without scratching the detectors, thus reducing the incidence of tribosignals. The rack can be placed in a normal ORNL film badge. These holders have been used successfully in some field tests for personnel and environmental radiation monitoring. Plug-type holders for the BeO made of nylon, Teflon, and polyethylene have also been tested in tritium-beta and neutron monitoring without triboeffects. Even with all precautions, however, there still are occasionally unexplainable, erratic results, and TSEE dosimetry cannot yet be considered a routinely easy matter to be transferred to other laboratories.

## GAS EFFECTS ON TSEE

Transient alterations in the TSEE response of BeO detectors can be induced by repetitive readouts in a short period of time or by changing the maximum readout temperature. The presence or absence of

ORNL-DWG 72-11269R

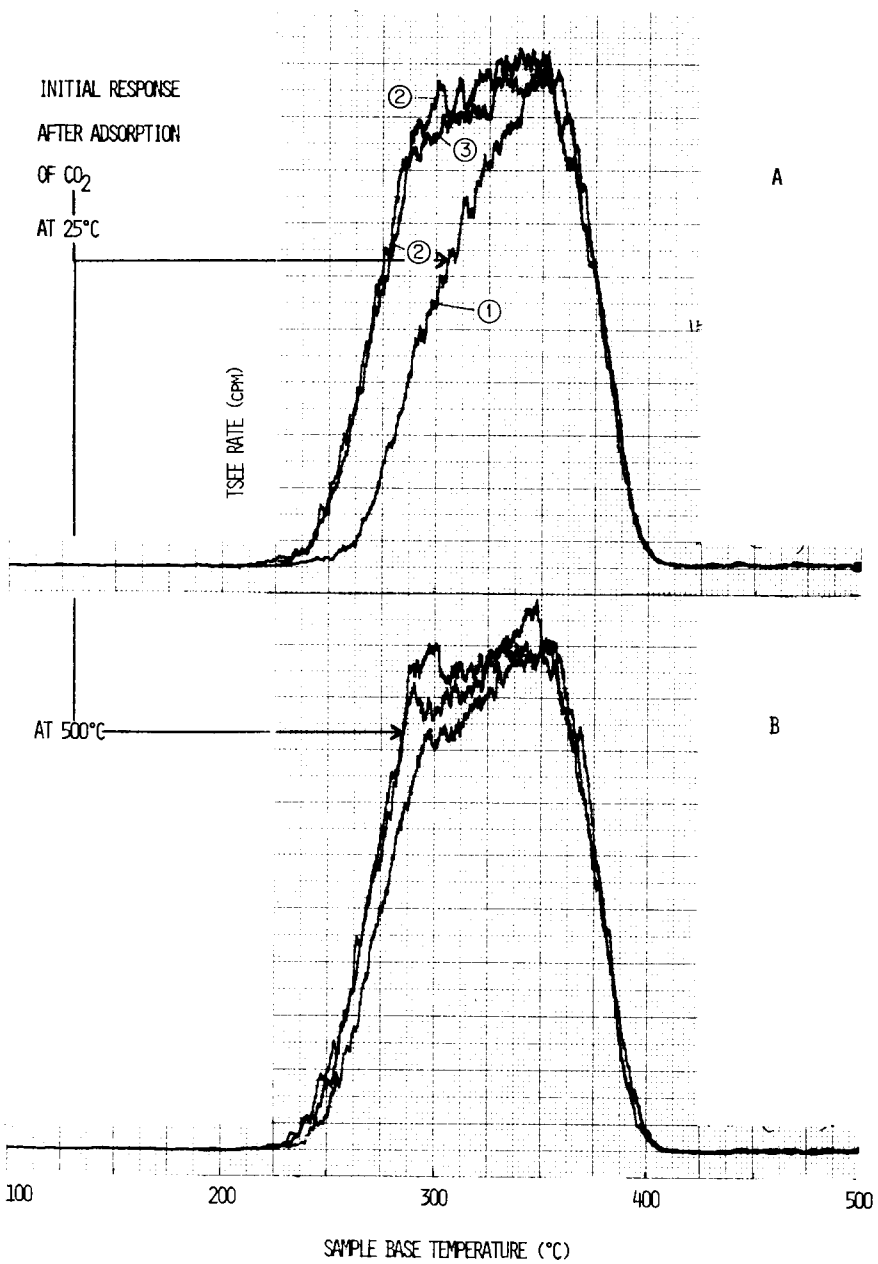


**Fig. 2.5. Recovery of exoelectron emission from Thermalox BeO 995 after outgassing in the counting gas followed by exposure to $CO_2$.** (*A*) At room temperature; (*B*) at 500°C.

adsorbed species in the surface or subsurface layers of the BeO has been suspected to be the cause of some of this behavior. Indeed, oxygen, water vapor, and carbon dioxide, acting singly or together, profoundly affect the exoelectron emission.[4] As shown in Fig. 2.5 for adsorbed $CO_2$, the sorption layers apparently render inoperative certain traps which would otherwise contribute to TSEE. After exposure of the BeO to these gases, the TSEE is dominated by a single peak at a surface temperature of ~275°C. Removal of the adsorbates by outgassing during readout causes the exoelectron emission to intensify and the TSEE curve to become more complex. If, after thorough degassing, inadequate time (less than several hours) is allowed for the BeO surface and subsurface to reequilibrate with the atmosphere, an anomalously high response may be observed.

The photon radiation effect on the dosimeter is caused by absorption of radiation in the dosimeter and in its environment. It has been generally thought that the contribution from electrons released from the environment predominates because the exoelectron layer is assumed to be quite thin (10 to 100 Å). As one of several possible methods to check this assumption, some tests have been made with different inert gases above the BeO surface and with x rays of energies where the photoelectric effect predominates. If absorptions in the gas are predominant, a substantial increase in sensitivity should be seen in switching from air to krypton ($Z$ = 36). At distances sufficient for electron equilibrium, the results of irradiations with 5.6- to 22-keV photons from $^{55}$Fe and $^{109}$Cd indicate that the influence of the gas is appreciably smaller than expected. Instead of a higher power dependence of the sensitivity on the atomic number of the gas, the dependence is less than a power of 1. For 22-keV photons, there is only a fivefold increase in TSEE response if helium is replaced by krypton. These findings suggest that absorption of radiation within the solid is a major factor in the processes leading to exoelectron trap filling.

## TSEE IN PERSONNEL AND ENVIRONMENTAL MONITORING

During the disassembly, examination, and reassembly of the core of the HPRR which took place last March, four persons were monitored daily for exposure to radiation by BeO disks held in a Lucite rack inserted into an ORNL film badge. Pocket meters and TSEE dosimeters were worn and read daily. A badge with film and an additional thermoluminescent (TL) detector was also worn as usual. The results are summarized in Table 2.2. A comparison of the TSEE and pocket meter readings on a daily basis shows satisfactory agreement. In general, the agreement between results for the exoelectron and other types of dosimeters is good (daily exposures, as measured by TSEE, ranged from 0.4 to 90 mR).

In a second field test lasting four weeks, three badges containing five detectors each were distributed, one to each of three people working in areas having a higher than normal radiation level. At the end of each week, two of the five detectors in each badge were read to obtain the weekly exposure. The remaining three BeO dosimeters were read at the end of the four-week period to obtain the accumulated exposure. The data are summarized in Table 2.3.

For the exoelectron dosimeters in the three badges the sum of the weekly exposures deviated from the one-month exposure by an average of 6%. As these field tests demonstrate, there is reasonable agreement (within 7%) between exposures measured by exoelectron dosimeters and film, TLD, and pocket dosimeters. A total of 154 TSEE readings were taken, and tribosignals

**Table 2.2. Field test of different personnel dosimeters**

| Person | Sum of daily readings (mR) | | Accumulated reading (mR) | | Ratio[a] |
|---|---|---|---|---|---|
| | Pocket dosimeter | TSEE | Film | TLD | |
| W.F.F. | 380 | 361 | 370 | 300 | 1.03 |
| H.W.D. | 130 | 118 | 103 | 123 | 0.99 |
| D.R.W. | 335 | 274 | 320 | 280 | 0.88 |
| L.B.H. | 220 | 172 | 215 | 195 | 0.82 |

[a]TSEE readings divided by the mean of film, pocket dosimeter, and TLD reading. Average ratio of the four cases is 0.93.

**Table 2.3. Comparison of TSEE and pocket ionization chamber personnel dosimeter readings**

| Carrier | TSEE dosimeter (mR) | | Pocket dosimeter (mR), sum of daily readings |
|---|---|---|---|
| | Sum of weekly readings | One-month reading | |
| J.M.P. | 38 | 38 | 55 |
| C.K.T. | 197 | 190 | 270 |
| W.M.S. | 77 | 66 | 80 |

4. J. S. Nagpal and R. B. Gammage, *Radiat. Eff.*, in press.

**Table 2.4. TSEE and TLD background measurements at various locations in and around Oak Ridge**

| Location | Exposure rate (microroentgens/hr) | |
|---|---|---|
| | TSEE | TLD |
| Home R.B.G. | 8.8 ± 0.2 | 9.3 ± 0.3 |
| Home K.B. | 7.1 ± 0.7 | 7.2 ± 0.3 |
| Home J.S.C. | 7.1 ± 0.6 | 9.7 ± 0.3 |
| Room 113, Building 7710 | 18.2 ± 1.3 | |
| Counting room, Building 7710 | 7.0 ± 0.6 | |

interfered in only two of these. The sensitivity of the detectors remained unchanged. A three-months intercomparison of film, TLD, and TSEE dosimeters worn by six ORNL radiation workers is presently in progress.

BeO detectors from different batches have also been used in environmental monitoring tests, usually involving storage times of one month at the DOSAR building and in private residences in and around Oak Ridge (Table 2.4), as well as at the AEC Headquarters building in Washington, where an average dose rate of 8.5 ± 0.5 microrads/hr was observed. The TSEE results agreed well with those measured with $CaSO_4$: Dy TL detectors. At one residence (RBG) the exposure rate was measured twice during periods separated by six months and found to be invariant. The high value for the room in DOSAR is due to operation of the nearby HPRR reactor. More field testing is planned to determine the performance capabilities and limitations of TSEE and TLD for environmental measurements.

## FAST-NEUTRON DOSIMETRY BY TSEE

As we reported previously,[5,6] use can be made of the response of inorganic TSEE dosimeters which exhibit a low inherent fast-neutron sensitivity to fast-neutron-induced recoil protons from external "radiators" for neutron dosimetry in mixed radiation fields. This is done by covering the front face of one ceramic BeO detector with a polyethylene layer, while that of a second dosimeter is covered with a nonhydrogenous low-$Z$ material such as graphite or Teflon. The lower practicable energy limit of the system is estimated to be less than 10 to 50 keV. We are currently investigating the possibility of extending the range to lower energies by covering a small fraction of the TSEE dosimeter with a material such as LiF (TLD-100) or $Li_2B_4O_7$, whose constituents undergo $(n,\alpha)$ reactions with the thermalized and backscattered neutrons from the human body. By properly balancing the respective contributions of recoil and albedo mechanisms to the total measured TSEE signal, it is hoped to obtain a smooth energy response over a large part of the neutron spectrum, at least for frontal neutron incidence on a detector worn on the surface of the thorax.

Also studied in some detail was the angular response of radiator-covered flat TSEE detectors. It can be seen in Fig. 2.6 that the sensitivity rapidly drops when approaching or exceeding an angle of neutron incidence of 90° (frontal exposure = 0°). As one would expect from the neutron energy dependence of the recoil proton range and the thickness of the sensitive layer in the BeO, this directional dependence becomes more pronounced with decreasing neutron energy. A simple modification can reduce this undesirable directional response. The hydrogenous radiator is sandwiched between two BeO disks. They are both evaluated by reading out the side facing the radiator, and the differences between each detector reading and that of the Teflon-covered one are added. As can be seen in Fig. 2.7, the resulting fast-neutron response becomes

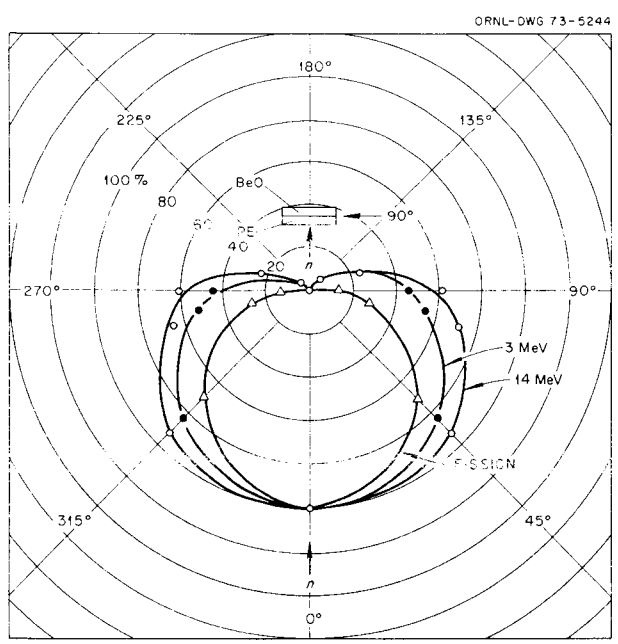


**Fig. 2.6. Directional response of a ceramic BeO disk TSEE dosimeter, covered with a thick polyethylene recoil proton radiator, for different neutron energies.**

5. K. Becker, *Proceedings of the Second International Conference on Luminescence Dosimetry,* CONF-680920, p. 205 (1968).

6. K. Becker and K. W. Crase, *Nucl. Instrum. Methods* 82, 297 (1970).

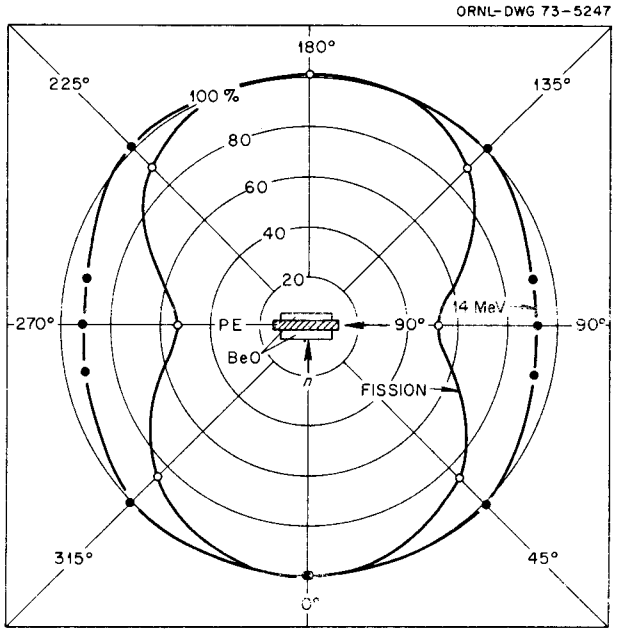


**Fig. 2.7. Directional response of a composite TSEE fast-neutron dosimeter consisting of two detectors sandwiching a thick radiator.**

quite independent of the direction of neutron incidence for higher neutron energies but still exhibits a dip around 90° for fission neutrons.

The response ratio between the two detectors obviously indicates whether the neutron exposure occurred from the front or the back. A more precise determination of the direction of neutron incidence is possible by using a cubical device with TSEE disks on all six faces; some of the dosimeters are covered by Teflon and others by polyethylene in order to measure neutrons and gamma rays.[7] It can be seen in Fig. 2.8 how the angular response of this detector depends on its location on the surface of a thorax phantom.

A TSEE fast-neutron dosimeter can also be easily transformed into a "poor man's fast-neutron spectrometer" based on the strong neutron energy dependence of the recoil proton range and, consequently, of the radiator thickness which is required to establish recoil proton equilibrium. With 14-MeV neutrons, for example, more than 2 mm of polyethylene is required to establish maximum recoil proton response, while only ~0.3 mm is necessary for the HPRR fission spectrum (Fig. 2.9). If a sequence of radiators with different thicknesses are placed between the detector and a nonhydrogenous medium, the shape of the resulting curve also indicates whether the neutrons are monoenergetic or not, a wide energy distribution such as in the fission spectrum resulting in a less steep rise of the curve. A modification of this method consists of an arrangement in which recoil proton absorbers such as aluminum or Teflon foils of varying thicknesses are

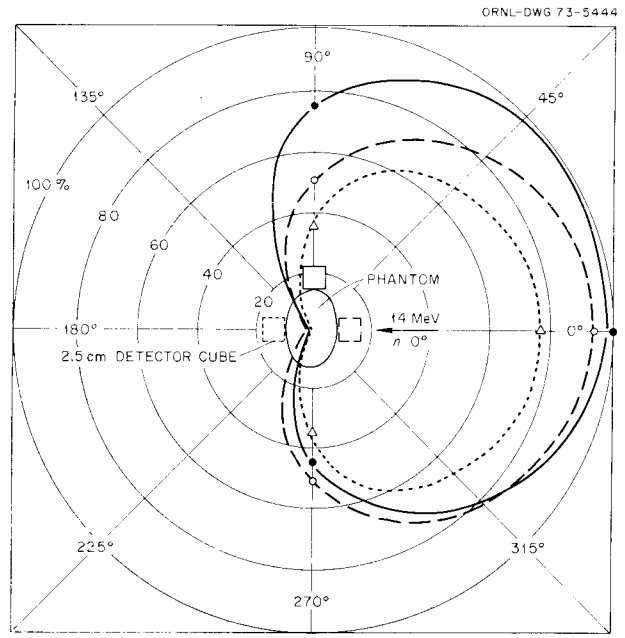


**Fig. 2.8. Fast-neutron-induced TSEE response of polyethylene-covered BeO detectors held in the four sides of a Teflon cube mounted on the front, back, and side of a thorax phantom.** The gamma response, which is nearly independent of the angle of incidence of the beam, was measured by Teflon-covered BeO detectors in the remaining two faces of the cube.

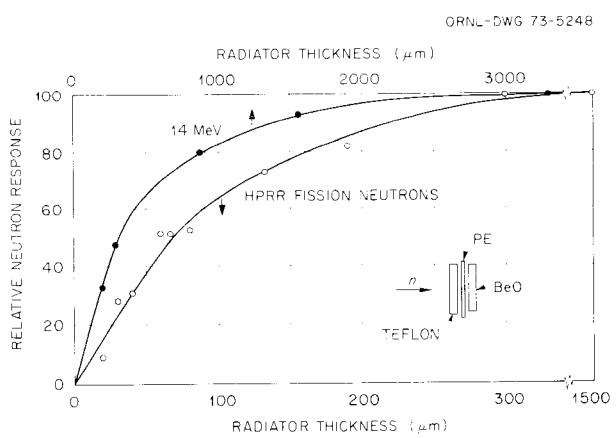


**Fig. 2.9. Relative fast-neutron response of TSEE dosimeters as a function of the thickness of the hydrogenous radiator (polyethylene) layer for two neutron energies and energy distributions.**

7. M. H. Lee, R. B. Gammage, and F. F. Haywood, to be published.

**Table 2.5. TSEE results for the ORNL Ninth Intercomparison Study of Nuclear Accident Dosimetry (July 1972), and average of other detectors (in parentheses)**

| Shielding of HPRR | Dose (rads) | |
|---|---|---|
| | Neutrons | Gamma |
| Bare | 250 (256) | 36.3 (35) |
| Steel | 74.2 (110) | 13.0 (13.5) |
| Lucite | 42.4 (45.4) | 31.8 (35.8) |
| Bare | 263 (272) | 40.2 (40.8) |

placed between a thick recoil proton radiator and the detector.[8]

With a pulse counter for evaluation of the dosimeters, fast-neutron doses as low as a few millirads can be measured. For high-dose-level accident dosimetry, the previously described[9] ionization-chamber-type TSEE counter should be used. The results which were obtained during the last DOSAR Intercomparison Study[7] are compared in Table 2.5 with the averages of the readings of three different dosimeter types as used by various other groups, showing excellent agreement in all but one neutron measurement behind heavy shielding.

## TSEE MONITORING OF BETA EMITTERS

An exoelectron radiation detector possesses the intrinsic advantage over bulk-type solid-state detectors in being able to detect efficiently weakly penetrating radiations such as low-energy beta rays. Efforts have been directed toward the detection of tritium either in air or on contaminated surfaces, where the present techniques for its measurement are cumbersome, expensive, or inaccurate. A gaseous tritium dosing apparatus (Reactor Chemistry Division) has been used for the tritium exposures. There is a linear TSEE response with exposure time at a concentration of 0.1 $\mu$Ci/cc of tritium in helium. Conversion to a 40-hr exposure indicates that 1/1000 of the occupational maximum permissible concentration would produce a TSEE signal several times higher than that caused by normal background radiation. The sensitivity is thus apparently high enough for the purposes of personnel protection.

Metal surfaces contaminated with tritium have been monitored by placing the BeO disk face down either in direct contact with, or about 0.1 mm away from, the metal surface. As an example of the detector's capability, a surface (smear tested to give 200 dis/min) produced a TSEE signal ten times higher than the noise level after an exposure time of 30 min. BeO detectors have also been placed in the exhaust of the vacuum pump of a 14-MeV neutron generator, and the tritium-induced signal was measured as a function of exposure time. As can also be seen in Fig. 2.10, tritium is able to penetrate a polyethylene encapsulation of the detectors after sufficient exposure time.

Before the TSEE signal is read, an exchange reaction in alcohol must be performed to remove the tritiated hydroxyls from the BeO surface. The adverse effect of not doing this is demonstrated by Fig. 2.11. Self-excitation is triggered in an erratic fashion at elevated temperature, and this emission interferes with the characteristic radiation-induced signal.

The measurement of a beta emitter in solution is possible by directly immersing the BeO detector, and Fig. 2.12 shows the results for a $^{204}$Tl solution of 0.184 $\mu$Ci/ml (50 millirads/hr to the surface of the BeO). Immersion for 40 hr in a solution containing the maximum permissible concentration of $^{204}$Tl would produce ~17,000 counts. The monitoring of such radionuclides over extended periods of time is a possibility, although the sensitivity changes and fading effects have still to be resolved. In particular, the immersion in water containing ions poses a dirt problem which causes anomalous effects in the exoelectron emission in much the same way that is found after the BeO has been exposed to tritium. The BeO disk must be

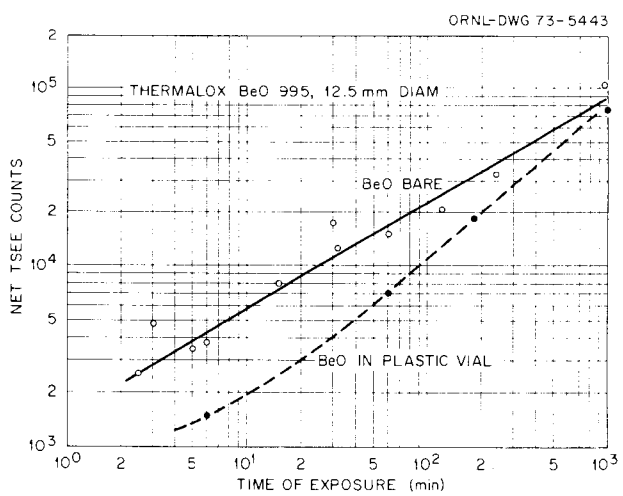


**Fig. 2.10. TSEE response of BeO detectors placed in the tritium-contaminated exhaust fumes from the vacuum pump of a 14-MeV neutron generator, with the detectors either bare or protected by a polyethylene vial.**

8. K. Becker and M. Abd-el Razek, *Nucl. Instrum. Methods*, in press (1973).

9. K. W. Crase, R. B. Gammage, and K. Becker, *Health Phys.* **22**, 402 (1972).

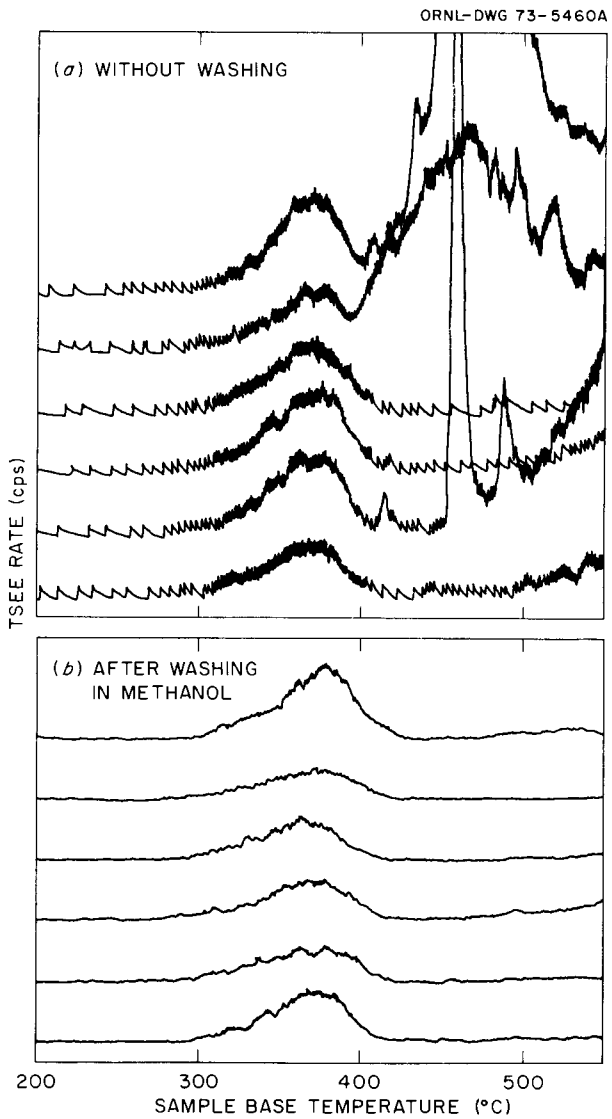


**Fig. 2.11. TSEE curves from six Thermalox 995 BeO detectors exposed to small concentrations of tritium gas in helium.** (*A*) Without any postirradiation treatment; (*B*) after postirradiation washing in alcohol.

thoroughly washed in distilled water and alcohol to remove adsorbed ions for avoiding the non-radiation-induced self-excitation signals and contamination of the reader.

## TLD AND FILM STABILITY STUDIES

Because of the increasing worldwide interest in personnel monitoring and environmental dosimetry, a postal intercomparison study was conducted by mailing detectors under warm and humid climatic conditions in many developing countries and the southern parts of

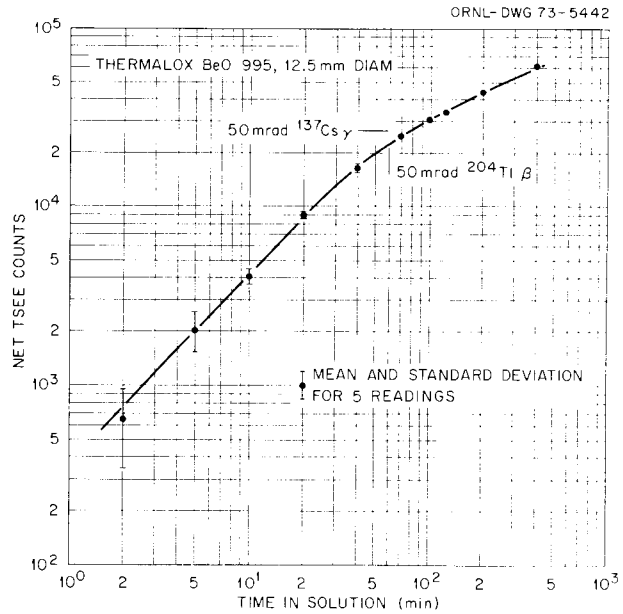


**Fig. 2.12. Normalized TSEE response of ceramic BeO detectors immersed in a 0.184-μCi/ml solution of $^{204}$Tl.** Mean responses to 50 millirads of 660-keV photons are also indicated.

the USA and Europe. The laboratory field testing of the long-term stability of various film and solid-state dosimeters (mostly TLD) has been continued. The work was partially supported by the World Health Organization and the Pan American Health Organization. For example, unexposed and gamma-irradiated film dosimeters with or without additional heat-sealing into aluminum-polymer compound foils, and LiF:Mg,Ti (TLD-100) and $CaSO_4$:Dy phosphors have been stored in seven different locations in Colombia, Ecuador, Chile, and Argentina for periods of about three months, prior to evaluation at ORNL and comparison with the readings of identically irradiated references which had been stored at −8°C and 0% relative humidity.

Some of the results of this intercomparison of detectors are compiled in Table 2.6. Not listed in Table 2.6 are other films such as Kodak PM type 3 and Agfa/Gevaert, which exhibit a very similar behavior, and the fog densities of unexposed films, which undergo up to 63% fading and 20% fogging relative to the controls (for a detailed discussion, see ref. 10). The tentative conclusions of these tests may be summarized as follows:

1. It is difficult to simulate field conditions in laboratory tests, mostly because it is more the extremes than the averages in temperature and humidity

10. K. Becker, ORNL-TM-4279 (1973).

**Table 2.6. Reading of gamma-irradiated film and TLD after storage for three months at different locations**

Normalized for controls kept under low-fading conditions

| Location | Average temperature (°C) | Average relative humidity (%) | Kodak PM type 2 | | TLD phosphors | |
|---|---|---|---|---|---|---|
| | | | Unsealed | Sealed | LiF:Mg,Ti (TLD-100) | $CaSO_4$:Dy |
| ORNL control | −8 | 0 | 100 | 100 | 100 | 100 |
| Bogota, Colombia | 16 | 70 | 97.5 | 97.5 | 89 | 94.7 |
| Cartagena, Colombia | 28 | 90 | 21.3 | 46.3 | 77.2 | 97.6 |
| Guayaquil, Ecuador | 20.7 | 71 | 0 | 11.3 | 86.2 | 94.6 |
| Santiago, Chile | 18.6 | 63 | 103.5 | 97.6 | 87.5 | 106 |
| Los Angeles, Chile | 29 | 82 | 102.9 | 96.5 | 92.7 | 109.5 |
| Buenos Aires, Argentina | 29.0 | 88 | 29 | 92 | 90.5 | 100 |
| Santa Fe, Argentina | 31.0 | 78 | 67 | 97.5 | 82.6 | 97 |

PHOTO 1036-73

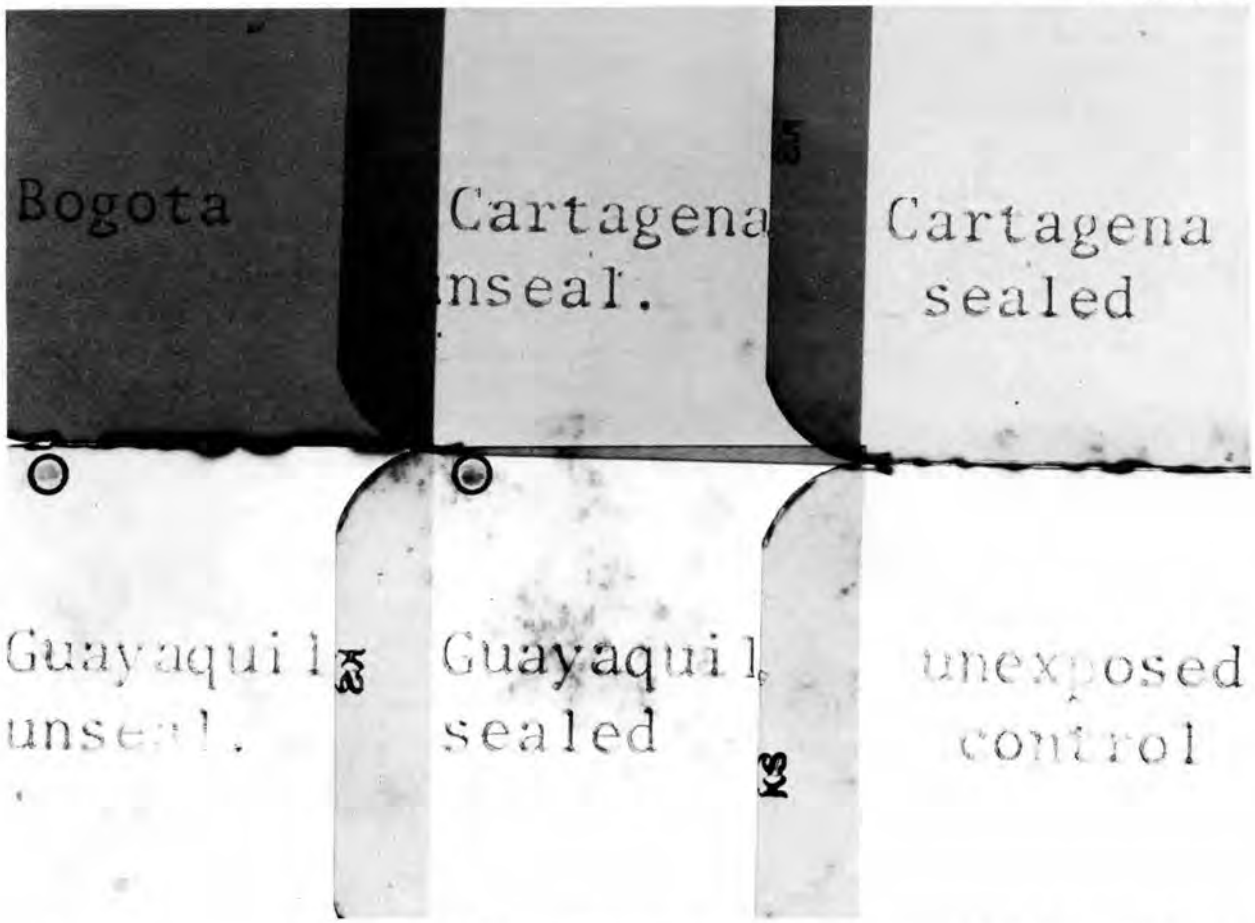


**Fig. 2.13. Appearance of the standard Kodak Personnel Monitoring type 2 film after exposure to 0.4 R of gamma radiation and three months of storage (from upper left to lower right) in Bogota, Colombia; in Cartagena, Colombia, without and with additional protective sealing; in Guayaquil, Ecuador, without and with sealing; and unexposed (background fog).**

which are responsible for most of the fading and fogging – high humidities being the dominant factor for the film instabilities and high temperatures for the fading in TLD.

2. In four out of seven locations, film dosimeters should not be used because fading of the gamma-radiation effect in the widely used Kodak type 2 film amounted to 33–100%. Even careful additional sealing did not protect the film sufficiently in two out of seven locations, namely, Cartagena in Colombia and Guayaquil in Ecuador (for the visual appearance of some of the stored films, see Fig. 2.13).
3. Under the same conditions, LiF:Mg,Ti (TLD-100) exhibited 7.3 to 22.8% fading and should, therefore, not be assumed to be perfectly stable under field conditions. More stable than LiF is $CaSO_4$:Dy, which is also 20 to 30 times more sensitive and has, consequently, been used widely for environmental monitoring work. In the 5-to-10-millirad range, accuracies of ±2 to 3% have been obtained routinely for $CaSO_4$:Dy with a commercial Harshaw 2000 reader (compensation for the photon energy dependence turned out to be not necessary because of the negligible contribution of <100-keV photons to total dose).

## TL DETECTOR DEVELOPMENT

Improved thermoluminescence dosimeters have been developed and are being tested in detail. A commercial TL reader was equipped with an ultraviolet-sensitive photomultiplier for the improved evaluation of the TL in ceramic BeO (Thermalox 995) disks known to emit a large fraction of their TL in the ultraviolet spectral region. This led to a sevenfold increase in detector sensitivity, and doses as low as 1 mR became detectable (doubling of background signal). The main TL peak is at 167°C for a 16°C/sec heating rate. Initially, the ceramic BeO exhibits only little light sensitivity, but an unusual self-induced TL signal was observed (peaking at ~190°C) after etching in HF; the signal grows in the dark and is enhanced by visible light.

A computer program has been developed which greatly simplifies the calculation of the photon energy response of solid-state detectors. It has been, or may easily be, applied to the matching of composite detectors to the energy dependence of air, water, soft tissue, bone, etc. For example, a mixture of 94% BeO and 6% $SiO_2$ has been calculated to be energy-independent within <1% between less than 10 keV and several MeV. This mixture forms a very hard and stable porcelain-like compound if the finely powdered constituents are heated to ~1400°C.

Finely powdered (<4 μm), highly sensitive TL phosphors such as $CaSO_4$:Dy and $CaSO_4$:Tm have been embedded into high-melting organics, for instance *p*-quaterphenyl or *p*-sexaphenyl (mp ~450°C), for fast-neutron dosimetry via recoil proton registration. If exposed to the mixed radiation field of the HPRR, such detectors exhibit a response three times higher than Teflon-embedded phosphors having the same gamma radiation sensitivity, the response difference being due to the fission neutrons. This indicates about 50% efficiency of the recoil protons in producing a TL signal in the phosphor. For 14-MeV neutrons from the (*d*,T) reaction, the response ratio is 10. The detectors are prepared by hot-pressing the constituents into reusable pellets. An increase in the visible light sensitivity was observed only in the *p*-sexaphenyl-embedded (not in the Teflon-embedded) material, probably due to electronic energy transfer from the organic luminescent material to the highly disperse thermoluminescent phosphor.

## OTHER RESEARCH

There are several other projects which should be mentioned. A more sophisticated "spark counter" for the evaluation of etched alpha and fission-fragment detector foils has been designed and built. It permits a better control of sparking conditions and is presently being used for systematic investigations on the influence of relative humidity, temperature, air pressure, etc., on the voltage vs spark count plateau and also on the accuracy and reproducibility of counting in general.

Initial work on the TL signals from ancient meso-American pottery has been carried out, with the goal being not so much the determination of unknown ages but the averaging of the environmental radiation background over very long periods of time in cases where the age of the sample is known. The principle of this method may be described (in a somewhat oversimplified way) by the equation

$$\text{average dose rate} = \frac{\text{accumulated TL}}{\text{sensitivity} \times \text{age}} .$$

Other work in progress includes high-resolution measurements of steep neutron and photon dose gradients at interfaces, for example, bone/tissue; the integrating dosimetry of biologically active ultraviolet light; and studies on the effect of controlled diffusion of impurities at temperatures up to 2700°C into high-melting metal oxides on their TSEE and TLD characteristics.

## INFORMATION AND EDUCATIONAL ACTIVITIES

During the past years, substantial efforts were devoted to training and to collection and dissemination of information in the field of solid-state dosimetry. Graduate students and guest scientists from this and ten foreign countries (Chile, Ecuador, Egypt, Germany, India, Mexico, Persia, Thailand, Taiwan, and Vietnam) received advanced training and worked with this group for extended periods, usually for one year. In cooperation with the Physics Department of the University of Tennessee, domestic and foreign students completed three M.S. and two Ph.D. dissertations on TSEE and track etching. Seminars and lectures on various aspects of solid-state dosimetry have been presented at about 40 universities and research institutes, not only in this country but also in Japan, Korea, Taiwan, Denmark, Belgium, England, Switzerland, Italy, Austria, Germany, Canada, Mexico, Colombia, Argentina, Chile, and Brazil. Courses on solid-state dosimetry were taught at National Tsing Hua University, Hsinchu, Taiwan; the Institute of Biophysics, Federal University, Rio de Janeiro, Brazil; and the National University (UNAM) of Mexico City. One group member served as member of a task group of ICRU, as vice-chairman of another task group of ICRP, and as a government advisor in health physics for IAEA and WHO in Taiwan, Brazil, Colombia, Chile, and Argentina.

A series of bibliographies on dosimetry covering about 12,000 references has been edited and published (ten reports). Numerous comprehensive critical reviews on various areas of solid-state dosimetry have been published, the most recent ones covering the whole field of solid-state dosimetry,[11] track etching,[12] and the stability of detectors for personnel and environmental dosimetry in warm and humid climates.[10] Members of the group have also been instrumental in the organization of the Second International Conference on Luminescence Dosimetry, Gatlinburg, 1968; a Symposium on the Future of Personnel Dosimetry, New York, 1971; the Third International Conference on Luminescence Dosimetry, Copenhagen, 1972; the International Conference on Exoelectrons, Prague (scheduled), 1973; and the Fourth International Conference on Luminescence Dosimetry, Cracow (scheduled), 1974. Preliminary work for establishing a formal Dosimetry Information Center in close cooperation with the Division's Information and Education Section has been completed (a key-word thesaurus is presently being prepared).

---

11. K. Becker, *Solid-State Dosimetry – Crystals, Glasses, and Polymers for the Integrating Measurement of Ionizing Radiation*, CRC Press, Cleveland, Ohio (1973).

12. K. Becker, "Dosimetric Applications of Track Etching," chapter 2 in *Topics in Radiation Dosimetry*, Suppl. I, Academic Press, 1972.

# 3. Atomic Physics

G. S. Hurst

W. R. Garrett[1] J. E. Talmage[2]
M. G. Payne E. B. Wagner

## TRANSPORT OF RESONANCE RADIATION

### Low-Pressure Theory

The combined experimental and theoretical study which is outlined here was stimulated by the important role played by resonance trapping[3-7] in determining the fate of energy deposited by fast charged particles in the inert gases. A great deal of information is available concerning these "energy pathways." In particular, detailed models have evolved for helium[3] and argon,[4-6] and these models are being subjected to detailed checks concerning predictions of time behavior of all inert-gas radiation that escapes from the gas, both for pure inert gases[4,5] and also for situations where impurities are added.[6] The models are also being checked for balance of energy among the various components of the energy emerging from the system.[5,6] At relatively low pressures, where photons are escaping to the walls of an apparatus, it is important to calculate the effect of initial conditions and the geometric peculiarities associated with the method of observing the emerging resonance photons. (At $P$ = pressure $\gtrsim$ 600 torr, the time behavior of the emerging radiation is insensitive to the wall losses because of the dominance of collision processes.)

We outline here the first part of a study whose objective is to find a correct transport theory, at least for the lower pressures, and to verify its predictions for as wide a range of pressures as possible. Our studies at lower pressures (i.e., $P < 10$ torr for the 1048-Å resonance line of argon) have contributed considerably to our understanding of how initial conditions and the geometrical arrangement for detecting emerging radiation affect the intensity and time behavior of the observed light. We have also found substantial deviations from a transport theory that assumes complete redistribution in frequency,[8,9] that is, a theory that assumes that any volume element of the gas emits photons with a frequency profile which is equal to the absorption profile.

Experimental studies of 1048-Å radiation in argon suggest that the following transport equation[10] is valid in the pressure range 0.002 torr $< P <$ 10 torr for container dimensions $>$ 1 cm:

$$\frac{\partial N(\mathbf{r}, x, t)}{\partial t} = -\gamma N(\mathbf{r}, x, t) - A\, N(\mathbf{r}, x, t) + S(\mathbf{r}, x, t) + \frac{\gamma \bar{k}}{4\pi} \int_{-\infty}^{\infty} dx' \int_{V} N(\mathbf{r}', x', t)\, \bar{R}(x', x) \times \exp\left\{ -\left[k(x') + l^{-1}\right] |\mathbf{r} - \mathbf{r}'| \right\} \frac{dV'}{|\mathbf{r} - \mathbf{r}'|^2}, \quad (1)$$

where $N(\mathbf{r}, x, t)\, dx\, dV$ = number of excited atoms in $dV$ at $\mathbf{r}$ and time $t$ which will emit photons in $dx$ at $x$,

1. Fundamental Health Physics Research Section.
2. Oak Ridge Graduate Fellow, University of Kentucky.
3. D. M. Bartell, G. S. Hurst, and E. B. Wagner, *Phys. Rev. A* 7, 1068 (1973).
4. N. Thonnard and G. S. Hurst, *Phys. Rev. A* **5**, 1110 (1972); T. E. Stewart, G. S. Hurst, T. E. Bortner, J. E. Parks, F. W. Martin, and H. L. Weidner, *J. Opt. Soc. Amer.* **60**, 1240 (1970).
5. J. E. Talmage, Ph.D. thesis, University of Kentucky, in preparation.
6. C. S. Hurst and E. B. Wagner (in preparation).
7. A. C. G. Mitchell and M. W. Zemansky, *Resonance Radiation and Excited Atoms*, The Macmillan Co., New York, 1934.
8. T. Holstein, *Phys. Rev.* **72**, 1212 (1947); T. Holstein, *Phys. Rev.* **83**, 1159 (1951).
9. L. M. Biberman, *Zh. Eks. Teor. Fiz.* **17**, 584 (1949).
10. J. E. Talmage, M. G. Payne, G. S. Hurst, and E. B. Wagner (to be published).

$\gamma$ = reciprocal natural lifetime for the resonance transition in question, $\nu_0$ = frequency of the center of the isolated line, $c$ = speed of light, $\lambda_0 = c/\nu_0$, $V_0$ = most probable velocity of the atoms, $x = (\nu - \nu_0)c/(\nu_0 V_0)$, $\nu$ = frequency, $g_2/g_1$ = ratio of statistical weights for the upper and lower levels, $N$ = number of atoms per unit volume, $A$ = volume rate constant for converting the energy of the resonance state to another form by way of collision with ground-state atoms or impurities, $l$ = mean free path for absorption of resonance photons by complexes other than ground-state atoms, $S(\mathbf{r}, x, t)\, dx$ = volume rate of production of resonantly excited atoms which will radiate in $dx$ at $x$ due to excitation processes other than absorption of resonance photons,

$$\gamma_c/\gamma = 0.9N\lambda_0{}^3(g_2/g_1)/6\pi^2 ,$$

$$a = (\gamma + \gamma_c)\lambda_0/(4\pi V_0) ,$$

$$k_0 = (\lambda_0{}^3\gamma/8\pi^{3/2})(g_2/g_1)(N/V_0) ,$$

$$\phi(x) = k(x)/\bar{k} ,$$

and

$$k(x) = k_0\pi^{-1/2}\int_0^\infty \times \exp\left[-aV - (V/2)^2\right] \cos Vx\, dV ,$$

$$\bar{k} = \int_{-\infty}^{\infty} k(x)\, dx ,$$

$$\bar{R}(x', x) \cong \frac{\gamma_c}{\gamma + \gamma_c}\phi(x)\,\phi(x') + \frac{\gamma}{\gamma + \gamma_c}R_{\mathrm{II}}(x', x) ,$$

with

$$R_{\mathrm{II}}(x', x) = \pi^{-3/2}\int_Z^\infty \times du\, e^{-u^2}(\tan^{-1} W_1 - \tan^{-1} W_2) ,$$

$$Z = |x - x'|/2 ,$$

$$W_1 = [u + \min(x, x')]/a ,$$

$$W_2 = [\max(x, x') - u]/a .$$

To obtain a complete transport theory, Eq. (1) is coupled with the assumption that if $P$ is sufficiently great for strong resonance trapping (i.e., $\gtrsim$ 0.002 torr for 1048-Å photons in argon) to occur, then emission from any volume element is isotropic. The strong trapping assumption limits the validity of Eq. (1) at low pressures, while at higher pressures one is limited by the fact that the derivation of Eq. (1) uses a theory for $\bar{R}(x', x)$ that includes only binary collisions and assumes that only the long-range part of the interaction between an excited atom and a ground-state atom is important.[11,12] At sufficiently high pressures, either higher-order collisions or the importance of the short-range part of the potential will cause Eq. (1) to fail. The derivation also assumes that there are no other atoms present that absorb the photons resonantly other than the ground-state atoms of the same isotope of the inert gas in question. The resonance level must be well isolated in energy from all others, and the density of excited atoms must be small.

Equation (1) was checked experimentally in the following way:[6]

1. Very pure argon was contained in a long cylinder of radius $R$ = 1.1 cm and was excited by a coaxial beam of protons.

2. The protons came in periodic pulses of duration $1.7 \times 10^{-8}$ sec, and the time between pulses was great enough (~128 $\mu$sec) so that essentially all energy associated with the $^1P_1$ level from one pulse had escaped before the next came.

3. The electronic arrangement described by Bartell, Hurst, and Wagner[3] was used to determine $I(t)$ = time profile of the protons detected due to excitation by a single pulse of protons. $I(t)$ was determined by accumulating photons from many proton pulses using a well-known technique.[4-6] Equation (1) can be used to show that with the detection geometry shown in Fig. 3.1 a nearly exponential decay of $I(t)$ will occur at both low and intermediate pressures if $y_0/2R \cong 0.34$. Further, if

$$I(t) = I(0)\, e^{-\beta t} ,$$

then

$$\beta = \gamma\int_{-\infty}^{\infty} dx' \left[P_c\,\phi(x') + (1 - P_c)\pi^{-1/2}e^{-x'^2}\right] \times \left[\lambda + (1 - \lambda)\, E_2(\tau_0/2) - (1 - \lambda)\, G(\tau_0/2, \lambda)\right] , \quad (2)$$

11. P. R. Berman and W. E. Lamb, *Phys. Rev.* **187**, 221 (1969).

12. D. L. Huber, *Phys. Rev.* **178**, 93 (1969).

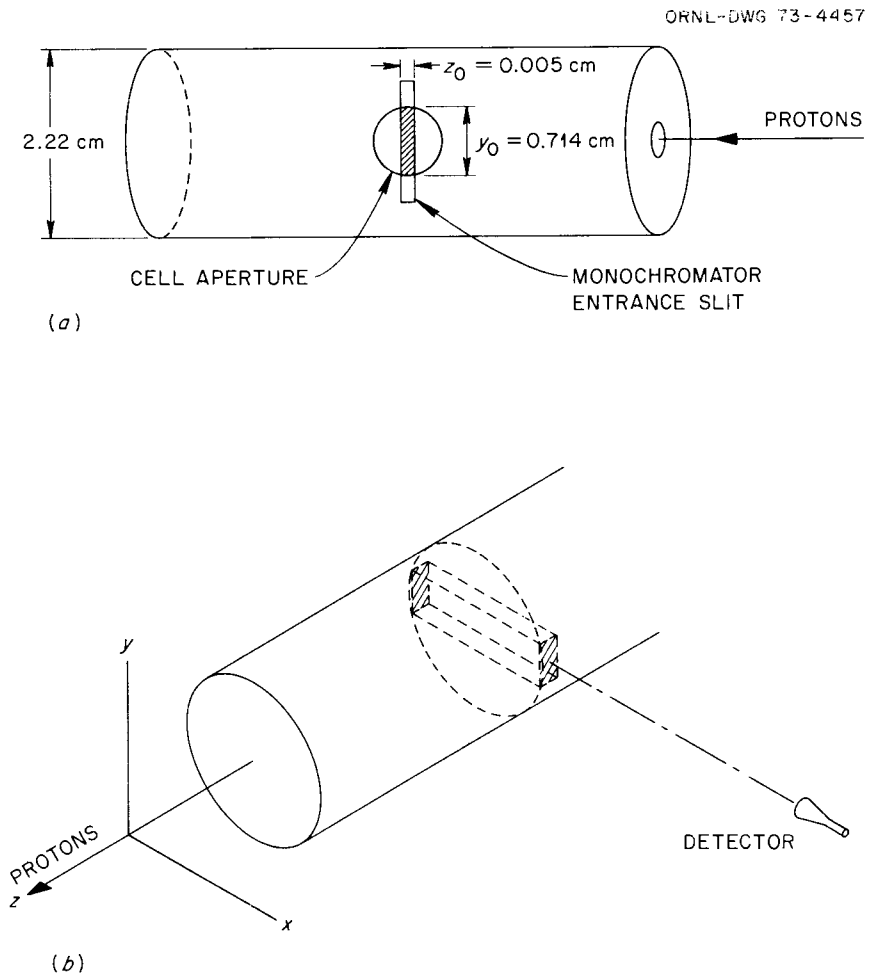


**Fig. 3.1. Detection geometry used in the measurement of $I(t)$ for the 1048-Å line of argon.**

where

$$P_c = \gamma_c/(\gamma + \gamma_c) ,$$

$$\lambda = (1 - P_c)[1 - b(x')] ,$$

$$b(x') = \pi^{-1/2} e^{-x'^2}/\phi(x') ,$$

$$\tau_0 = k(x')\, y_0 ,$$

and

$$E_2(x) = \int_1^\infty e^{-xy}\, dy/y^2 ,$$

$$G(x, \lambda) = \frac{\lambda}{\pi} \int_{-\infty}^{\infty} \frac{[R(|P|)]^2 \sin(Px)}{P[1 - \lambda R(|P|)]}\, dP ,$$

with $R(|P|) = \tan^{-1}(P)/P$. In Fig. 3.2 we show observed $I(t)$'s for several pressures, and in Fig. 3.3 we compare Eq. (2) with experiment over a wide pressure range. For 0.01 torr $< P <$ 0.3 torr, an approximation used in deriving Eq. (2) can be shown to lead to an underestimate of $\beta$. The approximations can be shown to be a good solution of Eq. (1), however, for 0.002 torr $< P <$ 0.01 and 0.3 torr $< P <$ 10 torr. Everywhere between 0.005 torr $< P <$ 0.25 torr a solution of the Holstein-Biberman equation with the absorption coefficient of Eq. (1) and emission profile $\phi(x) = k(x)/\bar{k}$ leads to an overestimate of $\beta$ by a factor of 2 or more.

## Effects of Photoabsorption on the Transport of Resonance Radiation

The effect of a finite mean free path for photoabsorption on the transport of resonance radiation has been calculated on the basis of the Holstein-Biberman equation. The latter equation is approximately correct at rather low pressures if there is still strong resonant

trapping but the wings of the absorption profile play no part. In the latter case the appropriate solution of the equation employs pure Doppler-broadened absorption and emission profiles. In addition, the Holstein-Biberman theory usually has a region of validity at intermediate pressures where $P_c \cong 1$ but the $R(x', x)$ of Eq. (1) is still valid. Thus, we will derive results for these two limiting cases.

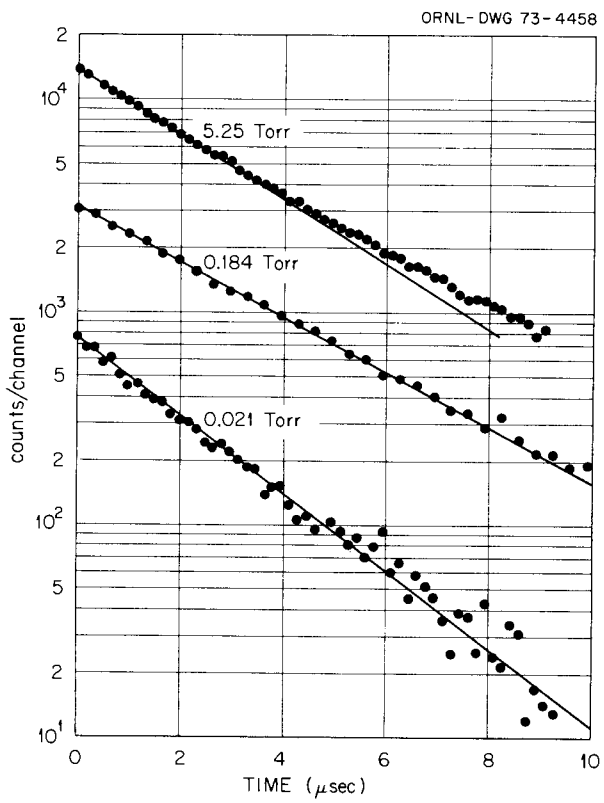


**Fig. 3.2. Typical $I(t)$ vs $t$ curves for the experiment on the 1048-Å line of argon.**

The Holstein-Biberman equation[8,9] including photoabsorption is

$$\frac{\partial N(\mathbf{r}, t)}{\partial t} = -\gamma N(\mathbf{r}, t) - A N(\mathbf{r}, t) - \gamma \int_V \frac{dV' \, N(\mathbf{r}', t)}{4\pi R^2} e^{-R/l} \frac{\partial T(R)}{\partial R}, \quad (3)$$

where

$$R = |\mathbf{r} - \mathbf{r}'|$$

and

$$T(R) = \int_{-\infty}^{\infty} \phi(x') \, e^{-k(x')R} \, dx' . \quad (4)$$

For simplicity, we restrict ourselves to slab geometry ($y_0$ = slab thickness) and assume that $N(\mathbf{r}', t)$ is strongly peaked near the slab center. The approximation of $N(\mathbf{r}', t)$ being sharply peaked near the slab center is appropriate to two limiting situations: (1) It is appropriate at very early times if at $t = 0$ all of the atoms in the resonance state are at the midplane of the slab. (2) It is appropriate at all times (and is also independent of the slab geometry assumption) if at $t = 0$ all excited atoms are at distances from the bounding container which are large compared with the mean free path $l$. In the latter situation the decay of the total number of resonance states is independent of the location of the excited

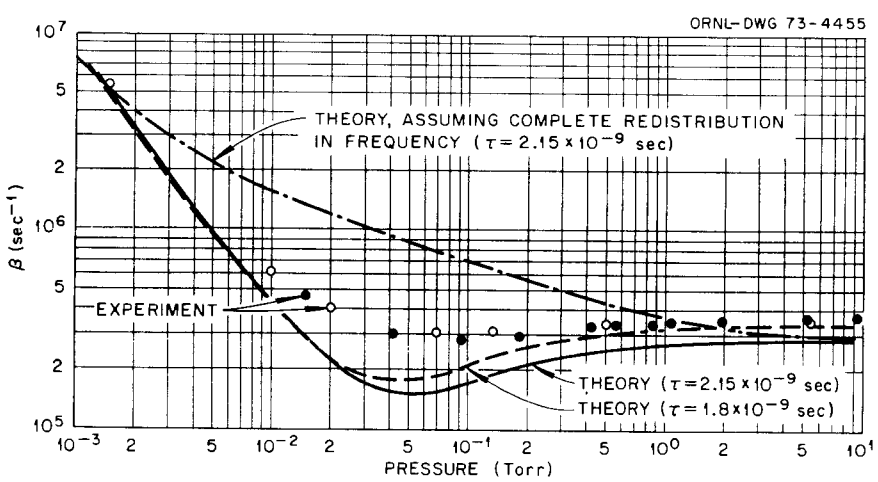


**Fig. 3.3. Decay constant $\beta$ vs pressure for the 1048-Å line of argon.** $I(t) = I(0) \exp(-\beta t)$.

atoms as long as the resonance photons cannot reach a surface before the energy is converted to another form. Thus, in either of the latter situations we find

$$N(t) = \int dV' \, N(\mathbf{r}', t)$$

directly from Eq. (3):

$$\frac{dN}{dt}(t) \approx -\beta N(t) , \tag{5}$$

where $\beta$ is given by

$$\beta = \gamma(P_e + P_\gamma) + A \tag{6}$$

and

$$P_\gamma = l^{-1} \int_0^{y_0/2} dy \int_1^\infty \frac{du}{d} T(yu) \, e^{-yu/l} , \tag{7}$$

$$P_e = T(y_0/2) \, E_{2+m} \, (y_0/2l) . \tag{8}$$

In Eq. (8) we have $m = 1$ for pure Doppler broadening and $m = \frac{1}{2}$ for pure impact broadening. The special function $E_s(x)$ is a generalization of the exponential integrals $E_n(x)$ to noninteger values of $n$:

$$E_s(x) = \int_1^\infty e^{-xy} \, dy/y^s . \tag{9}$$

For integer $s$ the properties of $E_s(x)$ are well known.[13] Using techniques that are similar to those used for integer $s$, we find

$$\frac{dE_s(x)}{dx} = -E_{s-1}(x) , \tag{10a}$$

$$E_{s+1}(x) = \frac{1}{s}[e^{-x} - x \, E_x(x)] , \tag{10b}$$

and for $s + x \gg 1$,

$$E_s(x) = \frac{e^{-x}}{s+x} \left\{ 1 + \frac{s}{(s+x)^2} + O[(s+x)^{-3}] \right\} . \tag{10c}$$

For $0 < s < 1$, we find

$$E_s(x) = x^{s-1} \, \Gamma(1-s) - \sum_{n=0}^{\infty} \frac{(-x)^n}{(n-s+1)n!} . \tag{10d}$$

13. Milton Abramowitz and Irene A. Stegun, eds., *Handbook of Mathematical Functions*, U.S. Government Printing Office, Washington, D.C., 1964.

We can readily evaluate $\beta$ in the more important limiting cases. In the special case of pure impact broadening:

$$\beta = \frac{2\gamma}{3} T\left(\frac{y_0}{2}\right) \left[ 1 + 3\frac{y_0}{2l} - \sqrt{\pi}\left(\frac{y_0}{2l}\right)^{3/2} + \frac{1}{2}\left(\frac{y_0}{2l}\right)^2 + O\left(\frac{y_0}{2l}\right)^3 \right] + A , \tag{11a}$$

for very early times and $y_0/2l < 0.2$. For all times and $y_0/2l > 2$, we have for impact broadening

$$\beta \approx \gamma \, T(y_0/2)(y_0\pi/2l)^{1/2} + A . \tag{11b}$$

$T(\rho)$ has been evaluated at large $k_P\rho$ by Holstein and is given by $T(\rho) = 1/(k_P\pi\rho)^{1/2}$, where

$$k_P = (\lambda_0{}^2 N)(g_2/g_1)(\gamma/\gamma_c)/2\pi .$$

With pure Doppler broadening, we obtain

$$\beta \cong \gamma \left\{ k_0 y_0 \, [\pi \ln (k_0 y_0/2)]^{1/2} \right\}^{-1} \times \left\{ 1 + [2 \ln (k_0 y_0/2) - 1](y_0/l) + O[(y_0/2l)^2 \ln (y_0/2l)] \right\} + A , \tag{11c}$$

for the limit of early times and $y_0/2l < 0.2$. In the Doppler limit with a container of dimensions which are large compared with $l$ we obtain at all times

$$\beta = 2\gamma(\ln k_0 l)^{1/2}/(\sqrt{\pi} k_0 l) + A . \tag{11d}$$

In most laboratory situations the effects of photoabsorption will probably be small because of the tendency of most impurities to contribute strongly to $A$ by way of collisional quenching of the resonance level. However, with a careful choice of impurity and resonance level and with a container of rather large dimensions, one can probably enhance the importance of photoabsorption considerably and check Eqs. (11) against experiment.

## DECAY OF RESONANCE PHOTONS IN ARGON GAS

The experimental work for the transport of 1048-Å resonance radiation in argon revealed an intense long-lifetime "tail" when one plots the relative intensity as a function of time (see Fig. 3.4). We observed that for proton excitation the long tail is more intense than for

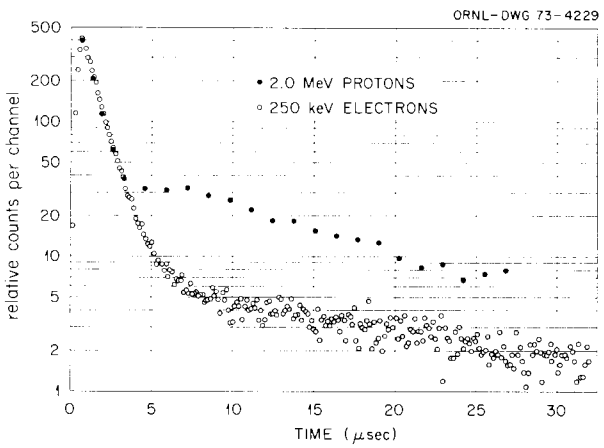


**Fig. 3.4. Decay of 1048-Å photons in argon at 600 torr.**

electron excitation.[14] This observation, as well as the observation that the long tail intensity is a nonlinear function of the number of protons in a single pulse, is consistent with the interpretation[15] that the time delay is due to a recombination process as follows:

$$Ar^+ + Ar(^1S_0) \rightarrow (Ar)_2^+ + Ar(^1S_0) ,$$

$$(Ar)_2^+ + e \rightarrow Ar^{**} + Ar ,$$

$$Ar^{**} \rightarrow Ar(^1P_1) + h\nu ,$$

which adds to the number of $Ar(^1P_1)$ states. These nonlinear effects are important to the practical realization of vacuum ultraviolet lasers and especially vital in predicting lasing efficiency.

Charged-particle excitation appears to be a useful approach to gas laser pumping. Excitation of high-pressure noble gases by accelerated electrons is one approach being intensively investigated. The work being pursued at ORNL on the energy pathways following proton interaction with a noble gas is, thus, very directly relevant to the laser problem. It has been shown, for instance, that fast charged particles excite the resonance states of these gases, whereas gas discharges cause mainly the excitation of optically forbidden (metastable) levels. Therefore, the large body of older literature on gas discharge excitation is not nearly so relevant to the laser problem as compared with proton excitation.

Our earlier observation[14] that, in general, noble-gas resonance states are converted to long-lived excited molecular states by three-body collisions has been used as the basis for looking for laser action in noble gases.[15,16] The exceptionally high yield of these diatomic species follows from the facts that the oscillator strengths for the resonance are large and that, once formed, all resonance states are converted to molecules at high pressure.

## QUENCHING OF RESONANCE EXCITED STATES WITH MOLECULES

Addition of molecular gas to excited noble gases and observation of the temporal changes in the emitted radiation appears to be a promising technique for the study of energy transfer. To cite an example of the direction of our work in this respect, we show in Fig. 3.5 the changes brought about in the lifetime of 1048-Å radiation by the addition of just 20 ppm of $C_2H_4$ to argon at 30 torr. The long tail is greatly diminished, and a slight increase in the rate of decay of the fast component is also observed. If the long tail is due to the dissociative recombination process described above, then the quenching of the tail does not alter the number of ion pairs observed in a normal $W$ measurement and hence cannot be responsible for the Jesse effect.

14. N. Thonnard and G. S. Hurst, *Phys. Rev. A* **5**, 1110 (1972).

15. D. C. Lorents and R. E. Olson, *Excimer Formation and Decay Processes in Rare Gases,* Semiannual Technical Report No. 1 Covering the Period June 1 to Nov. 30, 1972, Stanford Research Institute, Menlo Park, Calif. (Dec. 27, 1972).

16. *Laser-Fusion Program,* Semiannual Report – January–June 1972, Lawrence Livermore Laboratory report No. UCRL-50021-72-1 (July 12, 1972).

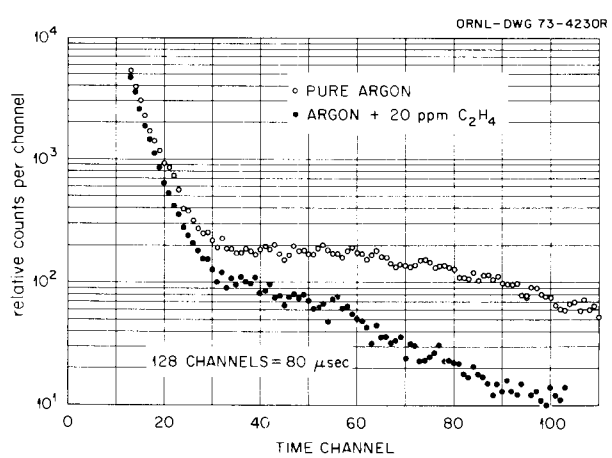


**Fig. 3.5. Decay of 1048-Å photons in argon at 30 torr.**

When larger concentrations of $C_2H_4$ were added, we were able to show that the pathways considerations are as follows:

*a*) $Ar(^1P_1) \rightleftharpoons Ar(^1S_0) + h\nu$ (1048 Å), which escapes to the wall at a rate $\beta_e$, and

*b*) $Ar(^1P_1) + 2Ar(^1S_0) \rightarrow (Ar)_2{}^* + Ar$,

so that the combined rate of decay of $^1P_1$ states is $\beta_0 = \beta_e + aP^2$, where $a$ is a constant and $P$ is the argon pressure. Now when $C_2H_4$ (for example) is added, a new pathway is open, since

*c*) $Ar(^1P_1) + C_2H_4 \rightarrow Ar(^1S_0) + (C_2H_4)^*$.

Therefore, plotting $\mu - \beta_0$ against $C_2H_4$ pressure gives a straight line, where $\mu$ is the rate of decay with the $C_2H_4$ added. Data plotted in this way were found to be independent of argon pressure and verify the kinetic scheme listed above as *a, b,* and *c*. We find the reaction rate for *c* to be $10.3 \times 10^{-10}$ cm$^3$/sec, compared with $10.3 \times 10^{-10}$ cm$^3$/sec obtained from a calculation based on the theory of Watanabe and Katsuura and $6.5 \times 10^{-10}$ cm$^3$/sec based on the interpretation of Jesse effects.[17] The reason for this low value (based on ionization experiments) is probably due to the fact that the Jesse effect in argon involves not only the $^1P_1$ state but also the $^3P_1$ state, where the cross section is, most likely, smaller.

## MATHEMATICAL FORMULATION OF RADIATION-STIMULATED BIOLOGICAL EFFECTS

The detailed processes by which specific biological effects are either induced or accelerated by ionizing radiation are extremely complex and poorly understood even in the simplest biological systems. A number of different approaches[18-22] have been taken in attempting to arrive at some understanding and/or a mathematical description of overall macroscopic biological response to ionizing radiation. Often two, three, or more theoretical interpretations have been offered to explain the same feature of certain experimental data. We have developed the thesis that greater insight might be gained in our understanding of the relationship between radiation insult and subsequent observation of macroscopic biological effects by directing careful attention to the kinetics of radiation-induced biological response.[18] The suggestion was made that a mathematical description of the biological kinetics be formulated on an operational basis where one foregoes a knowledge or description of microscopic molecular transitions which ultimately lead to observed macroscopic biological effects and starts with the overall dynamical response of the system. The idea is to model down toward a microscopic understanding of biological processes as opposed to starting with microscopic considerations and modeling up toward macroscopic effects.[18]

One of the most general pieces of information that can be obtained about a radiation effect is the probability that at time $t$ effect $i$ will exist in species $j$ at some recognizable level, given the particular chronological stage and environmental history of the specimen (including the external radiation field in which it has existed). By level we mean a recognizable physical or biological state of the system.

In the present work we specify and solve a rather general statistical model for a time-dependent probability function $P_{ij}(t, l)$, where $l$ is an integer which is assumed to be correlated in a one-to-one correspondence with an observable biological end point. The general model which we consider includes multihit–single-target and multitarget–single-hit models as special cases. It includes a simplified picture of both biological recovery and repair mechanisms and shares a number of points in common with some previous stochastic models of radiation reaction in living systems.[23-25] While the present model is more general than most of its predecessors, it by no means includes all the mechanisms which are known to be important in connection with some radiobiological effects. It does seem to describe with reasonable accuracy a number of experimental studies on cell survival as well as giving a schematic description of the available experimental data on cataracts in mice. Several possible applications of the theory have been worked out to illustrate its generality.

### Part A. Cell Survival – General Model

We first make special note of the schematic nature of the biological model which we choose as a basis for our

17. J. E. Parks, G. S. Hurst, T. E. Stewart, and H. L. Weidner, *J. Chem. Phys.* 57, 5467 (1972).
18. D. E. Lea, *Actions of Radiations on Living Cells*, Cambridge University Press, London, 1956.
19. A. M. Kellerer and H. Rossi, *Radiat. Res.* 47, 15 (1971).
20. G. M. Hahn and R. F. Kallman, *Radiat. Res.* 30, 702 (1967).
21. G. J. Dienes, *Radiat. Res.* 28, 185 (1966).
22. G. S. Hurst, W. R. Garrett, and M. G. Payne, submitted for publication to *Health Physics.*
23. J. Calkins, *Radiat. Res.* 45, 50 (1971).
24. R. Katz, B. Ackerson, M. Homayoonfar, and S. C. Sharma, *Radiat. Res.* 47, 402 (1971); J. J. Butts and R. Katz, *Radiat. Res.* 30, 855 (1967).
25. S. Curtis, private communication.

analysis. At this stage in our efforts to analyze biological response to ionizing radiation, we wish to construct a model which is mathematically tractable but at the same time sufficiently general to include a number of well-demonstrated macroscopic effects. Thus, we include a number of "components" in the model, along with a mathematical description of the interactions between these components, where the choices are based on biological information obtained from the dynamical response of biological systems to radiation exposure. However, we do not attempt to uniquely identify these components on a microscopic basis, that is, as to their physical or chemical identity. Emphasis is placed on the function of the components of the model in determining biological response to radiation, with careful attention being paid to the effect of radiation on these components and of the interactions between the components of the model.

We assume that the radiation-induced (or enhanced) processes in a biological subsystem can be described through the action of four active components. This is admittedly a gross oversimplification of the intricate biochemical machinery of any living system, but we are interested only in that fraction of the total machinery which, when affected by radiation, leads to a specific biological effect. Thus we consider the following elements.

The first component to be considered is one which we define as the critical component. This critical component is composed of entities which, if damaged and left unrepaired, lead to a specific observable effect. For purposes of identification, we call this component C, and the total number of elements which comprise this component will be denoted by $N_C$. In the model the integer $l$ is the number of damaged critical components. In some circumstances component C could clearly be identified as, say, DNA molecules or subunits thereof (e.g., in experiments on genetic damage). But in other cases the identification of the critical component in the manifestation of a given effect might be less clearly understood – for example, the critical disruptions which cause death in cell survival studies. Thus, we intentionally leave the identification uncertain.

The elements of component C can be damaged directly by radiation, or they may be damaged by a second component of the model which we label I. The reactive elements I are capable of interacting with a component C to damage it and thus increase $l$ by 1 (i.e., to cause one unit of damage). Component I might be pictured as reactive ions or radicals within a cell. These entities are created (or increased in concentration, $N_I$) by the interaction of radiation with otherwise innocuous molecules.

Table 3.1 is intended to help in keeping the possible reactions of the model clearly in mind. Thus, process 1 in Table 3.1 represents direct damage to critical component C by radiation to yield a damaged component C. Likewise, the second process in Table 3.1 represents the formation of a reactive component I as the result of radiation interaction with a molecule M. The third process represents indirect radiation damage to element C by the reactive component I which was formed by the process of step 2.

Now we introduce two additional components which serve to reverse the damage which results from the previous processes. The first of these is a component R which consists of elements which can repair component C directly. This repair mechanism is represented by process 4 in Table 3.1. The effect of the repair process in step 4 is to "undo" one unit of damage in component C and thus to decrease the level $l$ by 1. The component R would ordinarily be described as a repair enzyme, and its concentration, which we will denote by $N_R$, will generally depend on the time history of the radiation field, for the repair components themselves could be destroyed by radiation as depicted in process 5 of Table 3.1.

Finally, we introduce the second of the repair components, which is composed of elements which remove the reactive component I from the system. We label these elements S, and their concentration is indicated by $N_S$. The components of S might be identified as scavenger molecules in the usual chemical picture, which function by reacting with I to form nondamaging molecular complexes. This function is depicted by reaction 6 of Table 3.1.

The four active components just described can be used to form a differential equation whose solution will

**Table 3.1. Kinetic processes included in the general model**

| Process No. | Reaction | Description |
|---|---|---|
| 1 | C + radiation → ₵ | Damage of critical component C by radiation (₵ means damaged C) |
| 2 | M + radiation → I | Interaction of radiation with a molecule to form a reactive ion or radical |
| 3 | C + I → ₵ | Damage of C by component I |
| 4 | ₵ + R → C + R | Repair of damaged C by component R |
| 5 | R + radiation → ₨ | Destruction of R by radiation |
| 6 | I + S → M* | Removal of component I by S to form harmless complex M* |

yield the probability of observing any biological effect which is adequately described by the present model. In deriving the differential equation, we will neglect fluctuations in $N_I$, $N_R$, and $N_S$, since $N_S$ is a property of the system and the changes in the values of $N_I$ and $N_R$ due to radiation are large compared with unity [the fluctuations in $N_I$ and $N_R$ are proportional to 1/(No. of events)$^{1/2}$].

For the purpose of deriving an equation for $P_{ij}(t, l)$, we will assume that we have an ensemble of $N_0$ identical systems. $N_0$ can be chosen to be as large as we please, so that we may define the probability $P_{ij}(t, l)$ as the fraction of the systems in our ensemble which exhibit effect $i$ at level $l$ after time $t$. That is, if each system is exposed to identical radiation fields and a total number $N(t, l)$ exhibit effect $i$ at level $l$ at time $t$, then (with $N_0 \to \infty$),

$$P_{ij}(t, l) = N(t, l)/N_0 \equiv P(t, l) , \tag{12}$$

where we have suppressed the subscripts $i$ and $j$. Now if there are a number $N(t, l)$ of systems which have been damaged to the extent indicated by level $l$, we wish to determine how this number changes with time as a result of the processes discussed above. If we choose an interval of time $dt$ which is so small that it is very unlikely that $l$ will change by more than 1 (we restrict our considerations to low-LET radiation, where a single particle will produce no more than one unit of damage at a given site) or that the concentrations $N_I$, $N_R$, and $N_S$ will change appreciably, then we can write the following equation for a change in $N(t, l)$:

$$\begin{aligned} dN(t, l) = &- \alpha_I N_I(t) (N_C - l)\, dt\, N(l, t) \\ &+ \alpha_I N_I(t) [N_C - (l-1)]\, dt\, N(l-1, t) \\ &- (N_C - l)\, \beta(t)\, dt\, N(t, l) \\ &+ [N_C - (l-1)]\, \beta(t)\, dt\, N(t, l-1) \\ &- l\alpha_R N_R(t)\, dt\, N(t, l) \\ &+ (l+1)\, \alpha_R N_R(t)\, dt\, N(t, l+1) , \end{aligned} \tag{13}$$

where $N_C$ is the original number of undamaged critical elements or sites in the ensemble and $N_C - l$ is the number of undamaged elements remaining in an ensemble with level $l$ of damage. $\alpha_I$ is the rate constant (probability per unit time) for indirect damage (step 3 in Table 3.1), $\beta(t)$ is given by the flux of radiation and the cross section for producing damage (step 1 in Table 3.1), and $\alpha_R$ is the rate constant for repair of element C (step 4 in Table 3.1).

If we let

$$R(t) = \alpha_R N_R(t) \tag{14}$$

and

$$a(t) = \alpha_I N_I(t) + \beta(t) , \tag{15}$$

then divide Eq. (14) by $N_0$ and make use of Eq. (13), we get

$$\begin{aligned} \frac{dP(t, l)}{dt} = &- (N_C - l)\, a(t)\, P(t, l) \\ &+ (N_C - l + 1)\, a(t)\, P(t, l-1) \\ &+ R(t)\, [(l+1)\, P(t, l+1) - l P(t, l)] . \end{aligned} \tag{16}$$

We have suppressed the subscripts $i$ and $j$ in order to simplify the notation, but we understand that Eq. (16) is a differential equation for the probability of the appearance of effect $i$ at a given level (assumed in the model to be determined by the integer $l$) in a given organism $j$.

Analytic solutions to these equations may be readily obtained for two cases. If $N_C \gg l$, then Eq. (16) has the general solution

$$P(t, l) = \frac{g^l(t)}{l!} e^{-g(t)} , \tag{17}$$

where

$$g(t) = N_C \int_0^t a(t') \exp\, [\rho(t') - \rho(t)]\, dt' \tag{18}$$

and

$$\rho(t) = \int_0^t R(t')\, dt' . \tag{19}$$

Thus, with this model we have a Poisson distribution in $l$ with our average $l$ being given by $g(t)$.

Another special case can be solved completely – namely, that in which no direct repair is present [$R(t) = 0$]. Equation (13) can then be solved exactly to give

$$P(t, l) = \frac{N_C!}{(N_C - l)!\, l!} \left[1 - e^{-\mu(t)}\right]^l e^{-(N_C - l)\alpha(t)} , \tag{20}$$

where

$$\alpha(t) = \int_0^t a(t')\, dt' . \tag{21}$$

Thus, in this situation we have binomial statistics.

It should be emphasized that in many cases where this model may apply, one cannot easily measure $l$ directly. However, with analytic expressions for $P(t, l)$ one can treat $l$ as a parameter in the theory and choose it for best fit. The comparison with experiment is then achieved by comparing the time dependence of $P(t, l)$ with experiments for different time histories and amounts of incident radiation.

The model given here may be general enough to describe a number of results in radiation biology, but there will surely be many others which cannot be described by such a simple model. It seems to the present authors that an extensive team effort of model building along with careful and detailed experiments is needed if the puzzles inherent in some induced radiation effects are to be solved.

### Part B. Application of the General Model to the Analysis of an Experiment on Cell Survival

We offer here an alternative explanation for the data of Calkins[2,3] concerning cell survival experiments on stationary-phase *Tetrahymena pyriformis* irradiated by x rays. In the Calkins experiment it is assumed (and the experiment is consistent with the hypothesis) that caffeine stops repair while permitting the "fixation" of damage. Thus, the addition of caffeine to the cultures at different times after irradiation allows one to study cell survival for cases where the repair enzymes were allowed to perform their function for varying time. It is found, however, that the addition of caffeine at postradiation times greater than about 6 hr does not change the number of survivors. The experimental data and our theoretical curves which employ three adjustable parameters for purposes of calculating all five survival curves are shown in Fig. 3.6.

In the present model we follow Calkins in assuming that one hit by an x-ray photon can form a lesion of such a nature that the cell will be inactivated if even one such lesion is not repaired within a time called the fixation time, $t_F$. The present model does not allow for the possibility that a repair enzyme may be tied up in an enzyme-lesion complex for a period of time, but it does allow for the fact that irradiation may inactivate enzymes, so that after irradiation

$$R = R_0 e^{-\gamma D} ,$$

where $R_0$ is the unirradiated concentration of enzymes and $D$ is the x-ray dose which was given over a short period of time near $t = 0$. We assume the action of $N_I$ is very fast and that consequently we can take (see Part A)

$$a(t) = \beta\, dD/dt , \qquad t < \tau ,$$
$$= 0 , \qquad t \geqslant \tau ,$$

where $\tau$ is the time of irradiation and $dD/dt$ is the rate at which energy is deposited, and we will assume that $R\tau \ll 1$. $l$ is the number of potentially lethal lesions. Thus, the number of survivors $S$ divided by the initial number of bacteria $S_0$ is given by

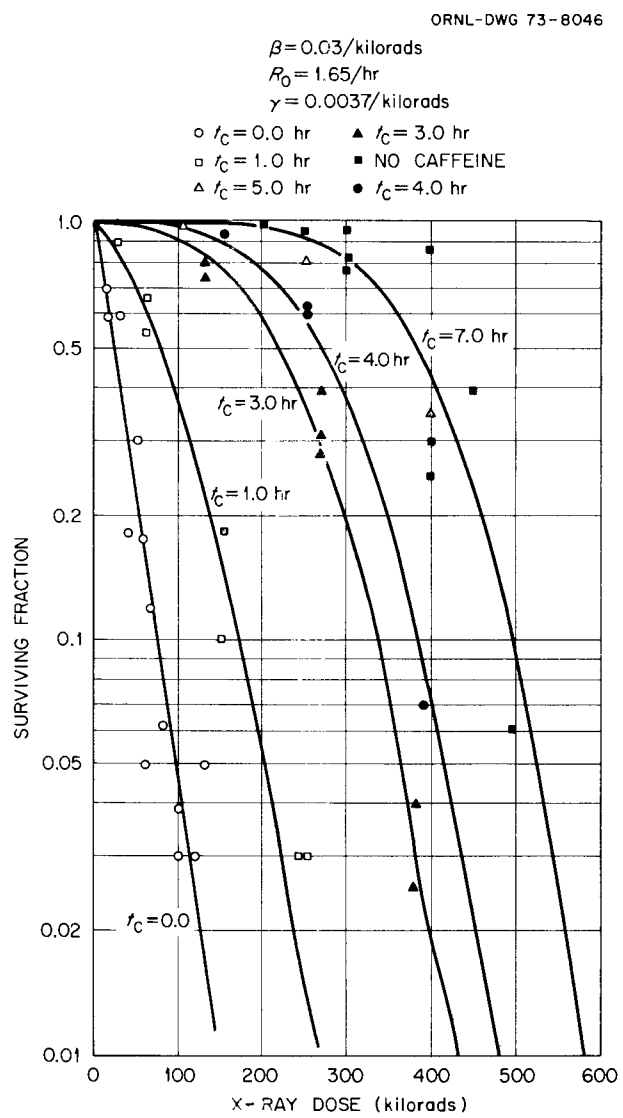


**Fig. 3.6. Surviving fraction as a function of x-ray dose for *Tetrahymena pyriformis* exposed to caffeine after various times $t_c$.** The solid lines are calculated from the present model.

$S/S_0$ = surviving fraction

= probability of no unrepaired lesions remaining after time $t_F$

$= P(t_c, 0)$

$= \exp\,[-g(t_c)]$ ,

where $t_c$ is the smaller of $t_F$ and the time at which the caffeine was added. From Eq. (18) ($\beta_0 = N_c\beta$),

$$g(t) = \beta_0 D \exp\,[-R_0 t \exp\,(-\gamma D)] \ .$$

Now, $t_c$ is known, and we need only choose $\beta_0$, $R_0$, and $\gamma$ in order to compare with experiment.

In the experiment a semilogarithmic graph of $S/S_0$ vs $D$ yields a straight line if the caffeine is added just after irradiation (i.e., $t_c = 0$). Thus, the slope of this line is $\beta_0$. The parameters $R_0$ and $\gamma$ were determined by making $S/S_0$ go through two points on the $t_c = 3$ curve. (Thus, two equations in two unknowns were obtained.)

We see that agreement with experiment is good. In fact, it is better than the fit obtained by Calkins with a much more complicated model which neglects enzyme inactivation but allows for the enzymes spending time tied up in an enzyme-lesion complex. The latter assumption introduces a feature into the probability problem which does not appear to lead to Poisson statistics as assumed by Calkins.

By including a set of assumptions about the kinetics of repair we have been able to describe the result of an experiment where repair was altered in a known way in terms of a single set of three parameters. In a multitarget–single-hit or a multihit–single-target cell survival model, it would be necessary to choose a new set of parameters for each $t_c$. Further, a model that includes kinetics of repair is more easily compared with experiment than is one that simulates repair in some way.

The model described in Part A can be easily generalized to include the possibility of lesions of different severity (which may be repaired at different rates, or not repaired at all), providing the events involved in producing the different types and in repairing them are statistically independent. It is also possible to allow for different sensitivities at different stages of the cell cycle in dealing with split dose or continuous irradiation experiments. Details will be described in a forthcoming publication.

## Part C. Generalization of the Katz Model of Cell Survival

When heavy ions interact with a condensed system, they send outward from their path a large number of electrons (delta rays) having a wide spectrum of energies. The ionization density in the case of heavy ions is thousands of times larger than that due to an electron of similar energy. When looked at in detail the ionization products along the path of an energetic electron are of low density, while in the region near the path of a heavy ion of similar energy a large density of ions, electrons, and subsequent reaction products are produced almost simultaneously, with the density of such products scaling with charge and velocity according to the parameter $Z^*/V$,[24,25] where $Z^*$ is the effective charge of a heavy ion of velocity $V$. As has been pointed out by Katz et al.,[24] a slowly moving ion of charge $10e$ liberates enough energy to vaporize water in a cylinder 100 Å in diameter about its path. Thus, in contrast to the situation with x rays or beta rays (even at large doses), there is a region about a heavy ion of relatively low energy in which the energy density is extremely large, and in this region there exists briefly a large concentration of radiation products. Consequently, Katz et al.[24] have suggested that there is an effective cross section about the path of an ion within which a "critical target" would be converted to an irreparable lesion and lead to cell death. The cross section $\sigma$ within which irreparable damage occurs is (for a particular type of cell) a function of $Z^*/V$. The part of the energy that does not get deposited in such concentrations as to produce such nonlinear effects as to cause irreparable damage is assumed by Katz to combine with the energy deposited by other ions in order to give an effective gamma-ray-like dose. Thus, one expects the surviving fraction to be given by an expression of the type

$$S/S_0 = e^{-\sigma n F}\, P(D_\gamma, D_\gamma') \ ,$$

where $D_\gamma = g(Z^*/V)\, D_I$ is the part of the ion dose $D_I$ which contributes to the production of x-ray-type lesions, $D_\gamma'$ is an equivalent x-ray dose due to ions which contribute to the inactivation of repair enzymes, and $F$ is the fluence of ions. The function $P(D_\gamma, D_\gamma')$ is the surviving fraction that would be obtained if the number of repairable lesions produced is the same as the number that would occur due to a dose $D_\gamma$ of x rays and if the number of repair enzymes were reduced by the amount that would occur with a dose $D_\gamma'$ of x rays.

The work that has been described above in a qualitative way is in its early stages, but it has as its objective a generalization of the work of Katz to incorporate the kinetics of repair and to permit prediction of survival for different time histories of the

radiation and for experiments where repair is interrupted at different times after irradiation. It is hoped that simultaneously one can find a way to predict response to heavy ions in terms of response to gamma rays plus a small number of parameters that are adjusted in such a way that $\sigma$ goes from a value near zero for low $Z^*/V$ to a biologically significant value for a proper larger $Z^*/V$ and simultaneously make $g(Z^*/V)$ close to zero for very large $Z^*/V$ but give a rise to near unity for proper $Z^*/V$.

We regard such a project as extremely important because at present the Katz theory requires a change of parameters to describe any situation except the one where all the radiation dose is given near $t = 0$ and the cell environment is kept fixed. Further, even though the Katz theory predicts much data in terms of a small number of parameters, it is basically a multitarget–single-hit theory, so that repair effects are merely simulated.

### Part D. Late Effects of Radiation

In the past year a cooperative effort between the Health Physics Division and the Biology Division of ORNL has been initiated. To date the study has involved cooperation in the study of radiation-induced lens opacification in mice, but other areas of cooperation are anticipated for the future.

Lens opacification in RF female mice[26] has been found to have the following features for 10 and 20% opacity levels and proton or x-ray doses less than 200 rads (or less than 15 rads for neutrons):

1. If the radiation is given in a short interval of time (say, less than one week) to young adult mice and $t_{1/2}$ is the time at which 50% of the mice reach the level of cataract in question, then

$$t_{1/2}^{-1} = \tau^{-1} + cD ,$$

where $D$ is dose and $\tau$ is the time (measured from time of irradiation) for 50% incidence for senile cataracts of the particular level. At doses of 300 rads or more for high-energy protons or for doses larger than about 20 rads for neutrons, $t_{1/2}$ becomes independent of dose [and Eq. (11) correspondingly fails] for x rays, protons, and neutrons and for 20% level cataracts[26] has a value of 70 to 80 days independent of type of radiation. Figures 3.7 and 3.8 show typical graphs of $t_{1/2}^{-1}$ vs $D$.

2. If $2\sigma_t$ is the time between ~16% incidence and 84% incidence, it is found that within experimental error (average deviation about 25%)

$$\sigma_t/t_{1/2} \cong \text{constant} .$$

The above relation was also noticed by Merriman, Bateman, Rossi, et al.[27] for lens opacification in another strain of mice.

3. There is some evidence[28] that essentially all variations in the time of incidence may be due to biological variability. This evidence is that the mean difference in opacity between the two lenses of the same animal at a particular time is much smaller than the mean difference in opacity between lenses of different animals at the same time. The effect persists even with proton data, where most of the radiation is directed to the lens and overall metabolic effects that might cause correlations between the two lenses of the same animal should be less probable.

The only late effect for which we have found the data to be sufficient to get an accurate determination of $\sigma_t$ (as in cataracts) is tumor induction on the ears of mice by ultraviolet radiation, as measured by Blum.[29] In this case the radiation was given periodically in equal doses up until 100% induction of tumors occurred. Depending on the dose rate (given in periodic lump amounts of variable magnitudes), the time for 50% incidence changes according to

$$t_{1/2}^{-2} = cd ,$$

where $d$ is the magnitude of a single one of the periodic doses. In the latter case it is again found that

$$\sigma_t/t_{1/2} = \text{constant} .$$

We will now give a qualitative argument for why the relation $\sigma_t/t_{1/2}$ = constant may be found to occur rather frequently for late effects where biological variability accounts for most of the magnitude of $\sigma_t$ and the effect occurs at 100% incidence before appreciable death occurs. In such a situation it is reasonable that for a particular animal in a carefully controlled experimental situation the time of incidence $t$ of the

26. E. B. Darden, Jr., K. W. Christenberry, J. J. Beauchamp, R. S. Bender, M. C. Jernigan, J. W. Conklin, and A. C. Upton, *Radiat. Res.* **43**, 598 (1970).

27. G. R. Merriam, Jr., B. J. Bivati, J. L. Bateman, H. H. Rossi, V. P. Bond, L. Goodman, and E. F. Focht, *Radiat. Res.* **25**, 123 (1968).

28. E. B. Darden, unpublished data.

29. H. F. Blum, *Carcinogenesis by Ultraviolet Light*, Princeton University Press, Princeton, N. J., 1959.

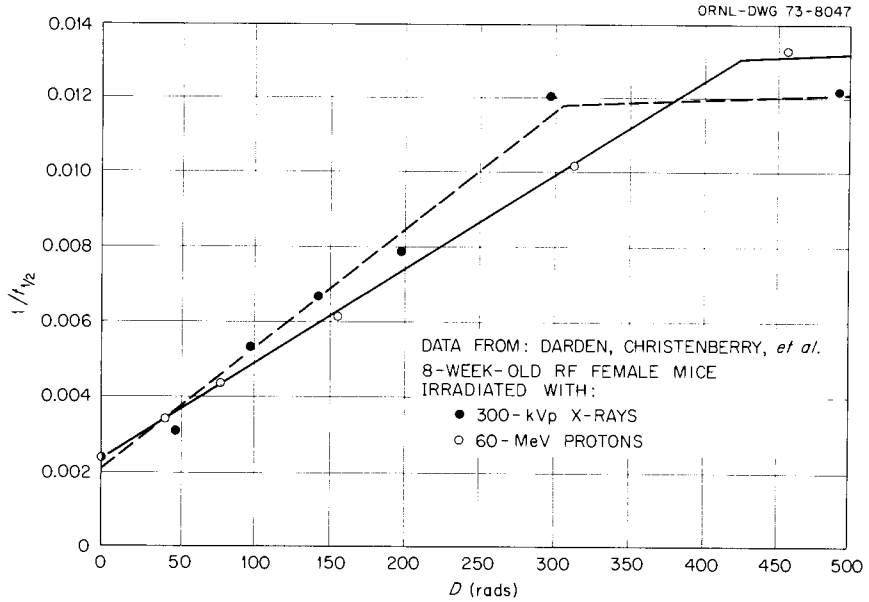


**Fig. 3.7. Reciprocal time for 50% incidence of level 20% cataract in RF female mice as a function of 60-MeV proton and 300-kVp x-ray dose.**

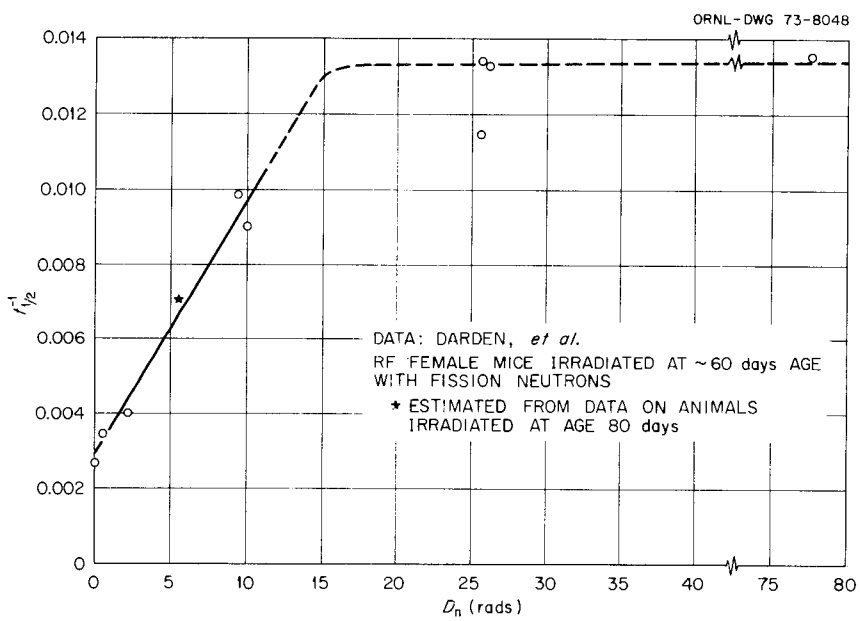


**Fig. 3.8. Reciprocal time for 50% incidence of level 20% cataract in RF female mice as a function of mean energy 1.3 MeV neutron dose.**

effect in question is given by

$$t = F_l(D, \gamma_1, \gamma_2, \ldots, \gamma_N) ,$$

where $D$ is dose, $l$ specifies the level of effect, and the $\gamma_i$ ($i = 1, 2, \ldots, N$) are independent parameters which determine the relative sensitivity of the animal to radiation. The radiation is given in a short time to young adult animals. Further, we assume that the probability of an animal chosen at random having $\gamma_i$ in the interval $d\gamma_i$ is $\overline{P}(\gamma_i)\, d\gamma_i$. Then, if $P_l(t)\, dt$ is the probability of the effect occurring in $dt$ at $t$,

$$P_l(t) = \int \cdots \int \left[ \prod_{i=1}^{N} d\gamma_i \overline{P}(\gamma_i) \right] \times \delta \left[ t - F_l(D, \gamma_1, \gamma_2, \ldots, \gamma_N) \right] ,$$

where $\delta$ is Dirac's generalized function. We assume that $\overline{P}(\gamma_i)$ is rather sharply peaked about $\overline{\gamma}_i$ ($i = 1, 2, \ldots, N$, and that $F_l(D, \gamma_1, \gamma_2, \ldots, \gamma_N)$ is approximately linear in $\gamma_i - \overline{\gamma}_i$ in the region where $\overline{P}(\gamma_i)$ is appreciably nonzero. Then, letting $\sigma_t^2 = (t - \overline{t})^2$ and $\sigma_j^2 = (\gamma_j - \overline{\gamma}_j)^2$ and suppressing the arguments of $F(D, \overline{\gamma}_1, \overline{\gamma}_2, \ldots, \overline{\gamma}_N)$,

$$\sigma_t^2 = \sum_{j=1}^{N} \left( \frac{\partial F}{\partial \gamma_j} \right)^2 \sigma_j^2$$

and

$$\overline{t} = F(D, \overline{\gamma}_1, \overline{\gamma}_2, \ldots, \overline{\gamma}_N) .$$

We now assume that

$$t = H(\gamma_1, \gamma_2, \ldots, \gamma_N)\, F(D) ,$$

where special cases of the above relation might be ones where $\overline{t}$ is found to satisfy [since $\overline{t} = H(\overline{\gamma}_1, \overline{\gamma}_2, \ldots, \overline{\gamma}_N)\, F(D)$]

$$\overline{t}^{-1} = c_1' + c_2' D^n ,$$

or

$$\overline{t} = b_1 + b_2 / D^n .$$

We get

$$\frac{\sigma_t^2}{\overline{t}^2} = \sum_{i=1}^{N} \left( \frac{\partial}{\partial \gamma_i} \ln H \right)^2 \sigma_i^2$$

$$= \text{constant} .$$

The same arguments can be given for cases where $D$ is replaced by dose rate and the radiation given continuously (or periodically in equal doses) until 100% incidence occurs. Thus, in cases where $\overline{t}^{-1} = F_1 + F_2 d^n$ or $\overline{t} = e_1 + e_2/d^n$, we might still expect $\sigma_t/\overline{t} \cong$ constant. The arguments given here in no way constitute a proof, since one can easily think of reasons why particular ones of the several assumptions would fail. However, it is suggested that $\sigma_t/\overline{t}$ = constant could be a commonly occurring relation for several late effects in different species and for different time histories of the radiation field.

# 4. Spectrometric Dosimetry

J. H. Thorngate

D. J. Christian W. H. Shinpaugh
P. T. Perdue M. M. Abd El-Razek[1]

## ORGANIC SCINTILLATOR RESEARCH

Work on the synthesis and purification of *p*-sexiphenyl (PSP) has continued. As an organic scintillator, this material promises to have a greater light output per unit of energy deposited than other available organic scintillators, thus allowing the measurement of charged particles of lower energy. Single crystals will be useful for neutron spectrum measurements, as will possible liquid scintillators made with PSP as a secondary solute.

Our research on the purification of PSP has been with the collaboration of W. H. Baldwin of the ORNL Chemistry Division. Several hundred grams of the crude material have been made using the Kovacic and Lange synthesis from *p*-terphenyl.[2] Considerable effort has gone into simplifying the purification procedure. For example, a clarification technique has been perfected using gas absorption chromatography with pretreated aluminum oxide. This method has been found effective in removing the light-absorbing chromophores, producing material with superior optical properties.

Melting point determinations with vacuum-distilled and *p*-xylene-extracted PSP have produced the smectic and nematic states observed by Nozaki et al.[3] At this purity (~95%), we have obtained a liquid crystal state at 434°C and a clear liquid state at 542°C. This is in good agreement with the temperatures observed by Nozaki (428–429°C and 543°C). We have reason to believe that this melting point range is due to a small quantity of impurity that cannot be removed by vacuum distillation.

The highest purity of PSP produced to date is 99%, as determined by mass spectroscopy. This purity was obtained by growing single crystals from purified material in a helium atmosphere. Zone refining has been hindered by the melting point range of the impure material and decomposition of the material at the temperature required. As experience has accumulated, we have found that controlling both the partial gas pressures and the length of the molten zone is necessary in order to use zone refining. Optical measurements on 99% PSP indicate that the light produced by $^{137}Cs$ gamma rays is approximately 1.25 times that produced by anthracene.

In the search for solvents for PSP, it was discovered that mixtures of *p*-xylene and *p*-dioxane would dissolve more PSP than either solvent would dissolve alone. Although PSP is so insoluble that no solvent can put more than 0.2 g/liter in solution, this combination dissolves enough to allow evaluation of PSP as a secondary solute in a liquid scintillator. It was found that these mixtures were effective for most of the common liquid scintillator solutes, thereby reducing the solubility limitations on a number of good solutes presently in use.

Recently, PSP was supplied to the Solid State Dosimetry Group for incorporation as a proton radiator in a thermoluminescent neutron dosimeter. The PSP has been mixed with suitable thermoluminescent detector (TLD) materials. This organic is a good choice for many reasons, one of which is the requirement that the mixtures be heated frequently to above 240°C in order to form reusable pellets. Although the TLD material is not light sensitive and PSP has no long-term light storage, the combination was found to be light sensitive, probably due to an electron transfer to the TLD from the PSP in the presence of light of wavelengths shorter than 450 nm.

1. Alien Guest, United Arab Republic Atomic Energy Establishment, Cairo, Egypt.

2. P. Kovacic and R. M. Lange, *J. Org. Chem.* **29**, 2416–20 (1964).

3. T. Nozaki, M. Tamura, Y. Harada, and K. Saito, *Bull. Chem. Soc. Jap.* 33, 1329–32 (1960).

Tests were made of PSP in a nitrogen atmosphere at temperatures up to 350°C, and no sublimation was found below 300°C for material at least 99% pure. Other organic scintillators we have tested, such as *p*-quaterphenyl and anthracene, cannot be used in applications where temperatures above 150°C are required due to sublimation.

## DISTRIBUTION OF CHARGED-PARTICLE STOPPING

How a charged particle imparts its energy as it slows down in some medium has been studied in a number of ways. One of the oldest techniques is to measure the energy of the particle before it enters the medium and after it emerges, but this gives a limited amount of information on the interactions involved. More detailed are measurements of the energy and angular distribution of electrons produced within the medium by the charged particles. Lying between these extremes of detail are measurements of the energy spectrum of the charged particles as they emerge from the medium. This technique has been chosen to study the interactions of protons with tissue constituent elements and their compounds. Protons with energies below 175 keV will be used, because some evidence exists that molecular binding affects energy losses in this region,[4,5] although there is not complete agreement on this.[6] This work began last year and is continuing. Since measurements are planned in both gases and foils, work was done in the design and testing of a differentially pumped gas cell and in the development of improved techniques of foil casting. Work on the calibration of the electrostatic analyzers that will be used to measure proton energies has also been completed.

Because of the low energy of the protons to be measured, 50 to 175 keV, they cannot be introduced into the gas to be measured through a foil, since they would lose too much energy in so doing and the foil would also produce distributions in the energy losses of the protons that would complicate the interpretation of the data. Therefore, the protons must enter and leave the gas cell through apertures, necessitating a system of differential pumping. A section on either side of the gas cell must be pumped with high-capacity pumps in order to keep the target gas from the rest of the vacuum system, and the pressures in these sections must be kept low enough so that the dimensions of the gas cell remain well defined.

Theoretical design of such systems is difficult, so the original design used apertures that were quite small, 0.34 mm in diameter, and had provisions for two sections of high-speed pumping on each side of the gas cell. Tests showed that only one pumping section would be required on each side and that the apertures could be increased in size to 0.71 mm. Together these changes simplify alignment of the proton beam and increase the size of the transmitted beam.

Techniques of foil casting are being developed that are modifications of those of Revell and Agar.[7] Also being developed are capacitive techniques for measuring the thickness of the resulting foils.

Because of the high resolutions possible, electrostatic analyzers were chosen to determine the energy of the protons incident on the stopping medium and to measure the energy distribution of the protons after they have passed through the stopping medium. In order to be able to relate the voltage applied to the plates of the electrostatic analyzers to the energy of the particle deflected, the analyzers need to be carefully calibrated. This was done using protons from a 600-keV accelerator (belonging to the ORNL Thermonuclear Division) that has a high-voltage supply regulated to one part in $10^5$ and a well-calibrated voltage divider that can be read out to the nearest 0.1 keV. The electrostatic analyzers were both cross-calibrated to the

4. J. T. Park and E. J. Zimmerman, *Phys. Rev.* **131**, 1611–18 (1963).

5. P. D. Bourland and D. Powers, *Phys. Rev.* **133**, 3635–41 (1971).

6. J. W. Williamson and D. E. Watt, *Phys. Med. Biol.* **17**, 486–92 (1972).

7. R. S. M. Revell and A. W. Agar, *Brit. J. Appl. Phys.* **6**, 23–25 (1955).

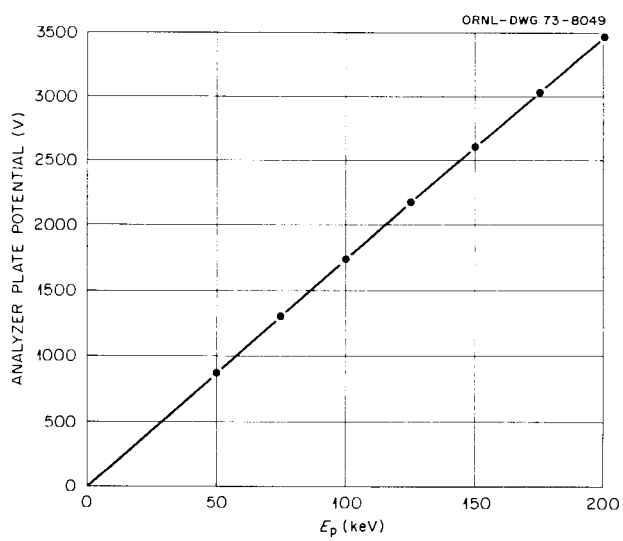


**Fig. 4.1. Electrostatic analyzer calibration.**

voltage divider, and then the divider was calibrated using $(p, \gamma)$ resonance reactions in $^{19}F$ and $^{27}Al$. Figure 4.1 shows typical calibration results. A weighted least-squares fit to a straight line was made to the data, with the result that the zero intercept was found to be 57 ± 0.2 eV, and the slope of the proton energy vs analyzer plate voltage was determined to a precision of 0.08% for the analyzer that will be used to measure the energy of the protons emerging from the gas cell or foil.

## HPRR NEUTRON AND GAMMA-RAY SPECTRUM INCIDENT ON THE ROOF OF THE DOSAR

In support of the program to measure the fast-neutron and gamma-ray spectra produced by the HPRR that are incident upon the roof of the DOSAR Control Building, computations of the proton spectrum and alpha spectrum produced in a 2 X 2 in. cylindrical NE213 scintillator, like that used for the neutron measurements, were made for neutron energies of 3 to 15 MeV.[8] It was planned that these would be used in conjunction with measurements of neutrons of these energies to determine the response of the scintillator as a function of neutron energy. This approach has not yet been completely successful.

Measurements of the fast-neutron spectra have been made as a function of angle for energies from about 200 keV to 2 MeV. Refined techniques are being developed to reduce these data that are based on unfolding techniques developed by Turner et al.[9]

The NaI pair spectrometer that was used to measure the high-energy gamma rays produced by the interaction of neutrons with air during Operation HENRE[10,11] was modernized with new electronics and has been tested preliminary to mounting it on the DOSAR roof to make measurements as a function of incident angle of the high-energy gamma rays produced by the interaction of HPRR neutrons with air. Improved setup techniques were developed for this instrument using an $^{22}Na$ source. Because this source has a positron emission followed by a gamma ray, its radiations satisfy all of the logical requirements of the coincidence system used with the spectrometer. As before, the 4.43-MeV gamma ray from the carbon deexcitation of an alpha-beryllium neutron source is used as the primary energy calibration standard.

## ALPHA AIR MONITOR ELECTRONICS

R. E. Coleman of the Radiation and Safety Surveys Section of the Health Physics Division has developed a system for determining small amounts of man-made alpha emitters in the presence of natural alpha emitters.[12] Essentially, the system measures the ratio of the total alpha activity to the high-energy alpha activity of an air sample. An elaborate electronic system, shown in the block diagram (Fig. 4.2), was developed in the Spectrometric Dosimetry Group to fulfill the requirements of this special alpha air monitor. The design parameters are simplicity, low cost, reliability, and accuracy.

The preamplifiers used are an integrating type designed originally for the NE213 neutron spectrometer. An integrated circuit dual differential comparator is used for pulse-height discrimination. Output pulses from the comparator are shaped by dual univibrator circuits composed of the circuits in an integrated circuit that has four "nor" gates. A simple count-rate circuit was designed around an integrated circuit dual operational amplifier. Another similar amplifier is used as a buffer to provide the individual count-rate information for external meters or recorders. These signals are also the input for an integrated circuit analog divider, the output of which provides the required ratio of the count-rate data.

Tests have shown that the circuit performs properly over an input pulse range from 1 count/min to 100 counts/sec. A long time constant is required in the count-rate circuits to provide satisfactory performance at low count rates. The linearity of the overall system is indicated in Fig. 4.3, which relates varying ratios of input pulse rates to the output voltage of the divider. An overnight run using standard alpha sources to irradiate the detectors showed no measurable drift.

## A CONVENIENT COUNTER FOR MEASURING THE ALPHA ACTIVITY OF AIR SAMPLES

A simplified alpha counter for air samples was one of the devices developed by this group in support of a study of the natural radiation environment that was the basis for a Ph.D. dissertation at the Georgia Institute of Technology.[13,14] An existing gas-flow proportional counter was modified to hold a surface-barrier semi-

---

8. S. N. Cramer, *Monte Carlo Analysis of an NE213 Detector,* ORNL-TM-4149 (March 1973).
9. J. E. Turner, V. E. Anderson, R. D. Birkhoff, and D. R. Johnson, *Health Phys.* 18, 15–24 (1970).
10. J. H. Thorngate, D. R. Johnson, and P. T. Perdue, *Energy and Angular Distribution of Neutrons and Gamma Rays – Operation HENRE,* CEX-65.11 (April 1969).
11. J. H. Thorngate, *Health Phys.* 18, 339–45 (1970).
12. R. E. Coleman, in preparation.
13. J. A. Auxier, *Contribution of Natural Terrestrial Sources to the Total Radiation Dose to Man,* doctoral thesis, Georgia Institute of Technology, December 1972.
14. P. T. Perdue, W. H. Shinpaugh, J. H. Thorngate, and J. A. Auxier, "A Convenient Counter for Measuring Alpha Activity of Smear and Air Samples," submitted to *Health Physics* for publication.

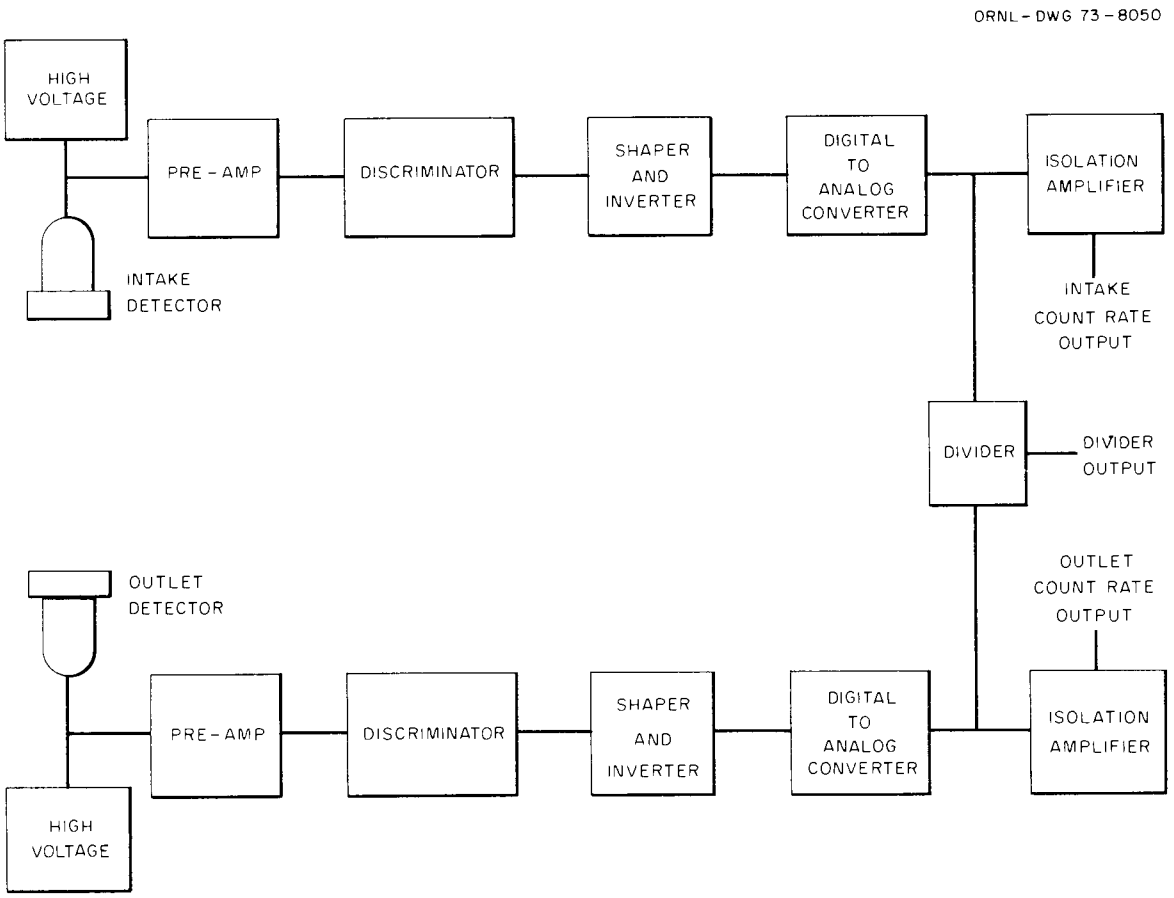


**Fig. 4.2. Block diagram of the electronics for an alpha air monitor.**

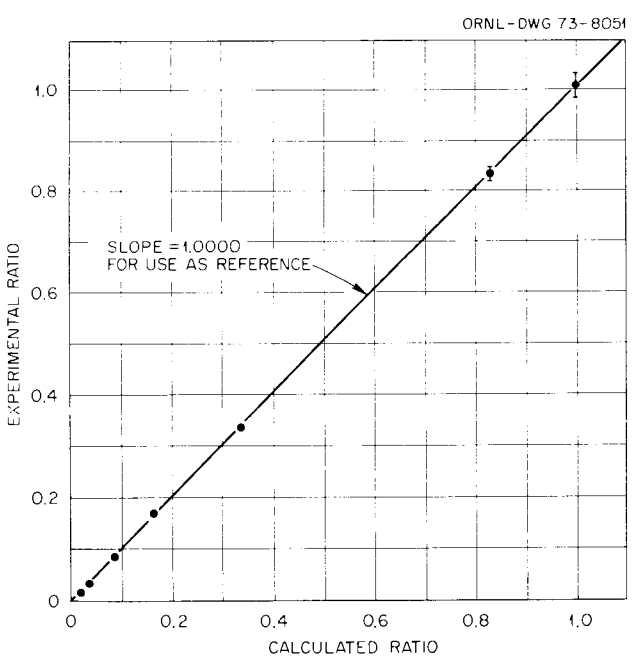


**Fig. 4.3. Comparison of measured and calculated count-rate ratios using the alpha air monitor electronics.**

conductor diode as close as possible to the air sample to be measured. Helium was flowed through the counter to reduce the energy lost by the alpha particles traversing the distance between the sample and the detector. Using a vacuum would minimize the energy loss, but vacuum operations greatly complicate sample changing and cause problems if the alpha emitter to be measured is an adsorbed gas. Moreover, semiconductor diodes break down at certain intermediate pressures, and so either they must be kept in a good vacuum or the bias voltage must be cycled. The first of those alternatives presents a mechanical problem in the design of the counting chamber, and the second results in a great deal of extra time required for a measurement. This counter, and the use of helium as a flow gas, presented a convenient, time-saving, rugged counter that was used successfully to measure air samples for thorium and radium decay products in air. Figure 4.4 shows an exploded view of the counter, and Fig. 4.5 compares the response of the diode to alpha particles with vacuum, air, and helium between the source and detector.

PHOTO 2909-72

**Fig. 4.4. Exploded view of the counter for alpha air samples.**

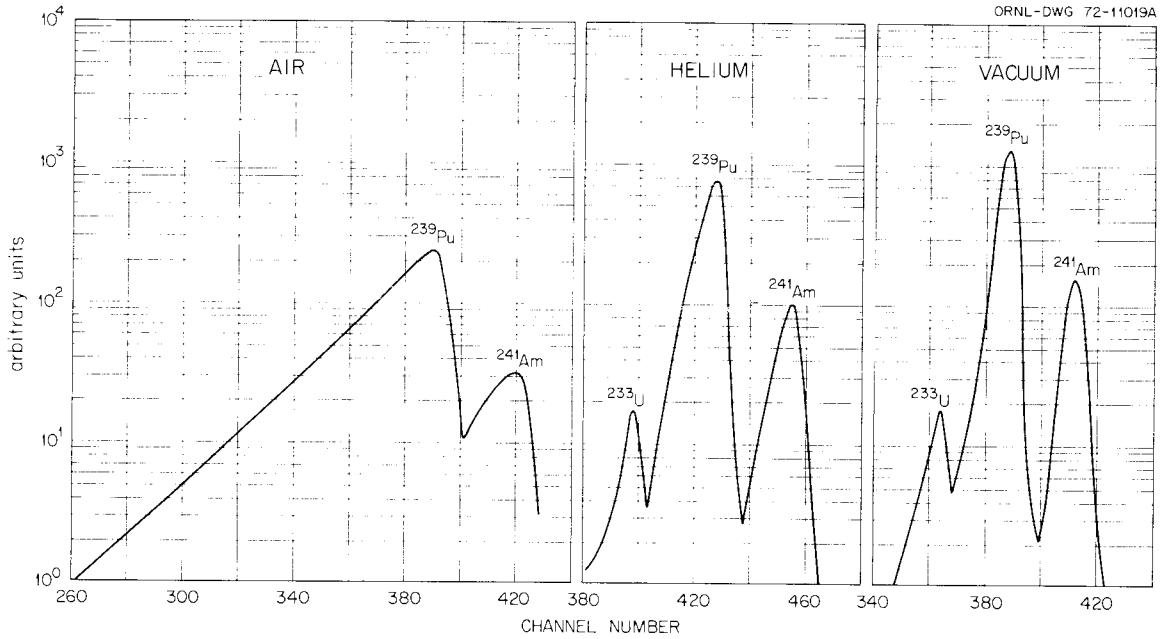


Fig. 4.5. Comparison of an alpha-particle spectrum measured with air, helium, or vacuum in the space between the source and the semiconductor diode detector.

# 5. HPRR and Accelerator Operations

D. R. Ward[1]
F. F. Haywood[2]
H. W. Dickson[2] C. P. Littleton[3]
W. F. Fox[2] R. L. Shoup[4]
J. W. Poston[5]

## HEALTH PHYSICS RESEARCH REACTOR OPERATIONS

As has been the case over the past several years, the Health Physics Research Reactor (HPRR) is continually used as a versatile radiation source for a growing number of dosimetry and radiobiology studies. Most of these studies are directed toward the correlation of biological response with absorbed dose. Some of the important continuing radiobiology experiments which utilized the HPRR this year were: determination of RBE for intestinal crypt cell survival, M-2 generation grain plant mutation studies, incidence of cancer in the mammary glands of Sprague-Dawley rats, lens opacities in mice exposed to fission neutrons, effects of neutrons on poinsettias and sweet potatoes, and the effects of small doses of neutrons on one-day-old mouse embryos. For other users, such studies as the pumping of gas lasers, determining detector responses, and the effect of sustained neutron exposure on platinum needles used for encapsulating $^{252}$Cf were conducted.

Some of the most important work involving the reactor this year was in direct support of the Japanese dosimetry program. The HPRR was operated for long periods of time in order that measurements of the angular distribution of neutrons and gamma rays incident on the HPRR Control Building could be made. The data from this study were used to develop a technique to be used in the ABCC Statistics Department for estimating the dose to survivors exposed in heavy concrete structures.

1. Neutron Physics Division.
2. Dual capacity.
3. Instrumentation and Controls Division.
4. National Science Foundation Presidential Intern.
5. Medical Physics and Internal Dosimetry Section.

The Ninth Dosimetry Intercomparison Study was held in July 1972. This study was planned specifically for representatives from companies which hold special nuclear materials licenses; however, there were only two participants in this category. Most of the participating organizations were AEC contractors. In addition, one naval laboratory, one private company, and one foreign laboratory (from Brazil) were represented. Results of this intercomparison bear out the fact that most organizations, which provide their own monitoring capability, are able to provide estimates of dose to within ±25% or better. The intercomparison program is being expanded to include periodic evaluations of the response of personnel monitoring devices when exposed to "standard" radiation fields similar in nature to those encountered in routine operations involving materials which emit both neutrons and gamma rays. No specific date has been set for the first experiment in this series, but it is expected to be carried out this calendar year.

## HIGH-DENSITY TRACK COUNTING USING AN ELECTRON BEAM

There exists a problem of counting high densities (>2000 tracks/cm$^2$) of etched charged-particle tracks in thin films (polycarbonate film 10 $\mu$ thick) reliably and quickly. The most accurate method, optical reading using a microscope, is time consuming. This report presents the results of measuring high track densities by recording the amount of 14-keV electron current transmitted through etched holes in the foil sample. The measurement period (<2 min) was independent of track density and had a linear response with the density. Various track densities were measured and compared with spark counting techniques.

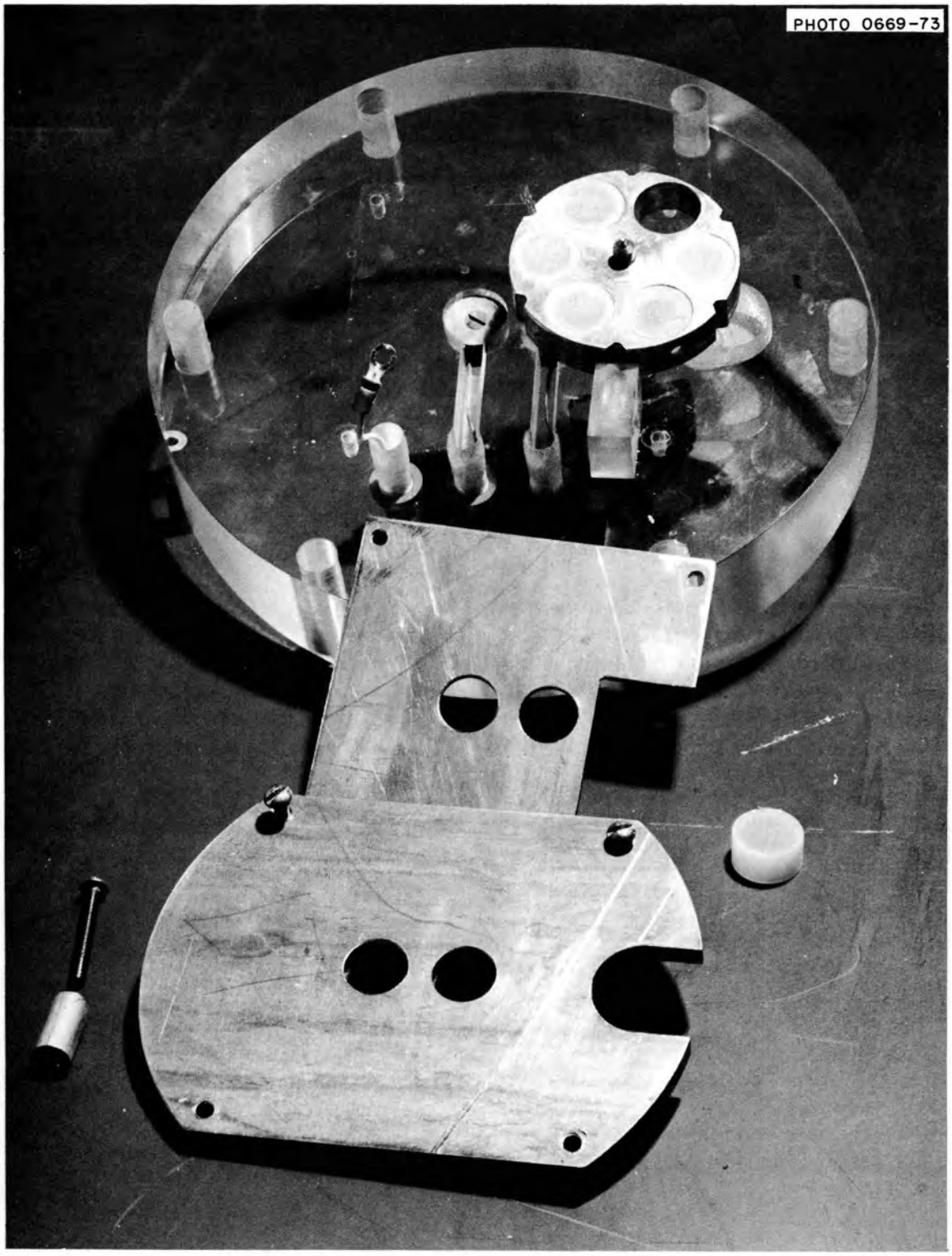


**Fig. 5.1.** View of sample holder and Faraday cup assembly used to measure electron current transmitted through 10-$\mu$ Kimfoil detectors.

An electron gun was used to produce a 14-keV, 1-$\mu$A electron beam. A magnetic deflection yoke was used to obtain a 1 X 2 in. image across two $^5/_8$-in.-diam holes drilled in a brass plate about 16 in. from the source. This brass plate is shown at the bottom of Fig. 5.1. The part of the beam that passed through the left-hand hole was collected on a Faraday cup; and on the right-hand side, the beam passed through a sample holder before being collected on an identical cup. The sample holder was a brass disk with six equally spaced eccentric holes. It was accurately positioned by an indexing mechanism.

With no sample in place, the beam was adjusted to read approximately the same currents on both Faraday cups with current integrators. A sample was then turned into position on the right-hand side, and the amount of transmitted current was measured.

Kimfoil samples that had been exposed to fission fragments from a $^{252}$Cf source for measured lengths of time were then etched, washed, and dried. The samples were counted in a spark counter several times, and then five samples at a time were loaded in the sample holder. The amount of current that passed through the small holes in each sample was measured several times, and the average percent of transmitted beam was calculated for each sample. The spark counting data and the electron transmission data are compared and shown in Fig. 5.2. The electron transmission data showed a linear response with the exposure time of the sample to the $^{252}$Cf source. Average errors were between 8 and 10% above 0.4% transmission and greater than 15% below 0.4%. The spark counting data were linear to about 2000 tracks/cm$^2$ and then leveled off.

The measurement of tracks using the percent of the electron beam transmitted is a good alternative for counting foils with high track densities. This technique overlaps readily with the region where spark counting techniques are used and is reliable in the range measured (<20,000 counts/cm$^2$).

This technique is, however, dependent upon foil etching and prior preparation; but no more so than other methods of counting high densities (other than use of optical microscopes).

Because of the bilateral symmetry of this system, a second sample holder can be easily added, and then ten samples can be loaded and easily measured with each measurement taking less than 2 min.

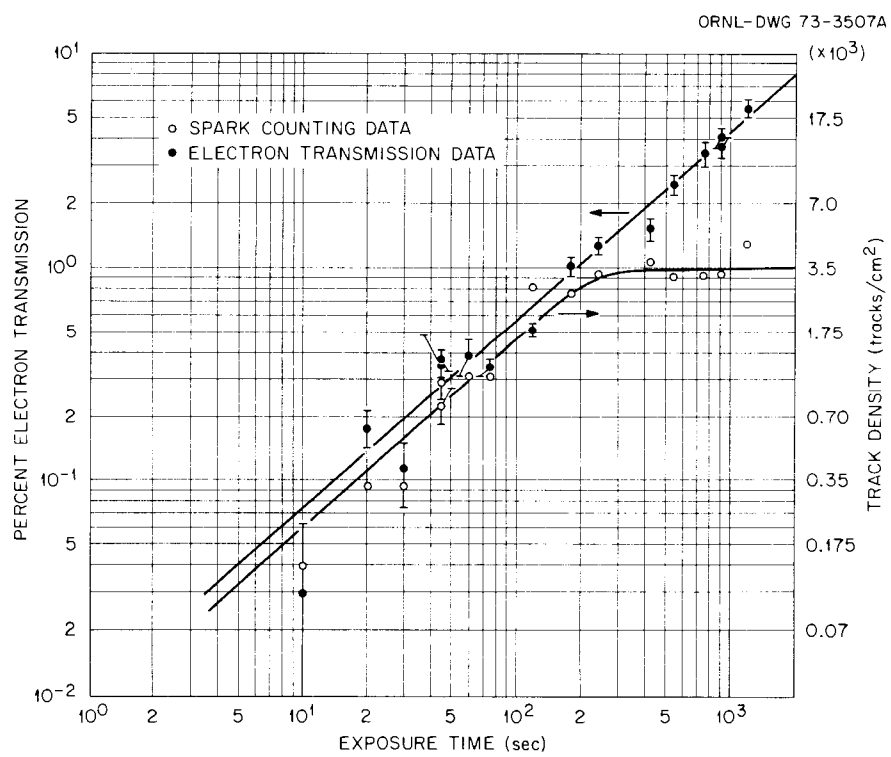


**Fig. 5.2. Electron transmission and fission fragment track density as a function of time of exposure to $^{252}$Cf fission fragments.**

## LONG-LIVED TRITIUM TARGETS FOR NEUTRON GENERATORS

A new concept in targets for neutron generators has been successfully tested at ORNL.[6] An alloy layer of palladium and silver, which was water-cooled, has been used as a substrate for a target occluder and as a valve to pass tritium into the target region. A prototype system has been operated for more than 10 hr at an average neutron yield of $2 \times 10^{10}$ neutrons $sec^{-1}$ $mA^{-1}$, which is over an order of magnitude greater than comparable yield for a commercially available target. The purpose of this research was to optimize the parameters of this new design for direct application to cancer therapy and general radiobiology research. In particular, the objective was to develop a target capable of handling high beam power and produce a high neutron yield for a long period with little risk to personnel from the health physics standpoint.

Six targets were fabricated. The target design is shown in Fig. 5.3. A palladium-silver alloy substrate is brazed over the concentric gas reservoir grooves cut in the front side of the target, and the rear of the target has 15 machined water-cooling channels. Tritium gas is introduced into the gas reservoir from a gas-handling manifold.

Four targets have been tested, and these results show no significant neutron yield dependence on the substrate composition and thickness (0.010 to 0.030 in.). An optimum neutron yield was obtained with a titanium occluder of thickness equal to the range of 200-keV deuterons in titanium (~500 $\mu g/cm^2$). The results are shown in Fig. 5.4. The half-life of this target was approximately 6 hr, with an average yield of $2 \times 10^{10}$ neutrons $mA^{-1}$ $sec^{-1}$. A target with an erbium occluder of similar thickness produced a neutron yield that was 66% of the yield of the titanium target. Both a bare substrate and a thick occluder (~1 $mg/cm^2$) produced neutron yields of only 25% of that of the titanium target.

Measurements of tritium diffusion through the targets and neutron yield show a loss rate of 2 to $3 \times 10^6$ tritium atoms per neutron produced for the titanium occluder and 5 to $6 \times 10^6$ tritium atoms per neutron for the erbium occluder. There are approximately 10 tritium atoms lost per incident deuteron on these targets. The losses in conventional neutron targets are $\sim 10^5$ tritium atoms per neutron and 1 tritium atom per incident deuteron.[7]

Heat removal tests were conducted on this target design and were compared with linear heat transfer

6. F. F. Haywood et al., *A Self-Replenishing Tritium Target for Neutron Generators*, ORNL-TM-3397 (June 1972).

7. D. O. Nellis et al., *Tritium Contamination in Particle Accelerator Operation*, U.S. Department of Health, Education, and Welfare, 1968.

PHOTO 1803-72

**Fig. 5.3. View of target assembly prior to brazing palladium-silver foil over tritium reservoir.**

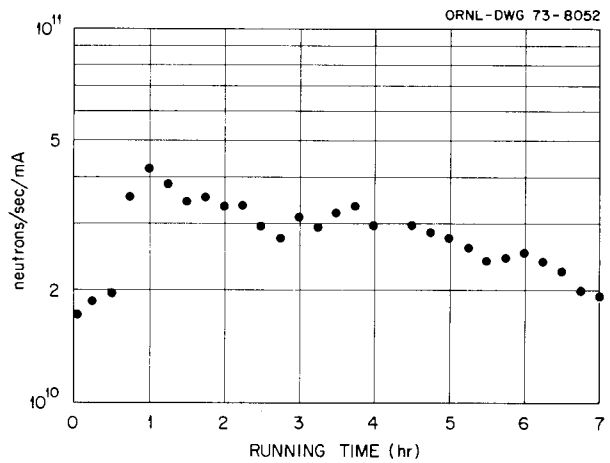


**Fig. 5.4. Neutron yield as a function of running time for 0.030-in. 80% palladium–20% silver foil covered with 515 $\mu g/cm^2$ titanium.**

calculations. An oxygen-acetylene torch adjusted to maximum power was used to heat the center of the target. Approximately 2 kW of heat was removed from the target with a cooling water flow of 3.5 liters/min. During this test, the back of the target remained at room temperature, the temperature at the back of the substrate was 100°C, and the target surface was about 350°C.

Tests of water flow rates through the targets show a maximum capacity of 10 liters/min under a head pressure of 45 psig. This rate is equivalent to a linear velocity of 9 m/sec (turbulent flow).

Linear heat removal calculations show that the present target design can dissipate 2.6 kW of power.[8] These calculations assume a water flow of 11 m/sec and that the target surface cannot be hotter than 200°C ($Ti\text{-}H_2$ is eutectic around 300°C).[9] These calculations correspond to a maximum beam power density of 1.4 $kW/cm^2$ or a 7-$mA/cm^2$ beam of 200-keV deuterons (present targets were run between 0.15 and 0.2 $kW/cm^2$). The problem is not heat dissipation but is one of controlling the temperature gradient between the target surface and cooling channel and the beam power density at the target.

New controls were fabricated, and modifications were made around the DOSAR Low Energy Accelerator to accommodate these sets of target tests.

A stainless steel uranium furnace and a gas manifold were built to store and handle the tritium gas. The manifold with the furnace and a target is shown in Fig. 5.5. The furnace (lower left) is a hollow finger filled with 5 g of uranium chips and has a 5-$\mu$ stainless steel filter above it. The low-volume manifold was evacuated either by a mechanical pump or by opening a valve and venting into the beam line of the accelerator. A precision Bourdon manometer gage (top center, Fig. 5.5) was used to measure the tritium gas pressure when the furnace was heated. When the manifold-target system was pressurized to 400 torr, it contained approximately 20 Ci of tritium gas.

A new beam line connector-insulator was built with a quick-coupling flange and is shown in Fig. 5.6. With this system, a complete target change takes less than 15 min. Smears before and after a target change showed no detectable tritium contamination.

For personnel safety and to prevent contamination of parts in case of an accidental tritium release, a hood was installed above the accelerator beam line and target area. The hood was vented through a stack extending 8 ft above the building, and a wind vane within the ductwork was interlocked into the accelerator control console. The air flow around the target ranges from 130 to 170 lin ft/min (well within industrial safety requirements).

The target's temperature was adjusted by a remotely controlled needle valve added to the target water cooling system. The diffusion rate of tritium through the substrate was controlled by this needle valve, since the palladium substrate acts as a heat-sensitive valve. Typical water flows and target temperatures are shown in Fig. 5.7.

In summary, the following observations were made:

1. The neutron yield was dependent on occluder thickness, may be dependent on occluder material, but appeared to be independent of substrate composition and thickness.

2. The neutron yield was varied by 10 to 20% by controlling the tritium diffusion rate through the substrate, but was independent of the tritium gas pressure over a range of 150 to 500 torr.

3. The present target design was capable of handling beam power densities up to 2.0 $kW/cm^2$ without reaching excessive target surface temperatures.

4. Present target and tritium handling procedures have not jeopardized personnel safety or produced any contamination during target changes and accelerator operations.

Additional studies of the half-life of this target design are being conducted. However, the present target appears to be capable of producing a neutron flux of $5 \times 10^{11}$ neutrons/sec with a 6-hr half-life if operated under a 2-kW beam (200 kV, 10 mA).

8. S. Benny, E.G.&G., Inc., Las Vegas, Nev., private communication, 1972.

9. G. A. Lenning et al., *J. Metals*, March 1954, p. 367.

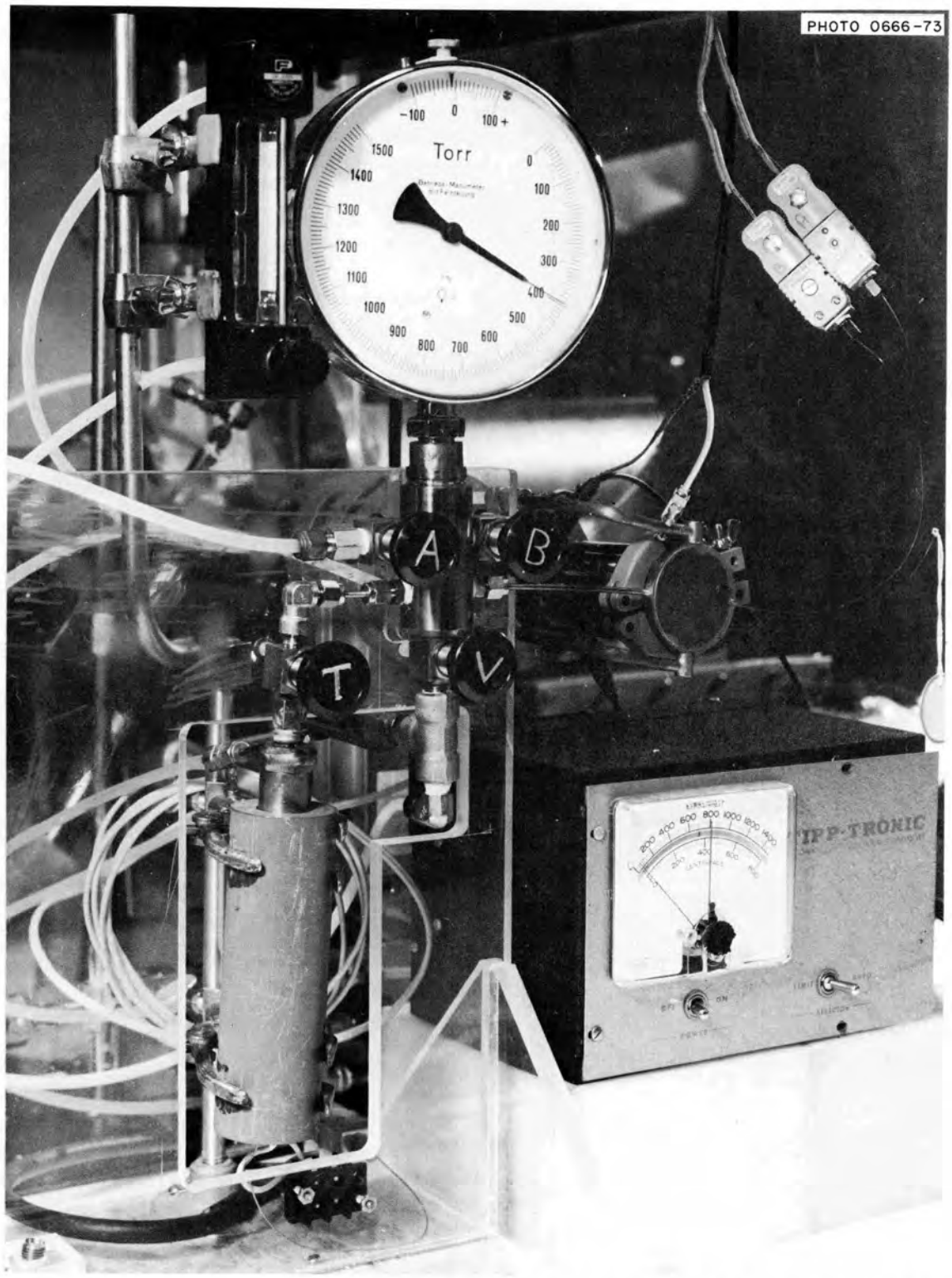


Fig. 5.5. Self-replenishing target assembly and uranium trap (tritium supply) shown attached to the accelerator beam tube.

**Fig. 5.6. View of self-replenishing target (far right), quick-coupling mechanism, and beam tube end piece.**

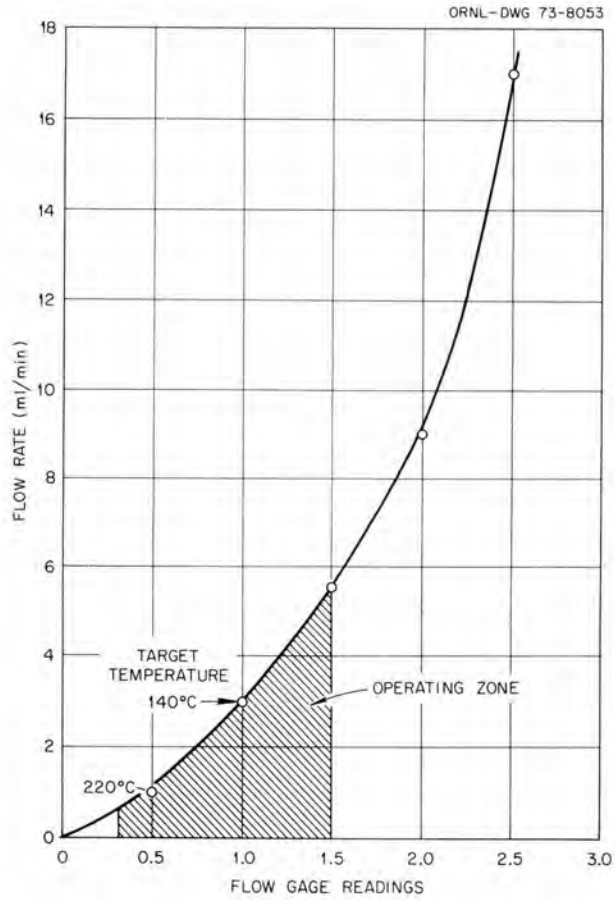


**Fig. 5.7. Diagram of coolant flow rate as a function of flow gage reading.**

# Part II. Fundamental Health Physics Research

R. D. Birkhoff R. H. Ritchie

## 6. Theoretical Radiation Physics

R. H. Ritchie

G. D. Alton[1] W. R. Garrett S. Y. Shieh[4]
V. E. Anderson[2] R. N. Hamm J. E. Turner
J. C. Ashley V. N. Neelavathi[1] R. B. Vora[1]
W. Brandt[3] J. Neufeld[4] C. E. Wheeler[1]
J. M. Elson[1] H. C. Schweinler H. A. Wright

### PION DOSIMETRY[5]

A description of the computer code used to calculate depth-dose curves for realistic pion beams incident on a cylindrical water target has been published.[6] As reported last year, good agreement was obtained between calculated values and curves measured by the Health Physics Group at the European Organization for Nuclear Research (CERN), with whom we are continuing collaborative work.

Additions have been made to the computer code, which is called PION-1, to make it more versatile. Calculations can now be carried out for multiregional targets, consisting of water, soft tissue, bone, and air cavities. Range straggling and an improved method of treating multiple Coulomb scattering have been incorporated into PION-1. Provision has also been made for obtaining the absorbed dose in various LET intervals at different positions in the target.

The dose distribution in an irradiated target is affected by various beam parameters, which can be varied within certain limits. Foremost among these are the mean momentum of pions in the beam, the magnitude of the momentum spread, and the size and degree of uniformity of the beam. Studies of the effects of varying these beam characteristics have been undertaken. Figure 6.1 shows, as an example, the depth-dose distribution in water for a typical pure pion beam with variable mean momentum $\bar{p}$. The momentum distribution, assumed Gaussian, had a spread $\Delta p$ such that one-half of the pions have momenta within 2% of $\bar{p}$. Other parameters will be varied and similar results compiled for several beam configurations.

Cell survival studies are important when considering the use of pions in radiotherapy. Based on RBE values of Todd[7] for heavy ions and of Berendsen and Broerse[8] for neutrons, a calculation of T-1 kidney cell survival was made[9] for the beam configuration used in ref. 6. The upper part of Fig. 6.2 shows the calculated mean values, $\overline{\mathrm{RBE}}$, averaged over all particle types within an axial cylindrical detector of 3 cm radius at various depths. The momentum spread of the beam was varied from 1 to 5% as indicated. The lower portion of the figure shows the corresponding depth-dose curves. The maximum value of $\overline{\mathrm{RBE}}$ is found to occur at a somewhat greater depth than the maximum dose. The most efficient position for killing cells is thus not that

1. Graduate student.
2. On loan from Mathematics Division, ORNL.
3. New York University.
4. Consultant.
5. Supported in part by the National Science Foundation.
6. J. E. Turner, J. Dutrannois, H. A. Wright, R. N. Hamm, J. Baarli, A. H. Sullivan, M. J. Berger, and S. M. Seltzer, *Radiat. Res.* 52, 229–46 (1972).
7. P. Todd, *Radiat. Res. Suppl.* 7, 196 (1967).
8. G. W. Barendsen and J. J. Boerse, *Proc. Int. Congr. Protection against Accel. Space Radiat.*, CERN 71-16.
9. J. R. Dutrannois, H. A. Wright, J. E. Turner, and R. N. Hamm, "Estimations of the RBE for $\pi^-$ and $\pi^+$ from Survival Data of T-1 Human Kidney Cells," *Int. J. Radiat. Biol.*, in press.

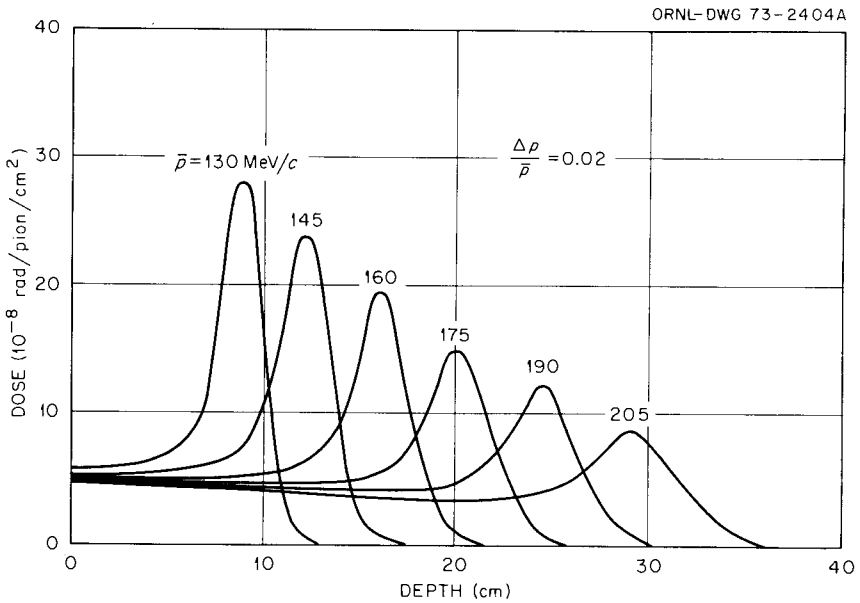


**Fig. 6.1. Variation of absorbed dose with mean momentum for a typical pion beam** [J. E. Turner et al., *Radiat. Res.* **52**, 229–46 (1972)] **with fixed momentum spread $\Delta p/\bar{p}$ of 2%.**

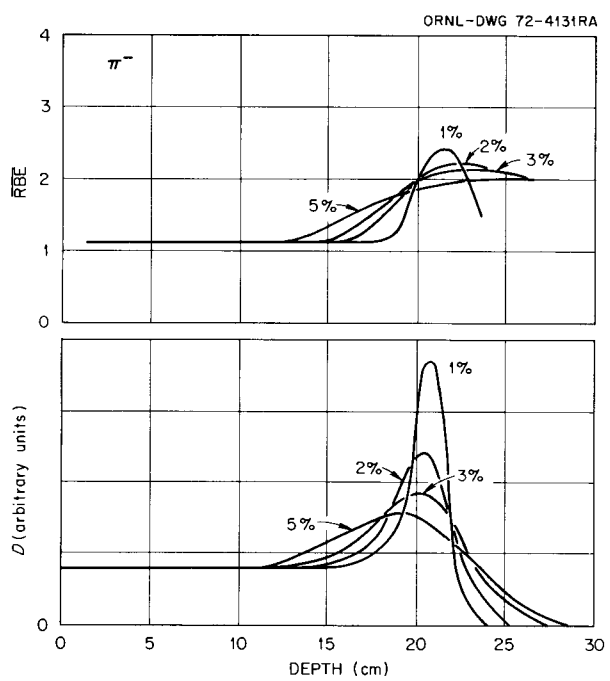


**Fig. 6.2. Variation of dose $D$ and $\overline{\text{RBE}}$ with momentum spread of a negative pion beam** [J. E. Turner et al., *Radiat. Res.* **52**, 229–46 (1972)]. Mean momentum is 175 MeV/$c$. Momentum spreads of 1, 2, 3, and 5% were used.

of maximum dose, but at a somewhat greater depth where relatively more pions stop.

A computer program was written to calculate two-dimensional isodata contours from the raw data generated by Monte Carlo programs, such as PION-1. Cylindrical symmetry is assumed, and the data are smoothed as functions of depth and radial distance from the beam axis. Figure 6.3 shows an example of absorbed dose contours, labeled as fractions of the peak dose, for a uniform, circular (radius 2 cm) beam of pions of mean momentum 153 MeV/$c$, with a Gaussian momentum distribution having a 2% spread. The pions are incident from the left with the beam axis at the zero position. The vertical scale gives distance from the beam axis in centimeters, and the horizontal scale gives the depth in the target (tissue) in centimeters.

## STOPPING POWER OF MATTER FOR NEUTRONS

The Bethe theory[10] of the stopping power of matter has been generalized to include the neutron as a projectile.[11,12] The neutron can lose relatively small amounts of energy through the interaction of its spin,

10. U. Fano, *Annu. Rev. Nucl. Sci.* **13**, 1 (1963).
11. J. E. Turner, V. N. Neelavathi, R. B. Vora, J. S. Bisht, R. K. Kher, and D. Arora, submitted to *Phys. Rev.*
12. J. E. Turner, R. K. Kher, D. Arora, J. S. Bisht, V. N. Neelavathi, and R. B. Vora, submitted to *Phys. Rev.*

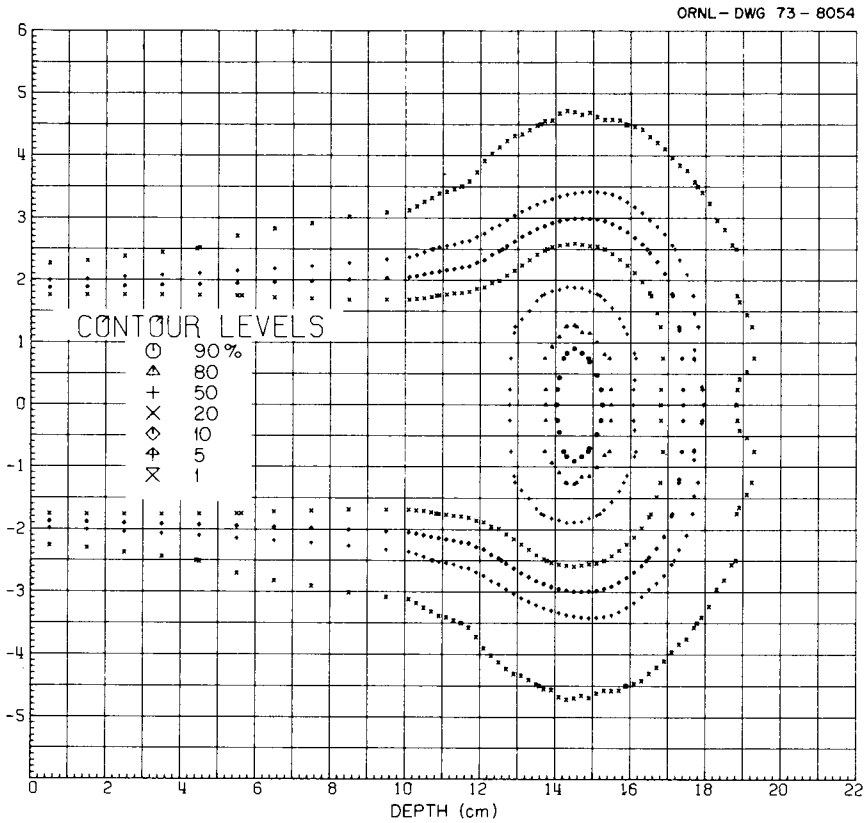


**Fig. 6.3. Isodose contours at the 90, 80, 50, 20, 10, 5, and 1% levels resulting from a 2-cm circular, uniform beam of negative pions with mean energy 153 MeV/*c* and 2% spread.**

anomalous magnetic moment, and finite charge distribution with the charge and spin of atomic electrons. The calculation, which was carried out quantum mechanically in the first Born approximation, replaces an earlier semiclassical estimation based on the impulse approximation.[13] The two methods of computation give comparable numerical results for neutron energies in the range 5 to 10 GeV, where they both apply. The quantum-mechanical formula shows a weaker energy dependence than that predicted by the semiclassical approximation.

The stopping power in an elemental medium of atomic number $Z$ at neutron energies between $4Z^{0.35}$ GeV and 500 GeV is given approximately by

$$-\frac{dE}{ds} = \frac{2\pi e^4 NZ\mu^2}{m\beta^2}\left(\frac{m}{M}\right)^2 \gamma^2\beta^2(1+\beta^2), \qquad (1)$$

the binding of the electrons in the medium being negligible. Here $e$ and $m$ are the electron's charge and mass; $N$ is the number of atoms per unit volume of the medium; $\mu$ is the magnetic moment of the neutron, expressed in nuclear magnetons; $M$ is the neutron's mass; $\beta$ is the speed of the neutron in units of the speed of light; and $\gamma = (1-\beta^2)^{-1/2}$. At 10 GeV, the stopping power of matter for neutrons is about $10^{-5}$ that for protons. Calculations were performed for neutron energies up to 7000 GeV. The stopping power increases by about a factor of 100 between $\gamma = 10$ and 100 and by another order of magnitude between $\gamma = 100$ and 1000. Thereafter, it rises only slightly when $\gamma$ is increased to 7000.

13. R. B. Vora, V. N. Neelavathi, J. E. Turner, T. S. Subramanian, and M. A. Prasad, *Phys. Rev. B* 3, 2929 (1971).

## THE CALCULATION OF THE $Z_1{}^3$-DEPENDENT STOPPING POWER CONTRIBUTION AND ITS INFLUENCE ON RANGES, MEAN EXCITATION POTENTIALS, AND SHELL CORRECTIONS

The theory of the $Z_1{}^3$-dependent contribution to the stopping power of matter for charged particles[14,15] has been cast into simple formulas for stopping powers and range-energy relations which apply in a comprehensive manner to all targets.[16] The stopping power $S$ of a medium of atomic number $Z_2$ for an incident particle of velocity $v_1$ and charge number $Z_1$, in terms of the stopping power in the first Born approximation $S_0$, can be written in the form

$$S(x) = S_0(x)\left[1 + \frac{Z_1}{Z_2{}^{1/2}}\frac{\kappa(b, x)}{x}\right] \qquad (2)$$

in terms of the reduced variable $x \equiv v_1{}^2/(v_0{}^2 Z_2)$, where $v_0$ is the Bohr velocity. Since $S_0(x) \propto Z_1{}^2$, the second term in this equation represents the $Z_1{}^3$ contribution. The function $\kappa(b, x)$, where $b$ is a parameter which can be fixed by experiment, has been derived and tabulated in earlier work.[15,16] This function varies slowly with $x$ and for many applications when $x > 1$ may be set equal to a constant with value approximately the mean of the distribution.

The $Z_1{}^3$ contribution to stopping power for a compound target may be derived under the assumption that Bragg's additivity rule of stopping power applies. For a target consisting of atomic constituents $Z_{2i}$, present in atomic concentrations $n_i$, the stopping power becomes

$$S_0 = \sum_i n_i S_{0i}(x_i)/\sum_i n_i,$$

where $x_i \equiv v_1{}^2/(v_0{}^2 Z_{2i})$. Since $S_{0i} \propto L(x_i)/x_i$, the $Z_1{}^3$ contribution takes the form

$$\frac{S - S_0}{S_0} \equiv \frac{\Delta S}{S_0} = Z_1\left(\frac{v_0}{v_1}\right)^2 \frac{\sum_i n_i Z_{2i}{}^{3/2} L(x_i)\ \kappa(b, x_i)}{\sum_i n_i Z_{2i} L(x_i)}, \qquad (3)$$

where the function $L(x_i) \approx \ln(x_i/q)$ for $x_i > 1$. The constant $q \approx 0.18$ for all materials. We illustrate the results of Eq. (3) for the important case of the "standard" nuclear emulsion.[17] The result is plotted in Fig. 6.4 in the form

$\beta^2\ \Delta S(\beta)/Z_1\ S_0(\beta)$ vs $\beta$, where $\beta \equiv v_1/c$.

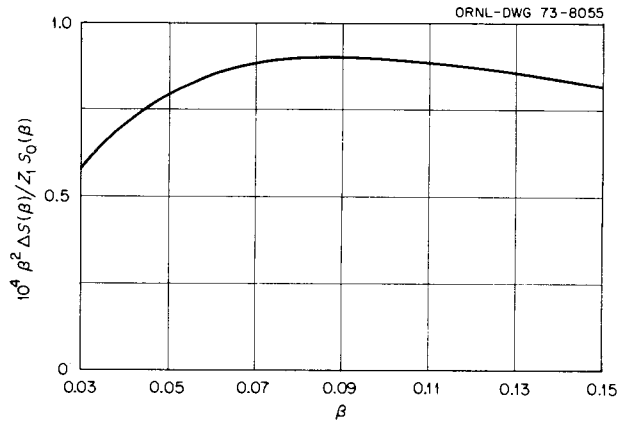


**Fig. 6.4. A function for calculating the fractional change in stopping power, $\Delta S/S_0$, due to the $Z_1{}^3$ effect in "standard" nuclear emulsions.**

Formulas for contributions to the range due to the $Z_1{}^3$ effect can be derived from Eq. (2) using the continuous slowing down approximation. The expressions for the range contributions are rather more complicated than the stopping power contributions.[16] We will illustrate some of the results graphically for the experimentally important case of the ranges of $\pi^+$ and $\pi^-$ mesons in nuclear emulsion. If $\Delta R_\pi$ is the difference in range of a $\pi^-$ meson, $R_{\pi^-}$, and the range of a $\pi^+$ meson, $R_{\pi^+}$, of the same initial energy, then Fig. 6.5 shows $\Delta R_\pi$ as a function of $R_{\pi^+}$ and the corresponding energy $E_{\pi^+}$. These results agree quite well with range differences measured by Barkas et al.[18] and Tovee et al.[19]

Evaluation of mean excitation potentials and shell corrections has been made for the elements $Z_2 = 20$ to 30 from very careful stopping power measurements[20] using theoretical expressions derived in the first Born approximation. Recently, however, both experiment[21]

14. *Health Phys. Div. Annu. Progr. Rep. July 31, 1971*, ORNL-4720.
15. J. C. Ashley, R. H. Ritchie, and W. Brandt, *Phys. Rev. B* **5**, 2393 (1972).
16. J. C. Ashley, R. H. Ritchie, and W. Brandt, to be published.
17. W. H. Barkas, *Nuovo Cim.* **8**, 201 (1958).
18. W. H. Barkas et al., *Phys. Rev.* **101**, 778 (1956); *Phys. Rev. Lett.* **11**, 26(1963); CERN Report 65-4 (unpublished).
19. D. N. Tovee et al., *Nucl. Phys.* **B33**, 493 (1971) (and private communication).
20. H. H. Andersen et al., *Phys. Rev.* **175**, 389 (1968); *Phys. Rev.* **180**, 373 (1969).
21. H. H. Andersen, H. Simonsen, and H. Sørensen, *Nucl. Phys.* **A125**, 171 (1969).

and theory[15] have shown that higher-order terms in the Born series, terms proportional to $Z_1^3$, where $Z_1$ is the charge of the incident particle, produce a significant contribution to the stopping power of heavy charged particles at low energies (e.g., protons of energy $\lesssim$ 15 MeV).

We have reexamined the work of ref. 20, including the $Z_1^3$ contributions. The reanalysis shows little change in the mean excitation potentials ($\lesssim$1.5%) for this range of $Z_2$ values but rather dramatic changes in the shell corrections. Plots of the shell correction term $C/Z_2$ as a function of incident proton energy over the range 2.5 to 12 MeV show a change in shape of the curve which results from studies reported in ref. 20 due to the addition of the $Z_1^3$ contribution to stopping power. In addition, an increase in the value of the shell correction by 20 to 25% occurs at the lower energies even though the $Z_1^3$ contribution to the stopping power is only 2 to 3% at the lower energies. This result is illustrated in Fig. 6.6 for the case of copper ($Z_2$ = 29), where the solid line represents the results of our reanalysis and the dashed line the results of ref. 20.

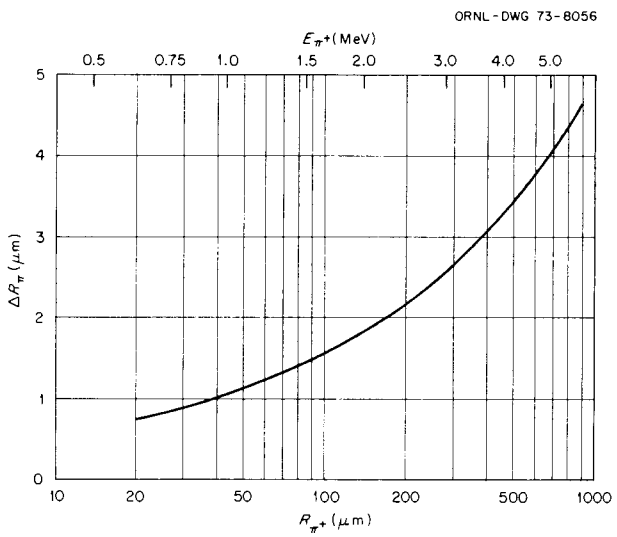


**Fig. 6.5. The range difference due to the $Z_1^3$ effect between $\pi^-$ and $\pi^+$ mesons, $\Delta R_\pi$, as a function of the range of $\pi^+$ or of the initial energy of the $\pi^+$.**

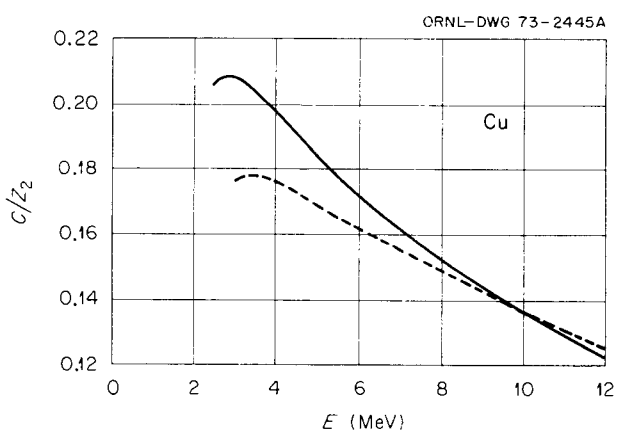


**Fig. 6.6. Shell correction for Cu ($Z_2$ = 29) as a function of energy of the incident proton.** The solid curve shows the results of our reanalysis of stopping power measurements, including the $Z_1^3$ contribution. The dashed curve represents the results of ref. 20.

## AN EXPERIMENTAL AND A COMPUTATIONAL PROGRAM FOR OBTAINING A RELATIONSHIP BETWEEN QUALITY FACTOR, $Q$, AND LINEAR ENERGY TRANSFER, LET

It is generally understood that the ICRP-recommended $Q$-LET dependence was obtained through a conservative estimate based on RBE-LET relationships. However, it has been recognized that RBE-LET relationships for various biological effects are difficult to determine for mammals, mainly because the current techniques (track segment and track average techniques) are not adequate for obtaining the relevant data. Also, the values of RBE appropriate for many end points with a long latent period pose great difficulties for animal experimentation. An experimental and computational program for obtaining the required information has been proposed. One performs a series of experiments on animals in a controlled radiation environment. By applying Monte Carlo procedures, one determines distributions of LET in critical organs of the animals. Then, using biological data for critical effects (e.g., cataract, impaired fertility, and defective development of the fetus), a set of linear equations is obtained in which the coefficients are the doses delivered in various intervals of LET and the unknowns are "biological weighting factors, λ." From these equations one can derive λ's for various LETs as they relate to the critical effects. It is assumed that radiation effects observed on animals are relevant to the assessment of occupational exposure. Then, using value judgments and combining calculated results with data observed on man, one can obtain a LET relationship which is more directly based on experimental evidence than that which is currently used. To obtain the relevant biological data, one extrapolates from observational information at high doses to presumed effects at low doses.

## THEORETICAL STUDIES OF RADIATION-STIMULATED BIOLOGICAL EFFECTS

Over the past year a new program has been developed between members of the Fundamental Health Physics and Radiation Research and Development sections of the Health Physics Division and the Pathology and Immunology sections of the Biology Division of ORNL. This work is described in Part I, Section 3.

## THE LINEAR RESPONSE FUNCTION OF A RANDOM ASSEMBLY OF MOLECULES

By making some approximations we have been able to derive an expression for the linear dielectric response function of a randomly distributed system of molecules. The resulting response function describes in a qualitative fashion both single electron-hole pair excitations and collective excitations (plasmons) in fairly dense systems. To our knowledge, this constitutes the first theoretical description of the plasmon in which a basis set of electron wave functions appropriate to individual molecules is employed and where the material described may have the properties of an insulator.

We make the following assumptions in arriving at the linear response function:

1. The overlap between electron clouds on neighboring molecules is neglected.
2. The correlation in position between neighboring molecules is neglected.
3. The existence of a space- and time-dependent, self-consistent scalar electric potential $\phi(\mathbf{r}, t)$ in the medium is postulated.

The many-body Schrödinger equation for the time development of the system under the influence of the assumed potential $\phi(\mathbf{r}, t)$ is solved in first-order time-dependent perturbation theory, neglecting exchange effects. The resulting electric charge density becomes the source of a scalar electric potential which by the usual self-consistency arguments is set equal to the originally assumed $\phi(\mathbf{r}, t)$. In summing the electric charge density from individual molecules an important cancellation in momentum transfer space occurs due to the assumed uncorrelated positions of molecules in the system. This cancellation is analogous to that which occurs in the theory of the electrical resistance of an electron gas which contains a completely random distribution of scattering centers.

We find that the dielectric response function of a random system of identical molecules may be written

$$\epsilon(\omega, \mathbf{q}) = 1 + \frac{\omega_p^{\,2}}{2} \sum_n \frac{f_{n0}(q)}{E_{n0}} \times \left[ \frac{1}{E_{n0} - (\omega + i\eta)} + \frac{1}{E_{n0} + (\omega + i\eta)} \right],$$

where the generalized oscillator strength (GOS)

$$f_{n0}(q) = \frac{2E_{n0}}{q^2} \left| \langle n | \sum_{i=1}^{Z_2} e^{i\mathbf{q}\cdot\mathbf{r}_i} | 0 \rangle \right|^2$$

and all quantities are in atomic units. Here $E_{n0}$ is the energy difference between the $n$th excited state and the ground state (in units of Ry $= e^2/a_0 = 27.2$ eV), and $\omega$ and $\mathbf{q}$ are the frequency and wave vector which appear in the argument of the dielectric function, respectively. Also $\mathbf{r}_i$ is the position vector of the $i$th electron in a given molecule, $Z_2$ is the number of electrons per molecule, and $|n\rangle$ is the eigenvector corresponding to the $n$th excited stationary state of the molecule. The quantity $\omega_p^{\,2} = 4\pi N$ in atomic units, where $N = Z_2 N_A$ and $N_A$ is the density of molecules in the system. The quantity $\eta$ is a positive infinitesimal. The summation over $n$ is understood to include an integration over continuum states as well as a sum over discrete states.

Since the exact GOS for the hydrogen atom is known, we have computed $\epsilon(\omega, \mathbf{q}) = \epsilon_1(\omega, q) + i\epsilon_2(\omega, \mathbf{q})$ for an assembly of hydrogen atoms from the equation above. The plasma energy $\omega_p$ is used as a parameter. Figure 6.7*a* shows a plot of $\epsilon_1$ and $\epsilon_2$ as a function of $\omega$ in the region in which only discrete, real transitions are possible; only the frequency range corresponding to the first two transitions has been plotted. The quantity $\eta$ has been taken equal to 0.01 in these calculations. Figure 6.7*b* shows the behavior of $\mathrm{Im}(-1/\epsilon)$ in the region of the longitudinal exciton-like resonance associated with the first excited state transition. Note that this resonance energy is about 10% higher in energy than that corresponding to the transition energy itself due to long-range interactions.

Figure 6.8 shows $\epsilon_1$, $\epsilon_2$, and $\mathrm{Im}(-1/\epsilon)$ as a function of $\omega$ in the region of the continuum. The plasmon resonance at $\omega \sim 0.9$ is clearly seen. The peak in $\mathrm{Im}(-1/\epsilon)$ at $\omega \sim 0.41$ again corresponds to the first excited state transition in the isolated atom.

Figure 6.9 shows the variation in the plasma resonance energy as the wave number $q$ is varied. The relation is seen to be nearly quadratic for small $q$. Such a quadratic relation is also found for the plasmon in an electron gas.

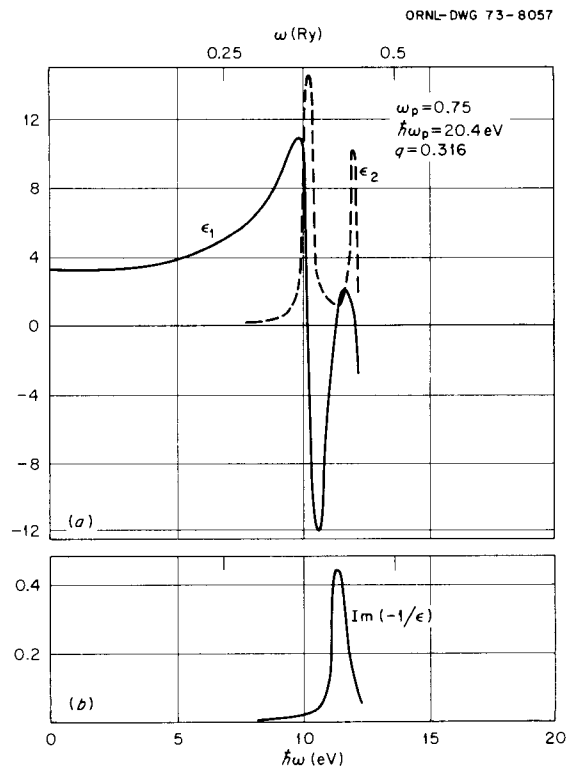


**Fig. 6.7. Dielectric functions for a gas of hydrogen atoms.** (*a*) The real ($\epsilon_1$) and imaginary ($\epsilon_2$) parts of the dielectric function for a gas of H in the region of discrete transitions in the isolated atom. Here $\omega_p = \sqrt{4\pi N} = 0.75$, $q = 0.316$, and $\eta = 0.01$. (*b*) The imaginary part of the reciprocal dielectric function for a gas of H atoms for $\omega_p = 0.75$, $q = 0.316$, and $\eta = 0.01$.

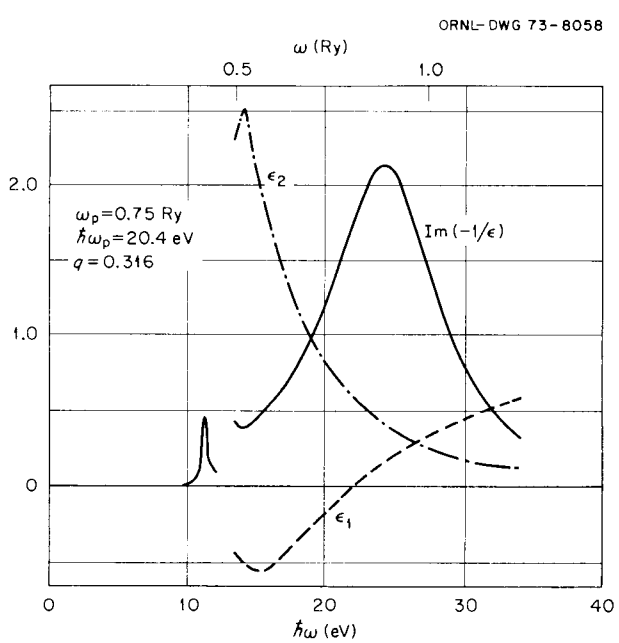


**Fig. 6.8.** $\epsilon_1(\omega)$, $\epsilon_2(\omega)$, **and Im** $(-1/\epsilon)$ **for a gas of H atoms in the continuum of final states for the isolated atom.** Here $\omega_p = 0.75$, $q = 0.316$, and $\eta = 0.01$.

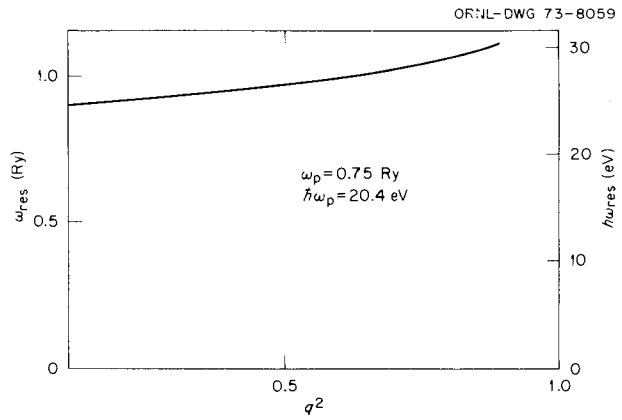


**Fig. 6.9. The plasmon dispersion relation for** $\omega_p = 0.75$ **and** $\eta = 0.01$.

## COMPLEX POTENTIAL METHODS FOR MOLECULAR SCATTERING

Further investigation is being made of the usefulness of Feshbach's[22] complex optical potential approach for multichannel scattering problems in atomic and molecular systems. Results have been reported previously[23,24] for the atomic scattering of electrons in the energy region above the ionization threshold but below the energy range where the Born approximation may be utilized. The theoretical analysis has been applied to a study of electron collisions with linear molecules in the fractional electron volt energy region where significant contributions to the total scattering cross sections come from rotational and vibrational excitation of the target molecule. The resultant integro-differential equations are amenable only to numerical solution. The extremely long-range nature of the interaction potential for charged particle scattering by a heteronuclear diatomic molecule has led to considerable difficulty in achieving numerical solutions with existing computer programs. Preliminary results have been obtained for CO, but further modifications in computational techniques are under way in order to achieve acceptable accuracy and to explore the potentialities of the method over a suitably wide energy range.

## ROTATIONAL RESONANCES IN MOLECULAR SCATTERING OF ULTRA-LOW-ENERGY ELECTRONS

The existence of rotational resonances in low-energy electron collisions with simple molecules has been

22. H. Feshbach, *Ann. Phys.* **5**, 357 (1958).
23. R. H. Ritchie et al., *Health Phys. Div. Annu. Progr. Rep. 1972*, ORNL-4811, p. 8.
24. G. D. Alton, W. R. Garrett, M. Reeves, and J. E. Turner, *Phys. Rev. A* **6**, 2138 (1972).

proposed[25] to explain anomalies in electron swarm experiments at very high pressures and in electron-beam transmission experiments with time-of-flight techniques.[26] The existence of temporary negative ions, or resonances, associated with electronically excited states of atomic or with electronically and vibrationally excited states of molecular systems are well known, but no theoretical demonstration has yet been made of such states associated with rotational excitation. Close coupling results for $e$-$H_2$ scattering failed to show any such phenomena,[27] though the experiments[25,26] seem to indicate their presence.

In order to explore the characteristics of rotational resonances in molecular scattering phenomena, we have considered the problem of electron scattering by a simple dipolar molecular system in the energy region below the first rotational threshold. The existence of Feshbach-type rotational resonances for this system is essentially guaranteed, and the binding properties of the target system in various rotational states have been well established.[28]

We consider a simple dipolar molecular system with moment of inertia $I$ and rotational energy levels $E_j = j(j+1)/2I$, which is composed of point charges of opposite sign separated by distance $R$. The system has dipole moment $D = eR$ and is capable of binding an electron to form a negative molecular ion in a state of total angular momentum $J$ only if the dipole moment exceeds a critical value $D_c{}^J$ as described in ref. 28.

The total wave function $\Psi_{jl}{}^{JM}$ for the system having total angular momentum $J$ can be written as

$$\Psi_{jl}{}^{JM}(\mathbf{r}, \hat{s}) = \sum_{j'l'} Y_{j'l'}{}^{JM}(\mathbf{r}, \hat{s})\, U_{j'l'}{}^{J}(r)/r, \qquad (4)$$

where $Y_{j'l'}{}^{JM}(\mathbf{r}, \hat{s})$ is the usual coupled spherical harmonic which is an eigenfunction of the rotational Hamiltonian and of $J^2$. The vector $\mathbf{r}$ designates the electron coordinate and $\hat{s}$ is the orientation vector of the molecular axis. The use of (4) in the time-independent Schroedinger equation for the total system leads to the set of radial equations

$$\left[ -\frac{d^2}{dr^2} + \frac{l'(l'+1)}{d^2} - k_{jj''}{}^2 \right] U_{j'l'}{}^{J}(r) + \sum_{j''}\sum_{l''}\sum_{\mu} f_\mu(j''l'';j'l'';J)\, V_\mu(r)\, U_{j''l''}{}^{J}(r) = 0. \qquad (5)$$

$U_{j'l'}{}^{J}(r)$ is the reduced radial function of the scattered electron whose orbital angular momentum at large distance is $l'$. The momentum $l'$ couples to the rotational angular momentum $j'$ of the target to give total angular momentum $J$. The coefficients $f_\mu(j''l'';j'l';J)$ result from angular integration over the functions $Y_{j'l'}{}^{JM}$ and over the angular part of the multipole component $V_\mu(r)$ of the interaction potential.[29]

In order to investigate the properties of rotational resonances, we consider solutions to (5) in the unusual energy regime $E < 1/I$ where energies are measured in Rydbergs. For these low energies all rotational excitational channels are closed, and only elastic scattering is possible. The boundary conditions on (5) for scattering from ground state molecules become

$$U_{j'l'}{}^{J}(r) \sim 0 \text{ for } j' > 0,$$

$$U_{0l'}{}^{J}(r) \sim \sin(k_0 r + \delta_{l'}), \quad j' = 0.$$

Thus, for molecular systems where $I \gtrsim 10^4\ m_e a_0{}^2$ units ($a_0$ = Bohr radius), the energy regime for rotational resonances is $E \lesssim 10^{-4}$ Ry ($\sim 10^{-3}$ eV).

In order to get a detailed picture of the behavior of the resonant phase shift, we first determine the nature of the background phase shift as a function of dipole strength. Thus, in Fig. 6.10 we show the phase shift for a fixed energy of $1 \times 10^{-6}$ Ry with $J = 0$ and $J = 1$ as a function of dipole moment. The phase shifts increase by $\pi$ radians as the dipole moment goes through its critical value for the particular choice of $J$ and $I$. (The critical moments are indicated in Fig. 6.10.) With this background information we can then study the phase shift for a given target system as a function of incident energy $E_0 = k_0{}^2$. Sample results are shown in Fig. 6.11. The phase shifts for $s$-wave electrons incident on a target dipolar system with $D = 0.75$ and for $p$-wave electrons on a system with $D = 0.85$ are shown over the energy range from $I = 10^{-6}$ Ry to the threshold for the first inelastic process. A rotational resonance in the $J = 1$ elastic channel is clearly demonstrated in the energy region just below $E_{\text{threshold}}$. We hasten to add that the appearance of

25. L. Frommhold, *Phys. Rev.* **172**, 118 (1968); W. N. Sams, L. Frommhold, and D. J. Kouri, *Phys. Rev. A* **6**, 1070 (1972).
26. W. Raith and J. E. Land, in *Proc. Third International Conference on Atomic Physics, Boulder, Colo., Aug. 7–11, 1972*, S. J. Smith and G. K. Walters, eds., Plenum, N. Y., 1973, p. 82.
27. R. J. W. Henry and N. F. Lane, *Phys. Rev.* **183**, 221 (1969).
28. W. R. Garrett, *Phys. Rev. A* **3**, 961 (1971).
29. W. R. Garrett, *Mol. Phys.* **24**, 465 (1972).

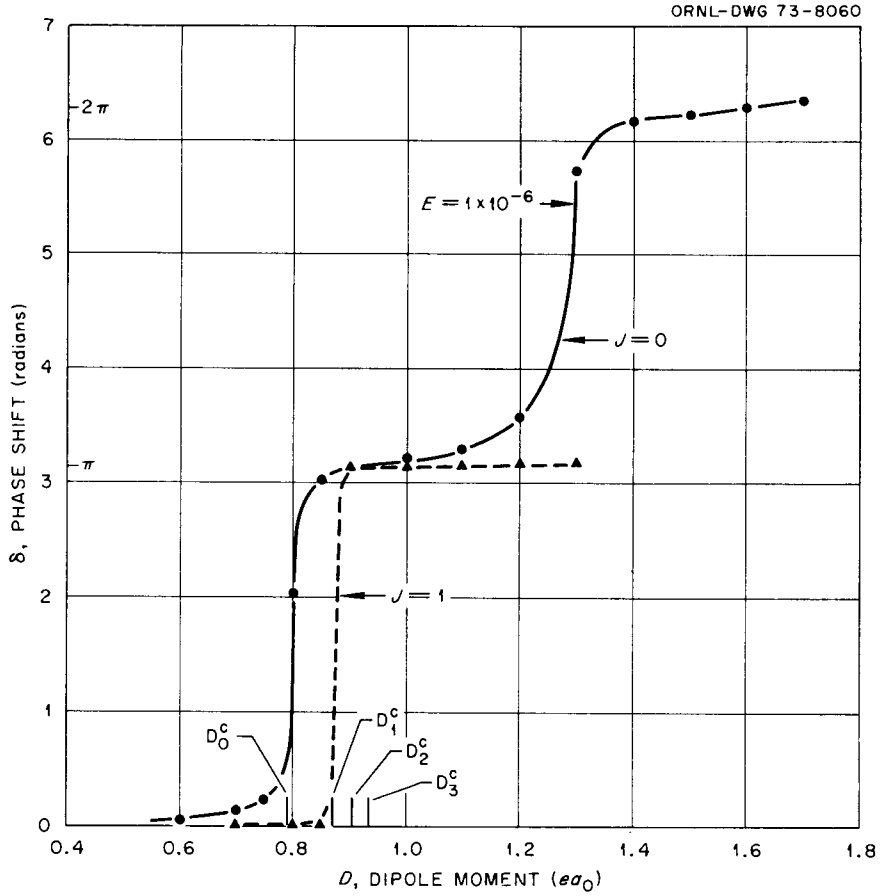


**Fig. 6.10. Phase shifts for fixed energy as a function of dipole moment.** *s*-wave ($J = 0$) curves for $E = 1 \times 19^{-6}$ and $1 \times 10^{-5}$ Ry; *p*-wave ($J = 1$) for $E = 1 \times 10^{-6}$ Ry.

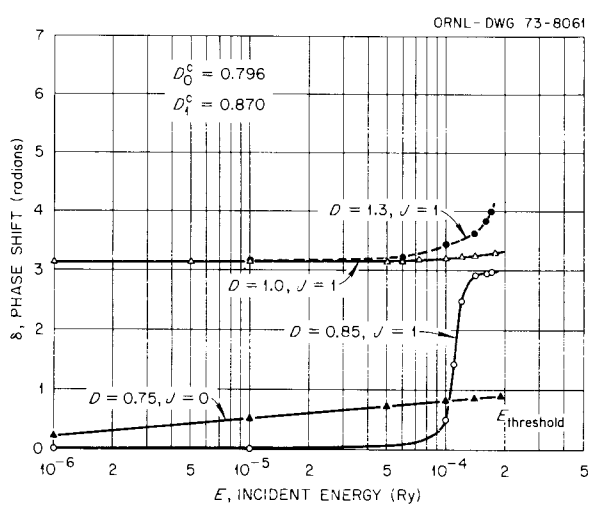


**Fig. 6.11. Elastic scattering phase shifts in the energy region below the first inelastic threshold.**

rotational resonances for the model system having a dipole moment near a critical value does not imply that polar molecules passing a dipole moment of comparable magnitude would show a similar resonance at the same energy. The dipole contribution in the total electron–polar-molecule interaction potential has been shown to give little information on the electron binding property or electron scattering cross sections for such systems, since other contributions to the interaction potential play a far from negligible role in the processes.[28]

Further study is under way on the properties of rotational resonances in electron scattering at extremely low energies.

## COLLISIONS OF ALKALI METAL ATOMS WITH ATOMIC OXYGEN[30]

A semiclassical approach was used to calculate excitation and charge-transfer cross sections in neutral

30. R. B. Vora, R. N. Compton, and J. E. Turner, ORNL-TM-4239 (1973). A summary of this work is being prepared for publication.

atom-atom collisions. Use of single-electron wave functions in a time-dependent perturbation theory gave a set of coupled differential equations, which were transformed into a tractable form in a three-state approximation. The formalism was applied to alkali-atom–oxygen collisions. The three states were taken to be the ground and the first excited ($^2P_{1/2}$) states of the alkali atom and the single stable state of the $O^-$ ion. Charge-transfer and excitation cross sections were calculated initially in two-state approximations for alkali-atom energies between 10 and 10,000 eV. The resulting charge-transfer cross sections generally agree with available results based on Landau-Zener theory. The transition probability for transfer at high velocities was found to vary as $1/v^2$, as in the Born approximation, rather than $1/v$, as predicted from Landau-Zener theory.

Calculations were performed in the three-state approximation to study the effects of the simultaneous existence of two final states on the charge-transfer and excitation cross sections. In the energy range 10 to 10,000 eV the charge-transfer cross sections were found to remain almost unaffected when the excited alkali state was included. The excitation cross sections were considerably altered by the presence of the ionic channel. In particular, at lower velocities they were found to be considerably higher than in the two-state approximation.

## CLASSICAL BINARY INELASTIC CROSS SECTIONS FOR EXCITATION AND IONIZATION OF ELECTRONS IN ATOMIC SYSTEMS

Much progress has been made in recent years toward theoretical construction of cross sections for atomic excitation and ionization. However, many such approaches involve detailed numerical solutions of the Schrödinger or Dirac equations in an assumed potential (usually self-consistent in some sense) and require separate studies for each shell in an atom.

At a more empirical level, studies of the classical binary collision (CBC) model have become popular following the papers of Gryzinski.

The CBC model has been applied to the problem of obtaining estimates of quantities such as stopping power for atomic systems for charged particles with low enough energy that the asymptotic Bethe-Bloch formula is not accurate. These efforts suffer from the defect that the CBC formulas used are based on the Gryzinski velocity distribution which is employed to characterize the ground state electrons; a number of workers have objected to this velocity distribution because of its unphysical, ad hoc character.

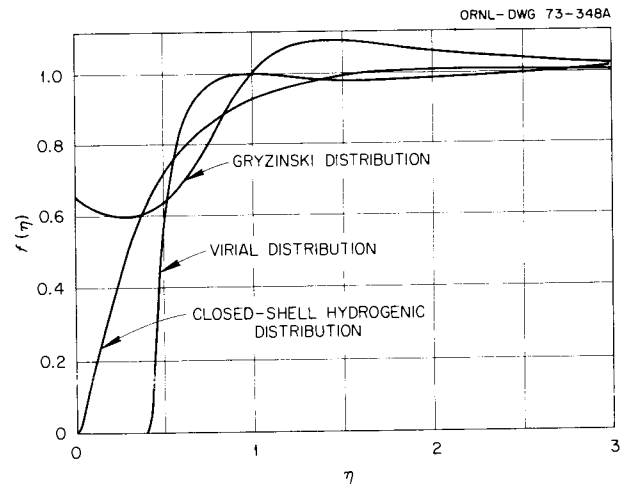


**Fig. 6.12. The Bethe sum rule integral $f(\eta)$ plotted as a function of $\eta$, where $\eta$ is momentum transfer measured in units of $\hbar a_0^{-1}$ and $a_0 = \hbar^2/me^2$.** $f(\eta)$ has been calculated from the CBC model using the original Gryzinski velocity distribution, the virial distribution, and the closed-shell hydrogenic distribution.

We have been concerned for some time with the study of electron slowing-down distributions in condensed matter at electron kinetic energies comparable with ionization energies in the atoms making up the material. In order to construct inelastic differential cross sections for such materials, we studied the CBC model in some detail. We have evolved certain simple semiempirical procedures for fitting CBC model cross sections in the large momentum transfer region, where they are most reliable, with information on cross sections in the region of small momentum transfer. These models may be employed to estimate charged particle inelastic cross sections, stopping power, mean angular deflections, etc., for complicated many-electron systems which should be useful to arbitrary energy.

We have computed the Bethe sum rule integral $f(\eta)$ for the generalized oscillator strength appropriate to CBC cross sections for three different velocity distributions: (1) the original Gryzinski distribution, (2) the "virial" distribution, and (3) the distribution of velocities appropriate to a closed-shell hydrogenic model. The quantity $\eta$ is the momentum transfer in units of $\hbar a_0^{-1}$. The results are shown in Fig. 6.12. From general quantum considerations, $f(\eta)$ should equal 1 in the present normalization for all $\eta$. All of these distributions yield $f(\eta)$ values which are deficient when $\eta < 1$.

We wish to retain the analytical simplicity of the CBC cross sections, but prefer to use cross sections for which the generalized oscillator strength (GOS) satisfies the

fundamental Bethe sum rule and possibly higher-order sum rules. The following simple procedure suggests itself in this connection. We note that optical oscillator strengths are known experimentally (and a few theoretically) for a number of atomic systems over a rather wide range of energies. Optical oscillator strengths $f_n(0)$ [or $df(0)/d\epsilon$ in the continuum] of an atom are equal to the GOS of that atom in the limit of zero momentum transfer. Suppose that $f_n(0)$ and $df(0)/d\epsilon$ are known for a given atom and that one may use CBC-GOS values in the region of large $n$ for a given shell of that atom. We suggest that the following approximation to the true GOS of a given shell should be useful:

$$\tilde{f}_n(q) \approx f_n(0)[1 - f_{\mathrm{CBC}}(\eta)] \tag{6}$$

in the region of discrete transitions, and

$$\frac{d\tilde{f}(\eta)}{d\epsilon} = \frac{df(0)}{d\epsilon}[1 - f_{\mathrm{CBC}}(\eta)] + \frac{df_{\mathrm{CBC}}}{d\epsilon} \tag{7}$$

in the continuum, where $\epsilon$ is the energy transfer variable. That is, we propose an interpolation scheme for the GOS which reduces to the known optical oscillator strength for small momentum transfers and which goes over into the CBC cross section, using closed-shell hydrogenic speed distributions, for large momentum transfer. There are at least two advantages to such a procedure: (1) the Bethe sum rule for $f_n$ and $df/d\epsilon$ is satisfied for all $\eta$; (2) the cross section resulting from this GOS yields a charged particle stopping power which reduces to the correct Bethe form for large (but nonrelativistic) velocities of the charged particle. Clearly, one may choose other differential GOS functions than $df_{\mathrm{CBC}}/d\epsilon$ for use in Eqs. (6) and (7); however, the analytical simplicity of this scheme is quite appealing. Also, this form should be fairly accurate for inner shells, particularly if one employs experimental values of the ionization energy $E_i$ of a given atomic shell and if one chooses the mean kinetic energy of electrons in that shell from Slater's rules.

As an indication of the usefulness of the procedure described above, we have plotted in Fig. 6.13 the exact differential GOS of the H atom, the CBC-GOS, and $df/d\epsilon$ from Eq. (7) in which $df(0)/d\epsilon$ is taken to be the exact optical oscillator strength of the H atom. All energies are expressed in terms of Ry = 13.6 eV, and momenta are expressed in units of $(a_0)^{-1}$ = (0.529 Å)$^{-1}$. The various GOS are plotted as a function of $\eta^2 = (a_0 q)^2$ and for several values of $\epsilon = E/\mathrm{Ry}$. One sees from this plot that $df/d\epsilon$ is definitely superior to $df_{\mathrm{CBC}}/d\epsilon$ and is a reasonable approximation to the exact GOS over the whole $\epsilon$-$\eta$ plane.

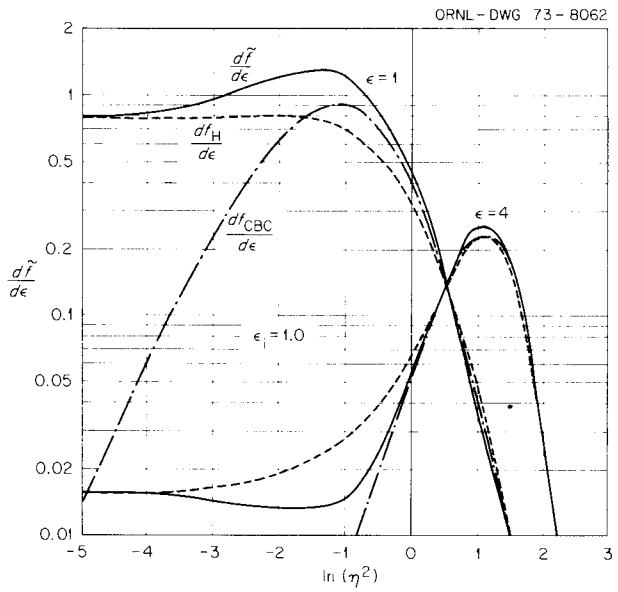


**Fig. 6.13. The differential GOS for two different values of energy transfer = $\epsilon$Ry and as a function of ln ($\eta^2$), where $\eta$ is momentum transfer measured in units of $\hbar a_0^{-1}$.** The GOS is computed for the CBC model (dot-dash lines), for the exact ground state hydrogen model (dashed line), and for the present model (solid line).

## HIGH-ENERGY SATELLITES IN AUGER ELECTRON SPECTRA FROM SOLIDS

Observations attributed to the interaction of Auger electrons with plasmons in a solid have been made by a number of experimenters. Jenkins and Chung[31] were apparently the first to suggest that high-energy satellites in the $L_{2,3}VV$ Auger lines in solid silicon appearing in their data might be explained by the gain of the plasmon quantum by an Auger electron. Other workers have attributed such structure to double ionization of the shell which gives rise to the primary Auger electron, thus resulting in a lowering of the vacancy energy by an amount which may be approximately equal to the plasmon energy in the solid. Jenkins and Zehner[32] have recently made observations on the $KVV$ Auger electron satellites in beryllium metal which seem to show that both the plasmon energy gain satellite and the double ionization satellite exist in this substance.

A theoretical explanation of the plasmon energy gain process must take into account the following. Suppose

31. L. H. Jenkins and M. F. Chung, *Surface Sci.* **26**, 151 (1971); **26**, 649 (1971); **28**, 409 (1971).

32. L. H. Jenkins and D. M. Zehner, *Bull. Amer. Phys. Soc.* **18**, 391 (1973).

for simplicity that an inner shell vacancy is produced in a solid at some instant of time. The sudden appearance of this vacancy may shock the valence electrons into oscillation. If a well-developed plasmon exists, then an oscillating potential field will be created in the neighborhood of the vacancy. An Auger electron, born in the immediate vicinity, may interact strongly with this plasmon field and thereby gain the plasmon energy.

The methods of many-body perturbation theory may be used to compute the probability of this process in a metal in a relatively straightforward way if the conduction electrons are represented in the electron gas model. Figure 6.14 shows some Feynman diagrams representing processes which contribute to the energy gain satellite. We simplify the situation by assuming that the inner shell is ionized initially by an x-ray photon. If a fast charged particle causes the vacancy, still other interactions must be considered. We are in the process of evaluating the probability of Auger energy gain by these methods.

Useful estimates may also be obtained in a simpler fashion if one is willing to approximate as follows: Assume (1) that the deep hole is infinitely heavy and (2) that the plasmon acting upon the Auger electron is just that associated with a classical expanding dipole formed by the inner shell vacancy and the ejected electron as it recedes from its parent ion. These assumptions lead one to the following equation for $P_{\text{gain}}$, the probability of plasmon energy gain,

$$P_{\text{gain}} = \frac{\pi}{[E_A(E_A + E_P)]^{1/2}} G(E_A, E_P, E_I) \frac{\Gamma_v}{\Gamma_v + \Gamma_p} .$$

The factor $G$, which depends upon Auger energy $E_A$, the energy of the ejected electron $E_I$, and the plasmon energy $E_P$, is

$$G = \frac{1}{4\pi} \left\{ \left[ \pi - \tan^{-1}\left(\frac{A}{B_-}\right) - \tan^{-1}\left(\frac{A}{B_+}\right) \right]^2 + \ln^2 \left[ \frac{B_-^2 + A^2}{B_+^2 + A^2} \right] \right\} ,$$

where $A = E_P/4E_I^{1/2}$ and $B_\pm = (E_A + E_P)^{1/2} E_A^{1/2}$. $\Gamma_v$ and $\Gamma_p$ are the decay rates of the vacancy and the plasmon, respectively. $G$ is of the order of unity and varies relatively little as its arguments are varied. The ratio of decay rates, $\Gamma_v/(\Gamma_v + \Gamma_p)$, is quite important here. In the metals with atomic number $\lesssim 30$ the vacancy decay rate is only a few percent of the plasmon decay rate; thus, the plasmon decays away before most Auger electrons are emitted.

ORNL-DWG 73-7526

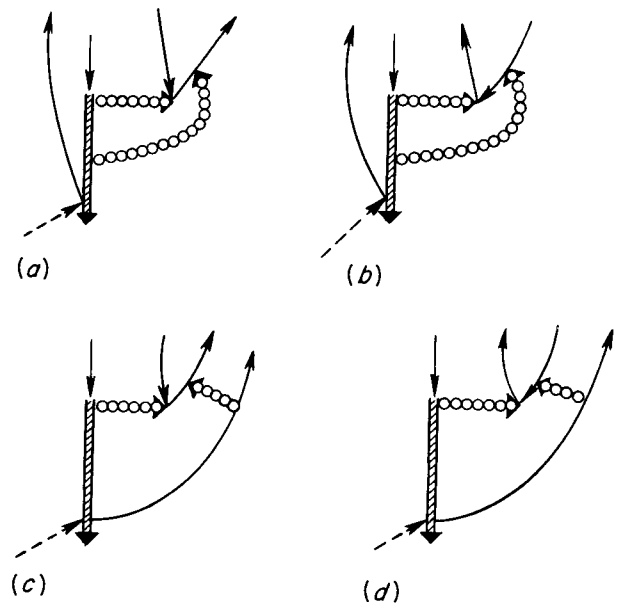


**Fig. 6.14. Feynman diagrams representing processes involving plasmon energy gain by an Auger electron generated in a metal.** The shaded double line represents the deep hole created in the metal by an x-ray photon, which is represented by a dashed line. A solid line directed upward represents an electron excited out of the Fermi sea, while a solid line directed downward represents a hole in the conduction band. The line of bubbles represents the Coulomb interaction between particles screened by polarization of the conduction electrons.

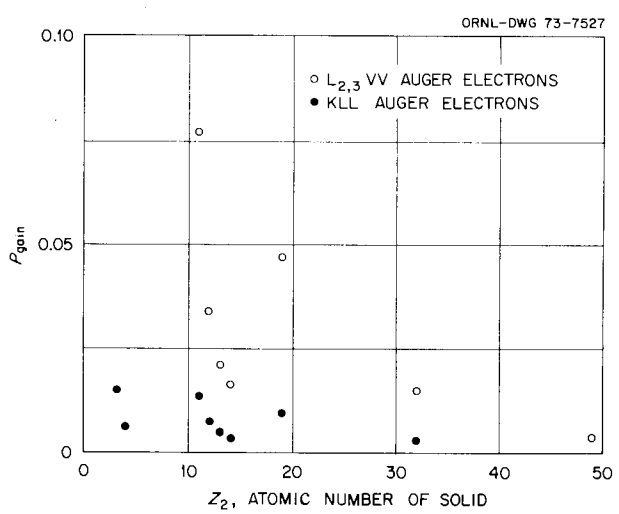


**Fig. 6.15. Probability of plasmon energy gain by various Auger electrons in several different metals.** The open circles correspond to $L_{2,3}VV$ Auger electrons and the closed circles to $KLL$ Auger electrons.

We have used this equation together with Auger and plasmon energies and approximate decay rates for several different metals. The results are displayed in Fig. 6.15. Sodium and magnesium are predicted to be the most favorable metals for displaying the energy gain effect. It should be noted that $\Gamma_v$, the vacancy decay rate, is not very well known for most materials. We have not yet compared these results in detail with experiment. The quantity $P_{gain}$ inferred from experimental data now available on the various metals does not seem to be obtainable with accuracy better than ~±50%. Our results seem to agree with experiment within these limits.

## DIFFUSE SCATTERING AND SURFACE PLASMON GENERATION BY PHOTONS AT A ROUGH DIELECTRIC SURFACE

First-order perturbation theory has been employed to derive formulas for (1) the probability of the scattering of photons on a plane, microscopically rough dielectric surface and (2) the probability of conversion of photons into surface plasma oscillations at such a surface. The calculation proceeds through a classical solution of Maxwell's equations. Transformation to a nonorthogonal system of coordinates is effected. The Green function tensor for the Hertz vector potential appropriate to two semi-infinite dielectric media separated by a plane boundary has been found and has been used to determine the fields scattered by the surface roughness. The results should be valid for arbitrarily large damping due to electronic transitions in the dielectric. This theory has been applied in the analysis of data on magnesium and is described in the section Interaction of Radiation with Liquids and Solids in this report.

## SURFACE PLASMONS IN CYLINDRICAL GEOMETRY

The existence of various modes of the electromagnetic field in which the fields are confined to a region near the surface (surface plasmons) has been investigated for spheres and plane surfaces but has apparently not been studied explicitly for the case of cylindrical geometry. To examine these modes one looks for solutions of Maxwell's equations corresponding to fields which decrease exponentially as one moves away from the surface. The application of the boundary conditions at the surface leads to an equation, or equations, relating the frequency $\omega$ and wave number $k$ for which solutions of the desired form exist. The equation giving $\omega$ as a function of $k$ is called the dispersion relation for the surface plasmons.

For a right circular cylinder of radius $a$ and infinite length, the dispersion relation for surface plasmons is given by

$$\nu^2\nu'^2(\nu'\epsilon\alpha_n - \nu\epsilon'\beta_n)(\nu'\alpha_n - \nu\beta_n) - \frac{n^2}{a^2}(\epsilon' - \epsilon)^2 k^2 \frac{\omega^2}{c^2} = 0 \text{ for } n = 0, 1, 2, \ldots, \quad (8)$$

where $c$ is the velocity of light, $\epsilon = \epsilon(\omega)$ is the dielectric function of the cylinder material, and $\epsilon' = \epsilon'(\omega)$ is the dielectric function of the medium filling the space outside the cylinder. We have also used the definitions:

$$\nu = \left(k^2 - \epsilon\frac{\omega^2}{c^2}\right)^{1/2},$$

$$\nu' = \left(k^2 - \epsilon'\frac{\omega^2}{c^2}\right)^{1/2},$$

$$\alpha_n = \frac{d}{d(\nu a)} \ln I_n(\nu a),$$

$$\beta_n = \frac{d}{d(\nu' a)} \ln K_n(\nu' a),$$

where $I_n$ and $K_n$ are the modified Bessel functions of the first and second kind of order $n$.

As an illustrative example we consider a free electron gas with a plasma frequency $\omega_p$ in the cylindrical region with vacuum outside. Thus $\epsilon' = 1$ and $\epsilon = 1 - (\omega_p/\omega)^2$. For $a = 80$ Å we show in Fig. 6.16 the surface plasmon dispersion relations for the modes $n = 0, 1, 2, 3, 10$. Also shown (dashed curve) is the dispersion relation for surface plasmons for an infinite plane boundary between a free electron gas and vacuum. For large $k/k_p$, where $k_p \equiv \omega_p/c$, the frequencies of the various modes approach the value for the flat surface. As $a \to \infty$, all the modes converge to the dashed curve in Fig. 6.16. Thus for large $k$ and/or large radii the cylinder surface appears "flat" for the surface plasmon.

## PRIMARY RADIATION PROCESSES IN THE PHYSICAL STAGE

A review has been made of physical processes which may occur in condensed matter at early times ($<10^{-13}$ sec) following the passage of a swift charged particle. Emphasis has been given to "nonscaling" aspects of

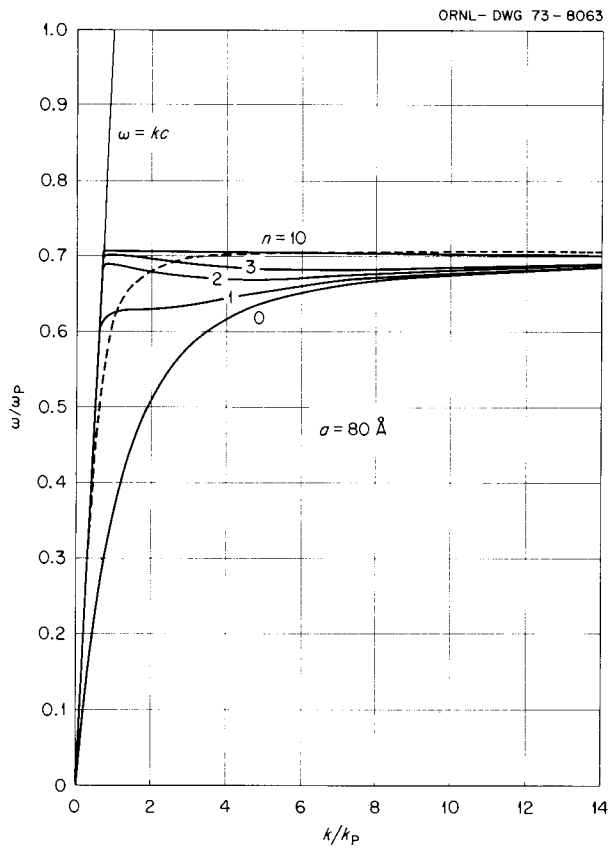


**Fig. 6.16. The $n$ = 0, 1, 2, 3, 10 surface plasmon modes for a cylindrical free electron gas in vacuum.** The radius of the cylinder is 80 Å. The dashed curve gives the surface plasmon dispersion relation at a plane boundary for a free electron gas. All curves are bounded on the left by the "light line," $\omega = kc$.

radiation interactions, that is, those occurring in condensed matter which cannot be described adequately by merely scaling, according to density, data relevant to the same phenomena in gases. We have considered the spatial distribution of collective excitations in the intratrack of a charged particle and the propagation and decay of these excitations. The high density of valence electrons which prevails in condensed media makes it quite likely that a high degree of collectivity exists in the response of such materials to ionizing radiation. It is also likely that interesting nonlinear interactions may occur among the products of excitation and ionization along a particle track even at these early times. We have considered specific models of certain of these interactions and have suggested how they may affect the course of the energy deposition process and how their occurrence may be detected experimentally.

This work was carried out in collaboration with Prof. Werner Brandt of New York University. An account will be published in the *Proceedings of the Conference on Physical Mechanisms in Radiation Biology,* held in Airlie, Virginia, October 11–14, 1972.

## SURFACE PLASMONS IN SOLIDS

A review of the properties of the dynamic electron polarization modes associated with surfaces of simple solids has been made. Significant progress has been made in recent years toward the systematic use of the surface plasmon as a diagnostic tool to characterize the state of matter at the surface and in the bulk of solids. Emphasis in this review has been given to the way in which these modes may give rise to observable effects in various experimental situations. The dispersion relations, that is, the dependence of the eigenfrequency of such modes upon this propagation vector, have been studied for plane geometries. This review has been published in *Surface Science* **34**, 1 (1973).

A shorter review of some of the properties of surface polaritons, with emphasis upon spatially dispersive media, will be published in the *Proceedings of the Taormina Conference on the Structure of Matter,* held in Taormina, Sicily, October 2–6, 1972.

# 7. Atomic and Molecular Radiation Physics

L. G. Christophorou

V. E. Anderson[1]
R. P. Blaunstein[2]
Ada E. Carter
J. G. Carter
J. T. Cox
C. E. Easterly[3]
Kathy S. Gant[4]
R. E. Goans[4]
A. Hadjiantoniou[4]
J. P. Johnson[4]
C. E. Klots
D. L. McCorkle[3]
M. N. Pisanias[4]
D. Pittman

## INTERACTION OF SLOW ELECTRONS WITH MOLECULES IN VERY-HIGH-PRESSURE ("QUASI-LIQUID") ENVIRONMENTS

Our electron-molecule work at very high gas densities ("quasi-liquid" media) continued in an effort to bridge the existing gap between isolated-molecule and condensed-phase behavior. A number of experimental problems have been overcome.

Our investigation of the capture of slow electrons by $O_2$ to form $O_2^-$ in gradually increasing densities of various gaseous media continued. The study of $O_2^-$ formation in $O_2$-$N_2$ mixtures has been extended to higher $N_2$ pressures, $P_{N_2}$ (see Figs. 7.1 and 7.2). The model proposed earlier[5] to account for the drastic increases in the magnitude and the changes in the energy dependence of the attachment rates with $P_{N_2}$ shown in Figs. 7.1 and 7.2 (and also for similar changes in the attachment cross section deduced[6] from the data in Fig. 7.1 through the swarm unfolding technique[7]) seems to hold over the entire range of $N_2$ pressures investigated. Thus, the prediction of this model that

$$\frac{(\alpha w)_0}{P_{N_2}} = A + BP_{N_2} , \qquad (1)$$

where $A$ and $B$ are constants and $(\alpha w)_0$ is the attachment rate for $O_2$ pressure $P_{O_2} \to 0$, is sustained, as is shown by the data in Fig. 7.3. In our model for $O_2$-$N_2$ mixtures, $N_2$ is assumed (1) to act as a stabilizing third body in "distant" collisions and (2) to be involved in "hard" collisions which result in a serious perturbation of the $O_2^-$ potential-energy curve during capture, with a possible formation of a transient complex ($O_2^{-*}$-$N_2$). On the basis of this model and the data in Figs. 7.1 and 7.3 the autodetachment lifetime of $O_2^{-*}$ at thermal electron energies has been estimated[5] to be $\lesssim 4 \times 10^{-12}$ sec.

Additionally, electron attachment to $O_2$ to form $O_2^-$ at thermal and near-thermal energies has been studied in mixtures with $C_2H_4$ (ethylene) (up to 14,000 torr) and $C_2H_6$ (ethane) (up to 16,000 torr). The observed changes in the magnitude of the attachment rate for the formation of $O_2^-$ with increasing density of these three media ($N_2$, $C_2H_4$, and $C_2H_6$) are very different, demonstrating the profound effect and importance of the environment on the electron attachment process. In all three media at low pressures, low-energy electron attachment to $O_2$ can be treated as a three-body process. However, as the density of the medium increases, each medium affects the capture process differently. Thus, for $N_2$, $(\alpha w)_0$ increases drastically (see Fig. 7.2) with $P_{N_2}$, while for $C_2H_4$, $(\alpha w)_0$ shows a less than linear increase for pressures $\gtrsim 1000$ torr (see Fig. 7.4), indicating a transition from a three-body to a

1. On loan from the Mathematics Division, ORNL.
2. Consultant.
3. Postdoctoral Fellow from the University of Tennessee.
4. Graduate student.
5. L. G. Christophorou, *J. Phys. Chem.* **76**, 3730 (1972).
6. D. L. McCorkle, L. G. Christophorou, and V. E. Anderson, *J. Phys. B* (At. Mol. Phys.) **5**, 1211 (1972).
7. L. G. Christophorou, D. L. McCorkle, and V. E. Anderson, *J. Phys. B* (At. Mol. Phys.) **4**, 1163 (1971).

two-body electron attachment process. From the data in Fig. 7.4 we deduced a lifetime for $O_2^{-*}$ of $\sim 2 \times 10^{-12}$ sec, which is in agreement with that estimated from the data on $O_2$-$N_2$ mixtures.

These studies are currently being extended to even higher gas densities and also to other "key" molecules. In this connection, evidence has been obtained that benzene captures electrons in mixtures with high pressures of $N_2$, although no such attachment was observed at low pressures.

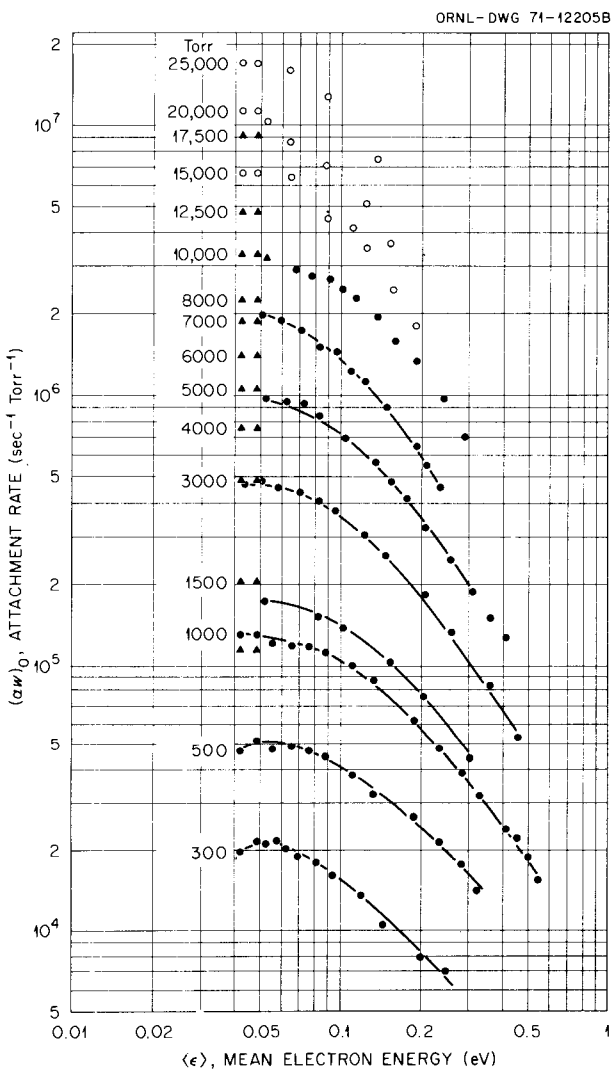


**Fig. 7.1.** $(\alpha w)_0$ **vs** $\langle\epsilon\rangle$ **for** $O_2$ **in** $N_2$ **(300** $\leqslant P_{N_2} \leqslant$ **25,000 torrs).** •, ref. 6; ▲ and ○, R. Goans and L. G. Christophorou, unpublished results.

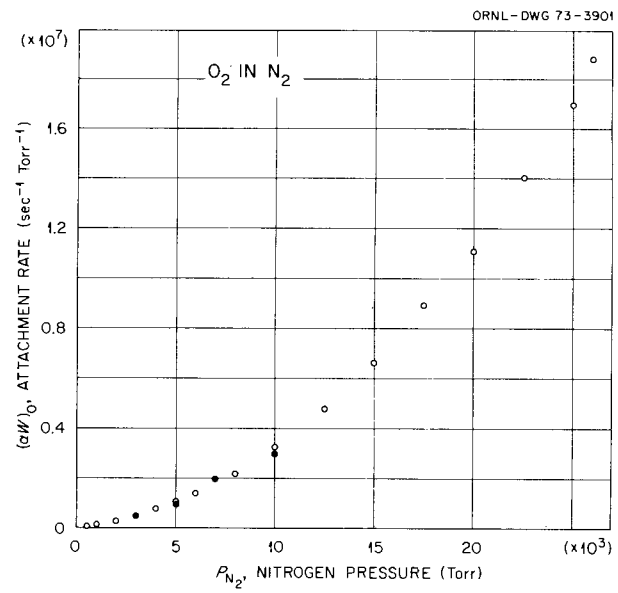


**Fig. 7.2.** $(\alpha w)_0$ **vs** $P_{N_2}$ **at** $\langle\epsilon\rangle \cong$ **0.04 eV.**

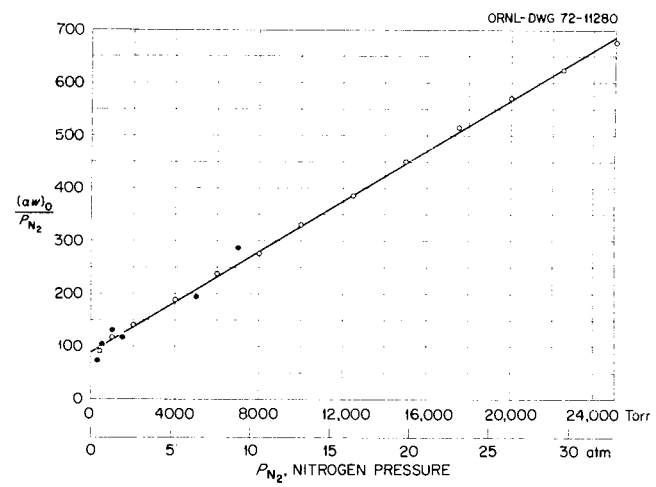


**Fig. 7.3.** $(\alpha w)_0/P_{N_2}$ **vs** $P_{N_2}$ **for** $O_2$-$N_2$ **mixtures.** •, ref. 6; ○, R. Goans and L. G. Christophorou, unpublished results.

## LONG-LIVED ORGANIC NEGATIVE IONS

We undertook a systematic study whereby we investigated and identified structures which capture thermal and epithermal electrons forming long-lived nuclear-excited Feshbach resonant states. Mass spectrometric studies and measurements of lifetimes of long-lived ($>10^{-6}$ sec) parent negative ions have been used to identify organic structures and specific functional groups which when contained in a large molecule

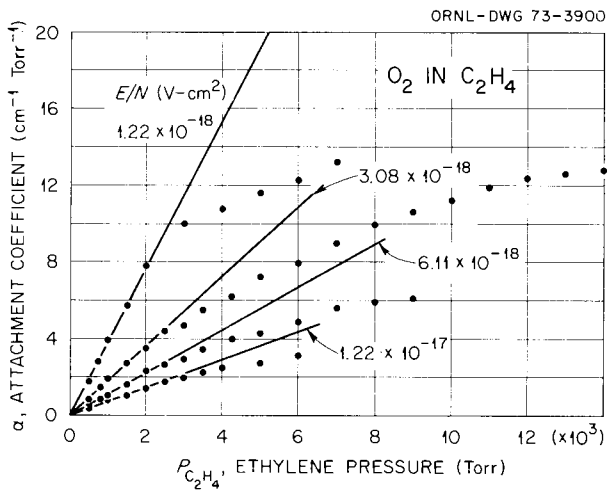


Fig. 7.4. $\alpha$ vs $P_{C_2H_4}$ for $O_2$ in $C_2H_4$.

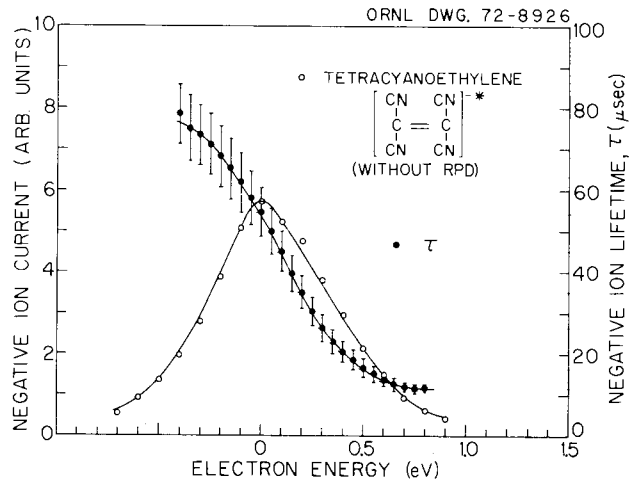


Fig. 7.5. Negative ion lifetime and negative ion current (without RPD) for $[C_2(CN)_4]^{-*}$ as a function of electron energy.

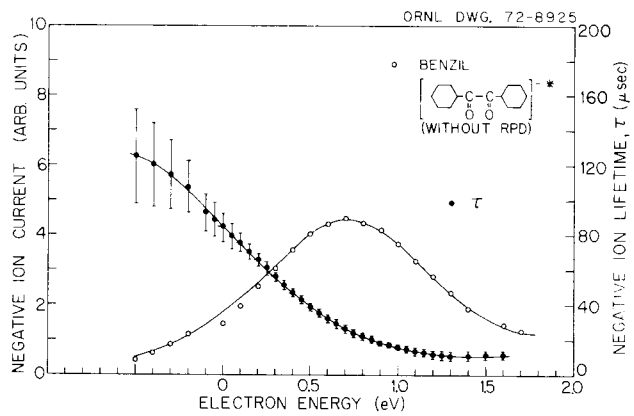


Fig. 7.6. Negative ion lifetime and negative ion current (without RPD) for $C_6H_5COCOC_6H_5^{-*}$ as a function of electron energy.

constitute the "electrophilic site" or "electron trapping center." From a study of "key" organic molecules of biological interest it has been concluded[8,9] that $NO_2$-containing benzene derivatives, CN-substituted organic molecules, higher aromatic hydrocarbons, strained structures, and organic molecules containing the functional groups –COCO–, –COCH(OH)–, –COOH, and =CHCHO–, capture thermal and near-thermal electrons very efficiently (often with a cross section >100 Å$^2$) and – in the absence of competing dissociative attachment processes which are usually very fast – form long-lived parent negative ions via nuclear-excited Feshbach resonances. For the majority of the organic molecules investigated, the cross section for parent negative ion formation peaked at thermal energies (see, for example, Fig. 7.5), but in a few cases (see, for example, Fig. 7.6) these peaked at energies in excess of thermal (still, however, below 1 eV).

Long-lived organic negative ions are initially formed in superexcited states and are thus subject to autoionization. The lifetimes of some of these extraordinarily long-lived species are listed in Table 7.1. The lifetime data for the $NO_2$-containing disubstituted benzene derivatives listed in Table 7.1 indicate that the parent-negative-ion lifetimes for these molecules depend on the electron donor-acceptor properties of the substituent groups and the intramolecular interaction between them, which is a function of their relative position around the benzene periphery.[8]

An important aspect of these studies has been the finding[10] that the autoionization lifetimes of the long-lived parent negative ions of *o*-nitrophenol ($o$-$C_6H_4OHNO_2$), benzil ($C_6H_5COCOC_6H_5$), and tetracyanoethylene $[C_2(CN)_4]$ – formed via nuclear-excited Feshbach resonances – decrease greatly with increasing incident electron energy (see Figs. 7.5 and 7.6). The lifetimes for $o$-$C_6H_4OHNO_2^{-*}$, $C_6H_5COCOC_6H_5^{-*}$, and $C_2(CN)_4^{-*}$ decrease from 420, 85, and 55 μsec at ~0.0 eV to 90, 10, and 11 μsec at 0.6, 1.5, and 0.8 eV, respectively. These lifetime variations, as well as the

8. A. Hadjiantoniou, L. G. Christophorou, and J. G. Carter, Part I, *Faraday Transactions* (Chemical Physics) (in press).

9. A. Hadjiantoniou, L. G. Christophorou, and J. G. Carter, Part II, *Faraday Transactions* (Chemical Physics) (in press).

10. L. G. Christophorou, A. Hadjiantoniou, and J. G. Carter, Part III, *Faraday Transactions* (Chemical Physics) (in press).

first such observation reported by us[11] over three years ago for 1,4-naphthoquinone (and *p*-benzoquinone[12]), have been theoretically treated.[10] They are attributed to the increase in the probability of autodetachment with increasing electron energy (which increases the compound negative ion's internal energy) due to the increase in the number of final neutral-molecule states to which the unstable compound negative ion can decay. From this theoretical analysis the autodetachment lifetime is calculated[10] to decrease much faster than experimentally measured (see Fig. 7.7).

**Table 7.1. Long-lived parent-negative-ion lifetimes of organic molecules formed via a nuclear-excited Feshbach resonance at thermal energies**

| Molecule | Formula | $\tau$($\mu$sec) |
|---|---|---|
| **A. Benzene derivatives** | | |
| *o*-Nitrotoluene | $o$-$C_6H_4CH_3NO_2$ | 13[a] |
| *m*-Nitrotoluene | $m$-$C_6H_4CH_3NO_2$ | 18.8[a] |
| *p*-Nitrotoluene | $p$-$C_6H_4CH_3NO_2$ | 14[a] |
| *o*-Nitrophenol | $o$-$C_6H_4OHNO_2$ | 460 ± 34[b,c] |
| *m*-Nitrophenol | $m$-$C_6H_4OHNO_2$ | 31 ± 1.3[c] |
| *p*-Nitrophenol | $p$-$C_6H_4OHNO_2$ | 13.9 ± 0.4[c] |
| *o*-Nitroaniline | $o$-$C_6H_4NH_2NO_2$ | 46 ± 2[c] |
| *m*-Nitroaniline | $m$-$C_6H_6NH_2NO_2$ | 21 ± 1[c] |
| *p*-Nitroaniline | $p$-$C_6H_4NH_2NO_2$ | 15 ± 0.8[c] |
| Cinnamaldehyde | $C_6H_5(CH)_2CHO$ | 12[a] |
| **B. Other aromatic molecules** | | |
| 1-Naphthaldehyde | 1-$C_{10}H_7CHO$ | 15 ± 0.5[d] |
| 2-Naphthaldehyde | 2-$C_{10}H_7CHO$ | 7.6 ± 0.3[d] |
| Benzoin | $C_6H_5CH(OH)COC_6H_5$ | 10 ± 0.5[d] |
| Benzil | $C_6H_5COCOC_6H_5$ | ~90[d,e] |
| Quinoline | $C_9H_7N$ | 632 ± 74[d,f] |
| Azulene | | 7 ± 1.5[g] |
| 1,4-Naphthoquinone | | 350[h] |
| **C. Nonaromatic organic molecules** | | |
| Tetracyanoethylene | $C_2(CN)_4$ | ~60[d,i] |
| 2,3-Pentanedione | 2,3-$CH_3CH_2COCOCH_3$ | 7 ± 0.3[d] |
| Acrolein | $CH_2CHCHO$ | 38 ± 3[d] |
| Acetic acid | $CH_3COOH$ | 326 ± 30[d] |
| Adipic acid | $HOOC(CH_2)_4COOH$ | 30 ± 3[d] |
| Malonic acid | $HOOCCH_2COOH$ | >1[d] |
| Hexafluoroacetone | $CF_3COCF_3$ | 60[j] |

[a]L. G. Christophorou, J. G. Carter, E. L. Chaney, and P. M. Collins, paper presented at the IVth International Congress of Radiation Research, Evian, France, June 1970, Gordon and Breach, in press.

[b]The lifetime decreases with electron energy.

[c]A. Hadjiantoniou, L. G. Christophorou, and J. G. Carter, Part I, *Faraday Transactions* (Chemical Physics) (in press).

[d]A. Hadjiantoniou, L. G. Christophorou, and J. G. Carter, Part II, *Faraday Transactions* (Chemical Physics) (in press).

[e]The lifetime decreases with electron energy (see Fig. 7.6).

[f]Measured at the resonance maximum at 0.6 eV; however $\tau$ was not found to change with electron energy.

[g]E. L. Chaney, L. G. Christophorou, P. M. Collins, and J. G. Carter, *J. Chem. Phys.* **52**, 4413 (1970).

[h]P. M. Collins, L. G. Christophorou, E. L. Chaney, and J. G. Carter, *Chem. Phys. Lett.* **4**, 646 (1970).

[i]The lifetime decreases with electron energy (see Fig. 7.5).

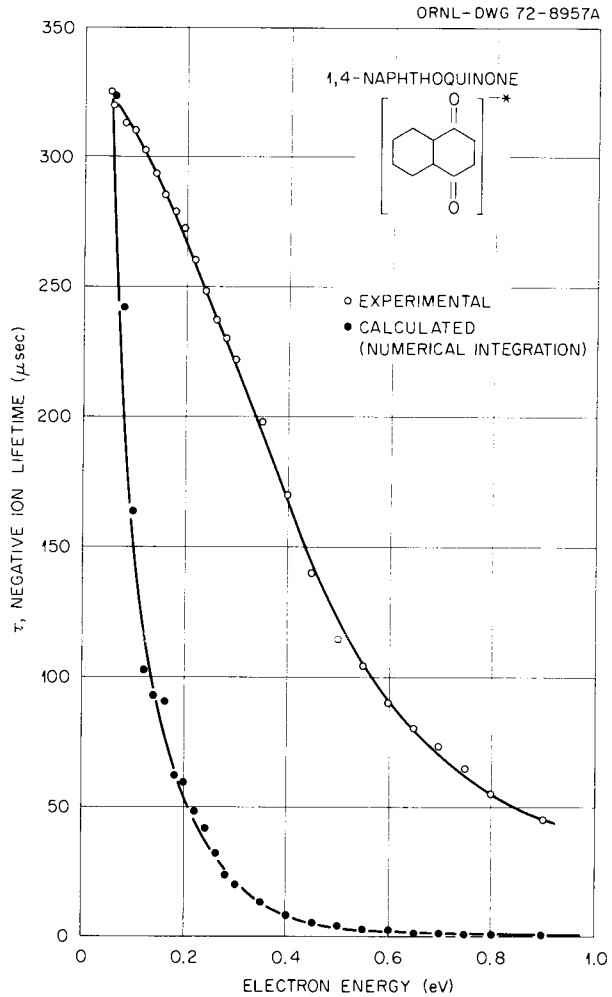


**Fig. 7.7. Experimental and calculated lifetimes for 1,4-$C_{10}H_6O_2^{-*}$ as a function of electron energy normalized at the lowest energy point (see ref. 10).**

11. P. M. Collins, L. G. Christophorou, E. L. Chaney, and J. G. Carter, *Chem. Phys. Lett.* 4, 646 (1970).

12. Collins et al. (ref. 11) have reported that the *p*-benzoquinone long-lived parent negative ion is formed via an electron-excited Feshbach resonance. No other long-lived electron-excited Feshbach resonance besides that of *p*-benzoquinone has yet been reported.

## EXTENSION OF OUR BASIC UNDERSTANDING OF PROCESSES ACCOMPANYING INTERACTION WITH MATTER FROM SIMPLE TO COMPLEX STRUCTURES

As part of our systematic effort to build up step by step our knowledge on electron-molecule interactions in complex molecular structures of radiobiological interest, we investigated[13] the compound-negative-ion resonance (CNIR) states and the threshold electron excitation spectra of the *N*-heterocyclic molecules pyridine, pyridazine, pyrimidine, pyrazine, and *sym*-triazine. Optically forbidden and $n \rightarrow \pi^*$ transitions have been observed. Two CNIR states ("shape" resonances) have been detected below the first excited electronic states of all *N*-heterocyclic molecules studied, except *sym*-triazine, for which only one CNIR state has been observed. The positions of the maxima of these CNIR states are given in Table 7.2. These CNIR states have been discussed[13] in terms of the effect of a perturbation introduced by the more electronegative nitrogen atom(s) in the benzene ring on the two lowest (degenerate) antibonding orbitals of benzene. In view of these results we have extended our investigation to monosubstituted benzene derivatives such as phenol and aniline. Two CNIR states with maxima at 0.61 and 1.67 eV for phenol and 0.55 and 1.88 eV for aniline have been observed, indicating that for these benzene derivatives too, the removal of the degeneracy of the two lowest (degenerate) antibonding orbitals of benzene – due to the perturbation introduced by the substituents – results in two CNIR states.

**Table 7.2. Positions of the maxima of the compound-negative-ion resonances in benzene and the *N*-heterocyclic benzene derivatives**

| Molecule | Peak energies(eV) |
|---|---|
| Benzene | 1.30[a] |
| | 1.40[b] |
| Pyridine | 0.84;[c] 1.30[c] |
| Pyridazine | 0.70;[c] 1.44[c] |
| Pyrimidine | 0.80;[c] 1.90[c] |
| Pyrazine | 1.10;[c] 1.53[c] |
| *sym*-Triazine | 1.54[c] |

[a]H. H. Brongersma, J. A. v.d. Hart, and L. J. Oosterhoff, in *Proceedings of Nobel Symposium 5*, Interscience, New York, 1967, p. 211.

[b]R. N. Compton, L. G. Christophorou, and R. H. Huebner, *Phys. Lett.* **23**, 656 (1966).

[c]Reference 13.

## THRESHOLD ELECTRON EXCITATION AND COMPOUND-NEGATIVE-ION FORMATION IN UNSATURATED HYDROCARBONS

The threshold electron excitation spectra of higher members of linear and branched unsaturated hydrocarbons (e.g., *n*-hexane and neopentane) have been investigated and compared with photoabsorption spectra and energy losses suffered by slow electrons scattered from thin films of these materials.[14] In the case of neopentane, two low-lying peaks at 0.85 and 2.47 eV have been observed and have been attributed to excitation of compound-negative-ion resonant states. This study is a continuation of our earlier work[15] on the lower members of the linear hydrocarbon series (e.g., methane, ethane, etc.).

## ELECTRON ATTACHMENT TO $c$-$C_4F_8$ AND $CCl_2F_2$ BELOW ~2 eV

As part of our investigation of electron attachment processes in polyatomic molecules we studied the perfluorocyclobutane ($c$-$C_4F_8$) and dichlorodifluoromethane ($CCl_2F_2$) molecules.

The variation of $\alpha w$ with mean electron energy $\langle \epsilon \rangle$ for $c$-$C_4F_8$ is shown in Fig. 7.8*A* along with the (thermal) value of $\alpha w$ obtained using the microwave method.[16] In addition to the attachment process at thermal energies, another attachment process exists below 1 eV with a maximum in $\alpha w$ at ~0.3 eV. This latter process has a broad and quite intense cross section. The total attachment cross section has been determined using the swarm unfolding technique[7] and is given in Fig. 7.8*B*.

The attachment rate $\alpha w$ as a function of $\langle \epsilon \rangle$ for $CCl_2F_2$ is shown in Fig. 7.9*A*. The microwave (thermal) value[16] of $\alpha w$ is also shown. In Fig. 7.9*B* the total attachment cross section is also given for 500, 1000, and 1500 iterations using the swarm unfolding method.[7] The agreement seen indicates clearly the convergence of the iterative procedure employed. In the same figure the monoenergetic attachment rate[7] is also shown. The cross sections derived earlier by Blaunstein

13. M. N. Pisanias, L. G. Christophorou, J. G. Carter, and D. L. McCorkle, *J. Chem. Phys.* **58**, 2110 (1973).
14. K. Hiraoka and W. H. Hamill, *J. Chem. Phys.* **57**, 3870 (1972).
15. M. N. Pisanias, L. G. Christophorou, and J. G. Carter, ORNL-TM-3904 (1972).
16. R. W. Fessenden, private communication (1972).

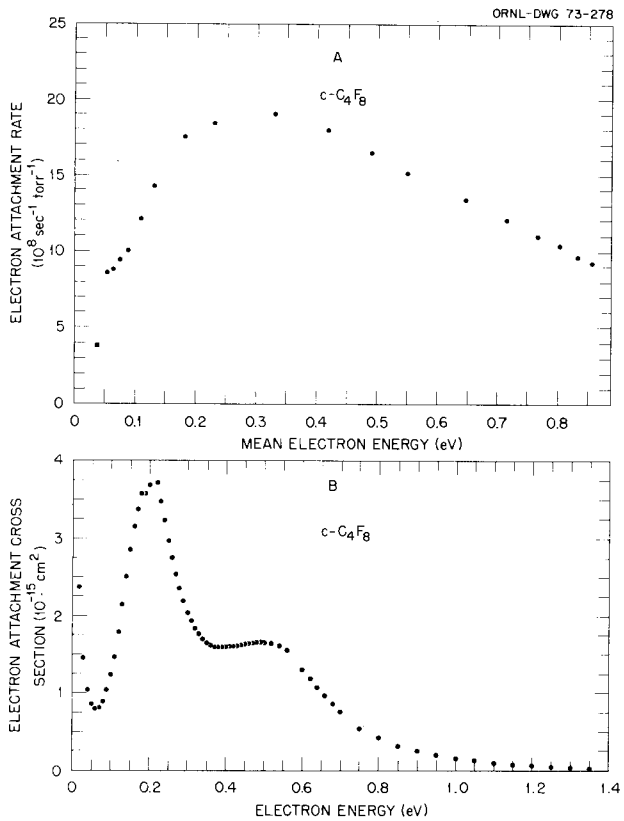


**Fig. 7.8.** Electron attachment for $c$-$C_4F_8$. (*A*) Electron attachment rate as a function of mean electron energy for $c$-$C_4F_8$. (•) Swarm data; (▪) microwave data. (*B*) Electron attachment cross section (total) as a function of electron energy for $c$-$C_4F_8$.

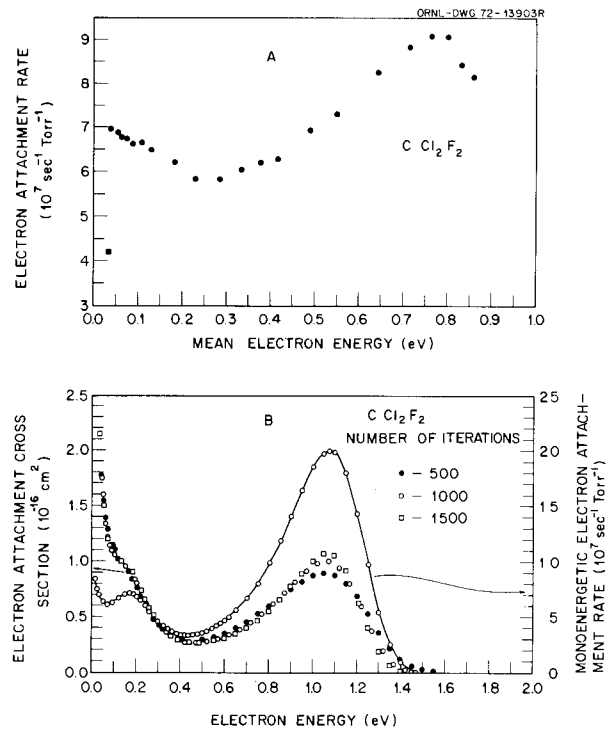


**Fig. 7.9.** Electron attachment for $CCl_2F_2$. (*A*) Electron attachment rate as a function of mean electron energy for $CCl_2F_2$. (•) Swarm data; (▪) microwave data. (*B*) Monoenergetic electron attachment rate as a function of electron energy for 1000 iterations and electron attachment cross section (total) as a function of electron energy for 500, 1000, and 1500 iterations. (L. G. Christophorou, D. L. McCorkle, and D. Pittman, submitted to *J. Chem. Phys.*)

and Christophorou[17] are in agreement with the present data, as are also the recent measurements by Chen and Chantry[18] which show the predominant ion at room temperature to be $Cl^-$.

## COMPARISON OF ELECTRON SWARM AND MICROWAVE MEASUREMENTS OF THE THERMAL RATE OF ELECTRON ATTACHMENT

Various methods for measuring electron attachment to molecules are in use. From these, our electron swarm method – in which the compound under investigation is studied in binary gas mixtures with an abundant carrier gas for which the electron energy distribution as a function of the pressure-reduced field $E/P$ is known – has been proven to be the most useful. This method not only allows measurement of the electron attachment rate as a function of $E/P$, but it also yields this quantity as a function of the mean electron energy. Recently, measurements have been made of the thermal value of the attachment rate for a number of molecules using microwave techniques. Some of these reported values are in agreement with those measured using the swarm method (see, for example, Fig. 7.10), but in some cases they differ appreciably (see, for example, Figs. 7.8 and 7.11). These differences have been investigated, and possible sources of error intrinsic in the microwave method have been indicated.[19]

17. R. P. Blaunstein and L. G. Christophorou, *J. Chem. Phys.* **49**, 1526 (1968).

18. C. L. Chen and P. J. Chantry, *Bull. Amer. Phys. Soc.* **17**, 1133 (1972).

19. L. G. Christophorou, D. L. McCorkle, and D. Pittman, submitted to *J. Chem. Phys.*

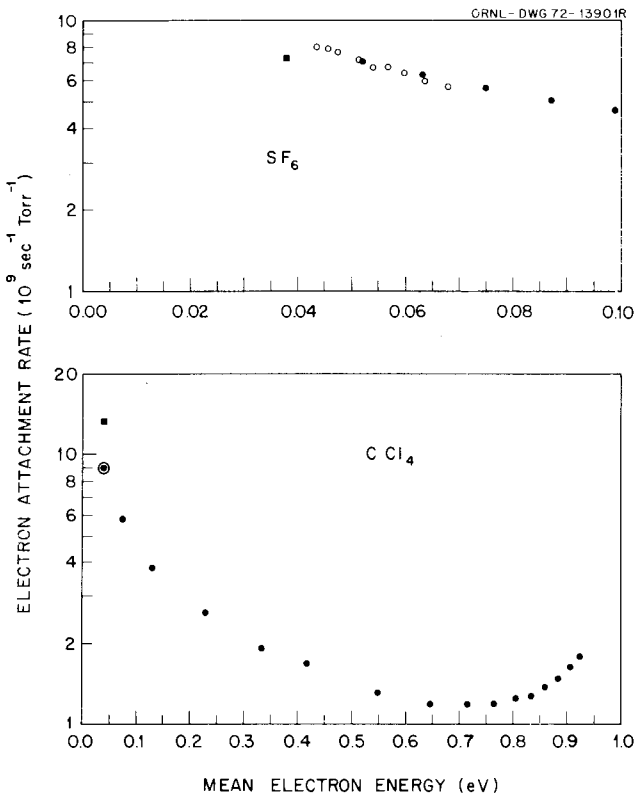


**Fig. 7.10. Electron attachment rate as a function of electron energy for $SF_6$ and $CCl_4$ (see ref. 19).** $SF_6$: (•) swarm data using $N_2$ as a carrier gas; (○) swarm data using $C_2H_4$ as a carrier gas; (▪) microwave data. $CCl_4$: (•) swarm data using $N_2$ as a carrier gas; (○) swarm data using $C_2H_4$, $CO_2$, and $CH_3OH$ as carrier gases; (▪) microwave data.

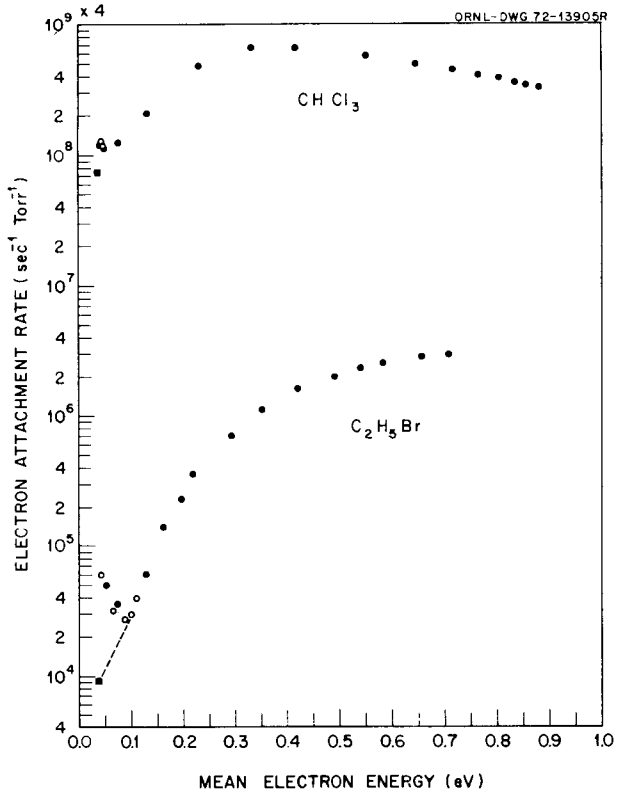


**Fig. 7.11. Electron attachment rate as a function of mean electron energy for $CHCl_3$ and $C_2H_5Br$ (see ref. 19).** $CHCl_3$: (•) swarm data using $N_2$ as a carrier gas; (○) swarm data using $C_2H_4$ as a carrier gas; (▪) microwave data. $C_2H_5Br$: (•) swarm data using $N_2$ as a carrier gas; (○) swarm data using $C_2H_4$ as a carrier gas; (▪) microwave data.

## MOBILITIES OF THERMAL ELECTRONS IN $\pi$-ELECTRON-CONTAINING ORGANIC GASES

The mobility $\mu$ of thermal electrons in molecular gases depends strongly on the magnitude of the molecular permanent electric dipole moment $D$.[20] For $D \rightarrow 0$, $\mu$ decreases with increasing static polarizability $\alpha$.[21] In addition to these macroscopic parameters, distinct microscopic characteristics of the molecular structure are known[20-22] to affect the scattering of slow electrons by molecules, and likewise $\mu$.

To ascertain the effect of induced $\pi$-orbital polarization on the scattering of slow electrons by – and the mobility of thermal electrons in – molecular gases we measured[23] the drift velocity $w$ ($=\mu E$; $E$ is the electric field in volts per centimeter) as a function of the pressure-reduced electric field $E/P$ (in volts per centimeter per torr) for three groups of $\pi$-electron-containing molecules – linear, cyclic, and aromatic hydrocarbons – for which $D$ is zero or very small and $\alpha$ is more or less constant. Table 7.3 summarizes our results and other pertinent quantities: $D$, $\alpha$, number of $\pi$ orbitals, and

$$\mu \left(=\frac{w}{E}=\frac{w}{E/P}\,\frac{1}{P}=S/P\right).$$

The slope $S$ was obtained[23] from a least-squares fit to the linear portion (low $E/P$ region) of the $w$ vs $E/P$ curves.

It is clear from the data presented in Table 7.3 that the scattering of thermal and near-thermal electrons is strongly affected by the number of $\pi$ orbitals contained in each molecule. For the linear hydrocarbons hexane,

20. L. G. Christophorou and A. A. Christodoulides, *J. Phys. B* (At. Mol. Phys.) **2**, 71 (1969).
21. L. G. Christophorou, G. S. Hurst, and A. Hadjiantoniou, *J. Chem. Phys.* **44**, 3506 (1966).
22. W. R. Garrett, *Mol. Phys.* **24**, 465 (1972).
23. L. G. Christophorou, R. P. Blaunstein, and D. Pittman, submitted to *Chem. Phys. Lett.*

**Table 7.3. Electric dipole moment $D$, static polarizability $\alpha$, and thermal electron mobility $\mu$ (=$S/P$; $P$ at 1 torr) for linear, cyclic, and aromatic hydrocarbons**

| Molecule | Formula or structure | $D$ (Debyes) | $\alpha^a$ ($10^{-24}$ cm$^3$) | Number of $\pi$ orbitals | $\mu$ ($10^5$ cm$^2$ V$^{-1}$ sec$^{-1}$) |
|---|---|---|---|---|---|
| | | **Linear hydrocarbons** | | | |
| Hexane | $CH_3(CH_2)_4CH_3$ | $0^b$; $0.05^c$ | 11.8 | 0 | 20.6 |
| 1-Hexene | $CH_3(CH_2)_3CH{=}CH_2$ | $0.4^c$ | | 1 | 10.0 |
| 1,2-Hexadiene | $CH_3CH_2CH_2CH{=}C{=}CH_2$ | | | 2 | 4.1 |
| 1,3-Hexadiene | $CH_3CH_2CH{=}CHCH{=}CH_2$ | | | 2 | 5.1 |
| 2,4-Hexadiene | $CH_3CH{=}CHCH{=}CHCH_3$ | $0.33^c$ | | 2 | 6.9 |
| 1,4-Hexadiene | $CH_3CH{=}CHCH_2CH{=}CH_2$ | | | 2 | 8.4 |
| 1,5-Hexadiene | $CH_2{=}CHCH_2CH_2CH{=}CH_2$ | | | 2 | 9.0 |
| | | **Cyclic nonaromatic hydrocarbons** | | | |
| Cyclohexane | 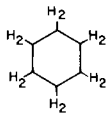 | $0.1^c$ | 10.9 | 0 | 14.7 |
| Cyclohexene | 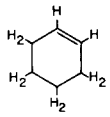 | $0.28^b$ | | 1 | 6.8 |
| 1,4-Cyclohexadiene | 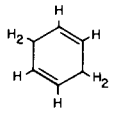 | | | 2 | 5.5 |
| 1,3,5-Cycloheptatriene | 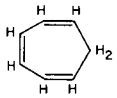 | $0.25^d$ | | 3 | 4.5 |
| | | **Aromatic hydrocarbons** | | | |
| Benzene | | $0^b$ | 10.3 | 3 | 5.2 |
| 1,4-Dimethylbenzene | | $0.04^b$<br>$0.13^c$ | 14.1 | 3 | 5.8 |
| 1,3,5-Trimethylbenzene | 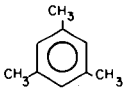 | $0^b$<br>$0.12^c$ | | 3 | 3.9 |
| 1.4-Diethylbenzene | 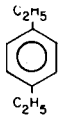 | $0^b$<br>$0.24^c$ | | 3 | 3.4 |
| Naphthalene | 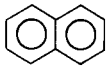 | $0^c$ | | 5 | 3.1 |
| 1,2-Diphenylethylene | 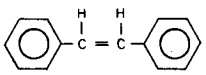 | $0^c$ | | 7 | ~0.9(?) |

[a]H. H. Landolt and R. Börnstein, "Tables of Chemical Data," *Zahlenwerte und Fünktionen,* Springer-Verlag, Berlin, 1951, vol. 1, part 3.

[b]Average of gaseous phase values given in A. L. McClellan, *Tables of Experimental Dipole Moments,* W. H. Freeman and Co., San Francisco, 1963.

[c]Average of values in benzene solutions; ref. *b*.

[d]*Handbook of Chemistry and Physics,* Chemical Rubber Co., 1969.

1-hexene, and 1,2-hexadiene or 1,3-hexadiene with zero, one, and two $\pi$ orbitals, respectively, $\mu$ decreases from 20.6 to 10 to about $5 \times 10^5$ cm$^2$ V$^{-1}$ sec$^{-1}$, and for the cyclic nonaromatic molecules, $\mu$ decreases from 14.7 to 6.8, 5.5, and $4.5 \times 10^5$ cm$^2$ V$^{-1}$ sec$^{-1}$ for molecules with zero, one, two, and three $\pi$ orbitals, respectively, indicating the direct influence of the microscopically induced $\pi$-orbital polarization on $\mu$. For these groups of molecules – especially for the cyclic ones in Table 7.3 – the effect of $\pi$-orbital polarization is not additive. This may suggest that the individual $\pi$-orbital polarization is influenced by that of the rest. It might be noted that for a fixed number of $\pi$ orbitals, some of the observed differences in $\mu$ may arise from small differences in $D$ and/or $\alpha$. It is also interesting to note that the value of $\mu$ for *p*-xylene (1,4-dimethylbenzene) is larger than that for benzene in spite of the fact that the values of $D$ and $\alpha$ for *p*-xylene are somewhat higher than those for benzene. This may indicate that the $CH_3$ groups in *p*-xylene interfere with the polarization of the $\pi$ orbitals and decrease the overall polarization compared with benzene.

The data on the linear hydrocarbons with two $\pi$ orbitals in Table 7.3 suggest that $\mu$ is a strong function of the separation of the two $\pi$ orbitals in the linear molecule; $\mu$ increases monotonically as the two $\pi$ orbitals become further apart. When the two $\pi$ orbitals are separated by four carbon atoms (1,5-hexadiene) the value, $9 \times 10^5$ cm$^2$ V$^{-1}$ sec$^{-1}$, of $\mu$ almost equals that of 1-hexene, $10 \times 10^5$ cm$^2$ V$^{-1}$ sec$^{-1}$, which has only one $\pi$ orbital. This increase in $\mu$ values for the 1,2-, the 1,3-, the 1,4-, and the 1,5-hexadiene molecules probably reflects a decrease in the overall $\pi$-orbital polarization with increasing separation of the two orbitals. The closeness of the values of $\mu$ for 1-hexene with one $\pi$ orbital and 1,5-hexadiene with two $\pi$ orbitals may indicate that when the two $\pi$ orbitals are well separated, the scattering of the impinging electron is influenced predominantly by one rather than by both $\pi$ orbitals.

For a given number of $\pi$ orbitals a comparison of the $\mu$ values for the three groups of molecules – linear, cyclic, and aromatic – in Table 7.3 indicates no profound differences in $\mu$.

It would be desirable to use the data in Table 7.3 to determine directly the scattering cross sections for these molecules at thermal and epithermal energies. There is no straightforward way to do this, mainly because the velocity dependence of the scattering cross section is not known. For elastic electron scattering and a Maxwellian distribution of electron velocities (such a distribution is reasonable to assume, especially for the linear portion of the $w$ vs $E/P$ curves), $\mu$ is related to the momentum transfer cross section $\sigma_m(\mathrm{v})$ by [20,24]

$$\mu = \frac{S}{P} = \frac{w}{E} = \left(\frac{2}{\pi}\right)^{1/2} \frac{e}{3NP} \frac{m^{3/2}}{(kT)^{5/2}} \int_0^\infty \frac{\mathrm{v}^3}{\sigma_m(\mathrm{v})} e^{-m\mathrm{v}^2/2kT}\, d\mathrm{v} . \quad (2)$$

In Eq. (2), $e$, $m$, and v are, respectively, the electron charge, mass, and velocity, $k$ is the Boltzmann constant, $T$ is the absolute temperature, $P$ is the pressure in torrs, $N$ is the number of molecules per cubic centimeter per torr, and the rest of the symbols are as defined earlier. On the basis of Eq. (2), relative changes in $\mu$ reflect relative changes in $\sigma_m$. An estimate of the scattering cross section can be obtained as follows: If we define an average cross section as[21]

$$\langle \sigma_m(\mathrm{v}) \rangle \equiv 4\pi \int_0^\infty \sigma_m(\mathrm{v})\, f_0(\mathrm{v})\, \mathrm{v}^2\, d\mathrm{v} , \quad (3)$$

where $4\pi\, f_0(\mathrm{v})\, \mathrm{v}^2$ is the normalized Maxwellian distribution, we have from Eqs. (2) and (3)

$$\langle \sigma_m(\mathrm{v}) \rangle_{\mathrm{v}} = \left(\frac{2}{m\pi kT}\right)^{1/2} \frac{e}{N} S^{-1} = \frac{3}{8} \langle \sigma_m(\mathrm{v}) \rangle_{\mathrm{v}^2} . \quad (4)$$

The averages $\langle \sigma_m(\mathrm{v}) \rangle_{\mathrm{v}}$ and $\langle \sigma_m(\mathrm{v}) \rangle_{\mathrm{v}^2}$ correspond, respectively, to an $A/\mathrm{v}$ and a $B/\mathrm{v}^2$ expression of $\sigma_m(\mathrm{v})$ ($A$ and $B$ are constants in units of cm$^3$ sec$^{-1}$ and cm$^4$ sec$^{-1}$, respectively), which in turn correspond, respectively, to an $R^{-4}$ and $R^{-2}$ scattering potential ($R$ is the electron-molecule interaction distance). If we use Eq. (4) and the data in Table 7.3, $\langle \sigma_m(\mathrm{v}) \rangle_{\mathrm{v}}$ is found equal to 4.4, 9.4, 11.7, and $14.4 \times 10^{-15}$ cm$^2$ for cyclohexane (zero $\pi$ orbitals), cyclohexene (one $\pi$ orbital), 1,4-cyclohexadiene (two $\pi$ orbitals), and 1,3,5-cycloheptatriene (three $\pi$ orbitals), respectively. Similarly, $\langle \sigma_m(\mathrm{v}) \rangle_{\mathrm{v}}$ increases from $12.5 \times 10^{-15}$ cm$^2$ for benzene to $20.7 \times 10^{-15}$ cm$^2$ for naphthalene. It is thus seen that the scattering cross sections increase with increasing number of $\pi$-electron orbitals and that although for these molecules $D \cong 0$, the scattering cross sections are large. This would indicate that double-bonded systems can effectively thermalize slow electrons, and that this property increases with increasing number of $\pi$ orbitals.

## UNIMOLECULAR DECOMPOSITIONS

Our previous work on the rates of decomposition of excited molecules has been extended to obtain expres-

24. W. P. Allis, *Hand. Phys.* **21**, 413 (1956).

sions for the dispersal of excitation energy among the various possible excited states of the reaction products. We find that, to a very good approximation, this dispersion can be described by a temperature, a straightforward function of the energy to be dissipated, and of the heat capacities of the products. This development makes the calculation of secondary decomposition probabilities especially simple.

This same temperature is expected to govern the kinetic energy distribution of the reaction fragments. We have applied this formalism to experimental measurements of these kinetic energies in order to extract the thermodynamic parameters governing the decomposition.[25] We find a number of decompositions which are nominally forbidden in terms of orbital symmetry selection rules and yet occur quite easily.

## ENERGY TRANSFER FROM ARGON TO XENON ATOMS

Previous studies in this laboratory have focused on energy transfer from excited atoms to atoms or molecules of low ionization potential. This work has implicated the dipole-dipole energy transfer mechanism as the origin of the well-known Jesse effect in irradiated gaseous mixtures. One outstanding anomaly is the much larger Jesse effect which occurs when xenon, rather than krypton, is added to argon. The origin of this anomaly has now been identified. Upon photoexcitation of argon to either of its resonance states, the reaction

$$Ar^* + Xe \rightarrow Ar + Xe^*$$

occurs, followed by a Hornbeck-Molnar reaction:

$$Xe^* + Xe \rightarrow Xe_2^+ + e\,.$$

The first step is of much interest. It is one of the few examples known of nonresonant energy transfer. Because excited states of xenon exist with energies within $kT$ of the excited argon state, the energy transfer occurs rapidly over large distances. The Hornbeck-Molnar reaction, meanwhile, is already known to proceed rapidly.

## EMISSION FROM THE FIRST AND SECOND EXCITED $\pi$-SINGLET STATES OF AROMATIC HYDROCARBONS IN SOLUTION AND THEIR TEMPERATURE DEPENDENCES

Detailed studies have been made[26] of the temperature dependence of the fluorescence emission from dilute deoxygenated *n*-heptane solutions of the aromatic hydrocarbons 1,12-benzperylene, 3,4-benzpyrene, 1,2-benzanthracene, 2′-methyl-1,2-benzanthracene, 7-methyl-1,2-benzanthracene, 3,4-benzotetraphene, and 3-methylpyrene, for which the energy separation $E_{S_{2,0}} - E_{S_{1,0}}$ between the first $S_1$ and second $S_2$ excited $\pi$-singlet states lies in the range 1200 to 2500 $cm^{-1}$. In all cases, fluorescence emission from $S_2$ to the ground state $S_{0,n}$ has been clearly observed. A new example is shown in Fig. 7.12. For a given molecule, the ratio of the integrated fluorescence intensity from $S_2$ to that from $S_1$ increases with increasing temperature; for the group of molecules studied, this ratio decreases – approximately exponentially – with increasing $E_{S_{2,0}} - E_{S_{1,0}}$. The experimental results indicated that (1) the $S_2$ fluorescence is primarily a result of thermal repopulation of $S_2$ from $S_1$ and (2) the $S_2$ fluorescence is quite important – especially at elevated temperatures – for aromatic molecules which have close-lying first and second excited $\pi$-singlet states. Furthermore, a model based on a two-electronic-level scheme describes the radiative and nonradiative deactivation processes from $S_2$ and $S_1$ reasonably well. On the basis of this model it was found that (1) the activation energy for the thermal repopulation of $S_2$ from $S_1$ is a factor of 2 to 3 times less than the actual $E_{S_{2,0}} - E_{S_{1,0}}$ energy separation, (2) the apparent lifetimes of $S_2$ are shorter – at 20°C by a factor of 10 to 50, depending on the molecule – than the radiative lifetimes of $S_2$ calculated from the absorption spectra; for a given molecule they increase with increasing temperature, and for the group of molecules studied they decrease with increasing $E_{S_{2,0}} - E_{S_{1,0}}$; and (3) the rate constants for nonradiative deactivation of $S_2$ to $S_1$ are about $10^{10}$ to $10^{11}$ $sec^{-1}$, that is, relatively small compared with earlier estimates of about $10^{12}$ to $10^{13}$ $sec^{-1}$.

25. C. E. Klots, *J. Chem. Phys.* (in press).
26. C. E. Easterly, L. G. Christophorou, and J. G. Carter, *Faraday Trans. II* (Chem. Phys.) **69**, 471 (1973).

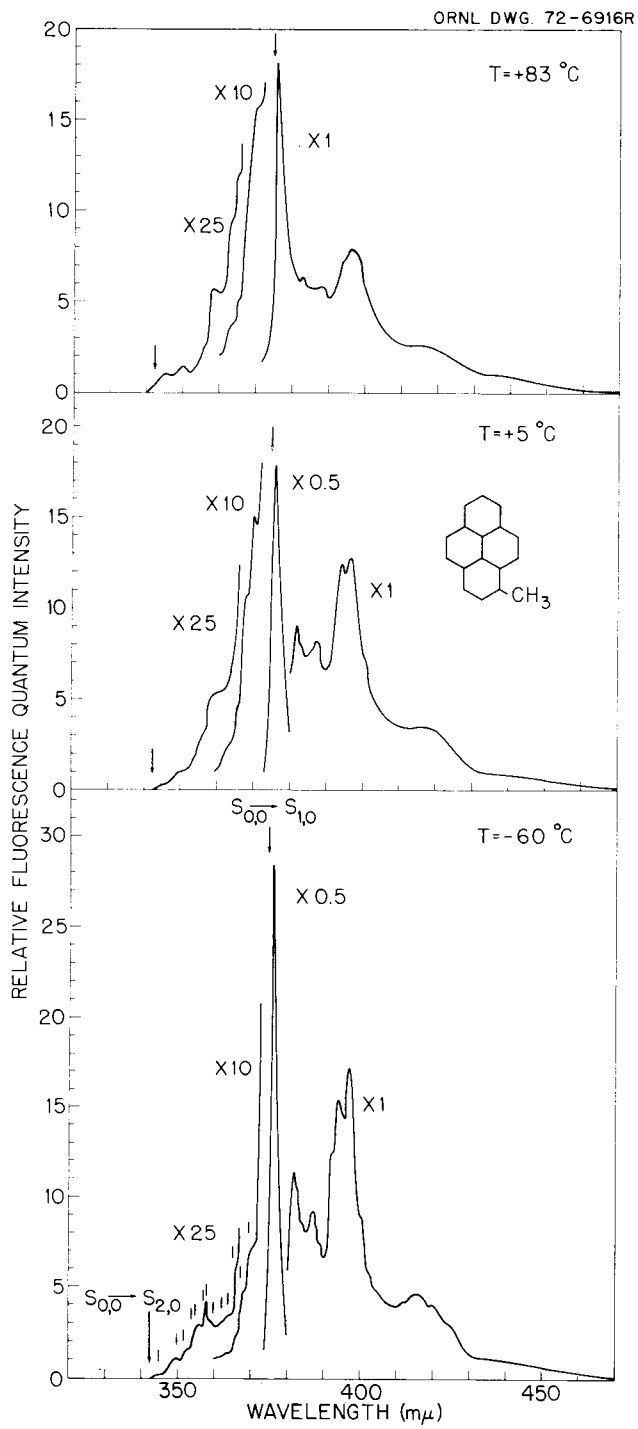


**Fig. 7.12.** The relative fluorescence quantum intensities as a function of wavelength, λ, for a $5 \times 10^{-6}$ *M* solution of 3-methylpyrene in *n*-heptane at −60, +5, and +83°C. The exciting light is the 2804-Å Hg line.

# 8. Interaction of Radiation with Liquids and Solids

E. T. Arakawa
R. D. Birkhoff[1]

A. J. Braundmeier, Jr.[2]
T. A. Callcott[2]
W. T. Cochran[3]
L. C. Emerson
R. A. MacRae[2]
Linda R. Painter[2]
I-Lan Tang[3]
C. E. Wheeler, Jr.[3]
Mary W. Williams

## PHOTON–SURFACE-PLASMON COUPLING IN THIN FILMS

In the last few years studies of surfaces have revealed electronic energy states unique to a surface, which are generated by the passage of ionizing radiation through or near the surface. It is known that volume plasmons (quantized collective electronic oscillations) are created in bulk material, and these have been studied extensively in previous years. This year, however, the emphasis has been on the investigation of surface plasmons since it is thought that these may be important in macromolecules such as DNA.

Surface plasmons are collective oscillations of electrons in solids or liquids which propagate as polarization waves along the surface of the medium. The basic problem in exciting surface plasmons by light consists in matching the phase velocity of the photons in the medium to that of the surface plasmons. This can be achieved by reducing the incident light's phase velocity by passing it through a material whose index of refraction is greater than unity, so that its phase velocity along the surface matches that of the surface plasmon and coupling can occur. The experimental arrangement is shown schematically in Fig. 8.1. A thin metal film is deposited by vacuum evaporation on the plane surface of a transparent semicylinder. Monochromatic light, incident through the semicylinder, is reflected at the semicylinder-metal interface and the reflectance measured as a function of angle of incidence. Figure 8.1 shows typical results of reflectance as a function of angle of incidence – in this case for a 15-nm aluminum film on a quartz semicylinder and for light of wavelength 550 nm and polarized in the plane of incidence. The dashed curve shows the reflectance of

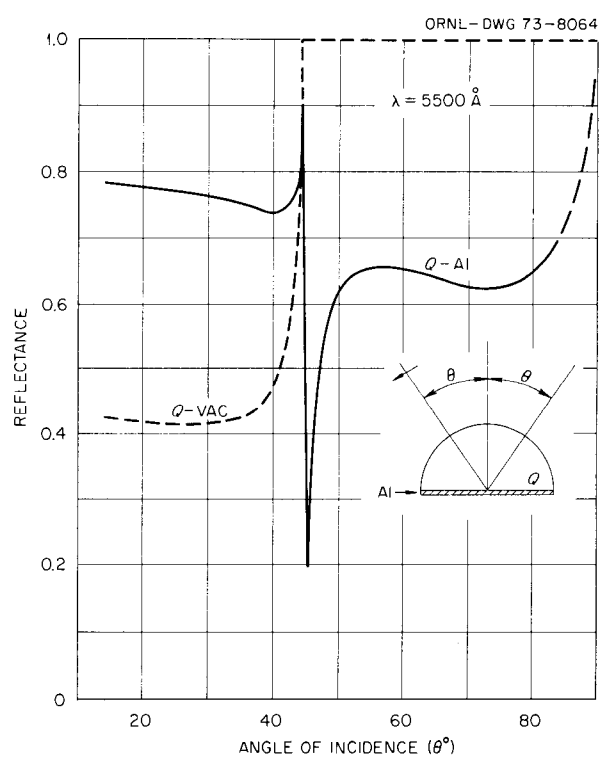


**Fig. 8.1. Reflectance vs photon angle of incidence at a quartz-aluminum interface.**

1. Also Chief of Fundamental Health Physics Research Section.
2. Consultant.
3. Graduate student.

the quartz-vacuum interface with no film present. There is a critical angle at 43°. However, with the film present (the solid curve) there is a marked difference. At an angle just greater than the critical angle for total internal reflection of the semicylinder, a very sharp minimum is seen in the reflectance. At this angle the photons refracted along the semicylinder-metal interface can excite surface plasmons associated with the metal-vacuum surface. Since no light is transmitted through the film for angles greater than the quartz critical angle, it is clear that the dip in reflectance represents a large increase in absorbance. This is a dramatic illustration of the excitation of surface plasmons.

### Measurement of Optical Constants

In the experimental arrangement described above, the classical Fresnel equations for reflectance predict the observed reflectance dip when the appropriate optical constants and thickness of metal film are used. Thus, reflectance as a function of angle of incidence may be used to determine the optical constants of the metal film. This method has been used to obtain the optical constants of silver. For a fixed wavelength, the reflectance vs angle of incidence curve was fitted by least squares to the theory, with the optical constants $n$ and $k$ of the metal as the two adjustable parameters. The sharp structure observed in reflectance makes this a sensitive method for determining $n$ and $k$. The optical constants obtained by this method are shown in Fig. 8.2 compared with values obtained by Huebner et al.[4] and Dujardin and Theye.[5]

### Dispersion Curves

The position of the minimum in reflectance yields the value of the surface plasmon wave vector for a given incident photon energy. Thus a surface plasmon dispersion curve of wave vector vs energy can be constructed directly from the position of the minima for different wavelengths. For small wave vectors we have observed dispersion curves as a function of the roughness of the metal-vacuum surface and find that the wave vector of a surface plasmon propagating on an irregular surface is greater than that for an equally energetic surface plasmon propagating on a planar surface. Dispersion curves for silver for different surface roughnesses are shown in Fig. 8.3. Silver was evaporated onto the plane

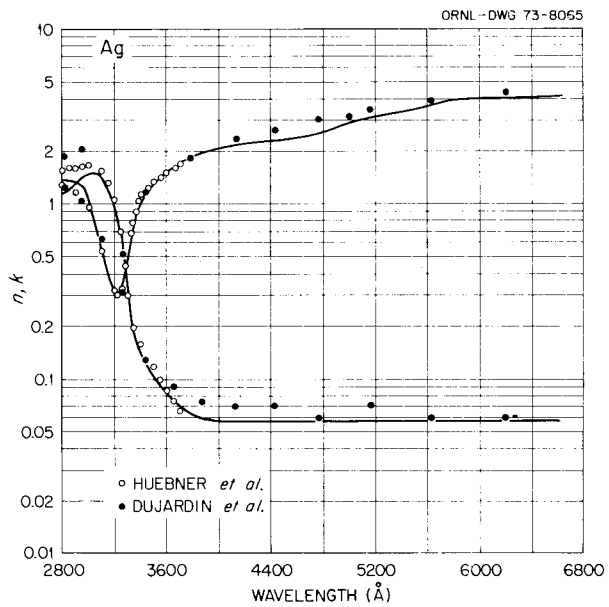


**Fig. 8.2. Optical properties of silver vs wavelength.**

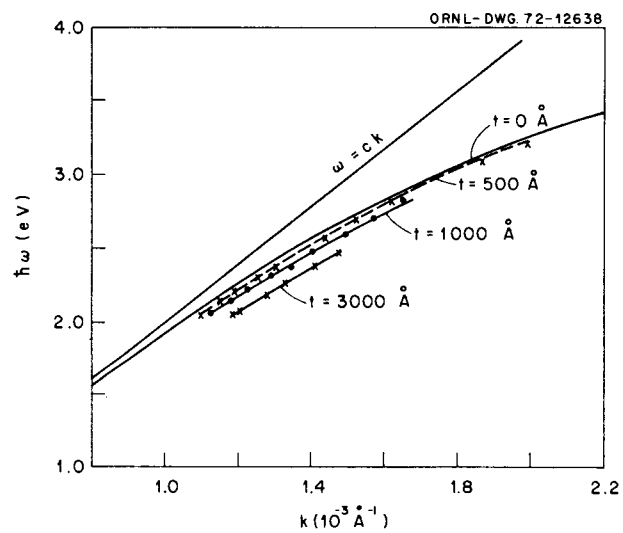


**Fig. 8.3. Surface plasmon dispersion curves for 300-Å-thick silver films of various roughness; the thickness of the $CaF_2$ layer is indicated beside each curve.** The curve labeled $t = 0$ is the measured dispersion curve for a smooth surface while the other curves are smooth fits to the experimental data from roughened surfaces.

surface of a quartz semicylinder which could be artifically roughened by depositing thin layers of $CaF_2$ on its surface. Although the absolute root mean square surface roughness is not known, it is known that increasing the thickness of $CaF_2$ increases the root mean square surface roughness height of the metal surface. The dispersion curves are labeled in terms of

4. R. H. Huebner, E. T. Arakawa, R. A. MacRae, and R. N. Hamm, *J. Opt. Soc. Amer.* **54**, 1434 (1964).

5. M. M. Dujardin and M. L. Theye, *J. Phys. Chem. Solids* **32**, 2033 (1971).

the thickness (0, 500, 1000, and 3000 Å) of the $CaF_2$ causing the surface roughness. These curves could not be extended to higher energies than shown because the reflectance minimum became poorly defined or nonexistent. They show that for a constant energy, increasing the roughness tends to enhance the excitation of plasmons which have larger wave vectors, that is, smaller phase velocities, and thus the asymptotic value of the surface plasmon energy also decreases. This latter effect is apparent from the following. It is seen from the dispersion relation for surface plasmons[6] $k = (\omega/c)[\epsilon_1/(\epsilon_1 + 1)]^{1/2}$ that $k \to \infty$ when $\epsilon_1 \to -1$. Thus, for a Drude-type metal with $\epsilon_1 = 1 - E_p{}^2/(E^2 + \gamma^2)$, where $E_p$ is the plasmon energy and $\gamma$ is the damping constant, the surface plasmon energy $E_s$ is given by

$$E_s = \left(\frac{1}{2}E_p{}^2 - \gamma^2\right)^{1/2},$$

for $\epsilon_1 = -1$. Therefore the surface plasmon energy is decreased if $\gamma$ is increased for whatever reason, as by surface roughness in this study.

### Photoelectric Yield

At the angular position of the dip in the reflectance it is observed that there is a maximum in the photoelectric yield from the metal-vacuum surface. This shows that at this angle the absorbed energy is concentrated along the metal-vacuum surface in the production of surface plasmons, which then can decay into single electron excitations which show up experimentally as an increase in photoelectric yield. This form of surface plasmon decay has been seen in magnesium and is reported in the next section of this report. Typical photoelectric yield data confirming this hypothesis for aluminum are shown in Fig. 8.4 for a thin film of aluminum on $MgF_2$.

## OPTICAL AND PHOTOELECTRIC PROPERTIES OF MAGNESIUM IN THE VACUUM ULTRAVIOLET

Recently there has been both experimental and theoretical interest in roughness-aided photon–surface-plasmon coupling in metallic surfaces and in the subsequent decay of the resulting "nonradiative" surface plasmons. Experimentally, roughness-aided photon–surface-plasmon coupling shows up as a decrease in reflectance at energies close to the nonradiative surface plasmon energy. A general theory due to Elson and Ritchie[7,8] gives a decrease in reflectance

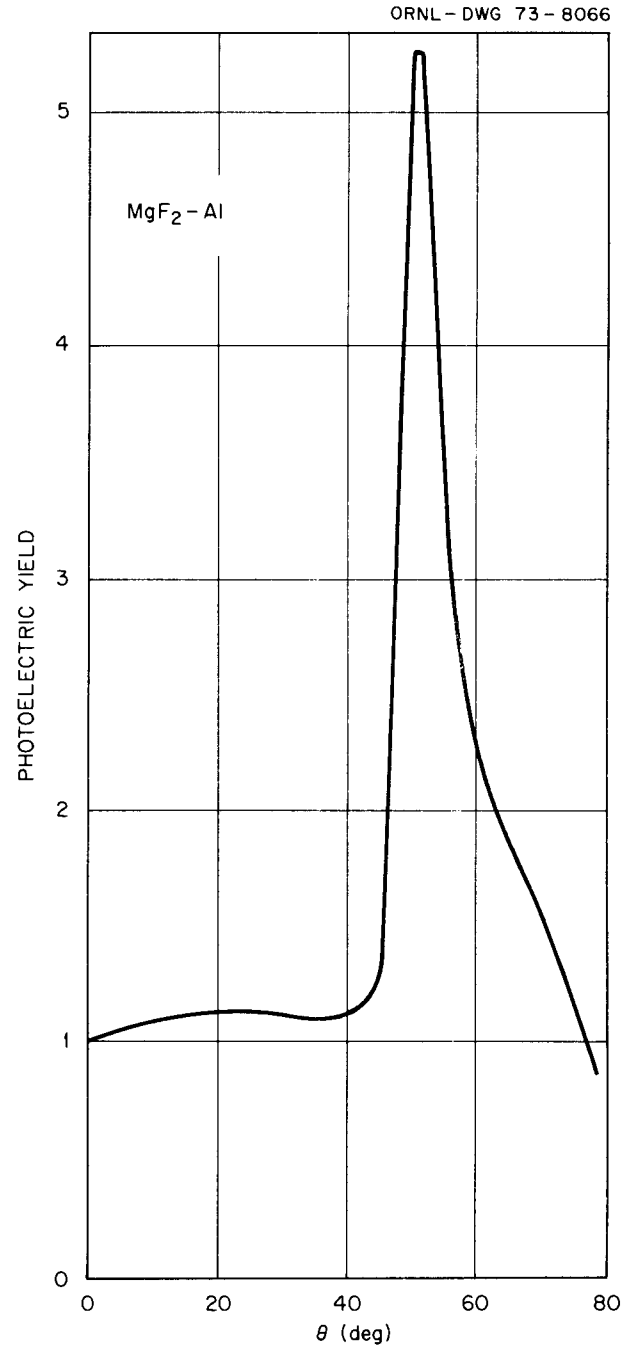


**Fig. 8.4. Photoelectric yield vs photon angle of incidence for a 220-Å-thick aluminum film on a $MgF_2$ semicylinder.** The photon wavelength was 2700 Å.

6. A. Otto, *Z. Physik* **224**, 65 (1969); A. Otto, *Phys. Status Solidi* **42**, K37 (1970).

7. J. M. Elson and R. H. Ritchie, *Phys. Lett.* **33A**, 255 (1970); *Phys. Rev.* **B4**, 4129 (1971).

8. J. M. Elson and R. H. Ritchie, to be published.

(due not only to surface plasmon excitation but also to scattering by the rough surface) that is in good agreement with the experimental data. This enables us to determine the surface roughness parameters, root mean square surface roughness height $\delta$ and autocorrelation length $\sigma$ (approximately the width of a "bump"), for each surface. The surface plasmon decay may then manifest itself as photon emission at the surface plasmon energy or, if the surface plasmon energy exceeds the work function of the metal, as an increase in photoelectric yield at this incident photon energy.

Near-normal-incidence reflectance measurements in the region 2 eV $\leqslant h\nu \leqslant$ 12 eV on five representative films deposited on a "super smooth" quartz substrate are shown in Figs. 8.5 and 8.6. The absolute values of reflectance for each film were obtained to within 2%, while the accuracy associated with the relative values was better, as indicated by the scatter of the experimental points. The films designated A, B, and D were about 450 Å thick while films C and E were about 1000 Å thick. All of the films were essentially of infinite thickness except near the plasma energy (~10.5 eV) where magnesium becomes transparent. In this region the thinner films exhibit anomalously high reflectances due to reflection from the substrate. The dashed line in Fig. 8.5 represents the measurements of Daudé et al.,[9] taken at 20° angle of incidence on ~2000-Å-thick films. The solid line is the reflectance

$$R_{\mathrm{Drude}} = \left| \frac{\sqrt{\epsilon - 1}}{\sqrt{\epsilon + 1}} \right|^2$$

calculated assuming a Drude model for a nearly free-electron metal with

$$\epsilon = \epsilon_1 + i\epsilon_2 = 1 - \frac{\omega_p^{\,2}}{\omega^2 + \gamma^2} + \frac{i\gamma}{\omega} \frac{\omega_p^{\,2}}{\omega^2 + \gamma^2} ,$$

where the plasma energy $\hbar\omega_p$ was set equal to 10.5 eV and the damping term $\hbar\gamma$ to 0.4 eV. It is apparent from Figs. 8.5 and 8.6 that magnesium exhibits the reflectance characteristics of a free-electron metal with slight damping except for the region from 6 to 8 eV. A prominent dip in the reflectance in this region is evident in our data and in the data of Daudé et al. In both cases

9. A. Daudé, M. Priol, and S. Robin, *C. R. Acad. Sc. Paris* **264**, 1489 (1967).

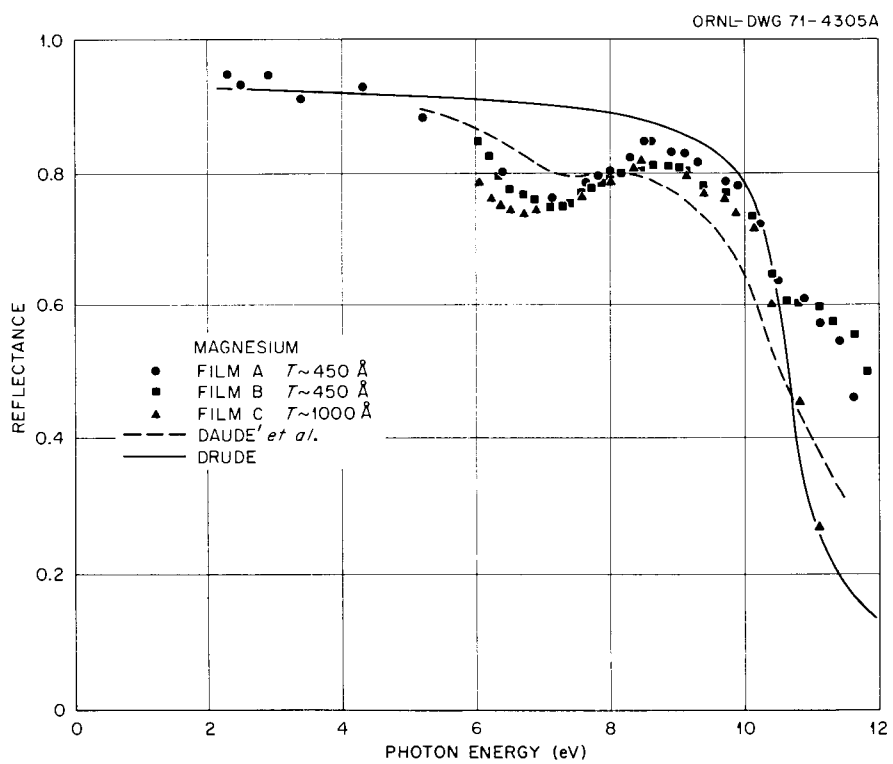


**Fig. 8.5. Near-normal-incidence reflectance of magnesium in the 2-to-12-eV range.**

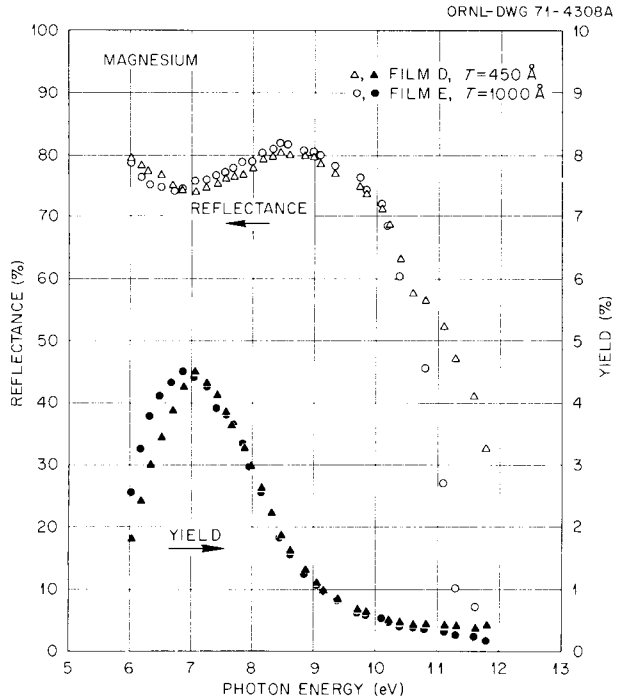


**Fig. 8.6. Simultaneously measured yield and reflectance data for magnesium.**

this dip is outside the limits of experimental scatter, and occurs at an energy near the surface plasmon energy for magnesium (7.1 eV).

Using the theories of Elson and Ritchie we calculated the reflectance from

$$R = R_{\mathrm{Drude}}\, e^{-(P'_{\mathrm{sp}} + P_{\mathrm{scat}})}, \qquad (1)$$

where $P'_{\mathrm{sp}}$, the probability that a photon incident on a rough metallic surface will create a surface plasmon, is in terms (refs. 7 and 8) of a damping term $\hbar\gamma'$ which includes the effects of all surface plasmon damping processes and $P_{\mathrm{scat}}$ is the probability for scattering out of the specular beam. Figure 8.7 gives measured reflectances for the five films, replotted from Figs. 8.5 and 8.6, and our best fitting values for $R$ calculated from Eq. (1). The energy at which the difference between the measured reflectance and $R_{\mathrm{Drude}}$, $\Delta R$, is a maximum was found to be sensitive to $\sigma$ but not to the other parameters. Hence values for $\sigma$ were obtained for each of the five films by fitting the minima in the observed reflectance curves. Holding these values of $\sigma$ constant, all of the curves could be fitted with $\hbar\gamma$=0.4 eV. With $\hbar\gamma$ and $\sigma$ fixed for each film, the width of the surface plasmon absorption is determined mainly by $\hbar\gamma'$, and the maximum value of $\Delta R$ mainly by $\delta$.

**Table 8.1. Table showing the autocorrelation length $\sigma$ and root mean square roughness $\delta$ for each of the films, as used in the fits for the reflectance shown in Fig. 8.7**

| Film | Thickness (Å) | Energy for $\Delta R$ = max (eV) | $\sigma$ (Å) | $\delta$ (Å) |
|---|---|---|---|---|
| B | ~450 | 7.35 | 160 | 29 |
| A | ~450 | 7.25 | 180 | 27 |
| D | ~450 | 7.1 | 275 | 36 |
| C | ~1000 | 6.9 | 375 | 45 |
| E | ~1000 | 6.7 | 475 | 49 |

Examination of the widths at half maximum of the surface plasmon absorption placed $\hbar\gamma'$ in the range 1.9 to 2.3 eV. For each of the films in Fig. 8.7 the measured reflectances are compared with $R$ calculated from Eq. (1) for $\hbar\omega_p$ = 10.5 eV, $\hbar\gamma$ = 0.4 eV, $\hbar\gamma'$=1.9, 2.1, and 2.3 eV, $\sigma$ as determined from the energy at which $\Delta R$ is a maximum, and a value of $\delta$ which best fits the magnitude of $\Delta R$ at its maximum. The constants associated with each film, and used to calculate the values of $R$ shown in Fig. 8.7, are given in Table 8.1. Also shown in Fig. 8.7 for film D, besides the curve for $\hbar\gamma'$ = 2.1 eV and $\delta$ = 36 Å, are curves for $\hbar\gamma'$ = 2.1 eV and $\delta$ = 34 and 38 Å. The data in Fig. 8.7 indicate that, in general, as the film thickness is increased, both $\delta$ and $\sigma$ increase while the peak position of $\Delta R$ decreases in energy. Figure 8.8 shows that within the accuracy of these measurements and the fitting procedure used, there is a linear relation between $\delta$ and $\sigma$.

Simultaneous measurements of quantum yield and reflectance are presented in Fig. 8.6 for films D and E. It is seen that the yield exhibits a strong maximum at an energy very close to that at which the reflectance drop due to nonradiative surface plasmon excitation is a maximum. Calculations based on the equation given by Berglund and Spicer[10] for photoemission of unscattered electrons from a semi-infinite isotropic photoemitter excited by normally incident photons fails to account for the magnitude of this peak in the photoelectric yield. For 7-eV photons the predicted yield per incident photon, calculated using the optical constants of magnesium presented by Daudé et al.[9] and the electron attenuation length predicted by Ritchie and Ashley,[11] is only 0.3% whereas the experimental yield

10. C. N. Berglund and W. E. Spicer, *Phys. Rev.* **A136**, 1030 (1964).

11. R. H. Ritchie and J. C. Ashley, *J. Phys. Chem. Solids* **26**, 1689 (1965).

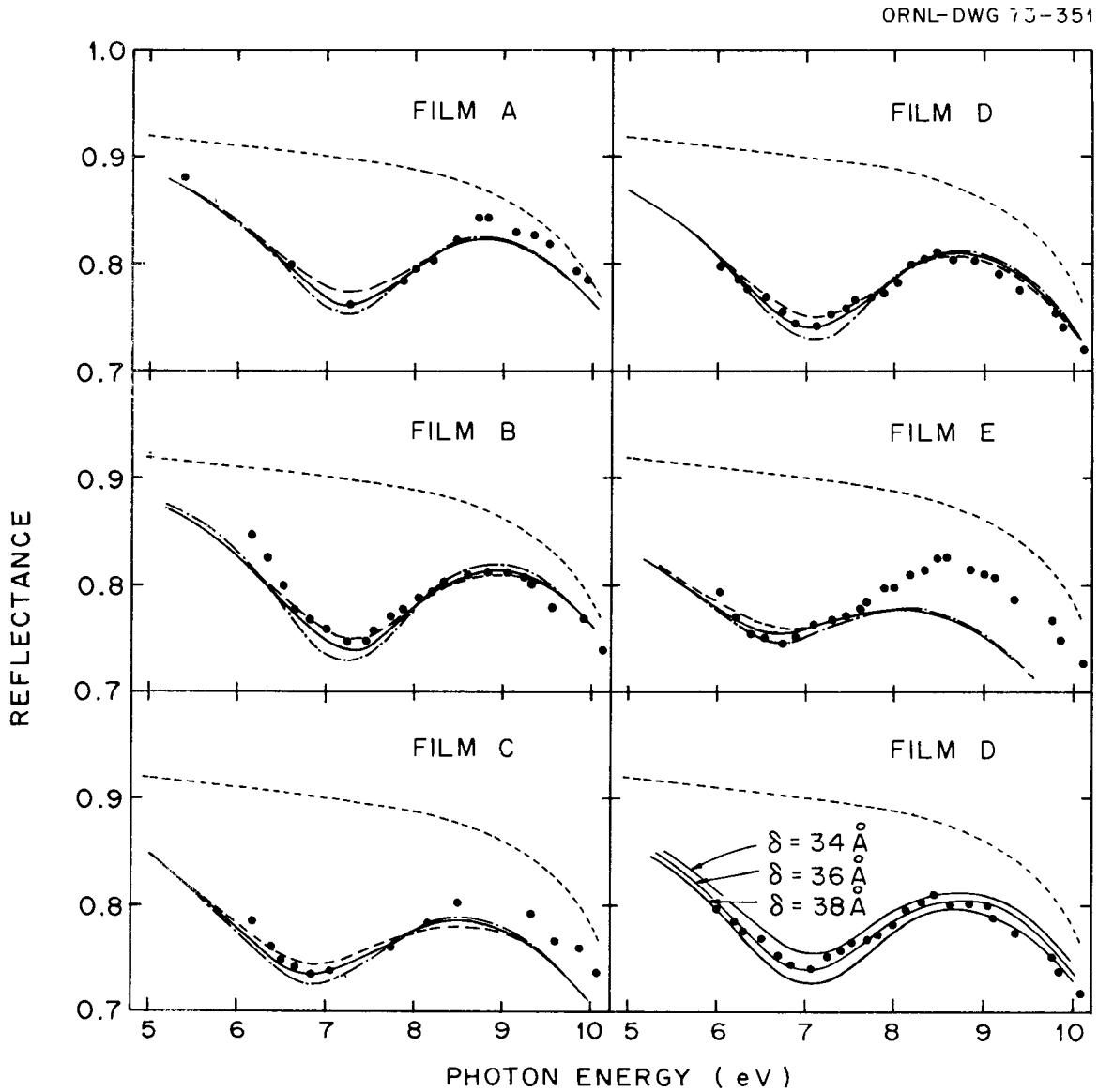


**Fig. 8.7. Experimental reflectance of magnesium for the five films of Figs. 8.5 and 8.6 together with theoretical fits to each.** Experimental, •; Drude reflectance calculated for $\hbar\omega_p$ = 10.5 eV and $\hbar\gamma$ = 0.4 eV, ----; theoretical fits for $\hbar\gamma'$ = 1.9 eV, –.–.–., $\hbar\gamma'$ = 2.1 eV, ———, and $\hbar\gamma'$ = 2.3 eV, – – –; and values of $\sigma$ and $\delta$ as given in Table 8.1 substituted into Eq. (1).

is 4.5%. We conclude that the large peak in the yield near 7 eV is due to the decay of nonradiative surface plasmons by one-electron excitations into observable electrons. Thus it appears that nonradiative surface plasmons can be several times more efficient than photons in creating external electrons. Similar results have been found for aluminum.[12]

12. J. G. Endriz and W. E. Spicer, *Phys. Rev.* **B4**, 4159 (1971).

## OPTICAL PROPERTIES AND ELECTRON ATTENUATION LENGTHS FROM PHOTOELECTRIC YIELD MEASUREMENTS

The variation with energy of the optical functions of a medium and of the attenuation length of photoexcited electrons can yield information about the electronic states and scattering processes, respectively, within the medium. We have developed a method of obtaining optical constants and/or electron attenuation lengths from photoelectric yield measurements which,

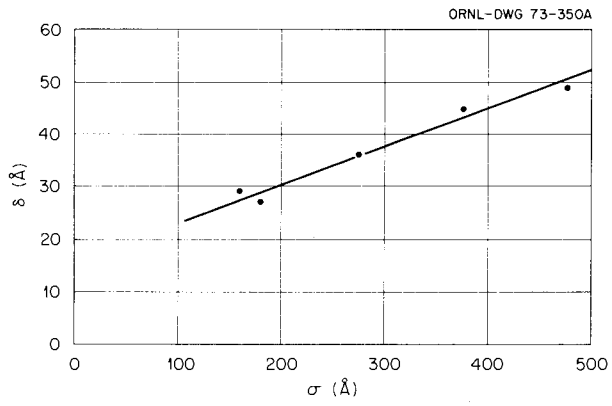


**Fig. 8.8. Experimental variation of $\delta$, the root mean square roughness height, with $\sigma$, the autocorrelation length.**

in certain energy regions, may enable us to obtain more accurate values of these quantities than can be obtained by other methods.

In the vacuum ultraviolet, optical constants of solids and liquids have usually been obtained from reflectance measurements, either by fitting the reflectance vs angle of incidence to Fresnel's equations or by performing a Kramers-Kronig analysis of normal-incidence reflectance. Frequently, however, there are difficulties associated with the accurate determination of optical constants by this technique. For weakly absorbing media which have refractive indices less than unity, we developed previously a more sensitive method based on the measurement of the critical angle.[13] In addition, absorption coefficients can be determined from transmission measurements. Conventionally, electron attenuation lengths are determined from electron transmission measurements through thin films. However, when electron attenuation lengths are short it is difficult to prepare sufficiently thin homogeneous films for these thin-film measurements. Also, when high-energy electrons interact with a solid, the points of origin and energies of secondary electrons are not well defined, and it is difficult to extract a meaningful electron attenuation length from such measurements. The method currently developed for obtaining optical constants and electron attenuation lengths avoids these difficulties. In many ways, photoelectric yield measurements are easier and more straightforward to make than are reflectance measurements. Thick films of the solid under investigation are used, avoiding the problems associated with making very thin homogeneous films. Photons of energy $h\nu$ incident on the solid and attenuated exponentially with distance into the solid generate electrons each with energy $h\nu$. Furthermore, the quantity analyzed is the photoelectric yield as a function of the photon angle of incidence relative to the photoelectric yield for normal incidence, so that absolute measurements are not required. Absolute photoelectric yields are difficult to measure accurately, but relative values are easy to obtain since virtually all photoelectrons emitted in any direction from the photoemitter can be collected if a sufficiently high potential difference is applied.

Pepper[14] has calculated the yield of an arbitrary photoemissive material as a function of the optical constants of the photoemitter and the substrate, the thickness of the photoemitter, the energy, the polarization and angle of incidence of the exciting light, and the attenuation length of the electrons in the photoemitter. Using this theory, Gesell and Arakawa[15] found the average attenuation length $L$ for all electrons photoemitted by 21.2-eV photons to lie in the range $4 \leqslant L \leqslant 12.8$ Å. They used thin aluminum films and found the yield to be sensitive to three parameters: the electron attenuation length $L$, the film thickness $d$, and the refractive index $n$ of the photoemitter.

Recently we have reexamined this method, using films that optically can be considered infinitely thick. Interference effects are eliminated, and the data are independent of $d$ and simpler to interpret. It is found that the photoelectric yield as a function of angle of incidence is a maximum at an angle very close to $\theta_c$ given by $n = \sin \theta_c$ and that the magnitude of the yield at this angle, relative to that for normal incidence, is dependent on $L$ and the extinction coefficient $k$ of the photoemitter.

Figure 8.9 shows typical curves of the relative yield $G(\theta)$ vs $\theta$ calculated for an infinitely thick photoemitter of refractive index $n = 0.9$ and for various values of the extinction coefficient $k$. In each case unpolarized incident light and an electron attenuation length of 10 Å in the photoemitter are assumed. Figure 8.9 shows that the angle at which the relative yield is a maximum is virtually independent of $k$, while the magnitude of the yield at this angle is dependent on $k$. There is a similar dependence of the yield on $L$ for constant $k$. Thus in energy regions where a critical angle is obtained

13. E. T. Arakawa et al., *Health Phys. Div. Annu. Progr. Rep. July 31, 1972*, ORNL-4811, pp. 16–17; U. S. Whang, R. N. Hamm, E. T. Arakawa, and M. W. Williams, *J. Opt. Soc. Amer.* **63**, 305 (1973).

14. S. V. Pepper, *J. Opt. Soc. Amer.* **60**, 805 (1970).

15. E. T. Arakawa et al., *Health Phys. Div. Annu. Progr. Rep. July 31, 1971*, ORNL-4720, pp. 48–50; T. F. Gesell and E. T. Arakawa, *Phys. Rev. Lett.* **26**, 377 (1971).

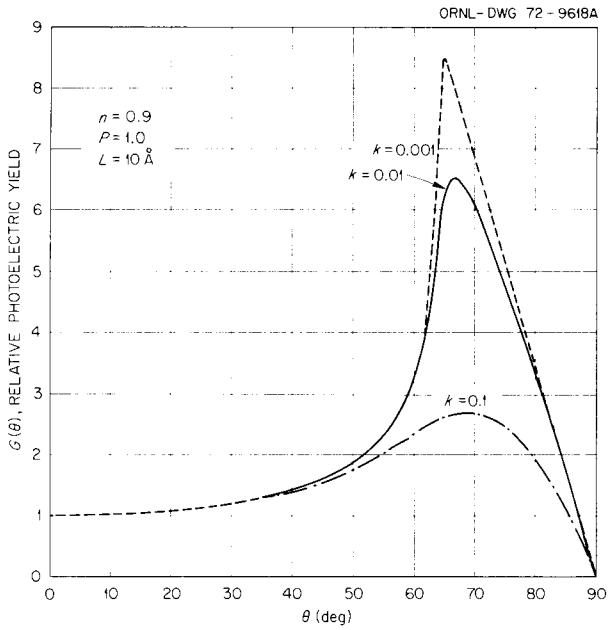


**Fig. 8.9. Calculated relative yield vs angle of incidence for an infinitely thick photoemitter of refractive index 0.90 and extinction coefficients of 0.001, 0.01, and 0.1.** An electron attenuation length in the photoemitter of 10 Å and unpolarized incident light are assumed.

for a photoemitter, $n$ may be obtained from the angle at which the yield is a maximum, and $k$ or $L$ may be obtained from the magnitude of the maximum yield if the other quantity is measured independently. In practice a least-squares fit of the photoelectric yield as a function of photon angle of incidence to the theoretical expression derived from Pepper's equations is made using $n$ and $L$ or $n$ and $k$ as adjustable parameters, depending on whether an independent measurement of $k$ or $L$ is available. It is assumed that the polarization of the incident light is known. If it is not, this introduces an additional parameter.

This method is most sensitive for the determination of optical constants when $n$ is close to, but less than, unity and $k$ and $L$ are small. These are just the conditions under which it is difficult to obtain accurate optical constants from reflectance measurements. However, when $k$ is small accurate values of $k$ can be obtained from transmission measurements, and this method becomes a useful tool for electron attenuation lengths.

## SATELLITES IN THE X-RAY EMISSION SPECTRA OF Li, Be, AND Na

The circumstances and the extent to which plasmons are involved in the production of x-ray satellites has continued to be of interest. Previously we studied[16] the high-energy x-ray satellites of the $L_{2,3}$ emission bands of Na, Mg, Al, and Si. Although the possibility of volume plasmon involvement could not be ruled out completely, the results indicated that the primary contribution to the high-energy satellite for each of these elements came from the radiative decay of a double ionization state, specifically, a double vacancy in the $L_{2,3}$ shell. On the other hand, satellites on the low-energy side of the $L_{2,3}$ emission bands of Na, Mg, and Al have been shown by Rooke[17] to be associated with volume plasmon creation.

In the past year the $K$ x-ray emission spectra of Li and Be and the $L_{2,3}$ x-ray emission spectrum of Na have been recorded. In each case a single low-energy and a single high-energy satellite associated with the main emission bands were observed. For Li the spectrum changed with time after the Li film was vacuum evaporated in situ. The spectrum recorded directly after film deposition is presented in Fig. 8.10 and shows a satellite about 7 eV below the main peak which had never been observed before and which became undetectable as the surface deteriorated with time. The volume plasmon energy in Li is about 7 eV, and this satellite is associated with volume plasmon creation. In

16. E. T. Arakawa et al., *Health Phys. Div. Annu. Progr. Rep. July 31, 1971*, ORNL-4720, pp. 46–47; W. F. Hanson and E. T. Arakawa, *Z. Physik* **251**, 271 (1972).
17. G. A. Rooke, *Phys. Lett.* **3**, 234 (1963).

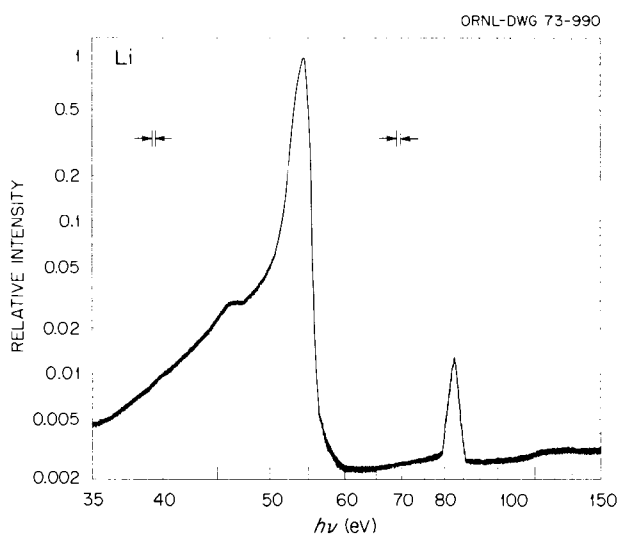


**Fig. 8.10. Recorder trace of $K$-emission spectrum of lithium taken less than 2 min after film deposition.** The electron energy was 2.5 keV, electron beam current 4.8 mA, and the chamber pressure $3 \times 10^{-7}$ torr. The slit width was 200 $\mu$, and the spectral slit width in electron volts is shown in the figure.

filling a vacancy in the Li $K$ shell the deexcitation energy is shared between a photon which is seen in the low-energy satellite and a volume plasmon which is created in the material. Similarly, low-energy satellites are seen about 18.5 eV below the main $K$ emission in Be (Fig. 8.11) and about 5.5 eV below the main $L_{2,3}$ emission in Na (Fig. 8.12). Both of these low-energy satellites are associated with volume plasmon creation. The high-energy satellites seen in Figs. 8.10–8.12 occur ~28.5, ~34.5, and ~11.3 eV above the main emissions in Li, Be, and Na, respectively. The origin of these satellites is of great interest. It is theoretically possible in filling a vacancy in a core level that the deexcitation energy may be augmented by the volume plasmon energy if a volume plasmon has been created in the vicinity of the excited atom to give a high-energy satellite. The observed energy separations of the high-energy x-ray satellites of Li, Be, and Na are not consistent with this type of volume plasmon involvement. However, the observed energy separations are consistent with values calculated from theories of double ionization decay of the relevant core levels.

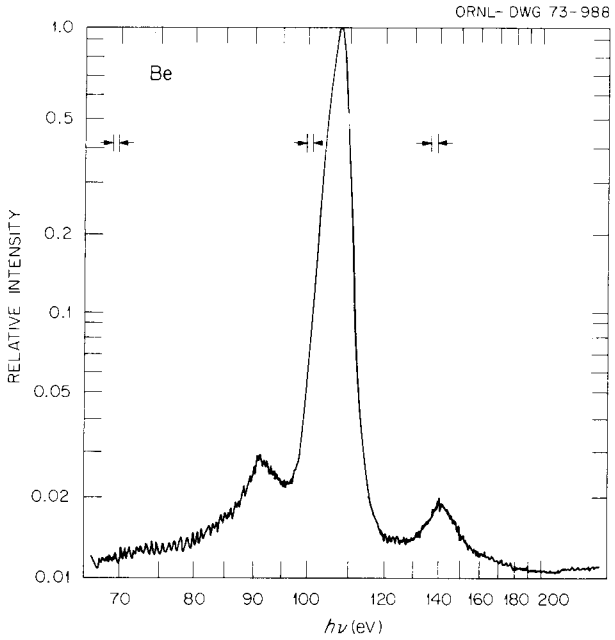


**Fig. 8.11. Recorder trace of $K$-emission spectrum of beryllium.** The electron energy was 2 keV, electron beam current 4.6 mA, and the chamber pressure $5 \times 10^{-7}$ torr.

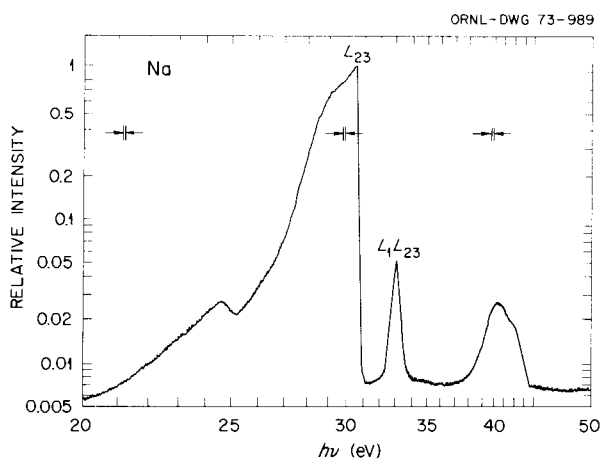


**Fig. 8.12. Recorder trace of $L$-emission spectrum of sodium.** The electron energy was 2.5 keV, the electron beam current 3.5 mA, and the chamber pressure $5 \times 10^{-7}$ torr.

The present studies show that for Li, Be, and Na low-energy satellites involve volume plasmon creation, while high-energy satellites result from double ionization decay and do not involve volume plasmons. Thus the present studies are consistent with the previous interpretations of x-ray spectra.

## STUDY OF THE OPTICAL PROPERTIES OF SOLIDS BY ELLIPSOMETRY

The alkali metals are electronically the simplest of all solids. Thus they serve as ideal testing grounds for theory and experiment of the electronic structure of matter.

Previously[18] we have reported measurements of the optical properties of Na, K, Rb, and Cs; now we have begun a similar study of lithium. A film of the metal was evaporated on the base of a 40°-70°-40° strain-free quartz isosceles prism. The evaporation was made from a tubular stainless steel boat and was carried out in the ellipsometer chamber at a base pressure of $5 \times 10^{-9}$ torr. The measurements were made at the metal-quartz interface to reduce the effects of a possible contaminating oxide film at the metal-vacuum interface.

The dielectric constants have been obtained in the energy region between 1.91 and 3.87 eV for one Li sample and are shown in Fig. 8.13. The scatter in the data at the higher energies results from the falloff in intensity of the quartz-iodine tungsten filament lamp coupled with the onset of absorption by the mica wave plate which is in the optical train. While these data are preliminary the shapes of curves generally agree with lithium data reported recently by others.[19] We plan to extend these measurements over a broader spectral region.

18. E. T. Arakawa et al., *Health Phys. Div. Annu. Progr. Rep. July 31, 1972*, ORNL-4811, pp. 13–15, and previous reports in this series.

19. J. Bosenberg, *Phys. Lett.* 41A, 185 (1972); A. G. Mathewson and H. P. Myers, *Phys. Scripta* 4, 291 (1971).

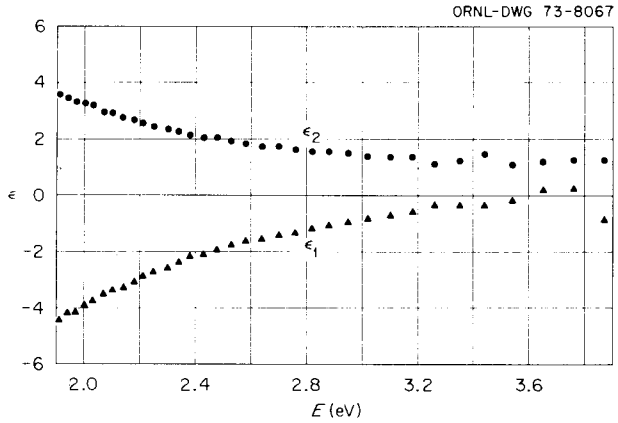


**Fig. 8.13. Dielectric constants of lithium.**

# 9. Electron and Ion Collision Physics

R. N. Compton

V. E. Anderson[1]
Ada Carter
C. D. Cooper[2]
J. T. Cox
F. J. Davis
Liliana Deleanu[3]
W. F. Frey[4]
W. R. Garrett
D. R. Nelson[5]
P. W. Reinhardt
H. C. Schweinler
J. C. Steelhammer[6]
J. A. Stockdale
J. F. Wilson[7]
J. M. Younkin[3]

## DISSOCIATIVE IONIZATION OF MOLECULES BY ELECTRON IMPACT

The dissociative ionization process

$$e + AB \rightarrow A^+ + B + e + e \qquad (1)$$

may often contribute a large fraction of the total ionization produced by electron impact on molecules.[8] However, since the pioneering work of Sasaki and Nakao,[9] who measured an anisotropic distribution of protons produced by impact of 85-eV electrons on $H_2$, the only detailed published studies of this process have been those of Dunn, Kieffer, and Van Brunt.[10] These workers have studied electron impact on $H_2$ and $N_2$ and have measured both the kinetic energies and angular distributions of the ionic products. There are two reasons why it is important to make measurements of at least this degree of completeness. First, the results shed light on the symmetries[11] and positions of the molecular states involved in the dissociation process; second, they are of fundamental importance to radiation chemistry and dosimetry since the nature and distribution of the final products of irradiation will be determined by the energies and angular distributions of the primary dissociation products.

Figure 9.1 shows schematically an apparatus which has been constructed to study the kinematics of molecular dissociation. It consists of a pulsed horizontal electron beam which intersects a vertical molecular gas beam. The electron gun can be rotated in the horizontal plane about the molecular beam and reaction products formed in the beam intersection region are detected by a fixed channeltron electron multiplier. Figure 9.2 shows sample time-of-flight distributions for positive ions obtained by impact of 70-eV electrons on $C_6H_6$ and $C_6D_6$. There are evident shifts to longer times of flight for the first three peaks in the deuterated case. In fact, the drift in the first (fastest) peak is consistent with it being $H^+$ ($D^+$) of energy 2.8 eV, while the second and third peaks are consistent with compositions of the form $C_nH_n^+$ and $C_{3n}H_{2n}^+$, respectively.

Figure 9.3 shows a set of $O^+$ time-of-flight spectra obtained for impact of 20- to 300-eV electrons on $O_2$ for an angle of 90° between electron beam and ion

1. On loan from Mathematics Division, ORNL.
2. Consultant from the University of Georgia.
3. Graduate student, University of Tennessee.
4. Research Participant from Davidson College.
5. On temporary assignment with the U.S. Atomic Energy Commission, Washington, D.C.
6. Postdoctoral Fellow.
7. Radiological Health Physics Fellow, University of Tennessee.
8. D. Rapp, P. Englander-Golden, and D. D. Briglia, *J. Chem. Phys.* **42**, 4081 (1965).
9. V. N. Sasaki and T. Nakao, *Proc. Imp. Acad. (Tokyo)* **11**, 413 (1935); **17**, 75 (1941).
10. G. H. Dunn and L. J. Kieffer, *Phys. Rev.* **132**, 2109 (1963); L. J. Kieffer and R. J. Van Brunt, *J. Chem. Phys.* **46**, 2728 (1967); R. J. Van Brunt and L. J. Kieffer, *Phys. Rev. A* **2**, 1293 (1970).
11. G. H. Dunn, *Phys. Rev. Lett.* **8**, 62 (1962).

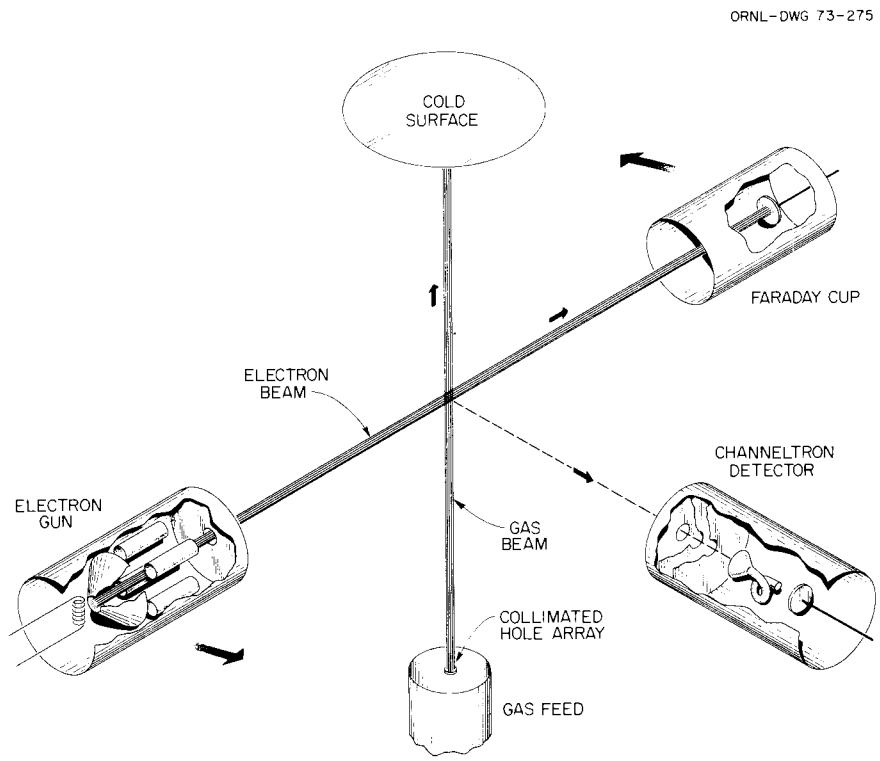


**Fig. 9.1. Schematic diagram of equipment for the study of the kinematics of molecular dissociation by electron impact.** Approximate apparatus parameters: beam pulse, 1.0 μsec repeated every 100 μsec; integrated beam current, $2 \times 10^{-8}$ A; angular resolution, ≤3°; pressure in flight region with beams operating, $\leq 5 \times 10^{-7}$ torr; angular range, 30° (forward direction) to 110°; ion flight distance, 20 cm.

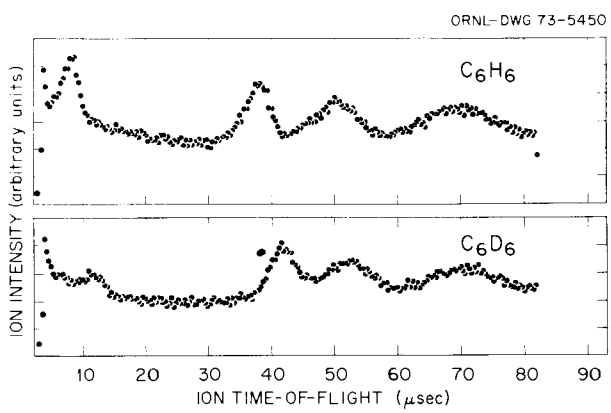


**Fig. 9.2. Time-of-flight spectra of positive ions from impact of 70-eV electrons on $C_6H_6$ and $C_6D_6$.** Electron-beam–ion-detector angle, 90°.

detector. These results illustrate the complexity and richness of the data. The spectrum for 50 eV, for example, contains four main groups of ions represented by the peaks near 24, 33, and 40 μsec and the group involved in the tail out to longer flight times. It is interesting to note also from these data that the cross section for production of fast $O^+$ ions – represented by the total area under the spectral curve – appears to peak in the neighborhood of 140 eV, as does the total ionization cross section. Figure 9.4 is a similar time-of-flight spectrum for $O^+/O_2$ at 50-eV electron impact energy obtained with improved resolution. Here, the four ion groups are somewhat better defined. Figure 9.5 is a computer-generated point-by-point conversion of the data of Fig. 9.4 to an energy scale and shows the four main $O^+$ groups to peak with 0.8-, 2.0-, 3.0-, and 5.0-eV kinetic energy. The positions of these peaks correlate well with data obtained from photoionization,[12] with peaks observed in time-of-flight spectra of high Rydberg state oxygen atoms from electron impact on $O_2$,[13] and with a measurement of $O^+$ produced by electron impact.[14]

12. P. H. Doolittle, R. I. Schoen, and K. E. Schubert, *J. Chem. Phys.* **49**, 5108 (1968).
13. R. S. Freund, *J. Chem. Phys.* **54**, 3125 (1971).
14. L. J. Kieffer, G. M. Lawrence, and J. M. Slater, in *Proc. VII ICPEAC*, Amsterdam, 1971, p. 574.

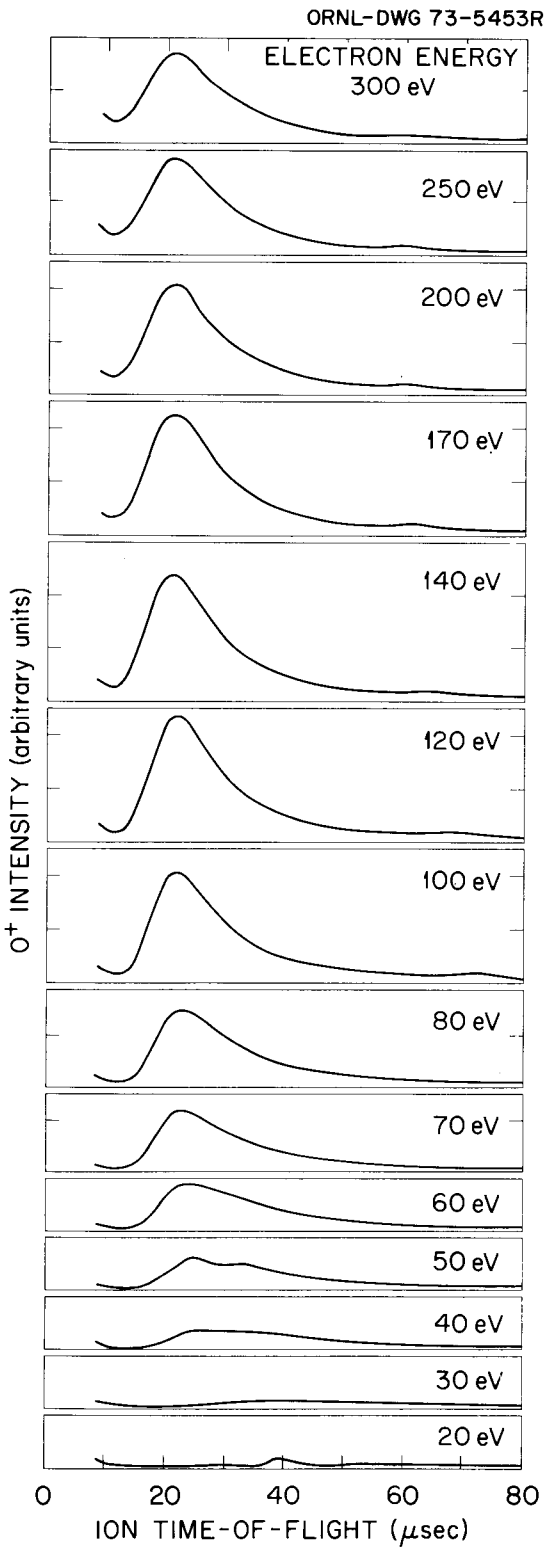


**Fig. 9.3. Time-of-flight spectra of $O^+$ ions produced by impact of 20- to 300-eV electrons on $O_2$.** Electron-beam–ion-detector angle, 90°.

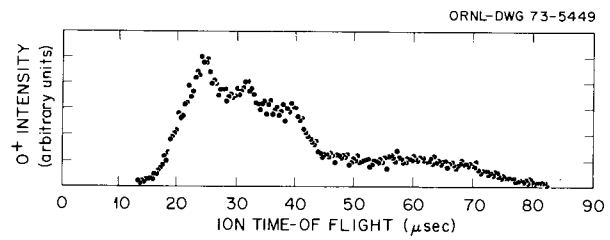


**Fig. 9.4. Time-of-flight spectra of $O^+$ ions produced by impact of 50-eV electrons on $O_2$.** Electron-beam–ion-detector angle, 90°.

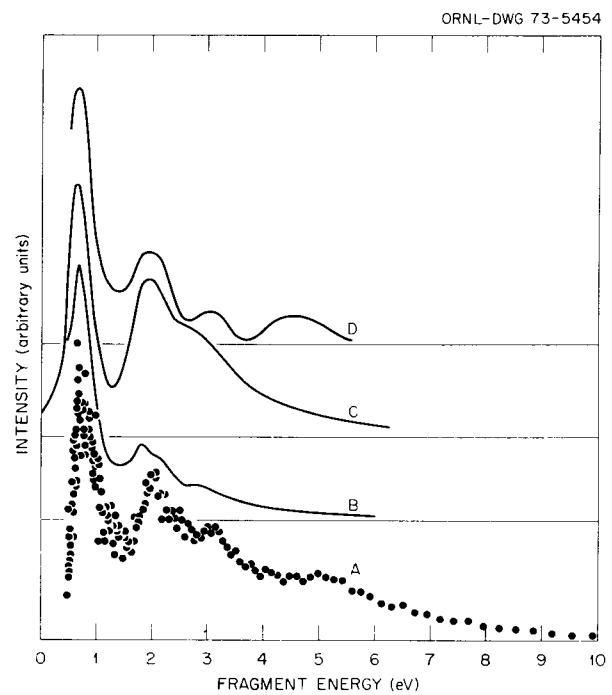


**Fig. 9.5. Energy spectra of oxygen fragments from $O_2$ dissociation.** (*A*) This work, 50-eV impact, $O^+$ detected; (*B*) Kieffer et al.,[14] 35-eV impact, $O^+$ detected; (*C*) Freund,[13] 39-eV impact; high Rydbergs detected; (*D*) Doolittle et al.,[12] 34.6-eV photons, $O^+$ detected.

Figure 9.6 shows angular distributions of the four $O^+/O_2$ peaks for 50-eV electron impact. For all four peaks the distributions are substantially isotropic. Doolittle, Schoen, and Schubert[12] and Freund[13] have suggested possible $O_2^+$ states involved as precursors of these peaks. The angular distributions of Fig. 9.6, when combined with the selection rules of Dunn,[11] tend to confirm these suggestions. For instance, Doolittle, Schoen, and Schubert[12] suggested that their 0.7-eV peak arose from predissociation of the $B^2\Sigma_g^-$ state of $O_2^+$. Dunn's selection rules imply that near threshold

the transition probability for excitation from the ground $^3\Sigma_g^-$ state of $O_2$ to an excited state $^2\Sigma_g^-$ of $O_2^+$ would be allowed for orientations of the internuclear axis of the oxygen molecules both parallel and perpendicular to the momentum vector of the input electrons. This would produce an isotropic angular distribution in dissociation. The times involved in transitions to the possible repulsive states $^2\Sigma_g^+$ and $^4\Pi_g$ involved in the predissociation would tend to encourage isotropy. Freund has suggested that the 5-eV peak may arise from initial ionization of $O_2$ to the $^2\Sigma_g^-$ and/or $^4\Sigma_g^-$ states formed by removal of the $\sigma_g 2s$ electron. An isotropic distribution such as that observed might be expected from either of these two states. Interpretation of the results of the 2- and 3-eV peaks is more speculative.[15]

Figure 9.7 shows an angular distribution for 2.9-eV $N^+$ ions from impact of 60-eV electrons on $N_2$. The results are in reasonable agreement with the measurements of Kieffer and Van Brunt, though the latter show a small rise in the forward and backward directions with respect to the electron beam. We have obtained similar results for 1-, 2-, and 4-eV $N^+/N_2$,[15] and have made preliminary studies of $H^+/H_2O$ and $H^+/CH_4$ kinetic energies and angular distributions.

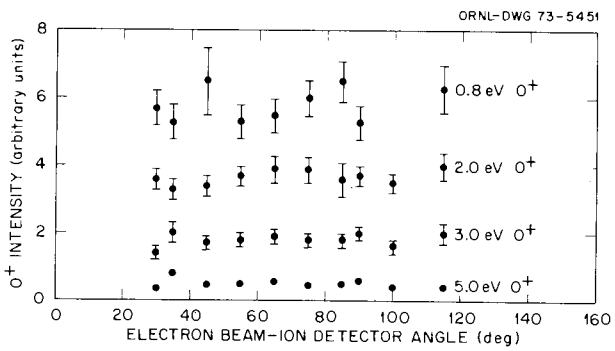


**Fig. 9.6. Angular distribution of 0.8-, 2.0-, 3.0-, and 5.0-eV $O^+$ ions from impact of 50-eV electrons on $O_2$.** Points are averages of data obtained with the electron gun located on the two symmetric opposite sides of the apparatus with respect to the ion detector.

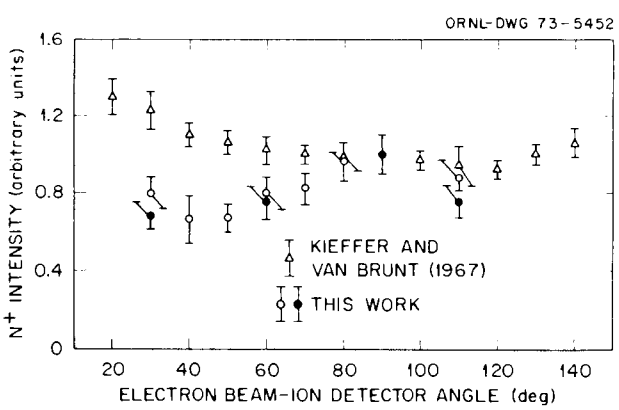


**Fig. 9.7. Angular distribution of 2.9-eV $N^+$ ions from impact of 60-eV electrons on $N_2$.** This work (○, electron gun on north side of detector; ●, electron gun on south side of detector); Δ, Kieffer and Van Brunt, 1967.

## LONGITUDINAL DIFFUSION COEFFICIENTS AND DRIFT VELOCITY MEASUREMENTS IN $H_2O$ AND $D_2O$

Measurements of longitudinal electron diffusion coefficients $D_L$ and electron drift velocities $w$ were reported for water vapor in the preceding annual report.[16] Identical measurements performed on deuterated water vapor have revealed significant differences in $D_L$ and $w$ from those obtained for $H_2O$. Water is anomalous in that the longitudinal diffusion coefficient is larger than the transverse, as shown in Fig. 9.8, where $D/\mu$ (ratio of diffusion coefficient to mobility) is plotted vs the electric field to pressure ratio $E/P$. The corresponding plot for $D_2O$ is also presented in Fig. 9.8, and a striking difference from the behavior of $H_2O$ is observed. $D/\mu$ is related to the mean energy of the electron swarm. The mean energies for $H_2O$ and $D_2O$ remain thermal up to an $E/P$ of approximately 5 V $cm^{-1}$ $torr^{-1}$. An abrupt increase in mean energy is observed above $E/P$ about 5 V $cm^{-1}$ $torr^{-1}$ for $D_2O$ and $E/P$ about 10 V $cm^{-1}$ $torr^{-1}$ for $H_2O$. A large isotope effect is also observed in the drift velocity measurements. Figure 9.9 shows that the electron drift velocity is considerably greater in $D_2O$ than in $H_2O$ for $E/P$ equal to 10 to 30 V $cm^{-1}$ $torr^{-1}$.

## MASS ANALYSIS OF NEGATIVE IONS PRODUCED IN SWARM EXPERIMENTS: ION CLUSTERING REACTIONS IN WATER VAPOR

In 1890, Wilson observed cloudy condensations produced by nucleation about gaseous phase ions in his now famous cloud chamber experiments. Since that time, ion nucleation is thought to be important in such areas as aerosol production in the presence of ionizing radiations, atmospheric processes (fog, rain, etc.), and ion solvation in liquids. In this connection we have studied the production of small cluster ions in water vapor, using mass spectrometric techniques.

15. J. A. D. Stockdale and Liliana Deleanu (to be published).
16. R. N. Compton et al., *Health Phys. Div. Annu. Progr. Rep. July 31, 1972,* ORNL-4811, pp. 32–33.

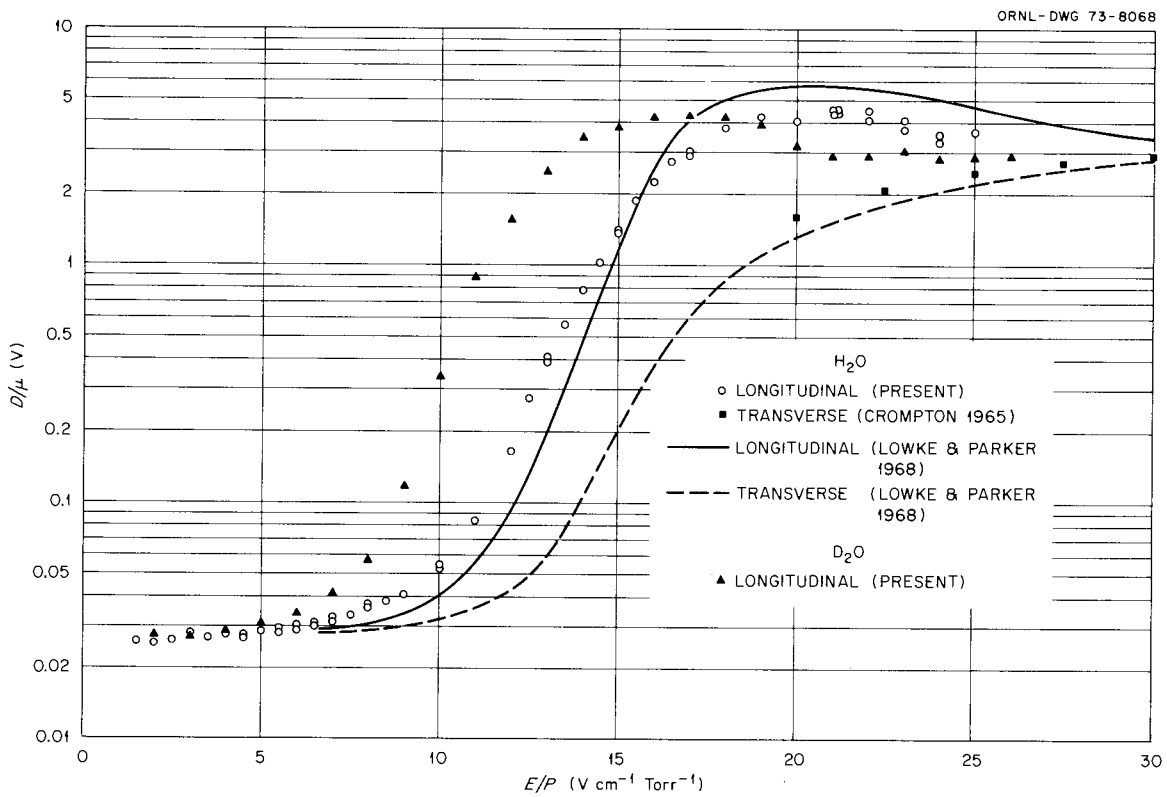


**Fig. 9.8. Ratio of electron diffusion coefficient to mobility vs the electric field to pressure ratio for water vapor and deuterated water vapor.**

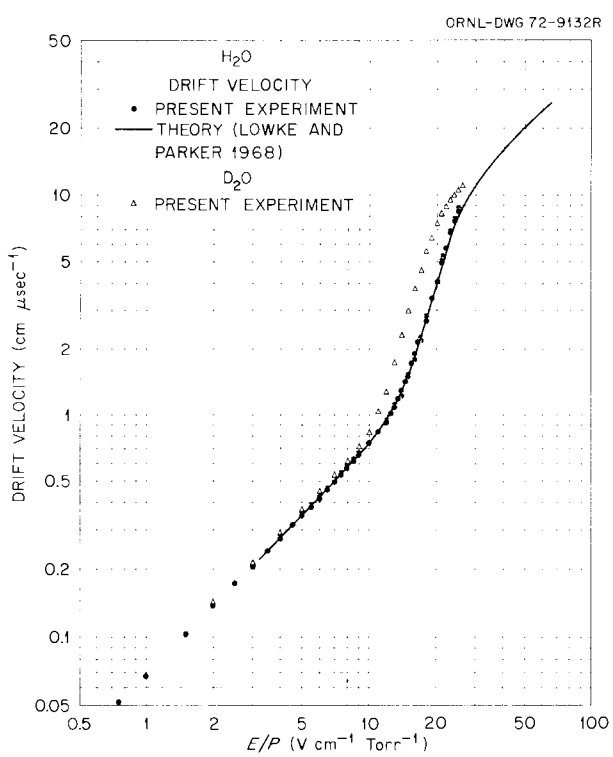


**Fig. 9.9. Drift velocity measurements as a function of the electric field to pressure $E/P$ ratio for $H_2O$ and $D_2O$.**

Negative ions with masses in the range from 1 to 200 amu produced by electron swarm interactions with water vapor at room temperature have been recorded as a function of $E/P$ from 0 to 70 V cm$^{-1}$ torr$^{-1}$ and pressures from 0.1 to 3 torr. Figure 9.10 shows the yield of $OH^-$ ions for two different pressures as a function of $E/P$. The primary process observed is[17]

$$e + H_2O \rightarrow H^- + OH\,. \tag{2}$$

The $H^-$ ion rapidly reacts to form $OH^-$ according to [18]

$$H^- + H_2O \rightarrow OH^- + H_2\,. \tag{3}$$

This reaction accounts for all of the $OH^-$ formed. Since the cross section for reaction (3) decreases rapidly as the $H^-$ ion energy decreases, we explain the rapid decrease in $OH^-$ with $E/P > 20$ to an increase in energy of the $H^-$ ion. The $OH^-$ "cluster" ions result from the

17. R. N. Compton and L. G. Christophorou, *Phys. Rev.* **154**, 110 (1967).

18. J. A. D. Stockdale, R. N. Compton, and P. W. Reinhardt, *Phys. Rev.* **184**, 81 (1969).

following three-body reactions:

$$OH^- + H_2O + H_2O \rightarrow OH^-\cdot(H_2O) + H_2O\ ,$$

$$OH^-\cdot(H_2O)_{n-1} + H_2O + H_2O \rightarrow OH^-\cdot(H_2O)_n + H_2O\ .$$

$OH^-\cdot(H_2O)_n$ clusters were observed with $n$ equal to 1 up to and including 7. The change in intensity of the $OH^-$ ion and the cluster ions $OH^-\cdot(H_2O)_n$ with $n$ = 1 to 6 as a function of $E/P$ for a constant water vapor pressure is shown in Fig. 9.11. Parallel studies with $D_2O$ have been performed.

Preliminary studies of electron attachment and ion-molecule three-body clustering reactions in high-pressure electron swarms are being carried out on the following molecules: $CCl_4$ (carbon tetrachloride); $CH_3NO_2$ (nitromethane); and $C_4F_8$ (perfluorobutene-2 and octofluorocyclobutane). Three-body reactions have been observed in $CCl_4$ when $Cl^-$ clusters with $CCl_4$ and $CHCl_3$. The $CHCl_3$ (chloroform) is present as an impurity in the $CCl_4$ sample. Clustering is found in

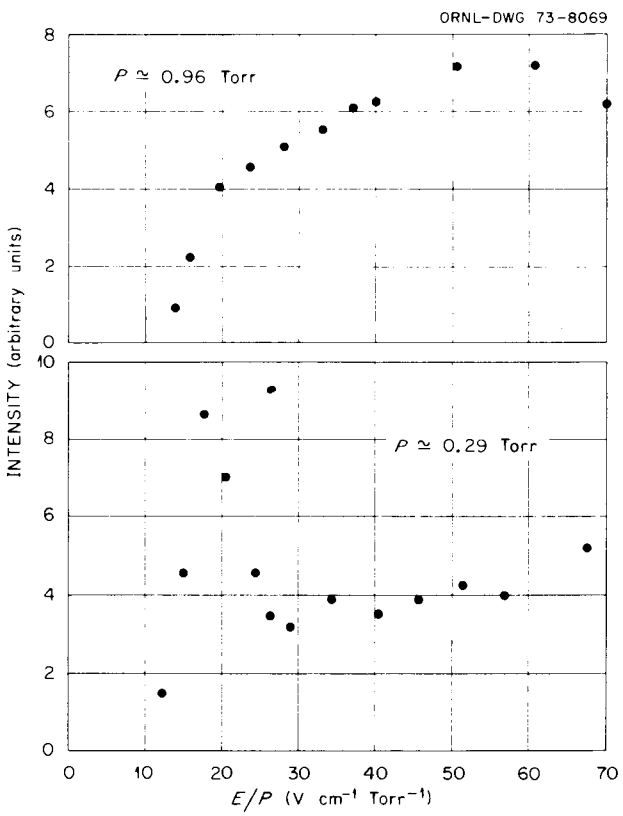


**Fig. 9.10. Production of $OH^-$ from the $H^- + H_2O$ reaction in pure water at two vapor pressures as a function of $E/P$.**

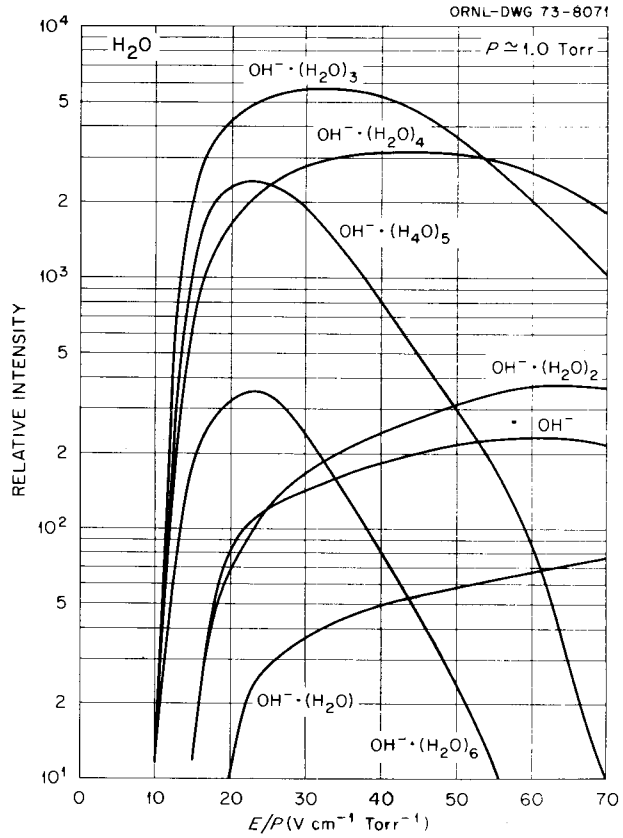


**Fig. 9.11. Relative intensities of the ions $OH^-$, $OH^-\cdot H_2O$, $OH^-\cdot 2H_2O$, $OH^-\cdot 3H_2O$, $OH^-\cdot 4H_2O$, $OH^-\cdot 5H_2O$, and $OH^-\cdot 6H_2O$ as a function of $E/P$.**

$CH_3NO_2$ with the ions $CH_2NO_2^-\cdot(CH_3NO_2)_n$($n$ = 1, 2, 3) being observed. Similar reactions from the ions of $C_4F_8$ have not yet been observed. The relationship of $C_4F_8^-$ from perfluorobutene-2 as a function of $E/P$ is shown in Fig. 9.12.

## THERMAL ENERGY ELECTRON ATTACHMENT RATE CONSTANTS FOR SOME POLYATOMIC MOLECULES

Rate constants for the attachment of thermal energy electrons to a number of polyatomic molecules have been determined by a new technique. The attachment rate constants $\alpha w$ are determined in an electron swarm experiment under zero electric field conditions where the electrons have a Maxwellian energy distribution corresponding to the temperature of the nonattaching diluent gas. Various diluent gases were used, and no significant differences in the attachment rate constants were found. Corrections to the attachment rate con-

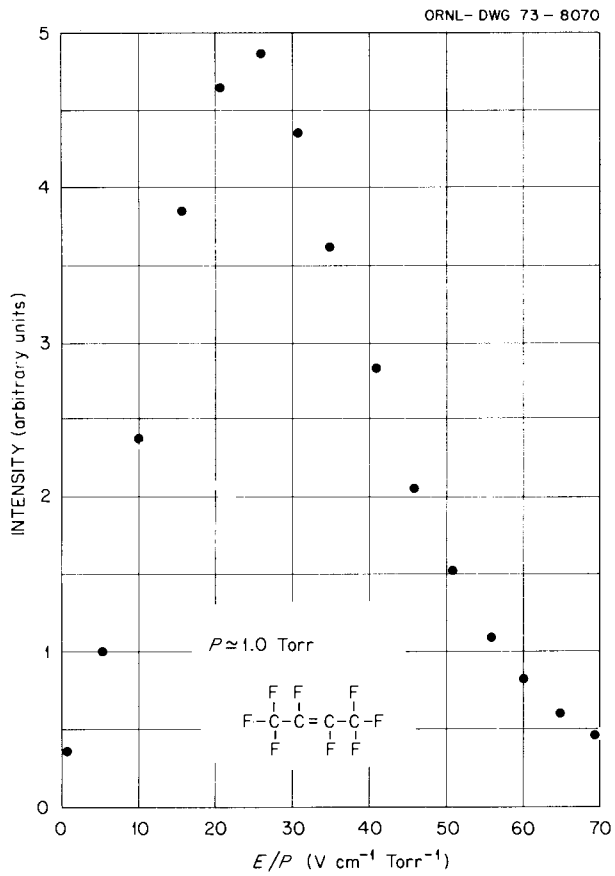


**Fig. 9.12. Negative ion production of $C_4F_8^-$ from perfluorobutene-2 as a function of *E/P*.**

stant measurements due to electron diffusion are small and are taken into account. Thermal energy attachment rate constants are reported for the following molecules (attachment rate constants are given in parentheses in units of cubic centimeters per second): $SeF_6$($1.27 \times 10^{-9}$), $CCl_4$($3.55 \times 10^{-7}$), $C_7F_{14}$($4.0 \times 10^{-8}$), $C_6F_6$($1.06 \times 10^{-7}$), $C_7F_8$($2.42 \times 10^{-7}$), $C_6F_{10}$($3.13 \times 10^{-7}$), $C_5F_8$($1.18 \times 10^{-7}$), $C_4F_8$($1.11 \times 10^{-8}$), $C_8H_8$($7.7 \times 10^{-10}$), and $SO_2F_2$($5.8 \times 10^{-10}$). Upper limits to the attachment rates for a number of molecules were obtained using pure gases, and the results are presented in Table 9.1. An upper limit of about $3 \times 10^{-12}$ $cm^3$/sec for the thermal electron attachment rate constant for HCl in a mixture with $N_2$ as a carrier gas is reported and is more than 100 times smaller than a previously reported value.[19]

19. L. G. Christophorou, R. N. Compton, and H. W. Dickson, *J. Chem. Phys.* 48, 1949 (1968).

**Table 9.1. Upper limits to the thermal electron attachment rate constants for various molecules**

| Molecule | Total pressure (torrs) | Attachment rate ($cm^3$/sec) |
|---|---|---|
| $CF_4$ | 2 | $<3.1 \times 10^{-13}$ |
| $C_2F_6$ | 2 | $<1.6 \times 10^{-13}$ |
| $C_3F_8$ | 2 | $<1.24 \times 10^{-12}$ |
| $CClF_3$ | 2 | $<3.1 \times 10^{-13}$ |
| $CHF_3$ | 2 | $<6.2 \times 10^{-14}$ |
| $CHClF_2$ | 2 | $<1.6 \times 10^{-13}$ |
| $C_2H_2F_2$ | 2 | $<2.2 \times 10^{-13}$ |
| $C_2H_4F_2$ | 1 | $<1.6 \times 10^{-12}$ |
| $C_2ClF_5$ | 1 | $<6.2 \times 10^{-12}$ |
| $TeF_6$ | 0.5 | $<2.0 \times 10^{-11}$ |
| $HCl + N_2$ | 5 | $<3.1 \times 10^{-12}$ |

## COLLISIONAL IONIZATION OF CESIUM BY MOLECULES: DETERMINATION OF MOLECULAR ELECTRON AFFINITIES

Studies of chemi-ionizing collisions between fast cesium atoms and molecules continue to yield important information on structures of molecular negative ions. The relative cross sections for the production of mass selected negative ions resulting from collisions of cesium with $SF_6$ and $TeF_6$ have been studied as a function of the incident cesium atom energy from 0 to 40 eV. Electron affinities (EA) for $SF_6$ and $TeF_6$ are derived from accurate measurements of the threshold for ion-pair production with the results $EA(SF_6) = (0.54^{+0.1}_{-0.17})$ eV and $EA(TeF_6) = (3.34 \pm 0.2)$ eV. Dissociative ionization studies resulted in $EA(SF_5) \geqslant (2.8 \pm 0.1)$ eV and the dissociation energy $D(SF_5^- - F) = (1.05 \pm 0.1)$ eV. Figure 9.13 shows the negative ion yields from $TeF_6$ as a function of the energy in the center-of-mass system. The rather large electron affinity for $TeF_6$ is surprising in view of the fact that $TeF_6$ does not attach thermal electrons (see previous article). Negative ion formation has also been studied for cesium collisions with $C_2F_4$, $CH_3Br$, HI, HF, $(CF_3)_2CO$ (hexafluoroacetone), $C_4F_6$ (perfluorobutene), $C_4F_4O_3$ (perfluorosuccinic anhydride), and $C_5F_6O_3$ (perfluoroglutaric anhydride).

## ELECTRON IMPACT STUDIES OF SOME CYCLIC HYDROCARBONS

In accord with Hückel's rule, organic molecules which contain $4n + 2$ ($n$ = integer) $\pi$ electrons are known to be

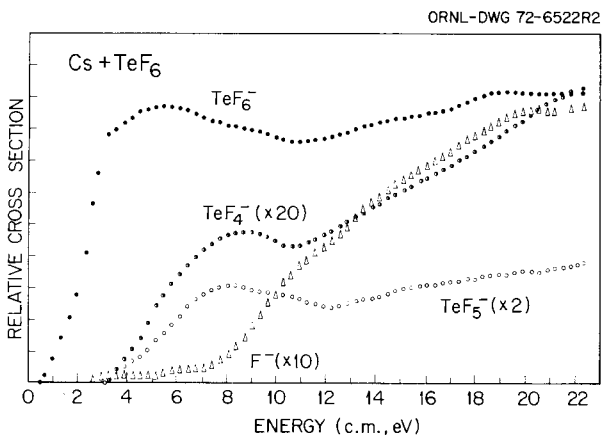


**Fig. 9.13. Relative cross section for the production of negative ions resulting from collisions between fast cesium atoms and $TeF_6$.**

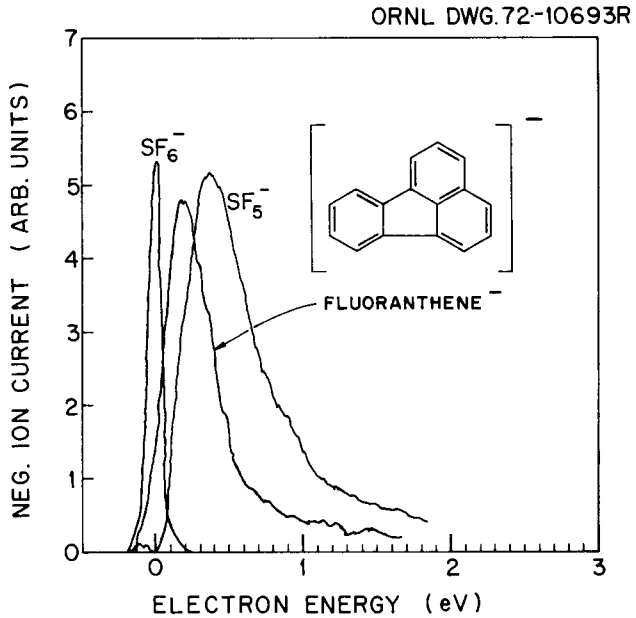


**Fig. 9.14. Metastable parent negative ion current of fluoranthene as a function of electron energy.** Energy scale is calibrated by $SF_6^-$ and $SF_5^-$ peaks from $SF_6$.

particularly stable. Also, we expect molecules that contain one or two electrons fewer than a "filled" Hückel's shell will form stable negative ions.

The formation of positive and negative ions by collisions of monoenergetic electrons with cyclo-öctatetraene, biphenylene, triphenylene, fluorene, indene, indole, acenaphthene, benzothiazole, carbazole, acenaphthylene, and fluoranthene was examined in the gas phase under single collision conditions. The data are analyzed with regard to Hückel's rule. Long-lived negative ions ($\tau > 1$ $\mu$sec) were observed in the cases of cycloöctatetraene (8 $\pi$ electrons) and acenaphthylene (16 $\pi$ electrons) at approximately zero energy with mean lifetimes of 6.4 and 88 $\mu$sec, respectively. The energy breadth of the negative ion resonances for these ions was equal to the electron energy resolution, and thus the measured lifetimes are averaged over the width of the resonances. Fluoranthene captures slow electrons with a maximum in the cross section at 0.2 eV, and the width of the resonance is approximately 0.4 eV (see Fig. 9.14). The lifetime was found to decrease from 180 $\mu$sec at about 0 eV to 80 $\mu$sec at about 1.0 eV, as shown in Fig. 9.15. A similar lifetime variation has been noted previously for *p*-benzoquinone.[20] Another compound state in fluoranthene was observed at 2 eV. Energy-loss processes were observed, using the $SF_6$ scavenger technique, in biphenylene and triphenylene at electron energies of 2.15 and 2.35 eV, respectively, and are attributed to compound negative ion states. Positive ion

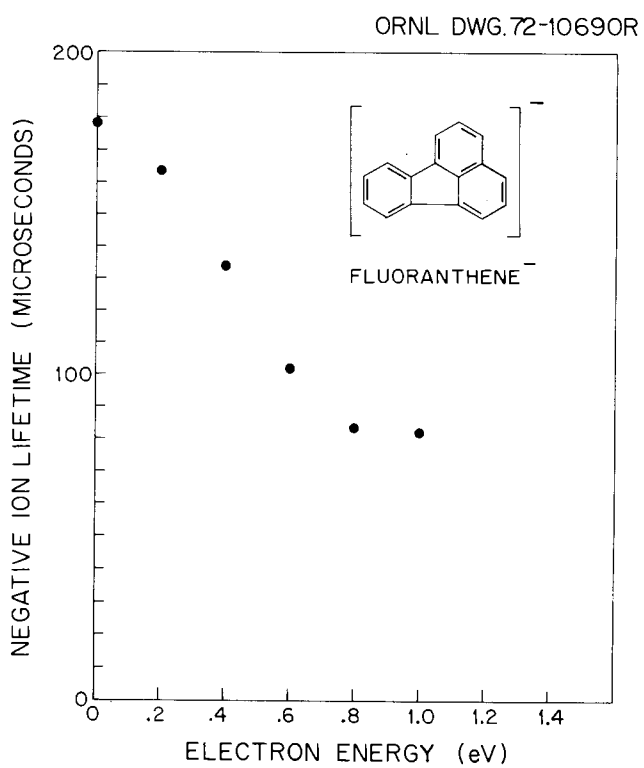


**Fig. 9.15. Variation of negative ion lifetime of fluoranthene negative ions as a function of incident electron energy.**

20. P. M. Collins, L. G. Christophorou, E. L. Chaney, and J. G. Carter, *Chem. Phys. Lett.* 4, 646 (1970).

**Table 9.2. First ionization potentials**

| Acenaphthylene | Fluoranthene | Fluorene | Indene | Acenaphthene | Ref. | Method[a] |
|---|---|---|---|---|---|---|
| | | | **Experimental** | | | |
| 8.15 ± 0.1 | 7.9 ± 0.1 | 8.1 ± 0.1 | 8.25 ± 0.1 | 7.8 ± 0.1 | *b* | ei |
| | | 8.63 | 8.81 | | *c* | ei |
| 8.02 | 7.80 | 7.93 | 8.14 | 7.73 | *d* | pes |
| | | | 8.08 | 7.76 | *e* | pi |
| | | | | 7.76 | *f* | pi |
| | 7.72 | 7.78 | | | *g* | ct |
| | | | | 7.76 | *h* | ct |
| | | | 8.13 | | *i* | pes |

[a]The various methods of ionization potential determination are designated: ei = electron impact; pi = direct photoionization; ct = charge transfer; pes = photoelectron spectroscopy.
[b]Present work.
[c]R. F. Pottie and F. P. Lossing, *J. Amer. Chem. Soc.* **85**, 269 (1963).
[d]M. J. S. Dewar, E. Haselbach, and S. D. Worley, *Proc. Roy. Soc. (London)* A**315**, 431 (1970).
[e]J. Aihara and H. Inokuchi, *Bull. Chem. Soc. Jap.* **43**, 1265 (1970).
[f]J. Aihara, M. Tsuda, and H. Inokuchi, *Bull. Chem. Soc. Jap.* **43**, 3067 (1970).
[g]M. A. Slifkin and A. C. Allison, *Nature* **215**, 949 (1967).
[h]M. Kinoshita, *Bull. Chem. Soc. Jap.* **35**, 1609 (1962).
[i]J. H. D. Eland and C. J. Danby, *Z. Naturforsch.* **23a**, 255 (1968).

appearance potentials (ionization potentials) for a number of cyclic hydrocarbons are reported in Table 9.2.

## LOW-ENERGY INDUCED SPUTTERING OF ALKALI HALIDES

Sputtering from the (100) face of air-cleaved KI, KCl, and NaCl crystals due to low-energy electron bombardment was studied in an ultrahigh vacuum environment. Such studies may be useful in determining the possible evolution of chlorine gas from the storage of radioactive materials in salt mine repositories. Electron energies were varied between 100 and 1000 eV, and surface temperatures ranged from room temperature to 500°C. Sputtering rates were determined with a quadrupole mass spectrometer for different orientations of the crystal. Ions of the form $A^+$, $X^+$, and $X_2^+$ (A = K and Na and X = I and Cl) were observed in the mass spectrometer originating from the crystal surface. The kinetic energies of the sputtered neutral particles were measured by a time-of-flight analysis. The kinetic energies for all particles A, X, and $X_2$ were found to be equal to that of the surface temperature of the crystal. These results are being considered in light of proposed mechanisms for *F*-center production in irradiated alkali halides.

## PROPERTIES OF CONSTITUENTS OF POSSIBLE SUPERCONDUCTORS

A program has been initiated to measure fundamental parameters of molecules which offer promise as components of organic superconductors. The organic salt consists of an ionic crystal of organic electron acceptor-donor molecules. One such electron donating species is tetrathiofulvalene (TTF) whose ionization potentials are expected to be quite low. The ionization potential is found to be (7.05 ± 0.05) eV, which is low but not startlingly so. A mass corresponding to $(TTF)^{2+}$ has also been identified, but its appearance potential remains obscure.

Electron attachment to TTF occurs rapidly at low energies via dissociative mechanisms. The appearance potentials for the negatively charged fragments, as well as the onset of fragmentation from $TTF^+$, should yield much new information on the stability of carbon-sulfur compounds. For example, the most facile decomposition of $TTF^+$ results in a species of mass equal to 159 (amu). This probably has a structure with two fused five-membered rings. Decomposition of metastable $TTF^+$ into a number of daughter ions was observed with both magnetic and time-of-flight mass spectrometers.

Work is presently under way to study the negative ion properties of the electron acceptor tetracyanoquinodimethan (TCNQ). Tetracyanoquinodimethan is found to

attach slow electrons to form long-lived parent negative ions. Peaks are observed in the attachment cross section at ~0, ~2, and 3.2 eV. The third resonance is metastable with respect to dissociation into HCN and $C_{11}H_3N_3^-$. The electron affinity of TCNQ is being determined with the cesium collisional ionization technique. These results will hopefully be useful in interpreting the peculiar properties of the charge transfer complexes.

## A CHEMICAL ACCELERATOR FOR STUDYING THE COLLISIONAL BEHAVIOR OF LARGE MOLECULES: $SF_6 + CO_2$

An accelerator for producing fast (500 eV to 10 keV) neutral beams of a class of large molecules has been constructed at Florida State University in a cooperative effort with ORNL. Total scattering cross sections are presently being measured by Dr. J. G. Skofronick at FSU. For $SF_6$ colliding with $CO_2$, a total effective cross section of about 40 $Å^2$ was obtained for an $SF_6$ kinetic energy of 1200 eV. These are the first such measurements for neutral-neutral molecular collisions. A preliminary report of their technique has been presented.[21]

21. J. G. Skofronick, D. B. Greene, E. A. Halprin, and R. N. Compton, "A Chemical Accelerator for Studying the Collisional Behavior of Large Molecules: $SF_6 + CO_2$ Total Cross Sections," VIII. International Conference on Electronic and Atomic Collisions Book of Abstracts, pp. 908, Beograd, Yugoslavia (1973).

# 10. Physics of Tissue Damage

E. T. Arakawa
R. D. Birkhoff[1]

W. T. Cochran[2]
L. C. Emerson
R. N. Hamm
R. A. MacRae[3]
R. H. Ritchie
Mary W. Williams

## ELECTRON-SLOWING-DOWN STUDIES

We have previously carried out an extensive series of studies on the electron-slowing-down spectra in a wide variety of metals and semiconductors.[4] Recently these studies were expanded to include insulating materials to determine the effect of a wide energy gap on the slowing-down cascade.

Because of its importance as an insulator and its ease of fabrication into forms suitable for experimental study, aluminum oxide was chosen for the investigation. The study has been carried out, concomitant with a theoretical investigation, using both polished and unpolished polycrystalline samples. It was necessary to dope the $Al_2O_3$ with a small amount of normal isotopic dysprosium which serves as the source of primary beta particles following activation by thermal neutron irradiation.

The target disks, containing 0.5 wt % dysprosium as the oxide, were fabricated by a coprecipitation technique. The disks were ground to final size using an aluminum oxide abrasive. Sources obtained in this manner exhibited a density of 87% of the theoretical value. The surfaces of the unpolished disks were covered with micropits and imperfections which had dimensions of the order of 0.001 in. The typical size of the individual crystals appeared to be under 0.005 in.

Results of the initial studies on the unpolished crystals were reported earlier.[5] The electron flux inside the material is inferred from that measured in the vacuum environment outside by dividing by a suitable barrier transmission factor which takes the form

$$T(E) = 1 - \sqrt{E_A/(E + E_A)} \ ,$$

where $E$ is the electron energy outside and $E_A$ is the electron affinity, equal to the difference between the work function and the gap energy. There exists considerable uncertainty in the value of $E_A$. A literature survey on aluminum oxide revealed values extended from 0 for amorphous $Al_2O_3$ to 1.8 eV for the crystalline form. The electron affinity for our polycrystalline sources would presumably fall near the lower end of this range, since this form more nearly resembles the amorphous material. In our work we have somewhat arbitrarily chosen an $E_A$ value of 0.5 eV.

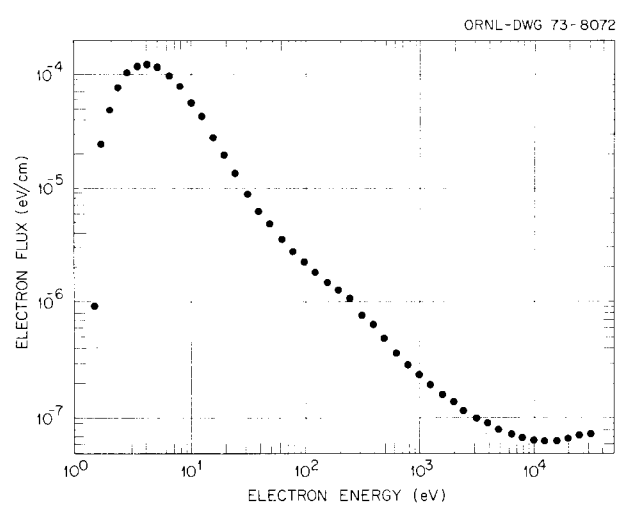


**Fig. 10.1. Electron-slowing-down spectrum of aluminum oxide.**

1. Also Chief of Fundamental Health Physics Research Section.
2. Graduate student.
3. Consultant.
4. See previous reports in this series.
5. E. T. Arakawa et al., *Health Phys. Div. Annu. Progr. Rep. July 31, 1972*, ORNL-4811, pp. 19–21.

The earlier studies were repeated using polished disks to eliminate possible effects of surface roughness on the experimentally determined flux. A diamond polishing compound was used to produce surfaces with a flatness of approximately one wavelength. The results for the electron flux inside the specimen, shown in Fig. 10.1, exhibit essentially the same shape as the results for the unpolished sources but are everywhere lower in absolute value. This difference is thought to be associated with the uncertainty in the thermal neutron flux in the irradiation facility rather than in the electron flux itself. The characteristics of the measured spectrum are similar to those found earlier for both metals and semiconductors. The most noteworthy difference is the somewhat more rapid buildup of secondary electrons at low energies in the case of the aluminum oxide.

Another phase of the electron-slowing-down studies is associated with the measurements initiated last year on the series of thin gold films. We have repeated a portion of this work to resolve a discrepancy in connection with one of the sources. This discrepancy consisted of an unaccountably large depression in the secondary electron flux in the region near $10^2$ eV for one of the four sources on which we had obtained data.[5] Two new gold films of approximately the same thickness were prepared by vacuum evaporation onto beryllium substrates, and the slowing-down spectra were investigated in the usual manner. The spectrum of neither source exhibited the previously noted discrepancy.

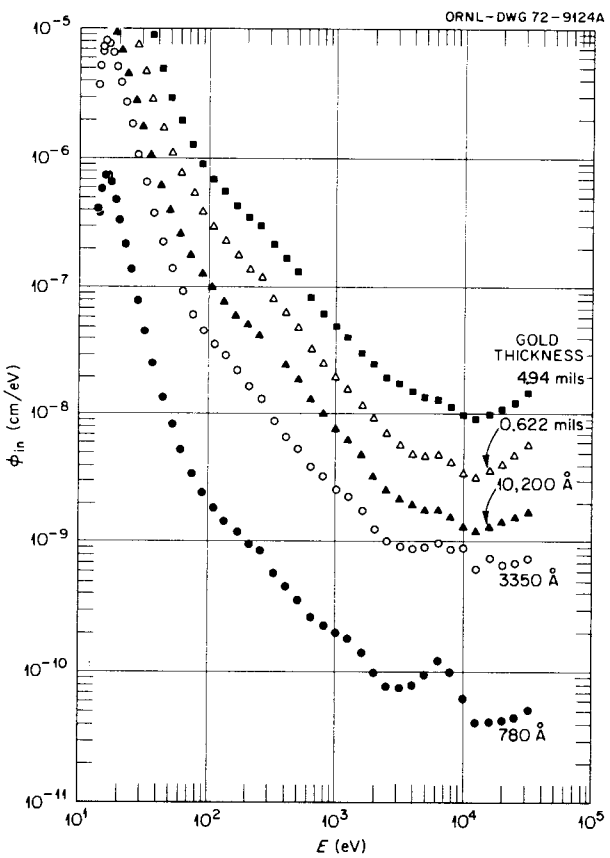


**Fig. 10.2. Variation of electron flux with energy from gold films of various thicknesses.**

These measurements have also been extended with gold films of different thicknesses to provide a more complete understanding of how the secondary electron flux depends on source thickness. The variation of the flux with thickness for five of the sources studied is shown in Fig. 10.2. The structure seen earlier at the *LMM* Auger energy is easily discernible in all but the thicker films. The more rapid rise in the secondary flux which was seen earlier in the very thin sources at low energies continues to be evident.

It is now clear that much information concerning the slowing-down processes can be obtained from studies of this type, particularly from very thin films. Although we have been unsuccessful in obtaining meaningful data from films with thicknesses less than 500 Å, we hope that by utilizing low-cross-section and high-purity source holders and optimizing the irradiation conditions we can obtain data for films as thin as 100 Å.

## OPTICAL PROPERTIES OF ORGANIC LIQUIDS

Since a large percentage of human tissue is in the liquid state, it is necessary to understand how ionizing radiations interact with simple, biologically related liquids in order to try to understand the more complicated interactions involved in tissue damage by ionizing radiations.

Several years ago a project was initiated to investigate the effects of substitutions and additions on the electronic properties of some simple aromatic molecules in the liquid state. Using a closed cell with a semicylindrical window, reflectance measurements as a function of photon angle of incidence were made on benzene ($C_6H_6$), pyridine ($C_5H_5N$), quinoline ($C_9H_7N$), and 2-ethylnaphthalene ($C_{10}H_7C_2H_5$) over the energy range 4 to 10.6 eV. The real and imaginary parts $n$ and $k$, respectively, of the refractive index were calculated for each liquid over the whole energy range studied, but it was found that when $k$ is small and $n$ large these reflectance measurements did not yield accurate values of $k$. Hence, transmission measurements have now been made on these liquids using a recently developed

transmission cell.[6] The $k$ values obtained for pyridine and quinoline from transmission measurements are shown in Figs. 10.3 and 10.4. When we used these $k$ values, self-consistent values of $n$ as a function of photon energy $E$ were calculated over the experimental energy range for $k$ from the following Kramers-Kronig relationship:

$$n(E) - 1 = \frac{2}{\pi}\int_0^\infty \frac{E'\,k(E')\,dE'}{(E')^2 - E^2}$$

$$= \frac{2}{\pi}\int_0^{E_0} \frac{E'\,k(E')\,dE'}{(E')^2 - E^2} + n_2(E)\,, \quad (1)$$

where $n_2(E)$ is the contribution to $n(E) - 1$ from the integral from $E_0$ to infinity. The experimentally determined values of $n(E)$ from reflectance measurements and $k(E)$ from transmittance measurements from 0 to $E_0$, the highest energy data point, were inserted into Eq. (1), and the quantity $n_2(E)$ was calculated. The quantity $n_2(E)$ should be a monotonically increasing function of $E$, and deviations from a smooth curve are interpreted as inconsistencies in $n(E)$ and/or $k(E)$. Since the $k$ values could be measured with good accuracy by the transmission method, any deviations in $n_2(E)$ from a smooth curve were considered to be caused by inconsistencies in the refractive indices. The refractive index values obtained from reflectance measurements were then corrected by the amounts that $n_2(E)$ deviated from a smooth curve. In this way self-consistent values of $n$ and $k$ have been obtained for benzene, pyridine, quinoline, and 2-ethylnaphthalene from 4 to 10.6 eV. The correct values of $n$, calculated by this Kramers-Kronig technique, are shown in Figs. 10.3 and 10.4 for pyridine and quinoline, respectively.

If we start with benzene, substitution of one carbon and one hydrogen by a nitrogen in the benzene ring gives pyridine. The optical properties of pyridine shown in Fig. 10.3 are very similar to those of benzene reported previously.[7] This is because the ultraviolet spectrum of benzene below about 9 eV is associated with the six $\pi$ electrons per molecule, which are still present in almost the same configuration in pyridine. We have previously identified a strong peak in $k$ at 6.5 eV for liquid benzene as due to the strongly allowed molecular excitation ${}^1A_{1g} - {}^1E_{1u}$ of the $\pi$ electrons in liquid benzene, that is, a $\pi - \pi^*$ excitation. We assume that the absorption shown in Fig. 10.3 for pyridine which peaks at 6.9 eV is due to the same $\pi - \pi^*$ excitation. Similarly, the absorption above about 9 eV is assumed to be due to $\sigma - \sigma^*$ excitations, as in benzene.

If we go to other aromatic compounds such as naphthalene, it is predicted[8] that the degeneracy due to the symmetry associated with the single ring in benzene and pyridine will be removed and the $\pi - \pi^*$ excitation will be split. As naphthalene is solid at room tempera-

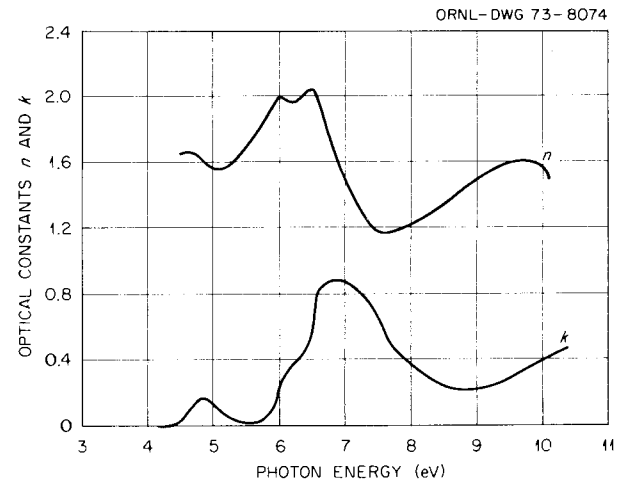


**Fig. 10.3. Optical constants of liquid pyridine vs photon energy.**

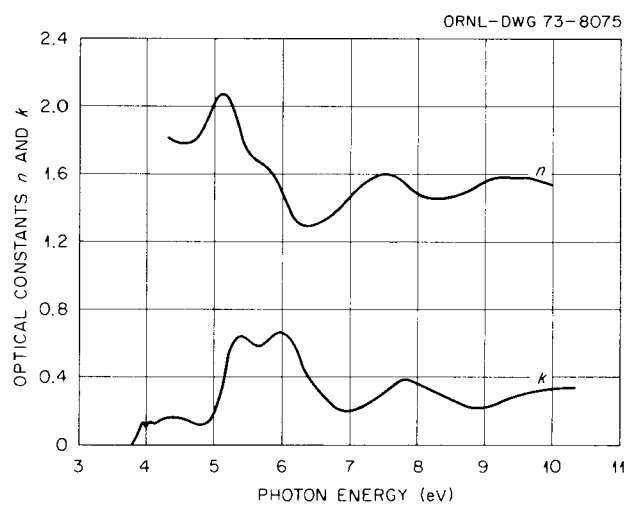


**Fig. 10.4. Optical constants of liquid quinoline vs photon energy.**

6. E. T. Arakawa et al., *Health Phys. Div. Annu. Progr. Rep. July 31, 1972,* ORNL-4811, pp. 21–23, and previous reports in this series.

7. M. W. Williams, R. A. MacRae, R. N. Hamm, and E. T. Arakawa, *Phys. Rev. Lett.* **22**, 1088 (1969).

ture, we chose to look at the two substituted systems, quinoline and 2-ethylnaphthalene, both of which are liquid at room temperature. It would be expected that both of these liquids would show basically the same structure as predicted for naphthalene in the vacuum ultraviolet. Klevens and Platt[8] predict $\pi - \pi^*$ absorption peaking at 5.64, 6.50, and 7.42 eV for naphthalene. We find in quinoline (Fig. 10.4) peaks in the absorption at 5.4, 6.0, and 7.85 eV, indicating that the degeneracy in the $\pi - \pi^*$ excitation is in fact removed as predicted. Similar results are obtained for 2-ethylnaphthalene.

The calculated energy loss functions $-\mathrm{Im}[1/\epsilon(E)]$, where $\epsilon = n^2 - k^2 + i2nk$, are shown for pyridine and quinoline in Figs. 10.5 and 10.6. The peaks in $-\mathrm{Im}(1/\epsilon)$ above about 5 eV are significantly displaced from the corresponding peaks in $k$ and thus show that conditions under which collective oscillations can occur in the liquids are satisfied. As for benzene,[7] presumably these collective oscillations would involve the same $\pi$ electrons as are involved in the $\pi - \pi^*$ excitations.

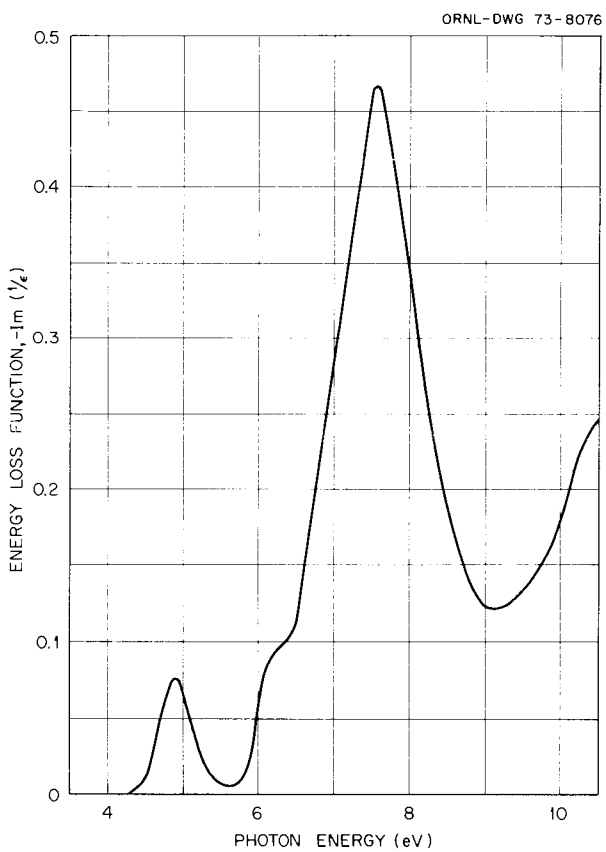


**Fig. 10.5. Energy-loss function, $-\mathrm{Im}(1/\epsilon)$, of liquid pyridine vs photon energy.**

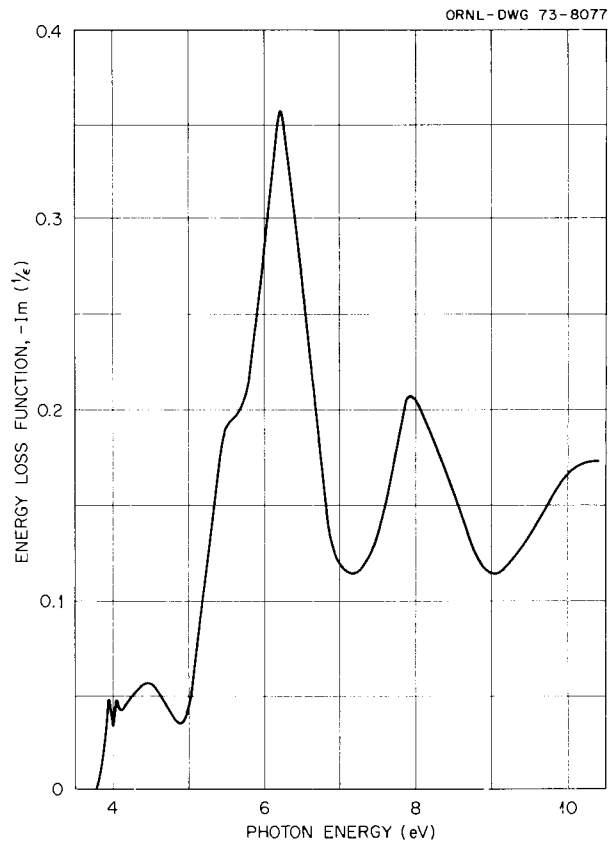


**Fig. 10.6. Energy-loss function, $-\mathrm{Im}(1/\epsilon)$, of liquid quinoline vs photon energy.**

## RADIATION INTERACTIONS WITH NUCLEIC ACID BASES

Characteristic electron energy-loss measurements, obtained using a scanning electron microscope equipped with a high-resolution magnetic spectrometer, have been reported in the literature for the nucleic acid bases. Eventually the aim is to refine this method so that the sequence of bases in a particular **DNA** molecule can be identified from the spectra of the individual bases. It has been thought that the results obtained might be affected by radiation damage done to the **DNA** molecule by the scanning electron beam. As a check on this, we have initiated a study of the optical properties of the nucleic acid bases which will enable us to calculate the energy-loss functions that can be compared directly with the measured electron energy-loss spectra.

8. H. B. Klevens and J. R. Platt, *J. Chem. Phys.* **17**, 470 (1949).

Previously we reported[9] the results of our initial studies on the optical and dielectric properties of the nucleic acid base guanine in the energy region extending from 14 to 82 eV. These data were obtained from an experimental study of the optical reflectance as a function of the angle of incidence. However, this method was insensitive to the optical constants below about 14 eV, necessitating the use of a different technique in this energy region. From 4 to 10 eV, $k$, the imaginary part of the refractive index, has been determined from measurements of transmittance as a function of film thickness for each experimental wavelength. These values of $k$ combined with the measured reflectance at 20° photon angle of incidence were then used to calculate $n$, the real part of the refractive index as a function of wavelength. These measurements were limited to the energy region below 10 eV by the absorption of the $CaF_2$ substrate.

Figure 10.7 shows the values of $k$ obtained over the wavelength range 1200 to 3200 Å for four different guanine films. These films were sublimed in vacuum onto the $CaF_2$ substrates, exposed to the atmosphere while being transferred to the monochromator, and measured with the films maintained in vacuum. There is virtually no experimental scatter associated with the $k$ data for a given film. The factors governing reproducibility of the transmission data from one film to the next are not yet understood. Inhomogeneities in the films, surface irregularities, and contamination are some of the factors which could be involved. Detailed experimentation on conditions affecting film structure, such as determination of optimum temperature and hence rate of sublimation, still has to be done. The near-normal-incidence reflectance is shown in Fig. 10.8. Also shown are $n$ values calculated at each wavelength from the reflectance and an averaged $k$ value from Fig. 10.7.

The energy-loss function $-\mathrm{Im}(1/\epsilon)$, where $\epsilon = n^2 - k^2 + i2nk$, has been calculated from the $n$ and $k$ values to compare with the electron energy-loss data of Johnson.[10] In Fig. 10.9 the values of $-\mathrm{Im}(1/\epsilon)$ from 0 to 10 eV obtained from the present study are shown along with the data reported earlier[9] covering the energy range from 14 to 80 eV. It is seen that there is fair agreement between the structure in $-\mathrm{Im}(1/\epsilon)$ and the structure in the electron energy-loss spectrum.

Similarly, exploratory transmission and normal incidence reflectance measurements have been made on

9. E. T. Arakawa et al., *Health Phys. Div. Annu. Progr. Rep. July 31, 1972*, ORNL-4811, pp. 23–24.
10. D. E. Johnson, *Radiat. Res.* 49, 63 (1972).

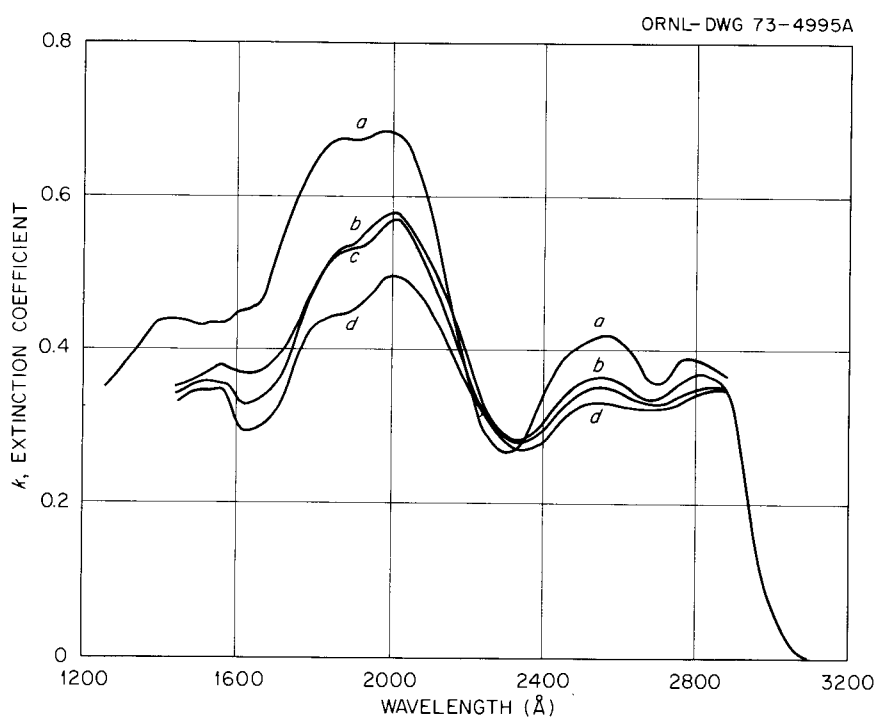


**Fig. 10.7. Extinction coefficient $k$ for guanine vs wavelength.**

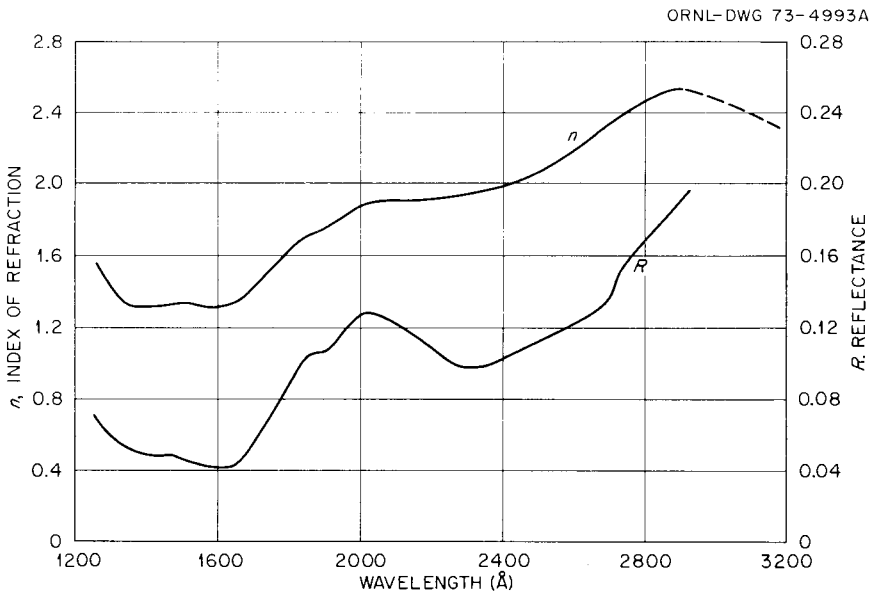


**Fig. 10.8. Refraction index $n$ and reflectance $R$ for guanine vs wavelength.**

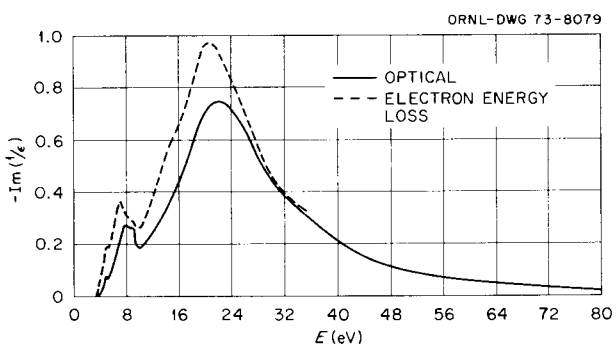


**Fig. 10.9. Energy-loss function for guanine: ——, calculated from optical data; ----, electron-energy-loss measurements.**

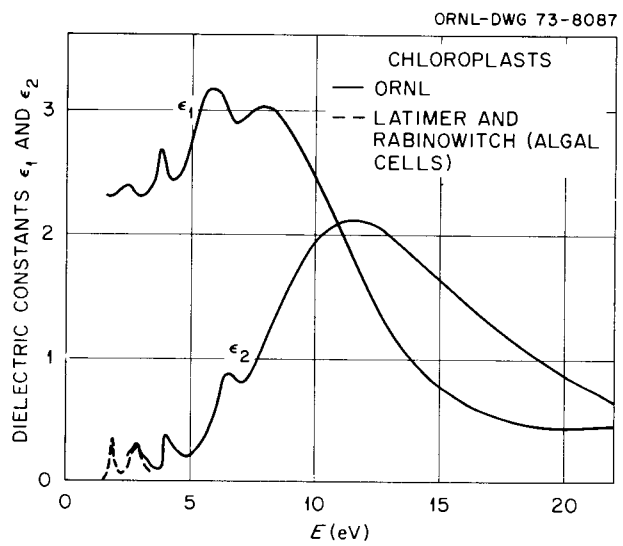


**Fig. 10.10. Dielectric constants of chloroplasts from 2 to 22 eV.**

thin films of adenine, cytosine, and thymine in the 4-to-10-eV energy region. When the problems associated with film preparation have been solved, measurements of the optical properties will be obtained over the full energy range from 0 to 80 eV.

## OPTICAL AND ELECTRONIC PROPERTIES OF CHLOROPHYLL

We have begun optical studies of chlorophyll in an attempt to improve our understanding of the optical and electronic processes involved in photosynthesis. Although photosynthesis occurs in the visible region of the spectrum, it may be influenced by electronic structure extending to much higher energies. Thus we have extended previous observations of the optical properties of chlorophyll into the ultraviolet energy region. Measurements have been made on chloroplasts – the chlorophyll-containing bodies in plant cells in which photosynthesis takes place – since in the chloroplasts the chlorophyll is protected from oxidation. The ORNL Biology Division has provided chloroplast samples in the form of films deposited on slides and on the flat side of a quartz semicylinder. We have measured the transmittance, reflectance as a function of

angle of incidence, and normal incidence reflectance and analyzed these measurements to obtain the optical and dielectric constants of chloroplasts in the energy region from 2 to 22 eV.

The chloroplast dielectric constants $\epsilon_1$ and $\epsilon_2$ are shown in Fig. 10.10 and are compared with the values of $\epsilon_2$ calculated from measurements obtained by Latimer and Rabinowitch[11] for visible light. The absorption peak in $\epsilon_2$ at 4 eV has been observed previously,[12] but the peak at 6.5 eV and the very broad absorption at about 11.5 eV have not been seen before.

We hope to be able to obtain smoother films in order to make better optical measurements and to make measurements on pure chlorophyll in order to determine what part of the absorption may be due to other constituents of the chloroplasts and what part is due to the chlorophyll itself.

---

11. P. Latimer and E. Rabinowitch, *J. Chem. Phys.* **24**, 480 (1956).

12. K. Sauer and R. B. Park, *Biochim. Biophys. Acta* 79, 476 (1964).

# Part III. Medical Physics and Internal Dosimetry

W. S. Snyder J. W. Poston

## 11. A Model for Exposure to a Semi-Infinite Cloud of a Photon Emitter

W. S. Snyder J. W. Poston L. T. Dillman[1]

Radionuclides present in the air may irradiate the body significantly as an external source in addition to the radiation received following inhalation or ingestion. In particular, the noble gases are of special importance due to the rapidity of their elimination from the body and the resulting low dose delivered from the internal source. In many cases the external source can be assumed to be infinite, particularly for radionuclides of long radioactive decay half-times, for example, $^{85}$Kr. Even when a finite cloud is assumed, one may be willing to accept the conservatism inherent in the assumption of an infinite cloud at a concentration approaching the maximum observed or assumed concentration rather than resort to more accurate, but much more complicated, calculations for the finite cloud. This study provided estimates of dose to body organs for monoenergetic photons emitted in the infinite cloud. These sources are for the same 12 energies used in the calculations reported in MIRD Pamphlet No. 5 and use the same type of phantom and the Monte Carlo techniques developed there.[2] It is expected that dose from photons emitted in the decay of a real radionuclide could be obtained by interpolation from these results. Previous results have usually been given only for a surface dose at the boundary of a half space containing no emitter. However, these results give no indication of the depth dose within the body or of dose to individual body organs, and it is not always conservative in that there may be a considerable contribution to dose from photons transmitted through the body.

If a hypothetical photon emitter emitting 1 photon of energy $E_0$ per disintegration is considered to be distributed uniformly in an infinite cloud with intensity of 1 $\mu$Ci per gram of air $\cong$ ($3.2 \times 10^9$ disintegrations/day) per gram of air, the dose rate in the air is $51E_0$ rads/day. If one considers an infinitesimal tissue element in the field, it will be irradiated by photons of a spectrum of energies not exceeding $E_0$. The first objective of the approach taken here is to calculate this energy spectrum. Because the initial photon may be assumed to be emitted isotropically, all succeeding generations of photons will also be distributed isotropically. Thus, one need only calculate the spectrum of energies in energy space. The program for calculating this energy spectrum has been developed by Dillman.[3]

Photons chosen randomly from this spectrum of energies were programmed to impinge randomly on the surface of the phantom, the distribution of angles being chosen to represent an isotropic emission of photons in the cloud; that is, the direction was chosen from the cumulative distribution:

$$\text{Probability } (\theta < \theta_0) = \sin^2 \theta_0,$$

$\theta$ being the acute angle the photon direction makes with the inward-pointing normal to the surface. The phantom[2] used was essentially that described in MIRD Pamphlet No. 5 with the modifications mentioned in the SEE report.[4] The photon energy was determined by

1. Consultant, Ohio Wesleyan University.
2. W. S. Snyder, M. R. Ford, G. G. Warner, and H. L. Fisher, Jr., *Estimates of Absorbed Fractions for Monoenergetic Photon Sources Uniformly Distributed in Various Organs of a Heterogeneous Phantom,* MIRD Suppl. No. 3, Pamphlet 5, August 1969.
3. L. T. Dillman, *Absorbed Gamma Dose for Immersion in a Semi-Infinite Radioactive Cloud,* in press.
4. W. S. Snyder et al., *Values of Specific Effective Energies for Selected Radionuclides,* in press.

independent selection from the calculated incident spectrum. A sample of 60,000 photons was used for each monoenergetic source, and the values of dose per photon incident on the phantom are tabulated in Table 11.1. The values not underscored had a coefficient of variation of less than 30% and were accepted on the basis of this calculation.

In Table 11.2 the results have been normalized to provide estimates of dose rate (rads/day) corresponding to a concentration in the cloud of 1 $\mu$Ci/m$^3$ of a hypothetical emitter with a yield of 1 photon per disintegration at the indicated energy. To do this, the absorbed dose per incident photon as determined by the Monte Carlo calculation has been multiplied by the surface area of the phantom, the photon flux density (as calculated by Dillman) incident on the exterior surface of the phantom, and the appropriate factors to convert time from seconds to days and source intensity from 1 $\mu$Ci/g of air to 1 $\mu$Ci/m$^3$ of air at STP. This result is then divided by a factor of 2 to account for the presence of the ground which removes essentially half the source strength. Although the energy and angular distribution of photons striking the phantom must differ somewhat from that in the infinite medium, the assumption that they differ by a constant factor seems consistent with the dosimetric data available (Dillman, 1973). The authors are not aware of a more exact treatment of the spectrum near an air-ground interface. The conversion factors are tabulated as a function of energy in Table 11.3.

To obtain more accurate estimates for calculated values with coefficients of variation greater than 30%, we plotted the average dose found in the Monte Carlo calculations for various regions of the phantom which are defined by a regular geometrical grid of surfaces. The average dose in each of these regions was used as an additional datum from the Monte Carlo calculations and had the advantage that, generally speaking, their coefficients of variation were smaller than those calculated for many of the particular organs. Moreover, their regular variations of size and of depth below the irradiated surfaces of the phantom undoubtedly produced considerable regularity in their joint statistical behavior.

The technique employed to provide the above-mentioned estimates was based on the use of these 85 geometrical subregions in the trunk of the adult phantom. These regions allow one to plot depth-dose

**Table 11.1. Absorbed dose for selected organs from cloud source**

| Organ | Absorbed dose (rads/photon) for initial photon energy of – | | | | | | | | | | | |
|---|---|---|---|---|---|---|---|---|---|---|---|---|
| | 0.01 MeV | 0.015 MeV | 0.02 MeV | 0.03 MeV | 0.05 MeV | 0.1 MeV | 0.2 MeV | 0.5 MeV | 1.0 MeV | 1.5 MeV | 2.0 MeV | 4.0 MeV |
| Bladder | 3.2–23 | 3.6–18 | 1.4–16 | 1.8–15 | 2.9–15 | 5.0–15 | 6.4–15 | 1.4–14 | 2.8–14 | 4.1–14 | 4.2–14 | 2.1–13 |
| Stomach | 4.5–16 | 1.8–16 | 5.2–16 | 2.1–15 | 3.9–15 | 4.7–15 | 6.5–15 | 1.8–14 | 2.6–14 | 4.1–14 | 5.5–14 | 7.7–14 |
| Small intestine | 3.5–19 | 1.1–17 | 1.0–16 | 9.2–16 | 2.7–15 | 4.7–15 | 7.0–15 | 1.3–14 | 2.4–14 | 3.4–14 | 4.7–14 | 1.1–13 |
| U.L.I | 6.1–19 | 2.7–18 | 1.8–16 | 1.3–15 | 3.0–15 | 4.6–15 | 7.2–15 | 1.4–14 | 2.8–14 | 4.5–14 | 7.2–14 | 1.3–13 |
| L.L.I. | 7.3–17 | 8.8–16 | 4.6–16 | 6.4–16 | 2.5–15 | 3.8–15 | 5.5–15 | 1.3–14 | 2.0–14 | 3.8–14 | 5.0–14 | 1.0–13 |
| Kidneys | 2.6–19 | 3.3–17 | 1.2–15 | 3.0–15 | 3.9–15 | 5.3–15 | 7.2–15 | 1.6–14 | 2.9–14 | 3.1–14 | 4.6–14 | 9.5–14 |
| Liver | 1.9–18 | 3.5–17 | 4.0–16 | 2.0–15 | 3.7–15 | 5.4–15 | 7.6–15 | 1.5–14 | 2.6–14 | 3.7–14 | 5.3–14 | 1.1–13 |
| Lungs | 1.8–16 | 3.8–16 | 6.3–16 | 2.7–15 | 4.5–15 | 6.1–15 | 8.8–15 | 1.7–14 | 2.9–14 | 4.2–14 | 5.7–14 | 1.1–13 |
| Marrow | 3.5–16 | 2.0–15 | 4.3–15 | 8.7–15 | 1.3–14 | 1.3–14 | 1.5–14 | 2.2–14 | 3.4–14 | 4.5–14 | 5.9–14 | 1.1–13 |
| Yellow | 4.3–16 | 2.4–15 | 5.1–15 | 1.0–14 | 1.4–14 | 1.4–14 | 1.6–14 | 2.3–14 | 3.6–14 | 4.7–14 | 6.3–14 | 1.2–13 |
| Red | 2.7–16 | 1.6–15 | 3.5–15 | 7.3–15 | 1.1–14 | 1.2–14 | 1.4–14 | 2.1–14 | 3.1–14 | 4.3–14 | 5.5–14 | 1.0–13 |
| Muscle | 7.4–16 | 2.5–15 | 3.8–15 | 4.9–15 | 5.3–15 | 6.3–15 | 9.1–15 | 1.8–14 | 3.1–14 | 4.4–14 | 5.9–14 | 1.2–13 |
| Ovaries | 9.5–17 | 1.7–16 | 6.2–16 | 1.9–15 | 3.8–15 | 3.1–15 | 5.4–15 | 6.6–15 | 1.9–14 | 4.1–14 | 6.3–14 | 1.2–13 |
| Pancreas | 1.3–16 | 2.8–16 | 8.5–16 | 6.6–16 | 2.7–15 | 3.8–15 | 5.9–15 | 1.1–14 | 3.1–14 | 3.8–14 | 6.2–14 | 2.1–13 |
| Skeleton | 3.3–16 | 1.9–15 | 4.0–15 | 8.1–15 | 1.2–14 | 1.3–14 | 1.5–14 | 2.2–14 | 3.4–14 | 4.6–14 | 6.1–14 | 1.2–13 |
| Skin | 4.1–14 | 3.0–14 | 2.0–14 | 1.2–14 | 8.5–15 | 8.4–15 | 1.2–14 | 2.2–14 | 4.0–14 | 4.8–14 | 7.2–14 | 1.3–13 |
| Spleen | 4.5–17 | 1.8–16 | 3.5–16 | 1.8–15 | 3.6–15 | 4.4–15 | 8.1–15 | 1.9–14 | 3.1–14 | 5.0–14 | 3.7–14 | 1.1–13 |
| Testes | 1.6–15 | 2.2–15 | 5.8–15 | 7.3–15 | 5.4–15 | 6.8–15 | 1.3–14 | 2.0–14 | 2.8–14 | 3.3–14 | 3.0–14 | 7.2–14 |
| Thymus | 2.7–20 | 1.7–17 | 3.0–16 | 2.8–15 | 4.0–15 | 3.8–15 | 8.1–15 | 1.1–14 | 2.1–14 | 4.1–14 | 6.2–14 | 2.0–13 |
| Thyroid | 9.1–17 | 1.4–17 | 1.5–15 | 5.6–15 | 6.1–15 | 8.9–15 | 9.5–15 | 1.5–14 | 2.3–14 | 4.4–14 | 5.5–14 | 2.1–13 |
| Uterus | 1.8–20 | 2.5–19 | 3.8–17 | 6.8–16 | 1.0–15 | 3.0–15 | 6.0–15 | 1.2–14 | 2.2–14 | 3.0–14 | 4.7–14 | 9.2–14 |
| Total body | 2.2–15 | 3.2–15 | 4.1–15 | 5.3–15 | 6.2–15 | 7.3–15 | 9.9–15 | 1.8–14 | 3.1–14 | 4.4–14 | 5.9–14 | 1.2–13 |

Note: underlining indicates values estimated by the technique described in text; Monte Carlo results for these organs and energies had coefficients of variation greater than 30%.

**Table 11.2. Absorbed dose rate for selected organs from cloud source**

Assumes 1 $\mu$Ci/m$^3$ in air

| Organ | Absorbed dose rate (rads/day) for initial photon energy of – | | | | | | | | | | | |
|---|---|---|---|---|---|---|---|---|---|---|---|---|
| | 0.01 MeV | 0.015 MeV | 0.02 MeV | 0.03 MeV | 0.05 MeV | 0.1 MeV | 0.2 MeV | 0.5 MeV | 1.0 MeV | 1.5 MeV | 2.0 MeV | 4.0 MeV |
| Bladder | 2.95–14 | 1.25–8 | 1.20–6 | 5.02–5 | 2.65–4 | 1.09–3 | 1.98–3 | 5.97–3 | 1.34–2 | 2.29–2 | 2.30–2 | 1.25–1 |
| Stomach | 5.24–7 | 6.00–7 | 4.65–6 | 6.03–5 | 3.61–4 | 1.00–3 | 2.06–3 | 7.47–3 | 1.26–2 | 2.32–2 | 2.97–2 | 4.50–2 |
| Small intestine | 3.30–10 | 3.80–8 | 8.00–7 | 2.65–5 | 2.52–4 | 1.00–3 | 2.19–3 | 5.48–3 | 1.15–2 | 1.91–2 | 2.61–2 | 6.50–2 |
| U.L.I. | 6.02–10 | 9.51–9 | 1.55–6 | 3.75–5 | 2.79–4 | 9.52–4 | 2.30–3 | 6.11–3 | 1.34–2 | 2.55–2 | 3.95–2 | 7.50–2 |
| L.L.I. | 6.99–8 | 3.05–6 | 3.85–6 | 1.85–5 | 2.29–4 | 8.13–3 | 1.75–3 | 5.51–3 | 9.49–3 | 2.15–2 | 2.75–2 | 6.03–2 |
| Kidneys | 2.45–10 | 1.10–7 | 1.01–5 | 8.49–5 | 3.61–4 | 1.12–3 | 2.29–3 | 6.51–3 | 1.41–2 | 1.75–2 | 2.50–2 | 5.49–2 |
| Liver | 1.80–9 | 1.20–7 | 3.45–6 | 6.01–5 | 3.40–4 | 1.17–3 | 2.42–3 | 6.48–3 | 1.26–2 | 2.09–2 | 2.93–2 | 6.50–2 |
| Lungs | 1.69–7 | 1.29–6 | 5.05–6 | 7.49–5 | 4.25–4 | 1.32–3 | 2.81–3 | 7.02–3 | 1.40–2 | 2.36–2 | 3.14–2 | 6.48–2 |
| Marrow | 3.30–7 | 7.03–6 | 3.69–5 | 2.51–4 | 1.19–3 | 2.79–3 | 4.70–3 | 9.19–3 | 1.67–2 | 2.55–2 | 3.27–2 | 6.52–2 |
| Yellow | 3.85–7 | 8.01–6 | 4.25–5 | 2.90–4 | 1.32–3 | 3.00–3 | 5.11–3 | 9.61–3 | 1.74–2 | 2.66–2 | 3.44–2 | 7.00–2 |
| Red | 2.50–7 | 5.49–6 | 2.98–5 | 2.09–4 | 1.00–3 | 2.55–3 | 4.41–3 | 8.77–3 | 1.50–2 | 2.45–2 | 3.00–2 | 5.97–2 |
| Muscle | 6.99–7 | 8.50–6 | 3.30–5 | 1.45–4 | 4.98–4 | 1.35–3 | 2.85–3 | 7.51–3 | 1.49–2 | 2.49–2 | 3.25–2 | 6.96–2 |
| Ovaries | 9.02–8 | 5.98–7 | 5.05–6 | 5.53–5 | 3.48–4 | 6.48–4 | 1.72–3 | 2.75–3 | 9.01–3 | 2.31–2 | 3.47–2 | 7.03–2 |
| Pancreas | 1.21–7 | 9.49–7 | 7.50–6 | 1.90–5 | 2.52–4 | 7.97–4 | 1.86–3 | 4.11–3 | 1.51–2 | 2.14–2 | 3.40–2 | 1.25–1 |
| Skeleton | 3.09–7 | 6.48–6 | 3.45–5 | 2.30–4 | 1.11–3 | 2.80–3 | 4.68–3 | 9.11–3 | 1.65–2 | 2.58–2 | 3.35–2 | 7.01–2 |
| Skin | 3.85–5 | 1.04–4 | 1.75–4 | 3.45–4 | 7.51–4 | 1.79–3 | 3.78–3 | 8.99–3 | 1.94–2 | 2.71–2 | 3.95–2 | 7.50–2 |
| Spleen | 4.25–8 | 6.00–7 | 3.00–6 | 5.02–5 | 3.30–4 | 9.52–4 | 2.55–3 | 8.00–3 | 1.48–2 | 2.82–2 | 2.05–2 | 6.47–2 |
| Testes | 1.50–6 | 7.51–6 | 5.01–5 | 2.09–4 | 5.01–4 | 1.45–3 | 4.08–3 | 8.49–3 | 1.35–2 | 1.85–2 | 1.65–2 | 4.20–2 |
| Thymus | 2.50–11 | 5.97–8 | 2.60–6 | 8.00–5 | 3.70–4 | 8.00–4 | 2.56–3 | 4.58–3 | 1.01–2 | 2.29–2 | 3.41–2 | 1.15–1 |
| Thyroid | 8.49–8 | 5.00–8 | 1.29–5 | 1.59–4 | 5.97–4 | 1.92–3 | 3.02–3 | 6.25–3 | 1.09–2 | 2.51–2 | 3.03–2 | 1.25–1 |
| Uterus | 1.68–11 | 8.50–10 | 3.30–7 | 1.95–5 | 9.49–5 | 6.49–4 | 1.88–3 | 5.03–3 | 1.04–2 | 1.68–2 | 2.59–2 | 5.51–2 |
| Total body | 2.05–6 | 1.10–5 | 3.50–5 | 1.49–4 | 6.02–4 | 1.55–3 | 3.15–3 | 7.52–3 | 1.48–2 | 2.49–2 | 3.25–2 | 7.00–2 |

Note: underlining indicates values estimated by the technique described in the text; Monte Carlo results for these organs and energies had coefficients of variation greater than 30%.

**Table 11.3. Number of photons per day impinging on phantom[a]**

Conversion factors for photon cloud source

| Initial energy (MeV) | Photon flux density (photons cm$^{-2}$ sec$^{-1}$) | Photons/day[b] | Photons/day[c] |
|---|---|---|---|
| 0.01 | $1.92 \times 10^3$ | $2.42 \times 10^{12}$ | $1.87 \times 10^9$ |
| 0.015 | $7.09 \times 10^3$ | $8.93 \times 10^{12}$ | $6.90 \times 10^9$ |
| 0.02 | $1.77 \times 10^4$ | $2.23 \times 10^{13}$ | $1.72 \times 10^{10}$ |
| 0.03 | $5.91 \times 10^4$ | $7.45 \times 10^{13}$ | $5.76 \times 10^{10}$ |
| 0.05 | $1.90 \times 10^5$ | $2.39 \times 10^{14}$ | $1.85 \times 10^{11}$ |
| 0.1 | $4.40 \times 10^5$ | $5.54 \times 10^{14}$ | $4.28 \times 10^{11}$ |
| 0.2 | $6.50 \times 10^5$ | $8.16 \times 10^{14}$ | $6.31 \times 10^{11}$ |
| 0.5 | $8.60 \times 10^5$ | $1.08 \times 10^{15}$ | $8.35 \times 10^{11}$ |
| 1.0 | $9.99 \times 10^5$ | $1.26 \times 10^{15}$ | $9.74 \times 10^{11}$ |
| 1.5 | $1.16 \times 10^6$ | $1.46 \times 10^{15}$ | $1.13 \times 10^{12}$ |
| 2.0 | $1.13 \times 10^6$ | $1.42 \times 10^{15}$ | $1.10 \times 10^{12}$ |
| 4.0 | $1.20 \times 10^6$ | $1.52 \times 10^{15}$ | $1.17 \times 10^{12}$ |

[a]Surface area of phantom, 14,576 cm$^2$.
[b]Assuming 1 $\mu$Ci/g of air at STP.
[c]Assuming 1 $\mu$Ci/m$^3$ of air at STP.

profiles in the phantom, along the major and minor axes of the elliptical cross section, for each of the five tiers in the trunk. These profiles were constructed for each photon energy. The data were fitted, by use of a computer, with a smooth curve, and the resulting sets of curves were used to provide estimates of the absorbed dose to the organs of interest. Typical depth-dose profiles in tier one (the lowest tier in the trunk), plotted for photon energies of 0.03 and 1 MeV, are shown in Fig. 11.1. A schematic drawing of each organ was prepared which gave the location of the organ in the tier and the subregions which comprised the tier. Figure 11.2 shows a view of tier one and the location of the bladder in the geometric volume elements. By combining these schematic drawings and the depth-dose profiles, an estimate of the absorbed dose to each organ or region was derived. These estimates of absorbed dose were used in the tables for organs which had a coefficient of variation in excess of 30%.

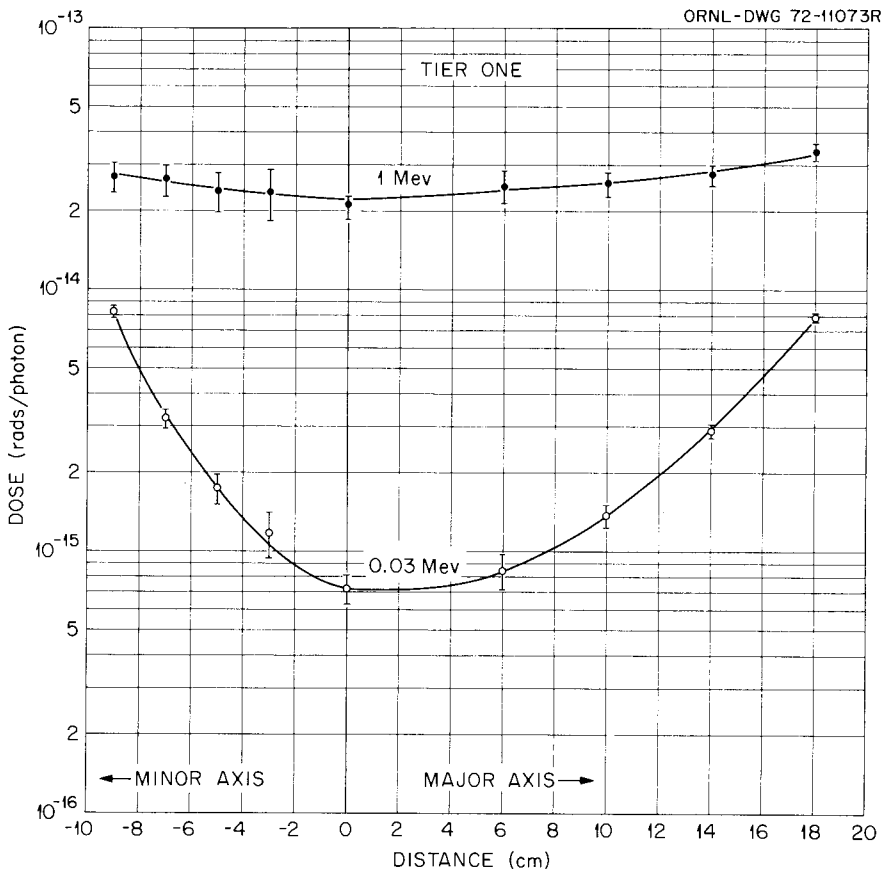


**Fig. 11.1. Dose per photon from infinite cloud.** Energies 1 and 0.03 MeV.

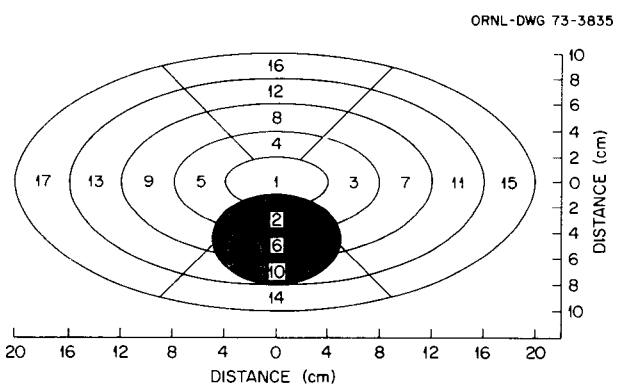


**Fig. 11.2. Schematic drawing of tier one showing locations of volume elements and the bladder.**

Before extensive use of this method was made in this study, a number of checks were made with statistically reliable data. The technique described above was used to provide estimates of absorbed dose to the major organs of the phantom for cases where the coefficients of variation were much less than 30%. These tests demonstrated that the technique could provide reliable estimates of absorbed dose for the majority of organs. Table 11.4 presents a comparison of absorbed dose from the Monte Carlo calculation and the absorbed dose estimated as described above. The photon energies of 0.2 and 2 MeV were chosen to illustrate this technique, since the Monte Carlo calculations gave results with coefficients of variation less than 30%; thus the calculated results were considered to be reliable. Organs for which estimates did not agree closely with calculated values were generally very complex (e.g., the upper large intestine) and extended into several tiers and many subregions of the phantom. However, by modifying the techniques, when applied to specific organs with very complex geometries, estimates of absorbed dose were derived which provided estimates of absorbed dose within 30% of the calculated values. After these checks were completed, the technique was applied to provide estimates of absorbed dose per incident photon (Table 11.1) and thus dose rate (Table

11.2) to complete the tabulations. As pointed out previously, these estimates have been underscored in Tables 11.1 and 11.2. It is readily apparent that, in general, these estimates were required for low-energy photons and/or for organs which had small volumes.

The absorbed dose from photons emitted in the decay of a real radionuclide may be obtained by interpolation or by extrapolation from these results. Clearly, the results will depend to some extent on the interpolation formula used, but for the extrapolated values it appears the linear extrapolation to 0 probably produces a conservative estimate of dose, since the dose vs energy curves we have examined appear to be concave upward in the energy region up to 50 keV.

**Acknowledgments.** The contributions of Mr. Billy L. Edge of the Georgia Institute of Technology in the preliminary analysis of the results are gratefully acknowledged.

**Table 11.4. Comparison of estimated and calculated absorbed dose to selected organs**

| Organ | Absorbed dose (rads/photon) from source in cloud[a] | | | | | |
|---|---|---|---|---|---|---|
| | 0.2 MeV | | | 2 MeV | | |
| | Monte Carlo calculation | Estimate from depth dose | Ratio MC/DD | Monte Carlo calculation | Estimate from depth dose | Ratio MC/DD |
| | $\times 10^{-15}$ | $\times 10^{-15}$ | | $\times 10^{-14}$ | $\times 10^{-14}$ | |
| Bladder | 6.35 | 7.52 | 0.844 | 4.18 | 5.20 | 0.804 |
| Stomach | 6.45 | 9.05 | 0.713 | 5.46 | 5.53 | 0.987 |
| ULI | 7.25 | 7.04 | 1.03 | 7.25 | 4.75 | 1.53 |
| LLI | 5.51 | 7.60 | 0.725 | 5.00 | 5.18 | 0.965 |
| Kidneys | 7.18 | 8.28 | 0.867 | 4.65 | 5.34 | 0.871 |
| Lungs | 8.82 | 8.30 | 1.06 | 5.69 | 5.38 | 1.06 |
| Ovaries | 5.44 | 7.82 | 0.696 | 6.29 | 5.24 | 1.20 |
| Pancreas | 5.94 | 8.05 | 0.737 | 6.17 | 5.31 | 1.16 |
| Spleen | 8.06 | 9.05 | 0.891 | 3.73 | 5.52 | 0.676 |
| Testes | 12.8 | 9.34 | 1.37 | 3.01 | 5.52 | 0.545 |
| Thymus | 8.15 | 8.08 | 1.01 | 6.20 | 5.27 | 1.18 |
| Thyroid | 9.49 | 10.4 | 0.913 | 5.55 | 5.50 | 1.01 |
| Uterus | 6.00 | 6.76 | 0.888 | 2.44 | 4.68 | 0.521 |

[a]Absorbed dose per photon impinging on the surface of the phantom.

# 12. Estimation of Dose and Dose Commitment to the Bladder Wall from a Photon Emitter Present in Urine

W. S. Snyder M. R. Ford

The bladder is one of the more variable organs of the body, and dose rate from a photon emitter present in urine may differ by up to an order of magnitude during the course of a filling.[1] Data published in ref. 1 provide a basis for a reasonably accurate estimate of dose from photons present in the urine in individual cases. That is, if one specifies a radionuclide, its rate of excretion in urine, the rate at which urine is produced, and the number of voids per day, one can apply the formulas to obtain an accurate estimate of dose. However, the practical implications of the fact that the dose depends on so many parameters have not been explored, and this is the problem discussed below. The choice of the radionuclide, and hence its model for excretion in the urine, will often be dictated by other considerations. In some cases the clinician may vary the amount of urine produced by varying the fluid intake. He may be able to influence the schedule for voidings, and, particularly, he may choose to administer the isotope when the bladder is nearly empty or he may administer the radionuclide when he estimates it to be partly filled. Although he cannot be expected to realize the precise situation for which dose is a minimum, the clinician may find it of interest to note the approximate ranges of the above variables where dose is significantly less than for other ranges.

The bladder is considered to be an ellipsoid with semiaxes in the directions of the $X$, $Y$, $Z$ axes proportional to 4:3:3, the $Z$ axis being directed upward, the $X$ axis to the left, and the $Y$ axis toward the back. The wall is considered to have a constant mass of 45 g, and its thickness varies approximately in the above ratios as the bladder expands. Dose to the bladder wall from photons emitted in urine has been computed by Monte Carlo techniques for the 12 energies of photons used in MIRD Pamphlet No. 5 and for bladder contents of 0, 50, 100, 200, 300, 400, and 500 ml. The dose received by the wall per photon emitted has been fitted with a two-exponential formula

$$D_p(V, E) = ae^{-\alpha V} + be^{-\beta V} \text{ (rads/photon)}, \qquad (1)$$

where $V$ is the volume of the bladder contents in ml, $E$ is the photon energy in MeV, and the values of $a$, $\alpha$, $b$, and $\beta$ are given in Table 12.1 together with the coefficient of variation of the result for the various energies.[1] It will be noted that the coefficient of variation of results for the different volumes ranges from about −11 to +11%, but when averaged over all the volumes representing a filling it is about 5% at most, and this is considered sufficiently accurate for clinical applications.

Consider a radionuclide excreted into the urine according to the formula

$$\sum_{i=1}^{n} A_i e^{-(\lambda_i+\lambda_r)t} \text{ (}\mu\text{Ci/day)}, \qquad (2)$$

where $\lambda_i$ represents the rate of biological elimination, $\lambda_r$ represents the constant rate of radioactive decay, and the coefficients $A_i$ represent the rate of urinary excretion into the bladder at time $t = 0$ from compartment $i$. For example, such an excretion formula arises whenever retention in the body is represented as a sum of exponential terms and all, or a fixed portion, of the excretion is by the bladder. If urine enters the bladder at a constant rate, say, $\gamma$ ml/day, and if $t_1$, $t_2$, ... $t_m$ represent times of successive voids, one can calculate the dose received by the bladder wall for one filling by the following considerations: The activity

1. W. S. Snyder, Mary R. Ford, and G. G. Warner, "Estimation of Dose and Dose Commitment to Bladder Wall from a Radionuclide Present in Urine," *Health Phys. Div. Annu. Progr. Rep. July 31, 1970,* ORNL-4584, p. 206.

Table 12.1. Parameter values for dose to bladder wall: $D_p(V) = ae^{-\alpha V} + be^{-\beta V}$ (rads/photon)

| $E$ (MeV) | $a$ | $\alpha$ | $b$ | $\beta$ | Deviation of function and data (%) | |
|---|---|---|---|---|---|---|
| | | | | | Average | Maximum |
| | $\times 10^{-12}$ | | $\times 10^{-12}$ | | | |
| 0.01 | 0.126 | 0.00168 | 3.474 | 0.0953 | ±2.51 | +4.8 |
| 0.015 | 0.479 | 0.00252 | 4.811 | 0.0631 | ±4.28 | +8.9 |
| 0.02 | 0.872 | 0.00292 | 5.301 | 0.0507 | ±4.44 | +8.7 |
| 0.03 | 0.977 | 0.00248 | 4.162 | 0.0388 | ±3.83 | +10.7 |
| 0.05 | 0.807 | 0.00218 | 2.172 | 0.0390 | ±3.65 | +8.6 |
| 0.1 | 0.766 | 0.00195 | 2.022 | 0.0378 | ±2.30 | −5.4 |
| 0.2 | 1.311 | 0.00187 | 4.124 | 0.0344 | ±4.04 | +9.0 |
| 0.5 | 3.284 | 0.00192 | 10.471 | 0.0342 | ±3.66 | −7.8 |
| 1.0 | 6.137 | 0.00213 | 19.916 | 0.0349 | ±2.56 | −4.6 |
| 1.5 | 8.274 | 0.00199 | 28.293 | 0.0377 | ±3.03 | −6.0 |
| 2.0 | 10.587 | 0.00198 | 34.723 | 0.0414 | ±2.04 | −4.6 |
| 4.0 | 19.086 | 0.00235 | 53.210 | 0.0380 | ±5.08 | −10.9 |

present in the bladder at time $t$ after $t_{m-1}$ is

$$\int_{t_{m-1}}^{t} d\tau \sum_{i=1}^{n} A_i e^{-(\lambda_i+\lambda_r)\tau} - e^{-\lambda_r(t-\tau)}$$

$$= \sum_{i=1}^{n} \frac{A_i e^{-\lambda_r t}(e^{-\lambda_i t_{m-1}} - e^{-\lambda_i t})}{\lambda_i}, \quad (3)$$

where $e^{-\lambda_r(t-\tau)}$ represents the effect of radioactive decay following the entry of activity into the bladder during the time interval $d\tau$. Since $D_p(V, E)$ is in units of rads per photon emitted, we have

$$D_m = 3.2 \times 10^9 \sum_{j=1}^{k} Y_j \int_{t_{m-1}}^{t_m} dt\, D_p[\gamma(t - t_{m-1}), E_j]$$

$$\times \sum_{i=1}^{m} \frac{A_i e^{-\lambda_r t}\,(e^{-\lambda_i t_{m-1}} - e^{-\lambda_i t})}{\lambda_i} \quad (4)$$

$$= 3.2 \times 10^9 \sum_{j=1}^{k} Y_j \int_{t_{m-1}}^{t_m} dt\,[a_j e^{-\alpha_j \gamma(t-t_{m-1})}$$

$$+ b_j e^{-\beta_j \gamma(t-t_{m-1})}]$$

$$\times \sum_{i=1}^{m} \frac{A_i e^{-\lambda_r t}\,(e^{-\lambda_i t_{m-1}} - e^{-\lambda_i t})}{\lambda_i} \text{(rads)}, \quad (5)$$

where $3.2 \times 10^9$ is the number of disintegrations per day/$\mu$Ci, $Y_j$ is the yield per disintegration of photons of a certain energy $E_j$, and one interpolates on $a_j$, $\alpha_j$, $b_j$, $\beta_j$ according to the energy of the photon. If the energy lies below 10 keV, one extrapolates linearly to zero on the energy in estimating the dose. Essentially, this formula is derived in ref. 1.

Formula (4) has been programmed for a digital computer to produce estimates of dose for one or for many fillings of the bladder. Clearly, the factor $e^{-(\lambda_r+\lambda_i)t_{m-1}}$ can be factored out of the terms in the final summation, and the remaining expression is then a function of $t - t_{m-1}$. This merely emphasizes that if the second voiding time equals the first, the dose due to compartment $i$ for the second time interval is $e^{-(\lambda_r+\lambda_i)t_1}$ multiplied by the dose from the first. This principle is used to produce a total dose for a given compartment by dividing the dose during the first day by $1 - e^{-(\lambda_i+\lambda_r)}$ to obtain the total dose.

This program has been used to estimate the dose received by the bladder as a function of: (1) the photon energy, the 12 energies used in MIRD Pamphlet No. 5 being used, that is, 0.01, 0.015, 0.02, 0.03, 0.05, 0.1, 0.2, 0.5, 1, 1.5, 2, and 4 MeV; (2) the rate of entry of urine into the bladder, $\gamma$ being taken equal to 1, 1.4, and 2 liters/day; (3) the rates of biological elimination $\lambda_i$ and of radioactive decay $\lambda_r$ being independently set equal to 1 hr, 2 hr, 4 hr, 8 hr, 1 day, 2 days, and 10 days; (4) the voiding schedule, regimes of 4 voids per day, 7 voids per day, and 10 voids per day being used.

Considering that the choice of radionuclide likely will be determined by other factors, we have sought answers to the following two questions:

1. What saving of dose results if the clinician can change the rate of formation of urine?
2. Assuming the clinician can arrange to administer the radionuclide at a time when the bladder is partly filled, what saving of dose results?

Initial volumes of 0.2, 0.4, 0.6, and 0.8 of the volume assigned for a void have been used for this purpose.

The answer to the first question is indicated in Fig. 12.1. Surprisingly, for all the energies tried, all the voiding schedules tried, and all the rates of biological elimination and radioactive decay programmed, the dose saved due to a doubling of the rate of formation of urine $\gamma$ (from 1 liter/day to 2 liters/day) always was at least 25% of the dose at the 1-liter/day rate and frequently approached a factor of 50%. More precisely, the total dose $D_2$ at the 2-liter/day rate and the total dose $D_1$ at the 1-liter/day rate always satisfied the conditions $0.5\ D_1 < D_2 < 0.75\ D_1$; that is, $D_2/D_1$ always fell within the shaded area of Fig. 12.1. It is not believed worth while to present the individual results more precisely. Clearly, for most radionuclides there will be a number of terms of various biological elimination half-times, but regardless of these, it appears likely that doubling the amount of urine to be voided will reduce the photon dose by 25 to 50%. The clinician might be willing to obtain this reduction in certain cases by persuading the patient to drink freely provided this does not interfere with other objectives of the test. In this connection we make two remarks:

1. The data based on the ratio of $D_2/D_1$ assume that the number of voids per day remains the same, and it may be that by taking in more fluid the number of voids will be increased. However, this only leads to a further reduction of dose as is indicated in Figs. 12.2*a* and 12.2*b*, where the total dose is compared for four, seven, and ten voids per day, all for a total output of 1400 ml/day. Although the reduction is not large, it appears that doses decrease regularly as the number of voids increases if the times of voiding are spaced rather regularly. A similar result holds for outputs of 1000 and 2000 ml/day.
2. It may not be practical to continue the enhanced rate of fluid intake for long periods, and that is one reason we have limited the range of exploration to half-times of ten days. In Fig. 12.1 are shown several examples of the saving in dose if the enhanced rate of 2 liters/day of output of urine is only maintained during the first day. As might be expected, when the radioactive half-life and the biological elimination half-time are both short, the saving in dose is essentially that indicated earlier, as after the first day little dose is delivered. However, as these half-times are increased, the saving of dose becomes increasingly smaller. Thus for radionuclides of short half-lives, one need only continue the enhanced rate of fluid intake during a day or so. However, many nuclides have an important amount of excretion coming out with a short biological elimination half-time, and to this portion of the total dose the reduction factor of 25 to 50% applies.

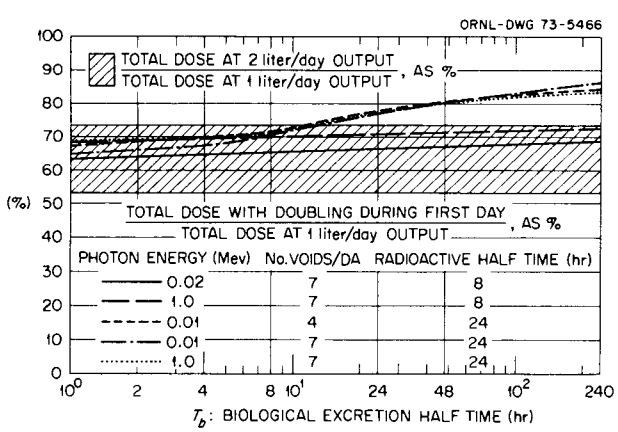


**Fig. 12.1. Effect of doubling urinary output.**

The answer to the second question is indicated in Fig. 12.3, where we have plotted the minimum dose received when the bladder is partly filled (0.2, 0.4, 0.6, 0.8) at time of administration of the nuclide as a fraction of the dose received when it is administered with the bladder empty. Although only the minimum dose is plotted, this minimum was attained either when it was 0.4 full or when it was 0.6 full in nearly all cases, and there is ample indication that this minimum is quite broad. Frequently, the dose was nearly the same for these two cases even to the second significant digit. Only a few of the many cases computed are indicated in the figure, but this behavior is typical of the cases computed. Thus the clinician might aim to deliver the radionuclide when the bladder is about half full, and even if he only realizes 40 to 60% of fullness, this will offer considerable dose reduction as the values in the tables indicate. When both the radioactive half-life and the biological elimination half-time are short, the dose is reduced by as much as 50%, but as these increase, the saving of dose diminishes and becomes finally less than 10%. Of course, when the urinary excretion is given as a sum of a number of exponentials (see formula 2), the saving of dose would largely be due to the portion excreted at the shorter half-times. Perhaps the principal importance of this is to emphasize that the fairly

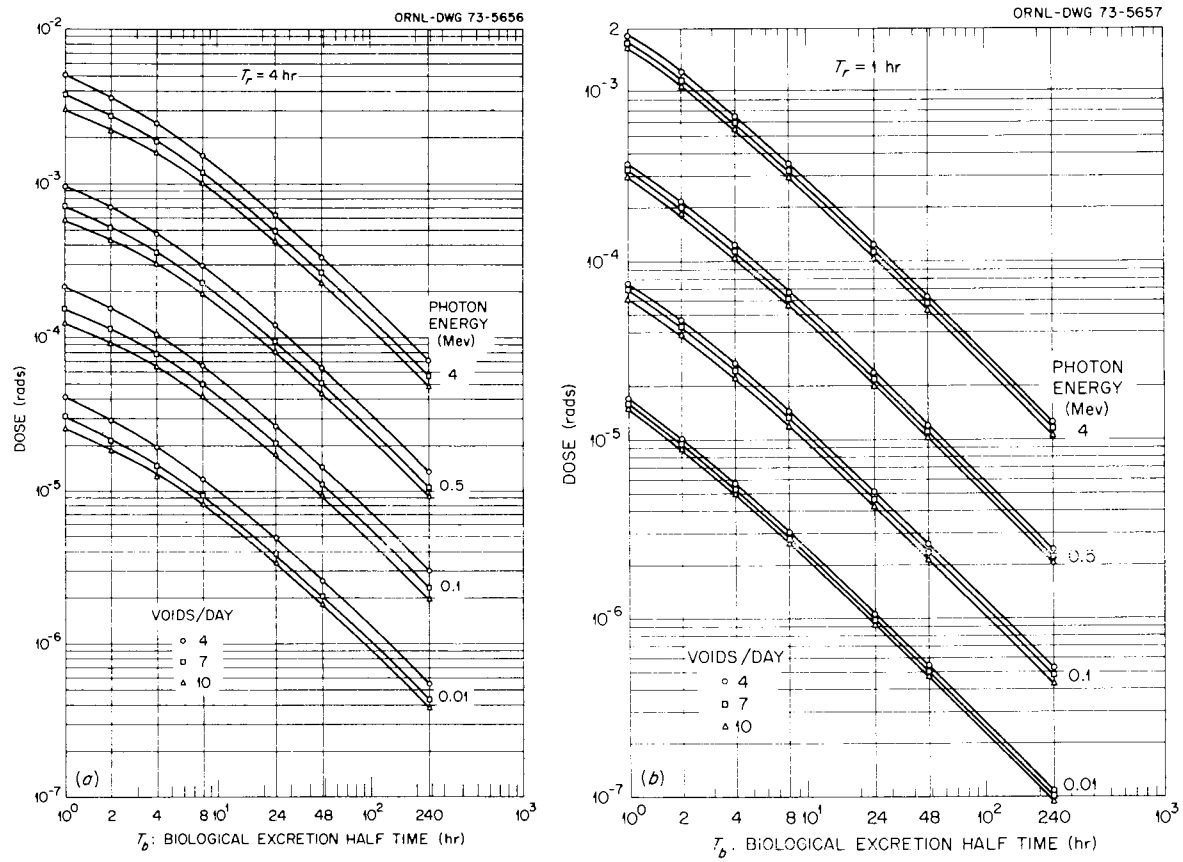


**Fig. 12.2. Variation of total dose for four, seven, and ten voids per day.** Urine volume, 1400 ml.

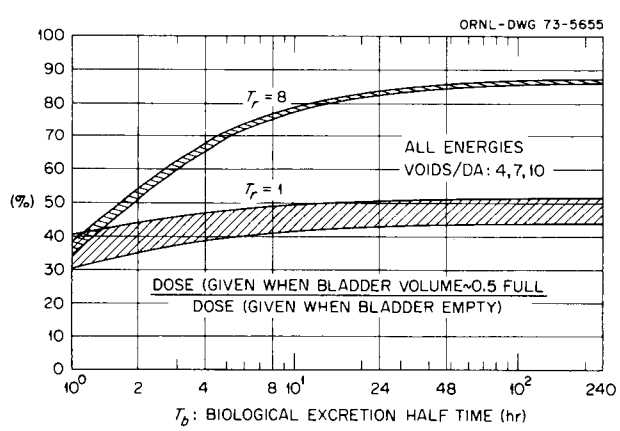


**Fig. 12.3. Effect on dose of choice of time of administration.** Urine volume, 1400 ml/day.

common practice of having a patient complete a void prior to administration of the nuclide in effect maximizes the dose received by the bladder. There may well be clinical situations where this is nevertheless desirable; but in the absence of such other reasons for the practice, the clinician might well aim to administer the nuclide when the bladder is approximately half full.

In summary, this study suggests that dose to the bladder may be significantly reduced if the fluid intake of the patient can be increased throughout the course of excretion and, for short-lived radionuclides, even during the first day following administration, and that a further reduction may be secured if one can administer the radionuclide when the bladder is approximately half full. The author realizes there may be clinical reasons why either practice may be impractical, and he is suggesting that clinicians consider this possibility only in the absence of such clinical reasons. For some radionuclides, the bladder may well be the critical tissue, for example, $^{99m}$Tc, and in such cases this reduction of dose may be of special importance. In a later publication the authors intend to treat the problem of dose from beta emitters, but preliminary indications are that dose from electrons and beta rays does not vary as greatly for the conditions explored here.

# 13. Dose from Photon Emitters Distributed Uniformly in the Total Body as a Function of Age

M. J. C. Hilyer G. S. Hill G. G. Warner[1]

In this paper we give specific absorbed fractions for photon emitters distributed uniformly in the total body, that is, the distribution is directly proportional to the density of the parts of the body. The total body becomes the source $S$, and any organ, including the total body, is a target organ $T$. The dose rate in the target organ is proportional to the specific absorbed fraction (SAF) or $\Phi$, which is defined as that fraction of the energy emitted which is absorbed per gram of the target organ. Thus

$$\Phi(T \leftarrow S) = \frac{\text{energy absorbed in } T}{(\text{energy released in } S)\,(\text{mass of } T \text{ in grams})}.$$

Estimates of the specific absorbed fractions were obtained by the Monte Carlo technique for a modified phantom basically similar to the anthropomorphic phantom[2] described in MIRD Pamphlet No. 5 (see Tables 13.1–13.6). These modifications are mentioned in Chap. 14 of this report. The calculation was for six monoenergetic sources of photons ranging from 20 keV to 2 MeV with a sample of 60,000 photons used for each monoenergetic source. The SAF and the dose rate were estimated for phantoms corresponding to ages 0 (newborn), 1, 5, 10, 15, and 20 (adult) years. The phantoms representing the various ages were obtained by transformation from the adult anthropomorphic phantom as described by Snyder and Cook.[3] The adult phantom was reduced by scale factors selected separately for the head, trunk, and leg sections of the phantom (Fig. 13.1). All organs and tissues within these sections were reduced by the scale factors for that particular section. Thus the loci of the organs which are nonintersecting in one phantom are nonintersecting in the other phantom.

In Fig. 13.2 the SAF as a function of age is shown for the red bone marrow for several monoenergetic photon sources uniformly distributed in the total body. When the source is the total body, the same general relationship for the SAF of the target organs seems to hold as when the source organ and the target organ are the same.[4] That is,

1. The SAF decreases as age increases. The newborn has the highest SAF, apparently due to the effect of the inverse square law.
2. The ratios of the SAF at a specific age to SAF for the adult decrease as the age increases. For instance, the SAF ratio for the newborn to the adult for 0.020 MeV differed by a factor of 20, while the same factor for the five year old to the adult was 4.
3. The SAF decreases as energy increases.

For a photon source distributed uniformly over the total body, the SAF (and hence the dose rate) to a target organ near the surface of the phantom is found to differ by approximately a factor of 2 from the SAF to a target organ near the central axis of the phantom. Figures 13.3 and 13.4 illustrate this relationship for the newborn and 20 year old (adult). The trunk skin was

1. Mathematics Division.
2. W. S. Snyder, Mary R. Ford, G. G. Warner, and H. L. Fisher, Jr., "Estimates of Absorbed Fractions for Monoenergetic Photon Sources Uniformly Distributed in Various Organs of a Heterogeneous Phantom," MIRD Pamphlet No. 5, *J. Nucl. Med. Suppl. No. 3:* 5 (1969).
3. W. S. Snyder and M. J. Cook, "Preliminary Indications of the Age Variation of the Specific Absorbed Fraction for Photons," *Health Phys. Div. Annu. Progr. Rep. July 31, 1971,* ORNL-4720, p. 116.
4. M. J. C. Hilyer, W. S. Snyder, and G. G. Warner, "Estimates of Doses to Infants and Children from a Photon Emitter in the Lungs," *Health Phys. Div. Annu. Progr. Rep. July 31, 1972,* ORNL-4811, p. 91.

Table 13.1. Specific absorbed fractions and coefficients of variation (%) for source in total body of newborn phantom

| | ENERGY (MEV) | | | | | | | | | | | |
|---|---|---|---|---|---|---|---|---|---|---|---|---|
| | 0.020 | | 0.050 | | 0.100 | | 0.500 | | 1.000 | | 2.000 | |
| | S.A.F. | C.V. | S.A.F. | C.V. | S.A.F. | C.V. | S.A.F. | C.V. | S.A.F. | C.V. | S.A.F. | C.V. |
| *ADRENALS | 3.1E-04 | 2.3E 01 | 7.5E-05 | 2.6E 01 | 8.1E-05 | 2.3E 01 | *8.5E-05 | 6.8E 00 | *8.9E-05 | 7.7E 00 | *7.4E-05 | 9.0E 00 |
| *BLADDER WALL | 3.4E-04 | 1.2E 01 | 9.8E-05 | 1.2E 01 | 5.6E-05 | 1.6E 01 | 7.6E-05 | 2.2E 01 | 5.2E-05 | 2.9E 01 | *8.8E-05 | 1.1E 01 |
| STOMACH WALL | 2.6E-04 | 7.7E 00 | 9.3E-05 | 7.3E 00 | 5.6E-05 | 9.0E 00 | 5.9E-05 | 1.4E 01 | 5.3E-05 | 1.6E 01 | 6.5E-05 | 1.6E 01 |
| SMALL INTESTINE | 3.0E-04 | 3.0E 00 | 1.0E-04 | 3.1E 00 | 6.5E-05 | 3.5E 00 | 6.9E-05 | 4.8E 00 | 6.5E-05 | 5.5E 00 | 5.1E-05 | 6.5E 00 |
| U.L.I. WALL | 3.0E-04 | 6.2E 00 | 1.1E-04 | 5.8E 00 | 6.5E-05 | 6.9E 00 | 6.5E-05 | 1.1E 01 | 5.6E-05 | 1.3E 01 | 7.1E-05 | 1.3E 01 |
| L.L.I. WALL | 2.7E-04 | 7.4E 00 | 1.1E-04 | 6.5E 00 | 5.9E-05 | 8.5E 00 | 6.8E-05 | 1.2E 01 | 6.3E-05 | 1.4E 01 | 4.4E-05 | 1.8E 01 |
| HEART | 2.7E-04 | 4.2E 00 | 1.2E-04 | 3.8E 00 | 7.4E-05 | 4.3E 00 | 8.5E-05 | 5.7E 00 | 8.5E-05 | 6.4E 00 | 6.5E-05 | 7.7E 00 |
| KIDNEYS | 2.1E-04 | 6.8E 00 | 8.2E-05 | 5.9E 00 | 5.6E-05 | 6.8E 00 | 6.3E-05 | 9.4E 00 | 5.6E-05 | 1.1E 01 | 5.2E-05 | 1.3E 01 |
| LIVER | 2.9E-04 | 2.4E 00 | 9.3E-05 | 2.6E 00 | 5.4E-05 | 3.0E 00 | 6.2E-05 | 3.9E 00 | 5.8E-05 | 4.5E 00 | 4.6E-05 | 5.3E 00 |
| LUNGS | 3.0E-04 | 2.9E 00 | 9.5E-05 | 3.0E 00 | 5.2E-05 | 3.7E 00 | 6.3E-05 | 5.0E 00 | 5.2E-05 | 6.3E 00 | 4.5E-05 | 7.3E 00 |
| RED MARROW | 3.1E-04 | 1.4E 00 | 1.5E-04 | 1.5E 00 | 5.4E-05 | 2.0E 00 | 3.3E-05 | 3.1E 00 | 3.1E-05 | 3.6E 00 | 2.6E-05 | 4.1E 00 |
| YELLOW MARROW | 4.3E-04 | 1.0E 00 | 1.9E-04 | 1.2E 00 | 6.4E-05 | 1.6E 00 | 4.3E-05 | 2.5E 00 | 4.0E-05 | 2.8E 00 | 3.4E-05 | 3.3E 00 |
| *OVARIES | *2.3E-04 | 5.7E 00 | 1.6E-04 | 2.4E 01 | 1.1E-04 | 2.7E 01 | *5.2E-05 | 9.2E 00 | *4.5E-05 | 1.1E 01 | *3.7E-05 | 1.8E 01 |
| PANCREAS | 3.2E-04 | 1.2E 01 | 1.1E-04 | 1.0E 01 | 5.1E-05 | 1.5E 01 | 7.4E-05 | 1.8E 01 | 5.5E-05 | 2.5E 01 | 6.7E-05 | 2.5E 01 |
| SKELETON | 3.2E-04 | 8.0E-01 | 1.5E-04 | 9.6E-01 | 5.1E-05 | 1.3E 00 | 3.5E-05 | 1.9E 00 | 3.2E-05 | 2.2E 00 | 2.6E-05 | 2.6E 00 |
| TOTAL SKIN | 1.1E-04 | 2.6E 00 | 3.6E-05 | 2.5E 00 | 2.4E-05 | 3.1E 00 | 2.9E-05 | 4.2E 00 | 3.0E-05 | 4.6E 00 | 2.3E-05 | 5.7E 00 |
| SPLEEN | 2.7E-04 | 7.5E 00 | 9.5E-05 | 7.5E 00 | 5.1E-05 | 9.5E 00 | 5.9E-05 | 1.3E 01 | 4.1E-05 | 1.7E 01 | 3.4E-05 | 2.0E 01 |
| *TESTES | 3.4E-04 | 1.8E 01 | 7.2E-05 | 2.0E 01 | 4.3E-05 | 2.9E 01 | *6.3E-05 | 1.5E 01 | 1.3E-04 | 2.7E 01 | *4.8E-05 | 2.0E 01 |
| *THYMUS | 2.6E-04 | 2.0E 01 | 7.8E-05 | 2.0E 01 | 5.1E-05 | 2.4E 01 | *6.5E-05 | 8.6E 00 | *5.8E-05 | 9.9E 00 | *5.6E-05 | 1.1E 01 |
| *THYROID | *1.3E-05 | 7.9E 00 | *1.3E-05 | 5.4E 00 | *7.2E-06 | 6.1E 00 | *1.0E-05 | 7.2E 00 | *8.8E-06 | 8.5E 00 | *6.9E-06 | 1.0E 01 |
| UTERUS | 2.4E-04 | 1.3E 01 | 9.3E-05 | 1.1E 01 | 6.9E-05 | 1.3E 01 | 8.1E-05 | 1.8E 01 | 6.1E-05 | 2.1E 01 | 4.1E-05 | 2.8E 01 |
| TOTAL BODY | 2.2E-04 | 2.2E-01 | 8.0E-05 | 4.9E-01 | 4.2E-05 | 6.0E-01 | 4.4E-05 | 6.9E-01 | 4.1E-05 | 7.8E-01 | 3.4E-05 | 9.2E-01 |

* S.A.F. to an appropriate subregion(s) is used instead of S.A.F.to the organ, because the coefficient of variation of the latter exceeded 30%.

Note: The digit following the symbol E indicates the power of ten by which each number is to be multiplied.

Table 13.2. Specific absorbed fractions and coefficients of variation (%) for source in total body of one-year-old phantom

| | ENERGY (MEV) | | | | | | | | | | | |
|---|---|---|---|---|---|---|---|---|---|---|---|---|
| | 0.020 | | 0.050 | | 0.100 | | 0.500 | | 1.000 | | 2.000 | |
| | S.A.F. | C.V. | S.A.F. | C.V. | S.A.F. | C.V. | S.A.F. | C.V. | S.A.F. | C.V. | S.A.F. | C.V. |
| *ADRENALS | 1.1E-04 | 2.3E 01 | 3.5E-05 | 1.8E 01 | 2.2E-05 | 2.1E 01 | *4.4E-05 | 5.6E 00 | *3.6E-05 | 7.0E 00 | *3.1E-05 | 8.1E 00 |
| BLADDER WALL | 1.1E-04 | 1.2E 01 | 5.2E-05 | 9.6E 00 | 2.7E-05 | 1.3E 01 | 4.1E-05 | 1.8E 01 | 2.8E-05 | 2.2E 01 | 2.2E-05 | 2.7E 01 |
| STOMACH WALL | 1.1E-04 | 7.2E 00 | 4.0E-05 | 6.5E 00 | 2.9E-05 | 7.2E 00 | 3.0E-05 | 1.1E 01 | 2.1E-05 | 1.4E 01 | 2.3E-05 | 1.5E 01 |
| SMALL INTESTINE | 1.0E-04 | 3.1E 00 | 5.1E-05 | 2.7E 00 | 3.3E-05 | 3.0E 00 | 3.1E-05 | 4.2E 00 | 2.9E-05 | 4.8E 00 | 2.7E-05 | 5.4E 00 |
| U.L.I. WALL | 1.0E-04 | 6.3E 00 | 5.1E-05 | 5.1E 00 | 3.4E-05 | 5.8E 00 | 3.1E-05 | 8.9E 00 | 3.3E-05 | 9.7E 00 | 2.7E-05 | 1.2E 01 |
| L.L.I. WALL | 9.8E-05 | 7.3E 00 | 5.0E-05 | 5.7E 00 | 3.1E-05 | 6.6E 00 | 2.9E-05 | 1.0E 01 | 2.9E-05 | 1.2E 01 | 2.7E-05 | 1.4E 01 |
| HEART | 1.2E-04 | 3.8E 00 | 6.7E-05 | 3.1E 00 | 4.0E-05 | 3.5E 00 | 4.2E-05 | 4.8E 00 | 4.5E-05 | 5.1E 00 | 3.0E-05 | 6.7E 00 |
| KIDNEYS | 9.8E-05 | 5.9E 00 | 4.3E-05 | 5.0E 00 | 2.7E-05 | 5.7E 00 | 2.8E-05 | 8.1E 00 | 2.6E-05 | 9.8E 00 | 2.0E-05 | 1.2E 01 |
| LIVER | 1.0E-04 | 2.4E 00 | 4.2E-05 | 2.4E 00 | 2.6E-05 | 2.7E 00 | 2.7E-05 | 3.5E 00 | 2.5E-05 | 4.0E 00 | 2.3E-05 | 4.5E 00 |
| LUNGS | 1.1E-04 | 2.8E 00 | 4.5E-05 | 2.6E 00 | 2.6E-05 | 3.1E 00 | 2.7E-05 | 4.4E 00 | 2.5E-05 | 5.2E 00 | 2.1E-05 | 6.0E 00 |
| RED MARROW | 1.1E-04 | 1.4E 00 | 7.5E-05 | 1.3E 00 | 3.0E-05 | 1.7E 00 | 1.7E-05 | 2.5E 00 | 1.6E-05 | 3.0E 00 | 1.4E-05 | 3.5E 00 |
| YELLOW MARROW | 1.4E-04 | 1.1E 00 | 8.5E-05 | 1.1E 00 | 3.2E-05 | 1.4E 00 | 2.0E-05 | 2.1E 00 | 1.9E-05 | 2.4E 00 | 1.6E-05 | 2.8E 00 |
| *OVARIES | *7.4E-05 | 6.0E 00 | 5.7E-05 | 2.3E 01 | 3.1E-05 | 2.8E 01 | *2.5E-05 | 7.5E 00 | *2.1E-05 | 9.5E 00 | *2.0E-05 | 1.0E 01 |
| PANCREAS | 1.2E-04 | 1.1E 01 | 4.8E-05 | 9.1E 00 | 3.6E-05 | 1.1E 01 | 3.1E-05 | 1.6E 01 | 3.1E-05 | 1.9E 01 | 1.8E-05 | 2.6E 01 |
| SKELETON | 1.1E-04 | 8.2E-01 | 7.0E-05 | 8.3E-01 | 2.7E-05 | 1.1E 00 | 1.7E-05 | 1.6E 00 | 1.6E-05 | 1.9E 00 | 1.3E-05 | 2.2E 00 |
| TOTAL SKIN | 4.4E-05 | 2.4E 00 | 1.6E-05 | 2.2E 00 | 1.1E-05 | 2.6E 00 | 1.4E-05 | 3.5E 00 | 1.3E-05 | 4.1E 00 | 1.1E-05 | 4.6E 00 |
| SPLEEN | 1.0E-04 | 7.6E 00 | 4.0E-05 | 6.8E 00 | 2.9E-05 | 7.3E 00 | 2.8E-05 | 1.0E 01 | 2.3E-05 | 1.3E 01 | 2.1E-05 | 1.5E 01 |
| *TESTES | 1.2E-04 | 1.6E 01 | 3.8E-05 | 1.6E 01 | 2.2E-05 | 2.0E 01 | 2.7E-05 | 2.7E 01 | *3.0E-05 | 1.3E 01 | *2.3E-05 | 1.5E 01 |
| *THYMUS | 9.2E-05 | 2.0E 01 | 4.3E-05 | 1.5E 01 | 2.6E-05 | 1.8E 01 | 4.2E-05 | 2.2E 01 | *2.6E-05 | 8.3E 00 | *2.6E-05 | 9.3E 00 |
| *THYROID | 1.4E-05 | 3.0E 01 | 5.4E-06 | 2.8E 01 | *4.1E-06 | 5.3E 00 | *4.6E-06 | 6.6E 00 | *4.8E-06 | 7.4E 00 | *3.9E-06 | 8.8E 00 |
| UTERUS | 1.1E-04 | 1.1E 01 | 4.5E-05 | 9.2E 00 | 3.7E-05 | 9.9E 00 | 2.4E-05 | 1.7E 01 | 3.1E-05 | 1.9E 01 | 1.7E-05 | 2.4E 01 |
| TOTAL BODY | 8.1E-05 | 1.9E-01 | 3.7E-05 | 4.1E-01 | 2.1E-05 | 5.2E-01 | 2.1E-05 | 5.7E-01 | 1.9E-05 | 6.5E-01 | 1.6E-05 | 7.6E-01 |

* (Same footnotes as on previous table)

Table 13.3. Specific absorbed fractions and coefficients of variation (%) for source in total body of five-year-old phantom

| | ENERGY (MEV) | | | | | | | | | | | |
|---|---|---|---|---|---|---|---|---|---|---|---|---|
| | 0.020 | | 0.050 | | 0.100 | | 0.500 | | 1.000 | | 2.000 | |
| | S.A.F. | C.V. | S.A.F. | C.V. | S.A.F. | C.V. | S.A.F. | C.V. | S.A.F. | C.V. | S.A.F. | C.V. |
| *ADRENALS | 4.7E-05 | 2.3E 01 | 2.0E-05 | 1.8E 01 | 1.5E-05 | 2.2E 01 | 2.2E-05 | 2.8E 01 | *1.7E-05 | 7.0E 00 | *1.6E-05 | 7.9E 00 |
| BLADDER WALL | 4.7E-05 | 1.3E 01 | 2.8E-05 | 9.4E 00 | 1.6E-05 | 1.1E 01 | 1.5E-05 | 1.9E 01 | 2.2E-05 | 1.9E 01 | 1.3E-05 | 2.6E 01 |
| STOMACH WALL | 4.8E-05 | 7.7E 00 | 2.8E-05 | 5.9E 00 | 1.6E-05 | 6.9E 00 | 1.7E-05 | 1.0E 01 | 1.4E-05 | 1.2E 01 | 1.3E-05 | 1.4E 01 |
| SMALL INTESTINE | 5.2E-05 | 3.1E 00 | 3.0E-05 | 2.6E 00 | 1.9E-05 | 2.8E 00 | 1.8E-05 | 3.8E 00 | 1.8E-05 | 4.3E 00 | 1.4E-05 | 5.3E 00 |
| U.L.I. WALL | 4.7E-05 | 6.6E 00 | 2.7E-05 | 4.7E 00 | 1.8E-05 | 5.5E 00 | 1.8E-05 | 8.5E 00 | 2.1E-05 | 8.9E 00 | 1.4E-05 | 1.2E 01 |
| L.L.I. WALL | 5.2E-05 | 7.4E 00 | 2.8E-05 | 5.5E 00 | 1.7E-05 | 6.2E 00 | 1.8E-05 | 9.5E 00 | 2.0E-05 | 1.1E 01 | 1.4E-05 | 1.3E 01 |
| HEART | 5.2E-05 | 4.2E 00 | 2.4E-05 | 3.7E 00 | 1.7E-05 | 3.9E 00 | 1.6E-05 | 5.6E 00 | 1.5E-05 | 6.3E 00 | 1.3E-05 | 7.3E 00 |
| KIDNEYS | 4.9E-05 | 6.0E 00 | 2.1E-05 | 5.1E 00 | 1.6E-05 | 5.5E 00 | 1.7E-05 | 7.6E 00 | 1.4E-05 | 9.1E 00 | 1.1E-05 | 1.1E 01 |
| LIVER | 5.0E-05 | 2.4E 00 | 2.5E-05 | 2.4E 00 | 1.5E-05 | 2.6E 00 | 1.7E-05 | 3.1E 00 | 1.5E-05 | 3.6E 00 | 1.2E-05 | 4.4E 00 |
| LUNGS | 5.7E-05 | 2.8E 00 | 2.6E-05 | 2.4E 00 | 1.7E-05 | 2.7E 00 | 1.7E-05 | 4.0E 00 | 1.5E-05 | 4.8E 00 | 1.2E-05 | 5.5E 00 |
| RED MARROW | 5.9E-05 | 1.4E 00 | 4.8E-05 | 1.3E 00 | 2.1E-05 | 1.6E 00 | 1.2E-05 | 2.3E 00 | 1.1E-05 | 2.7E 00 | 9.2E-06 | 3.2E 00 |
| YELLOW MARROW | 6.9E-05 | 1.1E 00 | 4.8E-05 | 1.0E 00 | 1.9E-05 | 1.3E 00 | 1.2E-05 | 1.9E 00 | 1.1E-05 | 2.2E 00 | 9.2E-06 | 2.6E 00 |
| *OVARIES | 6.4E-05 | 2.8E 01 | 2.4E-05 | 2.2E 01 | 2.2E-05 | 2.2E 01 | *1.7E-05 | 6.7E 00 | *1.5E-05 | 7.9E 00 | *1.3E-05 | 9.2E 00 |
| PANCREAS | 4.8E-05 | 1.3E 01 | 3.0E-05 | 8.6E 00 | 2.0E-05 | 1.0E 01 | 2.1E-05 | 1.4E 01 | 1.4E-05 | 2.0E 01 | 9.3E-06 | 2.6E 01 |
| SKELETON | 5.7E-05 | 8.4E-01 | 4.3E-05 | 7.9E-01 | 1.8E-05 | 1.0E 00 | 1.1E-05 | 1.5E 00 | 1.0E-05 | 1.7E 00 | 8.5E-06 | 2.0E 00 |
| TOTAL SKIN | 2.3E-05 | 2.5E 00 | 9.1E-06 | 2.0E 00 | 6.7E-06 | 2.3E 00 | 8.5E-06 | 3.2E 00 | 7.7E-06 | 3.7E 00 | 6.7E-06 | 4.3E 00 |
| SPLEEN | 4.6E-05 | 8.0E 00 | 2.4E-05 | 6.2E 00 | 1.5E-05 | 6.9E 00 | 1.2E-05 | 1.1E 01 | 1.2E-05 | 1.3E 01 | 1.3E-05 | 1.3E 01 |
| *TESTES | 4.4E-05 | 1.8E 01 | 1.9E-05 | 1.5E 01 | 1.5E-05 | 1.6E 01 | 1.1E-05 | 2.6E 01 | 1.5E-05 | 2.5E 01 | *1.2E-05 | 1.4E 01 |
| THYMUS | 5.9E-05 | 1.7E 01 | 3.2E-05 | 1.3E 01 | 1.4E-05 | 1.5E 01 | 1.6E-05 | 2.7E 01 | 2.1E-05 | 2.5E 01 | 3.1E-05 | 2.5E 01 |
| *THYROID | 1.4E-05 | 2.8E 01 | 9.9E-06 | 1.9E 01 | 4.3E-06 | 2.6E 01 | *3.2E-06 | 7.0E 00 | *2.6E-06 | 8.2E 00 | *2.2E-06 | 9.9E 00 |
| UTERUS | 6.3E-05 | 1.1E 01 | 3.2E-05 | 8.4E 00 | 2.0E-05 | 8.9E 00 | 1.6E-05 | 1.5E 01 | 1.8E-05 | 1.7E 01 | 1.3E-05 | 2.1E 01 |
| TOTAL BODY | 4.3E-05 | 1.7E-01 | 2.2E-05 | 3.7E-01 | 1.3E-05 | 4.7E-01 | 1.3E-05 | 5.2E-01 | 1.2E-05 | 5.8E-01 | 1.0E-05 | 6.9E-01 |

* S.A.F.to an appropriate subregion(s) is used instead of S.A.F.to the organ, because the coefficient of variation of the latter exceeded 30%.

Note: The digit following the symbol E indicates the power of ten by which each number is to be multiplied.

Table 13.4. Specific absorbed fractions and coefficients of variation (%) for source in total body of ten-year-old phantom

| | ENERGY (MEV) | | | | | | | | | | | |
|---|---|---|---|---|---|---|---|---|---|---|---|---|
| | 0.020 | | 0.050 | | 0.100 | | 0.500 | | 1.000 | | 2.000 | |
| | S.A.F. | C.V. | S.A.F. | C.V. | S.A.F. | C.V. | S.A.F. | C.V. | S.A.F. | C.V. | S.A.F. | C.V. |
| *ADRENALS | 3.0E-05 | 2.3E 01 | 1.6E-05 | 1.7E 01 | 1.2E-05 | 1.8E 01 | *1.1E-05 | 6.0E 00 | *1.0E-05 | 7.1E 00 | *7.5E-06 | 8.3E 00 |
| BLADDER WALL | 3.8E-05 | 1.2E 01 | 1.7E-05 | 9.4E 00 | 1.3E-05 | 1.0E 01 | 1.2E-05 | 1.7E 01 | 1.3E-05 | 1.8E 01 | 6.4E-06 | 2.8E 01 |
| STOMACH WALL | 3.2E-05 | 7.4E 00 | 1.7E-05 | 5.9E 00 | 1.2E-05 | 6.3E 00 | 1.1E-05 | 9.8E 00 | 1.1E-05 | 1.1E 01 | 6.8E-06 | 1.4E 01 |
| SMALL INTESTINE | 3.2E-05 | 3.1E 00 | 2.0E-05 | 2.6E 00 | 1.3E-05 | 2.8E 00 | 1.2E-05 | 3.7E 00 | 1.2E-05 | 4.2E 00 | 1.1E-05 | 4.8E 00 |
| U.L.I. WALL | 3.0E-05 | 6.5E 00 | 2.0E-05 | 4.6E 00 | 1.3E-05 | 5.0E 00 | 1.2E-05 | 7.7E 00 | 1.1E-05 | 9.2E 00 | 9.5E-06 | 1.1E 01 |
| L.L.I. WALL | 2.9E-05 | 7.6E 00 | 1.8E-05 | 5.3E 00 | 1.2E-05 | 5.7E 00 | 1.3E-05 | 8.5E 00 | 1.2E-05 | 1.0E 01 | 8.6E-06 | 1.3E 01 |
| HEART | 3.2E-05 | 4.2E 00 | 1.7E-05 | 3.8E 00 | 1.1E-05 | 4.1E 00 | 9.7E-06 | 5.6E 00 | 9.1E-06 | 6.3E 00 | 8.3E-06 | 7.1E 00 |
| KIDNEYS | 3.0E-05 | 6.1E 00 | 1.6E-05 | 5.0E 00 | 1.1E-05 | 5.2E 00 | 1.2E-05 | 7.2E 00 | 9.8E-06 | 8.8E 00 | 9.9E-06 | 9.3E 00 |
| LIVER | 3.1E-05 | 2.4E 00 | 1.7E-05 | 2.4E 00 | 1.1E-05 | 2.5E 00 | 1.1E-05 | 3.0E 00 | 9.9E-06 | 3.5E 00 | 8.1E-06 | 4.1E 00 |
| LUNGS | 3.4E-05 | 2.9E 00 | 1.7E-05 | 2.5E 00 | 1.1E-05 | 2.8E 00 | 1.0E-05 | 4.0E 00 | 9.3E-06 | 4.7E 00 | 7.7E-06 | 5.5E 00 |
| RED MARROW | 4.0E-05 | 1.4E 00 | 3.6E-05 | 1.2E 00 | 1.6E-05 | 1.4E 00 | 9.1E-06 | 2.1E 00 | 8.5E-06 | 2.5E 00 | 7.5E-06 | 2.8E 00 |
| YELLOW MARROW | 4.1E-05 | 1.1E 00 | 3.1E-05 | 9.7E-01 | 1.4E-05 | 1.2E 00 | 8.5E-06 | 1.8E 00 | 7.7E-06 | 2.0E 00 | 6.5E-06 | 2.4E 00 |
| *OVARIES | 4.1E-05 | 2.8E 01 | 1.8E-05 | 2.1E 01 | 1.7E-05 | 2.2E 01 | *1.3E-05 | 6.1E 00 | *1.2E-05 | 7.1E 00 | *1.0E-05 | 8.2E 00 |
| PANCREAS | 3.4E-05 | 1.2E 01 | 1.9E-05 | 8.8E 00 | 1.6E-05 | 8.9E 00 | 1.5E-05 | 1.4E 01 | 8.7E-06 | 1.8E 01 | 1.1E-05 | 1.9E 01 |
| SKELETON | 3.7E-05 | 8.3E-01 | 3.0E-05 | 7.5E-01 | 1.4E-05 | 9.5E-01 | 8.3E-06 | 1.3E 00 | 7.5E-06 | 1.6E 00 | 6.5E-06 | 1.8E 00 |
| TOTAL SKIN | 1.5E-05 | 2.4E 00 | 6.2E-06 | 2.0E 00 | 4.8E-06 | 2.1E 00 | 5.3E-06 | 3.1E 00 | 5.3E-06 | 3.5E 00 | 4.3E-06 | 4.2E 00 |
| SPLEEN | 2.9E-05 | 7.9E 00 | 1.7E-05 | 6.2E 00 | 1.3E-05 | 6.5E 00 | 8.6E-06 | 1.0E 01 | 8.8E-06 | 1.2E 01 | 7.5E-06 | 1.3E 01 |
| *TESTES | 2.5E-05 | 1.8E 01 | 1.4E-05 | 1.3E 01 | 8.6E-06 | 1.7E 01 | 1.0E-05 | 2.0E 01 | *6.3E-06 | 1.2E 01 | 7.8E-06 | 2.8E 01 |
| THYMUS | 2.2E-05 | 2.2E 01 | 2.2E-05 | 1.2E 01 | 1.5E-05 | 1.3E 01 | 2.1E-05 | 1.8E 01 | 1.7E-05 | 2.2E 01 | 1.3E-05 | 2.8E 01 |
| *THYROID | 1.5E-05 | 2.5E 01 | 5.3E-06 | 2.1E 01 | 3.9E-06 | 2.5E 01 | *2.6E-06 | 7.1E 00 | *3.0E-06 | 7.2E 00 | *2.3E-06 | 9.0E 00 |
| UTERUS | 3.3E-05 | 1.2E 01 | 2.3E-05 | 8.1E 00 | 1.3E-05 | 9.1E 00 | 1.5E-05 | 1.3E 01 | 9.2E-06 | 1.8E 01 | 1.1E-05 | 1.8E 01 |
| TOTAL BODY | 2.7E-05 | 1.5E-01 | 1.5E-05 | 3.4E-01 | 9.4E-06 | 4.4E-01 | 8.7E-06 | 4.8E-01 | 8.3E-06 | 5.4E-01 | 7.0E-06 | 6.4E-01 |

*(Same as footnotes on previous tables.)

Table 13.5. Specific absorbed fractions and coefficients of variation (%) for source in total body of 15-year-old phantom

| | ENERGY (MEV) | | | | | | | | | | | |
|---|---|---|---|---|---|---|---|---|---|---|---|---|
| | 0.020 | | 0.050 | | 0.100 | | 0.500 | | 1.000 | | 2.000 | |
| | S.A.F. | C.V. | S.A.F. | C.V. | S.A.F. | C.V. | S.A.F. | C.V. | S.A.F. | C.V. | S.A.F. | C.V. |
| *ADRENALS | 2.5E-05 | 2.1E 01 | 7.8E-06 | 1.7E 01 | 6.7E-06 | 1.9E 01 | 5.6E-06 | 2.8E 01 | *5.9E-06 | 7.7E 00 | *5.9E-06 | 7.6E 00 |
| BLADDER WALL | 2.0E-05 | 1.3E 01 | 1.2E-05 | 8.7E 00 | 8.3E-06 | 9.5E 00 | 9.5E-06 | 1.4E 01 | 9.3E-06 | 1.7E 01 | 6.4E-06 | 2.2E 01 |
| STOMACH WALL | 1.7E-05 | 7.8E 00 | 1.2E-05 | 5.4E 00 | 7.5E-06 | 6.1E 00 | 7.2E-06 | 8.9E 00 | 7.8E-06 | 1.0E 01 | 5.8E-06 | 1.2E 01 |
| SMALL INTESTINE | 1.8E-05 | 3.1E 00 | 1.3E-05 | 2.6E 00 | 9.3E-06 | 2.6E 00 | 8.4E-06 | 3.4E 00 | 7.9E-06 | 3.9E 00 | 6.0E-06 | 4.7E 00 |
| U.L.I. WALL | 2.1E-05 | 5.9E 00 | 1.3E-05 | 4.4E 00 | 8.6E-06 | 4.8E 00 | 8.2E-06 | 7.3E 00 | 7.6E-06 | 8.5E 00 | 6.1E-06 | 9.9E 00 |
| L.L.I. WALL | 1.9E-05 | 7.4E 00 | 1.1E-05 | 5.0E 00 | 8.6E-06 | 5.3E 00 | 7.8E-06 | 8.5E 00 | 7.2E-06 | 1.0E 01 | 7.3E-06 | 1.1E 01 |
| HEART | 1.8E-05 | 4.3E 00 | 1.1E-05 | 3.8E 00 | 7.2E-06 | 3.9E 00 | 6.8E-06 | 5.0E 00 | 6.2E-06 | 5.7E 00 | 5.6E-06 | 6.5E 00 |
| KIDNEYS | 1.7E-05 | 6.0E 00 | 1.1E-05 | 4.6E 00 | 7.1E-06 | 4.9E 00 | 8.2E-06 | 6.4E 00 | 7.2E-06 | 7.8E 00 | 5.8E-06 | 9.1E 00 |
| LIVER | 1.9E-05 | 2.4E 00 | 1.1E-05 | 2.3E 00 | 7.3E-06 | 2.4E 00 | 7.4E-06 | 2.9E 00 | 6.5E-06 | 3.3E 00 | 5.9E-06 | 3.7E 00 |
| LUNGS | 1.9E-05 | 3.0E 00 | 9.9E-06 | 2.5E 00 | 6.3E-06 | 2.7E 00 | 5.9E-06 | 3.9E 00 | 5.4E-06 | 4.7E 00 | 4.9E-06 | 5.2E 00 |
| RED MARROW | 2.5E-05 | 1.4E 00 | 2.4E-05 | 1.2E 00 | 1.2E-05 | 1.3E 00 | 6.7E-06 | 1.9E 00 | 6.1E-06 | 2.2E 00 | 4.9E-06 | 2.7E 00 |
| YELLOW MARROW | 2.4E-05 | 1.1E 00 | 2.0E-05 | 9.5E-01 | 9.4E-06 | 1.1E 00 | 5.5E-06 | 1.6E 00 | 5.1E-06 | 1.9E 00 | 4.3E-06 | 2.2E 00 |
| *OVARIES | *2.0E-05 | 5.2E 00 | 1.0E-05 | 2.1E 01 | 9.8E-06 | 2.0E 01 | *8.7E-06 | 5.5E 00 | *7.6E-06 | 6.5E 00 | *6.1E-06 | 7.7E 00 |
| PANCREAS | 1.6E-05 | 1.3E 01 | 1.2E-05 | 8.6E 00 | 8.2E-06 | 8.8E 00 | 6.9E-06 | 1.4E 01 | 7.2E-06 | 1.6E 01 | 4.8E-06 | 2.0E 01 |
| SKELETON | 2.3E-05 | 8.2E-01 | 2.0E-05 | 7.1E-01 | 1.0E-05 | 8.7E-01 | 5.8E-06 | 1.2E 00 | 5.3E-06 | 1.4E 00 | 4.5E-06 | 1.7E 00 |
| TOTAL SKIN | 9.5E-06 | 2.3E 00 | 4.2E-06 | 1.8E 00 | 3.2E-06 | 2.0E 00 | 3.9E-06 | 2.8E 00 | 3.7E-06 | 3.2E 00 | 3.1E-06 | 3.8E 00 |
| SPLEEN | 1.7E-05 | 7.9E 00 | 1.0E-05 | 6.0E 00 | 7.0E-06 | 6.7E 00 | 6.7E-06 | 9.3E 00 | 5.5E-06 | 1.1E 01 | 5.2E-06 | 1.2E 01 |
| TESTES | 1.7E-05 | 1.6E 01 | 7.9E-06 | 1.3E 01 | 6.2E-06 | 1.3E 01 | 6.2E-06 | 2.0E 01 | 5.2E-06 | 2.3E 01 | 7.9E-06 | 2.1E 01 |
| *THYMUS | 1.3E-05 | 2.1E 01 | 9.6E-06 | 1.4E 01 | 5.8E-06 | 1.7E 01 | 8.0E-06 | 2.0E 01 | 4.6E-06 | 2.8E 01 | *5.1E-06 | 8.8E 00 |
| *THYROID | 1.4E-05 | 2.4E 01 | 3.1E-06 | 2.3E 01 | 5.5E-06 | 1.7E 01 | *4.4E-06 | 5.1E 00 | *4.1E-06 | 5.7E 00 | *3.4E-06 | 6.6E 00 |
| UTERUS | 2.1E-05 | 1.2E 01 | 1.2E-05 | 8.3E 00 | 8.6E-06 | 8.3E 00 | 9.7E-06 | 1.2E 01 | 8.4E-06 | 1.5E 01 | 5.5E-06 | 2.0E 01 |
| TOTAL BODY | 1.7E-05 | 1.3E-01 | 9.9E-06 | 3.0E-01 | 6.4E-06 | 4.0E-01 | 5.9E-06 | 4.4E-01 | 5.6E-06 | 4.9E-01 | 4.8E-06 | 5.8E-01 |

*(Same as footnotes on previous tables.)

Table 13.6. Specific absorbed fractions and coefficients of variation (%) for source in total body of adult phantom

| | ENERGY (MEV) | | | | | | | | | | | |
|---|---|---|---|---|---|---|---|---|---|---|---|---|
| | 0.020 | | 0.050 | | 0.100 | | 0.500 | | 1.000 | | 2.000 | |
| | S.A.F. | C.V. | S.A.F. | C.V. | S.A.F. | C.V. | S.A.F. | C.V. | S.A.F. | C.V. | S.A.F. | C.V. |
| *ADRENALS | 8.4E-06 | 2.7E 01 | 5.3E-06 | 2.0E 01 | 6.4E-06 | 1.7E 01 | 7.9E-06 | 2.3E 01 | *5.8E-06 | 6.1E 00 | *4.3E-06 | 8.2E 00 |
| BLADDER WALL | 1.8E-05 | 1.2E 01 | 1.0E-05 | 8.0E 00 | 6.4E-06 | 9.1E 00 | 6.2E-06 | 1.5E 01 | 6.8E-06 | 1.7E 01 | 4.7E-06 | 2.2E 01 |
| STOMACH WALL | 1.5E-05 | 7.4E 00 | 8.6E-06 | 5.4E 00 | 5.7E-06 | 6.0E 00 | 6.1E-06 | 8.7E 00 | 5.5E-06 | 1.0E 01 | 4.5E-06 | 1.2E 01 |
| SMALL INTESTINE | 1.4E-05 | 3.2E 00 | 9.9E-06 | 2.6E 00 | 7.5E-06 | 2.6E 00 | 6.8E-06 | 3.3E 00 | 6.3E-06 | 3.7E 00 | 5.3E-06 | 4.4E 00 |
| U.L.I. WALL | 1.3E-05 | 6.5E 00 | 9.7E-06 | 4.4E 00 | 7.3E-06 | 4.6E 00 | 6.7E-06 | 6.8E 00 | 6.0E-06 | 8.2E 00 | 5.1E-06 | 9.8E 00 |
| L.L.I. WALL | 1.4E-05 | 7.5E 00 | 1.0E-05 | 4.9E 00 | 6.6E-06 | 5.2E 00 | 6.8E-06 | 7.9E 00 | 6.4E-06 | 9.2E 00 | 7.0E-06 | 9.7E 00 |
| HEART | 1.4E-05 | 4.2E 00 | 9.3E-06 | 3.5E 00 | 6.2E-06 | 3.7E 00 | 5.8E-06 | 4.8E 00 | 5.5E-06 | 5.4E 00 | 4.8E-06 | 6.2E 00 |
| KIDNEYS | 1.3E-05 | 6.2E 00 | 8.2E-06 | 4.7E 00 | 6.0E-06 | 4.9E 00 | 6.0E-06 | 6.4E 00 | 5.9E-06 | 7.2E 00 | 4.6E-06 | 8.8E 00 |
| LIVER | 1.4E-05 | 2.4E 00 | 9.0E-06 | 2.3E 00 | 6.2E-06 | 2.3E 00 | 6.0E-06 | 2.8E 00 | 5.9E-06 | 3.1E 00 | 4.7E-06 | 3.6E 00 |
| LUNGS | 1.4E-05 | 3.0E 00 | 8.4E-06 | 2.4E 00 | 5.4E-06 | 2.6E 00 | 5.3E-06 | 3.6E 00 | 4.6E-06 | 4.4E 00 | 3.8E-06 | 5.2E 00 |
| RED MARROW | 1.9E-05 | 1.4E 00 | 1.9E-05 | 1.1E 00 | 1.0E-05 | 1.3E 00 | 5.6E-06 | 1.9E 00 | 5.2E-06 | 2.2E 00 | 4.6E-06 | 2.5E 00 |
| YELLOW MARROW | 1.9E-05 | 1.1E 00 | 1.6E-05 | 9.4E-01 | 7.8E-06 | 1.1E 00 | 4.8E-06 | 1.6E 00 | 4.4E-06 | 1.8E 00 | 3.8E-06 | 2.1E 00 |
| *OVARIES | *1.3E-05 | 5.5E 00 | 8.1E-06 | 2.6E 01 | 7.0E-06 | 2.1E 01 | *6.5E-06 | 5.5E 00 | *6.6E-06 | 6.1E 00 | *5.7E-06 | 7.2E 00 |
| PANCREAS | 1.7E-05 | 1.1E 01 | 1.1E-05 | 8.2E 00 | 6.6E-06 | 8.5E 00 | 5.9E-06 | 1.3E 01 | 5.3E-06 | 1.6E 01 | 8.3E-06 | 1.4E 01 |
| SKELETON | 1.8E-05 | 8.1E-01 | 1.6E-05 | 7.0E-01 | 8.4E-06 | 8.5E-01 | 5.1E-06 | 1.2E 00 | 4.7E-06 | 1.4E 00 | 4.2E-06 | 1.5E 00 |
| TOTAL SKIN | 7.6E-06 | 2.3E 00 | 3.5E-06 | 1.8E 00 | 2.6E-06 | 1.9E 00 | 3.1E-06 | 2.8E 00 | 3.1E-06 | 3.1E 00 | 2.8E-06 | 3.6E 00 |
| SPLEEN | 1.3E-05 | 7.7E 00 | 8.4E-06 | 6.1E 00 | 6.1E-06 | 6.3E 00 | 6.1E-06 | 8.2E 00 | 5.7E-06 | 9.6E 00 | 4.2E-06 | 1.2E 01 |
| TESTES | 9.3E-06 | 1.9E 01 | 6.1E-06 | 1.3E 01 | 4.3E-06 | 1.3E 01 | 6.5E-06 | 1.8E 01 | 5.7E-06 | 2.0E 01 | 4.5E-06 | 2.6E 01 |
| THYMUS | 2.0E-05 | 1.6E 01 | 1.0E-05 | 1.3E 01 | 5.3E-06 | 1.5E 01 | 5.2E-06 | 2.2E 01 | 4.1E-06 | 2.8E 01 | 5.0E-06 | 2.9E 01 |
| *THYROID | 1.5E-05 | 2.0E 01 | 7.4E-06 | 1.7E 01 | 3.0E-06 | 2.3E 01 | 4.9E-06 | 2.7E 01 | 5.2E-06 | 2.9E 01 | *4.0E-06 | 5.9E 00 |
| UTERUS | 1.4E-05 | 1.2E 01 | 1.0E-05 | 8.1E 00 | 7.9E-06 | 8.5E 00 | 5.9E-06 | 1.3E 01 | 8.0E-06 | 1.4E 01 | 6.1E-06 | 1.6E 01 |
| TOTAL BODY | 1.3E-05 | 1.2E-01 | 8.1E-06 | 2.9E-01 | 5.4E-06 | 3.9E-01 | 4.9E-06 | 4.2E-01 | 4.7E-06 | 4.6E-01 | 4.1E-06 | 5.4E-01 |

*(Same as footnotes on previous tables.)

ORNL-DWG 66-6436R

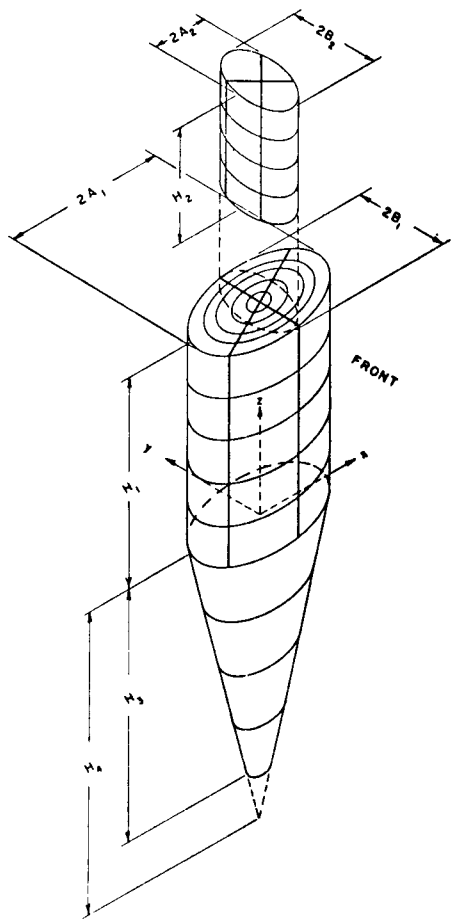


PHANTOM DIMENSIONS AND DOSE REGIONS

| Age (yr) | Mass (kg) | $H_1$ (cm) | $H_2$ (cm) | $H_3$ (cm) | $H_4$ (cm) | $A_1$ (cm) | $B_1$ (cm) | $A_2$ (cm) | $B_2$ (cm) |
|---|---|---|---|---|---|---|---|---|---|
| 0 | 3.473 | 23 | 13 | 15 | 20 | 5.5 | 5 | 4.5 | 5 |
| 1 | 10.171 | 33 | 16 | 27 | 36 | 8 | 7 | 6.5 | 7 |
| 5 | 19.654 | 45 | 20 | 46 | 57.5 | 11 | 7.5 | 6.5 | 7.5 |
| 10 | 31.902 | 54 | 22 | 64 | 80 | 14 | 8 | 6.5 | 8 |
| 15 | 54.041 | 65 | 23 | 78 | 97.5 | 18 | 9 | 7 | 9 |
| 20 | 70.037 | 70 | 24 | 80 | 100 | 20 | 10 | 7 | 10 |

**Fig. 13.1. Mass and dimensions for phantoms corresponding to various ages.**

selected as the surface organ, and the five subregions located along the central axis of the five tiers in the trunk of the appropriate age phantom were selected to simulate a central axis organ. The ratio of $\Phi$ averaged over the central axis subregions to the surface organ (trunk skin) is approximately 2:1. This ratio of a central axis organ dose rate to the dose rate of other organs will vary with the position of the organ relative to the central axis. In Fig. 13.5 this correlation is shown for the ovaries, testes, and skin for the ten-year-old phantom. The ovaries, which are positioned near the central axis, show a nearly 1:1 ratio with the central axis subregions of the trunk, while the testes, a more nearly surface organ, show a 1:1.5 ratio. Moreover, for larger organs, such as the liver, which extend from the center out toward the periphery of the body, the dose rate to that portion of the organ which is nearest the central axis will be somewhat higher than that part which lies near the surface.

Only data with a coefficient of variation less than 30% were used in the statistical evaluations. In some instances, such as the ovaries and testes, the coefficient of variation for the calculated specific absorbed fraction (SAF) was greater than 30%. In the case of the testes, for more reliable data the SAF for the genitalia were used in Fig. 13.5. For the ovaries, a technique described by Poston and Snyder[5] was used; here the SAF to the appropriate subregion or subregions of the phantom in which the organs lie was used to replace the SAF to the ovaries. It is believed these give a more reliable estimate of the SAF for these organs than do the Monte Carlo results.

The specific absorbed fraction (SAF) and coefficient of variation for some of the organs within the heterogeneous phantoms for ages 0, 1, 5, 10, 15, and 20 years

5. J. W. Poston and W. S. Snyder, *A Model for Exposure to a Semi-Infinite Cloud of a Photon Emitter*, in publication.

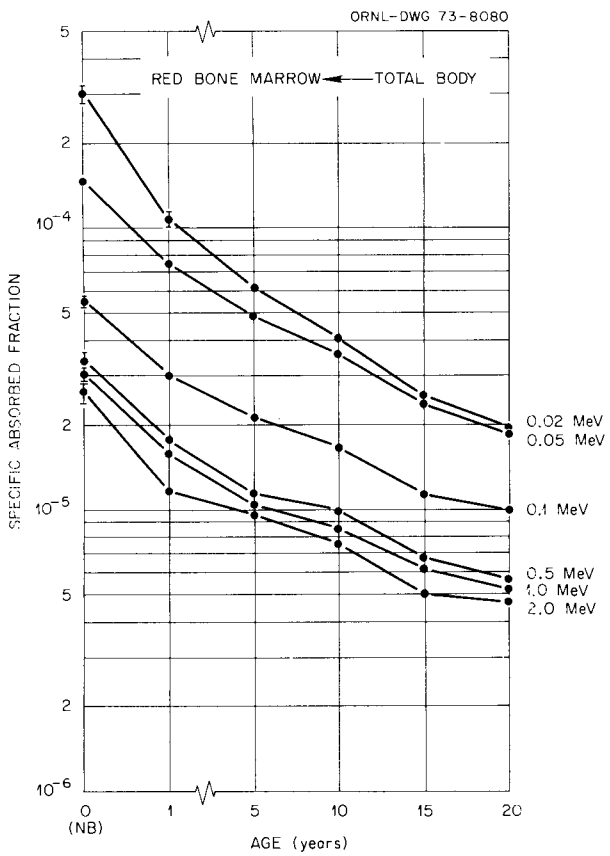


Fig. 13.2. Specific absorbed fraction of red bone marrow as a function of age and photon energy.

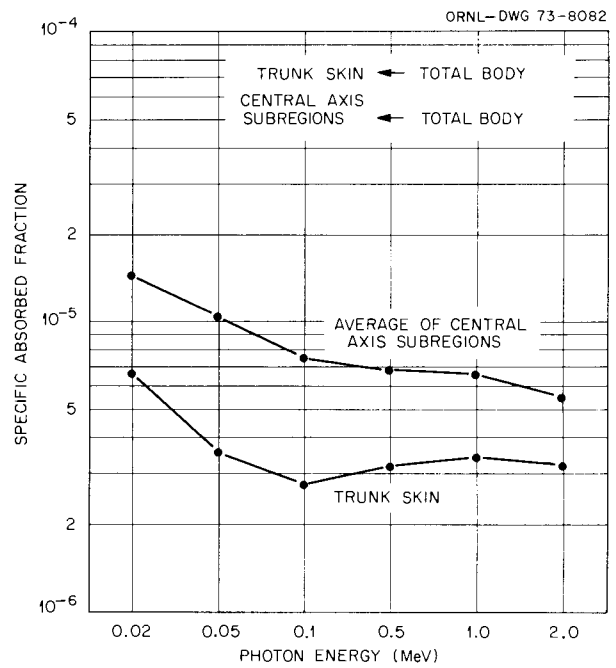


Fig. 13.4. Specific absorbed fraction as a function of photon energy and organ location for the adult (20 years).

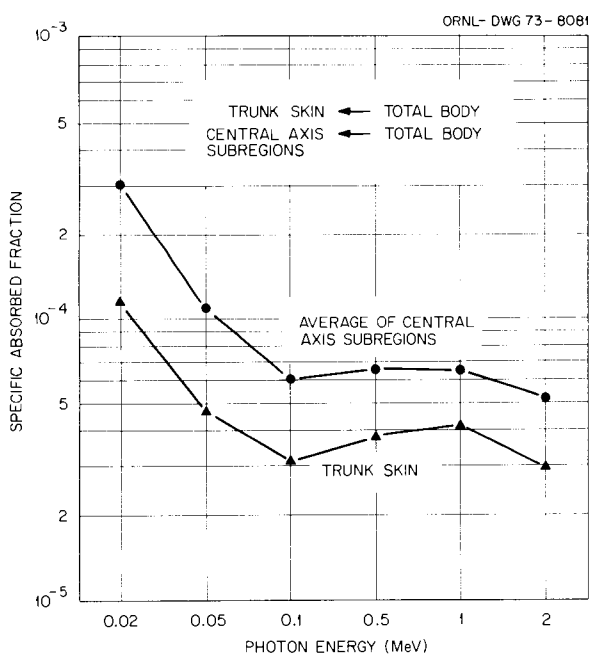


Fig. 13.3. Specific absorbed fraction as a function of photon energy and organ location for the newborn.

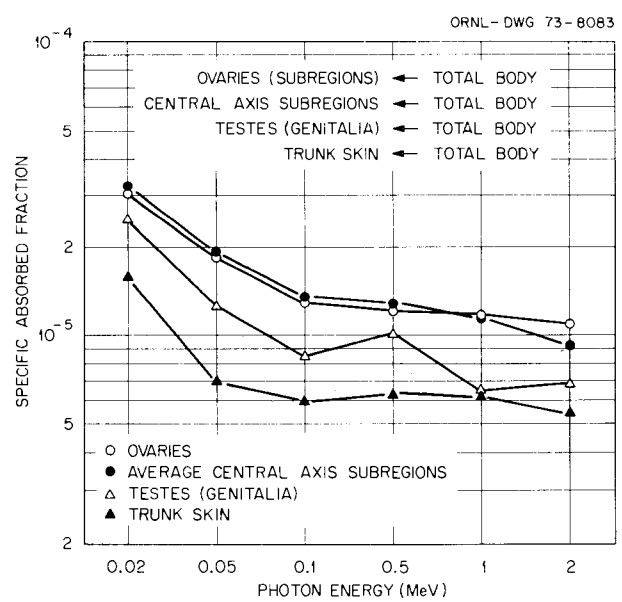


Fig. 13.5. Specific absorbed fraction as a function of photon energy and organ location for 10 year old.

are shown in Tables 13.1–13.6. In cases where the coefficients of variation were consistently greater than 30%, the corresponding data from the appropriate geometrical subregion or subregions in the phantoms in which the organ was located were substituted. The values are distinguished by an asterisk in the tables.

As previously reported,[6] when the source is distributed uniformly within an organ, the absorbed fraction (AF) for the organ might be expected to vary with the cube root of the mass, that is, $(AF)x \leftarrow y$ is proportional to $\mu_{ab}M^{1/3}$. In Figs. 13.6–13.8 the ratios of the AF to $\mu_{ab}M^{1/3}$ are plotted for various photon energies and organs. For energies of 0.100 MeV and higher, the ratio is found to be approximately a constant for all ages in the case of kidney and liver as well as for the total body. This behavior appears to hold also for other organs for which the Monte Carlo results are statistically significant, and thus the principle seems to be supported fairly well regardless of age. For lower energies, the rule does not appear to hold as might be expected from its derivation.

6. Walter S. Snyder, "Estimation of Absorbed Fraction of Energy from Photon Sources in Body Organs," in *Medical Radionuclides: Radiation Dose and Effects,* U.S. Atomic Energy Commission, Division of Technical Information, Oak Ridge, Tennessee, 1970, p. 33.

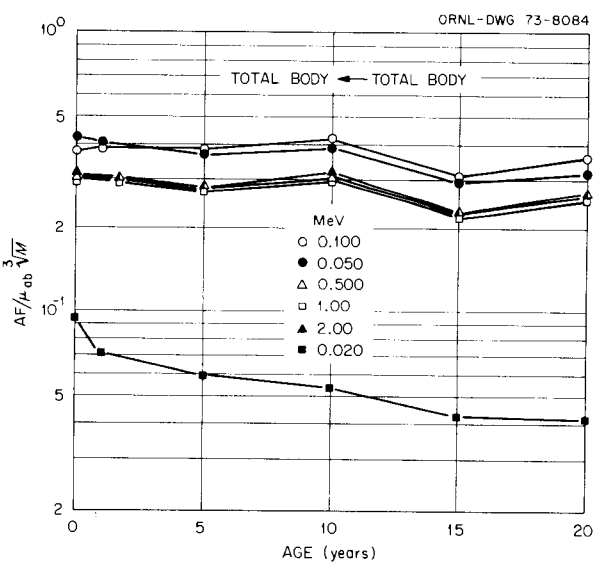


**Fig. 13.6. Absorbed fractions in total body as related to mass as a function of photon energy and age.**

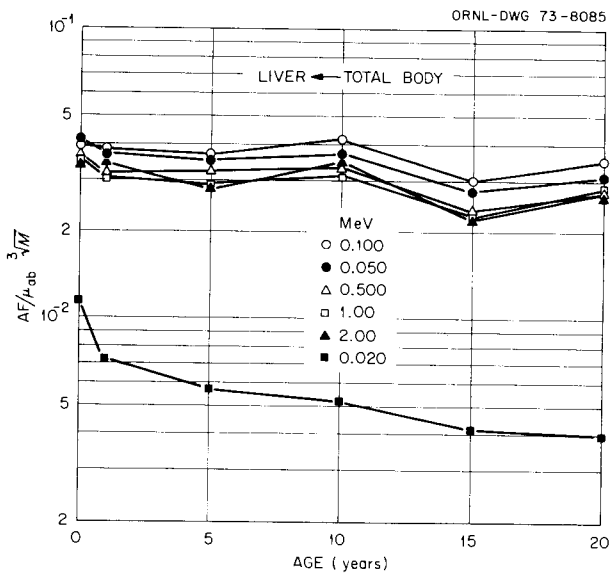


**Fig. 13.7. Absorbed fractions in liver as related to mass as a function of photon energy and age.**

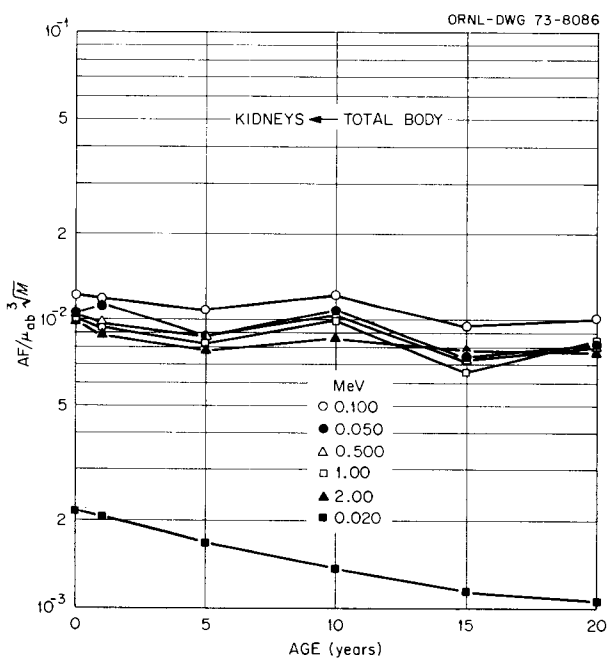


**Fig. 13.8. Absorbed fractions in kidneys as related to mass as a function of photon energy and age.**

# 14. Estimates of Dose Rate to Gonads of Infants and Children from a Photon Emitter in Various Organs of the Body

W. S. Snyder M. R. Ford

This paper provides some estimates of dose rates to gonads from sources of a photon emitter distributed uniformly in various organs of the body. The results are obtained by application of the reciprocity theorem to the Monte Carlo estimates of dose rate from gonads to large organs. Although only results for photon energies of 0.02, 0.05, 0.1, 0.5, 1, and 2 MeV are reported here, it is planned to complete the series, so the 12 monoenergetic sources used in MIRD Pamphlet No. 5[1] will be available for interpolation of other photon energies.

The basic phantoms used are essentially modifications of that reported in ref. 1. The modifications include specification of regions where active bone marrow is deposited in the adult, addition of clavicles and scapulae to the skeleton, rounding of the top of the head, separate legs for the phantom, and relocation of the testes. These modifications will be presented in detail in a separate publication.[2]

For these calculations, the head, trunk, and leg sections of the adult phantom were transformed by similitudes to form the new phantoms. Although all organs and regions in each of these sections were shrunk by the same factors, these factors were not identical for the three sections which were given overall dimensions typical for a given age. These factors are given in ref. 3. The phantoms produced by use of these transformations are referred to below as being those of ages 0 (newborn), 1, 5, 10, 15, and 20 (adult) years. The corresponding masses for the total body are approximately 3.4, 10, 19.5, 31.8, 54, and 70 kg.

Since the dose rates given below are based entirely on use of the reciprocity theorem, it is appropriate to consider the validity of this theorem in phantoms corresponding to the various ages. The validity in the adult phantom has been studied extensively and is reported in ref. 4. The theorem has been tested by programming sources of 60,000 photons at three widely separated regions of the phantom and at several energies. The three regions used were transforms of the central volumes (approximately elliptical cylinders of semiaxes 16 and 8 cm and height 14 cm) of the top, middle, and bottom fifths of the trunk of the adult phantom. The regions contain rather different amounts of bone and lung tissue so that the inhomogeneity of the phantom is well represented. Three source energies were chosen – 0.03, 0.1, and 0.5 MeV – and in all cases reciprocity held within 12%, generally being within a few percent in the corresponding cases. While far from the ideal solution of the problem, it is believed the values obtained for genetic dose by this means are sufficiently accurate for practical use, since the actual distances of the gonads from the various source organs will vary with the individual and will only be approximately specified in practical cases.

In Tables 14.1–14.12 are displayed the estimates of dose rate from various source organs to the ovaries and testes. As indicated above these values were obtained by Monte Carlo calculation and represent the dose to these organs from sources placed in the ovaries or testes, and thus the estimates given here are based on the use of reciprocity. The occurrence of a value zero in the table only indicates that the data are statistically uncertain. No values were accepted if the coefficient of variation of the estimate exceeded 30%. It is expected that more complete results will be published when the results for the 12 monoenergetic sources of photons are available.

---

1. W. S. Snyder et al., *J. Nucl. Med. Suppl. No. 3:* 5 (1969).
2. W. S. Snyder and M. R. Ford, ORNL report (in preparation).
3. J. C. Hilyer, G. S. Hill, and G. G. Warner, "Dose from Photon Emitters Distributed Uniformly in the Total Body as a Function of Age," this report.
4. W. S. Snyder, *Medical Radionuclides: Radiation Dose and Effects* (USAEC/DTI, Oak Ridge, Tennessee, 1970), p. 33.

Table 14.1. Doses (rads/photon) to ovaries and coefficients of variation (%) for source organs of the newborn phantom

| SOURCE ORGANS | ENERGY (MEV) 0.020 | | 0.050 | | 0.100 | | 0.500 | | 1.000 | | 2.000 | |
|---|---|---|---|---|---|---|---|---|---|---|---|---|
| | DOSE | C.V. | DOSE | C.V. | DOSE | C.V. | DOSE | C.V. | DOSE | C.V. | DOSE | C.V. |
| BLADDER WALL | 2.1E-13 | 8.1E 00 | 2.9E-13 | 6.2E 00 | 3.8E-13 | 7.7E 00 | 1.8E-12 | 1.2E 01 | 3.5E-12 | 1.4E 01 | 4.6E-12 | 1.8E 01 |
| STOMACH WALL | 7.9E-15 | 2.1E 01 | 6.1E-14 | 7.4E 00 | 7.5E-14 | 9.3E 00 | 3.3E-13 | 1.5E 01 | 5.7E-13 | 1.9E 01 | 9.5E-13 | 2.2E 01 |
| SMALL INTESTINE | 7.2E-13 | 1.0E 00 | 5.2E-13 | 1.2E 00 | 6.0E-13 | 1.4E 00 | 3.1E-12 | 2.1E 00 | 5.6E-12 | 2.4E 00 | 9.2E-12 | 2.8E 00 |
| U.L.I. WALL | 7.2E-13 | 2.2E 00 | 4.5E-13 | 2.5E 00 | 5.0E-13 | 3.3E 00 | 2.8E-12 | 4.7E 00 | 5.0E-12 | 5.6E 00 | 7.9E-12 | 6.7E 00 |
| L.L.I. WALL | 1.2E-12 | 2.0E 00 | 6.3E-13 | 2.4E 00 | 7.3E-13 | 3.1E 00 | 3.9E-12 | 4.6E 00 | 7.4E-12 | 5.3E 00 | 1.2E-11 | 6.4E 00 |
| HEART | 0.0 | 0.0 | 1.4E-14 | 8.7E 00 | 2.7E-14 | 8.6E 00 | 1.4E-13 | 1.2E 01 | 3.7E-13 | 1.2E 01 | 4.9E-13 | 1.5E 01 |
| KIDNEYS | 5.2E-15 | 2.1E 01 | 6.0E-14 | 6.1E 00 | 7.6E-14 | 7.3E 00 | 4.0E-13 | 1.1E 01 | 6.2E-13 | 1.3E 01 | 1.0E-12 | 1.5E 01 |
| LIVER | 4.2E-15 | 9.9E 00 | 4.4E-14 | 3.1E 00 | 6.2E-14 | 3.5E 00 | 2.8E-13 | 5.0E 00 | 5.4E-13 | 5.7E 00 | 8.5E-13 | 6.8E 00 |
| LUNGS | 0.0 | 0.0 | 1.2E-14 | 6.7E 00 | 2.0E-14 | 7.0E 00 | 1.2E-13 | 9.9E 00 | 2.5E-13 | 1.1E 01 | 4.8E-13 | 1.2E 01 |
| RED MARROW | 1.9E-13 | 1.1E 00 | 2.8E-13 | 1.1E 00 | 1.8E-13 | 1.5E 00 | 4.8E-13 | 2.6E 00 | 9.3E-13 | 3.0E 00 | 1.6E-12 | 3.5E 00 |
| YELLOW MARROW | 9.3E-14 | 1.1E 00 | 1.9E-13 | 1.0E 00 | 1.2E-13 | 1.4E 00 | 3.4E-13 | 2.4E 00 | 6.7E-13 | 2.8E 00 | 1.1E-12 | 3.3E 00 |
| OVARIES | 9.4E-11 | 9.8E-01 | 2.2E-11 | 1.8E 00 | 2.8E-11 | 2.3E 00 | 1.7E-10 | 3.1E 00 | 3.2E-10 | 3.6E 00 | 5.2E-10 | 4.2E 00 |
| PANCREAS | 0.0 | 0.0 | 3.8E-14 | 1.5E 01 | 7.0E-14 | 1.6E 01 | 3.4E-13 | 2.5E 01 | 8.3E-13 | 2.5E 01 | 0.0 | 0.0 |
| SKELETON | 5.4E-14 | 1.1E 00 | 1.1E-13 | 9.3E-01 | 7.8E-14 | 1.3E 00 | 2.1E-13 | 2.1E 00 | 4.1E-13 | 2.4E 00 | 6.9E-13 | 2.9E 00 |
| TOTAL SKIN | 2.4E-15 | 8.6E 00 | 2.1E-14 | 2.8E 00 | 2.8E-14 | 3.3E 00 | 1.5E-13 | 5.1E 00 | 2.9E-13 | 5.8E 00 | 5.1E-13 | 6.8E 00 |
| SPLEEN | 0.0 | 0.0 | 5.0E-14 | 8.4E 00 | 5.0E-14 | 1.1E 01 | 2.2E-13 | 1.7E 01 | 5.1E-13 | 1.8E 01 | 1.1E-12 | 2.0E 01 |
| UTERUS | 1.5E-12 | 2.7E 00 | 1.0E-12 | 3.1E 00 | 1.1E-12 | 4.0E 00 | 5.9E-12 | 5.8E 00 | 1.1E-11 | 6.9E 00 | 1.8E-11 | 8.0E 00 |
| TOTAL BODY | 9.1E-14 | 7.0E-02 | 9.2E-14 | 3.6E-01 | 1.0E-13 | 4.6E-01 | 5.0E-13 | 5.5E-01 | 9.2E-13 | 6.3E-01 | 1.5E-12 | 7.6E-01 |

Table 14.2. Doses (rads/photon) to ovaries and coefficients of variation (%) for source organs of the one-year-old phantom

| SOURCE ORGANS | ENERGY (MEV) 0.020 | | 0.050 | | 0.100 | | 0.500 | | 1.000 | | 2.000 | |
|---|---|---|---|---|---|---|---|---|---|---|---|---|
| | DOSE | C.V. | DOSE | C.V. | DOSE | C.V. | DOSE | C.V. | DOSE | C.V. | DOSE | C.V. |
| BLADDER WALL | 5.0E-14 | 9.6E 00 | 1.6E-13 | 5.0E 00 | 1.7E-13 | 6.5E 00 | 8.3E-13 | 1.0E 01 | 1.4E-12 | 1.3E 01 | 2.3E-12 | 1.5E 01 |
| STOMACH WALL | 0.0 | 0.0 | 2.5E-14 | 7.1E 00 | 3.2E-14 | 7.9E 00 | 1.6E-13 | 1.3E 01 | 3.2E-13 | 1.4E 01 | 6.7E-13 | 1.6E 01 |
| SMALL INTESTINE | 2.4E-13 | 1.0E 00 | 2.7E-13 | 1.0E 00 | 3.1E-13 | 1.2E 00 | 1.5E-12 | 1.7E 00 | 2.6E-12 | 2.0E 00 | 4.3E-12 | 2.4E 00 |
| U.L.I. WALL | 2.7E-13 | 2.1E 00 | 2.4E-13 | 2.1E 00 | 2.7E-13 | 2.6E 00 | 1.3E-12 | 4.0E 00 | 2.4E-12 | 4.6E 00 | 3.6E-12 | 5.8E 00 |
| L.L.I. WALL | 4.6E-13 | 1.9E 00 | 3.3E-13 | 2.0E 00 | 3.5E-13 | 2.6E 00 | 1.9E-12 | 3.8E 00 | 3.5E-12 | 4.4E 00 | 5.2E-12 | 5.5E 00 |
| HEART | 0.0 | 0.0 | 4.0E-15 | 1.0E 01 | 9.5E-15 | 8.6E 00 | 5.0E-14 | 1.1E 01 | 1.0E-13 | 1.3E 01 | 2.2E-13 | 1.3E 01 |
| KIDNEYS | 0.0 | 0.0 | 2.4E-14 | 5.5E 00 | 3.9E-14 | 5.6E 00 | 1.7E-13 | 8.9E 00 | 3.4E-13 | 1.0E 01 | 5.0E-13 | 1.3E 01 |
| LIVER | 3.3E-16 | 2.1E 01 | 1.8E-14 | 3.0E 00 | 2.7E-14 | 3.0E 00 | 1.2E-13 | 4.4E 00 | 2.2E-13 | 5.1E 00 | 4.2E-13 | 5.6E 00 |
| LUNGS | 0.0 | 0.0 | 3.3E-15 | 7.1E 00 | 6.6E-15 | 7.0E 00 | 4.3E-14 | 9.2E 00 | 1.0E-13 | 9.9E 00 | 1.8E-13 | 1.1E 01 |
| RED MARROW | 4.7E-14 | 1.3E 00 | 1.5E-13 | 9.1E-01 | 1.1E-13 | 1.2E 00 | 2.6E-13 | 2.1E 00 | 4.4E-13 | 2.6E 00 | 7.4E-13 | 3.0E 00 |
| YELLOW MARROW | 2.1E-14 | 1.3E 00 | 8.3E-14 | 8.8E-01 | 6.4E-14 | 1.2E 00 | 1.7E-13 | 2.0E 00 | 2.9E-13 | 2.4E 00 | 4.7E-13 | 2.9E 00 |
| OVARIES | 4.6E-11 | 7.9E-01 | 1.1E-11 | 1.5E 00 | 1.3E-11 | 1.9E 00 | 8.4E-11 | 2.6E 00 | 1.6E-10 | 3.0E 00 | 2.4E-10 | 3.6E 00 |
| PANCREAS | 0.0 | 0.0 | 2.0E-14 | 1.2E 01 | 3.6E-14 | 1.2E 01 | 1.0E-13 | 2.4E 01 | 3.7E-13 | 2.3E 01 | 0.0 | 0.0 |
| SKELETON | 1.3E-14 | 1.3E 00 | 5.1E-14 | 7.9E-01 | 4.1E-14 | 1.0E 00 | 1.1E-13 | 1.7E 00 | 1.8E-13 | 2.1E 00 | 3.1E-13 | 2.5E 00 |
| TOTAL SKIN | 3.9E-16 | 1.3E 01 | 7.9E-15 | 2.6E 00 | 1.2E-14 | 2.8E 00 | 7.2E-14 | 4.1E 00 | 1.4E-13 | 4.7E 00 | 2.5E-13 | 5.6E 00 |
| SPLEEN | 0.0 | 0.0 | 1.7E-14 | 8.3E 00 | 2.5E-14 | 9.2E 00 | 1.3E-13 | 1.3E 01 | 2.1E-13 | 1.7E 01 | 4.1E-13 | 1.9E 01 |
| UTERUS | 5.0E-13 | 2.8E 00 | 5.0E-13 | 2.6E 00 | 5.5E-13 | 3.3E 00 | 2.7E-12 | 5.0E 00 | 4.9E-12 | 5.9E 00 | 7.8E-12 | 7.2E 00 |
| TOTAL BODY | 3.1E-14 | 5.4E-02 | 4.3E-14 | 2.8E-01 | 5.1E-14 | 3.9E-01 | 2.3E-13 | 4.5E-01 | 4.3E-13 | 5.1E-01 | 7.1E-13 | 6.2E-01 |

Table 14.3. Doses (rads/photon) to ovaries and coefficients of variation (%) for source organs of the five-year-old phantom

| SOURCE ORGANS | ENERGY (MEV) 0.020 | | 0.050 | | 0.100 | | 0.500 | | 1.000 | | 2.000 | |
|---|---|---|---|---|---|---|---|---|---|---|---|---|
| | DOSE | C.V. | DOSE | C.V. | DOSE | C.V. | DOSE | C.V. | DOSE | C.V. | DOSE | C.V. |
| BLADDER WALL | 1.5E-14 | 1.2E 01 | 9.2E-14 | 4.6E 00 | 1.2E-13 | 5.4E 00 | 4.5E-13 | 9.7E 00 | 8.2E-13 | 1.2E 01 | 8.1E-13 | 1.6E 01 |
| STOMACH WALL | 0.0 | 0.0 | 9.9E-15 | 7.5E 00 | 1.8E-14 | 7.5E 00 | 7.8E-14 | 1.1E 01 | 1.4E-13 | 1.4E 01 | 2.8E-13 | 1.7E 01 |
| SMALL INTESTINE | 9.8E-14 | 1.1E 00 | 1.6E-13 | 9.7E-01 | 1.9E-13 | 1.1E 00 | 8.4E-13 | 1.6E 00 | 1.5E-12 | 1.9E 00 | 2.5E-12 | 2.2E 00 |
| U.L.I. WALL | 1.4E-13 | 2.1E 00 | 1.4E-13 | 2.0E 00 | 1.7E-13 | 2.3E 00 | 7.8E-13 | 3.6E 00 | 1.5E-12 | 4.2E 00 | 2.4E-12 | 5.1E 00 |
| L.L.I. WALL | 2.1E-13 | 2.0E 00 | 1.8E-13 | 1.9E 00 | 2.2E-13 | 2.3E 00 | 1.0E-12 | 3.6E 00 | 2.0E-12 | 4.2E 00 | 3.0E-12 | 5.2E 00 |
| HEART | 0.0 | 0.0 | 8.0E-16 | 1.7E 01 | 2.5E-15 | 1.2E 01 | 1.7E-14 | 1.3E 01 | 4.0E-14 | 1.5E 01 | 4.9E-14 | 1.8E 01 |
| KIDNEYS | 0.0 | 0.0 | 1.2E-14 | 5.7E 00 | 2.0E-14 | 5.7E 00 | 9.9E-14 | 7.9E 00 | 1.6E-13 | 1.0E 01 | 3.3E-13 | 1.1E 01 |
| LIVER | 0.0 | 0.0 | 7.1E-15 | 3.5E 00 | 1.3E-14 | 3.3E 00 | 6.3E-14 | 4.2E 00 | 1.2E-13 | 4.9E 00 | 2.1E-13 | 5.7E 00 |
| LUNGS | 0.0 | 0.0 | 9.3E-16 | 1.0E 01 | 2.4E-15 | 8.6E 00 | 1.7E-14 | 9.8E 00 | 4.2E-14 | 1.0E 01 | 7.6E-14 | 1.2E 01 |
| RED MARROW | 1.8E-14 | 1.6E 00 | 9.5E-14 | 8.5E-01 | 7.9E-14 | 1.1E 00 | 1.8E-13 | 1.9E 00 | 3.3E-13 | 2.3E 00 | 5.3E-13 | 2.7E 00 |
| YELLOW MARROW | 7.1E-15 | 1.6E 00 | 4.3E-14 | 8.4E-01 | 3.8E-14 | 1.1E 00 | 9.4E-14 | 1.8E 00 | 1.7E-13 | 2.2E 00 | 2.8E-13 | 2.6E 00 |
| OVARIES | 2.7E-11 | 7.1E-01 | 6.5E-12 | 1.4E 00 | 8.5E-12 | 1.7E 00 | 5.2E-11 | 2.3E 00 | 9.4E-11 | 2.7E 00 | 1.5E-10 | 3.2E 00 |
| PANCREAS | 0.0 | 0.0 | 6.8E-15 | 1.4E 01 | 1.2E-14 | 1.4E 01 | 4.9E-14 | 2.5E 01 | 1.2E-13 | 2.6E 01 | 2.4E-13 | 2.8E 01 |
| SKELETON | 4.6E-15 | 1.6E 00 | 2.8E-14 | 7.8E-01 | 2.6E-14 | 9.7E-01 | 6.5E-14 | 1.6E 00 | 1.2E-13 | 1.9E 00 | 1.9E-13 | 2.3E 00 |
| TOTAL SKIN | 6.7E-17 | 1.9E 01 | 4.4E-15 | 2.4E 00 | 7.6E-15 | 2.6E 00 | 4.0E-14 | 3.8E 00 | 9.3E-14 | 4.4E 00 | 1.5E-13 | 5.1E 00 |
| SPLEEN | 0.0 | 0.0 | 6.5E-15 | 9.5E 00 | 1.0E-14 | 1.0E 01 | 5.9E-14 | 1.3E 01 | 1.2E-13 | 1.5E 01 | 2.0E-13 | 1.8E 01 |
| UTERUS | 1.7E-13 | 3.3E 00 | 3.1E-13 | 2.4E 00 | 3.6E-13 | 3.0E 00 | 1.6E-12 | 4.5E 00 | 3.0E-12 | 5.3E 00 | 4.8E-12 | 6.5E 00 |
| TOTAL BODY | 1.6E-14 | 5.2E-02 | 2.5E-14 | 2.4E-01 | 3.2E-14 | 3.4E-01 | 1.4E-13 | 4.0E-01 | 2.6E-13 | 4.6E-01 | 4.4E-13 | 5.5E-01 |

Table 14.4. Doses (rads/photon) to ovaries and coefficients of variation (%) for source organs of the ten-year-old phantom

| SOURCE ORGANS | ENERGY (MEV) 0.020 | | 0.050 | | 0.100 | | 0.500 | | 1.000 | | 2.000 | |
|---|---|---|---|---|---|---|---|---|---|---|---|---|
| | DOSE | C.V. | DOSE | C.V. | DOSE | C.V. | DOSE | C.V. | DOSE | C.V. | DOSE | C.V. |
| BLADDER WALL | 4.9E-15 | 1.5E 01 | 6.8E-14 | 4.2E 00 | 7.6E-14 | 5.2E 00 | 3.2E-13 | 8.5E 00 | 5.8E-13 | 1.1E 01 | 9.7E-13 | 1.3E 01 |
| STOMACH WALL | 0.0 | 0.0 | 5.0E-15 | 8.2E 00 | 1.1E-14 | 7.1E 00 | 5.4E-14 | 1.2E 01 | 9.6E-14 | 1.4E 01 | 1.8E-13 | 1.6E 01 |
| SMALL INTESTINE | 5.2E-14 | 1.2E 00 | 1.1E-13 | 9.4E-01 | 1.3E-13 | 1.1E 00 | 5.7E-13 | 1.5E 00 | 1.0E-12 | 1.8E 00 | 1.7E-12 | 2.1E 00 |
| U.L.I. WALL | 8.5E-14 | 2.1E 00 | 9.1E-14 | 1.9E 00 | 1.2E-13 | 2.2E 00 | 5.1E-13 | 3.4E 00 | 9.8E-13 | 4.0E 00 | 1.8E-12 | 4.5E 00 |
| L.L.I. WALL | 1.2E-13 | 2.0E 00 | 1.3E-13 | 1.8E 00 | 1.6E-13 | 2.2E 00 | 7.5E-13 | 3.3E 00 | 1.3E-12 | 4.1E 00 | 2.2E-12 | 4.7E 00 |
| HEART | 0.0 | 0.0 | 4.6E-16 | 1.6E 01 | 1.0E-15 | 1.4E 01 | 1.0E-14 | 1.3E 01 | 1.9E-14 | 1.7E 01 | 4.2E-14 | 1.7E 01 |
| KIDNEYS | 0.0 | 0.0 | 5.3E-15 | 6.3E 00 | 1.3E-14 | 5.4E 00 | 6.2E-14 | 7.8E 00 | 1.1E-13 | 9.7E 00 | 1.8E-13 | 1.2E 01 |
| LIVER | 0.0 | 0.0 | 3.4E-15 | 4.0E 00 | 7.6E-15 | 3.4E 00 | 3.6E-14 | 4.3E 00 | 7.2E-14 | 4.9E 00 | 1.4E-13 | 5.4E 00 |
| LUNGS | 0.0 | 0.0 | 3.8E-16 | 1.3E 01 | 1.1E-15 | 9.2E 00 | 8.8E-15 | 1.0E 01 | 1.8E-14 | 1.1E 01 | 5.2E-14 | 1.1E 01 |
| RED MARROW | 8.2E-15 | 1.9E 00 | 7.0E-14 | 8.2E-01 | 6.2E-14 | 1.0E 00 | 1.4E-13 | 1.7E 00 | 2.5E-13 | 2.1E 00 | 4.0E-13 | 2.5E 00 |
| YELLOW MARROW | 2.9E-15 | 1.9E 00 | 2.7E-14 | 8.0E-01 | 2.6E-14 | 1.0E 00 | 6.1E-14 | 1.7E 00 | 1.1E-13 | 2.0E 00 | 1.9E-13 | 2.4E 00 |
| OVARIES | 1.9E-11 | 6.6E-01 | 4.9E-12 | 1.3E 00 | 6.0E-12 | 1.6E 00 | 3.5E-11 | 2.2E 00 | 7.0E-11 | 2.5E 00 | 1.1E-10 | 2.9E 00 |
| PANCREAS | 0.0 | 0.0 | 2.8E-15 | 1.6E 01 | 8.6E-15 | 1.2E 01 | 4.5E-14 | 2.1E 01 | 8.0E-14 | 2.3E 01 | 1.6E-13 | 2.6E 01 |
| SKELETON | 1.9E-15 | 1.9E 00 | 1.9E-14 | 7.7E-01 | 1.9E-14 | 9.2E-01 | 4.5E-14 | 1.5E 00 | 8.0E-14 | 1.8E 00 | 1.4E-13 | 2.2E 00 |
| TOTAL SKIN | 3.2E-17 | 2.1E 01 | 2.5E-15 | 2.5E 00 | 4.9E-15 | 2.4E 00 | 2.6E-14 | 3.7E 00 | 5.1E-14 | 4.3E 00 | 1.0E-13 | 4.7E 00 |
| SPLEEN | 0.0 | 0.0 | 2.3E-15 | 1.3E 01 | 7.1E-15 | 9.2E 00 | 3.6E-14 | 1.3E 01 | 7.4E-14 | 1.6E 01 | 1.3E-13 | 1.8E 01 |
| UTERUS | 7.5E-14 | 4.0E 00 | 2.0E-13 | 2.4E 00 | 2.4E-13 | 2.8E 00 | 9.9E-13 | 4.5E 00 | 2.0E-12 | 5.0E 00 | 3.2E-12 | 6.2E 00 |
| TOTAL BODY | 1.0E-14 | 5.1E-02 | 1.7E-14 | 2.1E-01 | 2.2E-14 | 3.2E-01 | 9.7E-14 | 3.7E-01 | 1.8E-13 | 4.2E-01 | 3.1E-13 | 5.1E-01 |

Table 14.5. Doses (rads/photon) to ovaries and coefficients of variation (%) for source organs of the 15-year-old phantom

| SOURCE ORGANS | ENERGY (MEV) 0.020 | | 0.050 | | 0.100 | | 0.500 | | 1.000 | | 2.000 | |
|---|---|---|---|---|---|---|---|---|---|---|---|---|
| | DOSE | C.V. | DOSE | C.V. | DOSE | C.V. | DOSE | C.V. | DOSE | C.V. | DOSE | C.V. |
| BLADDER WALL | 1.8E-15 | 2.1E 01 | 3.8E-14 | 4.0E 00 | 5.6E-14 | 4.5E 00 | 2.3E-13 | 7.8E 00 | 4.3E-13 | 9.2E 00 | 5.6E-13 | 1.2E 01 |
| STOMACH WALL | 0.0 | 0.0 | 2.7E-15 | 8.5E 00 | 6.3E-15 | 7.2E 00 | 2.8E-14 | 1.1E 01 | 6.3E-14 | 1.2E 01 | 1.1E-13 | 1.6E 01 |
| SMALL INTESTINE | 2.6E-14 | 1.3E 00 | 7.0E-14 | 9.0E-01 | 9.1E-14 | 9.9E-01 | 3.8E-13 | 1.4E 00 | 6.7E-13 | 1.7E 00 | 1.1E-12 | 1.9E 00 |
| U.L.I. WALL | 4.8E-14 | 2.2E 00 | 6.3E-14 | 1.8E 00 | 8.1E-14 | 2.0E 00 | 3.7E-13 | 3.1E 00 | 6.7E-13 | 3.7E 00 | 1.0E-12 | 4.5E 00 |
| L.L.I. WALL | 6.3E-14 | 2.1E 00 | 8.5E-14 | 1.7E 00 | 1.0E-13 | 2.0E 00 | 4.7E-13 | 3.1E 00 | 8.8E-13 | 3.7E 00 | 1.4E-12 | 4.5E 00 |
| HEART | 0.0 | 0.0 | 1.9E-16 | 2.6E 01 | 5.3E-16 | 1.4E 01 | 4.7E-15 | 1.5E 01 | 1.1E-14 | 1.6E 01 | 2.8E-14 | 1.5E 01 |
| KIDNEYS | 0.0 | 0.0 | 2.8E-15 | 7.1E 00 | 7.1E-15 | 5.6E 00 | 3.7E-14 | 7.5E 00 | 6.7E-14 | 9.1E 00 | 1.2E-13 | 1.1E 01 |
| LIVER | 0.0 | 0.0 | 1.4E-15 | 4.8E 00 | 3.9E-15 | 3.7E 00 | 2.2E-14 | 4.2E 00 | 4.7E-14 | 4.6E 00 | 8.5E-14 | 5.3E 00 |
| LUNGS | 0.0 | 0.0 | 1.2E-16 | 1.8E 01 | 4.6E-16 | 1.1E 01 | 4.3E-15 | 1.1E 01 | 1.2E-14 | 1.1E 01 | 2.1E-14 | 1.3E 01 |
| RED MARROW | 3.0E-15 | 2.5E 00 | 4.5E-14 | 8.0E-01 | 4.6E-14 | 9.4E-01 | 1.0E-13 | 1.6E 00 | 1.7E-13 | 2.0E 00 | 2.9E-13 | 2.3E 00 |
| YELLOW MARROW | 1.0E-15 | 2.5E 00 | 1.6E-14 | 7.9E-01 | 1.8E-14 | 9.2E-01 | 4.1E-14 | 1.6E 00 | 7.2E-14 | 1.9E 00 | 1.2E-13 | 2.3E 00 |
| OVARIES | 1.3E-11 | 6.1E-01 | 3.4E-12 | 1.2E 00 | 4.1E-12 | 1.5E 00 | 2.4E-11 | 2.0E 00 | 4.6E-11 | 2.3E 00 | 7.5E-11 | 2.7E 00 |
| PANCREAS | 0.0 | 0.0 | 1.7E-15 | 1.7E 01 | 4.5E-15 | 1.3E 01 | 2.1E-14 | 2.2E 01 | 3.0E-14 | 2.5E 01 | 1.2E-13 | 2.3E 01 |
| SKELETON | 7.1E-16 | 2.5E 00 | 1.1E-14 | 7.6E-01 | 1.3E-14 | 8.7E-01 | 3.1E-14 | 1.4E 00 | 5.4E-14 | 1.7E 00 | 9.2E-14 | 2.0E 00 |
| TOTAL SKIN | 1.3E-17 | 2.9E 01 | 1.5E-15 | 2.5E 00 | 3.0E-15 | 2.4E 00 | 1.8E-14 | 3.4E 00 | 3.5E-14 | 4.0E 00 | 6.8E-14 | 4.4E 00 |
| SPLEEN | 0.0 | 0.0 | 1.1E-15 | 1.4E 01 | 3.7E-15 | 9.9E 00 | 2.0E-14 | 1.3E 01 | 4.2E-14 | 1.5E 01 | 6.7E-14 | 1.7E 01 |
| UTERUS | 2.5E-14 | 5.1E 00 | 1.2E-13 | 2.4E 00 | 1.5E-13 | 2.7E 00 | 6.1E-13 | 4.3E 00 | 1.1E-12 | 5.1E 00 | 1.8E-12 | 6.1E 00 |
| TOTAL BODY | 5.9E-15 | 5.0E-02 | 1.1E-14 | 1.8E-01 | 1.5E-14 | 2.8E-01 | 6.5E-14 | 3.3E-01 | 1.2E-13 | 3.8E-01 | 2.1E-13 | 4.6E-01 |

Table 14.6. Doses (rads/photon) to ovaries and coefficients of variation (%) for source organs of the adult phantom

| SOURCE ORGANS | ENERGY (MEV) 0.020 | | 0.050 | | 0.100 | | 0.500 | | 1.000 | | 2.000 | |
|---|---|---|---|---|---|---|---|---|---|---|---|---|
| | DOSE | C.V. | DOSE | C.V. | DOSE | C.V. | DOSE | C.V. | DOSE | C.V. | DOSE | C.V. |
| BLADDER WALL | 1.1E-15 | 2.1E 01 | 3.2E-14 | 4.0E 00 | 4.6E-14 | 4.2E 00 | 1.8E-13 | 7.3E 00 | 3.6E-13 | 8.6E 00 | 5.4E-13 | 1.1E 01 |
| STOMACH WALL | 0.0 | 0.0 | 1.9E-15 | 9.0E 00 | 5.1E-15 | 7.0E 00 | 2.3E-14 | 1.1E 01 | 4.0E-14 | 1.3E 01 | 9.9E-14 | 1.5E 01 |
| SMALL INTESTINE | 1.9E-14 | 1.4E 00 | 5.8E-14 | 8.7E-01 | 7.6E-14 | 9.5E-01 | 3.2E-13 | 1.3E 00 | 5.7E-13 | 1.6E 00 | 9.9E-13 | 1.8E 00 |
| U.L.I. WALL | 3.4E-14 | 2.2E 00 | 5.1E-14 | 1.7E 00 | 6.6E-14 | 1.9E 00 | 3.0E-13 | 2.9E 00 | 5.4E-13 | 3.6E 00 | 9.4E-13 | 4.1E 00 |
| L.L.I. WALL | 4.6E-14 | 2.1E 00 | 7.1E-14 | 1.6E 00 | 8.9E-14 | 1.9E 00 | 3.9E-13 | 3.0E 00 | 6.8E-13 | 3.6E 00 | 1.2E-12 | 4.2E 00 |
| HEART | 0.0 | 0.0 | 7.0E-17 | 2.6E 01 | 3.6E-16 | 1.6E 01 | 3.3E-15 | 1.5E 01 | 9.0E-15 | 1.5E 01 | 1.4E-14 | 1.8E 01 |
| KIDNEYS | 0.0 | 0.0 | 2.1E-15 | 6.9E 00 | 5.6E-15 | 5.4E 00 | 3.1E-14 | 7.1E 00 | 5.8E-14 | 8.2E 00 | 1.1E-13 | 9.9E 00 |
| LIVER | 0.0 | 0.0 | 1.1E-15 | 4.8E 00 | 3.2E-15 | 3.7E 00 | 1.7E-14 | 4.1E 00 | 3.5E-14 | 4.6E 00 | 7.3E-14 | 5.0E 00 |
| LUNGS | 0.0 | 0.0 | 6.8E-17 | 2.1E 01 | 3.3E-16 | 1.1E 01 | 3.1E-15 | 1.1E 01 | 8.6E-15 | 1.1E 01 | 1.8E-14 | 1.2E 01 |
| RED MARROW | 1.9E-15 | 2.8E 00 | 3.6E-14 | 7.8E-01 | 4.0E-14 | 9.0E-01 | 8.4E-14 | 1.5E 00 | 1.5E-13 | 1.9E 00 | 2.5E-13 | 2.2E 00 |
| YELLOW MARROW | 6.2E-16 | 2.8E 00 | 1.3E-14 | 7.8E-01 | 1.5E-14 | 8.8E-01 | 3.4E-14 | 1.5E 00 | 6.1E-14 | 1.8E 00 | 1.1E-13 | 2.2E 00 |
| OVARIES | 1.0E-11 | 5.7E-01 | 2.9E-12 | 1.1E 00 | 3.5E-12 | 1.4E 00 | 2.1E-11 | 1.9E 00 | 3.9E-11 | 2.2E 00 | 6.7E-11 | 2.5E 00 |
| PANCREAS | 0.0 | 0.0 | 6.8E-16 | 2.3E 01 | 3.2E-15 | 1.4E 01 | 1.5E-14 | 1.9E 01 | 5.1E-14 | 1.9E 01 | 3.1E-14 | 2.7E 01 |
| SKELETON | 4.4E-16 | 2.8E 00 | 9.1E-15 | 7.6E-01 | 1.1E-14 | 8.3E-01 | 2.5E-14 | 1.4E 00 | 4.6E-14 | 1.6E 00 | 8.2E-14 | 1.9E 00 |
| TOTAL SKIN | 0.0 | 0.0 | 1.1E-15 | 2.6E 00 | 2.4E-15 | 2.3E 00 | 1.4E-14 | 3.3E 00 | 3.0E-14 | 3.7E 00 | 4.9E-14 | 4.6E 00 |
| SPLEEN | 0.0 | 0.0 | 8.2E-16 | 1.5E 01 | 2.8E-15 | 9.7E 00 | 1.9E-14 | 1.2E 01 | 3.3E-14 | 1.5E 01 | 8.0E-14 | 1.5E 01 |
| UTERUS | 1.6E-14 | 5.6E 00 | 1.0E-13 | 2.3E 00 | 1.3E-13 | 2.5E 00 | 4.9E-13 | 4.1E 00 | 8.5E-13 | 5.0E 00 | 1.5E-12 | 5.9E 00 |
| TOTAL BODY | 4.5E-15 | 5.0E-02 | 9.0E-15 | 1.6E-01 | 1.3E-14 | 2.6E-01 | 5.5E-14 | 3.1E-01 | 1.0E-13 | 3.5E-01 | 1.8E-13 | 4.2E-01 |

Table 14.7. Doses (rads/photon) to testes and coefficients of variation (%) for source organs of the newborn phantom

| SOURCE ORGANS | ENERGY (MEV) 0.020 | | 0.050 | | 0.100 | | 0.500 | | 1.000 | | 2.000 | |
|---|---|---|---|---|---|---|---|---|---|---|---|---|
| | DOSE | C.V. | DOSE | C.V. | DOSE | C.V. | DOSE | C.V. | DOSE | C.V. | DOSE | C.V. |
| BLADDER WALL | 1.9E-13 | 8.4E 00 | 2.3E-13 | 7.2E 00 | 3.4E-13 | 8.5E 00 | 1.7E-12 | 1.3E 01 | 2.9E-12 | 1.5E 01 | 5.0E-12 | 1.8E 01 |
| STOMACH WALL | 0.0 | 0.0 | 9.3E-15 | 2.0E 01 | 1.7E-14 | 2.1E 01 | 1.4E-13 | 2.5E 01 | 0.0 | 0.0 | 0.0 | 0.0 |
| SMALL INTESTINE | 1.3E-15 | 2.1E 01 | 3.3E-14 | 4.8E 00 | 4.2E-14 | 5.3E 00 | 2.2E-13 | 7.2E 00 | 5.0E-13 | 7.9E 00 | 6.4E-13 | 1.0E 01 |
| U.L.I. WALL | 0.0 | 0.0 | 3.2E-14 | 8.8E 00 | 4.1E-14 | 1.0E 01 | 2.3E-13 | 1.5E 01 | 4.9E-13 | 1.7E 01 | 7.8E-13 | 2.0E 01 |
| L.L.I. WALL | 2.1E-14 | 1.3E 01 | 9.9E-14 | 6.1E 00 | 1.3E-13 | 7.4E 00 | 6.1E-13 | 1.1E 01 | 1.0E-12 | 1.4E 01 | 1.9E-12 | 1.6E 01 |
| HEART | 0.0 | 0.0 | 3.0E-15 | 2.1E 01 | 5.4E-15 | 2.1E 01 | 4.0E-14 | 2.0E 01 | 1.0E-13 | 2.2E 01 | 2.4E-13 | 2.3E 01 |
| KIDNEYS | 0.0 | 0.0 | 5.5E-15 | 1.8E 01 | 1.0E-14 | 1.9E 01 | 6.7E-14 | 2.4E 01 | 1.7E-13 | 2.5E 01 | 2.8E-13 | 2.9E 01 |
| LIVER | 0.0 | 0.0 | 6.7E-15 | 8.4E 00 | 1.0E-14 | 8.4E 00 | 6.9E-14 | 9.5E 00 | 1.4E-13 | 1.1E 01 | 2.1E-13 | 1.3E 01 |
| LUNGS | 0.0 | 0.0 | 1.9E-15 | 1.7E 01 | 3.3E-15 | 1.7E 01 | 2.7E-14 | 1.9E 01 | 9.2E-14 | 1.7E 01 | 1.3E-13 | 2.0E 01 |
| RED MARROW | 4.5E-15 | 6.2E 00 | 4.4E-14 | 2.6E 00 | 3.5E-14 | 3.3E 00 | 1.1E-13 | 5.1E 00 | 1.7E-13 | 6.2E 00 | 3.1E-13 | 7.1E 00 |
| YELLOW MARROW | 3.8E-15 | 5.2E 00 | 4.7E-14 | 2.1E 00 | 3.6E-14 | 2.6E 00 | 1.2E-13 | 3.9E 00 | 2.3E-13 | 4.7E 00 | 4.2E-13 | 5.5E 00 |
| PANCREAS | 0.0 | 0.0 | 0.0 | 0.0 | 0.0 | 0.0 | 0.0 | 0.0 | 0.0 | 0.0 | 0.0 | 0.0 |
| SKELETON | 6.7E-15 | 3.0E 00 | 5.6E-14 | 1.4E 00 | 4.2E-14 | 1.9E 00 | 1.3E-13 | 2.7E 00 | 2.5E-13 | 3.1E 00 | 4.2E-13 | 3.7E 00 |
| TOTAL SKIN | 6.1E-14 | 1.9E 00 | 3.8E-14 | 2.2E 00 | 4.7E-14 | 2.8E 00 | 2.7E-13 | 3.9E 00 | 5.2E-13 | 4.5E 00 | 8.0E-13 | 5.5E 00 |
| SPLEEN | 0.0 | 0.0 | 8.5E-15 | 2.3E 01 | 1.4E-14 | 2.1E 01 | 0.0 | 0.0 | 0.0 | 0.0 | 0.0 | 0.0 |
| TESTES | 5.8E-11 | 7.2E-01 | 1.4E-11 | 1.4E 00 | 1.7E-11 | 1.8E 00 | 1.1E-10 | 2.4E 00 | 2.0E-10 | 2.8E 00 | 3.3E-10 | 3.2E 00 |
| UTERUS | 1.1E-14 | 2.8E 01 | 7.3E-14 | 1.1E 01 | 1.1E-13 | 1.2E 01 | 4.8E-13 | 2.0E 01 | 7.7E-13 | 2.5E 01 | 1.8E-12 | 2.6E 01 |
| TOTAL BODY | 6.7E-14 | 2.3E-01 | 5.4E-14 | 5.3E-01 | 6.2E-14 | 6.2E-01 | 3.3E-13 | 7.1E-01 | 6.3E-13 | 8.0E-01 | 1.0E-12 | 9.4E-01 |

Table 14.8. Doses (rads/photon) to testes and coefficients of variation (%) for source organs of the one-year-old phantom

| SOURCE ORGANS | ENERGY (MEV) 0.020 | | 0.050 | | 0.100 | | 0.500 | | 1.000 | | 2.000 | |
|---|---|---|---|---|---|---|---|---|---|---|---|---|
| | DOSE | C.V. | DOSE | C.V. | DOSE | C.V. | DOSE | C.V. | DOSE | C.V. | DOSE | C.V. |
| BLADDER WALL | 4.2E-14 | 1.1E 01 | 1.3E-13 | 5.7E 00 | 1.4E-13 | 7.4E 00 | 6.2E-13 | 1.2E 01 | 1.4E-12 | 1.3E 01 | 2.5E-12 | 1.5E 01 |
| STOMACH WALL | 0.0 | 0.0 | 2.1E-15 | 2.2E 01 | 8.3E-15 | 1.7E 01 | 3.7E-14 | 2.8E 01 | 0.0 | 0.0 | 0.0 | 0.0 |
| SMALL INTESTINE | 0.0 | 0.0 | 1.3E-14 | 4.4E 00 | 2.0E-14 | 4.6E 00 | 9.0E-14 | 6.6E 00 | 1.9E-13 | 7.3E 00 | 3.0E-13 | 8.7E 00 |
| U.L.I. WALL | 0.0 | 0.0 | 1.2E-14 | 8.9E 00 | 2.1E-14 | 8.4E 00 | 8.8E-14 | 1.4E 01 | 1.9E-13 | 1.7E 01 | 3.5E-13 | 1.8E 01 |
| L.L.I. WALL | 3.7E-15 | 1.8E 01 | 4.8E-14 | 5.1E 00 | 6.0E-14 | 6.0E 00 | 2.7E-13 | 9.6E 00 | 5.1E-13 | 1.1E 01 | 8.2E-13 | 1.3E 01 |
| HEART | 0.0 | 0.0 | 0.0 | 0.0 | 1.1E-15 | 2.3E 01 | 1.3E-14 | 2.2E 01 | 3.7E-14 | 2.0E 01 | 7.3E-14 | 2.2E 01 |
| KIDNEYS | 0.0 | 0.0 | 1.2E-15 | 2.4E 01 | 3.9E-15 | 1.6E 01 | 3.0E-14 | 2.1E 01 | 7.8E-14 | 2.2E 01 | 1.7E-13 | 2.3E 01 |
| LIVER | 0.0 | 0.0 | 1.7E-15 | 9.9E 00 | 4.0E-15 | 7.9E 00 | 2.3E-14 | 1.0E 01 | 5.9E-14 | 9.6E 00 | 1.1E-13 | 1.1E 01 |
| LUNGS | 0.0 | 0.0 | 2.8E-16 | 2.5E 01 | 1.6E-15 | 1.5E 01 | 1.2E-14 | 1.8E 01 | 3.0E-14 | 1.8E 01 | 7.5E-14 | 1.8E 01 |
| RED MARROW | 4.7E-16 | 1.0E 01 | 1.9E-14 | 2.4E 00 | 1.8E-14 | 2.7E 00 | 4.4E-14 | 4.5E 00 | 1.1E-13 | 4.9E 00 | 1.6E-13 | 5.9E 00 |
| YELLOW MARROW | 2.7E-16 | 9.5E 00 | 1.6E-14 | 2.1E 00 | 1.7E-14 | 2.3E 00 | 4.9E-14 | 3.6E 00 | 1.0E-13 | 4.0E 00 | 1.7E-13 | 4.7E 00 |
| PANCREAS | 0.0 | 0.0 | 0.0 | 0.0 | 0.0 | 0.0 | 0.0 | 0.0 | 0.0 | 0.0 | 0.0 | 0.0 |
| SKELETON | 8.6E-16 | 4.8E 00 | 2.4E-14 | 1.3E 00 | 2.4E-14 | 1.5E 00 | 6.4E-14 | 2.3E 00 | 1.2E-13 | 2.6E 00 | 2.1E-13 | 3.0E 00 |
| TOTAL SKIN | 2.1E-14 | 1.9E 00 | 1.7E-14 | 1.9E 00 | 2.3E-14 | 2.2E 00 | 1.3E-13 | 3.2E 00 | 2.5E-13 | 3.7E 00 | 4.5E-13 | 4.2E 00 |
| SPLEEN | 0.0 | 0.0 | 1.2E-15 | 2.8E 01 | 2.6E-15 | 2.6E 01 | 0.0 | 0.0 | 0.0 | 0.0 | 0.0 | 0.0 |
| TESTES | 2.3E-11 | 5.7E-01 | 6.2E-12 | 1.1E 00 | 7.6E-12 | 1.4E 00 | 4.6E-11 | 1.9E 00 | 8.1E-11 | 2.2E 00 | 1.4E-10 | 2.6E 00 |
| UTERUS | 0.0 | 0.0 | 3.6E-14 | 8.9E 00 | 4.9E-14 | 1.1E 01 | 2.4E-13 | 1.7E 01 | 4.0E-13 | 1.9E 01 | 6.3E-13 | 2.4E 01 |
| TOTAL BODY | 2.5E-14 | 1.9E-01 | 2.6E-14 | 4.5E-01 | 3.2E-14 | 5.3E-01 | 1.6E-13 | 5.9E-01 | 3.0E-13 | 6.6E-01 | 5.1E-13 | 7.7E-01 |

Table 14.9. Doses (rads/photon) to testes and coefficients of variation (%) for source organs of the five-year-old phantom

| SOURCE ORGANS | ENERGY (MEV) 0.020 | | 0.050 | | 0.100 | | 0.500 | | 1.000 | | 2.000 | |
|---|---|---|---|---|---|---|---|---|---|---|---|---|
| | DOSE | C.V. | DOSE | C.V. | DOSE | C.V. | DOSE | C.V. | DOSE | C.V. | DOSE | C.V. |
| BLADDER WALL | 8.4E-15 | 1.7E 01 | 6.5E-14 | 5.6E 00 | 8.1E-14 | 6.6E 00 | 4.4E-13 | 1.0E 01 | 7.4E-13 | 1.3E 01 | 1.3E-12 | 1.4E 01 |
| STOMACH WALL | 0.0 | 0.0 | 5.7E-16 | 2.9E 01 | 8.2E-16 | 2.9E 01 | 0.0 | 0.0 | 0.0 | 0.0 | 0.0 | 0.0 |
| SMALL INTESTINE | 0.0 | 0.0 | 4.5E-15 | 5.6E 00 | 9.2E-15 | 4.9E 00 | 4.8E-14 | 6.3E 00 | 9.7E-14 | 7.0E 00 | 1.9E-13 | 7.9E 00 |
| U.L.I. WALL | 0.0 | 0.0 | 4.1E-15 | 1.0E 01 | 7.0E-15 | 1.1E 01 | 4.9E-14 | 1.3E 01 | 9.2E-14 | 1.5E 01 | 2.1E-13 | 1.7E 01 |
| L.L.I. WALL | 2.7E-15 | 1.6E 01 | 3.0E-14 | 4.6E 00 | 3.9E-14 | 5.2E 00 | 1.9E-13 | 8.1E 00 | 4.0E-13 | 9.1E 00 | 5.9E-13 | 1.1E 01 |
| HEART | 0.0 | 0.0 | 0.0 | 0.0 | 0.0 | 0.0 | 4.3E-15 | 3.0E 01 | 9.5E-15 | 2.9E 01 | 2.3E-14 | 2.8E 01 |
| KIDNEYS | 0.0 | 0.0 | 5.1E-16 | 2.5E 01 | 1.4E-15 | 2.1E 01 | 9.3E-15 | 2.3E 01 | 2.9E-14 | 2.2E 01 | 4.8E-14 | 2.5E 01 |
| LIVER | 0.0 | 0.0 | 3.0E-16 | 1.4E 01 | 9.3E-16 | 1.3E 01 | 1.1E-14 | 1.1E 01 | 2.4E-14 | 1.1E 01 | 5.4E-14 | 1.1E 01 |
| LUNGS | 0.0 | 0.0 | 0.0 | 0.0 | 2.3E-16 | 2.5E 01 | 3.1E-15 | 2.1E 01 | 7.4E-15 | 2.1E 01 | 1.9E-14 | 2.2E 01 |
| RED MARROW | 1.2E-16 | 1.5E 01 | 1.2E-14 | 2.3E 00 | 1.4E-14 | 2.4E 00 | 3.5E-14 | 3.9E 00 | 6.9E-14 | 4.4E 00 | 1.1E-13 | 5.3E 00 |
| YELLOW MARROW | 5.3E-17 | 1.5E 01 | 6.7E-15 | 2.1E 00 | 8.7E-15 | 2.2E 00 | 2.6E-14 | 3.4E 00 | 5.4E-14 | 3.8E 00 | 9.4E-14 | 4.4E 00 |
| PANCREAS | 0.0 | 0.0 | 0.0 | 0.0 | 0.0 | 0.0 | 0.0 | 0.0 | 0.0 | 0.0 | 0.0 | 0.0 |
| SKELETON | 2.5E-16 | 6.3E 00 | 1.5E-14 | 1.2E 00 | 1.7E-14 | 1.4E 00 | 4.5E-14 | 2.0E 00 | 8.9E-14 | 2.2E 00 | 1.5E-13 | 2.7E 00 |
| TOTAL SKIN | 1.0E-14 | 1.9E 00 | 1.1E-14 | 1.7E 00 | 1.4E-14 | 2.0E 00 | 7.7E-14 | 3.0E 00 | 1.4E-13 | 3.5E 00 | 2.7E-13 | 3.9E 00 |
| SPLEEN | 0.0 | 0.0 | 0.0 | 0.0 | 1.1E-15 | 3.0E 01 | 0.0 | 0.0 | 0.0 | 0.0 | 0.0 | 0.0 |
| TESTES | 1.2E-11 | 4.9E-01 | 3.6E-12 | 9.8E-01 | 4.4E-12 | 1.2E 00 | 2.7E-11 | 1.6E 00 | 4.7E-11 | 1.9E 00 | 7.8E-11 | 2.2E 00 |
| UTERUS | 0.0 | 0.0 | 1.7E-14 | 1.0E 01 | 2.9E-14 | 9.5E 00 | 9.0E-14 | 1.6E 01 | 2.3E-13 | 1.8E 01 | 2.9E-13 | 2.5E 01 |
| TOTAL BODY | 1.4E-14 | 1.7E-01 | 1.6E-14 | 4.0E-01 | 2.0E-14 | 4.9E-01 | 1.0E-13 | 5.2E-01 | 1.9E-13 | 5.8E-01 | 3.2E-13 | 6.8E-01 |

Table 14.10. Doses (rads/photon) to testes and coefficients of variation (%) for source organs of the ten-year-old phantom

| SOURCE ORGANS | ENERGY (MEV) 0.020 | | 0.050 | | 0.100 | | 0.500 | | 1.000 | | 2.000 | |
|---|---|---|---|---|---|---|---|---|---|---|---|---|
| | DOSE | C.V. | DOSE | C.V. | DOSE | C.V. | DOSE | C.V. | DOSE | C.V. | DOSE | C.V. |
| BLADDER WALL | 2.9E-15 | 2.1E 01 | 4.0E-14 | 5.5E 00 | 5.5E-14 | 6.3E 00 | 2.8E-13 | 9.6E 00 | 3.1E-13 | 1.4E 01 | 6.6E-13 | 1.5E 01 |
| STOMACH WALL | 0.0 | 0.0 | 0.0 | 0.0 | 0.0 | 0.0 | 0.0 | 0.0 | 0.0 | 0.0 | 0.0 | 0.0 |
| SMALL INTESTINE | 0.0 | 0.0 | 2.1E-15 | 6.3E 00 | 4.9E-15 | 5.1E 00 | 3.0E-14 | 6.3E 00 | 6.5E-14 | 6.9E 00 | 1.2E-13 | 7.3E 00 |
| U.L.I. WALL | 0.0 | 0.0 | 1.9E-15 | 1.1E 01 | 4.4E-15 | 9.7E 00 | 2.0E-14 | 1.5E 01 | 4.4E-14 | 1.6E 01 | 7.2E-14 | 2.0E 01 |
| L.L.I. WALL | 9.9E-16 | 1.9E 01 | 2.1E-14 | 4.4E 00 | 3.0E-14 | 4.7E 00 | 1.6E-13 | 6.9E 00 | 2.2E-13 | 9.1E 00 | 4.8E-13 | 9.5E 00 |
| HEART | 0.0 | 0.0 | 0.0 | 0.0 | 0.0 | 0.0 | 0.0 | 0.0 | 0.0 | 0.0 | 1.4E-14 | 2.8E 01 |
| KIDNEYS | 0.0 | 0.0 | 0.0 | 0.0 | 6.6E-16 | 2.1E 01 | 8.8E-15 | 2.1E 01 | 1.1E-14 | 2.5E 01 | 2.8E-14 | 2.7E 01 |
| LIVER | 0.0 | 0.0 | 8.9E-17 | 2.1E 01 | 4.7E-16 | 1.3E 01 | 4.9E-15 | 1.2E 01 | 1.2E-14 | 1.2E 01 | 2.9E-14 | 1.2E 01 |
| LUNGS | 0.0 | 0.0 | 0.0 | 0.0 | 6.3E-17 | 2.9E 01 | 1.6E-15 | 2.7E 01 | 5.0E-15 | 2.3E 01 | 1.3E-14 | 2.3E 01 |
| RED MARROW | 2.2E-17 | 1.4E 01 | 6.9E-15 | 2.3E 00 | 9.5E-15 | 2.3E 00 | 2.5E-14 | 3.6E 00 | 5.0E-14 | 4.2E 00 | 8.6E-14 | 4.8E 00 |
| YELLOW MARROW | 8.2E-18 | 1.3E 01 | 3.2E-15 | 2.3E 00 | 4.8E-15 | 2.3E 00 | 1.4E-14 | 3.3E 00 | 3.0E-14 | 3.8E 00 | 6.1E-14 | 4.2E 00 |
| PANCREAS | 0.0 | 0.0 | 0.0 | 0.0 | 0.0 | 0.0 | 0.0 | 0.0 | 0.0 | 0.0 | 0.0 | 0.0 |
| SKELETON | 7.7E-17 | 9.2E 00 | 8.9E-15 | 1.2E 00 | 1.2E-14 | 1.3E 00 | 3.2E-14 | 1.9E 00 | 6.1E-14 | 2.1E 00 | 1.1E-13 | 2.4E 00 |
| TOTAL SKIN | 5.6E-15 | 2.0E 00 | 7.4E-15 | 1.6E 00 | 9.3E-15 | 1.9E 00 | 5.3E-14 | 2.8E 00 | 9.9E-14 | 3.2E 00 | 1.8E-13 | 3.7E 00 |
| SPLEEN | 0.0 | 0.0 | 0.0 | 0.0 | 5.1E-16 | 2.6E 01 | 0.0 | 0.0 | 0.0 | 0.0 | 0.0 | 0.0 |
| TESTES | 7.4E-12 | 4.4E-01 | 2.4E-12 | 9.0E-01 | 2.8E-12 | 1.1E 00 | 1.7E-11 | 1.5E 00 | 3.0E-11 | 1.7E 00 | 5.0E-11 | 2.0E 00 |
| UTERUS | 0.0 | 0.0 | 9.6E-15 | 9.9E 00 | 2.0E-14 | 8.9E 00 | 6.8E-14 | 1.6E 01 | 1.0E-13 | 1.8E 01 | 2.2E-13 | 2.2E 01 |
| TOTAL BODY | 8.5E-15 | 1.6E-01 | 1.1E-14 | 3.8E-01 | 1.4E-14 | 4.6E-01 | 7.0E-14 | 4.8E-01 | 1.3E-13 | 5.4E-01 | 2.3E-13 | 6.3E-01 |

Table 14.11. Doses (rads/photon) to testes and coefficients of variation (%) for source organs of the 15-year-old phantom

| SOURCE ORGANS | ENERGY (MEV) 0.020 | | 0.050 | | 0.100 | | 0.500 | | 1.000 | | 2.000 | |
|---|---|---|---|---|---|---|---|---|---|---|---|---|
| | DOSE | C.V. | DOSE | C.V. | DOSE | C.V. | DOSE | C.V. | DOSE | C.V. | DOSE | C.V. |
| BLADDER WALL | 0.0 | 0.0 | 2.8E-14 | 5.0E 00 | 3.9E-14 | 5.6E 00 | 1.6E-13 | 9.4E 00 | 3.2E-13 | 1.1E 01 | 5.2E-13 | 1.3E 01 |
| STOMACH WALL | 0.0 | 0.0 | 0.0 | 0.0 | 0.0 | 0.0 | 0.0 | 0.0 | 0.0 | 0.0 | 0.0 | 0.0 |
| SMALL INTESTINE | 0.0 | 0.0 | 8.9E-16 | 7.4E 00 | 2.8E-15 | 5.4E 00 | 1.8E-14 | 6.1E 00 | 3.7E-14 | 6.7E 00 | 7.0E-14 | 7.3E 00 |
| U.L.I. WALL | 0.0 | 0.0 | 5.2E-16 | 1.6E 01 | 2.2E-15 | 1.0E 01 | 1.6E-14 | 1.3E 01 | 3.3E-14 | 1.6E 01 | 5.2E-14 | 1.8E 01 |
| L.L.I. WALL | 5.4E-16 | 2.0E 01 | 1.3E-14 | 4.0E 00 | 1.9E-14 | 4.4E 00 | 1.0E-13 | 6.5E 00 | 1.8E-13 | 7.9E 00 | 2.9E-13 | 9.1E 00 |
| HEART | 0.0 | 0.0 | 0.0 | 0.0 | 0.0 | 0.0 | 0.0 | 0.0 | 0.0 | 0.0 | 1.2E-14 | 2.5E 01 |
| KIDNEYS | 0.0 | 0.0 | 0.0 | 0.0 | 3.4E-16 | 2.5E 01 | 2.4E-15 | 2.7E 01 | 1.3E-14 | 2.2E 01 | 2.2E-14 | 2.4E 01 |
| LIVER | 0.0 | 0.0 | 0.0 | 0.0 | 2.2E-16 | 1.5E 01 | 2.7E-15 | 1.1E 01 | 7.2E-15 | 1.1E 01 | 1.8E-14 | 1.1E 01 |
| LUNGS | 0.0 | 0.0 | 0.0 | 0.0 | 0.0 | 0.0 | 0.0 | 0.0 | 1.7E-15 | 2.8E 01 | 3.2E-15 | 2.7E 01 |
| RED MARROW | 4.9E-18 | 2.1E 01 | 3.7E-15 | 2.5E 00 | 6.6E-15 | 2.3E 00 | 1.7E-14 | 3.3E 00 | 3.2E-14 | 4.0E 00 | 5.8E-14 | 4.6E 00 |
| YELLOW MARROW | 2.0E-18 | 2.4E 01 | 1.5E-15 | 2.4E 00 | 2.9E-15 | 2.2E 00 | 9.0E-15 | 3.2E 00 | 1.8E-14 | 3.6E 00 | 3.6E-14 | 4.0E 00 |
| PANCREAS | 0.0 | 0.0 | 0.0 | 0.0 | 0.0 | 0.0 | 0.0 | 0.0 | 0.0 | 0.0 | 0.0 | 0.0 |
| SKELETON | 1.8E-17 | 1.5E 01 | 4.9E-15 | 1.3E 00 | 8.1E-15 | 1.3E 00 | 2.2E-14 | 1.8E 00 | 4.1E-14 | 2.0E 00 | 7.4E-14 | 2.3E 00 |
| TOTAL SKIN | 3.5E-15 | 2.0E 00 | 5.4E-15 | 1.5E 00 | 6.9E-15 | 1.7E 00 | 3.6E-14 | 2.6E 00 | 7.3E-14 | 2.9E 00 | 1.3E-13 | 3.4E 00 |
| SPLEEN | 0.0 | 0.0 | 0.0 | 0.0 | 0.0 | 0.0 | 0.0 | 0.0 | 0.0 | 0.0 | 0.0 | 0.0 |
| TESTES | 4.7E-12 | 4.0E-01 | 1.6E-12 | 8.3E-01 | 1.9E-12 | 1.0E 00 | 1.1E-11 | 1.3E 00 | 2.1E-11 | 1.6E 00 | 3.3E-11 | 1.9E 00 |
| UTERUS | 0.0 | 0.0 | 4.3E-15 | 1.1E 01 | 9.7E-15 | 9.4E 00 | 4.6E-14 | 1.4E 01 | 9.7E-14 | 1.6E 01 | 1.4E-13 | 2.0E 01 |
| TOTAL BODY | 5.1E-15 | 1.5E-01 | 6.8E-15 | 3.5E-01 | 9.7E-15 | 4.3E-01 | 4.7E-14 | 4.5E-01 | 9.1E-14 | 4.9E-01 | 1.5E-13 | 5.8E-01 |

Table 14.12. Doses (rads/photon) to testes and coefficients of variation (%) for source organs of the adult phantom

| SOURCE ORGANS | ENERGY (MEV) 0.020 | | 0.050 | | 0.100 | | 0.500 | | 1.000 | | 2.000 | |
|---|---|---|---|---|---|---|---|---|---|---|---|---|
| | DOSE | C.V. | DOSE | C.V. | DOSE | C.V. | DOSE | C.V. | DOSE | C.V. | DOSE | C.V. |
| BLADDER WALL | 7.2E-16 | 2.9E 01 | 2.0E-14 | 5.1E 00 | 3.0E-14 | 5.4E 00 | 1.4E-13 | 8.6E 00 | 2.8E-13 | 1.0E 01 | 4.3E-13 | 1.3E 01 |
| STOMACH WALL | 0.0 | 0.0 | 0.0 | 0.0 | 1.4E-16 | 3.0E 01 | 3.2E-15 | 3.0E 01 | 0.0 | 0.0 | 0.0 | 0.0 |
| SMALL INTESTINE | 0.0 | 0.0 | 6.4E-16 | 7.9E 00 | 2.0E-15 | 5.4E 00 | 1.5E-14 | 5.7E 00 | 2.8E-14 | 6.3E 00 | 5.9E-14 | 7.1E 00 |
| U.L.I. WALL | 0.0 | 0.0 | 5.3E-16 | 1.5E 01 | 1.7E-15 | 1.0E 01 | 8.8E-15 | 1.3E 01 | 2.2E-14 | 1.5E 01 | 7.3E-14 | 1.4E 01 |
| L.L.I. WALL | 2.5E-16 | 2.6E 01 | 1.0E-14 | 4.0E 00 | 1.7E-14 | 4.0E 00 | 7.8E-14 | 6.1E 00 | 1.2E-13 | 7.9E 00 | 2.3E-13 | 9.2E 00 |
| HEART | 0.0 | 0.0 | 0.0 | 0.0 | 0.0 | 0.0 | 0.0 | 0.0 | 0.0 | 0.0 | 4.1E-15 | 3.0E 01 |
| KIDNEYS | 0.0 | 0.0 | 0.0 | 0.0 | 1.8E-16 | 3.0E 01 | 2.8E-15 | 2.4E 01 | 8.1E-15 | 2.2E 01 | 1.3E-14 | 2.5E 01 |
| LIVER | 0.0 | 0.0 | 2.2E-17 | 2.9E 01 | 1.5E-16 | 1.7E 01 | 1.4E-15 | 1.3E 01 | 5.8E-15 | 1.1E 01 | 1.3E-14 | 1.2E 01 |
| LUNGS | 0.0 | 0.0 | 0.0 | 0.0 | 0.0 | 0.0 | 3.9E-16 | 2.8E 01 | 1.6E-15 | 2.7E 01 | 3.8E-15 | 2.5E 01 |
| RED MARROW | 0.0 | 0.0 | 2.6E-15 | 2.6E 00 | 5.0E-15 | 2.2E 00 | 1.4E-14 | 3.2E 00 | 2.7E-14 | 3.7E 00 | 5.1E-14 | 4.4E 00 |
| YELLOW MARROW | 0.0 | 0.0 | 1.1E-15 | 2.6E 00 | 2.3E-15 | 2.2E 00 | 7.8E-15 | 3.0E 00 | 1.5E-14 | 3.4E 00 | 3.2E-14 | 3.9E 00 |
| PANCREAS | 0.0 | 0.0 | 0.0 | 0.0 | 0.0 | 0.0 | 0.0 | 0.0 | 0.0 | 0.0 | 0.0 | 0.0 |
| SKELETON | 7.6E-18 | 1.8E 01 | 3.5E-15 | 1.4E 00 | 6.4E-15 | 1.3E 00 | 1.8E-14 | 1.7E 00 | 3.4E-14 | 1.9E 00 | 6.2E-14 | 2.2E 00 |
| TOTAL SKIN | 4.9E-15 | 1.5E 00 | 6.0E-15 | 1.2E 00 | 7.8E-15 | 1.5E 00 | 4.4E-14 | 2.1E 00 | 8.2E-14 | 2.4E 00 | 1.4E-13 | 2.8E 00 |
| SPLEEN | 0.0 | 0.0 | 0.0 | 0.0 | 0.0 | 0.0 | 3.6E-15 | 2.9E 01 | 0.0 | 0.0 | 0.0 | 0.0 |
| TESTES | 3.9E-12 | 3.9E-01 | 1.4E-12 | 7.9E-01 | 1.7E-12 | 9.6E-01 | 9.8E-12 | 1.3E 00 | 1.8E-11 | 1.5E 00 | 3.1E-11 | 1.7E 00 |
| UTERUS | 0.0 | 0.0 | 3.8E-15 | 1.1E 01 | 8.3E-15 | 8.9E 00 | 4.3E-14 | 1.2E 01 | 5.4E-14 | 1.6E 01 | 1.3E-13 | 1.9E 01 |
| TOTAL BODY | 4.0E-15 | 1.4E-01 | 5.5E-15 | 3.4E-01 | 8.0E-15 | 4.1E-01 | 3.9E-14 | 4.3E-01 | 7.5E-14 | 4.7E-01 | 1.3E-13 | 5.4E-01 |

# 15. A Human Metabolic Model for $^{14}C$-Labeled Metabolites Useful in Dose Estimation

S. R. Bernard

An average individual (70-kg man) takes in some 350 g of carbon per day, and his total body content of carbon is about 14 kg. Assuming uptake to blood is essentially complete, this corresponds to a mean residence time of 40 days. Metabolic models used in ICRP Publication 10[1] allow for a mean residence time of only 15 days for glycine and less than 1 day for $CO_2$. To be in agreement with the stable carbon data, one or more terms of longer half-lives are needed. Here a retention function $R(t)$ is suggested for glycine,

$$R(t) = 0.4e^{-0.693t/1} + 0.3e^{-0.693t/6} + 0.28e^{-0.693t/35} + 0.02e^{-0.693t/1100},$$

where $t$ is in days and the first three terms are essentially the retention given in ICRP Publication 10. The additional term produces a mean residence time more nearly that of stable dietary carbon. This model is conservative by about a factor of 3. Data of D. L. Buchanan[2] on uptake of $^{14}CO_2$ in mice indicate that the equilibrium level approached $10^{-4}$ times the specific activity in $^{14}CO_2$ in air, suggesting uptake of about 1% to blood with further dilution by dietary stable carbon of about 0.01. G. V. LeRoy et al.[3] have determined the retention of $^{14}CO_2$ in man during the first day, but need for a compartment of long biological half-life is indicated here also. Thus it is suggested that total body retention of $^{14}C$ administered as $NaH^{14}CO_3$ be taken as

$$R(t) = 0.54e^{-0.693t/0.01} + 0.44e^{-0.693t/0.25} + 0.02e^{-0.693t/1400}.$$

The first two terms constitute the model given in ICRP Publication 10, and the final term is chosen to give a mean residence of about 40 days for an uptake to blood of $^{14}C$ similar to that indicated in the experiment of Buchanan. When the above models are used in dose estimation for $CO_2$, it is found that ICRP Publication 2[4] overestimates the dose to the total body by a factor of about 30, while the ICRP Publication 10 model underestimates it by a factor indicated to be at least 16 and which might be as high as about 100. Probably the single exponential is an oversimplification and should be replaced by several exponentials of fairly long half-times, but to determine these, further data on man or on several species of animals would be desirable.

---

1. *Report of Committee IV on Evaluation of Radiation Doses to Body Tissues from Internal Contamination Due to Occupational Exposure,* Pergamon, England, 1968.
2. D. L. Buchanan, "Uptake and Retention of Fixed Carbon in Adult Mice," *J. Gen. Physiol.* **34,** 737–59 (1951).
3. G. V. LeRoy et al., personal communication (1965).
4. Report of ICRP Committee 2 on Permissible Dose for Internal Radiation, *Health Phys.* 3 (1960).

# 16. An Experimental Mockup of the Snyder-Fisher Phantom

S. M. Garry[1] P. S. Stansbury[2] J. W. Poston

A mathematical phantom has been described previously by Snyder et al.[3] for use in Monte Carlo calculations of absorbed dose. The Monte Carlo method utilizing this mathematical phantom has been accepted generally for providing an authoritative source of absorbed dose estimates in man for various radiation fields. An experimental program has been initiated to construct a physical phantom resembling the mathematical phantom employed in these calculations. This phantom has been built and is being used in a study to measure absorbed doses from various radiation fields.

The phantom was fabricated in three principal separable regions: (1) an elliptical cylinder representing the arms, torso, and hips; (2) a truncated elliptical cone representing both the legs and the feet; and (3) an elliptical cylinder representing the head and neck. Each region contains inhomogeneities characteristic of a heterogeneous phantom, that is, tissue, lung, and bone regions. All the regions of the phantom are confined by Lucite shells formed by conventional molding techniques. Certain perturbations were necessary in the design of the phantom to facilitate construction; however, care was taken to maintain original volumes and similar shapes.

Physical parameters were used to match the composition of each region with that given by Snyder et al. These parameters included the mass attenuation coefficients for each type of interaction, electron density, mass density, and percent elemental composition. The matching of these parameters provided construction materials which were "radiation equivalents" to the elemental compositions employed in the calculations. Materials simulating skeleton (density 1.5 g/cm$^3$) and tissue (density 1.0 g/cm$^3$) were in liquid form. The skeleton was simulated by combining 19.5% bone flour, 27% water, 39.5% sugar, 6% ammonium nitrate, and 8% ammonium phosphate. In addition, Sterox DJ,[4] a surfactant (25 drops per 200 g of bone flour), and Tergitol,[5] to reduce surface tension and foaming (2 drops per 200 g), were added to the mixture. The tissue region is 2% sugar, 78% water, and 20% methanol. The lung material is Shonka A-150 tissue-equivalent plastic[6] shavings which gave an effective density of 0.3 g/cm$^3$.

Experiments are planned with the phantom utilizing x-ray, gamma, and neutron radiation fields. Measurements of absorbed dose in phantom organs due to gamma sources uniformly distributed in organs are presently under way. Absorbed dose due to diagnostic x rays will be determined by an in-phantom spectrometry method. Measurements will be performed for organs both inside and outside the primary beam. Measurements of fast neutron depth dose and LET spectra due to 14-MeV neutron radiation on the phantom are planned. Experimental results from these three studies will be correlated with existing Monte Carlo estimates employing the mathematical phantom. A photograph of the phantom is shown in Fig. 16.1.

---

1. Health Physics Special Fellow, Oak Ridge Associated Universities.
2. Graduate Laboratory Participant, Oak Ridge Associated Universities.
3. W. S. Snyder et al., *Health Phys. Div. Annu. Progr. Rep. July 31, 1967,* ORNL-4168, pp. 245–57.
4. Monsanto Chemical Co., 710 N. 12th St., St. Louis, Mo.
5. Union Carbide Corporation, 17 Executive Park Dr., N.E., Atlanta, Ga.
6. J. J. Spokas, Illinois Benedictine College, Lisle, Ill.

PHOTO 1375 – 73

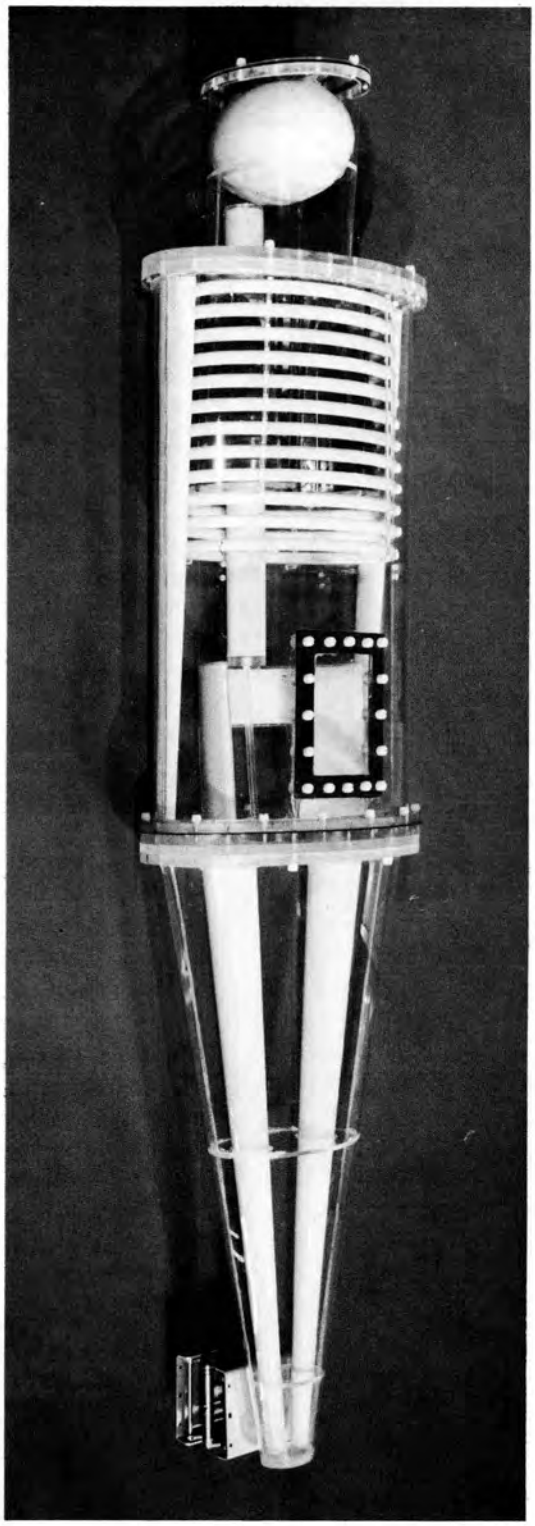

Fig. 16.1. The Snyder-Fisher phantom.

# 17. Medical X-Ray Dose Estimation Program

J. W. Poston G. G. Warner[1]

It is well established that x rays, particularly medical and dental x rays, contribute the largest exposure to the population of any man-made source of ionizing radiation. The fundamental objective of the medical use of radiation is to obtain optimum diagnostic information with minimum exposure to the patient, the radiological personnel concerned, and the general public. However, the problems posed when one attempts to estimate the doses received by various organs of the body from a medical exposure are among the most difficult problems the radiological physicist must face. The geometrical complexities and inhomogeneities of the body and the various organs make experimental simulation of the human body extremely difficult and usually unsatisfactory. A study was undertaken to determine the feasibility of calculating absorbed doses to internal organs from external sources of x-ray beams. The study was initiated as a result of an interagency agreement between the U.S. Atomic Energy Commission and the Food and Drug Administration.

The purpose of the present study is to obtain a complete set of basic dosimetry data for selected monoenergetic photon beams incident on a spatial grid from which one could construct certain organ doses from typical diagnostic x-ray exposures of specified average energy or energy spectrum and varying field size and location. Only the output for absorbed dose to the organs was obtained, and the organs of primary interest were the testes, ovaries, thyroid, red bone marrow, and the lens of the eye. These calculations made use of Monte Carlo techniques which trace energy deposition histories of photons incident on the phantom. Energy depositions were recorded in a mathematical representation of an anthropomorphic phantom containing 23 internal organs, skin, and a skeleton containing both red and yellow bone marrow (see Fig. 17.1). Details of the phantom and the techniques employed in this study have been reported previously.[2–7] Briefly, the phantom is comprised of essentially three regions: (1) a skeletal region, including bone, bone marrow, and other organic constituents; (2) a lung region; and (3) the remainder of the phantom. These regions are composed primarily of hydrogen, carbon, nitrogen, and oxygen. In the skeleton, additional elements amounted to about 18% of the total mass, with calcium and phosphorus accounting for most of this amount. In the lungs the composition is somewhat different from that of other soft tissues in the remainder of the phantom. The densities of the skeletal region (bone plus marrow), lungs, and the remainder of the phantom are approximately 1.5, 0.3, and 1.0 g/cm$^3$ respectively. In the calculation of absorbed dose in the bone marrow it is assumed that the bone and the bone marrow are mixed homogeneously in the skeleton of the phantom and that the red bone marrow absorbs energy as efficiently per gram as do the other constituents of bone. Photon energies chosen for this initial study were 30, 55, and 80 keV.

Three modifications were made in the existing phantom code to adapt it to the present study. First, the geometrical description of the phantom includes a simulation of the lenses of the eye. The normal lens is about 0.7 cm in diameter, 0.3 cm thick, and is located

1. Mathematics Division.

2. W. S. Snyder, M. R. Ford, G. G. Warner, and H. L. Fisher, Jr., "Estimates of Absorbed Fractions for Monoenergetic Photon Sources Uniformly Distributed in Various Organs of a Heterogeneous Phantom," *J. Nucl. Med., Suppl. No. 3,* **10** (August 1969).

3. T. D. Jones, J. A. Auxier, W. S. Snyder, and G. G. Warner, "Dose to Standard Reference Man from External Sources of Monoenergetic Photons," submitted to *Health Phys.*

4. G. G. Warner and A. M. Craig, Jr., *ALGAM, a Computer Program for Estimating Internal Dose from Gamma-Ray Sources in a Man Phantom,* ORNL-TM-2250 (June 10, 1968).

5. W. S. Snyder et al., *Health Phys. Div. Annu. Progr. Rep. July 31, 1970,* ORNL-4584, pp. 200–203.

6. J. W. Poston and G. G. Warner, *Medical X-Ray Dose Estimation Program,* ORNL-TM-3986 (October 1972).

7. J. W. Poston and G. G. Warner, *Medical X-Ray Dose Estimation Program,* ORNL-TM-4217 (April 1973).

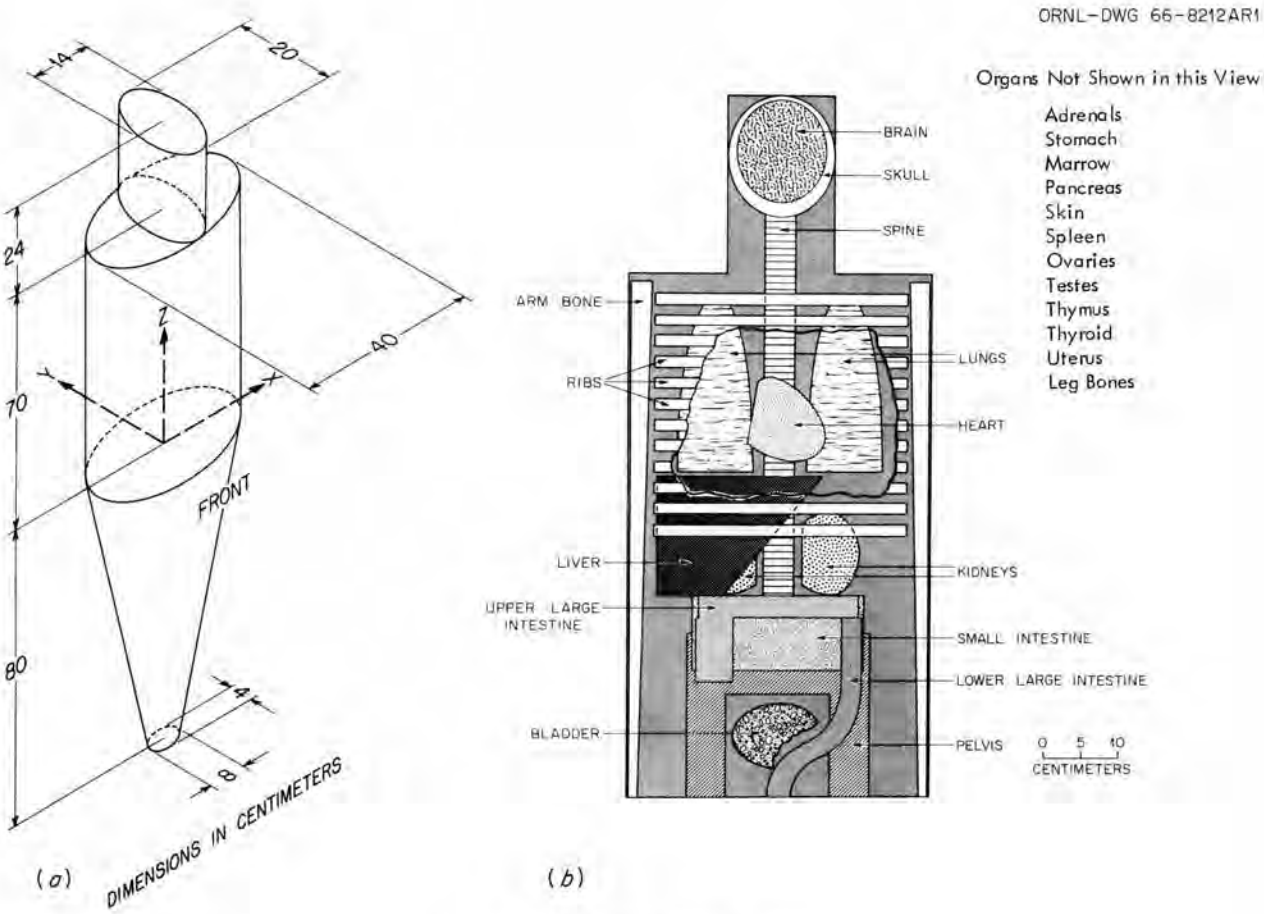


**Fig. 17.1. The adult human phantom.**

about 0.2 cm behind the cornea. Two distinct regions were added and subdivided into several smaller regions. Figure 17.2 gives a top view of these regions, while Fig. 17.3 shows a schematic drawing of these regions on the head of the phantom. One major region is located in the skin layer on the front surface of the head of the phantom and has the same thickness as the skin, 0.2 cm. This region is the projection of a 12-cm-wide, 4-cm-high rectangular area located on the *X-Z* plane. It is subdivided into projections of two 4 × 6 cm areas and further into projections of two 2 × 2 cm areas centered inside the 4 × 6 cm areas. The second major region is also 0.2 cm thick and located just inside the skull, which is 0.8 cm thick. It also contains the projection of the same large 4 × 12 cm area similarly subdivided into 4 × 6 cm areas. Therefore, various estimates of the average absorbed dose to the lenses of the eye can be obtained. The actual location of the lens of the eye is in an anatomically complex position that would fall between the two regions. These regions were selected to simulate energy deposition in the lens with respect to depth in the head, thickness of the lens, and the scattering and shielding effect of the skull.

Second, a typical diagnostic table was simulated in the phantom geometry to provide a backscattering medium similar to that encountered in actual diagnostic procedures. The table, which has dimensions of 184 × 70 × 1 cm, may be positioned either at the front or the rear of the phantom. To simplify the calculations, the composition of the table was initially the same as the tissue composition used in the code. The effect of the table on dose to some organs near the table was an increase. For example, the dose to the spine was increased by approximately 6%. For the organs of interest in this study, such an effect would be observed for the red bone marrow, testes, and lenses of the eye, depending on the location of the table.

The third modification was made in the existing composition of the thyroid gland by inclusion of 10 mg of iodine, to more accurately simulate its effective

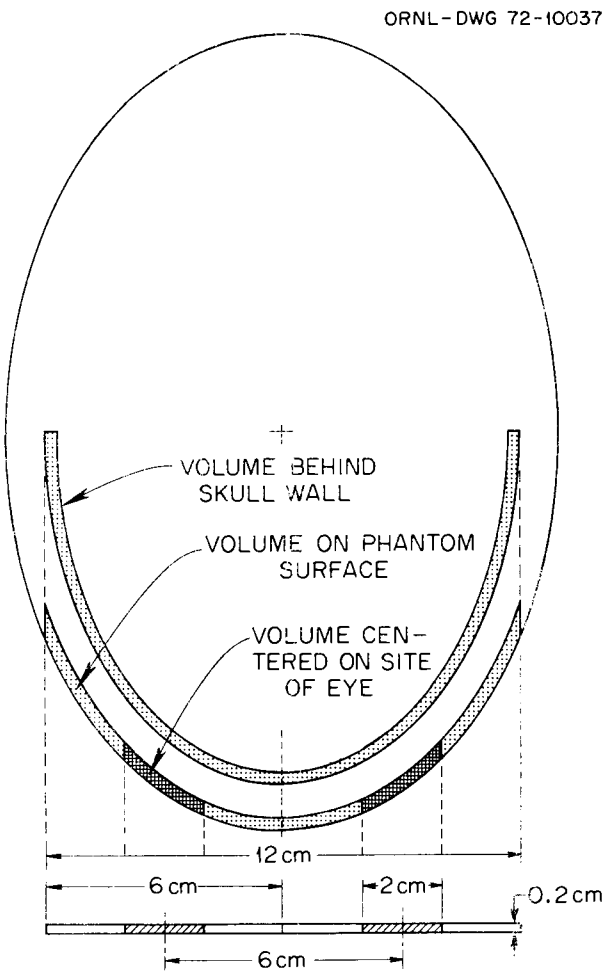


Fig. 17.2. Top view of lens of the eye regions.

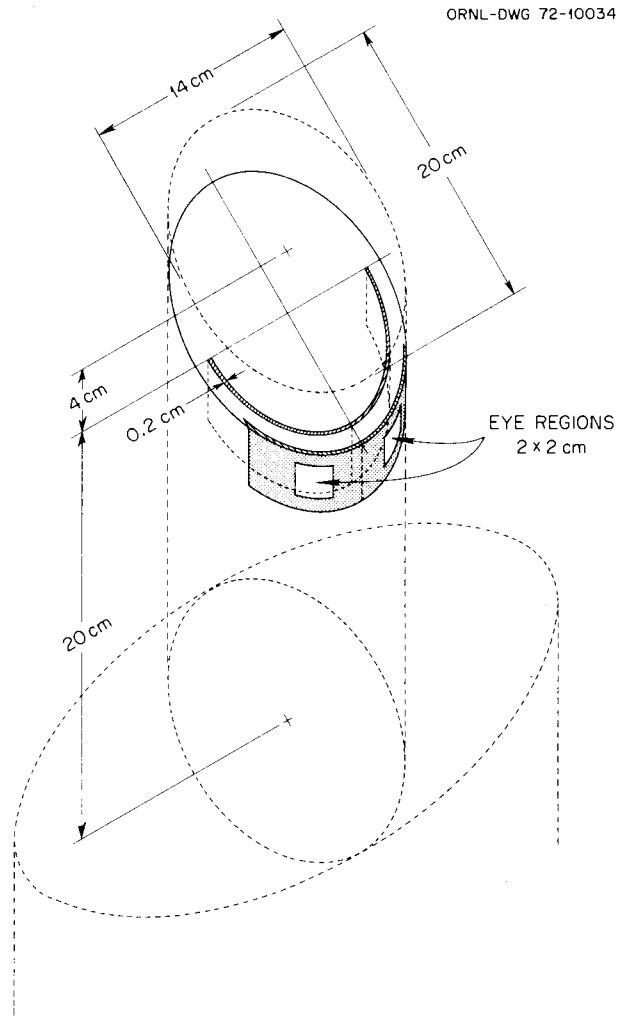


Fig. 17.3. Location of lens of the eye regions of the adult phantom.

atomic number and thus account for the increased energy absorption resulting from the high mass energy absorption coefficient of iodine for the energies under study, particularly at its $K$ absorption edge of 33.2 keV. The effective atomic number of the "iodated" thyroid is about 4% higher than the previously used tissue composition and agrees closely with the effective atomic number calculated from data on elemental composition of the thyroid from normal adult humans.[8] For example, the effect of replacing the tissue-equivalent thyroid with an "iodated" thyroid is an increase in the calculated absorbed dose of 12.5% for a 4 X 4 cm beam of 55-keV photons centered on the thyroid gland.

Since the organs of primary interest have symmetry about the vertical center line of the phantom (i.e., the $Z$ axis), the calculation schedule made use of left-right symmetry to reduce the number of computer runs. The radiation was collimated in a 4 X 4 cm beam and allowed to impinge at various anterior locations on the right side of the adult phantom. The centers of the first column of 4 X 4 cm locations are on the vertical center line of the phantom. The remaining 4 X 4 cm beams on the phantom cover the right side of the phantom with the exception of the lower 40 cm (legs). In all cases the beam impinged normal to the $X$-$Z$ plane (i.e., a parallel beam of photons traveling in the direction of positive $Y$).

8. I. H. Tipton, University of Tennessee, private communication.

Approximately 400 calculations have been completed for 4 X 4 cm beams incident on the anterior of the phantom (A-P incidence). Total number of grid locations (calculations) for each photon energy was: 30 keV, 95; 55 keV, 120; and 80 keV, 104. Each calculation was performed for 30,000 photon histories. Figure 17.4 gives a schematic representation of a typical calculation. Sample results for absorbed dose per unit surface radiation exposure (rads per roentgen) and their coefficients of variation for 30-keV photons are shown in Figs. 17.5 and 17.6 for both ovaries. Results for the 55-keV case are given in Figs. 17.7 and 17.8. The data in Figs. 17.5 and 17.7 have been rounded off to one significant digit and are limited to the regions contributing $10^{-2}$ to $10^{-4}$ rad/R. The data in Figs. 17.6 and 17.8 give the coefficients of variation for all beam locations considered. Coefficients of variation for the ovaries as well as the other smaller organs (testes, lens

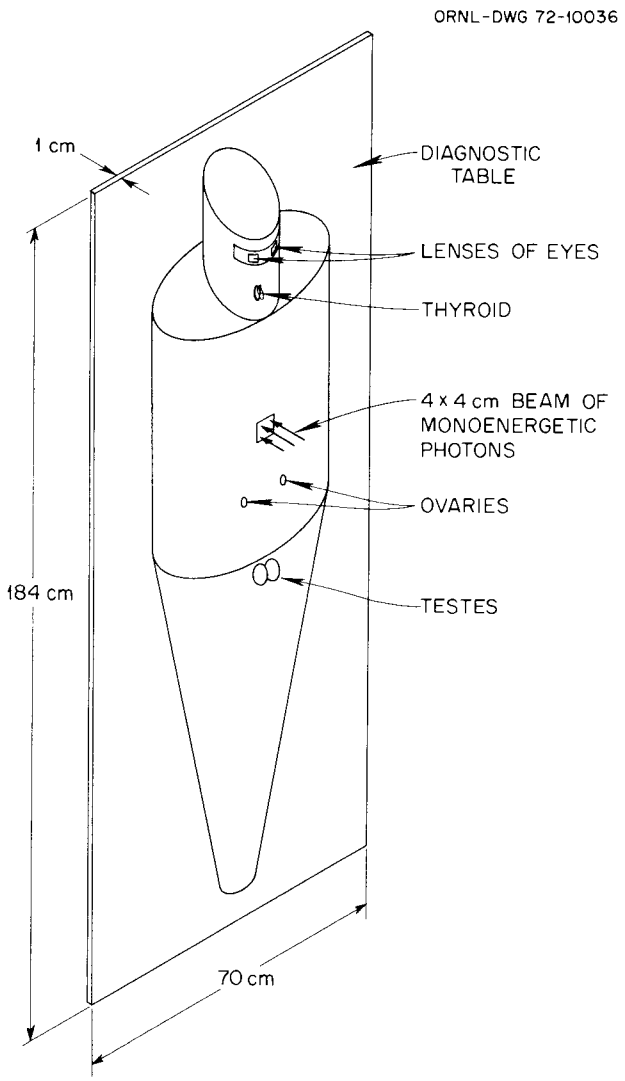


Fig. 17.4. General arrangement for typical monoenergetic photon calculation.

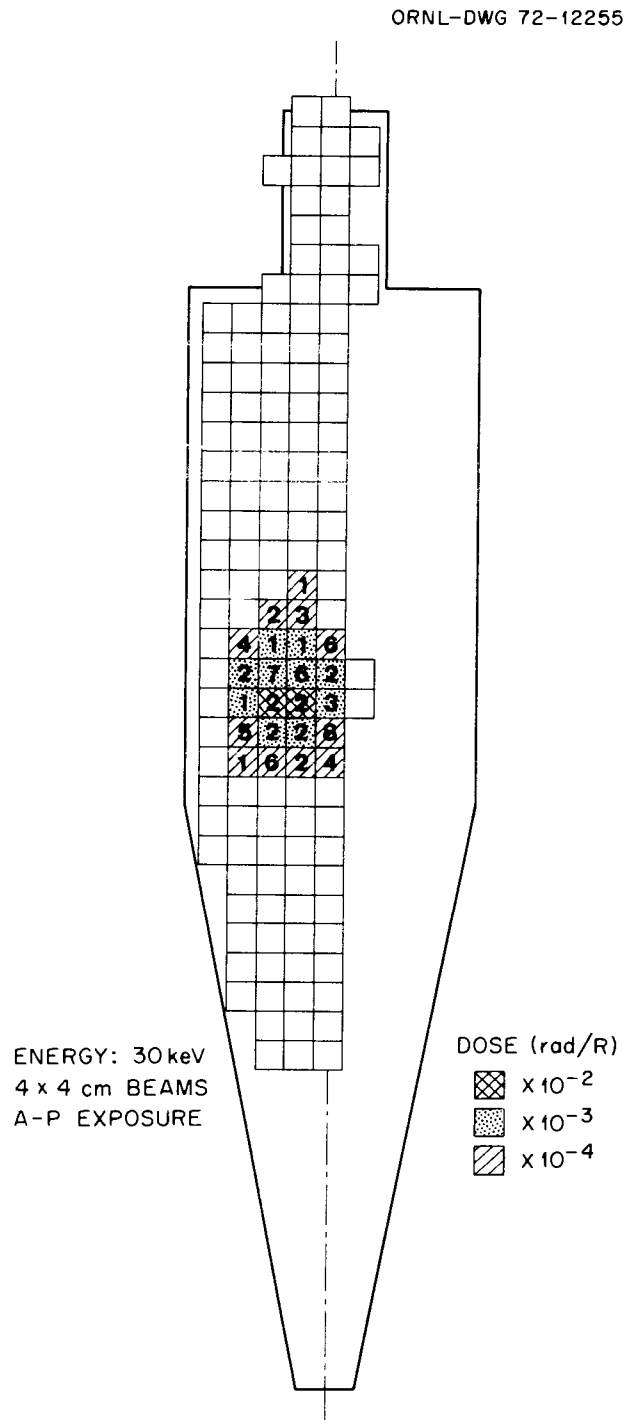


Fig. 17.5. Absorbed dose per unit exposure to the ovaries for 30-keV photon beams incident at various grid locations.

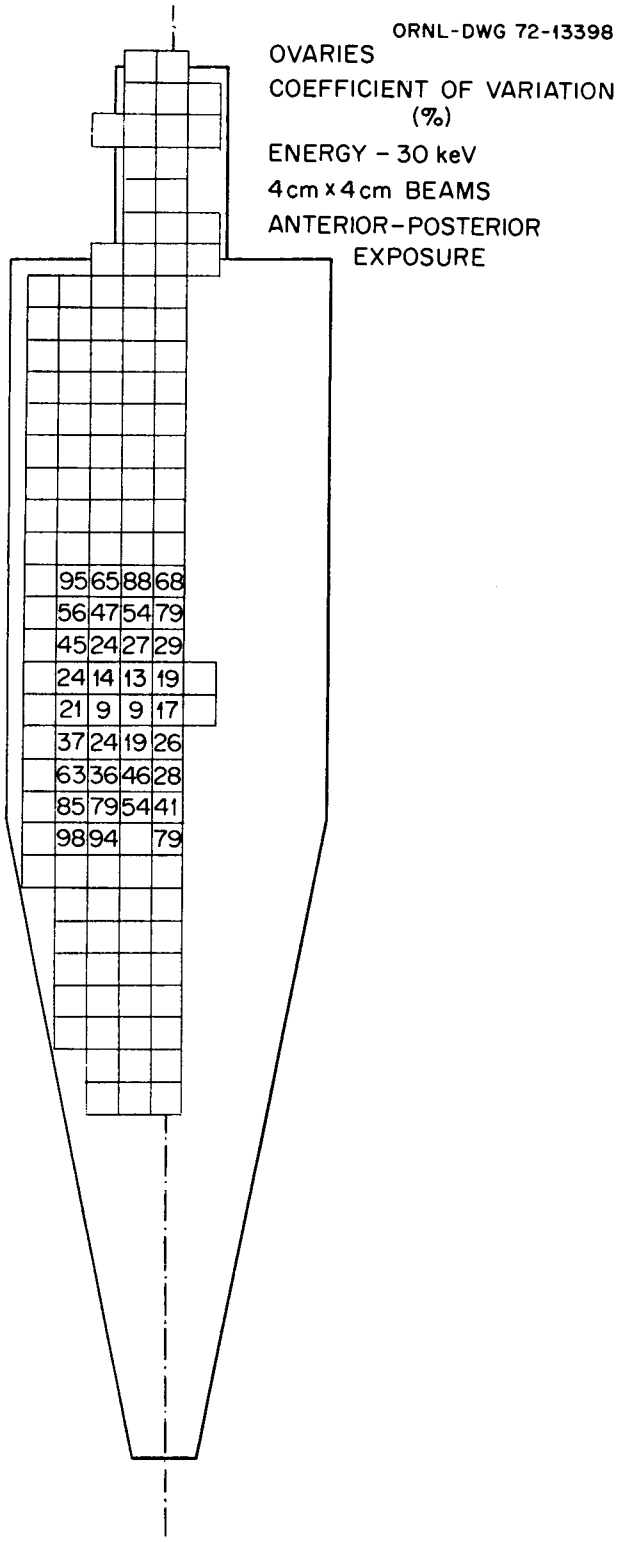


Fig. 17.6. The coefficients of variation (in percent) for the calculations shown in Fig. 17.5.

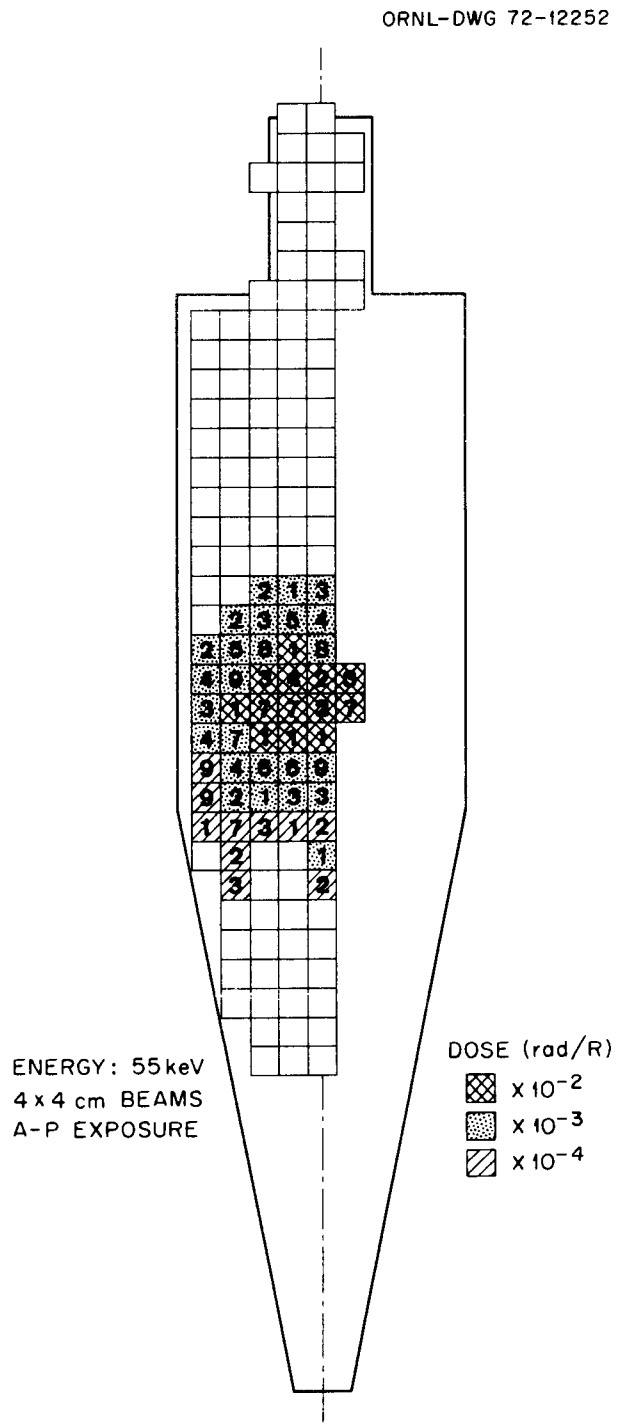


Fig. 17.7. Absorbed dose per unit exposure to the ovaries for 55-keV photon beams incident at various grid locations.

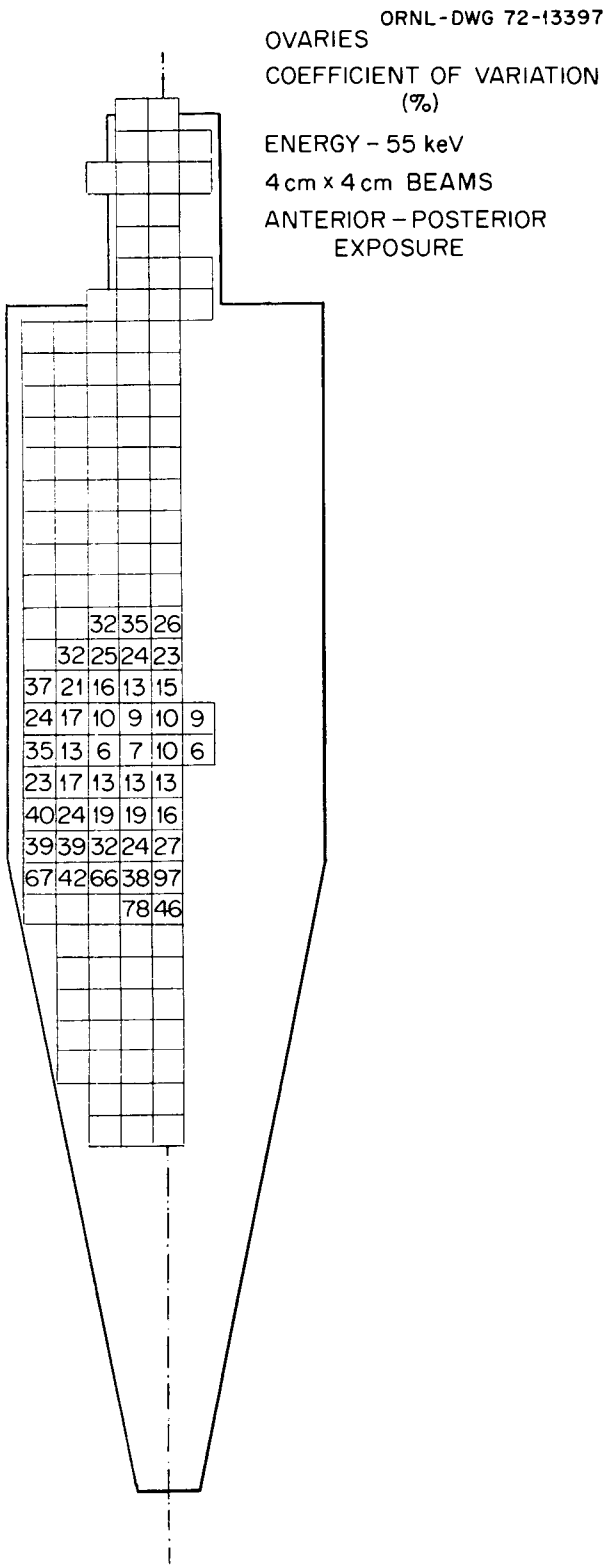


**Fig. 17.8. The coefficients of variation (in percent) for the calculations shown in Fig. 17.7.**

of the eye, and thyroid) rapidly exceed 25% as the beam is moved only a few beam locations away from the organ site due to the greatly reduced number of scattered photons interacting in the small volumes of the organs. Coefficients of variation for the red bone marrow are between 1 and 3% for all sites because of the greater mass of the tissue.

The effect of increasing the incident photon energy is apparent by comparing the absorbed dose per unit exposure for the 30- and 55-keV calculations. For example, compare Figs. 17.5 and 17.7. There are only two beam locations where the dose to the ovaries is greater than $10^{-2}$ rad/R for a photon energy of 30 keV. The right ovary is located at the intersection of these two 4 × 4 cm beams. In the 55-keV calculation there are 11 grid locations which contribute more than $10^{-2}$ rad/R to the ovaries. Only two of these locations can be considered to be irradiating the ovary directly. A similar comparison can be made for a dose of $10^{-3}$ rad/R, that is, nine beam locations at 30 keV and 25 beam locations at 55 keV. Therefore, for a photon energy of 30 keV, there are 11 beam locations where the dose to the ovaries is $10^{-3}$ rad/R or greater, while for 55 keV the total number of beam locations which fit this category is 36.

Additional calculations are planned for these same monoenergetic photon sources for posterior-anterior (P-A) incidence of the beam. Before such calculations are initiated the phantom geometry will be modified to provide a calculational geometry which is more realistic. The modifications include the relocation of the testes region, the separation of the legs of the phantom, and the rounding of the head of the phantom.

# Part IV. Urban Research

R. C. Taeuber

## 18. Background

The Urban Research Section began at the Oak Ridge National Laboratory in 1969 with a ten-week summer workshop during which an interdisciplinary group of 15 social scientists and 9 physical scientists and engineers explored the usefulness of the Laboratory's research and computer facilities for studies of population distribution. The workshop's findings appeared as "An Introduction to Urban Decentralization Research" (ORNL-HUD-3). Subsequently, a continuing project was funded at ORNL to study national urban growth patterns and to acquire the data base needed for such studies.

Results of a ten-week study could not be definitive, yet questions posed during that workshop still provide the basis for much of the Section's continuing research:

1. What are the trends in the distribution of population between and within regions: by size and type of place; by type of family, race, poverty, educational level, and other individual characteristics?
2. How is distribution of population related to distribution of employment? What are the trends in location of employment?
3. What is the impact of migration, the main component of internal population redistribution, upon the nation? Who migrates and why? How can one better estimate the volume and characteristics of migration streams?
4. How can alternative population distributions be evaluated? Which indices – health, infant mortality, income, success in school – best measure satisfactory living conditions or best indicate problem areas?
5. How can the effect of past programs upon population distribution and welfare be measured? Can national data and careful analysis identify differential impacts?
6. Can population growth be redirected? What are the available alternate policies, how effective would they be, and what would be their costs and benefits?

The summer project produced partial answers in all of these areas, and most have been pursued in subsequent work. Studies have dealt not only with numbers of people and their distribution, but also with the social and economic characteristics of these people. These studies have included measures of the changing concentration of people within states, of the population density of urbanized areas and central cities, and of demographic and social differentials between regions and within metropolitan areas.

A valuable by-product was the eight-volume series of "Demographic Profiles of the United States" which presented summary indicators from census data for each county in the U.S., indicators intended to give a quick general impression of the demographic structure of an area. Designed to be easy to interpret and relatively unambiguous, the indices cover: racial composition, place of residence, age and sex composition of the population, marital status, household structure, and housing.

While such studies of trends and characteristics have continued, the project's research has additionally focused on migration and, increasingly, on the impact of programs affecting population distribution. In the program impact area, various reports have been issued on the impact of the Interstate Highway Network on population redistribution and city growth. Reports also have been issued on studies on the characteristics of migrants and of data sources for estimates of migration flows. Appropriate highlights of these and other studies are given in the next chapter.

# 19. Program in Urban Research

R. C. Taeuber

B. L. Bishop
R. A. Bohm[1]
R. E. Kemper
E. S. Lee[1]
M. L. Levin[1]
K. P. Nelson
C. H. Patrick
W. W. Pendleton[1]
P. D. Postma[1]
P. N. Ritchey[1]
R. B. Sturgis[1]
M. M. Williams

## MIGRATION AND FERTILITY: A STUDY OF THE SOCIAL FACTORS INVOLVED[2]

The research reported in this monograph had two major thrusts: (1) to explore various aspects of the impact of migration on differentials in fertility and (2) among migrants, to examine relationships between fertility and characteristics associated with their residence histories. Study subjects were women 20 to 44 years old included in the 1967 Survey of Economic Opportunity.

Migration between rural and urban areas (regardless of direction) was related to those marital statuses with presumably greatest exposure to the risk of pregnancy. Thus, migrants disproportionately contribute to the overall level of fertility in the receiving area. The rural-urban differential in fertility is attenuated by the interchange of migration. Contrary to the implications of previous studies, the urban white-black differential in fertility cannot be attributed to urban black in-migrants with Southern rural background. The fertility of indigenous urban blacks exceeded that of whites by 25%.

The findings were used to appraise a conceptualization of migration producing a conflict between norms acquired in the area of origin and those in the area of destination. In general, the relationships expected on the basis of this model are consistent with data for white urban-to-rural and black rural-to-urban migrants, but not for white rural-to-urban migrants. The extent to which the model fits the facts, hopefully, will provide some impetus for future research and lead to a more adequate and broader explanatory system of the assimilation dimensions of migration and fertility.

## CHANGES IN POPULATION AND EMPLOYMENT AS PROCESSES IN REGIONAL DEVELOPMENT[3]

This study constructs a paradigm based on national trends showing the relationship of population and employment in the development of a region. Data for the Old Manufacturing Belt and the South are examined to determine if the processes evident at the national level are apparent in two subnational regions differing in their levels of economic development.

The results of the analysis of the data for the two regions are consistent with the interrelationships of employment and population changes and economic diversification depicted in the paradigm. The paradigm appears to be useful as a model for indicating the broad patterns of change which can be expected to occur as a region develops.

## CORRELATES OF CHILDLESSNESS AND EXPECTATION TO REMAIN CHILDLESS: U.S. 1967[4]

It is widely agreed that society has strong mores proscriptive of couples remaining childless. Nonetheless,

1. Consultant.
2. P. N. Ritchey, *Migration and Fertility: A Study of the Social Factors Involved*, ORNL-UR-101 (April 1973).
3. C. H. Patrick and P. N. Ritchey, Jr., *Changes in Population and Employment as Processes in Regional Development*, ORNL-UR-102 (April 1973).
4. P. N. Ritchey and C. Shannon Stokes, *Correlates of Childlessness and Expectation to Remain Childless: US 1967*, ORNL-UR-103 (April 1973).

childlessness varies regularly by a number of socio-demographic factors. Given the presumed universal acceptance of the norm concerning desirability of children, why does childlessness vary so widely among social aggregates?

First, it may simply be the case that this norm is not as universal as previously thought. Alternatively, if the norm is as universal as represented, various social structural influences may operate to selectively counter the prevailing norms and produce deviance.

Data from the 1967 Survey of Economic Opportunity for wives still in the childbearing years are used to explore these alternatives. Expectation data, interpreted as indicating the normative position of couples on remaining childless, are contrasted with current rates of childlessness for a number of factors. Comparisons are suggestive of the second alternative and directive of future research to include structural considerations.

## MEASURING PATTERNS OF URBAN GROWTH[5]

*Measuring Patterns of Urban Growth* is an overview of basic information about rural depopulation, urban migration, birth rates, city systems and size, metropolitan areas, population density, blacks, suburbs, and growth in transportation corridors. The focus is on new information from the 1970 Census and on analyses done by ORNL's Urban Research Section. The paper cites the need for studies of metropolitan dynamics as well as of areas as small as the neighborhood for use by governmental decision-makers.

## THE DECENTRALIZATION OF MANUFACTURING EMPLOYMENT[6]

This study indicates the magnitude of the decentralization of manufacturing employment which has occurred both regionally and by degree of urbanization since World War II. Since 1947, there has been a movement toward more equal geographic distribution of employment. Examining data for 1947–1963 and 1964–1969 reveals that in the latter period, manufacturing employment grew three times faster than in the former period. In both periods, growth of employment in the most urbanized areas was slower than in suburban areas, indicating a relative shift from the center to the periphery of metropolitan areas.

The decentralization of manufacturing (representing a movement toward equality in the proportion of employment located in the various regions of the U.S.) continued from 1964 to 1969 – the same general trend which was observed for 1947–1963. It is noteworthy that while growth rates were almost universally higher in all regions in the later period, the relative shift in proportions was lower, indicating to some extent a higher degree of stability in the later period.

## THE PROSPECTS FOR NEW CITIES: THE HISTORICAL VIEW[7]

If the development of new cities is not to be fraught with overwhelming problems, there should be instances of cities that have burst upon the scene lately and have rapidly grown to impressive but not alarming size. To assess such developments, a file of all incorporated places that had 10,000 or more inhabitants in 1970 was created, and each city was traced as far back as 1900, at which time settlement of the United States was virtually complete. We questioned whether our cities are predominantly old or new, whether they cluster around metropolises, and how growth is related to location and age. This survey of city formation and growth leads us to the conclusion that new places are increasingly located within the shadow of the metropolis, and as they grow they will coalesce into the mass megalopolitan. By and large our cities are old, they cluster together, and their very existence militates against the formation of any but satellites. To move against a trend of this magnitude, to establish new cities, that is, independent entities set away from already existing large cities, will require major efforts and vastly different attitudes from those which have prevailed in the past.

## AN URBAN CLASSIFICATION SCHEME: THE DEVELOPMENT OF A SIMPLE URBAN MODEL[8]

Small areas within a city can be compared along many social dimensions. Such dimensions may pertain to an area's economic and educational level, family and age structure, housing quality, crime rate, and so on – the list could be very extensive. There is, therefore, a very practical need to arrive at a few simple dimensions that

5. C. M. Taeuber, *Measuring Patterns of Urban Growth,* ORNL-UR-104 (April 1973).

6. C. H. Patrick, *The Decentralization of Manufacturing Employment,* ORNL-UR-105 (April 1973).

7. E. S. Lee and P. Neal Ritchey, *The Prospects for New Cities: The Historical View,* ORNL-UR-107, in press.

8. M. M. Williams, *An Urban Classification Scheme,* ORNL-UR-108 (April 1973).

somehow embrace many of the ways (or dimensions along which) areas within a city differ. Factor analysis and quartimax rotation were used to reduce 66 census, police, welfare, and educational achievement variables for each tract in the St. Louis Central City to three orthogonal factors. These factors were named impoverishment, nonfamily structure, and poor housing and explained 29, 44, and 59% of the total cumulated variance. Census tract factor scores are mapped and the resulting social implications discussed.

## SELECTED FACTORS INFLUENCING CITY GROWTH 1960–1970[9]

This paper examines the relationship between growth of cities over the past decade and five factors associated with growth: (1) city size in 1960, (2) metropolitan status, (3) distance from metropolitan areas, (4) interstate highway accessibility, and (5) presence or absence of annexation. It is the contention of the author that these variables can be seen as competitive advantages or disadvantages in attracting residents and that they are "underlying" conditions that provide the basis for industrial, occupational, economic, and educational developments – developments that do attract or repel residents. Some of the data included are: average growth rate of places 10,000 and over for the nation, regions, divisions, and states; growth by size in 1960 for all places 10,000 and over in 1960 for the U.S.; growth comparison of places inside and outside of Standard Metropolitan Statistical Areas (SMSA) by size in 1960; interstate highway accessibility of places 10,000 and over; annexation and SMSA status by growth of all places 10,000 and over in 1960.

A policy postscript is also included which briefly discusses policy as a concept and its relationship to the research.

## POVERTY AND MIGRATION FROM RURAL TO METROPOLITAN AREAS[10]

There is the widespread view that rural-to-urban migrants are saturating the ghetto areas of large cities and disproportionately contributing to poverty in urban areas. In this paper, data from the 1967 Survey of Economic Opportunity are analyzed to explore both dimensions of the presumed relationship of rural-urban migration and the plight of cities: (1) the location of rural migrants in urban areas and (2) the extent of their contribution to urban poverty. This paper compares the location and poverty of rural-urban migrants with that of indigenous urbanites in nonmetropolitan and metropolitan areas by size – including the metropolitan ring and poor and nonpoor areas of central cities. White-black differences are emphasized, and the relationship of poverty and previous or prolonged urban experience among migrants is also examined. The findings indicate that urban poverty and the problems of the central cities are the consequences of broader structural features of our society – the handicaps of age, of being a female head of household, or of the status ascribed to blacks – and not the product of rural-urban migration.

## LABOR MOBILITY AND URBAN GROWTH IN THE ATLANTA METROPOLITAN AREA[11]

A 1% sample of those in employment covered by Social Security was used to study the processes and patterns of urban change in the Atlanta Standard Metropolitan Statistical Area (SMSA) from 1962 to 1967. Migration, labor mobility, and economic growth, which are commonly thought to be basic to urban growth, were examined since the longitudinal nature of the data offers unique opportunities for studying migration streams and tracing, albeit imprecisely, changes in the spatial distribution of metropolitan employment.

The period was one of growth for the metropolitan area, and its workers benefited thereby. Labor force growth of 35% in the five-year period resulted from a sizable influx of new entrants and from net in-migration due largely to heavy in-migration from the rest of the Southern region. Three-fifths of the migration to and from Atlanta was intermetropolitan in nature. Blacks and females increased their share of the metropolitan labor force, as did workers less than 30 years old. The number of males earning less than $3000 declined, and positive returns from industrial mobility – implying a high degree of voluntary mobility – were found for both black and white males.

Suburbanization, however, accompanied growth. The location of employment shifted during the period: the central county's share of SMSA employment fell from 78 to 74%, with losses in the areas of manufacturing and both wholesale and retail trade. The share of employment accounted for by the central county fell for all sex and race groups, for workers of all ages, and

9. R. B. Sturgis, *Selected Factors Influencing City Growth 1960–1970,* ORNL-UR-109 (April 1973).

10. P. N. Ritchey, *Poverty and Migration from Rural to Metropolitan Areas,* ORNL-UR-110, in press.

11. K. P. Nelson, *Labor Mobility and Urban Growth in the Atlanta Metropolitan Area,* ORNL-UR-111, in press.

at all income levels. Declines in employment share were most striking for white females, workers with incomes above $9000, and the young and the old. The shift was primarily due both to SMSA stayers, who shifted jobs outward, and to new entrants, who found jobs disproportionately in suburban counties. Long-distance migration, on the other hand, favored the central county.

## EFFECTS OF CROWDING AND HIGH POPULATION DENSITY: AN ANNOTATED BIBLIOGRAPHY WITH PERMUTED TITLE AND SIMPLE AUTHOR, TITLE, KEY WORD, AND TAXONOMIC INDICES[12]

This bibliography contains 411 abstracted, keyworded references to publications that describe some demonstrable effect (rather than theoretical speculation) of crowding and/or population density. Publications are grouped into nine sections, depending on the major effects described: general effects; effects described in terms of future planning; animal behavior; physiology; population dynamics-mortality-fertility; human behavior; psychiatric disease; physical disease; and education.

All major English language and most other language publications since 1958 are hopefully included. Author, title, key-word-in-context, and taxonomic indices are given. The bibliography is part of the computerized ORNL Environmental Information System and may be searched by interested persons outside ORNL.

## A STATISTICAL PROCESSING SYSTEM FOR THE PUBLIC USE SAMPLES[13]

The Statistical Package for the Social Sciences (SPSS) is one of the most versatile and widely used of the statistical programming packages. To increase its usefulness, the SPSS override system (SOS) described here enables ready access to a generalized statistical processor for research with the U.S. Bureau of the Census's Public Use Samples. Through a series of modifications to the SPSS, provision is made to allow the user to read values from the Public Use Samples (PUS) directly into SPSS and consequently to gain access to its powerful and easy-to-use statistical capability. A data compression/decompression feature serving to reduce the physical size of the PUS is also provided. Users, at their option, can choose to employ this feature for any given application. The override system maintains the integrity of the PUS documentation.

Finally, with the exception of the compression/decompression feature, the system is not restricted to applications with the PUS. SOS allows the user to design ad hoc reading routines for any nonstandard file structure if the structure can be handled in a FORTRAN IV environment.

---

12. M. M. Williams, *Effects of Crowding and High Population Density: An Annotated Bibliography with Permuted Title and Simple Author, Title, Key Word, and Taxonomic Indices,* ORNL-UR-112 (June 1973).

13. M. L. Levin and Ruth E. Mellen, *A Statistical Processing System for the Public Use Samples,* ORNL-UR-113, in press.

# Part V. Civil Defense Research

## C. V. Chester

## 20. Strategic Defense

C. V. Chester C. M. Haaland
G. A. Cristy M. T. Heath[1]
J. S. Gailar C. H. Kearny
R. W. Manweiler

### SOVIET CIVIL DEFENSE STUDIES

The purpose of this research is to keep abreast of the Soviet civil defense effort in order that our own civil defense research can proceed in full cognizance of Soviet activities. Not only does the present Soviet civil defense program reflect their theories on the nature of possible future threats to them, but also reveals, by implication, the kinds of threats that they themselves could present in the event of an escalating crisis.

Awareness of the current Soviet civil defense effort has been gained primarily through three sources: (1) the *Translations on USSR Military Affairs*[2] and (2) the Foreign Broadcast Information Service's *Daily Report*[3] of broadcasts from the Soviet Union, both published in English, and (3) significant Soviet civil defense publications, which we have had translated and subsequently edited ourselves into grammatical, idiomatic English.

Our published translation of the 1969 Soviet manual *Civil Defense,*[4] which includes our own 16-page Preface presenting the highlights of each chapter, has resulted in or contributed to the following developments:

1. the entering of our Preface into the Congressional Record of June 16, 1971, by the Hon. Chet Holifield;
2. a new look at U.S. civil defense by influential government officials in the light of Soviet preparations to evacuate their cities within a few days;
3. the Richmond Study, initiated by the Defense Civil Preparedness Agency (DCPA), to devise a prototype evacuation plan;
4. Secretary of Defense Elliot Richardson's charge to DCPA in his FY 1974 message to "provide guidance to State and local governments in preparing plans for contingency evacuation or dispersal in case of natural disaster emergencies, as well as enemy attack";
5. briefings, which we gave by their request, to the Army General Staff and Joint Chiefs on Soviet civil defense preparations, based on information from our own edited translations and field experiments.

Moreover, our own experimental studies in expedient shelter construction have demonstrated the practicality of common Soviet designs discovered in the Soviet civil defense literature.

The usefulness of the 1969 Soviet handbook has led our project to undertake the translation of two other Soviet civil defense manuals: *Civil Defense* (1970),[5] which is in the process of being edited, and *Use of Shelters in Civil Defense,*[6] the editing of which will soon follow.

1. Mathematics Division.
2. *Translations on USSR Military Affairs,* Joint Publications Research Service, 1000 North Glebe Road, Arlington, Va.
3. *Daily Report: Soviet Union,* Foreign Broadcast Information Service, National Technical Information Service, U.S. Dept. of Commerce, Springfield, Va.
4. N. I. Akimov, ed., *Civil Defense* (*Grazhdanskaya Oborona*) (Moscow, 1969), translated from the Russian by S. J. Rimshaw and edited by J. S. Gailar and C. H. Kearny (ORNL-tr-2306), April 1971.
5. N. I. Alabin, P. T. Egorov, and I. A. Shlyakov, *Civil Defense* (*Grazhdanskaya Oborona*), Publishing House for Higher Education (Moscow, 1970).
6. Yu. Yu. Kammerer and A. Ye. Kharkevich, *The Operation of Civil Defense Shelters,* 2d ed., revised and supplemented, Construction Literature Press (Moscow, 1970).

Information on the current Soviet civil defense program is being supplied to those interested through *Survive, The American Journal of Civil Defense.*[7] Highlights of the current Soviet civil defense program, presented in this journal in a recent article, "What's New in Soviet Civil Defense?" include:

1. the upgrading of the position of Soviet Civil Defense Chief to Deputy Minister of Defense;
2. the inauguration of civil defense training in the second grade in schools throughout the Soviet Union;
3. greatly increased emphasis on decreasing the vulnerability of vital industries and their workers throughout the country so that they may continue to function in wartime;
4. ambitious and detailed civil defense exercises, including, for example, the evacuation of an entire fishing village, as well as the personnel of a number of industrial enterprises – all by a refrigeration fleet – from the port of Sevastopol and an exercise in shelter building for the collective and state farm directors throughout the Turkmen Republic.

The keystone of the Soviet civil defense program continues to be comprehensive evacuation and dispersal plans during periods of escalating crisis. According to these plans, the personnel, both operational and supervisory, of essential industries would be *dispersed* with their families to small towns and villages outside cities. The zones in which these towns and villages lie are selected on the basis of being far enough from target areas to be safe from the blast effects of nuclear weapons, but near enough that the workers and staff members could commute to work inside the cities, a distance of between 35 and 50 miles.

Retired people, educators, and workers in nonessential industries, and sometimes these industries as well, would be *evacuated* from cities to rural areas, where they would remain until the cessation of hostilities. Both evacuated and dispersed persons would be quartered with the rural residents and would be protected from fallout in hastily constructed shelters, which they would help their rural hosts to erect, or in reinforced cellars. It has been estimated by Professor Eugene P. Wigner that a retaliatory strike by the U.S. against the U.S.S.R., made after Russian cities had been evacuated and the population was in its expedient shelters, would not kill more than 6% of their population, less than they lost in World War II. This estimate was based on the assumption that the U.S. could and would retarget the strike to maximize casualties on the dispersed population. At the same time, with present protection, about 60% of our own population would be killed in an attack on our cities.

In addition to this overview of the Soviet civil defense program, detailed information on one single aspect of Soviet civil defense at a time is being presented in the journal *Survive* in a regular feature column: "The Soviet CD Scene."

## STRATEGIC CONSIDERATIONS IN PLANNING A COUNTEREVACUATION

The Soviet Union has highly developed plans to evacuate their population centers in a nuclear confrontation. Their plans include construction of expedient shelters in the outlying areas and continued operation of their essential industry by commuting workers. If they should successfully implement their plan, a subsequent nuclear exchange with the United States, assuming the U.S. does not retarget the weapons aimed at their cities, could cost them far fewer casualities than they suffered in World War II.[8] Under the same circumstances, the U.S. could lose from 50 to 70% of its population. This asymmetry would seriously weaken the bargaining position of the U.S. President. To restore the balance, a great reduction in the vulnerability of the U.S. population is required.

Under the present budgetary and political constraints, this reduction can be achieved most economically by planning a U.S. counterevacuation as a response to a Soviet evacuation. Because of the great differences in the two societies, the U.S. plan can only borrow a limited amount from the Russian plan. This preliminary study has been detailed enough to determine that the U.S. does have ample resources to move and shelter its population at least as effectively as the Soviet Union. The only critical disadvantage for the U.S. is the widespread misconception that effective survival measures are not possible.

The U.S. automobile inventory is so large that we have a tenfold advantage in passenger transportation, which will permit most cities to be evacuated in one day compared with three days for the Soviets. The road nets in even the most congested cities are adequate to make the evacuation in one day with only a bare

7. *Survive,* The American Journal of Civil Defense, published by the Association for Community-Wide Protection from Nuclear Attack, P.O. Box 910, Starke, Fla.

8. C. V. Chester et al., *Strategic Considerations in Planning a Counterevacuation,* ORNL-4888 (June 1973).

minimum of planning. The large Soviet weapon inventory and smaller area of the U.S. makes the fallout problem more acute for the U.S.; therefore, the construction of high-protection-factor expedient shelters will be necessary. Cristy[9] has shown that there will be ample supplies of tools and construction materials to accomplish this.

Private ownership of housing, especially rural, is a disadvantage to a U.S. evacuation. It could nucleate resistance to the evacuation unless redirection of food distribution to the rural area is clearly evident to the host population.

The Soviet provision for maintaining essential production in the evacuated posture by a commuting work force will require that the U.S. do the same. Otherwise, prolonging the evacuation for more than a few days will put great economic pressure on the U.S. to the disadvantage of its bargaining position.

The disciplined Soviet population and authoritarian government will permit cycling the Soviet plans. One or two false alarms will render the U.S. plans completely ineffective. Hence, the U.S. plan should be designed for one time only. Then advantage can be taken of the change produced by an evacuation in the political climate and national priorities to build a shelter system that, with only tactical warning, will give protection comparable to the Soviet evacuation, and will permit operation of the economy during a crisis. This will require that the U.S. recognize, as does the Soviet Union, that protection of its productive population is part of its strategic deterrent.

9. G. A. Cristy, *Expedient Shelters Survey,* ORNL-4860 (June 1973).

## MAPPING OF POPULATION DENSITY

An analysis of population distribution and mapping of population density was prepared to provide guidance for planning of evacuation from areas of potential disaster, either natural or man-made, and to indicate areas of greatest population risk in the event of nuclear war. Maps of population density are also useful in selecting sites for nuclear power plants.

The Bureau of Census listing of geographical coordinates of centroids of all 255,627 enumeration districts together with population count from the U.S. 1970 Census of Population was used to construct via computer five nationwide geographical grids of population density with sector dimensions of 0.01, 0.02, 0.04, 0.1, and 0.25° of latitude and longitude. The entire popula-

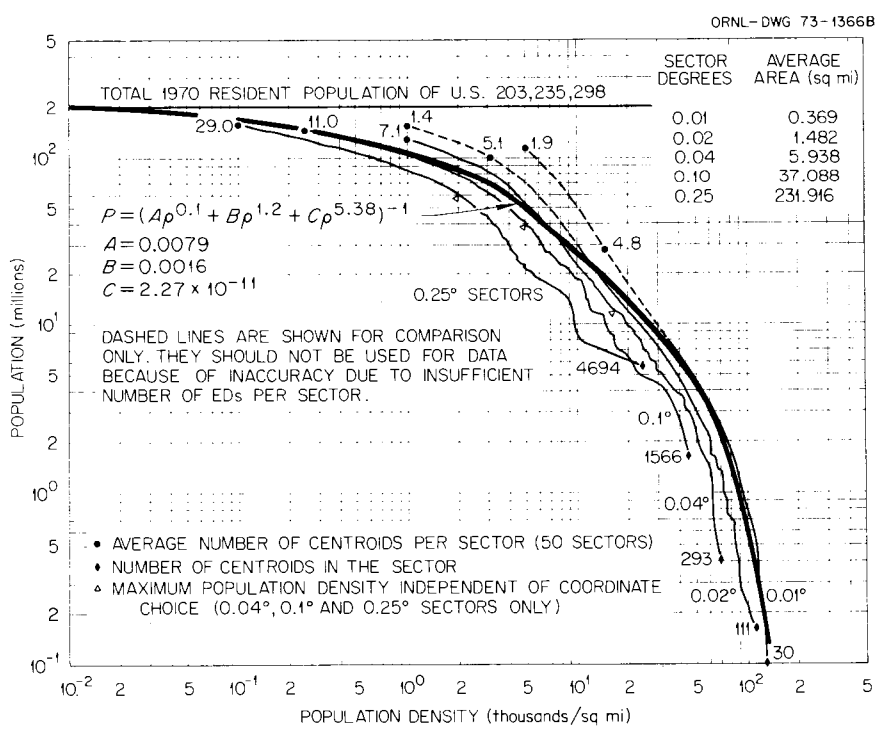


**Fig. 20.1. U.S. residential population, 1970 Census, as a function of population density, for various size sectors.**

tion of a district was assigned to a sector if the coordinates of the district centroid fell within the boundaries of the sector. The sectors were then rank-ordered according to population density, and listings were made of sector population, population density, geographical location, cumulative population, area of sector, and cumulative area.

Curves showing population as a function of population density are shown in Fig. 20.1. The heavy curve synthesizes the data obtained by rank-ordering density in the five different sector sizes. Curves showing population as a function of area, together with a synthesizing curve, are shown in Fig. 20.2.

From these data it was found, for example, that about 800,000 people live in 19 sectors of 0.01° dimensions with a population density of 100,000 people per square mile or greater (nearly all in Manhattan); about 10,000,000 live in 183 sectors of 0.02° dimensions with a population density of 23,000 per square mile or greater; and about half of the total U.S. population, that is, about 100,000,000 people, reside within about 0.6% of the area of the U.S., that is, within 20,000 square miles.

Two representative maps of population density are shown in Figs. 20.3 and 20.4, one for the Northeast Corridor and one for the vicinity of Richmond, Virginia. Isometric projections of population density for the Detroit and New York Standard Metropolitan Statistical Areas are shown for 1960 and 1970 in Figs. 20.5–20.8.

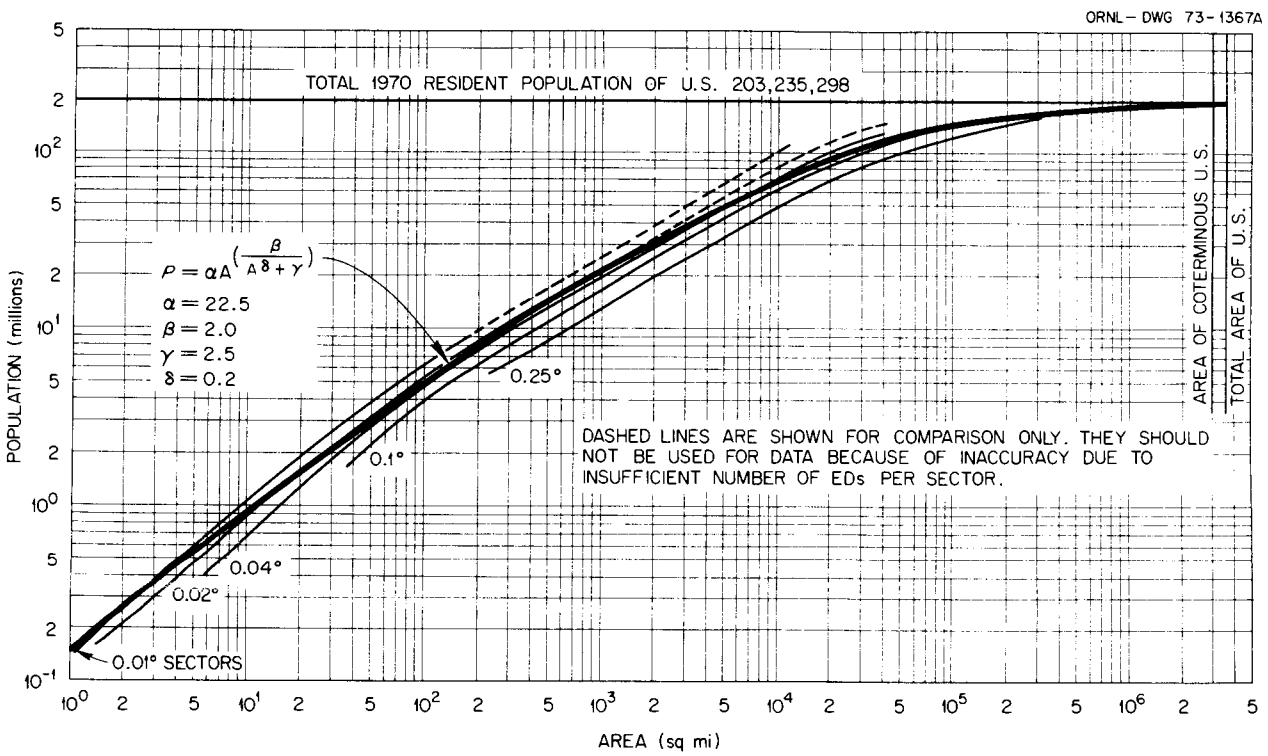


**Fig. 20.2. U.S. population, 1970 Census, as a function of area occupied in residence, for various size sectors.**

ORNL-DWG 73-8088

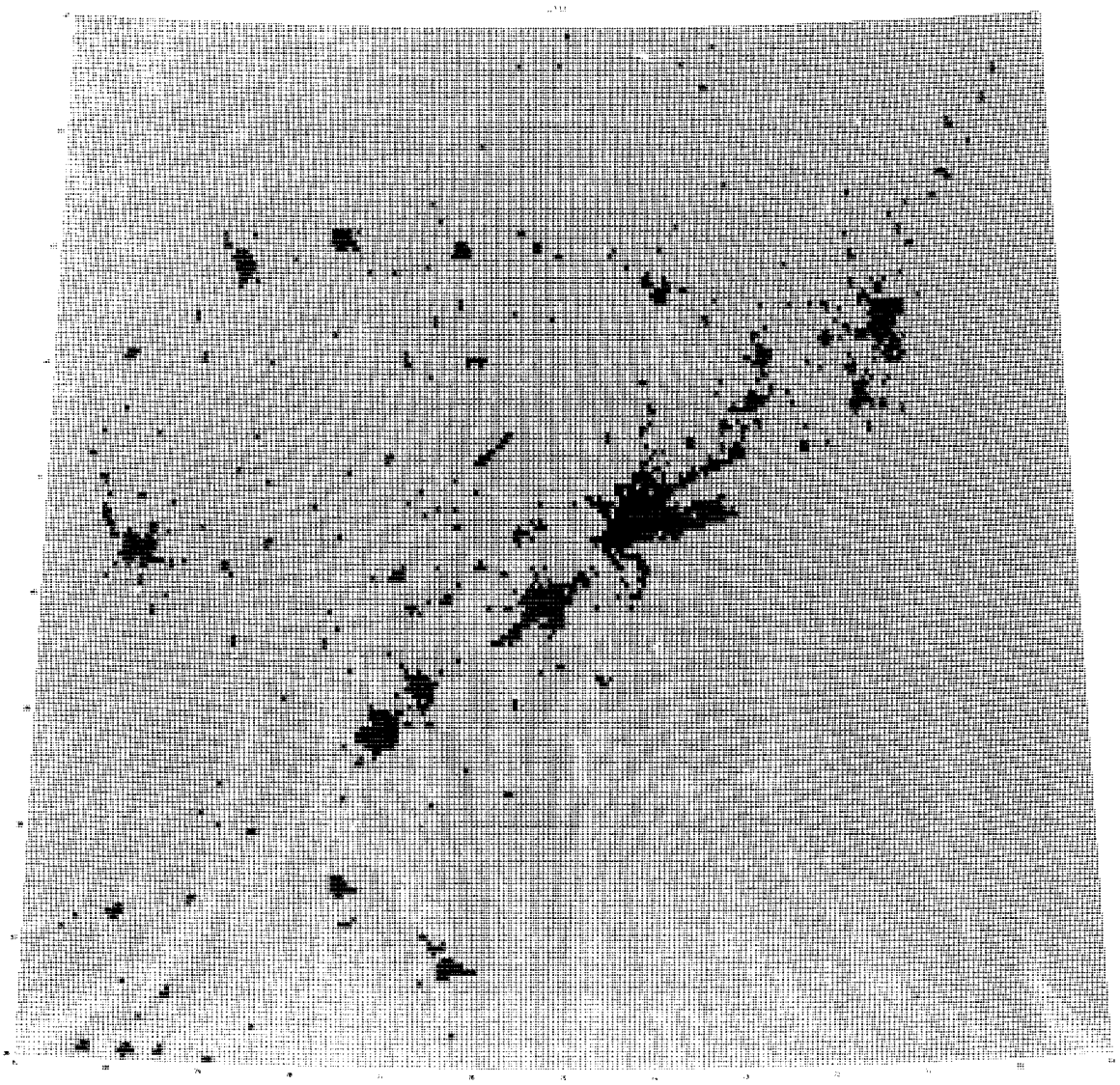

Fig. 20.3. Albers equal area projection of a 0.05° mesh of latitude and longitude lines for the Northeastern U.S., with asterisks placed in sectors in which the population density exceeds 1000 people per square mile.

ORNL DWG. 72-13741

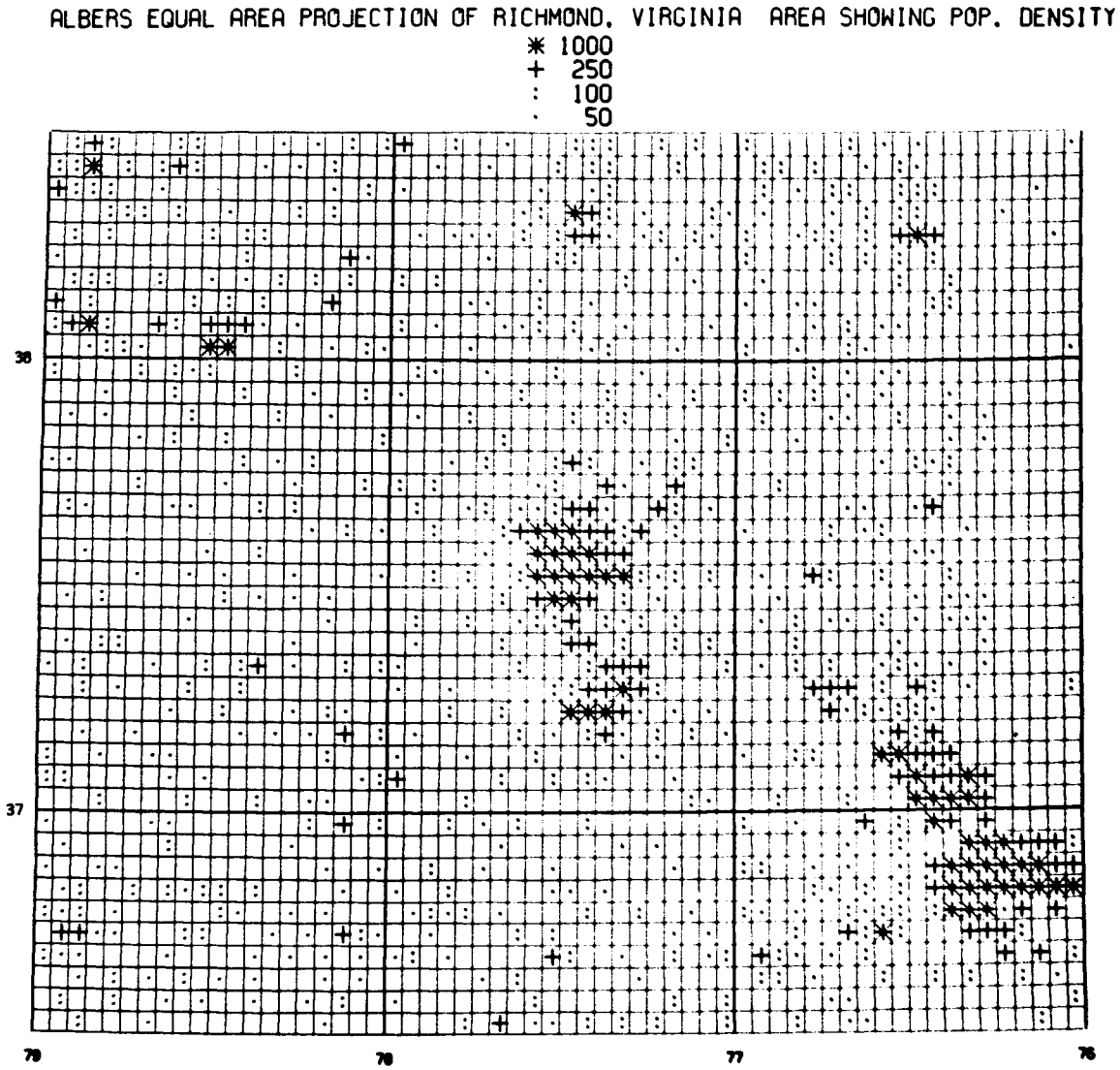


**Fig. 20.4. Albers equal area projection of area surrounding Richmond, Virginia, with population density indicated in 0.05° sectors.** An asterisk indicates population density exceeding 1000 people per square mile, a plus sign indicates density between 250 and 1000 people per square mile, two dots indicate density between 100 and 250 people per square mile, one dot, between 50 and 100, and the density is less than 50 people per square mile where there is no dot.

PHOTO 0952-73A

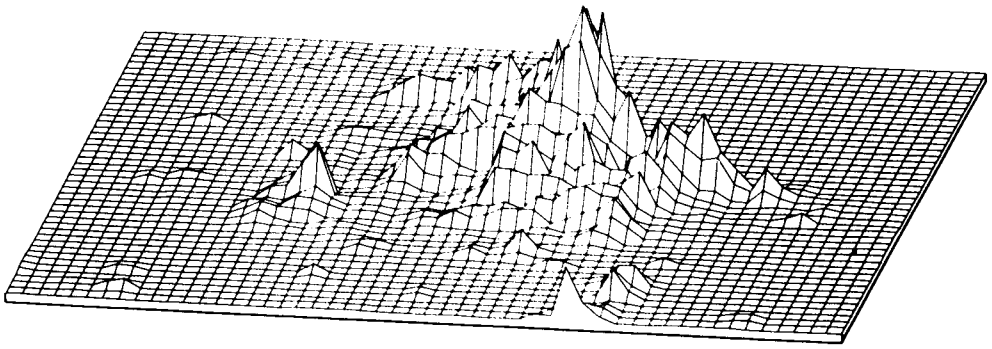

DETROIT, MICHIGAN 1960

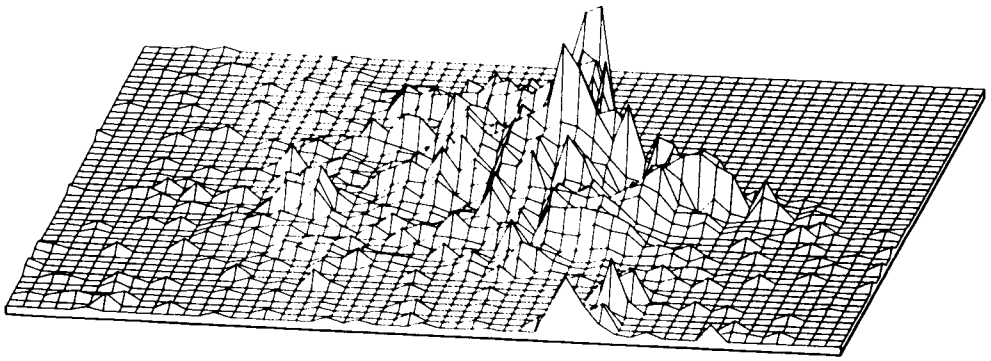

DETROIT, MICHIGAN 1970

**Fig. 20.5. Isometric projection of population density of Detroit Metropolitan Area on 2-km squares, seen from the west, with Ann Arbor peak in the foreground, for 1960 and 1970, at the same scale.**

PHOTO 0953-73A

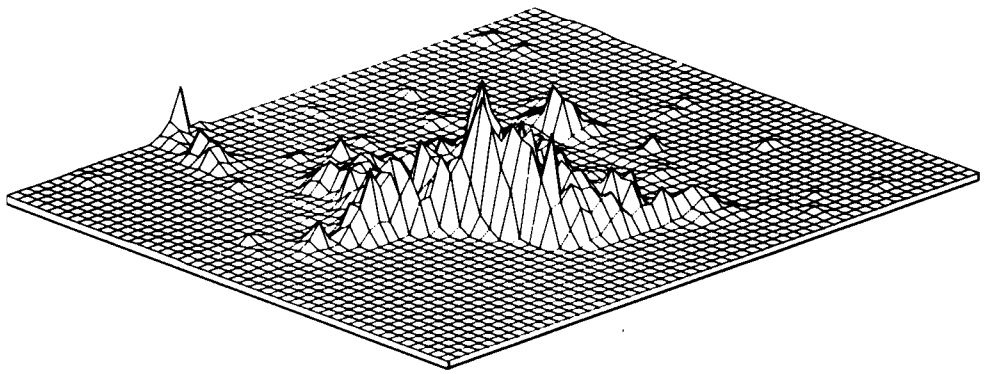

DETROIT, MICHIGAN 1960

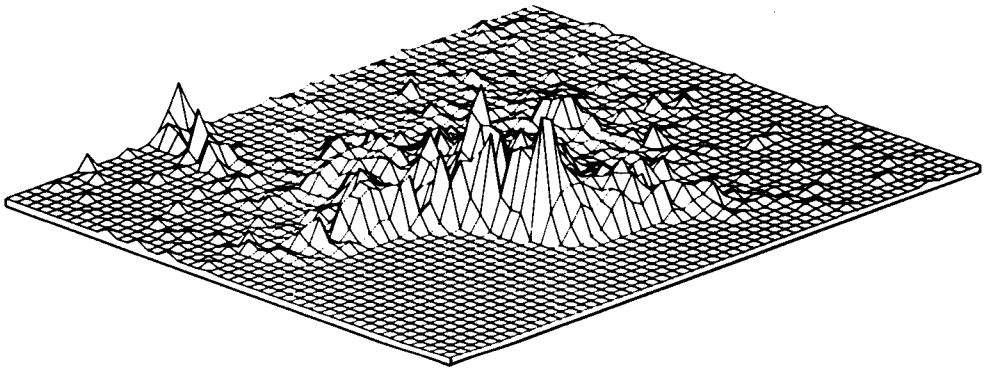

DETROIT, MICHIGAN 1970

**Fig. 20.6. Same as Fig. 20.5, seen from the southeast, from Canada.**

PHOTO 0800-73A

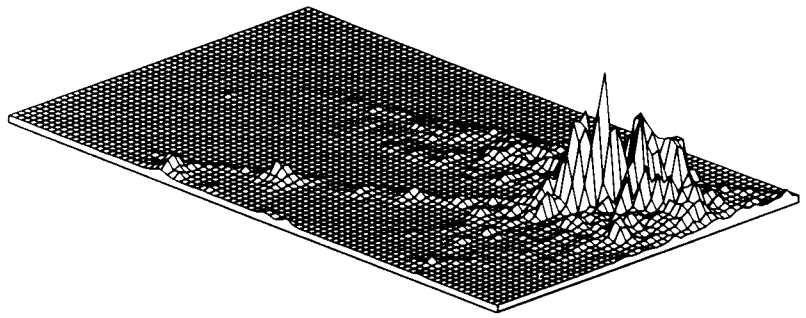

NEW YORK CITY 1960

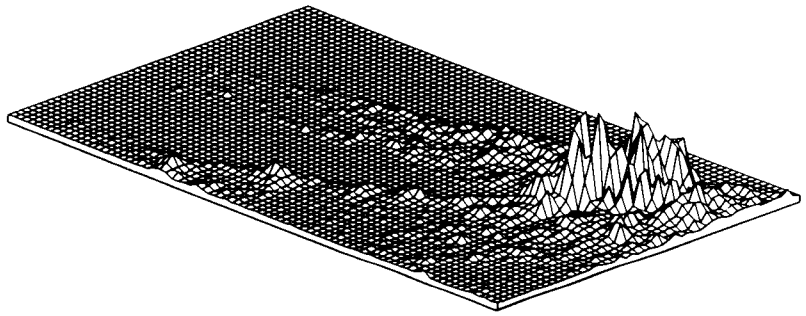

NEW YORK CITY 1970

**Fig. 20.7. Isometric projection of population density of New York City Metropolitan Area on 2-km squares, seen from the northeast, for 1960 and 1970.** The Connecticut coastline is in the foreground extending from left to right, and Long Island is discernible beyond Long Island Sound.

PHOTO 0803-73A

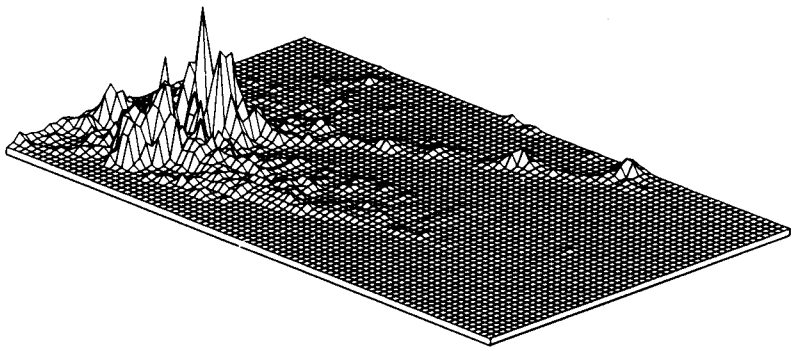

NEW YORK CITY 1960

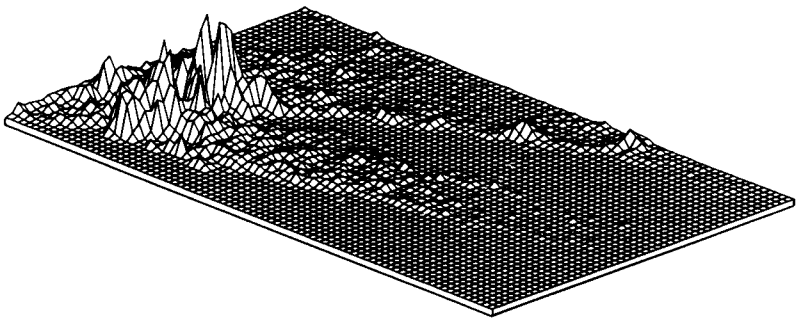

NEW YORK CITY 1970

**Fig. 20.8. Same as Fig. 20.7, seen from the southeast.**

## EXPEDIENT SHELTER SURVEY

The state of the art of expedient shelter building was reviewed and reported[10] to the Defense Civil Preparedness Agency (DCPA). This review is part of a long-range program being pursued by the Civil Defense Section under an interagency agreement between the AEC and DCPA. The goal of the interagency program is to develop a viable U.S. response to the inferred threat posed by the continuing refinement of the evacuation and dispersal doctrine of the Union of Soviet Socialist Republics.

The review of the art of expedient shelter building involved a comprehensive review of all available U.S. literature on shelter building and the selection of a number of the most promising designs to be included in a proposed expedient shelter manual for assistance to civil defense planners and for any other person who might need (or wish) to build such a shelter. An expedient shelter was defined to be one that could be built by a crew of mostly inexperienced labor in a period of not more than 48 hr. Designs of 15 shelters were selected as being appropriate to be included in the proposed handbook. Six of the designs were the six types developed at ORNL (see "Blast Resistance of Expedient Shelters," this report). This selection will allow builders a wide choice of designs covering most conditions of availability of building sites, construction materials, and tools.

The shelters include fully buried, semiburied, and aboveground models. Some can be used only in firm (self-supporting) ground; others provide shoring for support for the surrounding earth. Many of the designs are based on dimensioned lumber, but several use logs or small poles. The wire catenary design, which uses fence posts and fence wire, was developed for areas where lumber and timber are scarce. Another very promising design uses interior doors to cover a trench. Doors should be the most readily available of all shelter-building materials.

In addition to the review of designs, a preliminary evaluation of the availability of equipment, tools, and building materials was made. It was concluded that the rural and suburban residents will have enough tools to build all the expedient shelters they need for themselves. However, in an evacuation situation, the influx of urban residents would cause a serious shortage of tools unless the evacuees brought tools with them. This indicates that some prior planning should be done by civil defense organizations particularly in the urban areas before an evacuation starts.

A sample survey of excavation equipment indicated that there probably would be enough such equipment to do the excavation for shelters for about one-third of the population in any specific area. When the requirement for expedient shelter exceeds that, the remainder must be excavated by hand.

The supply of lumber available in lumber yards will be insufficient in many areas to provide adequate shelters for the evacuated population. This can be alleviated by using shelters made of small poles in areas where forested areas are within easy reach of the urban population. Data obtained from the U.S. Forestry Service Survey were used to evaluate the availability of timber resources. It was assumed that all evacuation of urban areas would be into rural areas within the same OBE area.[11] The results are shown in Fig. 20.9 (map) and Table 20.1.

In Fig. 20.9, the darkest green areas represent OBE areas that would require less than 1% of the timber resources to build small-pole shelters for *all* the population within the OBE; the medium green areas represent areas where from 1 to 10% of the timber resources would be needed.

Table 20.1 lists the OBE areas in order of the percentage of timber needed to shelter *all* the population and shows the cumulative population which can be sheltered using the tabulated percentage. For example: 32% of the U.S. population resides in the OBE areas which can shelter *all* their population with 1% or less of the timber available, and nearly 70% of the U.S. population resides in the OBE areas which can shelter *all* their population with 10% or less of the available timber. Naturally, only a fraction of the population in any OBE area would need to have expedient shelters built. For comparison, the annual cut of trees for lumber and for pulpwood, as reported by the U.S. Forest Service, normally amounts to from 1 to 5% of the total growing stock.

When timber and lumber supplies are exhausted, or not available, use can be made of the wire catenary design or the interior-door-over-trench design, using doors from the shelterees' dwellings.

Work has been started on the proposed Expedient Shelter Manual.

10. G. A. Cristy, *Expedient Shelters Survey*, ORNL-4860 (June 1973).

11. One of the 183 areas identified by the U.S. Department of Commerce Office of Business Economics (OBE) as being an established trade area.

ORNL-DWG 72-9785B

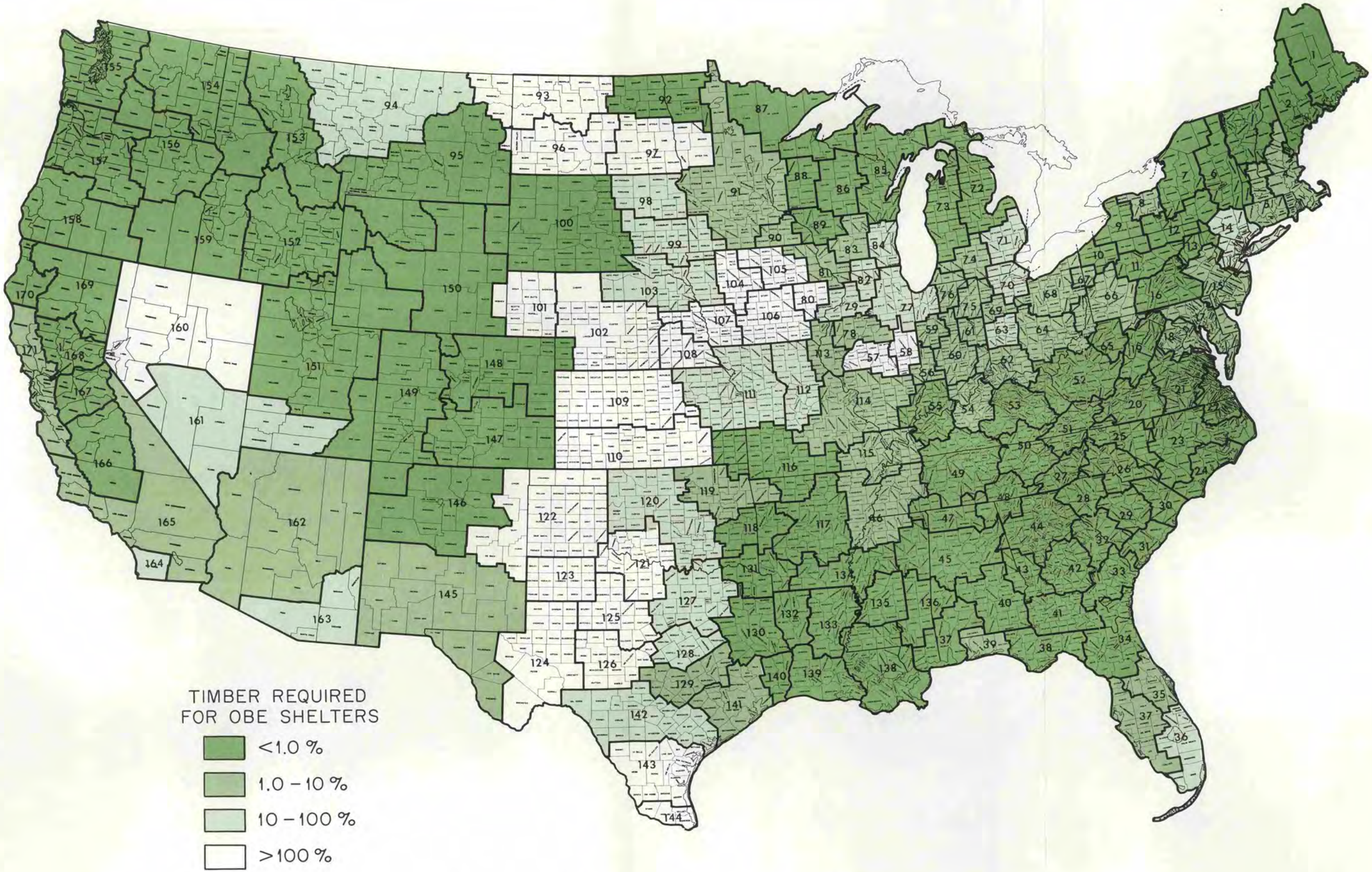


Adequacy of Timber for Expedient Shelters

**Table 20.1. Timber resources for expedient shelters by OBE area in order of percent timber needed**

| OBE No. | OBE name | Population (thousands) | Population density (persons per sq mile) | Percent of timber needed | Cumulative population (%) |
|---|---|---|---|---|---|
| 169 | Redding, CA | 176 | 7.0 | 0.01 | 0.1 |
| 157 | Portland, OR | 1,635 | 55.9 | 0.02 | 0.9 |
| 146 | Albuquerque, NM | 572 | 14.4 | 0.02 | 1.2 |
| 158 | Eugene, OR | 543 | 17.3 | 0.02 | 1.5 |
| 170 | Eureka, CA | 121 | 15.7 | 0.02 | 1.5 |
| 156 | Yakima, WA | 406 | 12.8 | 0.03 | 1.7 |
| 153 | Butte, MT | 234 | 6.9 | 0.03 | 1.8 |
| 155 | Seattle, WA | 2,363 | 112.4 | 0.04 | 3.0 |
| 154 | Spokane, WA | 687 | 13.7 | 0.04 | 3.3 |
| 1 | Bangor, ME | 321 | 17.0 | 0.04 | 3.5 |
| 152 | Idaho Falls, ID | 300 | 7.3 | 0.04 | 3.7 |
| 159 | Boise City, ID | 265 | 6.4 | 0.05 | 3.8 |
| 149 | Grand Junction, CO | 251 | 4.8 | 0.06 | 3.9 |
| 87 | Duluth, MI | 429 | 18.6 | 0.09 | 4.1 |
| 150 | Cheyenne, WY | 229 | 4.5 | 0.13 | 4.2 |
| 136 | Meridian, MS | 393 | 35.8 | 0.15 | 4.4 |
| 131 | Texarkana, TX | 329 | 29.3 | 0.15 | 4.6 |
| 2 | Portland, ME | 740 | 59.9 | 0.16 | 5.0 |
| 11 | Williamsport, PA | 419 | 62.5 | 0.16 | 5.2 |
| 116 | Springfield, MO | 830 | 31.9 | 0.17 | 5.6 |
| 134 | Greenville, MS | 506 | 35.0 | 0.17 | 5.8 |
| 3 | Burlington, VT | 502 | 42.2 | 0.17 | 6.1 |
| 133 | Monroe, LA | 532 | 43.0 | 0.18 | 6.3 |
| 42 | Macon, GA | 496 | 50.9 | 0.20 | 6.6 |
| 19 | Staunton, VA | 395 | 48.1 | 0.20 | 6.8 |
| 118 | Ft Smith, AR | 289 | 25.4 | 0.20 | 6.9 |
| 117 | Little Rock, AR | 864 | 41.9 | 0.21 | 7.4 |
| 167 | Stockton, CA | 643 | 58.9 | 0.21 | 7.7 |
| 130 | Tyler, TX | 553 | 38.8 | 0.21 | 8.0 |
| 33 | Savannah, GA | 417 | 49.1 | 0.22 | 8.2 |
| 147 | Pueblo, CO | 509 | 14.5 | 0.23 | 8.4 |
| 32 | Augusta, GA | 461 | 55.6 | 0.24 | 8.6 |
| 27 | Asheville, NC | 391 | 69.3 | 0.24 | 8.8 |
| 85 | Green Bay, WI | 926 | 46.6 | 0.25 | 9.3 |
| 41 | Albany, GA | 461 | 42.4 | 0.25 | 9.5 |
| 140 | Beaumont, TX | 394 | 79.2 | 0.26 | 9.7 |
| 135 | Jackson, MS | 510 | 56.2 | 0.27 | 10.0 |
| 132 | Shreveport, LA | 453 | 61.1 | 0.27 | 10.2 |
| 95 | Billings, MT | 246 | 3.7 | 0.27 | 10.3 |
| 52 | Huntington, WV | 1,309 | 72.8 | 0.28 | 11.0 |
| 72 | Saginaw, MI | 798 | 50.0 | 0.28 | 11.4 |
| 30 | Florence, SC | 400 | 62.5 | 0.28 | 11.6 |
| 168 | Sacramento, CA | 1,089 | 94.9 | 0.29 | 12.1 |
| 21 | Richmond, VA | 1,010 | 85.5 | 0.30 | 12.6 |
| 137 | Mobile, AL | 724 | 66.6 | 0.30 | 13.0 |
| 86 | Wausau, WI | 350 | 33.7 | 0.30 | 13.1 |
| 65 | Clarksville, WV | 326 | 68.5 | 0.30 | 13.3 |
| 20 | Roanoke, VA | 735 | 70.7 | 0.32 | 13.7 |
| 24 | Wilmington, NJ | 482 | 70.1 | 0.32 | 13.9 |
| 50 | Knoxville, TN | 904 | 84.3 | 0.36 | 14.4 |
| 31 | Charleston, SC | 430 | 89.6 | 0.36 | 14.6 |
| 43 | Columbus, OH | 488 | 72.1 | 0.37 | 14.8 |
| 23 | Raleigh, NC | 1,621 | 102.8 | 0.38 | 15.6 |
| 34 | Jacksonville, FL | 1,051 | 67.1 | 0.38 | 16.1 |

Table 20.1 (continued)

| OBE No. | OBE name | Population (thousands) | Population density (persons per sq mile) | Percent of timber needed | Cumulative population (%) |
|---|---|---|---|---|---|
| 100 | Rapid City, SD | 231 | 4.4 | 0.38 | 16.3 |
| 12 | Binghampton, NY | 765 | 77.5 | 0.39 | 16.6 |
| 88 | Eau Claire, WI | 219 | 33.3 | 0.39 | 16.7 |
| 10 | Erie, PA | 459 | 120.2 | 0.41 | 17.0 |
| 40 | Montgomery, AL | 687 | 49.4 | 0.42 | 17.3 |
| 51 | Bristol, VA | 774 | 90.9 | 0.45 | 17.7 |
| 89 | La Crosse, WI | 269 | 41.0 | 0.46 | 17.8 |
| 166 | Fresno, CA | 1,036 | 46.1 | 0.48 | 18.3 |
| 138 | New Orleans, LA | 2,175 | 109.2 | 0.51 | 19.4 |
| 49 | Nashville, TN | 1,426 | 70.4 | 0.52 | 20.1 |
| 53 | Lexington, KY | 753 | 64.7 | 0.55 | 20.5 |
| 139 | Lake Charles, LA | 748 | 61.3 | 0.55 | 20.9 |
| 29 | Columbia, SC | 592 | 88.0 | 0.57 | 21.2 |
| 22 | Norfolk, VA | 1,232 | 217.5 | 0.59 | 21.8 |
| 48 | Chattanooga, TN | 718 | 87.8 | 0.60 | 22.1 |
| 6 | Albany, NY | 1,332 | 102.6 | 0.61 | 22.8 |
| 73 | Grand Rapids, MI | 1,124 | 91.1 | 0.62 | 23.4 |
| 151 | Salt Lake City, UT | 1,061 | 13.7 | 0.63 | 23.9 |
| 25 | Greensboro, NC | 1,142 | 133.4 | 0.64 | 24.5 |
| 45 | Birmingham, AL | 1,743 | 76.1 | 0.65 | 25.3 |
| 47 | Huntsville, AL | 671 | 75.0 | 0.65 | 25.7 |
| 44 | Atlanta, GA | 2,296 | 151.0 | 0.66 | 26.8 |
| 7 | Syracuse, NY | 1,445 | 104.9 | 0.70 | 27.5 |
| 16 | Harrisburg, PA | 1,723 | 171.6 | 0.82 | 28.4 |
| 28 | Greenville, SC | 817 | 129.2 | 0.83 | 28.8 |
| 13 | Wilkes Barre, PA | 692 | 197.4 | 0.84 | 29.1 |
| 148 | Denver, CO | 1,523 | 44.3 | 0.86 | 29.9 |
| 92 | Grand Forks, ND | 220 | 11.8 | 0.89 | 30.0 |
| 26 | Charlotte, NC | 1,489 | 152.7 | 0.92 | 30.7 |
| 55 | Evansville, IN | 771 | 68.7 | 0.96 | 31.1 |
| 9 | Buffalo, NY | 1,789 | 217.7 | 1.00 | 32.0 |
| 145 | El Paso, TX | 681 | 9.3 | 1.07 | 32.3 |
| 38 | Tallahassa, FL | 344 | 36.7 | 1.08 | 32.5 |
| 171 | San Francisco, CA | 5,090 | 300.8 | 1.14 | 35.0 |
| 115 | Paducah, KY | 558 | 43.5 | 1.21 | 35.3 |
| 56 | Terra Haute, IN | 252 | 73.4 | 1.21 | 35.4 |
| 97 | Fargo, ND | 335 | 14.6 | 1.28 | 35.6 |
| 35 | Orlando, FL | 941 | 142.5 | 1.35 | 36.1 |
| 83 | Madison, WI | 455 | 73.0 | 1.35 | 36.3 |
| 91 | Minneapolis, MN | 2,942 | 69.8 | 1.40 | 37.8 |
| 46 | Memphis, TN | 1,678 | 79.8 | 1.42 | 38.6 |
| 66 | Pittsburgh, PA | 3,716 | 275.6 | 1.47 | 40.4 |
| 141 | Houston, TX | 2,362 | 150.5 | 1.49 | 41.6 |
| 54 | Louisville, KY | 1,220 | 145.1 | 1.54 | 42.2 |
| 64 | Columbus, OH | 1,763 | 153.3 | 1.55 | 43.1 |
| 17 | Baltimore, MD | 1,764 | 205.7 | 1.62 | 44.0 |
| 81 | Dubuque, IA | 301 | 41.0 | 1.78 | 44.1 |
| 39 | Pensacola, FL | 382 | 82.1 | 1.84 | 44.3 |
| 119 | Tulsa, OK | 1,012 | 64.7 | 2.13 | 44.8 |
| 113 | Quincy, IL | 299 | 43.3 | 2.56 | 45.0 |
| 60 | Indianapolis, IN | 1,613 | 188.9 | 2.67 | 45.8 |
| 18 | Washington, DC | 3,404 | 610.8 | 2.81 | 47.4 |
| 90 | Rochester, MN | 245 | 57.0 | 3.35 | 47.6 |
| 37 | Tampa, FL | 1,798 | 149.3 | 3.37 | 48.5 |
| 74 | Lansing, MI | 1,034 | 174.4 | 3.48 | 49.0 |

Table 20.1 (continued)

| OBE No. | OBE name | Population (thousands) | Population density (persons per sq mile) | Percent of timber needed | Cumulative population (%) |
|---|---|---|---|---|---|
| 8 | Rochester, NY | 1,016 | 279.3 | 3.78 | 49.5 |
| 62 | Cincinnati, OH | 1,889 | 217.9 | 3.79 | 50.4 |
| 59 | Lafayette, IN | 250 | 72.5 | 3.97 | 50.5 |
| 67 | Youngstown, OH | 771 | 374.6 | 4.33 | 50.9 |
| 75 | Fort Wayne, IN | 597 | 123.8 | 4.46 | 51.2 |
| 76 | South Bend, IN | 747 | 176.1 | 4.98 | 51.6 |
| 112 | Columbia, MO | 397 | 29.8 | 5.33 | 51.8 |
| 129 | Austin, TX | 559 | 42.9 | 5.42 | 52.1 |
| 114 | St Louis, MO | 3,248 | 117.9 | 5.47 | 53.7 |
| 78 | Peoria, IL | 628 | 98.4 | 5.67 | 54.0 |
| 4 | Boston, MA | 6,339 | 638.8 | 5.71 | 57.1 |
| 5 | Hartford, CN | 2,966 | 390.8 | 6.69 | 58.6 |
| 69 | Lima, OH | 276 | 105.7 | 6.83 | 58.7 |
| 68 | Cleveland, OH | 4,255 | 399.3 | 7.57 | 60.9 |
| 165 | Los Angeles, CA | 10,436 | 182.1 | 7.93 | 66.0 |
| 15 | Philadelphia, PA | 7,281 | 682.4 | 8.73 | 69.7 |
| 61 | Muncie, IN | 551 | 178.8 | 9.64 | 69.9 |
| 70 | Toledo, OH | 1,054 | 217.5 | 10.98 | 70.5 |
| 162 | Phoenix, AR | 1,316 | 14.6 | 13.24 | 71.1 |
| 82 | Rockford, IL | 560 | 134.7 | 13.46 | 71.4 |
| 128 | Waco, TX | 403 | 43.8 | 13.84 | 71.6 |
| 79 | Davenport, IO | 605 | 104.2 | 14.11 | 71.9 |
| 98 | Aberdeen, SD | 132 | 10.3 | 16.16 | 71.9 |
| 63 | Dayton, OH | 1,162 | 289.4 | 16.29 | 72.5 |
| 163 | Tucson, AR | 454 | 19.6 | 17.57 | 72.8 |
| 164 | San Diego, CA | 1,357 | 318.7 | 17.90 | 73.4 |
| 71 | Detroit, MI | 5,207 | 769.2 | 18.22 | 76.0 |
| 111 | Kansas City, MO | 2,249 | 74.2 | 18.59 | 77.1 |
| 99 | Sioux Falls, SD | 351 | 21.3 | 18.77 | 77.3 |
| 14 | New York, NY | 18,272 | 1830.9 | 19.35 | 86.4 |
| 120 | Oklahoma City, OK | 1,158 | 38.4 | 20.17 | 86.9 |
| 36 | Miami, FL | 2,430 | 227.6 | 20.35 | 88.2 |
| 94 | Great Falls, MT | 222 | 4.3 | 32.68 | 88.3 |
| 84 | Milwaukee, WI | 2,066 | 389.5 | 37.90 | 89.3 |
| 142 | San Antonio, TX | 1,229 | 42.5 | 48.05 | 89.9 |
| 127 | Dallas, TX | 2,736 | 140.0 | 53.68 | 91.3 |
| 161 | Las Vegas, NV | 317 | 5.5 | 69.28 | 91.4 |
| 103 | Sioux City, IA | 452 | 20.5 | 74.70 | 91.6 |
| 77 | Chicago, IL | 8,193 | 654.3 | 94.12 | 95.7 |
| 107 | Omaha, NE | 794 | 75.7 | >100 | 96.1 |
| 106 | Des Moines, IA | 782 | 56.0 | >100 | 96.5 |
| 110 | Wichita, KA | 728 | 24.4 | >100 | 96.9 |
| 143 | Corpus Christi, TX | 516 | 26.2 | >100 | 97.1 |
| 57 | Springfield, IL | 490 | 77.9 | >100 | 97.4 |
| 121 | Wichita Falls, TX | 455 | 24.3 | >100 | 97.6 |
| 122 | Amarillo, TX | 437 | 9.0 | >100 | 97.8 |
| 105 | Waterloo, IA | 426 | 47.7 | >100 | 98.0 |
| 58 | Champaign, IL | 390 | 82.6 | >100 | 98.2 |
| 144 | Brownsville, TX | 355 | 83.7 | >100 | 98.4 |
| 109 | Salina, KS | 349 | 10.8 | >100 | 98.6 |
| 80 | Cedar Rapids, IA | 330 | 75.4 | >100 | 98.7 |
| 123 | Lubbock, TX | 328 | 24.0 | >100 | 98.9 |
| 102 | Grand Island, NE | 323 | 9.4 | >100 | 99.0 |
| 108 | Lincoln, NE | 323 | 37.9 | >100 | 99.2 |
| 124 | Odessa, TX | 319 | 9.5 | >100 | 99.4 |

Table 20.1 (continued)

| OBE No. | OBE name | Population (thousands) | Population density (persons per sq mile) | Percent of timber needed | Cumulative population (%) |
|---|---|---|---|---|---|
| 104 | Ft Dodge, IA | 266 | 32.2 | >100 | 99.5 |
| 125 | Abilene, TX | 264 | 16.7 | >100 | 99.6 |
| 160 | Reno, NV | 206 | 3.0 | >100 | 99.7 |
| 93 | Minot, ND | 182 | 6.7 | >100 | 99.8 |
| 96 | Bismarck, ND | 144 | 6.0 | >100 | 99.9 |
| 126 | San Angelo, TX | 124 | 8.2 | >100 | 99.9 |
| 101 | Scottsbluff, NE | 105 | 6.5 | >100 | 100.0 |

## BLAST RESISTANCE OF EXPEDIENT SHELTERS

ORNL field tests of expedient shelters during the past three years resulted in the selection and development of six types of expedient shelters deemed the most practical for average rural and small-town Americans to build in the principal environmental regions of the United States. Each type of shelter can be built within 48 hr[12] by average family groups of such Americans to provide all members with high-protective-factor shelter. In order to evaluate the blast protection afforded by these six types of expedient shelters, they were blast-tested as a part of Defense Nuclear Agency's Mixed Company event, a 500-ton TNT detonation, which was equivalent in its air-blast effects to a 1.0 to 1.8 kiloton nuclear burst.

A total of 12 shelters, representing six expedient types, were subjected to blast effects at surface overpressures ranging from 30 to 3 psi.[13,14] All except the two door-covered trench shelters were tested as *closed* shelters. Only one shelter was damaged, the door-covered trench shelter that was tested as an *open* shelter at 5 psi.

The six types of shelters, tested at the following measured surface overpressures, were: (1) two small-pole shelters, at 29 psi (see Fig. 20.10); (2) three wire-catenary-roofed shelters, at 29 and 13 psi; (3) one aboveground A-frame pole shelter, at 17 psi; (4) one shored-trench shelter, at 13 psi; (5) two log-covered trench shelters, at 17 psi; (6) two door-covered trench shelters, at 5 and 3 psi.

Seven of the shelters tested had a sufficient thickness of earth cover to result in effective earth arching under blast loading, as proved by measurements of roof deflections. For example, a half-scale model of the wire-catenary-roofed shelter (see Fig. 20.11), tested *closed* at a surface overpressure of 29 psi, had the center of its wire "catenary" ceiling permanently depressed only ¼ in. Calculations based on the lab-tested strength of the wire showed that if earth arching had been totally ineffective, this half-scale wire roof would have been broken and collapsed by an overpressure of only about 15 psi. In this test, earth arching carried almost all the load.

A new design of quickly closable expedient blast door was tested at 29, 17, and 13 psi surface overpressure ranges. Only the door at 17 psi was damaged, and even it remained intact and securely closed. Preliminary tests in Alabama of this blast door had demonstrated that shelter occupants, within about 4 sec of their seeing a light flashed on the shelter door, can close and secure this expedient blast door. The very bright light from a large nuclear explosion would be seen more than 4 sec before the arrival of the blast wave at distances far enough from the explosion to permit expedient shelters to survive the blast effects. Therefore, shelter entryways equipped with such blast doors could be left open to serve as low-resistance air ducts and to provide for ventilation-cooling, except for the short periods of blast hazards and the worst fallout dangers.

Two new types of expedient blast valves were installed and tested in the entrances of underground chambers at sites where the measured overpressures

12. "Hasty Shelter Construction Studies," chap. 21 of *Annual Progress Report, Civil Defense Research Project, March 1970–March 1971*. ORNL-4679.

13. C. H. Kearny and C. V. Chester, "Expedient Shelter Test," a paper in the forthcoming summary of the Preliminary Results Meeting for Defense Nuclear Agency Mixed Company event.

14. C. H. Kearny and C. V. Chester, *Expedient Blast Shelters*, a forthcoming ORNL report.

**Fig. 20.10. One of two half-scale small-pole shelters (shown partially completed) that were successfully tested, *closed*, at the 29-psi range.** The air-blast effects were approximately equivalent to those experienced by a full-scale model subjected to 29 psi by a ten-kiloton surface burst.

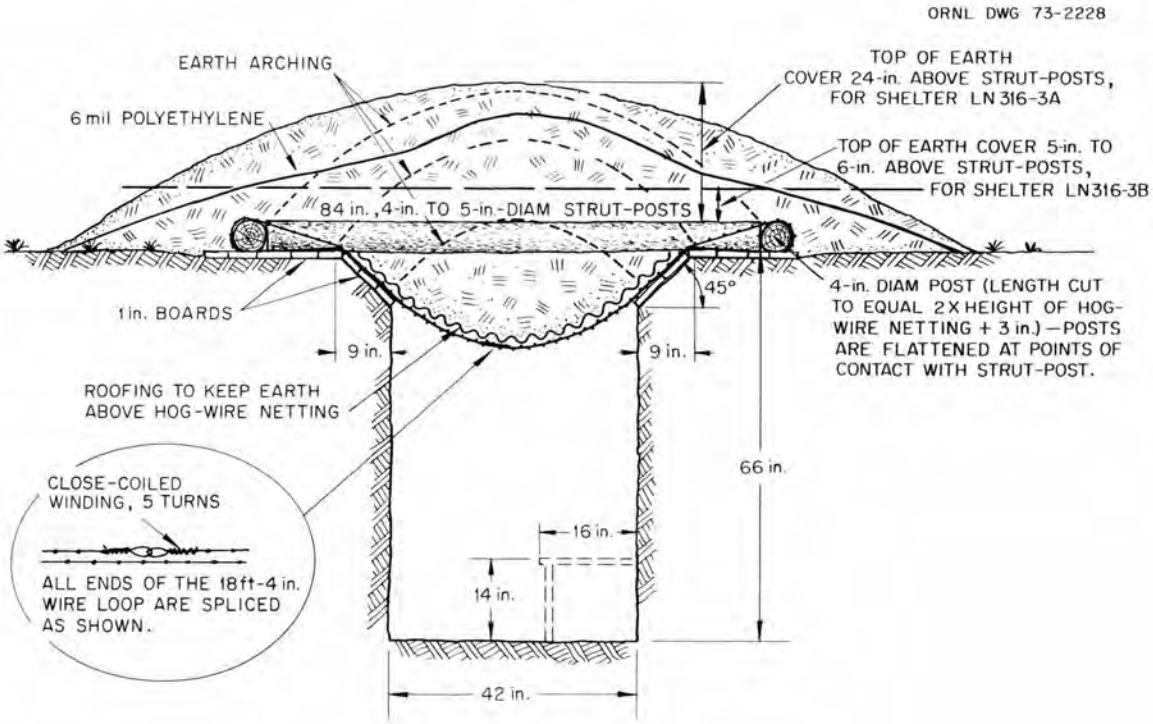


**Fig. 20.11. Wire-catenary-roofed shelter.**

were about 35 and 68 psi.[15] They performed satisfactorily. The most practical valve – built only of valve strips cut from worn tire treads, 2 × 12 in. boards, and nails – was undamaged by a 68-psi surface overpressure (see Fig. 20.12). Prior shock tube tests at ORNL had shown that this low-resistance expedient blast valve closes tightly in less than 2 msec when struck head-on by a 100-psi shock wave.

15. R. W. Manweiler, C. V. Chester, and C. H. Kearny, *Measurement of Shock Overpressure in Air by a Yielding Foil Membrane Blast Gauge*, ORNL-4868 (in preparation).

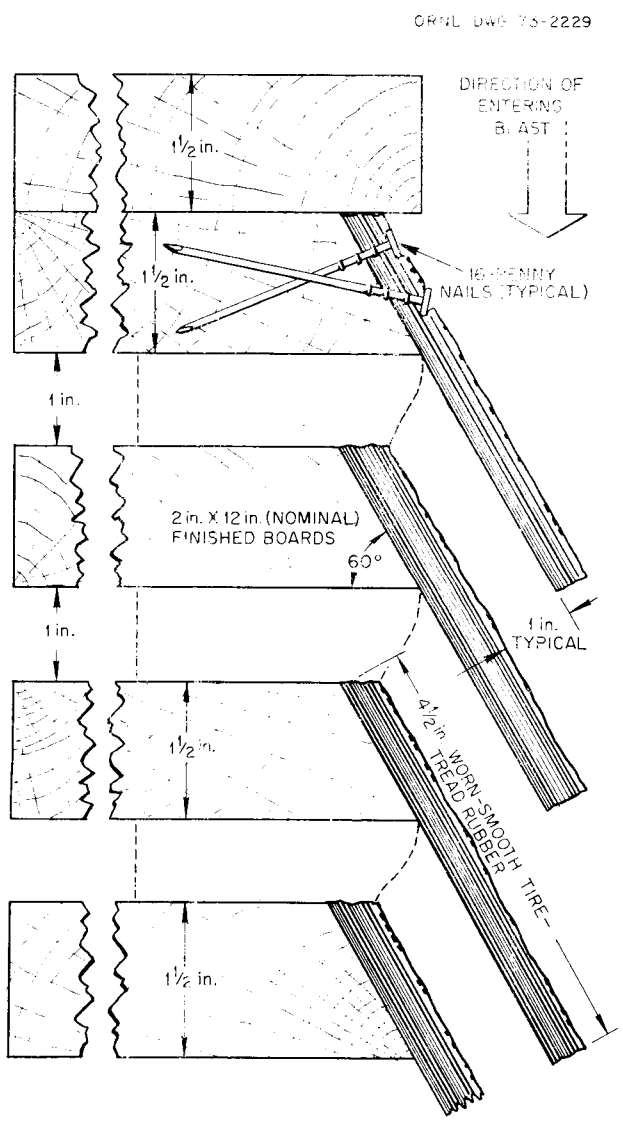


Fig. 20.12. Expedient blast valve.

## MEASUREMENT OF SHOCK OVERPRESSURE IN AIR BY A YIELDING FOIL MEMBRANE BLAST GAGE

### Introduction

An inexpensive yet accurate pressure gage was designed[15] making use of the relationship between the peak pressure of a single-step shock loading and the permanent plastic deformation of thin foil membranes when subjected to shock loading. The gage is of extremely simple design, is easy to use, and requires no electronic equipment. Peak shock overpressures from a few psi to hundreds of psi can be measured to about 10% accuracy.

This gage differs from membrane-rupture gages used early in the weapons program in that it gives continuous pressure readings over its range rather than interval limits. It is also at least one order of magnitude cheaper due to the use of epoxy adhesive to secure the membrane rather than a mechanical clamp. The gage has been successfully field-tested in a realistic experimental environment.

### Theory of Foil Membranes

Dresner[16] has shown that for a shock wave of instantaneous rise time and of infinite duration with normal incidence upon a circular foil membrane, the stress $\sigma$ and incident pressure $P$ (both measured in psi) are related by

$$\frac{\sigma}{P} = 0.138\,\frac{(D/T)^2}{h/T}\,, \tag{1}$$

where $D$ is the membrane's diameter (in inches), $T$ is the thickness (in mils), and $h$ is the maximum permanent deformation of the foil membrane (in inches). For normal incidence of the shock wave, the average linear strain $\eta$ is given by[16,17]

$$\eta = 1.8(h/D)^2\,. \tag{2}$$

The stress-strain curve for the foil can be determined using Eqs. (1) and (2) by a series of experiments each exposing the foil to a shock and measuring the pressure and the membrane deformation. Conversely, if the

16. L. Dresner, *Plastic Deformation of Circular Foils under Shock Loading*, ORNL-TM-2485 (1969).

17. L. Dresner, *J. Appl. Phys.* **41**, 2542 (1970).

stress-strain curve is known, the pressure as a function of the deformation can be calculated:

$$P = 7.25 \frac{T}{D^2} h\sigma \,. \tag{3}$$

For large strain, the stress is nearly constant and the pressure is nearly linear in the deformation. The interested reader should refer to ref. 16 for a discussion of both the validity and the limitations of Eqs. (1) through (3) for tangentially incident shock waves.

Experiments using a shock tube[18] were performed in order to determine the pressure as a function of the permanent maximum deformation for various diameters and thicknesses. Once the pressure as a function of the deformation is found, it is then possible to use Eqs. (1) and (2) to determine the stress-strain curve for the particular aluminum foil used. Finally, once the stress-strain curve is determined for a particular membrane thickness, one can calculate the pressure as a function of the deformation for any membrane diameter.

The experimental points for various membrane diameters have been plotted with different symbols in Fig. 20.13. Figure 20.14 shows the pressure as a function of the deformation for several membrane diameters. The plotted points are experimental values as determined directly from the shock tube measurements, while the curves are theoretical values as calculated from the *experimentally* determined stress-strain curves and using Eqs. (2) and (3).

18. L. Dresner and C. V. Chester, *A Four-Inch Shock Tube Driven by an Exploding Gas Mixture*, ORNL-TM-2094 (1968).

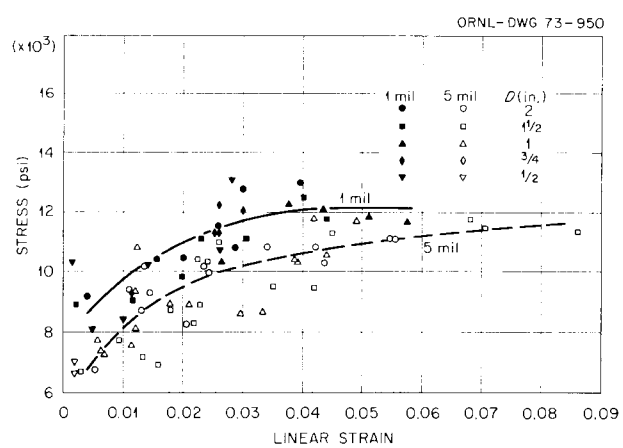


**Fig. 20.13. Stress-strain curves for 0.005- and 0.001-in.-thick aluminum foil.**

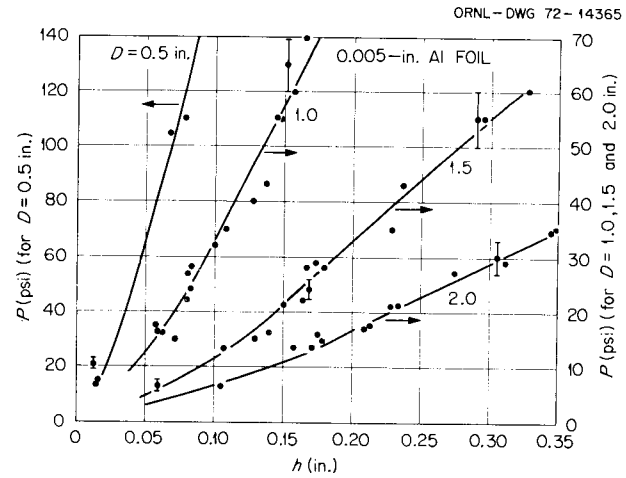


**Fig. 20.14. Pressure as a function of permanent deformation for 0.005-in.-thick aluminum foil.**

## Design of the Gage

The pressure gage was designed for low cost and ease of fabrication. No electronic equipment of any kind is needed in the operation of the gage. A typical gage is shown side-on in Fig. 20.15, and Fig. 20.16 shows the assembled gage and a smaller (6-in. steel pipe) gage.

The topmost protective plate prevents debris accelerated by the blast from puncturing the foil membranes, and it also assures that the shock wave is incident tangentially upon the membranes. The aluminum foil is sandwiched between ¼- and ⅛-in. plates; it is secured to the ¼-in. plate with an epoxy adhesive. Both 0.005- and 0.001-in. aluminum foil was used. A typical membrane plate should have several membranes with diameters between ½ and 2 in. After the shock wave, $h$ can easily be measured using an optical micrometer from either side of the membrane plate after disassembly.

## Experimental Field Results

Fourteen aluminum-foil pressure gages have been tested at the Mixed Company event, a detonation[19] of 500 tons of TNT on November 13, 1972. The gages were placed at predicted pressures ranging from 5 to 100 psi and, in two cases, in the immediate vicinity of standard transducer gages so that the technique could be compared with standard methods.

19. Middle North Series, Mixed Company Event, Technical and Administrative Document, Defense Nuclear Agency, Kirtland Air Force Base, April 1972.

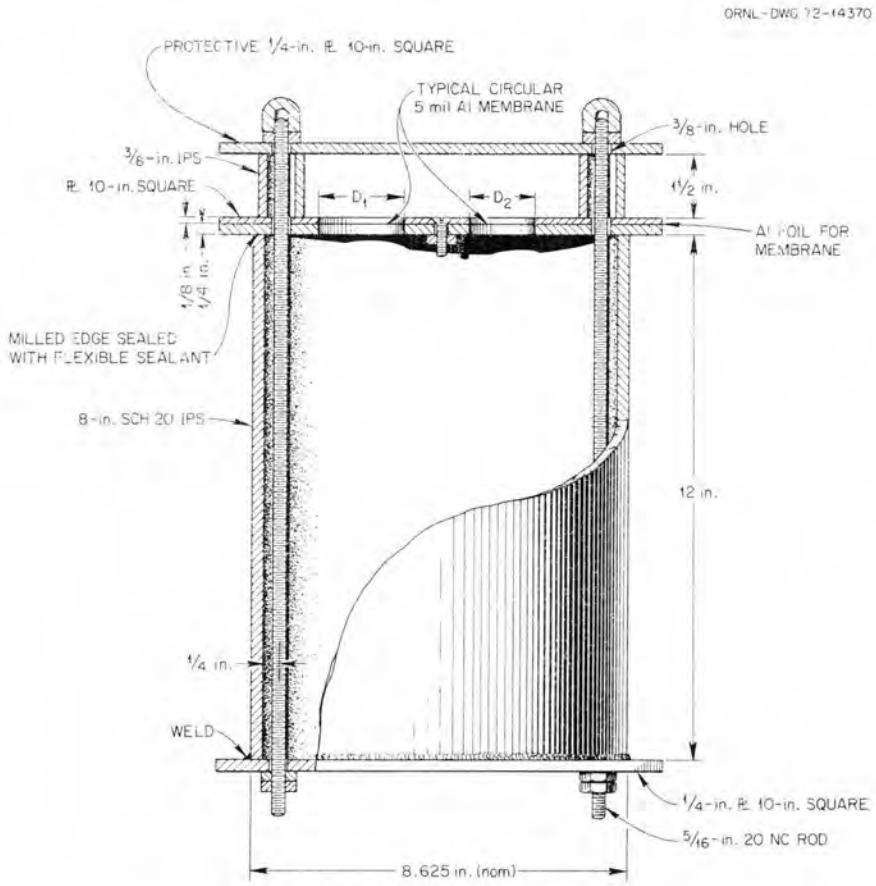


Fig. 20.15. Mechanical drawing (side view) of pressure gage.

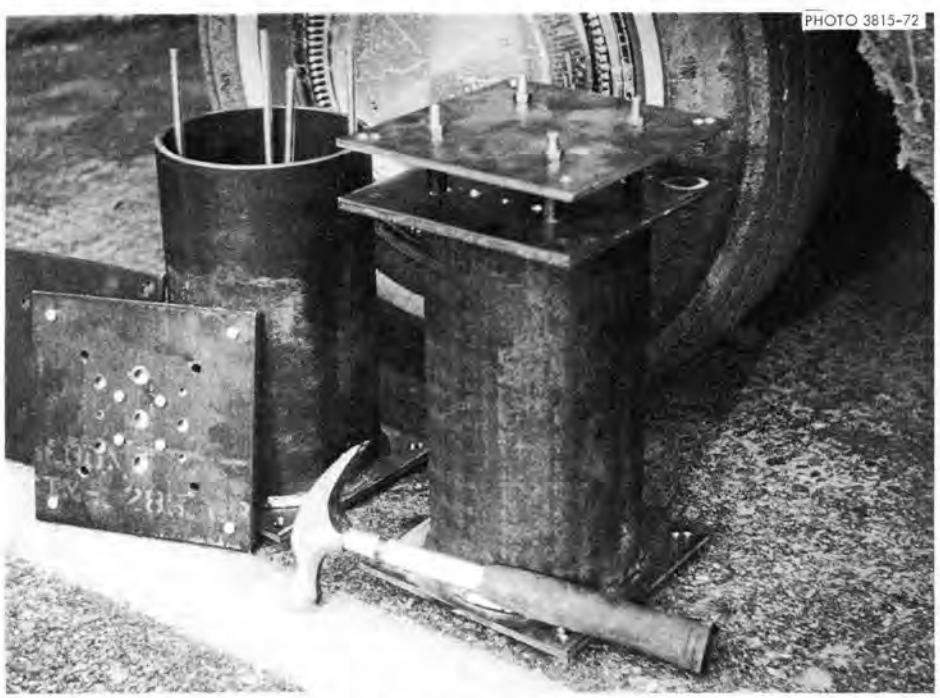


Fig. 20.16. Assembled 8-in. gage and a smaller (6-in.) gage shown partially assembled.

Approximately 75 membranes were tested. Figure 20.17 shows the ORNL foil membrane gage results, as well as the two transducer gage readings adjacent to two ORNL gages. The theoretical predicted pressure vs range curve is also shown. The agreement of the measurements is very good, with all accepted readings being well within the experimental errors.

The peak pressure at a particular location can be determined to an accuracy of about 10%, providing that the gage has several membranes. The data and the analysis are described more fully in ref. 15. A limitation of this method is its unreliability for recording a slowly rising overpressure (longer than 60 $\mu$sec), such as may occur inside a blast shelter with a small opening to the outside. Inaccurate readings can also result from multiple-step air shocks.

This gage should be designed with multiple membranes having diameters ranging between 2 in. and $\frac{1}{2}$ in. The stress-strain calibration curves given in this report and in more detail in ref. 15 can be used to make a reasonable estimate of the calibration for gages with aluminum-foil membranes of similar membrane thickness and diameter, provided that the shock wave is tangentially incident upon circular membranes.

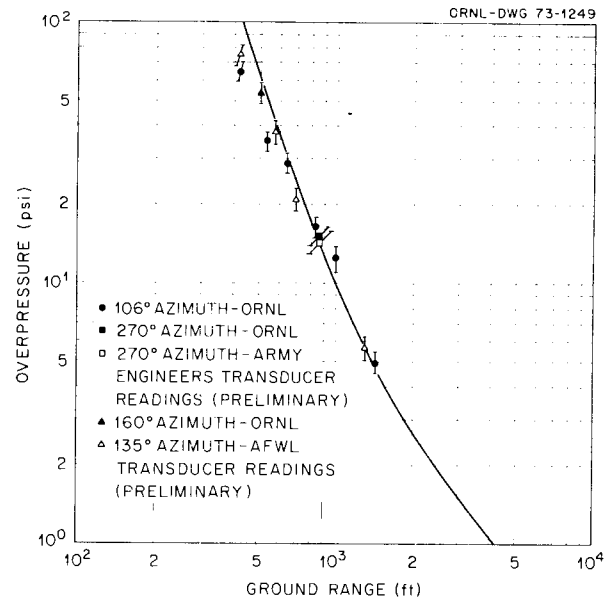


**Fig. 20.17. Recorded overpressures compared with predicted pressure-distance curve (ref. 19).** The ORNL membrane-gage experimental readings are shown as shaded symbols. The transducer readings are shown as unshaded symbols, for comparison. A 10% uncertainty was assigned to the transducer readings.

# 21. Effects on Civilian Systems from High-Altitude Detonations

J. K. Baird R. W. Manweiler
P. R. Barnes J. H. Marable
D. B. Nelson

## SURGES INDUCED IN TRANSMISSION SYSTEMS

An analysis of the effects of an electromagnetic pulse (EMP) from a high-altitude nuclear detonation on electrical systems may be broken into three parts: (1) a determination of the electromagnetic environment which can arrive at the energy-collecting parts of the system, (2) the calculation of the resulting current and voltage surges which are induced in the system by the incident wave, and (3) the effects of these surges on the system. These effects may imply a need for protective measures.

A comprehensive computer program has been developed which computes the important quantities in the first two of the above three parts. In particular, it computes currents and voltages in transmission systems as functions of time. In order to achieve this a number of essential subroutines were developed including Gaussian integration in the complex plane and the calculation of Bessel functions in the complex plane. The program is described as follows.

The determination of the electromagnetic environment consists mainly in (1) a choice of an incoming plane wave and (2) the reflection of the wave from the ground. The time dependence of the incoming wave is usually represented by a difference between two exponentials. Parameters of such a form have been reported previously.[1] Step functions are also of interest, and these options are also available in the program. Additional important parameters are the direction of propagation and the angle of polarization of the electric field.

The program has several options with respect to treatment of the ground reflection. It may be neglected or it may be based on a number of models. It can be specified by a given dielectric constant and a given conductivity or by given complex reflection factors, one for each of two independent polarizations. For example, a perfect conductor has reflection factors $-1$ and $+1$ for horizontal and vertical polarizations, respectively. The program can also provide a more realistic ground model with frequency-dependent dielectric constants and conductivity based on experimental measurements.

The transmission system is assumed to be made up of pieces consisting of transmission line segments and various lumped impedances. The transmission line segments are characterized by height, radius, and conductivity of the wire as well as the direction and length of the line. The impedances are circuit models of various components, mostly transformers and loads.

According to transmission line theory the currents and voltages in the system are related to the original EMP source through a set of intermediate quantities. These intermediate quantities are the currents which would be produced in each of the transmission lines if they were infinite in extent instead of being finite segments. They can be calculated on the basis of transmission line theory or as rigorous solutions to Maxwell's equations. Both options are available in the program.

Figure 21.1 shows the magnitude of the electric field of a representative EMP as a function of time. Figure 21.2 shows the component of the total (incident and reflected) electric field along a horizontal line in the plane of incidence 4 m above the ground. The incident EMP is assumed to come in 10° above the horizon with an electric field polarization 30° from the horizontal. The ground has frequency-dependent properties characterized by a low-frequency conductivity of 2 millimhos/m.

The voltage in Fig. 21.3 is that induced at the junction of a semi-infinite copper wire of radius 0.35

1. J. H. Marable, J. K. Baird, and D. B. Nelson, *Effects of Electromagnetic Pulse (EMP) on a Power System,* ORNL-4836 (1972).

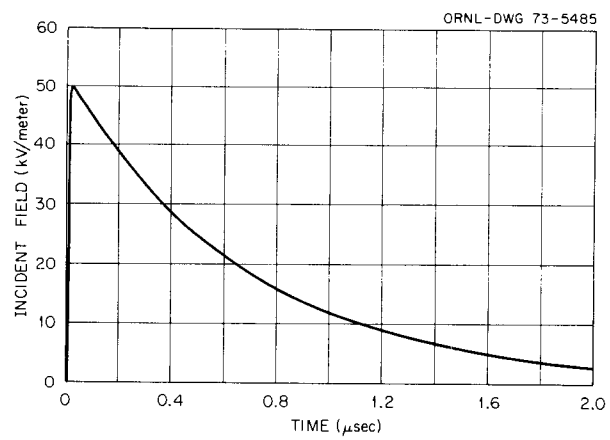


**Fig. 21.1. The magnitude of the incident electric field.**

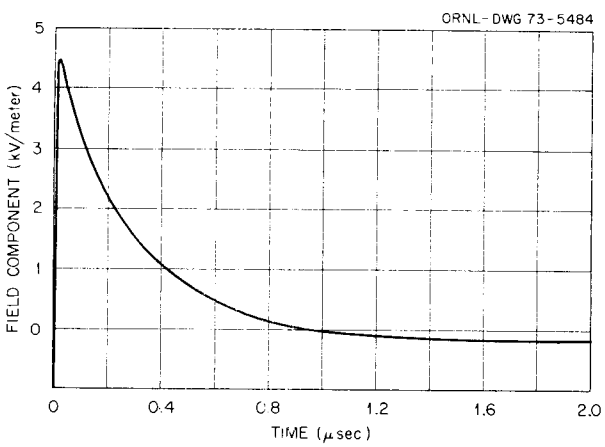


**Fig. 21.2. The component along the wire of the incident reflected electric field.**

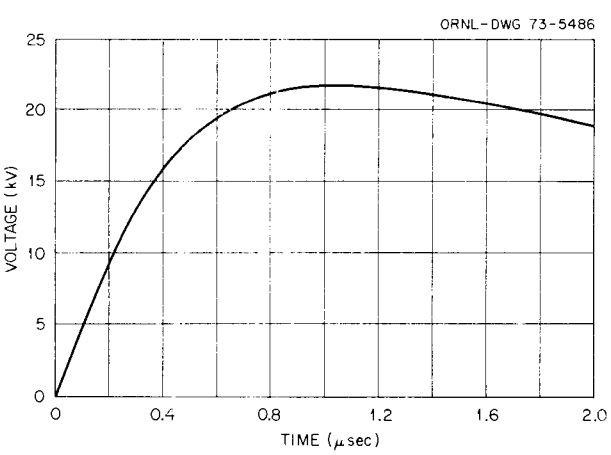


**Fig. 21.3. The voltage induced by the EMP at the junction of the line and the transformer coupled load.**

mm and a 600-Ω load coupled through a transformer. The variation of resistance with frequency is important in this case and is taken into account by the program. Note that transmission systems in general are more sensitive to low-frequency components than to high-frequency components. This is indicated for this specific case by the voltage of Fig. 21.3 having a slower time response than the EMP fields shown in Figs. 21.1 and 21.2.

Several modifications are presently being made on the program. They include (1) the induction of currents into vertical lines, (2) the addition of the voltage of the incident field to the induced voltage to obtain a total voltage, (3) the coupling between common mode and differential modes for multiple wire transmission systems, and (4) the induction and transmission of voltages and currents in underground lines.

## EFFECTS OF EMP ON THE SUPERVISORY CONTROL EQUIPMENT OF A POWER STATION

A previous study of the power system has shown that large currents and high voltages are likely to be induced in power lines by an incident EMP wave.[1] That study prompted this investigation of the supervisory control equipment associated with a power system.

The investigation confined itself to the following points of entry of the EMP into the supervisory control circuitry:

1. Induction of traveling currents in the power lines, which in turn induce electromotive forces in the secondary circuits of the current transformers monitoring the lines.
2. Direct induction of currents in exposed outdoor relay wiring.
3. Direct induction of currents in relay wiring contained in control houses.

The three points of entry were analyzed as follows:

1. A laboratory-scale experiment was performed to establish the transfer function of a typical current transformer. This was combined with calculations of the current induced in a power line[1] and the corresponding current and voltage in the secondary circuit of the transformer.
2. A typical outdoor relay wiring scheme was idealized as a loop circuit, and the current induced in the loop by the EMP magnetic field was calculated assuming a quasi-static approximation. This limited consideration to loops no larger than 1.2 m in diameter.

3. The shielding of relay circuitry contained in a metal control house was calculated using standard electromagnetic shielding data.[2] EMP fields leaking through nonconducting windows and doors penetrating the control house were also estimated. The relay circuits were idealized as before.

Damage to relays connected to the above circuits was assessed. It was found that if the relays were entirely electromechanical, damage which would prevent their further functioning was extremely unlikely, nor was it very likely that the currents induced in the circuits feeding the relays would cause them to operate falsely because of their great mechanical inertia. On the other hand, if the relays were constructed from semiconductor components, damage and false operation were very likely.

The following countermeasures were recommended:

1. Avoid routing relay control wiring along paths which form loops.
2. Use circuits with high intrinsic impedance with semiconductor relays to limit the current which can be induced in the loop.
3. Eliminate openings in control houses larger than 1 m on a side. Without these openings, only insignificant electromagnetic fields penetrate the control house.
4. Use surge arresters with high current capacity, preferably vacuum tube type.
5. When employing redundant relaying, run the wiring of the relays at right angles. Since the current induced in the wiring depends upon the polarization of the incident EMP and the orientation of the circuit, it is unlikely that the EMP will induce destructive currents in each of two circuits which travel in different directions.
6. Use logic circuitry to prevent false operation. EMP is likely to induce signals on all wires leading to a relay. By the addition of two transistors to a semiconductor relay, these common mode signals can be distinguished from the ordinary operating signals. This also protects the relay from the effects of its ordinary noise environment.

## THE STABILITY OF THE ELECTRIC POWER SYSTEM IN A NUCLEAR ELECTROMAGNETIC ENVIRONMENT

The stability of the electric power system in a nuclear electromagnetic pulse (EMP) environment is being studied. The electric power system may be perturbed by EMP to the extent that synchronism is lost, that is, the system becomes unstable.

The possible perturbations caused by EMP include[1] faults, that is, short circuits, on the low-voltage distribution systems or the high-voltage transmission system, relay malfunctions which would cause lines to open unnecessarily, loss of generation, and load shedding, that is, loss of load. The effects of the different types of perturbations are being studied using a digital stability computer program[3] which models the transmission system of the Eastern and Central states.

In order to simulate EMP effects, we have found that it is essential to study perturbations applied to extensive geographic areas, instead of severe perturbations in local areas. The effect of the geographic extent of the perturbation is illustrated in Fig. 21.4, which compares machine (i.e., generator) angles after different types of perturbations. Since the power transfer from a machine depends upon sin $\delta$, where $\delta$ is the machine angle, synchronism will be lost if the relative angles of connected machines differ greatly.

Figure 21.4 compares the effect of local vs widespread loss of load. The dashed curves show the machine angles after load reduction of 50% on a dozen busses – a severe perturbation, but still rather local. (A bus is a point where lines connect to other lines, loads, or machines.) The solid curves show the same machines after a load reduction of 50% on all major TVA busses. Note that even on bus 1740, which is a distant reference machine, there is a substantial difference between the two cases. This is primarily due, not to the increase in net load shed, but rather to the larger geographical extent of the perturbation. For when a local perturbation occurs, the remainder of the system helps to stabilize the perturbed area, even for a severe perturbation; that is, there is a large source to maintain the stability. But when the area of perturbation is extensive, such as is likely in an EMP environment, there is no unperturbed area to stabilize the system.

The stability program has also been used to calculate the following perturbation which could result from EMP. A fault was applied to a bus connected to the major 161-kV TVA busses through a pure reactance of 10 to 15%. This model should simulate the effect on

2. *DASA EMP (Electromagnetic Pulse) Handbook,* DASA 2114-1, DASA Information and Analysis Center, General Electric Company, TEMPO, Santa Barbara, Calif., September 1968, Chapter 9.

3. W. W. Maslin, S. T. Matraszek, C. H. Rush, and J. G. Irwin, *IEEE Summer Power Meeting and EHV Conference,* July 12–17, 1970; paper No. CP 684-PWR.

the TVA transmission system from *multiple faulting* of the 13.8-kV lines of the *distribution* system. After 0.2 sec the fault was removed and the system returned to normal for 0.3 sec. Then the bus was again faulted for a second time for 0.15 sec. After the second fault was removed the load on both the TVA and the major connecting transmission systems was reduced by 30% in order to simulate load shedding due to permanent opening of distribution lines. Three machine angles are plotted in Fig. 21.5. Note that machines No. 2 and No. 3 have lost synchronism with No. 1 (most of the system remained in synchronism with No. 1).

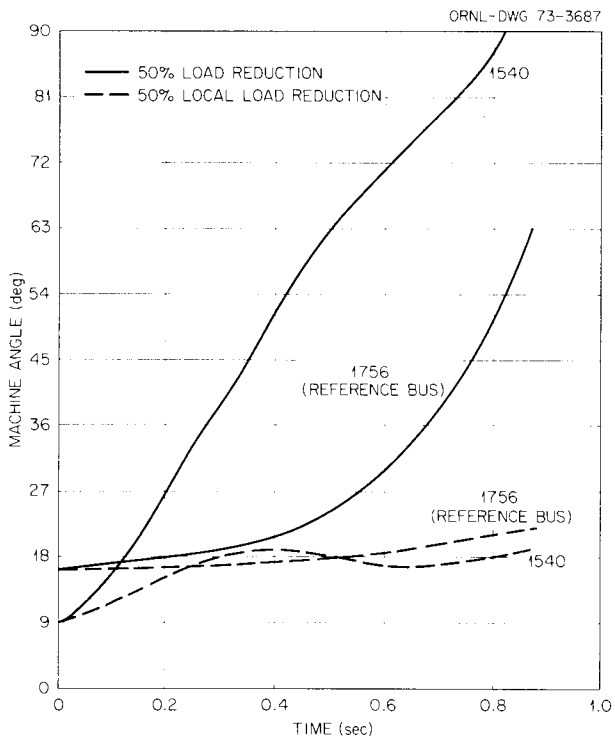


**Fig. 21.4. Machine angle as a function of time after load shedding.**

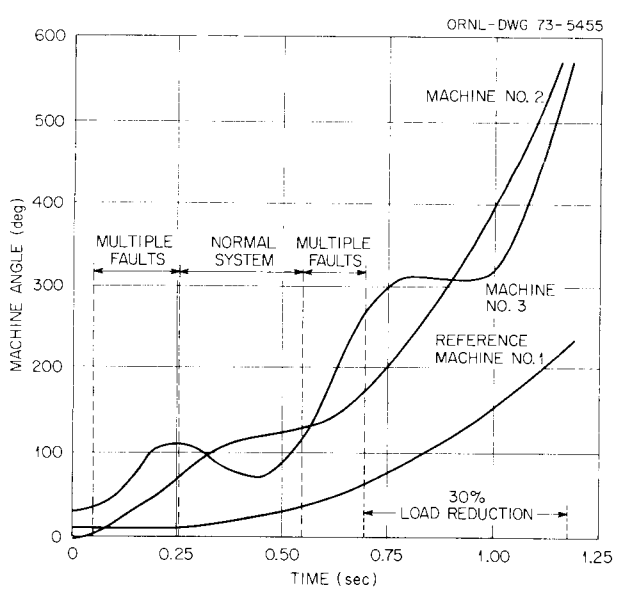


**Fig. 21.5. Machine angle as a function of time.** The fault characteristics are indicated on the time scale.

Consequently, it is possible that the extensive geographical perturbations induced by EMP on the distribution system may cause the transmission system to lose stability and to segment or necessitate the cessation of power generation until the power system can be brought back up. Our investigation is continuing in order to determine more precisely what possible EMP perturbations may occur and the effects which they will have upon the power system's overall stability.

## EFFECTS OF ELECTROMAGNETIC PULSE ON RADIO COMMUNICATIONS

Communications are essential to civil defense operations that provide the necessary emergency services to ensure national survival during and following a nuclear attack. Since much of the telecommunications, except in some local areas, are likely to be damaged by the attack, two-way radio communications will be required to fulfill much of the communications requirements. The available two-way radio communications for civil defense activities are primarily those communication networks in the land mobile class, owned by government, medical services, and utilities companies as well as those of the amateur and citizen's radio services. Most of these communication systems will be subjected to the intense transient electromagnetic pulse (EMP) environment created by both distant and near nuclear detonations.

The nuclear EMP has a large portion of its energy within the radio frequency spectrum. A portion of this energy will couple to the sensitive electronic circuits of communication systems with the possible result of system malfunction or failure. The major coupling mechanisms are antennas, control links, and the commercial power lines, all of which perform as inadvertent antennas to the EMP. Other coupling mechanisms include ground loops, direct electromagnetic interaction with equipment circuitry, and indirect coupling by the reradiation of energy collected by long metal structures such as pipes.

The EMP-induced surges available to communications equipment from power lines and phone line control links are similar to those caused by lightning. Voltage

peaks associated with these surges are likely to range from several kilovolts to about 50 kV. Conventional lightning arresters on the lines probably will not respond in time to significantly suppress these surges. Thus, to protect against EMP's additional surge suppressors are required at points near where power and phone lines are connected to equipment.

Antennas respond well to the EMP environment since they are designed for the transmission and reception of electromagnetic energy. The dominant EMP energy collected by the antenna has frequency components near the antenna's design frequency. Thus, this energy is well coupled to the receiver or transmitter connected to the antenna. For antennas in the HF, VHF, and UHF bands, the EMP energy received is approximately inversely proportional to the cube of the rf carrier frequency and ranges from several microjoules to about 50 J.

The EMP-induced voltage transients at the antenna's terminals have peak values that range from about 100 V for UHF unity gain antennas to about 200 kV for HF monopole antennas. Direct ground and standard air-gap antenna lightning protection is essentially no protection against these EMP-induced surges. To protect equipment circuitry against EMP-induced transients, a fast-response surge suppressor is required. Since EMP energy is also collected by the antenna feed-line cable, the protection should be provided near where the cable is connected to the equipment.

The probabilities of failure, in general terms, for typical communication systems without EMP protection are: (1) moderate for HF tube-type amateur systems, (2) moderately high for citizen's band and VHF low-band systems with solid-state receivers, (3) moderate for VHF high-band systems with solid-state receivers, and (4) moderately low for UHF systems. However, the probability of communications failure for these systems can be reduced to near zero by providing EMP protection and emergency backup equipment for some essential system components.

## THE VOLTAGE INDUCED IN INFINITE, LOSSLESS, TWO-WIRE TRANSMISSION LINE BY PARALLEL FINITE CURRENT SOURCES

The problem of a terminated two-wire transmission line illuminated by an external electromagnetic field has been treated in the frequency domain using transmission line theory by Taylor, Satterwhite, and Harrison.[4] Using these authors' results and ignoring losses, it is possible to obtain one-dimensional wave equations for the current and voltage, which can be integrated in the time domain by d'Alembert's method. These equations are

$$\frac{\partial V(z,t)}{\partial z} + L\frac{\partial I(z,t)}{\partial t} = \frac{\partial}{\partial t}\int_0^b B^i{}_y(x,0,z,t)\,dx\,, \qquad (1a)$$

$$\frac{\partial I(z,t)}{\partial z} + C\frac{\partial V(z,t)}{\partial t} = -C\frac{\partial}{\partial t}\int_0^b E^i{}_x(x,0,z,t)\,dx\,, \qquad (1b)$$

where $V(z, t)$ and $I(z, t)$ are the transmission line voltage and current, $L$ and $C$ are the inductance and capacitance per unit length of the line, $B^i{}_y(x, y, z, t)$ is the $y$ component of the incident magnetic field, $E^i{}_x(x, y, z, t)$ is the $x$ component of the incident electric field, and $t$ is the time. The spatial coordinates, the orientation of the line, and the spacing $b$ are as defined in Fig. 21.6.

We examine some of the consequences of these equations. Consider an infinitely long, lossless, two-wire transmission line immersed in an external electromagnetic field whose source is a current density $\mathbf{J}(x, y, z, t)$. If the transverse components of $\mathbf{J}$ are zero, that is, $J_x = J_y = 0$, then $V(z, t)$ and $I(z, t)$ satisfy the one-dimensional wave equations

$$\Box_z^2 V(z,t) = 0\,, \qquad (2a)$$

$$\Box_z^2 I(z,t) + u^2 C A^i{}_z(x,0,z,t)\Big|_{x=0}^{x=b} = 0\,, \qquad (2b)$$

respectively, where

$$\Box_z^2 \equiv \frac{\partial^2}{\partial z^2} - \frac{1}{u^2}\frac{\partial^2}{\partial t^2}\,,$$

4. C. D. Taylor, R. S. Satterwhite, and C. W. Harrison, Jr., "The Response of a Terminated Two-Wire Transmission Line Excited by a Nonuniform Electromagnetic Field," *IEEE Trans. Antennas Propagat.* **AP-13**, 987–89 (1965).

ORNL-DWG 73-408A

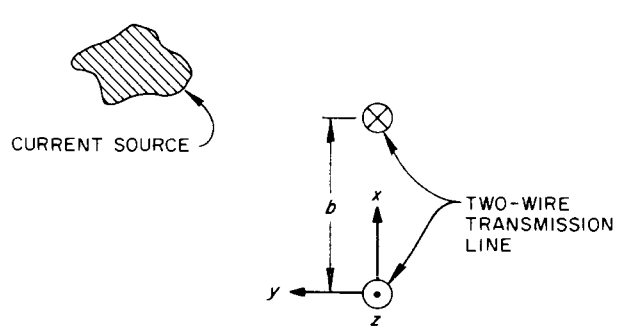


**Fig. 21.6. Two-wire transmission line and source of external fields.**

$A^i{}_z(x, y, z, t)$ is the $z$ component of the vector potential $\mathbf{A}^i(x, y, z, t)$ produced by $\mathbf{J}$, $u^2 = (LC)^{-1}$ is the speed of light in the medium containing the transmission line, and

$$A^i{}_z(x, 0, z, t) \Big|_{x=0}^{x=b} = A^i{}_z(b, 0, z, t) - A^i{}_z(0, 0, z, t).$$

Moreover, if $V(z, t)$ and $I(z, t)$ satisfy the homogeneous initial conditions

$$V(z, 0) = \frac{\partial V(z, 0)}{\partial t} = 0\,, \tag{3a}$$

$$I(z, 0) = \frac{\partial I(z, 0)}{\partial t} = 0\,, \tag{3b}$$

then the solutions to Eqs. (2) are

$$V(z, t) \equiv 0\,, \tag{4a}$$

$$I(z, t) = -u^2 C A^i{}_z(x, 0, z, t) \Big|_{x=0}^{x=b}\,, \tag{4b}$$

respectively.

It is a curiosity that the voltage on the line can be identically zero, while the current remains finite. To understand this apparent anomaly, we must recognize that $V(z, t)$ is a total voltage made up to a part due to the electric field scattered from the line and a part due to the incident field. For the situation of source and line described here, these two parts cancel one another exactly.

Equation (4*a*) may also be calculated directly from Maxwell's equations without reference to Eqs. (1). In this proof there are established vector and scalar potentials $\mathbf{A}(x, y, z, t)$ and $\Phi(x, y, z, t)$ from which the sum of the incident and scattered electromagnetic fields may be derived. We assume the wires making up the transmission line are thin so that they carry current only in the $z$ direction, which is also the direction of the source current. This implies that $\mathbf{A}$ has only a $z$ component and satisfies the Lorentz condition

$$\frac{\partial A_z(x, y, z, t)}{\partial z} + \frac{1}{u^2}\,\frac{\partial \Phi(x, y, z, t)}{\partial t} = 0\,. \tag{5}$$

Moreover, the $z$ component of the total electric field $E(x, y, z, t)$

$$\mathbf{E}(x, y, z, t) = -\frac{\partial \mathbf{A}(x, y, z, t)}{\partial t} - \nabla\Phi(x, y, z, t) \tag{6}$$

must be zero at the surface of either of the wires. Evaluating Eqs. (5) and (6) at the surfaces of the wires and eliminating the vector potential leads to the equations

$$\Box_z^2\, \Phi(b, 0, z, t) = 0\,, \tag{7a}$$

$$\Box_z^2\, \Phi(0, 0, z, t) = 0\,. \tag{7b}$$

If we assume that the total fields $\mathbf{E}(x, y, z, t)$ and $\mathbf{B}(x, y, z, t)$ are initially zero, it is sufficient for $\Phi$ to satisfy the initial conditions

$$\Phi(x, y, z, 0) = 0\,, \tag{8a}$$

$$\frac{\partial \Phi(x, y, z, 0)}{\partial t} = 0\,. \tag{8b}$$

These conditions plus Eqs. (7) require $\Phi$ to be identically zero at the surfaces of both wires. We calculate the transmission line voltage in terms of $\Phi$ as

$$V(z, t) = -\int_0^b E_x(x, 0, z, t)\, dx$$

$$= \int_0^b \frac{\partial \Phi(x, 0, z, t)}{\partial x}\, dx = \Phi(x, 0, z, t) \Big|_{x=0}^{x=b}\,.$$

Since $\Phi$ is zero at the surfaces of the wires $V(z, t)$ is identically zero, which is in agreement with the result from transmission theory given in Eq. (4*a*).

# 22. Emergency Planning for Accidental Radioactivity Releases from a Licensed Nuclear Facility[1]

R. O. Chester C. V. Chester

A few topics which affect the handling of an accidental radioactivity release from a nuclear power plant are discussed. The intent is to provide practical suggestions to supplement existing emergency plans and procedures. Pre-incident and the first few hours post-incident are the times of interest.

## TIME AVAILABLE TO INSTITUTE EMERGENCY PROCEDURES

Representatives of power companies with licensed nuclear facilities have indicated that backup emergency personnel would arrive no later than 1 hr after notification of an incident.[2,3] They also indicated that 3 hr after an incident at least temporary remedial procedures could be in effect. Reliance on backup personnel assumes that the entire complement of onsite personnel are unable to institute emergency actions. Calculations of fission product release from even a severe accident situation indicate that, if emergency personnel can restore or ensure the integrity of at least one level of containment in 1 to 3 hr from the time the release starts, only a very small fraction of the isotopes available for release will have escaped.[4] The considerable utility of badly damaged containment and an additional containment building are also demonstrated by these calculations.

## CHEMICAL PROPHYLAXIS

A number of chemical compounds can be ingested before or shortly after exposure to radioactive aerosols and gases to prevent the biological assimilation of the inhaled radioisotopes.[5] Radioiodine, radiostrontium, and radiocesium, in particular, were considered. While prophylaxis for radiostrontium and for radiocesium have been demonstrated, more work needs to be done with human volunteers to develop a workable schedule of prophylactic doses. In most imaginable accidents, radiostrontium and radiocesium would probably not be serious offsite hazards, and prophylactic compounds for those radioisotopes would be mainly of interest to emergency personnel involved in onsite operations.[6]

Radioiodine is usually considered a more credible offsite threat, and as a result more effort has gone into prophylactic radioiodine research. The English, for example, have stockpiles of stable iodine, as potassium iodate tablets, to be used in the event of a reactor accident. Since potassium iodate has not yet been approved for human use by the FDA in the United States, potassium iodide, a less stable and foul-tasting compound, is being considered for use in the U.S. In addition to potassium iodide and potassium iodate, a number of even more stable iodine-containing compounds that could be used for radioiodine prophylaxis were investigated. These have been used by the Morton Salt Company as an additive to salt for farm animals. A large fraction of Morton's salt is sold for use in animal husbandry; therefore, they have done research to identify iodine additive compounds that remain stable when the salt is left exposed to the weather. Table 22.1 (taken from ref. 1) lists the most promising radioiodine prophylactic compounds.

The problem of distributing prophylactic compounds has been considered. The effectiveness of the compounds is greatest if taken shortly before or at most

1. J. A. Auxier and R. O. Chester, *Report of the Clinch Valley Study, May 15–June 2, 1972,* ORNL-4835 (January 1973).
2. Ibid., p. 19, and personal communication, E. A. Belvin, Tennessee Valley Authority, Muscle Shoals, Ala.
3. Personal communication, S. A. Kingsbury, Florida Power and Light Co., Miami, Fla.
4. Ref. 1, Appendix 6.
5. Ref. 1, Appendix 4.
6. *Emergency Core Cooling Report of Advisory Task Force on Power Reactor Emergency Cooling,* W. K. Ergen, Chairman, TID-24226 (1971).

Table 22.1. Possible prophylactic iodine compounds

| Compound[a,b,c] | Solubility in Cold Water g/100 ml | Single Thyroid Blocking Dose | Toxicity Probable Lethal Dose 70 kg Adult | Taste | Stability in Storage | Current Use |
|---|---|---|---|---|---|---|
| KI, Potassium Iodide | 127.5 | 100 mg[d] | 35,000 to 350,000 mg[e] (similar to NaCl and sodium bicarbonate). | Strong, nauseating. May be difficult to give to infants and children. | Slightly delequiescent in moist air. Decomposes and discolors with long exposure to air, light, and moisture.[f,g] | Table salt additive in the USA (used in about 50% of iodized table salt). |
| $KIO_3$, Potassium Iodate | 4.74 | 130 mg | 80,000 mg[h] | Nearly tasteless | Iodates are much more stable in air, light, and moisture than iodides. The iodates are listed in order of increasing stability.[i] | Recommended by World Health Organization for table salt additive (used in about 50% of iodized table salt[e,j]). |
| $Ca(IO_3)_2$, Calcium Iodate | 0.427[c] | 120 mg | 25,000 mg[h] This toxicity group is similar to aspirin and quinine.[e] | | | Salt additives for farm animals.[i,j] |
| $Ca_5(IO_6)_2$, Pentacalcium Orthoperiodate[k] | 0.0063[c] | 200 mg | 50,000 mg[h] | | | |

[a]All the listed compounds make iodine available to the thyroid equally rapidly.[b,c]

[b]J. K. Miller, UT-AEC Agricultural Research Laboratory, Oak Ridge, Tennessee (personal communications).

[c]H. W. Fiedelman, Morton Salt Company, Woodstock, Illinois (personal communications).

[d]D. Ramsden, F. H. Passant, C. O. Peabody, and R. G. Speight, Health Phys. 13, 633-646 (1967).

[e]Gleason, Gosselin, Hodge, and Smith, Compilers, Clinical Toxicology of Commercial Products, Third Edition (The Williams and Wilkins Co., Baltimore, Md., 1969).

[f]Paul G. Stecher, Ed., The Merck Index, Eighth Edition (Merck and Co., Inc., Rahway, N. J., 1968).

[g]As a table salt additive, KI is stabilized by adding 0.04% dextrose and a trace of bicarbonate. With the additives the iodide is still not as stable as the iodate.

[h]E. J. Kuhajek and G. F. Andelfinger, J. Animal Sci. 31, 51-58 (1970).

[i]J. K. Miller, B. R. Moss, E. W. Swanson, P. W. Aschbacher, and R. G. Cragle, J. Dairy Sci. 51(11), 1831-1835 (1968).

[j]Iodates are not yet approved for human use in the USA by the FDA. The main objection the FDA has to the use of $KIO_3$ is that the required two-year feeding studies on two species of animals have not been carried out. The approximate cost of the studies would be $50,000.[c]

[k]Patent applied for by the Morton Chemical Co., Division of Morton International, Inc.

within a half-hour after exposure.[7] While it might be possible to reach the population at risk by radio, TV, or telephone within this time, it might *not* be possible to distribute the chemical compound within that time. One specific suggestion is to use the electric meter on each household as a pre-positioning storage point. That is, enough potassium iodate in tablet form to supply an average family could be sealed in a plastic tag and attached to the electric meter for each family. The tag could be installed and inspected regularly by the electric company with very little additional effort or cost. Repeated tampering could be discouraged by slightly increasing that month's electric bill when the tag has to be replaced. Pre-positioning the compounds particularly in a higher-risk area such as the low-population zone immediately surrounding the reactor might be worth while. The tag might also be utilized more widely in areas that are regularly isolated, such as areas that are snowed in each year.

## IMPROVISED RESPIRATORY PROTECTION

One good way to prevent the ingestion of radioisotopes is to filter air before breathing it. Experiments carried out at Fort Detrick in 1958 have shown that quite good respiratory protection can be improvised from household materials.[8] For example, two layers of bath towel filter out about 85% of particles that would be inhaled. Wetting the towel does not increase the filtering efficiency but rather just makes it necessary to use extra effort inhaling and exhaling. Many of the problems of stockpiling and distributing equipment could be avoided if common household items could be used in a time of emergency.

Some mention has been made recently of using civil defense shelters in the event of the release of radioactivity from a reactor.[9] If this suggestion is implemented, improvised respiratory protection might prove valuable in such shelters. In a reactor accident, it is probable that much of the danger would be from inhalation of radioactive aerosols, and civil defense shelters are usually designed for blast and fallout protection with no filtering of the air intake.

## DOSE AND DEPOSITION ESTIMATION

A method has been developed for estimating the dose from inhalation of radioactive aerosols as well as the amount of radioactive material deposited on the ground during and after a release. The output gives dose as a function of time after release and spatial position with respect to the release point. The plume created by the aerosol as it is released is followed through changes in wind direction, wind speed, and atmospheric stability conditions. The quantity of radioactive material assumed to be released under various conditions is taken from the Clinch Valley Study.[1]

Actual hourly meteorological data near the assumed release point are reviewed for a number of years, and conditions which give worst inhalation dose are determined. These more realistic doses are significantly lower than the worst inhalation doses obtained from two other previously accepted estimation procedures: those given in WASH-740 and licensing guidance on reactor siting.[10,11] These older procedures assume unrealistic persistence of slow dispersion conditions.

---

7. *Radiobiology Forum on Radioiodine,* March 3, 1970, Medical Research Council, 20 Crescent, London WIN 4 AL.

8. H. G. Guyton, H. M. Decker, and G. T. Anton, "Emergency Respiratory Protection against Radiological and Biological Aerosols," *AMA Arch. Ind. Health* **20,** 91–95 (August 1959).

9. Personal communication, C. R. Siebentritt, Defense Civil Preparedness Agency, Pentagon, Washington, D.C.

10. *Theoretical Possibilities and Consequences of Major Accidents in Large Nuclear Power Plants,* WASH-740 (1957).

11. J. J. DiNunno, F. D. Anderson, R. E. Baker, and R. L. Waterfield, *Calculation of Distance Factors for Power Test Reactor Sites,* TID-14844 (1962).

# Part VI. Education and Information

J. E. Turner

The Education and Information Section was formed in July 1972 to plan and coordinate the Division's educational programs and to develop a Health Physics Information System to serve the needs of the Division, the AEC, and the profession of health physics.

## 23. Education and Vocational Training

M. F. Fair J. C. Hart
J. E. Turner

Demands for training in health physics have continued to grow. Education at the Ph.D. level is required to provide personnel for positions of leadership in industrial, academic, and medical institutions. Training at the master's level is needed to provide the leaders in the applied health physics field with emphasis on instrumentation and procedures. The needs of the reactor and other nuclear-related professions must be met by large numbers of technicians with a B.S. degree. Over the past year, special efforts have been devoted in the Division to a program to train health physics technologists at this level.

A recent survey[1] shows that only 49 undergraduates were enrolled in the fall of 1971 in all subfields of radiation protection among the principal schools that offer radiological training programs. (In contrast, there were 559 graduate students enrolled.) Four bachelor's (and 201 graduate) degrees were awarded in radiation protection fields between July 1, 1970, and June 30, 1971.

Our estimates of the numbers of new health physics technologists needed for various activities by 1985 are shown in Table 23.1. Over the next 12 years until 1985, the average number of new technologists needed annually is between 275 and 500. Based on Table 23.1, the needs will occur rather evenly for each activity. The nuclear power program, including fuel recycling operations, will require between 950 and 1500 persons. Nuclear medicine and "other" nuclear applications will utilize between 1200 and 2500. The increasing Federal, State, and local regulatory activities will require an additional 500 to 1000 technologists. Between 650 and 1000 additional persons will be needed to replace present workers who will retire, die, or change their specialty.

To help meet the growing demands for radiation protection specialists, the Health Physics Division developed and proposed to the AEC a "Cooperative Training Program for Bachelor of Science Students – Health Physics Technologists." Under this program, undergraduate students come to ORNL from any university in the United States for a 12-week (one academic quarter) on-the-job training period, to be followed by a second such period at a later time during their undergraduate studies. The students are required to be science or engineering majors. The Oak Ridge training is given in addition to the students' normal academic requirements

**Table 23.1. Estimated numbers of newly trained health physics technologists needed for various activities by 1985**

| | Minimum | Maximum |
|---|---|---|
| Nuclear medicine | 500 | 1500 |
| Nuclear power | 750 | 1000 |
| Replacements for present personnel | 650 | 1000 |
| Regulatory | 500 | 1000 |
| Fuel cycles | 200 | 500 |
| Other nuclear applications | 700 | 1000 |
| | 3300 | 6000 |

1. *Radiation Protection Enrollment and Degree Survey,* U.S. Atomic Energy Commission, Division of Nuclear Education and Training, November 1972 [WASH-1229(72)].

for a bachelor's degree at the university in which they are enrolled.

Beginning in FY 1973 this program was funded by the AEC. A single recruiting trip was made in the fall of 1972 to several universities in the Appalachian region. There was enthusiastic response to the program by the students and faculty contacted. An initial group of seven students (from the Virginia Polytechnic Institute and the Georgia Institute of Technology) came to ORNL in January of this year. Five of these students returned in May 1973 for their second period of training. In addition, five new students were selected for training in FY 1974.

The Division provided assistance to the staff of the University of Tennessee in updating and teaching its graduate curriculum in health physics. The Division staff gave courses in General Health Physics, Radiation Chemical Physics, the Physics of Polyatomic Molecules, the Interaction of Electrons with Gases, the Interaction of Electrons with Solids, and the Interaction of Radiation with Matter. This curriculum has attracted students in both the master's and Ph.D. programs.

Assistance and consultation are available to any school desiring to set up a health physics program or institute courses in this field. Queries in this regard have been received from numerous schools throughout the country. Assistance was given the University of Tennessee in the preparation of qualifying examinations in health physics. A visit to ORNL with lectures and tours was provided for students in health physics from the University of Arkansas. Several universities were visited, and ORNL health physics research and educational activities were discussed.

There were a number of Oak Ridge Graduate Fellows, AEC Fellows, USPHS students, and others working on theses for advanced degrees under the supervision of the staff of the Fundamental Health Physics Research Section and the Radiation Research and Development Section. Their names, thesis titles, and universities are listed elsewhere in this report.

Assistance was given to Oak Ridge Associated Universities (ORAU) in the presentation of a ten-week course in health physics.

Two student trainees spent the summer of 1972 in the Division as research participants sponsored by ORAU. Five student trainees spent the summer of 1973 in the Division.

Several staff members of the Fundamental Health Physics Research Section of the Health Physics Division worked with the University of Tennessee faculty in preparing preliminary examinations for the Ph.D. degree and in grading the examinations. Four of our staff hold Ford Foundation appointments at the University and in this capacity participate in student advising on matters of curricula and research. They were also active on the University Committee on Graduate Education. Our staff took part in the faculty meetings of the University of Tennessee Physics Staff.

Nine students were enrolled in the General Health Physics undergraduate course (Physics 4710-20-30) taught by a member of the Division at the University of Tennessee. This was a three-quarter course which met 3 hr/week.

Seven Fellows participated in the summer training program at ORNL during July and August 1972 – two from the University of Kentucky, three from Vanderbilt University, one from the Georgia Institute of Technology, and one from the University of Tennessee. Two Fellows were in training during May and June 1973. The summer training began with a three-day orientation program, which was followed by five weeks with the applied health physics group and five weeks with the research health physics groups. The students spent one week at the Special Training Division of ORAU performing health physics experiments. Numerous seminars were held throughout the summer, highlighting recent advances in health physics and closely allied fields. Many of the seminar speakers were from laboratories and universities from around the world.

In the applied health physics training, the student gains practical experience in many phases of radiation protection under the supervision of a senior health physicist. In health physics research the students are first given a brief summary of all the research projects in progress in the Division. They then choose the group in which they remain for a five-week period. They thus become part of a team and are truly engaged in doing health physics research under senior-scientist supervision.

The summer program gives the student sufficient experience in applied health physics to enable him to take a position in this field, where with only a little additional experience he will soon qualify for a position of responsibility in radiation protection. Also, he learns of the tremendous breadth of research in health physics and is made aware of the diverse problems available for thesis work, should he decide to continue his education for the M.S. or the Ph.D. degree.

The AEC Radiation Science and Protection Fellowship program, which was started in 1950 to provide first-year graduate-level training in health physics, was terminated as of June 30, 1973.

A staff member from the Fundamental Health Physics Research Section was a consultant to the International

Atomic Energy Agency from mid-July to mid-September 1972. He presented a series of special lectures on Radiation Interactions in Condensed Media to the staff at the Directorate of Radiation Protection at the Bhabha Atomic Research Centre, Bombay, India. He also acted as consultant to the staff of the Directorate. Another staff member, assigned both to the Fundamental Health Physics Research and the Education and Information sections, was a consultant to the World Health Organization during January and February 1973 at the Bhabha Centre. He assisted in teaching a course in Hospital Physics for the Directorate of Radiation Protection.

# 24. Health Physics Information System

K. Becker
S. R. Bernard
J. C. Hart
C. F. Holoway
B. L. Houser
J. E. Turner

Until this year, the only formally organized information group in the Health Physics Division was the Information Center for Internal Exposure (ICIE). This activity, beginning in 1948, was organized as a Center in 1965 and was partially computerized, starting in 1970, through existing facilities of the Nuclear Safety Information Center. The scope of ICIE has been the estimation of dose received by the tissues of man from internally deposited radionuclides derived from natural background, weapons fallout, mining operations, industrial manufacture, nuclear power operations, nuclear fuel reprocessing, and medical therapy and diagnosis – in other words, from all radionuclides that constitute an internal hazard to man. The services of this Center include answering technical internal-exposure inquiries, preparing data compilations, and constructing mathematical models of metabolic processes. The Center has provided interpretations and recommendations, based upon the metabolic literature, to a number of government agencies, the National Council on Radiation Protection and Measurements (NCRP), and the International Commission on Radiological Protection (ICRP).

The formation of the Education and Information Section brought into focus the desirability of utilizing the Division's resources and expanding its information activities into other areas of health physics. A number of the staff, who have engaged in such activities as a normal part of their research, provided guidance in the design of a comprehensive system to satisfy the diverse needs of the Division. By January 1973, a Health Physics Information System (HPIS) had become operational on a pilot scale. The HPIS utilizes the extensive computer software and hardware systems available at ORNL – in particular, those of the Environmental Information System and the Nuclear Safety Information Center.[1] The HPIS is compatible with these systems. Although it exists now only on a pilot scale, the HPIS is designed so that it can expand as support warrants into virtually any area of health physics, for example, solid-state dosimetry; neutron dosimetry; the interaction of radiation with gases, liquids, and solids; mathematical modeling; radiotherapeutic properties of ions; and the demographics of power-source siting.

The Health Physics Information System possesses some unique features, not common to all information centers. It stresses quality of input, rather than quantity. Experts in various fields from within the Division provide the primary guidance in the selection of units (i.e., papers, reports, and personal scientific files) to be considered for HPIS. Interested scientists themselves will provide the input to HPIS and use it in their work. For the generalist or specialist outside a given field, supplemental material is entered to increase the usefulness of HPIS.

1. We gratefully acknowledge the assistance of the Environmental Information System and the Nuclear Safety Information Center.

# Theses, Papers, Publications, and Lectures

## Theses

Gerald D. Alton
*Electron Scattering from Simple Atomic and Molecular Systems: A Study of the Phenomenological and Microscopic Optical Models,* ORNL-TM-4826 (November 1972) (University of Tennessee)

D. M. Bartell
*Time-Dependent Vacuum Ultraviolet Emission of Helium,* ORNL-TM-3918 (September 1972) (University of Kentucky)

Liliana Deleanu
*Dissociative Ionization of Molecules by Electron Impact* (in preparation) (University of Tennessee)

C. E. Easterly
*Fluorescence Emission from the Second Excited π-Singlet States of Aromatic Molecules in Solution,* ORNL-TM-2616 (May 1973) (University of Tennessee)

K. Gant
*Electron Capture and Drift in Organic Liquids* (in preparation) (University of Tennessee)

R. E. Goans
*Electron Attachment to Molecules in High Pressure Gases* (in preparation) (University of Tennessee)

A. Hadjiantoniou
*Long-Lived Parent Negative Ions of Polyatomic Molecules Formed via Nuclear-Excited Feshbach Resonances,* ORNL-TM-3990 (April 1973) (University of Tennessee)

J. Johnson
*Organic Negative Ions* (in preparation) (University of Tennessee)

D. L. McCorkle
*Study of Low-Energy Electron Attachment to Molecules at High Densities,* ORNL-TM-3839 (July 1972) (University of Tennessee)

V. N. Neelavathi
*Collective Effects in Charged Particle Track Structure* (in preparation) (University of Tennessee)

M. N. Pisanias
*Threshold-Electron Excitation and Compound Negative Ion Formation in Polyatomic Molecules,* ORNL-TM-3904 (August 1972) (University of Tennessee)

J. E. Talmage
*Transport of Resonance Radiation in Argon* (in preparation) (University of Kentucky)

I-Lan Tang
*Optical Properties of Guanine, Thymine, Adenine, and Cytosine* (in preparation) (University of Tennessee)

R. B. Vora
*Theory of Single Electron Excitation and Transfer in Neutral Atom-Atom Collisions,* ORNL-TM-4239 (University of Tennessee)

C. Wheeler
*Experimental Studies of the Interaction of Electrons with Diffraction Gratings: The Smith-Purcell Effect* (in preparation) (University of Tennessee)

J. F. Wilson
*Mass Analysis of Ions Formed in Electron Swarm Experiments* (in preparation) (University of Tennessee)

# Papers

E. T. Arakawa
*Satellites in the K X-Ray Emission Spectra of Li and Be,* American Physical Society, March 19–22, 1973, San Diego, California.

J. K. Baird
*The Electromagnetic Pulse and the Electric Power System,* North American Power Systems Interconnection Committee Meeting, Jackson, Mississippi, March 15, 1973.

P. R. Barnes
*On the Singularity Expansion Method as Applied to the Cylindrical Dipole Receiving Antenna,* IEEE/G-AP Symposium, University of Colorado, August 21–24, 1973.

D. M. Bartell and G. S. Hurst
*Excitation and Ionization of Helium by Fast Protons and by Their Associated Secondary Electrons,* 25th Annual Gaseous Electronics Conference, October 17–20, 1972, London, Ontario, Canada (presented by D. M. Bartell).

K. Becker
*Progress in Solid-State Fast Neutron Dosimetry at ORNL,* IAEA Symposium on Neutron Monitoring for Radiation Protection Purposes, Vienna, Austria, December 11–15, 1972.

*Recent Progress in Solid-State Dosimetry Research and Applications,* USAEC Biomedical Directors' Meeting, ORNL, April 9–10, 1973.

*The Publication Explosion – Distill or Drown,* Health Physics Society Annual Meeting, Miami, Florida, June 17–21, 1973.

*Solid-State Neutron Personnel Dosimetry Research at ORNL,* Fourth USAEC Workshop on Personnel Neutron Dosimetry, Miami, Florida, June 14–15, 1973.

K. Becker, J. S. Nagpal, J. S. Cheka, and M. Sohrabi
*Fading of Solid-State Dosimeters and Film at Increased Temperatures and Humidities,* Third International Conference on Medical Physics, Göteborg, Sweden, July 30–August 4, 1972 (presented by K. Becker).

Werner Brandt and R. H. Ritchie
*Interaction Mechanisms in the Physical Stage,* Conference on Physical Mechanisms in Radiation Biology, October 11–14, 1972, Arlie, Virginia.

C. V. Chester and L. Dresner
*Attenuation of Shock Waves in Long Pipes by Orifice Plates, Rough Walls, and Cylindrical Obstacles,* Third International Symposium on Military Applications of Blast Simulators, September 19–21, 1972, Schwetsingen, Germany.

C. V. Chester and R. O. Chester
*Interaction of the Structure of a Selected Reactor Containment with Near Kilobar Nuclear Weapon Shock-Waves in Air,* Third International Symposium on Military Applications of Blast Simulators, September 19–21, 1972, Schwetsingen, Germany.

R. O. Chester and C. V. Chester
*A Protective Containment System for Large Nuclear Power Plants,* Health Physics Society Meeting, June 17–21, 1973.

L. G. Christophorou
*Photon and Electron Interactions with Organic Molecules,* Radiological Physics Contractors Meeting, February 15–16, 1973, Tallahassee, Florida.

*Electron Mobilities in Gases and Liquids,* Miller Conference, April 9–13, 1973, North Wales.

*Long-Lived Organic Negative Ions,* Miller Conference, April 9–13, 1973, North Wales.

R. N. Compton, C. D. Cooper, W. T. Divver, and P. W. Reinhardt
*Molecular Electron Affinities from Collisional Ionization of Cesium: $SF_6$ and $TeF_6$,* 25th Annual Gaseous Electronics Conference, October 17–20, 1972, London, Ontario.

C. D. Cooper and R. N. Compton
*Dissociative Electron Attachment Cross Sections of $\sim 10^{-14}$ $cm^2$ Observed for $C_4F_4O_3$ and $C_5F_6O_3$,* American Physical Society, Southeastern Section, November 16–18, 1972, Birmingham, Alabama.

G. A. Cristy, J. C. Bresee, and W. C. McClain
*Some Comparisons of Continuous and Pulsed Jets for Excavation,* First International Symposium on Jet Cutting Technology, Coventry, England, Paper B-9, April 1972.

F. J. Davis and D. R. Nelson
*Longitudinal Diffusion Coefficient and Drift Velocity Measurements,* 25th Annual Gaseous Electronics Conference, October 17–20, 1972, London, Ontario (presented by R. N. Compton).

H. W. Dickson
*Short Training Courses,* Combined Meeting of the Atlanta and East Tennessee Chapters, Health Physics Society, Chattanooga State Technical Institute, October 20–21, 1972.

C. E. Easterly and L. G. Christophorou
*Temperature Dependence of the Fluorescence Emission from the First- and Second-Excited π-Singlet States of Aromatic Hydrocarbons in Solution,* Radiation Research Society, April 29–May 3, 1973, St. Louis, Missouri.

M. M. A. El Razek, R. B. Gammage, and K. Becker
*Directional Response of TSEE Fast Neutron Dosimeters,* Health Physics Society Annual Meeting, Miami, Florida, June 17–21, 1973 (presented by M. M. A. El Razek).

R. B. Gammage and J. S. Cheka
*Toward a Practical TSEE Dosimetry System Using BeO Ceramic Detectors,* Health Physics Society Annual Meeting, Mimai Beach, Florida, June 17–21, 1973 (presented by R. B. Gammage).

R. B. Gammage, H. F. Holmes, E. L. Fuller, Jr., and D. R. Glasson
*Pore Structures Induced by Water Vapor Adsorbed on Nonporous Lunar Fines and Ground Calcite,* 47th National Colloid Symposium, Carlton University, Ontario, Canada, June 18–20, 1973 (presented by H. F. Holmes).

R. E. Goans and L. G. Christophorou
*Electron Attachment to Molecules in High-Pressure Gases,* Radiation Research Society, April 29–May 3, 1973, St. Louis, Missouri.

C. M. Haaland
*Mapping of Population Density,* Southern Sociological Society Meeting, Atlanta, Georgia, April 13, 1973.

R. N. Hamm, H. A. Wright, and J. E. Turner
*Calculation of Dose from Negative Pions in Soft Tissue and Bone,* Health Physics Society, June 17–21, 1973, Miami Beach, Florida.

F. F. Haywood
*Intercomparisons of Neutron Monitors under Conditions of Simulated Nuclear Accidents,* IAEA Symposium on Neutron Monitoring for Radiation Protection Purposes, Vienna, Austria, December 11–15, 1972.

*Radiation Research and Development – Overview,* USAEC Biomedical Directors' Meeting, ORNL, April 9–10, 1973.

Mary Jane Hilyer and W. S. Snyder
*Estimates of Dose from Xenon-133 to Infants and Children for Immersion in an Infinite Cloud and for Medical Uses,* 7th Midyear Topical Symposium of the Health Physics Society, "Health Physics in the Healing Arts," December 11–14, 1972, San Juan, Puerto Rico.

G. S. Hurst
*Excited States and Energy Pathways in Noble Gases,* 21st Annual Meeting of the Radiation Research Society, April 29–May 3, 1973, St. Louis, Missouri.

G. S. Hurst, D. M. Bartell, and E. B. Wagner
*Model for Vacuum Ultraviolet Emission and Energy Pathways Following Proton Excitation of Helium,* 25th Annual Gaseous Electronics Conference, October 17–20, 1972, London, Ontario, Canada (presented by D. M. Bartell).

G. S. Hurst and W. R. Garrett
*An Operational Approach to Radiation Protection,* Health Physics Society's Mid-Year Topical Symposium, San Juan, Puerto Rico, December 11–14, 1972 (presented by W. R. Garrett).

T. D. Jones
*The Effects of Energy and Beam Collimation on the Treatment of Neoplasms Injected with a Thermal Neutron Receptive Isotope,* Health Physics Society's Seventh Mid-Year Topical Symposium, San Juan, Puerto Rico, December 11–14, 1972.

C. H. Kearny
*Expedient Shelter Test,* Defense Nuclear Agency's MIXED COMPANY Event, DOD Nuclear Information and Analysis Center Symposium, Santa Barbara, California, March 12–15, 1973.

C. E. Klots
*Thermochemical and Kinetic Information from Metastable Decompositions of Ions,* 21st Annual Conference on Mass Spectrometry and Allied Topics, May 20–25, 1973, San Francisco, California.

E. S. Lee and R. C. Taeuber
"Organizing Census Results for Use by Social Scientists," *Proceedings of Social Science Section, American Statistical Association,* 1972 Meetings, March 1973.

D. B. Nelson
*Effects of EMP on Power Systems,* Defense Electric Power Administrators Seminar, Atlanta, Georgia, March 1, 1973.

K. P. Nelson
"Urban Growth Patterns: The Atlanta Experience," presented at the Symposium on the Labor Force: Migration, Earnings, and Growth, Muscle Shoals, Alabama, June 22–23, 1972.

M. N. Pisanias, L. G. Christophorou, J. G. Carter, and D. L. McCorkle
*Compound-Negative Ion Resonance States and Threshold-Electron Excitation Spectra of N-Heterocyclic Molecules: Pyridine, Pyridazine, Pyrimidine, Pyrazine, and sym-Triazine,* 4th Annual Meeting of American Physical Society, Division of Electron and Atomic Physics, November 29–December 1, 1972, Menlo Park, California (presented by D. L. McCorkle).

J. W. Poston
*Health Physics Challenges in the Southeast: Research and Industry,* Joint Meeting of the Atlanta and East Tennessee Chapters of the Health Physics Society on Health Physics Challenges in the Southeast, October 20–21, 1972, Chattanooga State Technical Institute, Chattanooga, Tennessee.

J. W. Poston, G. G. Warner, M. Rosenstein, and R. H. Schneider
*Calculation of Dose to Selected Organs from Monoenergetic X-Ray Beams Incident on a Heterogeneous and Anthropomorphic Phantom,* Health Physics Society, Seventh Mid-Year Symposium "Health Physics in the Healing Arts," December 11–14, 1972, San Juan, Puerto Rico.

R. H. Ritchie

*Surface Excitations in Solids,* Structure of Matter Conference on "Polaritons," October 2–6, 1972, Taormina, Sicily.

*Plasma Oscillations in Thin Films,* 9th Annual Symposium of the New Mexico Chapter of American Vacuum Society, April 9–11, 1973, Albuquerque, New Mexico.

J. G. Skofronick, D. B. Greene, E. A. Halprin, and R. N. Compton

*A Chemical Accelerator for Studying the Collisional Behavior of Large Molecules: $SF_6$ + $CO_2$ Total Cross Sections,* VIII International Conference on the Physics of Electronic and Atomic Collisions, July 16–20, 1973, Belgrade, Yugoslavia.

W. S. Snyder

*Evaluating a Plutonium Exposure (A Plea for the Health Physicist),* AEC and AEC-Contractor Health Protection Meeting, December 8–9, 1972, San Juan, Puerto Rico.

*Phantoms and People,* Western Pennsylvania Chapter of the Health Physics Society, May 14, 1973, Pittsburgh, Pennsylvania.

J. A. D. Stockdale and R. N. Compton

*Time-of-Flight Velocity Analysis of $O^+$ Ions Produced through Electron Impact Ionization of $O_2$,* American Physical Society, January 29–February 1, 1973, New York, N.Y.

J. A. D. Stockdale, Liliana Deleanu, and R. N. Compton

*Dissociative Ionization of Molecules by Electron Impact,* Impact Ionization Conference, July 23–26, 1973, Surrey, England (presented by R. N. Compton).

R. C. Taeuber

"The Oak Ridge Program," *Proceedings of the 14th National Meeting of the Public Health Conference on Records and Statistics,* Washington, D.C., June 1972.

"Some Comments on Methods and Ethics of Access," *Proceedings of Conference on the Current Population Survey, Pennsylvania State University,* September 1972.

M. M. Williams

"Race, Poverty, and Educational Achievement in an Urban Environment," *Proceedings, 80th Annual Convention, American Psychological Association,* Honolulu, September 1972, October 1972.

M. W. Williams, R. N. Hamm, and E. T. Arakawa

*Optical Constants from Photoelectric Yield,* American Physical Society, Southeastern Section, November 16–18, 1972, Birmingham, Alabama.

H. A. Wright, R. N. Hamm, and J. E. Turner

*$^{11}C$ Activity to Dose and Dose Equivalent Conversion Factors,* Health Physics Society, June 17–21, 1973, Miami Beach, Florida.

# Publications

G. D. Alton, W. R. Garrett, M. Reeves, and J. E. Turner

"Microscopic Optical-Model Analysis of Electron Scattering from Hydrogen," *Phys. Rev. A* **6**, 2138–46 (1972).

E. T. Arakawa, R. N. Hamm, and M. W. Williams

"Optical Properties and Electron Attenuation Lengths from Photoelectric Yield Measurements," submitted for publication in the *Journal of the Optical Society of America.*

J. C. Ashley, V. E. Anderson, R. H. Ritchie, and Werner Brandt

"$Z_1^3$ Effects in the Stopping Power of Matter for Charged Particles: Tables of Functions," submitted for publication to National Auxiliary Publications Service.

J. C. Ashley and R. H. Ritchie
"Contribution of Surface Losses to the Stopping Power of Matter for Charged Particles," *Phys. Rev. B* **5**, 3485–87 (1972).

J. C. Ashley, R. H. Ritchie, and Werner Brandt
"$Z_1{}^3$-Dependent Stopping Power and Range Contributions," submitted for publication in *The Physical Review.*

J. A. Auxier and R. O. Chester, eds.
*Report of the Clinch Valley Study,* May 15–June 2, 1972, ORNL-4835 (1973).

J. K. Baird
"Infinite, Lossless, Two-Wire Transmission Line Illuminated by the Fields of a Parallel Current," to be published in *IEEE Transactions on Electromagnetic Compatibility,* 1973.

"The Electromagnetic Pulse and the Electric Power System," *Proceedings North American Power Systems Interconnection Committee Meeting,* Jackson, Mississippi, March 15–16, 1973.

J. K. Baird and Nicholas J. Frigo
*EMP Effects on a Power System Supervisory Control Circuitry,* ORNL-4899 (1973).

P. R. Barnes
*The Effects of Nuclear Electromagnetic Pulse (EMP) on Civil Defense Two-Way Radio Communications,* ORNL-4873 (June 1973).

*The Analysis and Simulation of the Electric Dipole Antenna Response to EMP,* ORNL-TM-4086 (in preparation).

"On the Singularity Expansion Method as Applied to the Cylindrical Dipole Receiving Antenna," *Proceedings IEEE/G-AP Symposium,* University of Colorado, August 21–24, 1973.

D. M. Bartell, G. S. Hurst, and E. B. Wagner
"Time-Dependent Studies of Vacuum Ultraviolet Emission from Helium," *Phys. Rev. A* 7, 1068–78 (1973).

K. Becker
"Dosimetric Applications of Track Etching," Chap. 2 in *Topics in Radiation Dosimetry,* ed. by F. H. Attix, Academic, New York, 1972.

"Progress in Luminescence Dosimetry," *Science* **177**, 539–40 (August 11, 1972).

"The Future of Personnel Dosimetry," *Health Phys.* **23**, 729–37 (November 1972).

"Principles of Personnel Dosimetry" and "New Developments in Solid-State Dosimetry" in *Proceedings of First Latin American Conference on Physics in Medicine and Radiation Protection,* Sao Paulo, Brazil, February 28–March 3, 1972.

"Environmental Monitoring with TLD," *Nucl. Instrum. Methods* **104**, 405–7 (1972).

(Book) *Solid State Dosimetry,* CRC Press, Cleveland, Ohio, in press.

"Progress in Solid-State Fast Neutron Personnel Dosimetry," *Proceedings of the Symposium on Neutron Monitoring for Radiation Protection Purposes,* IAEA, Vienna, Austria, December 11–15, 1972.

(Book Review) "On the Possible Application of Exoelectrons in Dosimetry," *Proceedings of a Workshop, Braunschweig, 1972,* ed. by H. Riskat and H. Seguin, EUR-4904, 187 pages, *Health Phys.*, in press.

"Photographic, Chemical, and Solid-State Bibliography," AED-C-21-08, ZAED Karlsruhe, Germany, 1971.

"Internal Dosimetry Bibliography," AED-C-21-09, ZAED Karlsruhe, Germany, 1972.

"Dosimetry – Electrometric Techniques; Bibliography," AED-C-21-10, ZAED Karlsruhe, Germany, 1972.

"Report on Foreign Travel to Colombia, Chile, and Argentina, November 26–December 19, 1972," ORNL-CF-73-2-20 (February 14, 1973).

"Report on Foreign Travel to Sweden, Germany, and Switzerland, July 18–August 6, 1972," ORNL-CF-72-8-42 (August 14, 1972).

G. M. Begun and R. N. Compton
"Electron Impact Ionization Studies of Ferrocene, Cobaltocene, Nickelocene, and Magnesocene," *J. Chem. Phys.* **58**, 2271–80 (1973).

R. D. Birkhoff
"Review of ICRU Report 21: 'Radiation Dosimetry; Electrons with Initial Energies between 1 and 50 eV,' " submitted for publication in *Nuclear Safety.*

R. A. Bohm and D. A. Patterson
"An Analysis of Population Concentration and Dispersal in the United States, 1940–1970," *Civil Defense Research Project Annu. Progr. Rep. March 1971–March 1972,* ORNL-4784 (December 1972).

"Interstate Highway Location and County Population Growth," *Civil Defense Research Project Annu. Progr. Rep. March 1971–March 1972,* ORNL-4784 (December 1972).

Werner Brandt and R. H. Ritchie
"Primary Processes in the Physical Stage," in *Proceedings of Conference on Physical Mechanisms in Radiation Biology, Airlie, Virginia, October 10–14, 1972* (in press).

A. J. Braundmeier and E. T. Arakawa
"Effect of Surface Roughness on Surface Plasmon Resonance Absorption," submitted for publication in the *Journal of Physics and Chemistry of Solids.*

A. J. Braundmeier, Jr., M. W. Williams, E. T. Arakawa, and R. H. Ritchie
"Radiative Decay of Surface Plasmons from Al," *Phys. Rev. B* **5**, 2754–63 (1972).

D. G. Brown and F. F. Haywood
"14 MeV Neutron Irradiation of Swine," *Health Phys.* **24**(6) (1973).

C. V. Chester and R. O. Chester
*Civil Defense Implications of an LMFBR in a Thermonuclear Target Area,* ORNL-CF-72-5-31 (June 1972).

"Interaction of the Structure of a Selected Reactor Containment with Near Kilobar Nuclear Weapon Shock-Waves in Air," *Third International Symposium on Military Applications of Blast Simulators, Proceedings,* September 19–21, 1972, Schwetzingen, Germany, 1973.

C. V. Chester and L. Dresner
"Attenuation of Shock Waves in Long Pipes by Orifice Plates, Rough Walls, and Cylindrical Obstacles," *Third International Symposium on Military Applications of Blast Simulators, Proceedings,* September 19–21, 1972, Schwetzingen, Germany, 1973.

C. V. Chester, G. A. Cristy, and C. M. Haaland
*Strategic Considerations in Planning a Counterevacuation,* ORNL-4888 (in preparation).

R. O. Chester and C. V. Chester
"A Protective Containment System for Large Nuclear Power Plants," *Health Physics Society, Proceedings,* June 17–21, 1973.

L. G. Christophorou
"Intermediate Phase Studies for Understanding Radiation Interaction with Condensed Media. The Electron Attachment Process," *J. Phys. Chem.* **76**, 3730–34 (1972).

"Recent Studies on Electron Attachment," pp. 123–46, vol. 1, in *Proceedings of Third Tihany Conference on Radiation Chemistry,* ed. by J. Dubó and P. Hedvig, *Tihany, Hungary, May 10–17, 1971,* Akadémiai Kiadó, Budapest, 1972.

L. G. Christophorou, R. P. Blaunstein, and D. Pittman
"Mobilities of Thermal Electrons in Gases and Liquids," *Chem. Phys. Lett.* **18**, 509–14 (1973).

L. G. Christophorou, A. A. Hadjiantoniou, and J. G. Carter
"Long-Lived Parent Negative Ions Formed via Nuclear-Excited Feshbach Resonances. Part III – Variation of the Autodetachment Lifetime with Incident Electron Energy," submitted for publication in *The Journal of Chemical Physics.*

L. G. Christophorou, D. L. McCorkle, and D. Pittman
"Electron Attachment to $c$-$C_4F_8$, $CCl_2F_2$, and $C_2H_5Cl$ below ~2 eV; a Comparison of the Electron Swarm and the Microwave Methods," *J. Chem. Phys.* (in press).

R. N. Compton and C. D. Cooper
"Molecular Electron Affinities from Collisional Ionization of Cesium: $SF_6$ and $TeF_6$," submitted for publication in *The Journal of Chemical Physics.*

C. D. Cooper and R. N. Compton
"Electron Attachment to Cyclic Anhydrides and Related Compounds," submitted for publication in *The Journal of Chemical Physics.*

"Metastable Anions of $CO_2$," *Chem. Phys. Lett.* **14**, 29–32 (1972).

G. A. Christy
*Blast Shelter Potential in New Government Buildings,* ORNL-4849 (February 1973).

*Expedient Shelter Survey – Final Report,* ORNL-4860 (June 1973).

"Blast Shelters? Why Not?" *Survive* (1973).

F. J. Davis, R. N. Compton, and D. R. Nelson
"Thermal Energy Electron Attachment Rates for Some Polyatomic Molecules," submitted for publication in *The Journal of Chemical Physics.*

J. R. Dutrannois, R. N. Hamm, J. E. Turner, and H. A. Wright
"Analysis of Energy Deposition in Water around the Site of Capture of a Negative Pion by an Oxygen or Carbon Nucleus," *Phys. Med. Biol.* **17**, 765–70 (1972).

C. E. Easterly, L. G. Christophorou, and J. G. Carter
"Fluorescence from the Second Excited $\pi$-Singlet State of Aromatic Hydrocarbons in Solution," *J. Chem. Soc., Faraday Trans. II* **69**, 471–83 (1973).

J. M. Elson and R. H. Ritchie
"Diffuse Scattering and Surface Plasmon Generation by Photons at a Rough Dielectric Surface," submitted for publication in *Physical Review B.*

L. C. Emerson
"Automatic Data Processing Using Tape Cassettes," submitted for publication in the *Programmer.*

L. C. Emerson, R. D. Birkhoff, V. E. Anderson, and R. H. Ritchie
"Electron Slowing-Down Spectrum in Irradiated Silicon," *Phys. Rev. B* **7**, 1798–1811 (1973).

W. F. Frey, R. N. Compton, W. T. Naff, and H. C. Schweinler
"Electron Impact Studies of Some Cyclic Hydrocarbons," *Int. J. Mass Spectrom. Ion Phys.* (in press).

J. S. Gailar
"What's New in Soviet Civil Defense?," *Survive* **6**(2) (March–April 1973).

"Sevastopol Evacuation Exercises," *Survive* **6**(3) (May–June 1973).

"Soviet Civil Defense: The Importance of CD in the U.S.S.R.," *Survive* **6**(4) (July–August 1973).

R. B. Gammage and J. S. Nagpal
"Adsorbed Gases, Atmospheric, and Temperature Effects on TSEE from BeO," *Radiat. Eff.,* in press.

R. B. Gammage, H. F. Holmes, E. L. Fuller, Jr., and D. R. Glasson
"Pore Structures Induced by Water Vapor Adsorbed on Nonporous Lunar Fines and Ground Calcite," *J. Colloid Interface Sci.,* in press.

W. R. Garrett
Book Review: "Silent Slaughter," Joel Griffiths and Richard Ballentine, Henry Regnery Co., 1972, submitted for publication in *Health Physics.*

"Low-Energy Electron Scattering by Polar Molecules," *Mol. Phys.* **24**, 465–87 (1972).

T. F. Gesell and E. T. Arakawa
"Work Function Changes during Oxygen Chemosorption on Fresh Magnesium Surfaces," *Surface Sci.* **33**, 419–21 (1972).

T. F. Gesell, E. T. Arakawa, and M. W. Williams
"Optical and Photoelectric Properties of Mg in the Vacuum UV," submitted for publication in *The Physical Review.*

J. T. Grissom, R. N. Compton, and W. R. Garrett
"Slow Electrons from Electron Impact Ionization of He, Ne, and Ar," *Phys. Rev. A* **6**, 977–87 (1972).

C. M. Haaland
"Book Review of When War Comes (by Martin Caidin)," *Survive* **5**(5) (September–October 1972).

"Protection from Initial Nuclear Radiation," *Survive* **6**(3) (May–June 1973).

C. M. Haaland and M. T. Heath
*Passive-Active Defense Studies for the Detroit Metropolitan Area, Final Report, December 1972,* ORNL-4818 (December 1972).

"Mapping of Population Density," submitted to *Demography,* June 1973.

*Mapping of Population Density,* ORNL-TM-4246 (in press).

C. M. Haaland, E. P. Wigner, and J. V. Wilson
*Active and Passive Defense Interaction Studies, Vol. I: Summary, Models, and Calculations,* ORNL-TM-3485 (December 1971).

A. Hadjiantoniou, L. G. Christophorou, and J. G. Carter
"Long-Lived Parent Negative Ions Formed via Nuclear-Excited Feshbach Resonances. Part I – Benzene Derivatives," submitted for publication in *The Journal of Chemical Physics.*

"Long-Lived Parent Negative Ions Formed via Nuclear-Excited Feshbach Resonances. Part II – Aromatic Molecules Other than Benzene Derivatives and Non-Aromatic Organic Structures," submitted for publication in *The Journal of Chemical Physics.*

W. F. Hanson, E. T. Arakawa, and M. W. Williams
"Optical Properties of MgO and $MgF_2$ in the Extreme Ultraviolet Region," *J. Appl. Phys.* **43**, 1661–65 (1972).

F. F. Haywood
"Intercomparisons of Neutron Monitors under Conditions of Simulated Nuclear Accidents," *Proceedings of the Symposium on Neutron Monitoring for Radiation Protection Purposes,* IAEA, Vienna, Austria, December 11–15, 1972.

*Report of Foreign Travel – Vienna, Austria, December 11–22, 1972,* ORNL-CF-73-1-44 (January 29, 1973).

J. M. Heller, R. D. Birkhoff, M. W. Williams, and L. R. Painter
"Optical Properties of Glycerol in the Vacuum Ultraviolet," *Radiat. Res.* **52**, 25–31 (1972).

H. F. Holmes, E. L. Fuller, Jr., and R. B. Gammage
"Alteration of an Apollo 12 Sample by Adsorption of Water Vapor," *Earth Planet. Sci.* **19**, 90 (1973).

"Interaction of Gases with Lunar Materials: Apollo 12, 14, and 16 Samples," *Proceedings of the Fourth Lunar Science Conference,* in press.

R. H. Huebner, W. F. Frey, and R. N. Compton
"Threshold Electron Excitation of Azulene," submitted for publication in *Chemical Physics Letters.*

G. S. Hurst
"Radiation Protection," *Health Phys.* **23**, 747 (1972).

G. S. Hurst, W. R. Garrett, and M. G. Payne
"An Operational Logic for Radiation Biology and Radiation Protection," *Health Phys.*, in press.

J. E. Jobst, Z. G. Burson, and F. F. Haywood
"A Self-Replenishing Tritium Target," *ANS Trans.* **15**(1), 155 (1972).

T. D. Jones
"Solid Geometry vs. Plane Geometry for $^{252}$Cf Sources," *Phys. Med. Biol.* **17**(6), 858–59 (1972).

T. D. Jones and J. A. Auxier
"Local Dose from Neutron Produced Recoil Ions in the Region of a Therapeutic $^{252}$Cf Needle," *Radiology* **104**, 187–89 (1972).

T. D. Jones, J. A. Auxier, W. S. Snyder, and G. G. Warner
"Dose to Standard Reference Man from External Sources of Monoenergetic Photons," *Health Phys.* **24**(2) 241–55 (1973).

C. H. Kearny
*How to Make and Use a Homemade, Large-Volume, Efficient Ventilating Pump: The Kearny Air Pump,* ORNL-TM-3916 (August 1972).

"Expedient Shelter Test," *Defense Nuclear Agency's MIXED COMPANY/Middle Gust Results Meeting, Proceedings,* Santa Barbara, California, March 15, 1973.

G. D. Kerr, R. N. Hamm, M. W. Williams, R. D. Birkhoff, and L. R. Painter
"Optical and Dielectric Properties of Water in the Vacuum Ultraviolet," *Phys. Rev. A* **5**, 2523–27 (1972).

C. E. Klots
Book Review: "Fundamentals of Radiation Chemistry," A. R. Denaro and G. S. Jayson, Butterworths, London, 1972, *Health Phys.* **24**, 457–58 (1973).

"Thermochemical and Kinetic Information from Metastable Decompositions," *J. Chem. Phys.* (in press).

E. S. Lee
"How Cities Grow," *Civil Defense Research Project Annu. Progr. Rep. March 1971–March 1972,* ORNL-4784 (December 1972).

M. H. Lee
*Some Notes on the Use of TSEE and the Ionization Chamber for the Measurement of High Doses of Fast Neutron and Gamma Radiations,* ORNL-CF-72-11-16 (December 7, 1972).

M. L. Levin and W. W. Pendleton
"Growth of Urbanized Areas," *Civil Defense Research Project Annu. Progr. Rep. March 1971–March 1972,* ORNL-4784 (December 1972).

R. W. Manweiler, C. V. Chester, and C. H. Kearny
*Measurement of Shock Overpressure in Air by a Yielding Foil Membrane Blast Gauge,* ORNL-4868 (June 1973).

J. H. Marable, J. K. Baird, and D. B. Nelson
*Effects of Electromagnetic Pulse (EMP) on a Power System,* ORNL-4836 (December 1972).

D. L. McCorkle, L. G. Christophorou, and V. E. Anderson
"Low Energy ($\lesssim 1$ eV) Electron Attachment to Molecules at Very High Gas Densities: $O_2$," *J. Phys. B* **5**, 1211–20 (1972).

A. Moreno y Moreno, J. S. Cheka, J. A. Nagpal, R. B. Gammage, and K. Becker
"Further Studies on TSEE Activators in BeO," *Rev. Mex. Fis.* **21**, 123–38 (1972).

K. Z. Morgan and J. E. Turner
"Health Physics," pp. 8-291–8-315 in *American Institute of Physics Handbook,* ed. by Dwight E. Gray (Coordinating Editor), McGraw-Hill, New York, 1972.

W. T. Naff, R. N. Compton, and C. D. Cooper
"Electron Attachment and Excitation Processes in Selected Carbonyl Compounds," *J. Chem. Phys.* **57**, 1303–7 (1972).

S. J. Nalley, R. N. Compton, H. C. Schweinler, and V. E. Anderson
"Molecular Electron Affinities from Collisional Ionization of Cesium. Part I. NO, $NO_2$, and $N_2O$," submitted for publication in *The Journal of Chemical Physics.*

D. B. Nelson
*A Program to Counter the Effects of Nuclear Electromagnetic Pulse in Commercial Power Systems, Part I,* ORNL-TM-3552 (October 1972).

D. R. Nelson and F. J. Davis
"Thermal and Near Thermal Electron Transport Coefficients in $O_2$ Determined with a Time-of-Flight Swarm Experiment Using a Drift-Dwell-Drift Technique," *J. Chem. Phys.* **57**, 4079–84 (1972).

K. P. Nelson
"Social Security Data and Urban Growth Patterns," *Civil Defense Research Project Annu. Progr. Rep. March 1971–March 1972,* ORNL-4784 (December 1972).

J. Neufeld
"Absorbed Dose and Tissue Dose," *Health Phys.* **24**, 101–3 (1973).

"Dose Equivalent Index," *Health Phys.* **23**, 862–63 (1972).

"Comments on the Theory of Radiation Risk, Parts 1 and 2," submitted for publication in *Health Physics.*

Jacob Neufeld and Harvel Wright
"Radiation Levels and Fluence Conversion Factors," *Health Phys.* **23**, 183–86 (1972).

Y. Okamoto, H. Yamada, J. S. Cheka, and H. H. Hubbell, Jr.
"A Technique for the Estimation of Radiation Exposure to Japanese Survivors Shielded by Reinforced Concrete Structure," ORNL-CF-72-10-1 (February 5, 1973).

J. E. Parks, G. S. Hurst, T. E. Stewart, and H. L. Weidner
"Ionization of Noble Gases by Protons: Jesse Effects as a Function of Pressure," *J. Chem. Phys.* **57**, 5467–74 (1972).

C. H. Patrick
"Changes in the Concentration of Employment in Metropolitan Areas, 1964–1969," *Civil Defense Research Project Annu. Progr. Rep. March 1971–March 1972,* ORNL-4784 (December 1972).

*The Decentralization of Manufacturing Employment,* ORNL-UR-105 (April 1973).

C. H. Patrick and P. N. Ritchey, Jr.
*Changes in Population and Employment as Processes in Regional Development,* ORNL-UR-102 (April 1973)

M. G. Payne, W. R. Garrett, and G. S. Hurst
"Phenomenological Model for a Restricted Class of Radiation Stimulated Biological Effects," *Radiat. Res.,* in press.

M. G. Payne, J. E. Talmage, G. S. Hurst, and E. B. Wagner
"The Effect of Incomplete Redistribution in Frequency on the Transport of Resonance Radiation," *Phys. Rev.,* in press.

W. W. Pendleton and M. L. Levin
"Blacks and Suburbanization in Atlanta," *Civil Defense Research Project Annu. Progr. Rep. March 1971–March 1972,* ORNL-4784 (December 1972).

"An Examination of Black Suburban Residence," *Civil Defense Research Project Annu. Progr. Rep. March 1971–March 1972,* ORNL-4784 (December 1972).

P. T. Perdue, W. H. Shinpaugh, J. H. Thorngate, and J. A. Auxier
"A Convenient Counter for Measuring Alpha Activity of Smear and Air Samples," *Health Phys.,* in press.

M. N. Pisanias, L. G. Christophorou, J. G. Carter, and D. L. McCorkle
"Compound-Negative-Ion-Resonance States and Threshold-Electron Excitation Spectra of N-Heterocyclic Molecules: Pyridine, Pyridazine, Pyrimidine, Pyrazine, and *sym*-Triazine," *J. Chem. Phys.* **58**, 2110–24 (1973).

M. N. Pisanias, L. G. Christophorou, and J. G. Carter
"Compound Negative Ion Resonances and Threshold-Electron Excitation Spectra of Quinoline and Isoquinoline," *Chem. Phys. Lett.* **13**, 433–38 (1972).

J. W. Poston and W. F. Fox
"Comparison of IAEA Ionization Chambers with Other Dosimeters," *Neutron Irradiation of Seeds III,* Technical Reports Series 141, IAEA, 1972.

J. W. Poston, J. R. Knight, and G. E. Whitesides
"Calculation of the HPRR Neutron Spectrum for Simulated Nuclear Accident Conditions," 1972, to be published in *Health Physics.*

J. W. Poston and W. S. Snyder
"A Model for Exposure to a Semi-Infinite Cloud of a Photon Emitter," to be published in *Health Physics,* 1973.

P. N. Ritchey
"The Fertility of Negroes without Southern Rural Experience: A Reexamination of the 1960 GAF Study Findings with 1967 SEO Data," *Civil Defense Research Project Annu. Progr. Rep. March 1971–March 1972,* ORNL-4784 (December 1972).

"The Intervening Effects of Marital Status on the Fertility of Rural-Urban and Urban-Rural Migrants," *Civil Defense Research Project Annu. Progr. Rep. March 1971–March 1972,* ORNL-4784 (December 1972).

*Migration and Fertility: A Study of the Social Factors Involved,* ORNL-UR-101 (April 1973).

"Effects of Marital Status on the Fertility of Rural-Urban and Urban-Rural Migrants," *Rural Sociol.* (April 1973).

"The Fertility of Blacks without Southern Rural Experience: A Reexamination of the 1960 GAF Study Findings with 1967 SEO Data," *Population Stud.* (April 1973).

P. N. Ritchey and C. Shannon Stokes
*Correlates of Childlessness and Expectation to Remain Childless: U.S. 1967,* ORNL-UR-103 (April 1973).

R. H. Ritchie
Book Review: "High-Energy Electromagnetic Processes in Condensed Media," M. L. Ter-Mikaelian, Wiley-Interscience Tracts on Physics and Astronomy, No. 29, 1972, *Nucl. Technol.* (in press).

"Isotropic Incident Flux in Monte Carlo Calculations," *Health Phys.* **24**, 571–72 (1973).

"Plasmons in Solids," in *Proceedings NATO Advanced Study Institute, Istanbul, Turkey, August 16–27, 1971* (in press).

"Surface Plasmons in Solids," *Surface Sci.* **34**, 1–19 (1973).

"Surface Polaritons," in *Proceedings of Taormina Research Conference on the Structure of Matter, Taormina, Sicily, October 2–6, 1972* (in press).

R. H. Ritchie, Werner Brandt, and George Basbas
"Inner Shell Excitation of Atoms by Heavy Charged Particles," *Phys. Rev.* (in press).

W. S. Snyder
"A Method of Interpreting Excretion Data Which Allows for Statistical Fluctuation of the Data," *Assessment of Radioactive Contamination in Man* (IAEA, Vienna, 1972), p. 485.

W. S. Snyder, Mary R. Ford, J. R. Muir, and G. G. Warner
"Fluctuations of Daily Excretion of Plutonium and Their Interpretation for Estimation of the Body Burden," *Health Physics Operational Monitoring* (Gordon and Breach, New York, 1972), Vol. 1, p. 711.

M. Sohrabi and K. Becker
"Fast Neutron Personnel Monitoring by Fission Fragment Registration from $^{237}$Np," *Nucl. Instrum. Methods* **104**, 409–11 (1972).

B. L. Sowers, R. D. Birkhoff, and E. T. Arakawa
"Optical Absorption of Liquid Water in the Vacuum Ultraviolet," *J. Chem. Phys.* **57**, 583–84 (1972).

B. L. Sowers, M. W. Williams, R. N. Hamm, and E. T. Arakawa
"Optical Properties of Liquid Carbon Tetrachloride, *n*-Hexane, and Cyclohexane in the Vacuum Ultraviolet," *J. Chem. Phys.* **57**, 167–70 (1972).

J. A. D. Stockdale
"Thermal Energy Ion Condensation Reactions in Benzene Vapor," *J. Chem. Phys.* **58**, 3881–83 (1973).

J. A. D. Stockdale and Liliana Deleanu
"Dissociative Ionization of $O_2$ and $N_2$ by Electron Impact: $N^+$ and $O^+$ Energies and Angular Distributions," submitted for publication in *Chemical Physics Letters.*

R. B. Sturgis
*Selective Factors Influencing City Growth 1960–1970,* ORNL-UR-109 (April 1973).

C. M. Taeuber
*Measuring Patterns of Urban Growth,* ORNL-UR-104 (April 1973).

J. H. Thorngate
"Advances in Physical and Biological Radiation Detectors," *Proceedings of a Symposium, Vienna, November 23–27, 1970, IAEA,* Unipub, Vienna, 1971 (Book Review), *Health Phys.* **24**(5) 589 (1973).

J. H. Thorngate and P. T. Perdue
"A Stable Pulsed Light Source Using Low-Cost Light-Emitting Diodes," *Nucl. Instrum. Methods* **105**, 57 (1972).

J. E. Turner
Book Review: "Strahlenschutz an Hochenergiebeschleunigern," Eberhard Freytag, G. Braun, Publisher, Karlsruhe 1, Germany, 1972, submitted for publication in *Health Physics.*

J. E. Turner and J. A. Auxier
"Symposium on Radiation Standards and Regulations," *Health Phys.* **23**, 445–46 (1972).

J. E. Turner, J. Dutrannois, H. A. Wright, R. N. Hamm, J. Baarli, A. H. Sullivan, M. J. Berger, and S. M. Seltzer
"The Computation of Pion Depth-Dose Curves in Water and Comparison with Experiment," *Radiat. Res.* **52**, 229–46 (1972).

R. B. Vora, J. E. Turner, and R. N. Compton
"Single-Electron Excitation and Transfer in Collisions of Alkali-Metal and Oxygen Atoms," submitted for publication in *The Physical Review.*

U. S. Whang, E. T. Arakawa, and T. A. Callcott
"Optical Properties of K between 4 and 10.7 eV and Comparison with Na, Rb, and Cs," *Phys. Rev. B* **6**, 2109–18 (1972).

U. S. Whang, R. N. Hamm, E. T. Arakawa, and M. W. Williams
"A Slope Method for Determining Extinction Coefficients," *J. Opt. Soc. Amer.* **63**, 305–8 (1973).

M. M. Williams
"Race, Poverty, and Educational Achievement in an Urban Environment," *Civil Defense Research Project Annu. Progr. Rep. March 1971–March 1972,* ORNL-4784 (December 1972).

*An Urban Classification Scheme,* ORNL-UR-108 (April 1973).

M. W. Williams and E. T. Arakawa
"Optical Properties of Glassy Carbon from 0 to 82 eV," *J. Appl. Phys.* **43**, 3460–63 (1972).

H. Yamada and T. D. Jones
"An Examination of A-Bomb Survivors Exposed to Fallout Rain and a Comparison to a Similar Control Population," ORNL-TM-4017 (December 1972).

# Lectures

J. K. Baird
*Feasibility of a Power Supply Which Is the Thevinin Equivalent of a Semi-Infinite Transmission Line Driven by an Electromagnetic Pulse (EMP) Space Wave,* National Academy of Sciences, Advisory Committee on Civil Defense, Subcommittee on EMP Effects in Civilian Power Systems, September 19, 1972, Washington, D.C.

*Electromagnetic Pulse (EMP) Effects in Power Systems,* Annual Meeting, Virginia Civil Defense Association, August 18, 1972, Bristol, Virginia.

*The Electromagnetic Pulse and the Electric Power System,* Annual Meeting, South Central Systems, North American Power Systems Interconnection Committee, March 16, 1973, Jackson, Mississippi.

*The Current Status of Power System Electromagnetic Pulse Research,* Meeting of U.S. Defense Civil Preparedness Administration and Federal Republic of Germany Departments of Economic Affairs and Effective Utilization of Terrain, Construction Engineering and Urban Construction, April 3, 1973, Washington, D.C.

*Future Research Goals for the Understanding of Electromagnetic Pulse Effects in Power Systems,* Meeting of Electric Power Research Committee, Office of Science and Technology, April 28, 1972, Philadelphia, Pennsylvania.

K. Becker

*Progress in Solid-State Dosimetry Research at ORNL,* University of Giessen, West Germany, July 26, 1972.

*The Present Status and Future Trends in Personnel Radiation Dosimetry,* Instituto Nacional para Programs Especiales de Salud, Bogota, Colombia, November 30, 1972.

*The Present Status and Future Trends in Personnel Radiation Dosimetry,* Instituto de Higiena Trabajo y Contaminacion Atmosferica, Santiago, Chile, December 6, 1972.

*The Present Status and Future Trends in Personnel Radiation Dosimetry,* National Protection Service, Ministry of Social Welfare, Buenos Aires, Argentina, December 13, 1972.

*Progress in Solid-State Dosimetry,* Georgia Institute of Technology, Atlanta, Georgia, February 1, 1973.

*Nuclear Track Etching in Solids and Its Applications,* Mexican National Institute of Nuclear Energy, Salazar, March 1973.

*Photographic Film Dosimetry and Solid-State Techniques in Archaeometry,* Department of Physics, University of Mexico (UNAM), Mexico City, March 1973.

*Principles and Applications of Solid-State Dosimetry,* Department of Physics, University of Mexico (UNAM), Mexico City, March 1973.

*Thermoluminescence Dosimetry,* Department of Physics, University of Mexico (UNAM), Mexico City, March 1973.

*Exoelectron and Radiophotoluminescence Dosimetry,* Department of Physics, University of Mexico (UNAM), Mexico City, March 1973.

*Track Etching and Miscellaneous Other Techniques of Solid-State Dosimetry,* Department of Physics, University of Mexico (UNAM), Mexico City, March 1973.

J. S. Cheka

*Radiophotoluminescence – Glass Dosimetry,* ORAU-ORNL Ten-Week Health Physics Course, Oak Ridge Associated Universities, March 12, 1972.

C. V. Chester

*Civil Defense Research Program,* U.S. Atomic Energy Commission, Division of Biomedical and Environmental Research, Program Directors Meeting, April 9–10, 1973, Oak Ridge National Laboratory, Oak Ridge, Tennessee.

R. O. Chester

*Time Available for Emergency Actions after a Radioactivity Release from a Licensed Nuclear Facility,* Radiation Control Program Directors Meeting, May 7, 1973, Portland, Oregon.

L. G. Christophorou

*The Cultural and Educational Value of Basic Science,* National Research Center, January 12, 1973, Athens, Greece.

*Current Research in Atomic and Molecular Radiation Physics,* University of Athens, January 23, 1973, Athens, Greece.

R. N. Compton

*The Formation and Structure of Negative Ions,* Columbia University, November 10, 1972, New York, N.Y.

G. S. Hurst

*Some Elementary Effects of Ionizing Radiation,* Ball State University, Muncie, Indiana, November 9, 1972.

*Charged Particle Excitation of Helium,* University of Kentucky, Lexington, November 10, 1972.

C. H. Kearny

*Hasty Nuclear Blast/Fallout Shelters,* Briefing for the Joint Chiefs of Staff, April 20, 1972, The Pentagon.

*Expedient Blast Shelter Tests,* Briefing for Army General Staff, including General Bruce Palmer, Vice Chief of Staff, Lieutenant General D. H. Cowles, Deputy Chief of Staff for Operations, December 5, 1972, The Pentagon.

*Soviet Civil Defense and ORNL Expedient Shelter Experiments,* Briefing for Brigadier General G. D. Eggars, Deputy Director for Operations, Office of the Joint Chiefs of Staff, February 2, 1973, The Pentagon.

*Expedient Blast Shelter Tests,* Briefing for Hon. John E. Davis, Director, Defense Civil Preparedness Agency and Staff, February 2, 1973, The Pentagon.

*Expedient Blast Shelters,* U.S. Atomic Energy Commission, Division of Biomedical and Environmental Research, Program Directors Meeting, April 9–10, 1973, Oak Ridge National Laboratory, Oak Ridge, Tennessee.

G. D. Kerr

*Estimating Regional Radiological Impacts from the Nuclear Power Industry,* Georgia Institute of Technology, Atlanta, April 27, 1972.

R. W. Manweiler

*The Effects of Nuclear Electromagnetic Pulse (EMP) on the Electric Power System,* U.S. Atomic Energy Commission, Division of Biomedical and Environmental Research, Program Directors Meeting, April 9–10, 1973, Oak Ridge National Laboratory, Oak Ridge, Tennessee.

R. H. Ritchie

*Health Physics Research at Oak Ridge National Laboratory,* Directorate of Radiation Protection, August 2, 1972, Trombay, Bombay, India.

*The Interaction of Charged Particles with Condensed Matter,* Directorate of Radiation Protection, August 4, 1972, Trombay, Bombay, India.

*Dielectric Theory of Condensed Matter,* Directorate of Radiation Protection, August 9, 1972, Trombay, Bombay, India.

*Interactions in a Condensed Medium,* Directorate of Radiation Protection, August 11, 1972, Trombay, Bombay, India.

*Transverse Field Contributions to Stopping Power,* Directorate of Radiation Protection, August 16, 1972, Trombay, Bombay, India.

*Collective Effects in Stopping Power Theory,* Directorate of Radiation Protection, August 18, 1972, Trombay, Bombay, India.

*The Statistical Atom Model in Stopping Power Theory,* Directorate of Radiation Protection, August 23, 1972, Trombay, Bombay, India.

*Characterization of a Charged Particle Track in Condensed Matter,* Directorate of Radiation Protection, August 25, 1972, Trombay, Bombay, India.

*Track Effects,* Directorate of Radiation Protection, August 30, 1972, Trombay, Bombay, India.

*The Impact Parameter Representation,* Directorate of Radiation Protection, September 1, 1972, Trombay, Bombay, India.

*Interactions between Products of Excitation and Ionization in Charged Particle Tracks,* Directorate of Radiation Protection, September 5, 1972, Trombay, Bombay, India.

*Delta-Ray Effects in Track Structure,* Directorate of Radiation Protection, September 7, 1972, and continued on September 12, 1972, Trombay, Bombay, India.

*Beyond the First Born Approximation in Stopping Power,* Directorate of Radiation Protection, September 13, 1972, Trombay, Bombay, India.

*Collective Electron Modes in Solids,* University of Missouri, April 12, 1973, Rolla, Missouri.

H. C. Schweinler

*Super-High Conductivity in Molecular Ionic Crystals at 60°K,* Clemson University, June 7, 1973, Clemson, South Carolina.

*Super-High Conductivity in Molecular Ionic Crystals at 60°K,* University of Tennessee, April 10, 1973, Knoxville.

W. S. Snyder

*Environmental Pathways from Reactor to Man,* Traveling Lecture, Texas A&M, College Station, January 18, 1973; Northeast Louisiana University, Monroe, January 19, 1973; Valdosta State College, Valdosta, Georgia, May 10, 1973.

*Estimation of Absorbed Dose per Unit Intake of a Radionuclide: A Problem of Medicine, of Health Physics, and of Reactor Siting,* Traveling Lecture, Northeast Louisiana State, Monroe, January 19, 1973.

*Estimates of Specific Effective Energy for Internal Emitters,* National Radiological Protection Board, Harwell, England, April 26, 1973.

J. E. Turner

*Lecture Series in Selected Topics in Radiation Dosimetry,* Directorate of Radiation Protection, January 5–February 16, 1973, Trombay, Bombay, India.

*Energy Transfer by Heavy Charged Particles in Condensed Media,* Directorate of Radiation Protection, February 5, 1973, Trombay, Bombay, India.

*Health Physics at ORNL,* Directorate of Radiation Protection, February 15, 1973, Trombay, Bombay, India.

☆U.S. GOVERNMENT PRINTING OFFICE: 1973-747-302/34

# HEALTH PHYSICS DIVISION

**JULY 1, 1973**

J. A. AUXIER, DIRECTOR
W. S. SNYDER,* ASSISTANT DIRECTOR
D. M. DAVIS,* ASSISTANT DIRECTOR

**FINANCE OFFICER**
V. B. ISHAM

**SECRETARIAL STAFF**
JEANNE S. CARVER**
ANNA L. McCRAY

**HEALTH PHYSICS JOURNAL EDITORIAL OFFICE**
J. A. AUXIER*
GEORGE KERR*
W. S. SNYDER*
NATALIE TARR*

**OUTSIDE ASSIGNMENTS**
K. E. COWSER
B. L. HOUSER*
D. G. JACOBS

**ENGINEERING AND MAINTENANCE**
C. H. ABNER[7]
E. T. LOY
J. L. MALONE**[7]

**SENIOR RESEARCH ADVISORS**
K. Z. MORGAN
E. P. WIGNER

## RADIATION MONITORING
E. D. GUPTON*

**SECRETARIAL STAFF**
DOT GADDIS

**CALIBRATIONS**
D. R. CLARK
S. W. NICHOLS

**DOSE DATA**
J. R. MUIR
M. C. BENTLEY
I. T. FANN
D. M. SOARD

**ENVIRONS**
E. D. GUPTON*
G. L. ARTHUR
J. M. DAVIS
C. R. HENSON
P. M. LANTZ
J. P. SPRAIN

**INTERNAL**
W. W. PARKINSON
P. E. BROWN
L. B. FARABEE
L. S. GOMEZ

**PERSONNEL METERS**
J. C. LEDBETTER*
G. L. DOWNS
E. W. JOHNSON
M. R. MATTHEWS
R. C. WOOD

**RADIOCHEMISTRY GROUP**
L. C. HENLEY
M. J. AILOR
J. C. ANDERSON
A. J. SOARD

## RADIATION AND SAFETY SURVEYS
R. L. CLARK

**SECRETARIAL STAFF**
CAROLYN MILLER*

**Y-12 OPERATIONS**
D. E. ARTHUR
A. CARDWELL
H. R. CRAFT
G. R. PATTERSON
J. A. WESTBROOK

**BLDG. SURVEYS GP. I**
B. T. WALTERS

**CENTRAL**
A. J. SMITH
B. C. BURRELL
R. E. KENY
R. D. PARTEN

**SOUTH CENTRAL**
C. A. GOLDEN
A. C. BUTLER
J. V. HILYER
J. H. SPENCE

**EAST**
H. M. BUTLER**[11]
W. D. CARDEN
R. C. COOPER
P. E. COX
A. B. ELDRIDGE
C. E. HAYNES
R. E. MILLSPAUGH*
W. F. OHNESORGE*
K. M. WALLACE

**SOUTH EAST**
E. L. SHARP
T. G. CLARK
J. C. DAVIS

**SHIFT AND AREA SURVEYS**
C. R. GUINN

**SHIFT SUPERVISORS**
D. D. AUSMUS
R. B. MALCOLM
W. T. MARTIN
D. G. NOE

**SHIFT SURVEYS**
J. S. ADDISON
H. R. CALDWELL
R. L. JEFFERS
W. M. JOHNSON

**AREA SURVEYS**
C. F. SMITH
I. H. WIGGINS

**BLDG. SURVEYS GP. II**
L. C. JOHNSON

**NORTH WEST**
C. H. MILLER
J. BURDEN
W. D. COTTRELL
W. A. McLOUD
E. M. ROBINSON
C. F. ZAMZOW

**NORTH CENTRAL**
J. A. WORTH
J. H. PEMBERTON

**MELTON VALLEY**
R. E. COLEMAN
J. C. RICHTER
R. L. WALKER
R. P. WARD

## SAFETY ENGINEERING AND SPECIAL PROJECTS
D. M. DAVIS*

**SECRETARIAL STAFF**
CAROLYN MILLER*
EMILY RUCKART

**BALANCE AREA REPRESENTATIVE**
A. D. WARDEN*

**INDUSTRIAL SAFETY ENGINEERING**
D. C. GARY‡
J. C. LEDBETTER*
R. E. MILLSPAUGH*
J. W. SHUEY

**INSTRUMENTS**
E. D. GUPTON*

**ORIENTATION AND TRAINING**
R. E. MILLSPAUGH*

**RECORDS AND REPORTS (EPIDEMIOLOGICAL STUDIES)**
J. C. HART*

**SAFETY REVIEWS OF FACILITIES AND PROGRAMS**
T. J. BURNETT

**SAFETY REVIEWS OF X-RAY AND MICROWAVE EQUIPMENT**
W. F. OHNESORGE*

**STANDARDS AND PROCEDURES**
A. D. WARDEN*

**TRANSURANIUM HEALTH PHYSICS AND SAFETY PROCEDURES**
C. E. HAYNES*

## RADIATION RESEARCH AND DEVELOPMENT
F. F. HAYWOOD
J. H. THORNGATE*

**SECRETARIAL STAFF**
NORMA BRASHIER*
JO BROWN
AUDREY GILLIS

**APPLIED HEALTH PHYSICS AND SAFETY**
R. P. WARD*

**TECHNICAL SUPPORT**
J. E. JACKSON
C. E. FRITZ[8]
L. A. LEE[8]

**ATOMIC PHYSICS**
G. S. HURST
M. G. PAYNE
J. TALMAGE[4]
E. B. WAGNER

**DOSIMETRY FOR HUMAN EXPOSURES AND RADIOLOGICAL IMPACT**
G. D. KERR*
J. S. CHEKA*
S. L. CHU[6]
H. W. DICKSON*
W. F. FOX
T. D. JONES*
S. B. LUPICA
J. J. SHONKA*[4]

**HPRR AND ACCEL. OPERATIONS**
F. F. HAYWOOD*
D. R. WARD[9]
H. W. DICKSON*
C. P. LITTLETON[8]
J. W. POSTON*
R. L. SHOUP[11]

**SOLID STATE DOSIMETRY**
K. BECKER
J. S. CHEKA*
R. B. GAMMAGE
M. H. LEE[6]
M. EL RAZEK[6]*

**SPECTROMETRIC DOSIMETRY**
J. H. THORNGATE*
D. J. CHRISTIAN
P. T. PERDUE
M. EL RAZEK[6]*
W. H. SHINPAUGH, JR.
G. K. SUMNER[10]

**CONSULTANTS**
K. CRASE
D. G. WILHOIT

## FUNDAMENTAL HEALTH PHYSICS RESEARCH
R. D. BIRKHOFF
R. H. RITCHIE

**SECRETARIAL STAFF**
NORMA BRASHIER*
BEVERLY VARNADORE

**DESIGN ENGINEER**
J. T. COX

**TECHNICAL SUPPORT**
ADA E. CARTER
D. PITTMAN

**ATOMIC AND MOLECULAR RADIATION PHYSICS**
L. G. CHRISTOPHOROU
J. G. CARTER
C. E. EASTERLY[2,3]
K. S. GANT*
R. E. GOANS[4]
J. P. JOHNSON*
C. E. KLOTS
D. L. McCORKLE[2]

**ELECTRON AND ION COLLISION PHYSICS**
R. N. COMPTON
J. K. BAIRD
L. DELEANER*
D. R. NELSON[11]
P. W. REINHARDT
J. C. STEELHAMMER[2,3]
J. A. STOCKDALE
J. F. WILSON*
J. M. YOUNKIN*

**INTERACTION OF RADIATION WITH LIQUIDS AND SOLIDS**
E. T. ARAKAWA
R. D. BIRKHOFF*
W. T. COCHRAN[4]
L. C. EMERSON
M. F. FAIR*
I-LAN TANG[4]
C. E. WHEELER, JR.[4]
M. W. WILLIAMS

**MATHEMATICAL ANALYSIS**
V. E. ANDERSON[1]

**THEORETICAL RADIATION PHYSICS**
R. H. RITCHIE
J. C. ASHLEY
W. R. GARRETT
R. N. HAMM
V. N. NEELAVATHI[4]
H. C. SCHWERLER
J. E. TURNER*
H. A. WRIGHT

**CONSULTANTS**
A. J. BRAUNDMEIER, JR.
T. A. CALLCOTT
C. CHEN
W. F. FREY
H. H. HUBBELL
R. A. MacRAE
J. NEUFELD
L. R. PAINTER
S. Y. SHIEH

## MEDICAL PHYSICS AND INTERNAL DOSIMETRY
W. S. SNYDER*
J. W. POSTON*
S. R. BERNARD*
M. R. FORD
S. M. GARRY[4]
J. P. HICKEY
G. S. HILL
C. F. HOLOWAY*
D. Y. HSIA[6]
T. D. JONES*
J. A. SCARBOROUGH[5]
J. J. SHONKA*[4]
P. S. STANSBURY[8]

**SECRETARIAL STAFF**
KAY M. BRANAM
SALLY S. STOCKSTILL

**CONSULTANTS**
L. T. DILLMAN
F. C. VONDER LAGE

## URBAN RESEARCH
R. C. TAEUBER
R. J. ALLEN
O. F. BURCH
M. F. CLIFT
K. P. NELSON
C. H. PATRICK
P. N. RITCHEY[12]

**SECRETARIAL STAFF**
ADA F. MISEK
LINDA C. SPARKS

**COMPUTER SERVICE GROUP**
B. L. BISHOP
N. S. MALTHOUSE

**LIBRARIANS**
BRENDA RUTHERFORD*
PHYLLIS B. ZUSCHNEID*

**CONSULTANTS**
R. A. BOHM
E. S. LEE
M. L. LEVIN
D. O. PRICE

## CIVIL DEFENSE RESEARCH
C. V. CHESTER

**SECRETARIAL STAFF**
MARGARET A. CHRISMON
RUBY N. THURMER

**TECHNICAL SUPPORT**
S. D. ATTAYA[10]
C. B. BROOKS
N. J. FRIGO[10]

**LIBRARIANS**
BRENDA RUTHERFORD*
PHYLLIS B. ZUSCHNEID*

**ELECTROMAGNETIC PULSE**
J. H. MARABLE
P. R. BARNES
R. W. MANWEILER
D. B. NELSON[13]
G. L. RAGAN

**STRATEGIC DEFENSE**
G. A. CRISTY
R. O. CHESTER
J. S. GAILAR
C. M. HAALAND
C. H. KEARNY

## EDUCATION AND INFORMATION
J. E. TURNER*
K. BECKER*
S. R. BERNARD*
M. F. FAIR*
J. C. HART*
C. F. HOLOWAY*
B. L. HOUSER*

**SECRETARIAL STAFF**
NATALIE TARR*

**HEALTH PHYSICS DIVISION ADVISORY COMMITTEE**

GEORGE COWPER
ATOMIC ENERGY OF CANADA
CHALK RIVER, ONTARIO
CANADA

HENRY DAVID
NATIONAL ACADEMY OF SCIENCES
WASHINGTON, D.C.

EDWARD GERJUOY
UNIVERSITY OF PITTSBURGH
PITTSBURGH, PA.

HOWARD HARRENSTIEN
UNIVERSITY OF MIAMI
MIAMI, FLA.

L. V. SPENCER
NATIONAL BUREAU OF STANDARDS
WASHINGTON, D.C.

R. C. THOMPSON
BATTELLE NORTHWEST
RICHLAND, WASHINGTON

**HEALTH PHYSICS DIVISION LONG RANGE PLANNING COMMITTEE**

J. E. TURNER, CHAIRMAN
J. R. MUIR, VICE CHAIRMAN
G. A. CRISTY
G. S. HURST
C. H. MILLER
C. H. PATRICK
J. W. POSTON
E. G. STRUXNESS[14]
J. H. THORNGATE

*DUAL CAPACITY
*ALTERNATE FINANCE OFFICER
°QUALITY ASSURANCE COORDINATOR
‡RADIATION CONTROL OFFICER
‡DIVISION SAFETY OFFICER
[1]ON LOAN FROM MATHEMATICS DIVISION
[2]POSTDOCTORAL FELLOW
[3]ON LOAN TO ENVIRONMENTAL IMPACT STUDIES
[4]STUDENT
[5]VISITING PROFESSOR
[6]ALIEN GUEST
[7]PLANT AND EQUIPMENT DIVISION
[8]INSTRUMENTATION AND CONTROLS DIVISION
[9]NEUTRON PHYSICS DIVISION
[10]SUMMER EMPLOYEE
[11]ON LOAN TO AEC, WASHINGTON
[12]ON LOAN FROM ORAU
[13]THERMONUCLEAR DIVISION
[14]ENVIRONMENTAL SCIENCES DIVISION